



**BINDING SERVICES**  
Tel +44 (0)29 2087 4949  
Fax +44 (0)29 20371921  
e-mail [bindery@cardiff.ac.uk](mailto:bindery@cardiff.ac.uk)



**Seasonally laminated Late Quaternary  
Antarctic sediments**

**Eleanor Jane Maddison**

**School of Earth, Ocean and Planetary Sciences  
Cardiff University**

UMI Number: U584807

All rights reserved

INFORMATION TO ALL USERS

The quality of this reproduction is dependent upon the quality of the copy submitted.

In the unlikely event that the author did not send a complete manuscript and there are missing pages, these will be noted. Also, if material had to be removed, a note will indicate the deletion.



UMI U584807

Published by ProQuest LLC 2013. Copyright in the Dissertation held by the Author.  
Microform Edition © ProQuest LLC.

All rights reserved. This work is protected against  
unauthorized copying under Title 17, United States Code.



ProQuest LLC  
789 East Eisenhower Parkway  
P.O. Box 1346  
Ann Arbor, MI 48106-1346

**DECLARATION**

This work has not previously been accepted for any degree and is not concurrently submitted in candidature for any degree.

Signed.....*J. Ma*..... (candidate)

Date.....*2nd March 2006*.....

**STATEMENT 1**

This thesis is the result of my own investigations, except where otherwise stated. Other sources are acknowledged by footnotes giving explicit references. A bibliography is appended.

Signed.....*J. Ma*..... (candidate)

Date.....*2nd March 2006*.....

**STATEMENT 2**

I hereby give consent for my thesis, if accepted, to be available for photocopying and for inter-library loan, and for the title and summary to be made available to outside organisations.

Signed.....*J. Ma*..... (candidate)

Date.....*2nd March 2006*.....

**DECLARATION**

This work has not previously been accepted for any degree and is not concurrently submitted in candidature for any degree.

Signed.....J. Ma..... (candidate)

Date.....2nd March 2006.....

**STATEMENT 1**

This thesis is the result of my own investigations, except where otherwise stated. Other sources are acknowledged by footnotes giving explicit references. A bibliography is appended.

Signed.....J. Ma..... (candidate)

Date.....2nd March 2006.....

**STATEMENT 2**

I hereby give consent for my thesis, if accepted, to be available for photocopying and for inter-library loan, and for the title and summary to be made available to outside organisations.

Signed.....J. Ma..... (candidate)

Date.....2nd March 2006.....

## Summary

Quaternary diatom-rich laminated sediments, found in Antarctic inner shelf depressions, contain high-resolution records of climate change. Diatom assemblages and sediment fabric of four laminated intervals were examined with a scanning electron microscope (using backscattered and secondary electron imagery) and light microscope in this study.

Deglacial Palmer Deep laminated sediments (western Antarctic Peninsula) are composed of alternating biogenic diatom ooze and diatom-bearing terrigenous laminae. These laminae are interpreted as spring and summer signals respectively, with negligible winter deposition. Sub-seasonal species specific sub-laminae are observed repeatedly through the summer laminae. Tidal cycles, high storm intensities and / or intrusion of Circumpolar Deep Water onto the continental shelf create variation in shelf waters, enhancing species specific productivity through the summer.

Post-glacial Mertz Ninnis Trough laminated sediments (East Antarctic Margin) are composed of five lamina and one sub-lamina types. During deposition the Mertz Glacier Polynya was active and Adélie Land Bottom Water formation was strong.

Mid-Holocene Mertz Ninnis Trough laminated sediments are composed of five lamina types. Sea ice cover and sea ice formation was reduced relative to post-glacial times. The Mertz Glacier Polynya was not as active as in the post-glacial and Adélie Land Bottom Water formation was lower.

Late-Holocene Durmont d'Urville Trough laminated sediments (East Antarctic Margin) are composed of eight lamina and one sub-lamina types. Sea ice cover was extensive and persistent in the late-Holocene. Warmer periods occurred during the transition from mid-Holocene Climatic Optimum to cooler late-Holocene climatic conditions.

The types of lamina and sub-lamina formed in all four laminated intervals are controlled by seasonal sea ice cover, nutrient levels and light levels, which are in turn influenced by climate and oceanography. The Western Antarctic Peninsula and East Antarctic Margin laminated sediments give an insight into oceanographic responses to climatic change and variation through the Quaternary around the Antarctic margin.

## Acknowledgements

Firstly, I would like to express my gratitude to my main supervisor Dr Jennifer Pike, for her enthusiastic guidance, continuous support and scientific discussion throughout this study. I could not have imagined a better supervisor for my PhD. I am also grateful to Dr Amy Leventer for her supervision on this project and diatom taxonomy coaching.

Thanks to Dr Catherine Stickley for our diatom discussions and proof reading of thesis chapters. I thank Dr Xavier Crosta for making me very welcome on the *R/V Marion DuFresne* and for interesting dialogue on ecological preferences of diatom species (plus French lessons!). I would like to thank Rob Dunbar for the AMS-radiocarbon dates. I am grateful to Dr Leanne Armand for the diatom taxonomy lessons on board the *R/V Marion DuFresne*. Thanks to Dr Ian MacMillan for his assistance in identifying foraminifera from BSEI photographs. The opportunity to participate on the French CADO cruise to Antarctica is appreciated.

I would like to thank Pete Fisher for his instruction on the use of SEM 360 and ESEM facilities, showing me which buttons to press (and not to press!). I would also like to thank Laurence Badham for preparing polished thin sections, Lindsay Axe for light microscope assistance, Alun Rogers for his invaluable advice on Corel Draw and Andrew Wiltshire for IT support.

I acknowledge receipt of Natural Environment Research Council postgraduate research studentship NER/S/A/2002/10350. Thanks also go to The Micropalaeontological Society and the Quaternary Research Association for additional financial support.

I thank my office mates for making me laugh all the way through this PhD. Thanks to my parents, brother, Jess and Sarah for their encouragement and support. Lastly, I must thank Neil for keeping me sane over the last three years, and being a gentleman by allowing me to finish first!



## List of Abbreviations

AABW	Antarctic Bottom Water
AAIW	Antarctic Intermediate Water
AASW	Antarctic Surface Waters
ACC	Antarctic Circumpolar Current
ACoastC	Antarctic Coastal Current
ACR	Antarctic Cold Reversal
AG	Astrolabe Glacier
ALBW	Adélie Land Bottom Water
AZ	Antarctic Zone
BSEI	Backscattered Electron Imagery
CDW	Circumpolar Deep Water
CRS	<i>Hyalochaete Chaetoceros</i> spp. resting spores
CPT	Circumpolar Trough
DER	Diglycidol Ether of Polypropyleneglycol
DMAE	Dimethylaminoethanol
DUT	Durmont d'Urville Trough
EAIS	East Antarctic Ice Sheet
ESEM	Environmental Scanning Electron Microscope
HSSW	High Salinity Shelf Water
ISW	Ice-Shelf Water
LCDW	Lower Circumpolar Deepwater
LGM	Last Glacial Maximum
mbsf	Metres below sea floor
mcd	Metres composite depth
MCDW	Modified Circumpolar Deepwater
MGT	Mertz Glacier Tongue
MGP	Mertz Glacier Polynya
MNT	Mertz Ninnis Trough
NADW	North Atlantic Deepwater
NSA	Nonenyl Succinic Anhydride
PD	Palmer Deep
PF	Polar Front
PFZ	Polar Frontal Zone
RS	Resting Spore
SAF	Subantarctic Front
SEI	Secondary Electron Imagery
SEM	Scanning Electron Microscope
SIZ	Seasonal Ice Zone
STF	Subtropical Front
UCDW	Upper Circumpolar Deepwater
VCD	Vinocyclohexene Dioxide
WAIS	West Antarctic Ice Sheet
WDW	Warm Deep Water
WW	Winter Water
YD	Younger Dryas
ZG	Zélée Glacier

## List of Contents

Declaration .....	i
Summary .....	ii
Acknowledgements .....	iii
List of Abbreviations .....	iv
List of Contents .....	v
List of Tables .....	xii
List of Figures .....	xv

### CHAPTER 1

<b>1. Introduction.....</b>	<b>1</b>
1.1 Background.....	1
1.2 Thesis objectives.....	1
1.3 Thesis format.....	3

### CHAPTER 2

<b>2. Location background.....</b>	<b>4</b>
2.1 Geology of the Southern Ocean and Antarctic.....	4
2.2 Antarctic Ice Sheet History.....	6
2.3 Southern Ocean Oceanography.....	7
2.3.1 Zones of the Southern Ocean.....	7
2.3.2 Southern Ocean Water Masses and Currents.....	9
2.3.2.1 Antarctic Zone and Continental Margin.....	9
2.3.2.2 Subantarctic Zone.....	10
2.4 Palaeoclimate and Present Climate.....	10
2.4.1 Last Glacial .....	10
2.4.2 The Last Deglaciation.....	11
2.4.3 Holocene.....	13
2.4.4 Modern Antarctic Climate.....	15
2.5 Study Regions.....	16
2.5.1 Palmer Deep, Western Antarctic Peninsula.....	16
2.5.1.1 Geology.....	16
2.5.1.2 Glaciology.....	16
2.5.1.3 Regional Oceanography.....	19
2.5.1.4 Climate.....	20
2.5.2 Mertz Ninnis Trough, East Antarctic Margin.....	21
2.5.2.1 Geology.....	21
2.5.2.2 Glaciology.....	21
2.5.2.3 Mertz Glacier Polynya and Regional Oceanography.....	23
2.5.2.4 Climate.....	28
2.5.3 Durmont d’Urville Trough, East Antarctic Margin.....	28
2.5.3.1 Geology.....	28
2.5.3.2 Glaciology.....	28
2.5.3.3 Regional Oceanography.....	29
2.5.3.4 Climate.....	29
2.6 Summary.....	29

### CHAPTER 3

<b>3. Diatoms in the Southern Ocean.....</b>	<b>30</b>
3.1 Introduction.....	30
3.2 Environmental Controls on Diatom Assemblage Distribution.....	31
3.2.1 Sea Ice Zone.....	32
3.2.2 Marginal Ice Zone.....	33
3.2.3 Open Ocean Zone.....	34
3.2.4 Polar Front Zone.....	35
3.3 Preservation Controls on Diatom Assemblage Distribution.....	35
3.3.1 Dissolution.....	35
3.3.2 Aggregation.....	36
3.3.3 Advection.....	37
3.4 Antarctic Laminated Sediments.....	37
3.5 Species Ecology.....	39
3.5.1 <i>Actinocyclus actinochilus</i> (Ehrenberg) Simonsen.....	39
3.5.2 Genus <i>Astermophalus</i> Ehrenberg.....	39
3.5.3 Genus <i>Chaetoceros</i> Ehrenberg.....	41
3.5.3.1 Sub-genus <i>Hyalochaete</i> <i>Chaetoceros</i> Gran.....	41
3.5.3.2 Sub-genus <i>Phaeoceros</i> <i>Chaetoceros</i> Gran.....	41
3.5.4 Genus <i>Cocconeis</i> Ehrenberg.....	42
3.5.5 <i>Corethron pennatum</i> (Grunow) Ostenfeld.....	42
3.5.6 <i>Coscinodiscus bouvet</i> Karsten.....	42
3.5.7 <i>Eucampia antarctica</i> (Castracane) Mangin.....	43
3.5.8 <i>Fragilariopsis curta</i> (Van Heurck) Hustedt.....	43
3.5.9 <i>Fragilariopsis cylindrus</i> (Grunow) Krieger.....	44
3.5.10 <i>Fragilariopsis kerguelensis</i> (O'Meara) Hustedt.....	44
3.5.11 <i>Fragilariopsis obliquecostata</i> (Van Heurck) Heiden.....	45
3.5.12 <i>Fragilariopsis rhombica</i> (O'Meara) Hustedt.....	46
3.5.13 <i>Fragilariopsis ritscheri</i> (Hustedt) Hasle.....	46
3.5.14 <i>Fragilariopsis separanda</i> Hustedt.....	46
3.5.15 <i>Fragilariopsis sublinearis</i> (Van Heurck) Heiden.....	47
3.5.16 <i>Fragilariopsis vanheuckii</i> (M.Pergallo) Hustedt.....	47
3.5.17 Genus <i>Navicula</i> Bory de st-Vincent.....	47
3.5.18 <i>Odontella weissflogii</i> (Janisch) Grunow.....	47
3.5.19 Genus <i>Porosira</i> Jørgensen.....	48
3.5.20 Genus <i>Proboscia</i> Sunström.....	48
3.5.21 Genus <i>Rhizosolenia</i> Brightwell.....	49
3.5.22 <i>Stellarima microtrias</i> (Ehrenberg) Hasle & Sims.....	50
3.5.23 <i>Thalassiosira antarctica</i> Comber.....	50
3.5.24 <i>Thalassiosira gracilis</i> (Karsten) Hustedt.....	51
3.5.25 <i>Thalassiosira gravida</i> Cleve.....	51
3.5.26 <i>Thalassiosira lentiginosa</i> (Janisch) Fryxell.....	52
3.5.27 <i>Thalassiosira oliverana</i> (O'Meara) Makarova & Nikolaev.....	52
3.5.28 <i>Thalassiosira oestrupii</i> (Ostenfeld) Hasle.....	52
3.5.29 <i>Thalassiosira tumida</i> (Janisch) Hasle.....	53
3.5.30 <i>Thalassiothrix antarctica</i> Schimper ex Karsten.....	53
3.5.31 <i>Trichotoxon reinboldii</i> (Van Heurck) Reid & Round.....	53
3.5.32 <i>Trigonium arcticum</i> (Brightwell) Cleve.....	54
3.6 Summary.....	54

## CHAPTER 4

<b>4. Core site data.....</b>	<b>55</b>
4.1 Palmer Deep, Western Antarctic Peninsula.....	55
4.1.1 Bathymetry.....	55
4.1.2 Core Type and Sediment Description.....	57
4.1.3 Age.....	57
4.2 Mertz Ninnis Trough, East Antarctic Margin.....	61
4.2.1 Bathymetry.....	61
4.2.2 Core Type and Sediment Description.....	63
4.2.3 Age.....	66
4.3 Durmont d'Urville Trough, East Antarctic Margin.....	70
4.3.1 Bathymetry.....	70
4.3.2 Core Type and Sediment Description.....	71
4.3.3 Age.....	71
4.4 Summary.....	75

## CHAPTER 5

<b>5. Methods.....</b>	<b>76</b>
5.1 Sampling Strategy.....	76
5.2 Sample Preparation.....	76
5.2.1 Polished Thin Sections.....	76
5.2.2 Sediment Stubs.....	78
5.2.3 Quantitative Diatom Analysis.....	79
5.3 Data Collection.....	81
5.3.1 Backscattered Electron Imagery (BSEI).....	81
5.3.2 Secondary Electron Imagery (SEI).....	82
5.3.3 Quantitative Diatom Counts.....	82
5.4 Summary.....	86

## CHAPTER 6

<b>6. Palmer Deep.....</b>	<b>87</b>
6.1 Results.....	87
6.1.1 Orange-brown Biogenic Laminae.....	88
6.1.2 Blue-grey Terrigenous Laminae.....	92
6.1.3 Lamina Relationships.....	94
6.1.4 Sub-laminae within Blue-grey Laminae (Terrigenous).....	96
6.1.5 Sub-lamina Relationships.....	103
6.1.6 Lamina and Sub-lamina Relationships.....	104
6.1.7 Other Observations.....	105
6.2 Interpretation.....	108
6.2.1 Spring: Orange-brown Biogenic Laminae.....	108
6.2.2 Summer: Blue-grey Terrigenous Laminae.....	109
6.2.3 Winter.....	111
6.2.4 Annual Signal.....	111
6.2.5 Sub-seasonal Signal.....	111
6.2.6 Sub-seasonal and Seasonal Relationship.....	113
6.2.7 Discussion of Other Observations.....	115
6.3 Conclusions.....	116

## CHAPTER 7

7.	<b>Mertz Ninnis Trough.....</b>	<b>118</b>
7.1	Results NBP0101 JPC10.....	118
7.1.1	Biogenic Laminae.....	119
7.1.1.1	Near-monogeneric <i>Hyalochaete Chaetoceros</i> spp. Resting Spore Laminae.....	119
7.1.1.2	Laminae Characterised by <i>Corethron pennatum</i> .....	120
7.1.1.3	Laminae Characterised by <i>Rhizosolenia</i> spp. ....	126
7.1.1.4	Mixed Diatom Assemblage Laminae.....	126
7.1.2	Terrigenous Laminae.....	127
7.1.2.1	Mixed Diatom Assemblage Terrigenous Laminae.....	127
7.1.2.2	Terrigenous Sub-laminae Characterised by <i>Porosira glacialis</i> Resting Spores.....	128
7.1.3	Lamina Relationships.....	129
7.2	Interpretation and Discussion NBP0101 JPC10.....	131
7.2.1	Seasonal Signal.....	131
7.2.1.1	Spring: Near-monogeneric <i>Hyalochaete Chaetoceros</i> spp. Resting Spore Laminae.....	132
7.2.1.2	Summer: Laminae Characterised by <i>Corethron pennatum</i> or <i>Rhizosolenia</i> spp. ....	132
7.2.1.3	Summer: Mixed Diatom Assemblage Biogenic Laminae.....	133
7.2.1.4	Summer/Autumn: Mixed Diatom Assemblage Terrigenous Laminae...	133
7.2.1.5	Autumn: Terrigenous Sub-laminae Characterised by <i>Porosira glacialis</i> Resting Spores.....	134
7.2.2	Lamina Relationships.....	135
7.2.3	Polynya Model for Mertz Ninnis Trough Laminated Sediments.....	136
7.2.3.1	Spring.....	136
7.2.3.2	Summer.....	138
7.2.3.3	Summer/Autumn.....	138
7.2.3.4	Autumn.....	139
7.2.3.5	Winter.....	139
7.3	Conclusions NBP0101 JPC10.....	140
7.4	Results NBP0101 KC10A.....	141
7.4.1	Biogenic Laminae.....	141
7.4.1.1	Biogenic Laminae Characterised by <i>Fragilariopsis</i> spp. ....	141
7.4.2	Terrigenous Laminae.....	143
7.4.2.1	Terrigenous Laminae Characterised by <i>Fragilariopsis</i> spp. ....	143
7.4.3	Lamina Relationships.....	144
7.5	Interpretation and Discussion NBP0101 KC10A.....	148
7.5.1	Seasonal Signal.....	148
7.5.1.1	Spring/Summer: Biogenic Laminae.....	148
7.5.1.2	Summer/Autumn: Terrigenous Laminae.....	148
7.5.2	Lamina Relationships.....	149
7.6	Conclusions NBP0101 KC10A.....	150
7.7	Summary.....	151

## CHAPTER 8

<b>8.</b>	<b>Durmont d'Urville Trough.....</b>	<b>152</b>
8.1	Results.....	152
8.1.1	Laminae Characterised by <i>Hyalochaete Chaetoceros</i> spp. Resting Spores.....	153
8.1.2	Laminae Characterised by <i>Hyalochaete Chaetoceros</i> spp. Resting Spores and <i>Fragilariopsis</i> spp. ....	160
8.1.3	Laminae Characterised by <i>Fragilariopsis</i> spp. ....	160
8.1.4	Laminae Characterised by <i>Corethron pennatum</i> and <i>Rhizosolenia</i> spp...	161
8.1.5	Laminae Characterised by <i>Corethron pennatum</i> .....	165
8.1.6	Laminae Characterised by <i>Rhizosolenia</i> spp. ....	167
8.1.7	Mixed Diatom Assemblage Laminae.....	169
8.1.8	Sub-laminae Characterised by <i>Porosira glacialis</i> Resting Spores.....	171
8.1.9	Laminae Characterised by <i>Stellarima microtrias</i> Resting Spores, <i>Porosira glacialis</i> Resting Spores and / or <i>Coscinodiscus bouvet</i> .....	174
8.1.10	Lamina Relationships.....	176
8.2	Interpretation and Discussion.....	178
8.2.1	Seasonal Signal.....	178
8.2.1.1	Spring: Laminae Characterised by <i>Hyalochaete Chaetoceros</i> spp. Resting Spores and / or <i>Fragilariopsis</i> spp.....	178
8.2.1.2	Summer: Laminae Characterised by <i>Corethron pennatum</i> and / or <i>Rhizosolenia</i> spp. ....	179
8.2.1.3	Summer: Mixed Diatom Assemblage.....	180
8.2.1.4	Autumn/Spring Transition: Sub-lamina Characterised by <i>Porosira glacialis</i> Resting Spores.....	181
8.2.1.5	Autumn/Spring Transition: Laminae Characterised by <i>Stellarima microtrias</i> Resting Spores, <i>Porosira glacialis</i> Resting Spores and / or <i>Coscinodiscus bouvet</i> .....	181
8.2.2	Lamina Relationships.....	182
8.3	Conclusions.....	186

## CHAPTER 9

<b>9.</b>	<b>Core site comparison.....</b>	<b>187</b>
9.1	Deglacial and Post-glacial Laminated Sediment Comparison.....	187
9.1.1	Comparison.....	187
9.1.1.1	Position of Core Sites.....	187
9.1.1.2	Annual Cycle of Lamina and Sub-lamina Deposition.....	188
9.1.1.3	Lamina Types.....	191
9.1.1.4	Sub-lamina Types.....	192
9.1.2	Implications.....	193
9.2	Post-glacial and Mid-Holocene Laminated Sediment Comparison.....	195
9.2.1	Comparison.....	195
9.2.1.1	Position of Core Sites.....	195
9.2.1.2	Annual Cycle of Lamina and Sub-lamina Deposition.....	196
9.2.1.3	Lamina Types.....	196
9.2.1.4	Sub-lamina Types.....	197
9.2.2	Implications.....	197
9.3	Post-glacial and Late-Holocene Laminated Sediment Comparison.....	198
9.3.1	Comparison.....	198
9.3.1.1	Position of Core Sites.....	198

9.3.1.2	Annual Cycle of Lamina and Sub-lamina Deposition.....	199
9.3.1.3	Lamina Types.....	199
9.3.1.4	Sub-lamina Types.....	201
9.3.2	Implications.....	201
9.4	Mid-Holocene and Late-Holocene Laminated Sediment Comparison.....	205
9.4.1	Comparison.....	205
9.4.1.1	Annual Cycle of Lamina and Sub-lamina Deposition.....	205
9.4.1.2	Lamina Types.....	206
9.4.1.3	Sub-lamina Types.....	206
9.4.2	Implications.....	207
9.5	Comparison of all Four Laminated Sediments.....	207
9.5.1	Temporal Change in Absolute Abundance of Diatoms.....	207
9.5.2	Species Distribution Circum-Antarctica.....	208
9.5.3	Temporal Oceanographic Changes.....	210
9.5.4	Temporal Sedimentary Record Change.....	210
9.5.5	Temporal Climate Change.....	211
9.6	Summary.....	212

## CHAPTER 10

<b>10.</b>	<b>Conclusions and future research.....</b>	<b>213</b>
10.1	Main Conclusions.....	213
10.1.1	Deglacial Laminated Sediment, Palmer Deep, Western Antarctic Peninsula.....	213
10.1.2	Post-glacial Laminated Sediment, Mertz Ninnis Trough, East Antarctic Margin.....	213
10.1.3	Mid-Holocene Laminated Sediment, Mertz Ninnis Trough, East Antarctic Margin.....	214
10.1.4	Late-Holocene Laminated Sediment, Durmont d'Urville Trough, East Antarctic Margin.....	215
10.1.5	Wider Implications.....	216
10.1.6	Summary.....	216
10.2	Future Research.....	217

## APPENDICES

<b>A.1</b>	<b>Diatom Taxonomy.....</b>	<b>219</b>
<b>A.2</b>	<b>Diatom Images.....</b>	<b>224</b>
<b>A.3</b>	<b>Lamina type and thickness data.....</b>	<b>234</b>
A.3.1	Palmer Deep, Western Antarctic Peninsula.....	235
A.3.1.1	ODP Core 178-1098A-6H.....	236
A.3.1.2	ODP Core 178-1098A-6H and -1098C-5H.....	240
A.3.2	Mertz Ninnis Trough, East Antarctic Margin.....	244
A.3.2.1	NBP0101 JPC10.....	245
A.3.2.2	NBP0101 KC10A.....	251
A.3.3	Durmont D'Urville Trough, East Antarctic Margin.....	252
A.3.3.1	MD03 2597.....	253
<b>A.4</b>	<b>Quantitative diatom abundance data.....</b>	<b>260</b>
A.4.1	Palmer Deep, Western Antarctic Peninsula.....	260
A.4.1.1	ODP Core 178-1098A-6H.....	260
A.4.2	Mertz Ninnis Trough, East Antarctic Margin.....	266
A.4.2.1	NBP0101 JPC10.....	266
A.4.2.2	NBP0101 KC10A.....	271
A.4.3	Durmont D'Urville Trough, East Antarctic Margin.....	273
A.4.3.1	MD03 2597.....	273
<b>A.5</b>	<b>Markov chain analysis.....</b>	<b>282</b>
	<b>REFERENCES.....</b>	<b>288</b>



## List of Tables

### Chapter 2: Location background

2.1	Water mass properties in the vicinity of Palmer Deep.....	20
2.2	Water mass properties (area-averaged) for Mertz Ninnis Trough region.....	28

### Chapter 4: Core site data

4.1	Summary of core data.....	55
4.2	Palmer Deep core sample depths.....	57
4.3	Radiocarbon dates for Palmer Deep, ODP Leg 178.....	60
4.4	Mertz Ninnis Trough sample depths.....	63
4.5	Uncorrected radiocarbon dates for NBP0101 JPC10 and JPC 11, Mertz Ninnis Trough, corrected age was derived by subtracting the average core top age (2516±60 <sup>14</sup> C yrs) from adjacent cores sites. Ages calibrated with CALIB 5.0.....	67
4.6	Uncorrected radiocarbon dates for NBP0101 KC10A, Mertz Ninnis Trough, corrected age was derived by subtracting the average core top age (2516 ± 60 <sup>14</sup> C yrs) from adjacent cores sites. Ages calibrated with CALIB 5.0.....	68
4.7	Durmont d'Urville Trough core sample depths.....	71
4.8	Uncorrected radiocarbon dates for MD03 2597, Durmont d'Urville Trough, calibrated with CALIB 5.0.....	74

### Chapter 5: Methods

5.1	Amounts of Spurr resin constituents and acetone used in preparation of sediment samples. Order and number of additions.....	78
-----	---	----

### Chapter 6: Palmer Deep

6.1	Relative abundance of all diatom species in eight orange-brown biogenic laminae, Palmer Deep, ODP core 178-1098A.....	90
6.2	Relative abundance of <i>Hyalochaete Chaetcoeros</i> spp. free diatom assemblages in eight orange-brown biogenic laminae, Palmer Deep, ODP core 178-1098A.....	90
6.3	Absolute abundance of diatom species (valves per gramme x10 <sup>6</sup> of dry sediment) in eight orange-brown biogenic laminae, Palmer Deep, ODP core 178-1098A.....	92
6.4	Relative abundance of all diatom species in seven blue-grey terrigenous laminae, Palmer Deep, ODP core 178-1098A.....	93
6.5	Relative abundance of <i>Hyalochaete Chaetoceros</i> spp. free diatom assemblages in seven blue-grey, terrigenous laminae, Palmer Deep, ODP core 178-1098A.....	93

6.6	Absolute abundance of diatom species (valves per gramme x10 <sup>6</sup> of dry sediment) in seven blue-grey terrigenous laminae, Palmer Deep, ODP core 178-1098A.....	94
6.7	Relative abundance of all diatom species from terrigenous sub-laminae, Palmer Deep, ODP core 178-1098A.....	98
6.8	Relative abundance of <i>Hyalochaete Chaetcoeros</i> spp. free diatom assemblages from terrigenous sub-laminae, Palmer Deep, ODP core 178-1098A.....	99
6.9	Absolute abundance of diatom species (valves per gramme x10 <sup>6</sup> of dry sediment) from terrigenous sub-laminae, Palmer Deep, ODP core 178-1098A.....	99

### Chapter 7: Mertz Ninnis Trough

7.1	Relative abundance of all diatom species by lamina type, Mertz Ninnis Trough, NBP0101 JPC10.....	119
7.2	Relative abundance of <i>Chaetoceros</i> spp. free diatom assemblage by lamina type, Mertz Ninnis Trough, NBP0101 JPC10.....	120
7.3	Absolute abundance of diatom species (valves per gramme of dry sediment x10 <sup>6</sup> ) by lamina type, Mertz Ninnis Trough, NBP0101 JPC10.....	127
7.4	Relative abundance of all diatom species by lamina type, Mertz Ninnis Trough, NBP0101 KC10A.....	142
7.5	Relative abundance of <i>Chaetoceros</i> spp. free diatom assemblage by lamina type, Mertz Ninnis Trough, NBP0101 KC10A.....	142
7.6	Absolute abundance of diatom species (valves per gramme of dry sediment x10 <sup>6</sup> ) by lamina type, Mertz Ninnis Trough, NBP0101 KC10A.....	143

### Chapter 8: Durmont d'Urville Trough

8.1	Relative abundance of all diatom species by lamina type, Duromont d'Urville Trough, MD03 2597.....	155
8.2	Relative abundance of <i>Hyalochaete Chaetcoeros</i> spp. free counts by lamina type, Duromnt d'Urville Trough, MD03 2597.....	156
8.3	Absolute abundance of all diatom species (x10 <sup>6</sup> valves per gramme of dry sediment) by lamina type, Duromnt d'Urville Trough, MD03 2597.....	157

### Appendix 3: Lamina type and thickness data

A3.1.1	ODP Core 178-1098A-6H.....	236
A3.1.2	ODP Core 178-1098A-6H & -1098C-5H (combined).....	240
A3.2.1	NBP0101 JPC10.....	245
A3.2.1	NBP0101 KC10A.....	251
A3.3.1	MD03 2597.....	253

#### Appendix 4: Quantitative diatom abundance data

A4.1.1.1	Palmer Deep, ODP Core 178-1098A-6H, biogenic laminae quantitative diatom abundance counts, all species.....	260
A4.1.1.2	Palmer Deep, ODP Core 178-1098A-6H, biogenic laminae quantitative diatom abundance counts, <i>Hyalochaete Chaetoceros</i> spp. free.....	261
A4.1.1.3	Palmer Deep, ODP Core 178-1098A-6H, terrigenous laminae quantitative diatom abundance counts, all species.....	262
A4.1.1.4	Palmer Deep, ODP Core 178-1098A-6H, terrigenous laminae quantitative diatom abundance counts, <i>Hyalochaete Chaetoceros</i> spp. free.....	263
A4.1.1.5	Palmer Deep, ODP Core 178-1098A-6H, terrigenous sub-laminae quantitative diatom abundance counts, all species.....	264
A4.1.1.6	Palmer Deep, ODP Core 178-1098A-6H, terrigenous sub-laminae quantitative diatom abundance counts, <i>Hyalochaete Chaetoceros</i> spp. free.....	265
A4.2.1.1	Mertz Ninnis Trough, NBP0101 JPC10, biogenic laminae quantitative counts, all species.....	267
A4.2.1.2	Mertz Ninnis Trough, NBP0101 JPC10, biogenic laminae quantitative counts, <i>Chaetoceros</i> spp. free.....	268
A4.2.1.3	Mertz Ninnis Trough, NBP0101 JPC10, terrigenous lamina and sub-lamina quantitative counts, all species.....	269
A4.2.1.4	Mertz Ninnis Trough, NBP0101 JPC10, terrigenous lamina and sub-lamina quantitative counts, <i>Chaetoceros</i> spp. free.....	270
A4.2.2.1	Mertz Ninnis Trough, NBP0101 KC10A, quantitative diatom abundance counts, all species.....	271
A4.2.2.2	Mertz Ninnis Trough, NBP0101 KC10A, quantitative diatom abundance counts, <i>Chaetoceros</i> spp. free.....	272
A4.3.1.1	Durmont d'Urville Trough, MD03 2597, quantitative diatom abundance counts of all species.....	274
A4.3.1.2	Durmont d'Urville Trough, MD03 2597, quantitative diatom abundance <i>Hyalochaete Chaetoceros</i> spp. free counts.....	278

## List of Figures

### Chapter 1: Introduction

- 1.1 Locations of Antarctic laminated sediments.....2

### Chapter 2: Location background

- 2.1 Gondwana reconstruction from Early Jurassic (200 Ma) to present day.....5
- 2.2 Last Glacial Maximum ice sheet reconstruction for Antarctica..... 8
- 2.3 Schematic block diagram showing the surface currents and vertical motion of water masses in the Southern Ocean pole-ward of 40°S..... 8
- 2.4 Changes in the annual average sea surface temperatures (Last Glacial Maximum (LGM) – modern), with geographic distribution of LGM seasonal and perennial sea ice, and LGM land ice, based on seasonal estimates of CLIMAP..... 12
- 2.5 Stable isotope profiles from GISP2, Byrd and Vostok..... 12
- 2.6 Stratigraphic succession of Palmer Deep, Antarctic Peninsula, indicating Holocene palaeointervals..... 14
- 2.7 Geographic locations of the three core sites: Palmer Deep, Mertz Ninnis Trough and Durmont d’Urville Trough.....14
- 2.8 Schematic geological cross-section across Palmer Deep and the Gerlache Strait.....17
- 2.9 Cartoon illustrating various stages of glaciation of the Palmer Deep Basin I..... 17
- 2.10 Last Glacial Maximum reconstruction and palaeodrainage map for the Antarctic Peninsula region showing geomorphic features..... 18
- 2.11 Oceanographic regime of the Antarctic Peninsula..... 18
- 2.12 Geological map of George V Land and Terre Adélie.....22
- 2.13 Late Pleistocene ice sheet reconstructions for the Wilkes Land continental shelf.....22
- 2.14 Map showing facies on the George V shelf.....24
- 2.15 Cartoons showing the extent and retreat of the Mertz Glacier Tongue during the Last Glacial Maximum (LGM) and after the LGM..... 24
- 2.16 The position of the Mertz and Ninnis Glacier Tongues in 1913, 1962 and 1993...25
- 2.17 Oceanographic regime off the George V Coast.....25
- 2.18 Schematic representation of physical processes taking place in deep water and shelf water polynyas..... 26
- 2.19 Oceanographic regime off the Terre Adélie Coast..... 26

### Chapter 3: Diatoms in the Southern Ocean

- 3.1 Map of sediment type distribution around Antarctica..... 31
- 3.2 Schematic representation of the extent of the four Southern Ocean zones; Sea Ice Zone, Marginal Ice Zone, Open Ocean Zone and Polar Front Zone..... 32
- 3.3 Highly idealised schematic illustrations of (a) fast ice and (b) pack ice ecosystems in Antarctica showing the location of the major ice algal communities..... 33

3.4	(a) Schematic map showing Southern Ocean circulation. (b) Diagrammatic circulation transect through 135°E in the southeast Indian Ocean.....	40
3.5	Mean monthly sea ice concentrations for February (austral summer) and October (austral winter) averaged over 8.8 years between 1978-1987.....	45

#### Chapter 4: Core site data

4.1	Geographic locations of the three core sites: Palmer Deep, Mertz Ninnis Trough and Durmont d'Urville Trough.....	56
4.2	(a) Location map of ODP Site 1098, Palmer Deep on the Antarctic Peninsula continental margin. (b) Map of the three fault bound basins that make up Palmer Deep and the site of Leg 178 Site 1098.....	56
4.3	Core photograph of ODP Core 178-1098A-6H .....	58
4.4	Lithographic logs of ODP 178 1098A, MD03 2597, NBP0101 JPC10 and NBP0101 KC10A.....	59
4.5	Age model for the lower 25 m of ODP Core 178 1098, Palmer Deep.....	61
4.6	Location maps of NBP0101 JPC10, KC10A and JPC11. (a) JPC10, KC10A and JPC11 core locations within the Mertz Ninnis Trough, George V Coast. (b) Seabeam Swath map of highlighted area in (a) of the JPC10, KC10A and JPC11 core sites.....	62
4.7	Core photographs of NBP0101 JPC10 from the Mertz Ninnis Trough.....	64
4.8	Core photograph of NBP0101 KC10A from the Mertz Ninnis Trough.....	65
4.9	Comparison of NBP0101 JPC10 and JPC11 bulk density plots. Dates plotted are raw uncorrected radiocarbon ages.....	65
4.10	Age model for NBP0101 JPC10 and JPC11, Mertz Ninnis Trough.....	69
4.11	Age model for NBP0101 KC10A, Mertz Ninnis Trough.....	70
4.12	(a) Bathymetry of the Adélie continental margin. Position of core MD03 2597 indicated. (b) Seabeam Swath map of highlighted are in (a).....	72
4.13	Core photographs of MD03 2597 from the Durmont d'Urville Trough.....	73
4.14	Age model for MD03 2597, Durmont d'Urville Trough.....	74

#### Chapter 5: Methods

5.1	Summary of core preparation and analysis techniques.....	77
5.2	(a) Schematic of apparatus used in the preparation of quantitative light microscope slides. (b) Photograph of apparatus in (a).....	80
5.3	A low magnification backscattered electron imagery (BSEI) photomosaic base map showing alternating laminae of biogenic diatom ooze (dark) and diatom-bearing terrigenous laminae (bright).....	82
5.4	(a) Secondary electron imagery (SEI) photograph of a sediment block mounted on a standard scanning electron microscope (SEM) stub. (b) SEI photograph of <i>Hyalochaete Chaetoceros</i> spp. resting spores, taken on surface parallel to sedimentary laminated fabric.....	83

5.5	Light microscope photograph of <i>Fragilariopsis curta</i> and <i>Hyalochaete Chaetoceros</i> spp. resting spores.....	83
5.6	Counting methodology for fragmented valves.....	85
5.7	Counting methodology for <i>Chaetoceros</i> spp. valves.....	85

**Chapter 6: Palmer Deep**

6.1	Location map of ODP Site 1098, Palmer Deep on the Antarctic Peninsula continental margin.....	87
6.2	(a) Photograph of Core 178 1098A 6H, depth ~ 42.55 to 42.75 metres composite depth (mcd), showing alternating orange-brown laminae (biogenic) and blue-grey laminae (terrigenous). Red box indicates location of (b). (b) Backscattered secondary electron imagery (BSEI) photomosaic of alternating diatom ooze biogenic laminae (dark: spring) and diatom-bearing terrigenous laminae (light: summer) from 42.66 to 42.63 mcd. (c)/(d) and (e)/(f) refer to annotation on (b). (c) BSEI photograph of diatom ooze biogenic laminae composed of <i>Hyalochaete Chaetoceros</i> spp. resting spores. (d) Secondary electron imagery (SEI) photograph of <i>Hyalochaete Chaetoceros</i> spp. resting spores from biogenic laminae. (e) BSEI photograph of terrigenous laminae. (f) SEI photograph of terrigenous laminae with mixed diatom assemblage.....	89
6.3	Graph showing the thicknesses of different types of lamina from Palmer Deep, ODP 178-1098A and -1098C. Individual thicknesses are displayed as coloured bars within the total thickness of each lamina type.....	91
6.4	(a) Graph showing biogenic lamina thicknesses through part of the deglacial interval, 44.967 - 40.664 metres composite depth (mcd). (b) Graph to show terrigenous laminae thickness through part of the deglacial interval, 45.03 - 40.634 mcd.....	91
6.5	Types of lamina boundaries observed in ODP 178-1098A Palmer Deep deglacial laminated interval. (a) Backscattered secondary electron imagery (BSEI) photograph of sharp boundary between summer (terrigenous) and spring (biogenic) laminae. (b) BSEI photograph of bioturbated boundary between summer (terrigenous) and spring (biogenic) laminae. (c) BSEI photograph of gradational boundary between spring (biogenic) and summer (terrigenous) laminae.....	95
6.6	Graph illustrating the distribution of the different terrigenous sub-lamina types, Palmer Deep ODP 178-1098A, between 45.03 and 42.51 metres composite depth (mcd).....	96
6.7	Backscattered secondary electron imagery (BSEI) photomosaic of multiple sub-laminae within the terrigenous laminae, ODP 178-1098A Palmer Deep (~ 43.12 to 43.09 mcd). Scale bar = 3 mm.....	100
6.8	Sub-laminae species associated with Figure 6.7. (a) Backscattered electron imagery (BSEI) photograph of <i>Odontella weissflogii</i> resting spore (RS) sub-lamina. (b) Secondary electron imagery (SEI) photograph of <i>O. weissflogii</i> RS sub-lamina. (c) BSEI photograph of <i>Thalassiosira antarctica</i> RS sub-lamina. (d) SEI photograph of <i>T. antarctica</i> RS sub-lamina. (e) BSEI photograph of <i>Corethron pennatum</i> sub-lamina. (f) SEI photograph of <i>C. pennatum</i> sub-lamina. (g) BSEI photograph of <i>Coscinodiscus bouvet</i> sub-lamina. (h) SEI photograph of <i>C. bouvet</i> sub-lamina.....	101

6.9	Location of sub-laminae within the blue-grey terrigenous laminae in the deglacial laminated interval, 45.03-42.51 metres composite depth (mcd), ODP 1098A Palmer Deep.....	103
6.10	Secondary electron imagery (SEI) and backscattered electron imagery (BSEI) photographs of pyrite in deglacial laminated sediments, Palmer Deep, ODP site 1098A. (a) SEI photograph of <i>Corethron pennatum</i> filled with balls of pyrite. (b) SEI photograph of close up of balls of pyrite in (a). (c) BSEI photograph of <i>C. pennatum</i> surrounded with <i>Hyalochaete Chaetoceros</i> spp. resting spores. Balls of pyrite within the <i>C. pennatum</i> frustule.....	106
6.11	Backscattered electron imagery (BSEI) photograph of an agglutinated foraminifera in an orange-brown biogenic laminae.....	107
6.12	Schematic representation of the sub-seasonal sub-laminae within the terrigenous laminae, Palmer Deep. Compiled from backscattered electron imagery (BSEI) data.....	107

## Chapter 7: Mertz Ninnis Trough

7.1	Location map of NBP0101 JPC10 and KC10A, Mertz Ninnis Trough, George V Coast.....	118
7.2	Backscattered electron imagery (BSEI) and secondary electron imagery (SEI) photographs of five lamina types and one sub-lamina type, Mertz Ninnis Trough, NBP0101 JPC10. (a) BSEI photograph of near-monogeneric <i>Hyalochaete Chaetoceros</i> spp. resting spore (CRS) laminae. (b) SEI photograph of near-monogeneric CRS laminae. (c) BSEI photograph of laminae characterised by <i>Corethron pennatum</i> . (d) SEI photograph of laminae characterised by <i>C. pennatum</i> . (e) BSEI photograph of laminae characterised by <i>Rhizosolenia</i> spp.. (f) SEI photograph of laminae characterised by <i>Rhizosolenia</i> spp.. (g) BSEI photograph of mixed diatom assemblage laminae. (h) SEI photograph of mixed diatom assemblage laminae. (i) BSEI photograph of mixed diatom assemblage terrigenous laminae. (j) SEI photograph of mixed diatom assemblage terrigenous laminae. (k) BSEI photograph of terrigenous sub-laminae characterised by <i>P. glacialis</i> RS. (l) SEI photograph of terrigenous sub-laminae characterised by <i>P. glacialis</i> RS.....	121
7.3	Graph showing the thicknesses of different types of lamina and sub-lamina from Mertz Ninnis Trough (NBP0101 JPC10). Individual thicknesses are displayed as coloured bars within the total thickness of each lamina type.....	124
7.4	Graph illustrating the distribution of the different lamina and sub-lamina types, Mertz Ninnis Trough NBP0101 JPC10, between 17.36 and 20.60 metres below sea floor (mbsf).....	125
7.5	Backscattered electron imagery (BSEI) photomosaic of diatom ooze laminae (biogenic) and diatom-bearing terrigenous laminae (terrigenous), NBP0101 JPC10, Mertz Ninnis Trough.....	130
7.6	Schematic representation of the biogenic and terrigenous laminae and terrigenous sub-laminae succession in laminated interval, Mertz Ninnis Trough, NBP0101 JPC10.....	131
7.7	Summary table displaying polynya model and seasonal information responsible for the formation of multiple types of laminae through the deglaciation.....	137

7.8	Graph illustrating the distribution of the different lamina types, Mertz Ninnis Trough NBP0101 KC10A, Between 2.05 and 2.38 metres below sea floor (mbsf).....	145
7.9	Graph showing the thicknesses of different types of lamina from Mertz Ninnis Trough (NBP0101 KC10A). Individual thicknesses are displayed as coloured bars within the total thicknesses of each lamina type.....	145
7.10	Backscattered electron imagery (BSEI) and secondary electron imagery (SEI) photographs of laminae characterised by <i>Fragilariopsis</i> spp., Mertz Ninnis Trough, NBP0101 KC10A.....	146
7.11	Backscattered electron imagery (BSEI) photomosaics of biogenic laminae and terrigenous laminae, NBP0101 KC10A.....	147

## Chapter 8: Durmont d'Urville Trough

8.1	Location map of MD03-2597, Durmont d'Urville Trough on the Terre Adélie continental margin.....	152
8.2	Backscattered electron imagery (BSEI) and secondary electron imagery (SEI) photographs of biogenic and terrigenous laminae characterise by <i>Hyalochaete Chaetoceros</i> spp. resting spore (CRS), Durmont d'Urville Trough.....	154
8.3	Graph illustrating the distribution of different lamina types, Durmont d'Urville Trough MD03-2597, in discrete intervals between 18.75 and 56.80 metres below sea floor (mbsf) (see table 3.7).....	158
8.4	Graph showing the thicknesses of different types of lamina from Durmont d'Urville Trough, MD03 2597. Individual thicknesses are displayed as coloured bars within the total thickness of each lamina type.....	159
8.5	Backscattered electron imagery (BSEI) and secondary electron imagery (SEI) photographs of biogenic and terrigenous laminae characterised by <i>Hyalochaete Chaetoceros</i> spp. resting spores (CRS) and <i>Fragilariopsis</i> spp., Durmont d'Urville Trough.....	162
8.6	Backscattered electron imagery (BSEI) and secondary electron imagery (SEI) photographs of biogenic laminae characterised by <i>Fragilariopsis</i> spp., Durmont d'Urville Trough.....	163
8.7	Backscattered electron imagery (BSEI) and secondary electron imagery (SEI) photographs of biogenic laminae characterised by <i>Corethron pennatum</i> and <i>Rhizosolenia</i> spp., Durmont d'Urville Trough.....	164
8.8	Backscattered electron imagery (BSEI) and secondary electron imagery (SEI) photographs of biogenic and terrigenous laminae characterised by <i>Corethron pennatum</i> , Durmont d'Urville Trough.....	166
8.9	Backscattered electron imagery (BSEI) and secondary electron imagery (SEI) photographs of biogenic and terrigenous laminae characterised by <i>Rhizosolenia</i> spp., Durmont d'Urville Trough.....	168
8.10	Backscattered electron imagery (BSEI) and secondary electron imagery (SEI) photographs of mixed diatom assemblage biogenic and terrigenous laminae, Durmont d'Urville Trough.....	170
8.11	Backscattered electron imagery (BSEI) and secondary electron imagery (SEI) photographs of biogenic and terrigenous sub-laminae characterised by <i>Porosira glacialis</i> resting spores (RS), Durmont d'Urville Trough.....	172
8.12	Backscattered electron imagery (BSEI) photomosaics of laminated sediments, Durmont d'Urville Trough.....	173



8.13	Backscattered electron imagery (BSEI) and secondary electron imagery (SEI) photographs of biogenic and terrigenous laminae characterised by <i>Stellarima microtrias</i> resting spores (RS), <i>Porosira glacialis</i> RS and / or <i>Coscinodiscus bouvet</i> , Durmont d'Urville Trough.....	175
8.14	Schematic diagram showing the sequence of lamina type deposition, Durmont d'Urville Trough.....	177
8.15	Schematic representation of an annual succession of lamina types, Durmont d'Urville Trough. Compiled from backscattered electron imagery (BSEI) data.....	184
8.16	Polar stereographic satellite MODIS (Moderate Resolution Imaging Spectroradiometer) images of Adélie and George V coast, East Antarctica, from spring to autumn.....	185

## Chapter 9: Core site comparison

9.1	Continental shelf bathymetric profiles crossing through Palmer Deep, West Antarctica, Mertz Ninnis Trough and Durmont d'Urville Trough, East Antarctica. Core sites indicated on continental shelf profiles.....	188
9.2	Schematic representation of different types of lamina in the four Antarctic core sites.....	189
9.3	Schematic representation of annual diatom-rich laminated sediment deposited in (a) ODP 178 1098A Palmer Deep, (b) NBP0101 JPC10 Mertz Ninnis Trough, (c) NBP0101 KC10A Mertz Ninnis Trough and (d) MD03 2597 Durmont d'Urville Trough. Compiled from Backscattered electron imagery (BSEI) data.....	190
9.4	Comparison of absolute abundances of lamina types from post-glacial (NBP0101 JPC10 Mertz Ninnis Trough) and late-Holocene (MD03 2597 Durmont d'Urville Trough) laminated interval. Absolute abundance data from tables 7.3 and 8.3 and original count data in appendix 4.....	202
9.5	Schematic displaying absolute abundance changes in <i>Fragilariopsis</i> spp. and <i>Hyalochaete Chaetoceros</i> spp. resting spores from the deglacial to the late-Holocene. Temperature, sea ice cover and Adélie Bottom Water formation is also displayed.....	208

## 1. Introduction

This chapter presents the background and objectives for this study, and a summary of the thesis structure.

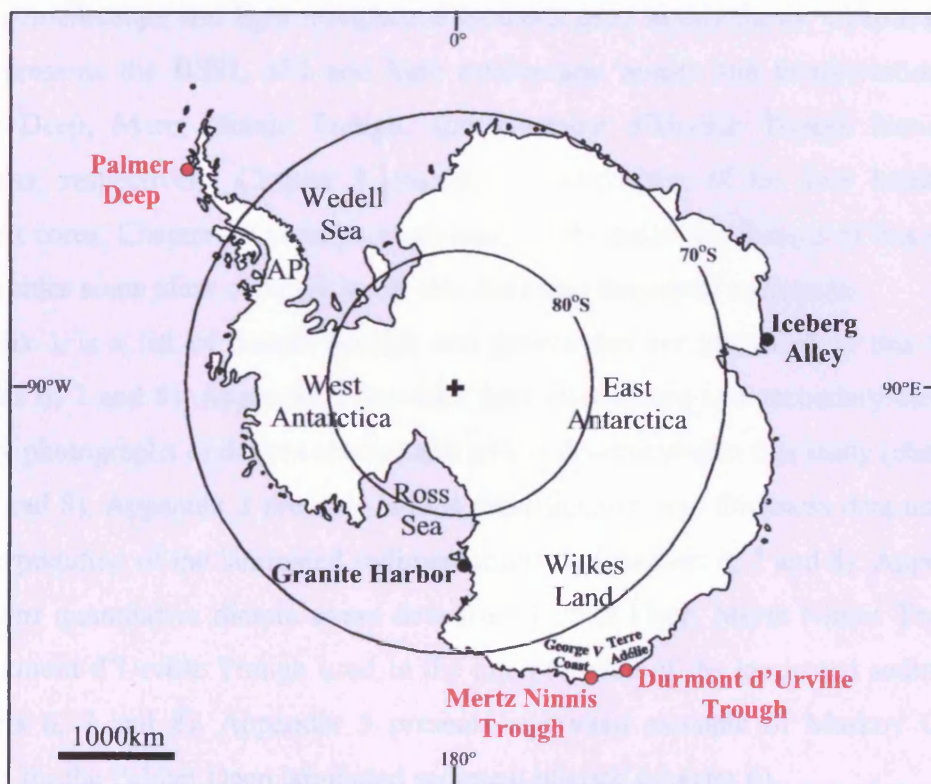
### 1.1. Background

Ultra-high resolution records from high southern latitudes are required to understand the complexities of Holocene and late Pleistocene climate in Antarctica. Marine sediment cores from the Antarctic continental shelf contain a useful high-resolution record of climatic fluctuations along the margin of the continent (Domack *et al.*, 1991). Highly diatom-rich laminated sediments are found in inner shelf basins such as Palmer Deep (Antarctic Peninsula; Leventer *et al.*, 1996; Domack and Mayewski, 1999; Barker *et al.*, 1999a; Leventer *et al.*, 2002), Granite Harbor (Ross Sea; Leventer *et al.*, 1993), Mertz Ninnis Trough (Wilkes Land Margin; Domack and Anderson, 1983; Domack, 1988; Brancolini and Harris, 2000) and Iceberg Alley (Mac.Robertson shelf; Harris *et al.*, 1997; Taylor, 1999a; Sedwick *et al.*, 2001; Stickley *et al.*, 2005) (Figure 1.1), protected from glacial scour. The value of diatoms as indicators of climate change is widely known in palaeoecological studies (e.g. Burckle, 1972; Truesdale and Kellogg, 1979; DeFelice and Wise, 1981; Leventer *et al.*, 1993; 1996) as many diatom species have specific requirements for temperature, pH, salinity and nutrient levels. Despite aggregation, dissolution and advection, the diatom record in laminated sediments preserve diatom flux events, reflecting surface water productivity (Leventer and Dunbar, 1996; Zielinski and Gersonde, 1997). Therefore, questions about Holocene and Late Pleistocene climate change can be addressed by examining and using palaeoecological information stored in laminated sediments.

### 1.2. Thesis objectives

The main objective of this study was to evaluate whether diatom assemblages and sedimentary fabrics can be used to determine whether a seasonal and/or annual signal is present in Antarctic deglacial and Holocene diatom-rich laminated sediments. A second objective of this investigation was to evaluate whether diatom assemblages in the laminated sediments can reveal climatic, environmental and oceanographic changes. Laminated sediments from three inner shelf basins, Palmer Deep (western

Antarctic Peninsula, West Antarctic Margin), Mertz-Ninnis Trough (George V Coast, East Antarctic Margin) and Durmont d'Urville Trough (Terre Adélie Coast, East Antarctic Margin) (Figure 1.1) were examined, assessed and compared. The sediments were analysed primarily using scanning electron microscopy (SEM) backscattered electron imagery (BSEI) and secondary electron imagery (SEI). Detailed BSEI analysis of laminated sequences was used to provide information on intra- and inter-annual variability in the water column. SEI analysis of selected laminae was used to assist in diatom species identification. The diatom species assemblage and terrigenous content of laminae was used to give an insight into spatial and temporal environmental, oceanographic and depositional variation on the continental shelf. Quantitative diatom assemblage analysis was conducted on key laminae to determine absolute diatom concentration and relative abundances of species within the total diatom assemblage.



**Figure 1.1**

Locations of Antarctic laminated sediments. Those in red are the three core sites studied in thesis: Palmer Deep, Mertz Ninnis Trough and Durmont d'Urville Trough. AP=Antarctic Peninsula.

### 1.3. Thesis format

The structure of this thesis is outlined in this section, and the content of each chapter and appendix summarised.

Chapters 2, 3 and 4 present the necessary background information for the later results chapters. Chapter 2 describes the geological history, oceanography and palaeoclimate of the Southern Ocean, followed by that of the core sites Palmer Deep, Mertz Ninnis Trough and Durmont d'Urville Trough. Chapter 3 contains an introduction to diatoms, areas of diatom deposition in the Southern Ocean, environmental controls and preservation of diatoms, and includes a brief summary of previous research conducted on diatom-rich Antarctic laminated sediments. Ecological details of Southern Ocean diatom genera and species encountered in this study are also provided in this chapter. Chapter 4 describes the bathymetric setting of the core sites, core lithologies and age models. Chapter 5 contains details of sample preparation, scanning electron microscope and light microscope methods used in this thesis. Chapters 6, 7 and 8 presents the BSEI, SEI and light microscope results and interpretations of Palmer Deep, Mertz Ninnis Trough, and Durmont d'Urville Trough laminated sediments, respectively. Chapter 9 provides a comparison of the four laminated sediment cores. Chapter 10 presents a summary of the main conclusions of this study and provides some ideas of future work into Antarctic laminated sediments.

Appendix 1 is a list of diatom species and genera that are identified in this study (chapters 6, 7 and 8). Appendix 2 provides light microscope and secondary electron imagery photographs of diatom species and genera documented in this study (chapters 3, 6, 7 and 8). Appendix 3 presents lamina classifications and thickness data used in the interpretation of the laminated sediment intervals (chapters 6, 7 and 8). Appendix 4 contains quantitative diatom count data from Palmer Deep, Mertz Ninnis Trough, and Durmont d'Urville Trough used in the interpretation of the laminated sediments (chapters 6, 7 and 8). Appendix 5 presents a worked example of Markov Chain analysis for the Palmer Deep laminated sediment interval (chapter 6).

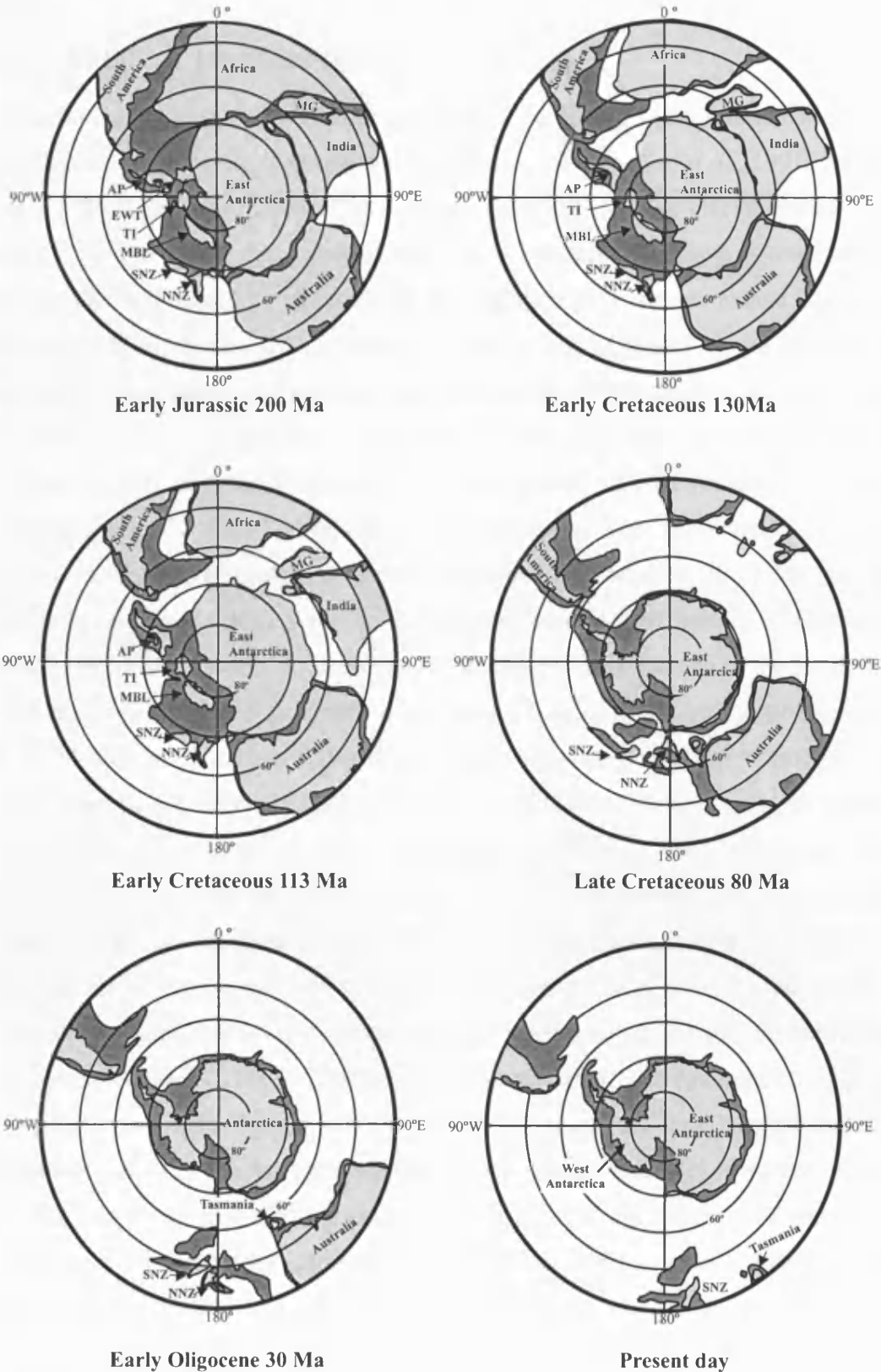
## 2. Location background

This chapter outlines the general geological, oceanographic and climatic settings of the Southern Ocean and the core sites in Palmer Deep, Mertz Ninnis Trough and Durmont d'Urville Trough.

### 2.1. Geology of the Southern Ocean and Antarctic

Antarctica consists of two distinct continental blocks. East Antarctica (Figure 2.1) is a large stable continental craton composed mainly of Precambrian metamorphic basement rocks with granitic intrusions that are unconformably overlain by generally flat-lying sedimentary rocks (Anderson, 1999). West Antarctica (Figure 2.1) is an archipelago composed of several micro-plates with volcanic and metamorphic terranes (Anderson, 1999). East and West Antarctica are separated by the Transantarctic Mountain range which spans nearly 3500 km.

Along with South America, Africa, Madagascar, India and Australia, Antarctica was a major component of the supercontinent Gondwana (Figure 2.1). A rift system developed in the early to mid Jurassic, separating East Antarctica from Madagascar and Africa. This rift system marked the initial separation of East Gondwana from West Gondwana. By the late Cretaceous, rifting of the New Zealand blocks and eastern Australia had begun, allowing circulation between Indian and Pacific oceans. The final separation of West Antarctica and New Zealand occurred ~ 72 Ma (Stock and Molnar, 1987). Timing of the deepening of Tasman Gateway, south of Australia, is well constrained across the Eocene-Oligocene boundary; it began around 35.5 Ma and by ~30.2 Ma the separation of Australia from Antarctica was sufficient for pelagic deposition (Stickley *et al.*, 2004). Two time frames for the opening of the Drake Passage (between the Antarctic Peninsula and South America) have been suggested; Early Oligocene ~31-28.5 Ma (Lawver and Gahagan, 2003) and Early Miocene ~22-17 Ma (Barker, 2001). Pfuhl and McCave (2005) have recently suggested that the establishment of the Antarctic Circumpolar Current (ACC) circuit around Antarctica occurred in the latest Oligocene after about 23.95 Ma.



**Figure 2.1**

Gondwana reconstruction from the Early Jurassic (200 Ma) to present day. Blocks are moved relative to a “fixed” East Antarctica. MG = Madagascar. AP = Antarctic Peninsula block. EWT = Ellsworth-Whitmore Mountains block. MBL = Marie Byrd Land block. NNZ = North New Zealand. SNZ = South New Zealand. TI = Thurston Island block. Adapted from Anderson (1999).

## 2.2. Antarctic Ice Sheet History

Significant permanent ice sheets first appeared on Antarctica at the Eocene/Oligocene boundary at about 34 Ma (Kennett and Shackleton, 1976; Miller *et al.*, 1991; Zachos *et al.*, 1996; Lear *et al.*, 2000). The stepwise onset of Antarctic glaciation has been linked to jumps in the deepening of the calcite compensation depth (Coxall *et al.*, 2005). There is debate on what caused the initiation of major permanent Cenozoic ice-sheets on Antarctica. One hypothesis is that it was triggered by the opening of Southern Ocean gateways (Kennett and Shackleton, 1976); another is that it was caused by a threshold response to long-term Cenozoic decline in atmospheric carbon dioxide levels (DeConto and Pollard, 2003). A permanent East Antarctic Ice Sheet (EAIS) persisted until 26-27 Ma, when a warming trend reduced Antarctic ice extent (Zachos *et al.*, 1996). Global ice volume remained low between 26-27 Ma and the middle Miocene (~15 Ma), with the exception of several brief periods of glaciation (Wright and Miller, 1993). At about 14 Ma there was major growth of the EAIS and since this time the EAIS has been a permanent feature of the continent (Kennett, 1978; Flower and Kennett, 1994). Between the Oligocene and early Miocene, the West Antarctic Ice Sheet (WAIS) consisted of a number of isolated ice caps centred over islands and continental blocks (Anderson and Shipp, 2001). These ice caps coalesced to form the WAIS, advancing onto the continental shelf on several occasions from late Miocene through the Pleistocene (Anderson and Shipp, 2001).

The last glacial maximum (LGM) (between 23 and 19 cal kyr) is the most recent interval when global ice sheets reached their maximum integrated volume during the last glacial (Mix *et al.*, 2001). The overall extent of ice cover in Antarctica during the last glacial maximum is not well known. Some reconstructions suggest that the peripheral domes of the Antarctic Ice Sheet were 500-1000 m thicker than at present and that ice extended out to the continental shelf break around most of Antarctica (Clark and Lingle, 1979; Hughes *et al.*, 1981; Denton *et al.*, 1991). Other reconstructions indicate a smaller extent; Mayewski (1975) proposed that the WAIS was only slightly, if at all, larger than today and interpretation of East Antarctic data indicates that ice did not extend to the shelf edge (Goodwin, 1993, Anderson *et al.*, 2002).

The retreat of the EAIS during deglaciation appears to have been diachronous around the East Antarctic Margin (Berkman *et al.*, 1998; Anderson, 1999) and in some areas,

retreat occurred prior to the LGM (Anderson *et al.*, 2002) (Figure 2.2). Retreat from the West Antarctic shelf appears to have occurred at about the same time all around West Antarctica, between 15 and 12, ka. In the Ross Sea and the Antarctic Peninsula regions, retreat continued well into the Holocene.

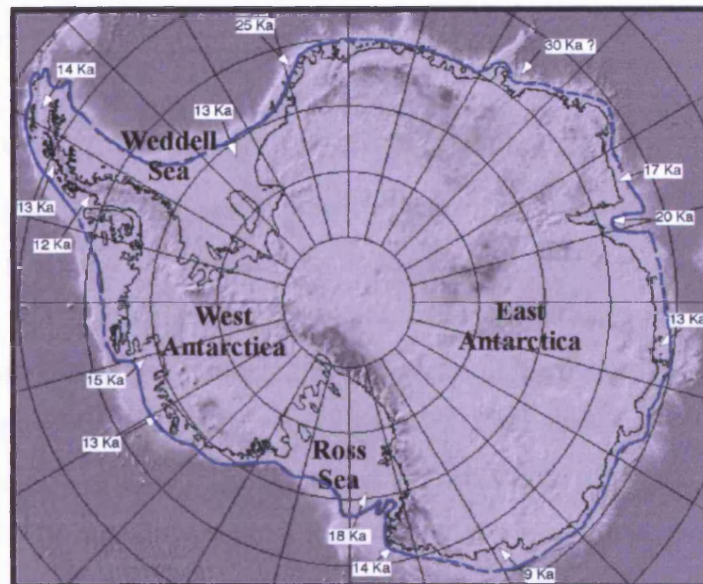
### **2.3. Southern Ocean Oceanography**

The Southern Ocean plays a central role in the global thermohaline circulation, mixing and exchanging heat and salts between the major oceanic basins; it maintains thermal isolation of the Antarctic continent and Antarctic ice sheets from subtropical waters to the north. The unique geography of the Southern Ocean makes it the only place where ocean currents can flow uninterrupted around the globe.

#### **2.3.1. Zones of the Southern Ocean**

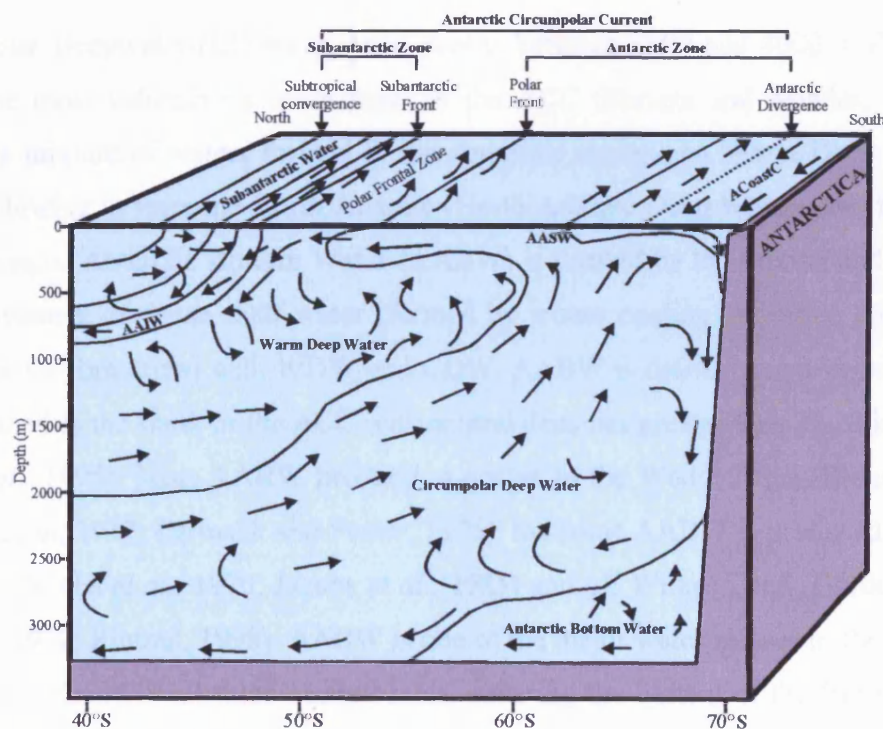
The Southern Ocean has no continental limits to the north; Australia, New Zealand and South America encroach on the Southern Ocean without limiting it, and Antarctica bounds the Southern Ocean to the south. The Southern Ocean has well defined characteristics that run approximately parallel to latitude. The Southern Ocean can be divided into two key zones, the Antarctic Zone (adjacent to Antarctica) and the Subantarctic Zone (further north) (Figure 2.3). The division between these two zones is not a sharp boundary, but rather a transition named the Polar Frontal Zone (PFZ) (Figure 2.3) and is located at approximately at 50°S in the Atlantic and Indian Oceans and at approximately 60°S in the Pacific. The PFZ is bound to the south by the Polar Front (PF) (also called the Antarctic Convergence) and to the north by the Subantarctic Front (SAF) and varies in width around Antarctica (narrower in the Drake Passage, wider in the South Atlantic) (Figure 2.3). The Antarctic Zone is characterised by colder and fresher surface temperatures than the Subantarctic Zone (Anderson, 1999). The southern boundary of the Antarctic Zone is marked by the Antarctic Divergence (Figure 2.3). The northern boundary of the Subantarctic zone, at 40°S, is the Subtropical Convergence and is the boundary between the Southern Ocean and the rest of the world ocean (Figure 2.3).





**Figure 2.2**

Last glacial maximum (LGM) ice sheet reconstruction for Antarctica. Blue line indicates minimum grounding line based on the presence of subglacial geomorphic features and/or till. Dates indicate the approximate times when the ice sheet retreated from the shelf, based on radiocarbon ages of glacial-marine sediment resting above till. Deeper grey indicate the continental slope and abyssal plain. From Anderson *et al.* (2002).



**Figure 2.3**

Schematic block diagram showing the surface currents and vertical motion of water masses in the Southern Ocean pole-ward of 40°S. AAIW = Antarctic Intermediate Water. AASW = Antarctic Surface Water. ACoastC = Antarctic Coastal Current. Adapted from Open University Course Team (1998) and Anderson (1999).

## 2.3.2. Southern Ocean Water Masses and Currents

### 2.3.2.1. Antarctic Zone and Continental Margin

Antarctic Coastal Current (ACoastC) flows westward in a narrow zone close to the Antarctic coast (Figure 2.3). This current follows the line of the coast and deviates due to changes in the coastline such as bays, capes or glacial protrusions. Further north, the Southern Ocean is dominated by the Antarctic Circumpolar Current (ACC), a deep, strong, eastward flowing current (Figure 2.3). The surface flow of the ACC is primarily driven by the frictional stress of westerly winds on the ocean surface. Wind stress combined with the Coriolis force contributes to a northward component of the surface current, resulting in the formation of fronts and a complex set of narrow jets within the PFZ (Pickard and Emery, 1990). Antarctic Surface Water (AASW) south of the PF originates near the continent and flows northward until it encounters Subantarctic surface waters, where it begins to sink (Figure 2.3). AASW properties are determined by ice melting in the summer and by cooling and ice formation in the winter.

Circumpolar Deepwater (CDW) at water depths between 1000 and 4000 m (Figure 2.3) is the most voluminous water mass in the ACC (Sievers and Nowlin, 1984). CDW is a mixture of waters formed in the Antarctic region and Warm Deep Water (WDW) flowing in from the North Atlantic (North Atlantic Deep Water), Pacific and Indian Oceans. Antarctic Bottom Water (AABW) is created by the mixing and down slope movement of dense shelf water (formed by winter cooling and brine rejection during sea ice formation) with WDW and CDW. AABW is defined as all volumes of water formed to the south of the ACC with neutral densities greater than  $27.28 \text{ kg / m}^3$  (Orsi *et al.*, 1995). Most AABW production occurs in the Weddell Sea (Brennecke, 1921; Deacon, 1937; Carmack and Foster, 1975), but some AABW is produced in the Ross Sea (Jacobs *et al.*, 1970; Jacobs *et al.*, 1985) and off Wilkes Land (Gordon and Tchernia, 1972; Rintoul, 1998). AABW is one of the major water masses of the world ocean and is found in all three ocean basins, covering the bottom of the Pacific and Indian Oceans and most of the bottom of the Atlantic Ocean. This water mass ventilates most of the deep waters in the rest of the world ocean, therefore, the strength of the southern source of cold bottom waters and subsequent equatorward flow are key elements of the global thermohaline circulation (Orsi *et al.*, 1995).

### 2.3.2.2. Subantarctic Zone

Water masses in this zone originate from inside and outside the Southern Ocean. Subantarctic Upper Water occupies the upper 500 m and has a southward motion (Figure 2.3). Below this water mass is the Antarctic Intermediate Water which includes surface water from the Antarctic Zone and is formed by mixing below the surface in the PFZ.

## 2.4. Palaeoclimate and Present Climate

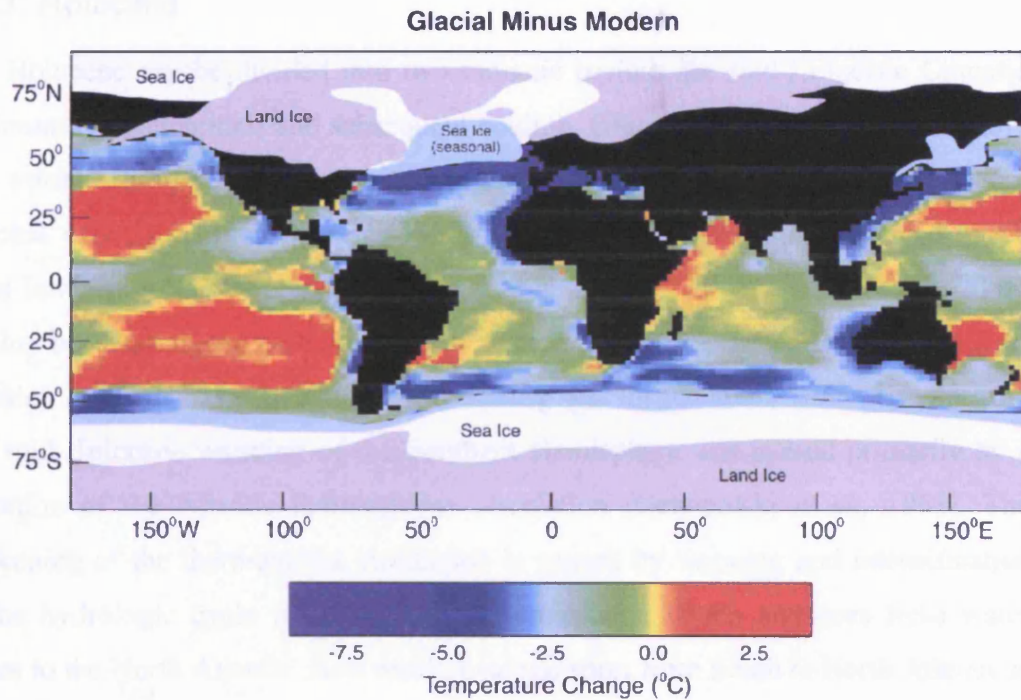
### 2.4.1. Last Glacial

Oxygen isotope records from deep-ocean sediments and ice cores indicate that major land ice masses developed during the last glacial (e.g. Martinson *et al.*, 1987; Jouzel *et al.*, 1987). The ocean circulation was notably different to today; deep water formation in the Atlantic was probably reduced and the global thermohaline circulation, therefore, was much slower (Duplessy *et al.*, 1984; Boyle, 1986; Lynch-Steiglitz *et al.*, 1999). The CLIMAP (Climate Long-range Investigation, Mapping And Prediction) project (1981) determined that temperature change during the LGM was different between regions and not globally uniform (Figure 2.4). The tropical oceans were  $3 \pm 1^\circ\text{C}$  colder than at present (Pierrehumbert, 1999) and air temperatures averaged about  $15^\circ\text{C}$  colder than now (Cuffey and Clow, 1997). The Southern Hemisphere was drier (Damuth and Fairbridge, 1970; Bowler, 1976; Sarnthein, 1978), which led to the shrinking of forests and expansion of deserts (deserts between  $30^\circ\text{N}$  and  $30^\circ\text{S}$  were five times larger than today) (Sarnthein, 1978), increasing albedo effects (Peterson *et al.*, 1979). A drop in sea level of approximately 120 m during the last glacial (Shackleton, 1987) exposed continental shelves creating another source of atmospheric dust, in addition to the increase in desert size (Petit *et al.*, 1981). The last glacial maximum (LGM) may have occurred earlier in the Southern Hemisphere than the Northern Hemisphere, the early onset in the Southern Hemisphere was driven by the minimum in regional insolation reached 35 – 30 kys BP (Vandergoes *et al.*, 2005). During the glacial, atmospheric circulation was much more vigorous from the tropical zone towards Antarctica than today (Petit *et al.*, 1981). Ice and deep-sea core studies have shown that the latitudinal thermal gradient

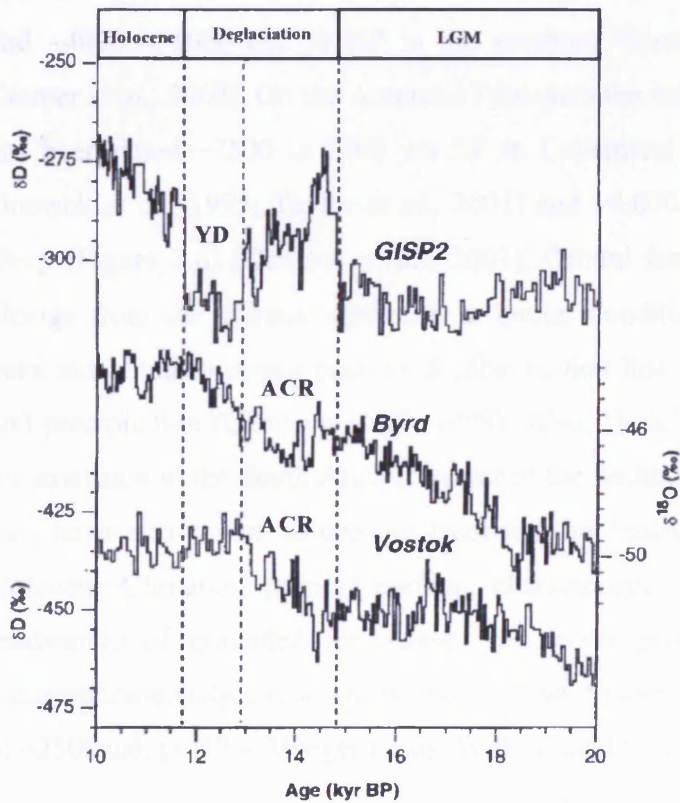
was greater during the LGM than at present (Wilson and Hendy, 1971; Luz, 1977). Diatom and radiolarian transfer functions have been used in the Southern Ocean to improve knowledge of past open ocean temperatures (e.g. Pichon *et al.*, 1992a; Brathauer and Abelmann, 1999). During the glacial, the surface of the ocean in the Subantarctic and Polar Frontal Zone was approximately 3° - 5°C cooler than today, which indicates there was a northward displacement of isotherms about 2° - 4° of latitudes with respect to modern positions (Brathauer and Abelmann, 1999). Diatom floral evidence indicates that sea ice was not perennial during the LGM (Burckle *et al.*, 1982; Burckle, 1984a; Crosta *et al.*, 1998).

#### 2.4.2. The Last Deglaciation

The last deglaciation (~20-10 cal kyr BP) is generally assumed to have been forced by the increase in Northern Hemisphere summer insolation between 24 and 10 kyr (Imbrie *et al.*, 1992). The insolation changes alone cannot explain the amplitude and global character of this climatic transition. The increase in atmospheric concentrations of the greenhouse gas CO<sub>2</sub> could have accounted for up to half of the glacial-interglacial warming (Manabe and Broccoli, 1985). Ice core data reveals that warming in the Southern Hemisphere after the LGM probably preceded Northern Hemisphere warming (Petit *et al.*, 1999). The gradual increase in temperature recorded in Antarctic ice cores is interrupted by a short cooling period, the Antarctic Cold Reversal (ACR; Jouzel *et al.*, 2001), ~13 to 15 kyrs BP. A return to near glacial conditions in the Northern Hemisphere ~ 11 to 10 kyrs BP, the Younger Dryas (YD) (Lowe and Walker, 1997) is considered to be an equivalent of the ACR (Johnsen *et al.*, 1992; Grootes *et al.*, 1993) (Figure 2.5). The cause of the ACR is uncertain, but a suggested cause for this cooling is the intense meltwater event, mwp 1A, occurring during the first step of deglaciation (Fairbanks, 1989). Weaver *et al.* (2003) propose that mwp 1A was created by the partial collapse of the Antarctic Ice Sheet, a result of prolonged warming in the Southern Hemisphere that began ~19,000 yr BP (Blunier and Brook, 2001). This could have triggered a seesaw mechanism (Broecker, 1998); Antarctic Bottom Water formation suppression would have turned on the Northern Hemisphere thermohaline circulation, warming the Northern Hemisphere (Bølling-Allerød warm period) and cooling the southern hemisphere (Weaver *et al.*, 2003).

**Figure 2.4**

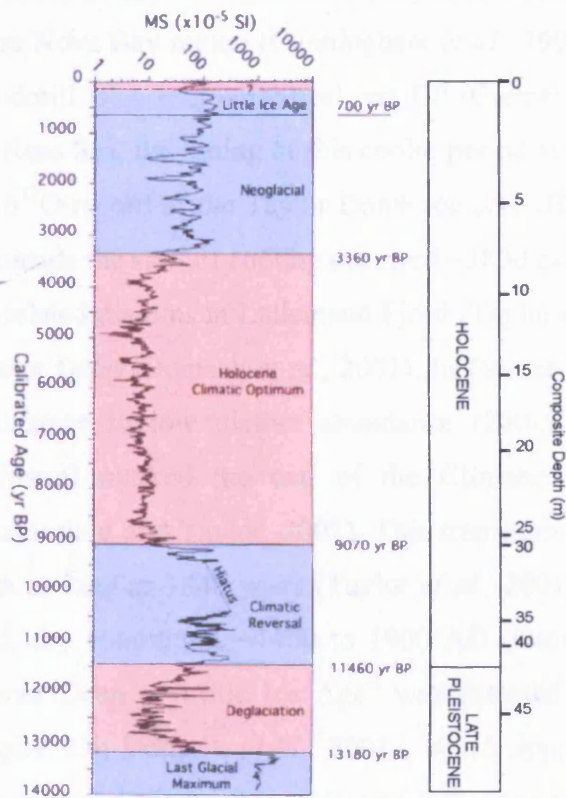
Changes in the annual average sea surface temperatures (last glacial maximum (LGM) - modern), with geographic distribution of LGM seasonal and perennial sea ice, and LGM land ice, based on seasonal estimates of CLIMAP (1981). From Mix *et al.* (2001).

**Figure 2.5**

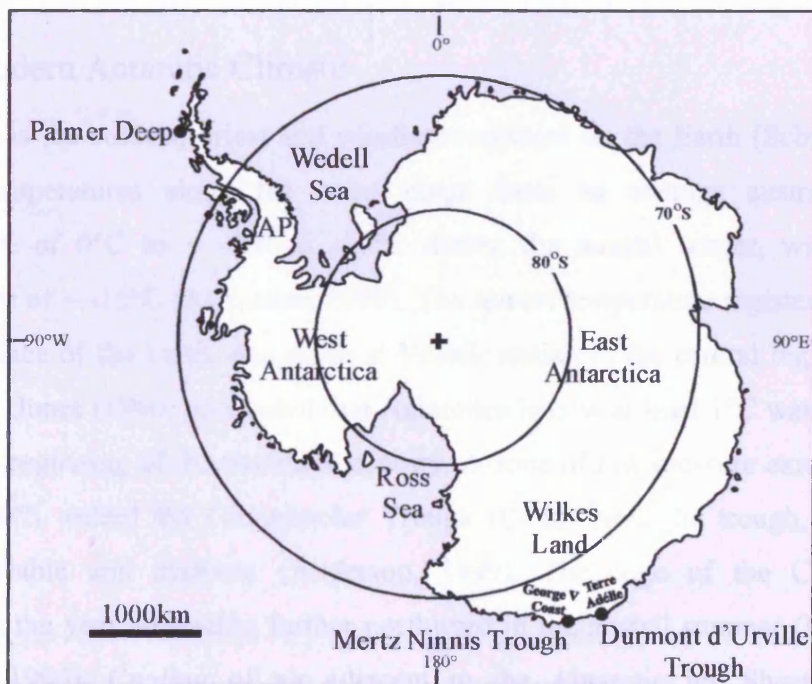
Stable isotope profiles from GISP2, Byrd, and Vostok adapted from Steig *et al.* (1998). Boundaries of climate intervals, as defined in the GISP2 record, are shown by dashed vertical lines; YD, Younger Dryas; LGM, last glacial maximum. ACR is the Antarctic Cold Reversal as defined at Byrd (Blunier *et al.*, 1997; 1998).

### 2.4.3. Holocene

The Holocene can be divided into two climatic periods the mid-Holocene Climatic Optimum (Hypsithermal) and subsequent cooling. Global temperatures were possibly 1°C warmer during the Climatic Optimum than today (Bigg, 2001) with significant regional variation (Mitchell *et al.*, 1988). The Climatic Optimum is detected in ice cores from the Antarctic polar plateau (e.g. Masson *et al.*, 2000; Vimeux *et al.*, 2001) and has been associated with the collapse of at least one Antarctic Peninsula ice shelf (Bentley *et al.*, 2005) which suggests warming was an Antarctic wide phenomenon. The mid-Holocene warming of the Southern Hemisphere was caused primarily by a reduction of the Atlantic thermohaline circulation (Ganopolski *et al.*, 1998). The weakening of the thermohaline circulation is caused by warming and intensification of the hydrologic cycle in the Northern Hemisphere, which enhances fresh water fluxes to the North Atlantic. As a result, heat transport from South to North Atlantic is reduced, which produces a negative feedback for Northern Hemisphere warming but raises mean annual temperature in the Southern Hemisphere by 0.7°C (Ganopolski *et al.*, 1998). Sea ice cover is reduced in the Southern Ocean, which amplifies the warming near Antarctica (Hodell *et al.*, 2001). In East Antarctica, this climatic optimum occurred between 3500 – 2500 yr BP at Bunger Oasis (Kulbe *et al.*, 2001) and ~4000 – 1000 cal. yr BP in the southern Windmill Islands (Goodwin, 1996; Cremer *et al.*, 2003). On the Antarctic Peninsula the mid-Holocene Climatic Optimum has been dated ~7500 to 5800 yrs BP in Lallemand Fjord (Shevenell *et al.*, 1996; Domack *et al.*, 1995; Taylor *et al.*, 2001) and ~9,070 to 3,360 cal. yr BP in Palmer Deep (Figure 2.6) (Domack *et al.*, 2001). Orbital forcing cannot solely explain the change from the climatic optimum to cooler conditions; the climate transition has been attributed to strong positive feedbacks that link subtropical vegetation, albedo, and precipitation (Claussen *et al.*, 1999). Also, Hodell *et al.* (2001) suggest that sea ice extension in the South Atlantic sector of the Southern Ocean about 5000 cal. yr BP may have also served as oceanic feedback that hastened climate change. Post mid-Holocene Climatic Optimum cooling, characterised by increased sea ice coverage, readvances of grounded ice masses and lower precipitation, did not commence contemporaneously circum-Antarctic. In East Antarctica this cool stage commenced at ~2500 cal. yr BP in Bunger Oasis, Wilkes Land (Kulbe *et al.*, 2001), at 2600 <sup>14</sup>C yr



**Figure 2.6**  
Stratigraphic succession of the composite record of Palmer Deep, Antarctic Peninsula from ODP Leg 178 Site 1098 (cores A-C) with magnetic susceptibility (MS) versus age and composite depth in the core. Holocene palaeointervals are indicated. Adapted from Domack *et al.* (2001).



**Figure 2.7**  
Geographic locations of the three core sites: Palmer Deep, Mertz Ninnis Trough and Durmont d'Urville Trough. AP=Antarctic Peninsula

BP in Prydz Bay, Vestfold Hills (Taylor and McMinn, 2002), at 3000  $^{14}\text{C}$  yr BP in the Terra Nova Bay region (Cunningham *et al.*, 1999) and relatively later in the southern Windmill Islands at  $\sim 1000$  cal. yrs BP (Cremer *et al.*, 2003). At the western edge of the Ross Sea, the timing of this cooler period at  $\sim 5000$  cal. yrs BP was determined by the  $\delta^{18}\text{O}$  record of the Taylor Dome ice core (Hoddell *et al.*, 2001). On the Antarctic Peninsula the start of cooling occurred  $\sim 3800$  cal. yrs BP determined by an increase in ice-related diatoms in Lallemand Fjord (Taylor *et al.*, 2001) and at 3360 cal. yr BP in Palmer Deep (Domack *et al.*, 2001). In Palmer Deep the transition from high diatom abundance to low diatom abundance ( $250\text{-}500 \times 10^6$  valves per gramme of dry sediment) marked the end of the Climatic Optimum and start of the cooling (Sjunneskog and Taylor, 2002). This transition on the Antarctic Peninsula may have been as long as 1340 years (Taylor *et al.*, 2001). The Little Ice Age was a period of cold, dry conditions,  $\sim 1400$  to 1900 AD (Grove, 1988). In marine sediments from Palmer Deep a “Little Ice Age” was detected between  $\sim 700$  to  $\sim 100$  cal yrs BP (Figure 2.6; Domack *et al.*, 2001), which approximately correlates with the GISP2 (Domack and Mayewski, 1999) and Siple Dome (Kreutz *et al.*, 1997) records.

#### 2.4.4. Modern Antarctic Climate

Antarctica is the coldest, driest and windiest continent on the Earth (Schwerdtfeger, 1984). Temperatures along the coast range from an average austral summer temperature of  $0^\circ\text{C}$  to  $\sim -20^\circ$  to  $-30^\circ\text{C}$  during the austral winter, with a mean temperature of  $\sim -15^\circ\text{C}$  (Anderson, 1999). The lowest temperature registered ( $-88^\circ\text{C}$ ) on the surface of the Earth was made at Vostok station in the central region of East Antarctica. Jones (1990) concluded that Antarctica is now at least  $1^\circ\text{C}$  warmer than it was at the beginning of the twentieth century. A zone of low pressure exists between  $65^\circ$  and  $70^\circ\text{S}$ , called the Circumpolar Trough (CPT). Near the trough, winds are highly variable and cyclonic (Anderson, 1999). The edge of the CPT moves throughout the year advancing further northward in the austral summer (Mullan and Hickman, 1990). Cooling of air adjacent to the Antarctic Ice Sheet creates a temperature inversion on the high polar plateau. The cooled air flows from the continental interior towards the coast due to gravity, an inversion wind. Topographic funnelling of this air intensifies flow speed, resulting in katabatic winds (Anderson, 1999). The areal extent of sea ice around Antarctica is roughly twice the size of the



Antarctic Ice Sheet and experiences a five-fold increase annually (Mullan and Hickmann, 1990), changing in area from roughly  $3 \times 10^6 \text{ km}^2$  in the austral spring to  $20 \times 10^6 \text{ km}^2$  in the austral autumn (Mullan and Hickman, 1990). This seasonal variability in the sea ice coverage is one of the most significant factors regulating the energy balance of the Southern Hemisphere atmosphere and ocean (Mullan and Hickman, 1990; Martinson and Iannuzzi, 1998). This influence is due to the large albedo difference between sea ice and the sea surface, which allows the sea ice to serve as a barrier to energy exchange between the atmosphere and ocean (Anderson, 1999). Over the last eleven years observations have shown that the East Antarctic Ice Sheet is thickening north of  $81.6^\circ\text{S}$  (Davis *et al.*, 2005). If the ice sheet continues to grow, then this thickening may counteract a proportion of future sea level rise.

## 2.5. Study Regions

In this section the three core sites, Palmer Deep, Mertz Ninnis Trough and Durmont d'Urville Trough (Figure 2.7), are discussed in a geological, glaciological, oceanographic and climatic framework.

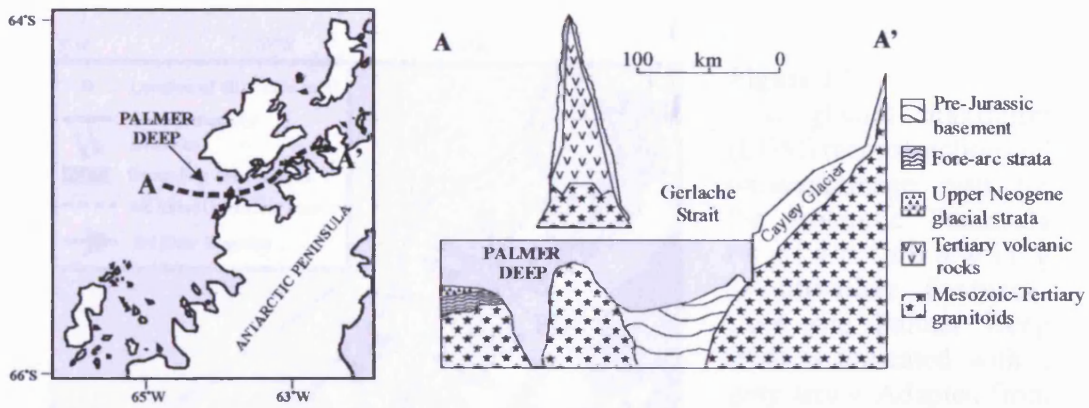
### 2.5.1. Palmer Deep, Western Antarctic Peninsula

#### 2.5.1.1. Geology

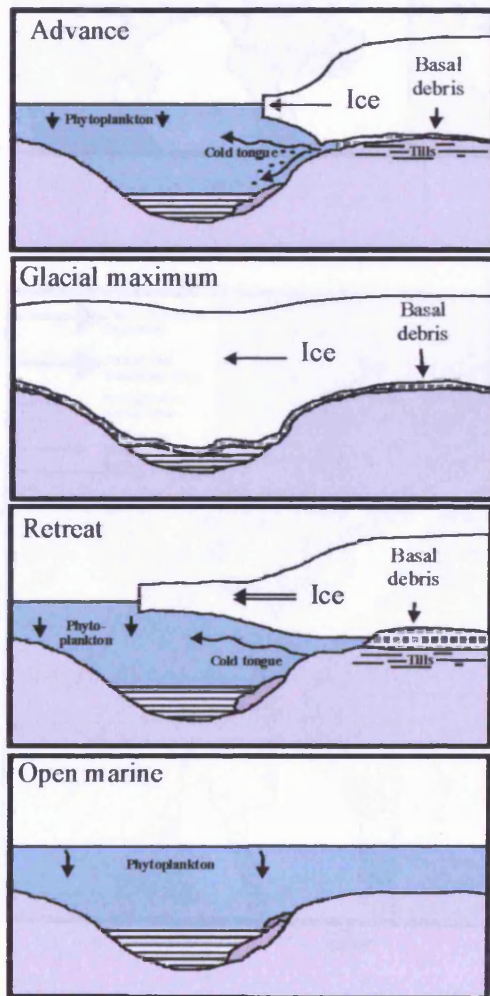
The Antarctic Peninsula consists largely of igneous plutons and related metavolcanics (Domack *et al.*, 2003) (Figure 2.8) of a Mesozoic-Cenozoic magmatic arc. Fore-arc basin sedimentary rocks are found to the west of the peninsula.

#### 2.5.1.2. Glaciology

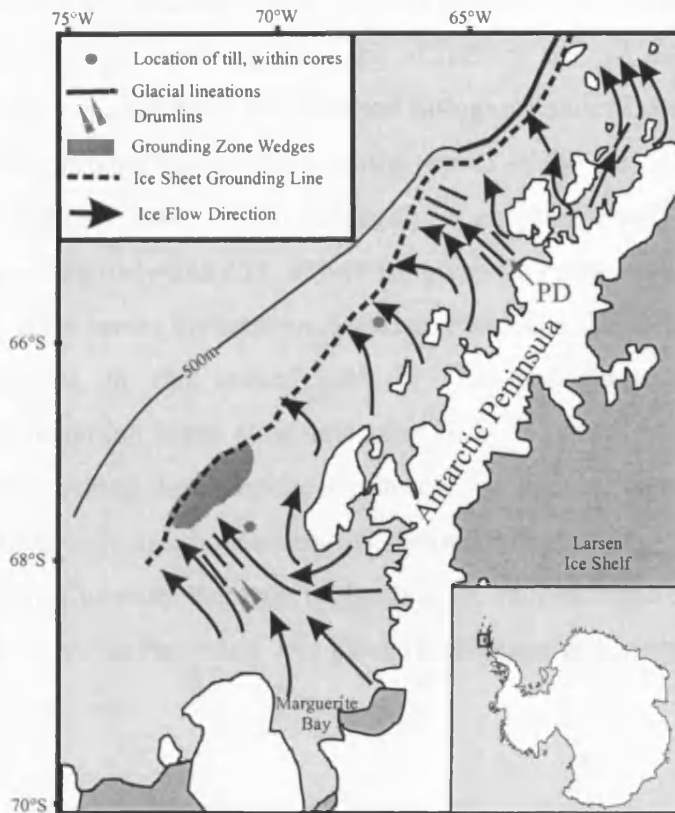
The Antarctic Peninsula ice sheet is part of the marine-based West Antarctic Ice Sheet (WAIS), where sea level is a major control on ice volume. During the last glacial maximum (LGM) the WAIS extended onto the continental shelf (Bart and Anderson, 1996; Pudsey *et al.*, 1994; Larter and Vanneste, 1995; Anderson *et al.*, 2002; Ingólfsson *et al.*, 2003) (Figure 2.9). The head of a major ice drainage system lay within Palmer Deep (Pudsey *et al.*, 1994; Rebesco *et al.*, 1998a). Coastal glaciers



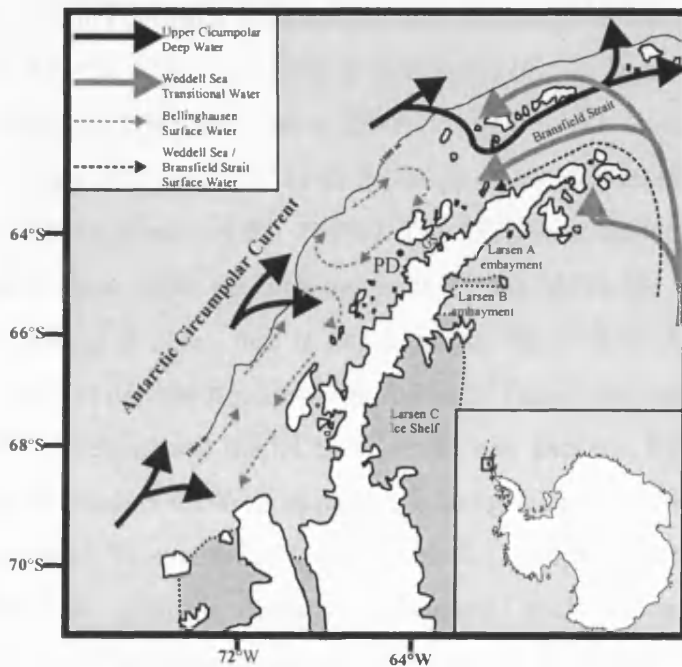
**Figure 2.8**  
Schematic geological cross-section (A-A') across Palmer Deep and the Gerlache Strait. Adapted from Domack *et al.* (2003).



**Figure 2.9**  
Cartoon illustrating various stages of glaciation of the Palmer Deep Basin I. Adapted from Rebesco *et al.* (1998b).



**Figure 2.10**  
Last glacial maximum (LGM) reconstruction and palaeodrainage map for the Antarctic Peninsula region showing geomorphic features. Core site Palmer Deep (PD) is indicated with a grey arrow. Adapted from Anderson *et al.* (2002). Inset is location of study area.



**Figure 2.11**  
Oceanographic regime of the Antarctic Peninsula. From Domack *et al.* (2003). PD = Palmer Deep. GS = Gerlache Strait. Inset is location of study area.

draining off the peninsula plateau and Anvers Island ice cap converged in the past in Palmer Deep (Rebesco *et al.*, 1998a) (Figure 2.10). Iceberg furrows between 350 and 500 m water depth are evidence of iceberg calving as the ice sheet front retreated (Pudsey *et al.*, 1994). Radiocarbon dating of Palmer Deep sediments by Domack *et al.* (2001) provided constraints on the retreat of the ice sheet to Palmer Deep at around 13,000 cal. yr BP, which is roughly in agreement with the uncalibrated radiocarbon age of approximately 11,000 yr BP given by Pudsey *et al.* (1994) for the retreat of the ice sheet across the western Antarctic Peninsula shelf. Radiocarbon ages from a core collected in the central part of Gerlache Strait indicate that glacial-marine sedimentation began sometime after 8000  $^{14}\text{C}$  yr BP (uncorrected date; Harden *et al.*, 1992). Along the Antarctic Peninsula, ice shelves exist up to a climatic limit which corresponds to the mean annual temperature isotherm of  $-8^{\circ}\text{C}$  (Vaughan and Doake, 1996). Currently there are no floating ice shelves north of  $69^{\circ}\text{S}$  on the western side of the Antarctic Peninsula, and glaciers terminate well within fjords (Pudsey *et al.*, 1994) (Figure 2.10).

### 2.5.1.3. Regional Oceanography

General oceanographic conditions for the modern western continental shelf of the Antarctic Peninsula are dominated by Circumpolar Deep Water (CDW) (Figure 2.11). Within the ACC, the CDW is composed of two types of oceanic water mass, Upper CDW (UCDW) and Lower CDW (LCDW). The core of the LCDW mass is found between 800 and 1000 m at the edge of the continental shelf west of the Antarctic Peninsula (Smith *et al.*, 1999a). The UCDW is derived from off-slope upwelling in association with the impingement of the Antarctic Circumpolar Current (ACC), appearing at 200 – 400 m depth, above the western Antarctic Peninsula shelf break (Smith *et al.*, 1999a). Since the Antarctic Peninsula continental shelf is relatively deep (300 - 500 m) and the UCDW is relatively shallow, this oceanic water mass is found on the shelf. UCDW is modified, mixing with Antarctic Surface Waters (AASW) on the shelf. This modified water (Table 2.1) supplies heat, salt and low oxygen water to the west Antarctic Peninsula continental shelf region below 200 m (Smith *et al.*, 1999a). The amounts of CDW in this region may have fluctuated through time (Ishman, 1990).

**Table 2.1** Water mass properties in the vicinity of Palmer Deep. From Hofmann and Klinck (1998a).

Water mass	Temperature (°C)	Salinity (psu)
Antarctic Surface Water (AASW)	0.0 to -1.5	34.0-34.4
Winter Water (WW)	< -1.5	34.0-34.4
Circumpolar Deep Water (CDW)	>0	34.6-34.73
Upper Circumpolar Deep Water (UCDW)	1.5-2.0	34.6-34.7
Lower Circumpolar Deep Water (LCDW)	1.3-1.6	34.7-34.73
Modified Circumpolar Deep Water (MCDW)	1.0-1.4	34.6-34.7
Shelf Water	<-1.8	34.2-34.9

#### 2.5.1.4. Climate

Climate observations in the last century have revealed that the Antarctic Peninsula has responded quickly to climate change over the last half century (Smith *et al.*, 1999b). The elevated Antarctic Peninsula acts as a major barrier to tropospheric circulation, experiencing a relatively mild maritime climate to the west and north of the peninsula and a harsher more continental climate to the east and south (King *et al.*, 2003). The peninsula currently receives a relatively high snowfall (500 to 1000 mm/yr), almost four times the continental average (Reynolds, 1981; Drewry and Morris, 1992). The peninsula is the only Antarctic region where the mean position of the Antarctic Circumpolar Trough (CPT) crosses land (Smith *et al.*, 1999b). The variability of the mean position of cyclones, as the CPT seasonally and inter-annually moves along the Antarctic Peninsula, strongly influences winds, temperature and sea ice distribution. Temperatures in the peninsula have increased markedly over the last 50 years, a 1.0–2.5°C increase in summer surface air temperatures (Jones *et al.*, 1993; King *et al.*, 2003), while temperature increases from around the rest of the continent have been generally small (Vaughan *et al.*, 2003). Several mechanisms have been suggested for this warming; changes in atmospheric circulation and temperature advection patterns across the Antarctic Peninsula; changing oceanographic processes which enhance CDW upwelling; and changes in surface energy balance (King, 1994; Vaughan *et al.*, 2001; Smith *et al.*, 2003). This warming trend coincided with a significant reduction in the size of the Larsen and George VI ice shelves (Potter and Paren, 1985; Rott *et al.*, 1996) and the disappearance of the smaller Wordie Ice Shelf (Doake and Vaughan, 1991) and Müller Ice Shelf (Domack *et al.*, 1995) in the Antarctic Peninsula region. Since 1980 ice shelves from the Antarctic Peninsula, on average, have retreated by  $\sim 300 \text{ km}^2$  (Vaughan and Doake, 1996). This gradual retreat has been

punctuated by two catastrophic collapses on the eastern Antarctic Peninsula. Larsen A and B ice shelves collapsed in January 1995 and March 2002 respectively (Doake *et al.*, 1998; Skvarca and De Angelis, 2003). The recent break-up of the Larsen B Ice Shelf is unprecedented in the Holocene history of this glacial system (Domack *et al.*, 2005). Speculation on the cause of the Larsen Ice Shelf collapse has concentrated on the destabilising effects of increased surface melt-water (Mercer, 1978; Rott *et al.*, 1998; Scambos *et al.*, 2000) which may have enhanced the process of crevasse fracture (Weertman, 1973). Shepherd *et al.* (2003) have shown that the Larsen Ice Shelf may have become susceptible to crevasse fracture through a sustained ice thinning by basal melting.

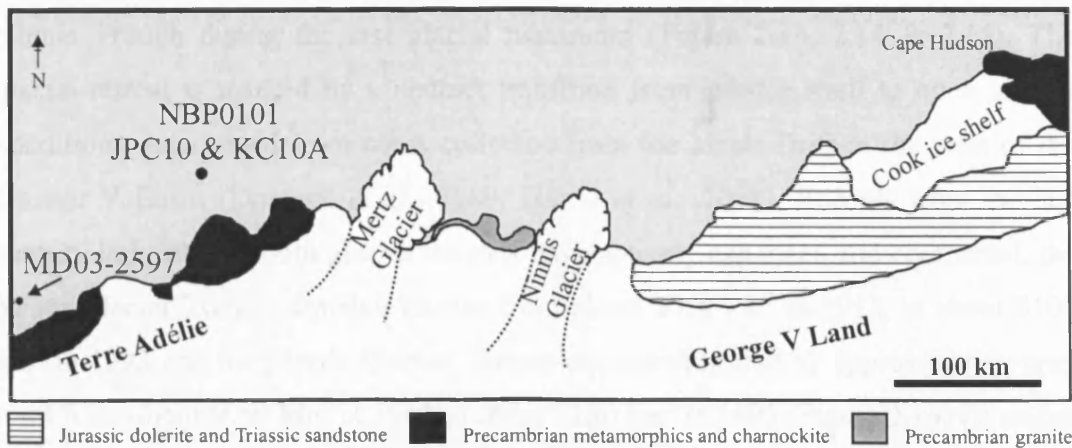
## 2.5.2. Mertz Ninnis Trough, East Antarctic Margin

### 2.5.2.1. Geology

The only exposed bedrocks on the George V Coast are coastal cliffs and nunataks. A geologic boundary occurs at about 147°E, west of the Mertz Glacier, which separates Precambrian metamorphic and igneous rocks from Mesozoic sedimentary and igneous rocks (Figure 2.12) (Craddock, 1972; Kleinschmidt and Talarico, 2000). The Mertz Ninnis Trough was excavated along the contact between crystalline basement rocks and sedimentary strata by ice streams that advanced from an expanded EAIS during the past glacial maxima (Domack, 1982; Domack and Anderson, 1983; Anderson, 1999).

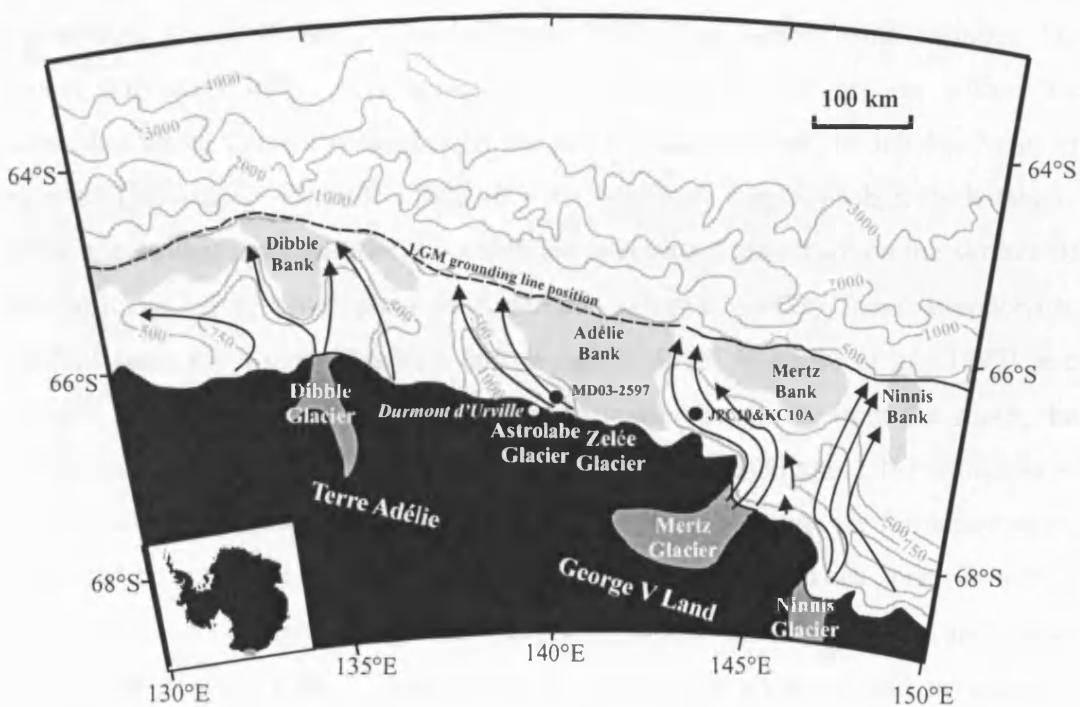
### 2.5.2.2. Glaciology

The George V Coast, East Antarctic Margin, is characterised by ice cliffs with the exception of the Mertz and Ninnis Glacier Tongues (Figure 2.12). These two glacier tongues drain a combined area of over  $4 \times 10^5 \text{ km}^2$  (Anderson, 1999). The Mertz Ninnis Trough is a deep linear basin of glacial origin which parallels the coast on the narrow, deep inner continental shelf. The Mertz Ninnis Trough reaches depths greater than 1300 m just west of the Ninnis Glacier Tongue. Fluted surfaces in the Mertz Ninnis Trough (Barnes, 1987), lateral moraines (Barnes, 1987) and terminal moraines (Domack *et al.*, 1991) indicate that the Mertz Glacier Tongue flowed ESE-WNW



**Figure 2.12**

Geological map of George V Land and Terre Adélie. Adapted from Craddock (1972). Mertz Ninnis Trough core site (NBP0101 JPC10 & KC10A) and Durmont d'Urville Trough core site (MD03-2597) are marked.



**Figure 2.13**

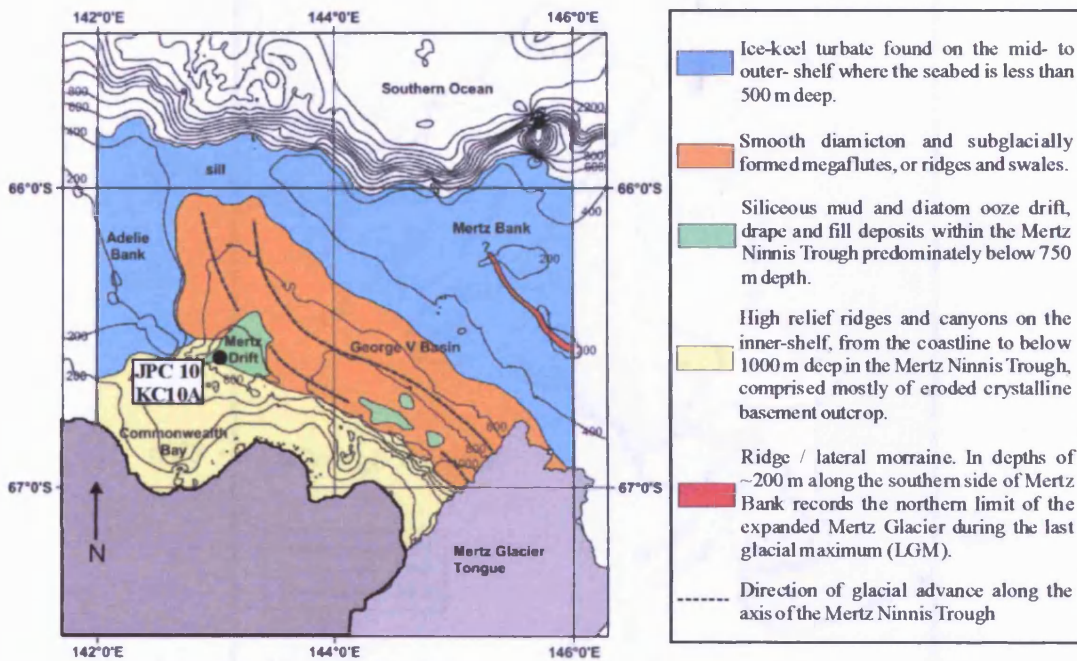
Late Pleistocene ice sheet reconstruction for the Wilkes Land continental shelf adapted from Anderson (1999). Arrows indicate palaeo ice stream flow (modified from Eittrheim *et al.*, 1995). Based on till petrography (Domack, 1982), side-scan sonar (Barnes, 1987) and seismic stratigraphy (Eittrheim *et al.*, 1995). Bathymetry from Chase *et al.* (1987). Core sites, NBP0101 JPC10 & KC10A and MD03-2597 are indicated.

during the late Pleistocene (Domack *et al.*, 1989) and expanded across the Mertz Ninnis Trough during the last glacial maximum (Figure 2.13, 2.14 & 2.15). The glacial retreat is marked by a distinct transition from sub-ice shelf to open marine conditions, interpreted from cores collected from the Mertz Drift in the west of the George V Basin (Domack *et al.*, 1989; Harris *et al.*, 2001). Records from the last century indicate that both glacier tongues have actively expanded and contracted; the Mertz Glacier Tongue doubled its size from about 3830 km<sup>2</sup> in 1913, to about 8100 km<sup>2</sup> in 1993 and the Ninnis Glacier Tongue decreased in size by approximately one-third from about 6060 km<sup>2</sup> in 1913 to about 2150 km<sup>2</sup> in 1993 (Figure 2.16) (Wendler *et al.*, 1996a; 1996b). In 2000 the Ninnis Glacier Tongue underwent a massive calving event which removed half of the floating tongue (Rignot, 2002).

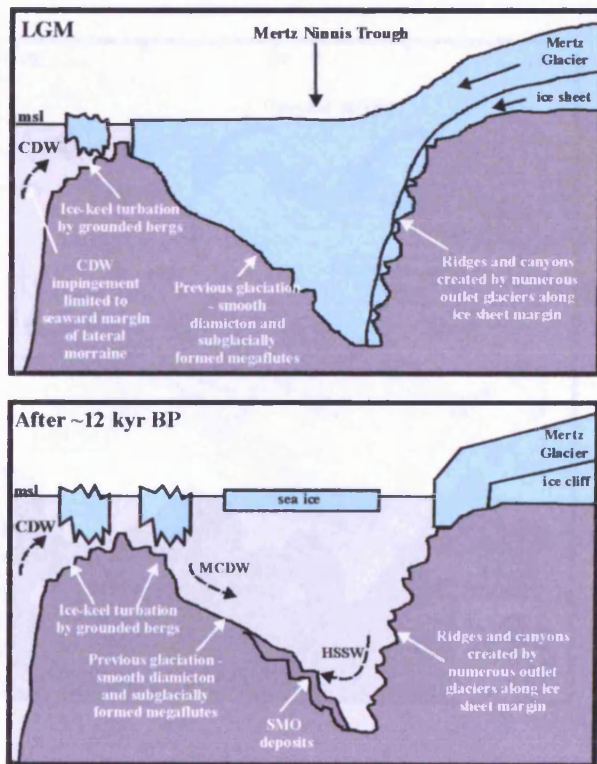
### 2.5.2.3. Mertz Glacier Polynya and Regional Oceanography

The Mertz Glacier Tongue (MGT) is associated with a coastal polynya, the Mertz Glacier Polynya (centred on 67°S, 145°E), an open area of water enclosed in sea ice approximately 20,000 km<sup>2</sup> in size (Figure 2.17). Two mechanisms maintain the coastal polynya. Firstly, near coastal westward advection of sea ice within the Antarctic Coastal Current is blocked by the MGT and associated grounded icebergs to the north (Massom *et al.*, 2001). Secondly, the George V Coast is subject to katabatic winds, the strength and duration of which are unequalled anywhere on the surface of the Earth, including other parts of Antarctica (Loewe, 1972). These directionally constant katabatic winds (Adolphs and Wendler, 1995; Wendler *et al.*, 1997) and synoptic winds provide mechanical forcing to remove ice away from the shore, the western edge of the glacier tongue and grounded icebergs (Figure 2.18) (Massom *et al.*, 2001). Coastal polynyas are “ice factories” and have large sea ice formation rates, which can be up to ten times greater than in the surrounding sea ice zone (Zwally *et al.*, 1985). The ice formation rates depend on local wind speed, air and water temperature and the area of open water (function of wind speed and persistence) (Cavalieri and Martin, 1985; Zwally *et al.*, 1985). Massom *et al.* (1998) have shown that the Mertz Glacier Polynya is a persistent, recurrent feature throughout the year and is believed to have the greatest ice production and therefore, highest rate of salt production in East Antarctica (Cavalieri and Martin, 1985). The fastest rate of areal growth of the polynya occurs during August/September (Bindoff *et al.*, 2001).

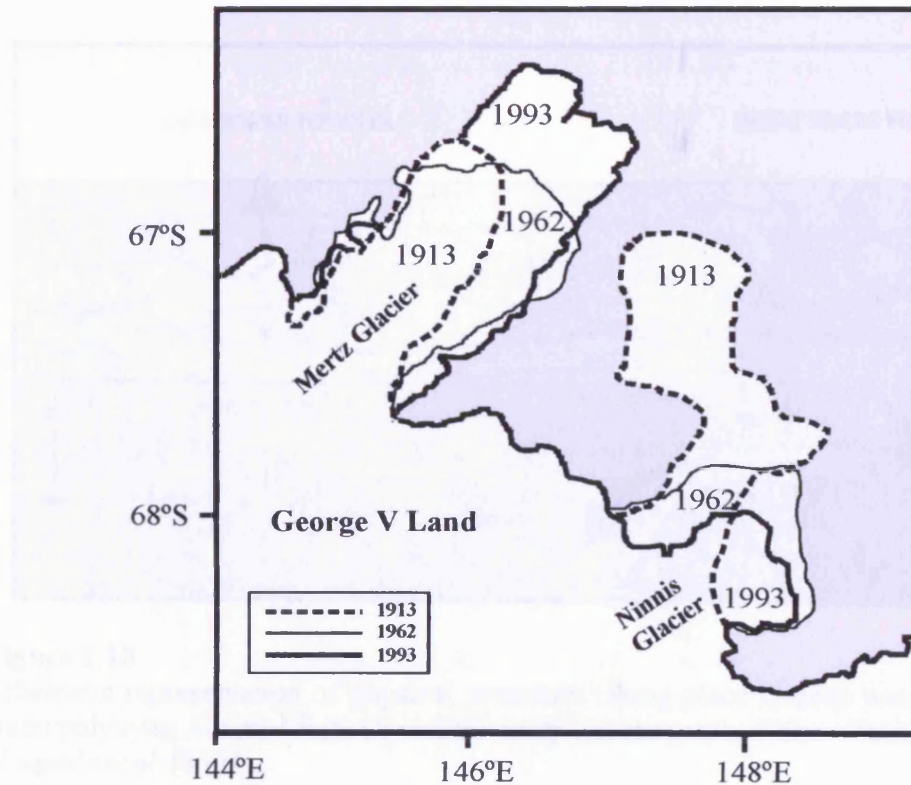




**Figure 2.14**  
Map showing facies on the George V shelf. Core site NBP0101 JPC10 and KC10A indicated. (George V Basin = Mertz Ninnis Trough). Adapted from Beaman and Harris (2003).

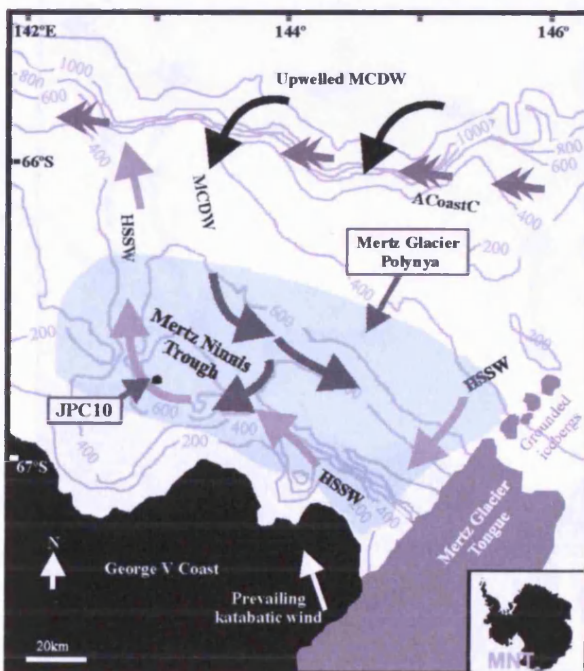


**Figure 2.15**  
Cartoons showing the extent and retreat of the Mertz Glacier Tongue during the last glacial maximum (LGM) and after the LGM (~12 kyr BP). msl = mean sea level. SMO = siliceous mud and diatom ooze. Adapted from Beaman and Harris (2003).



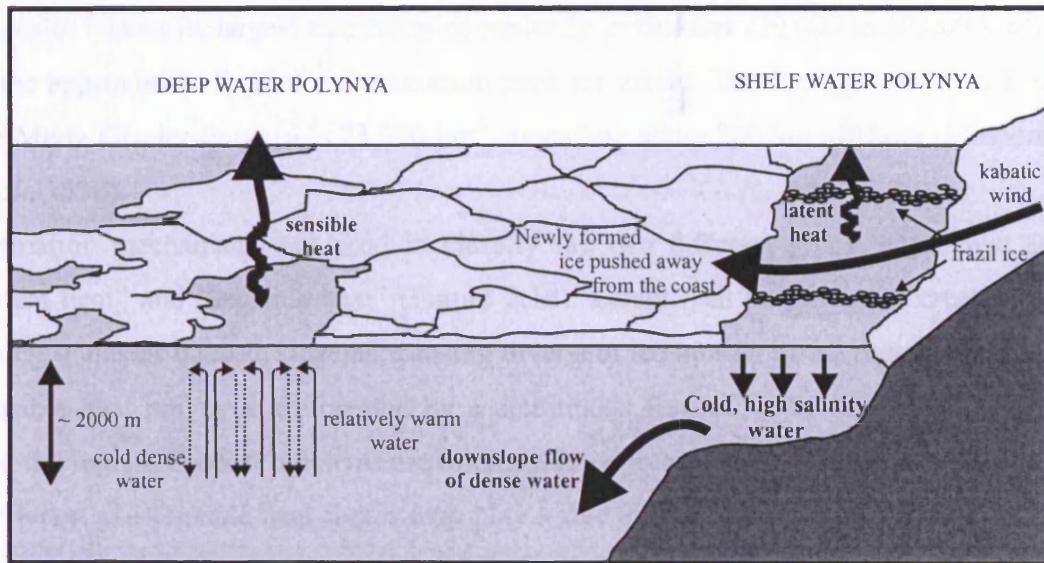
**Figure 2.16**

The position of the Mertz and Ninnis Glacier Tongues in 1913, 1962 and 1993. From Wendler *et al.* (1996a).

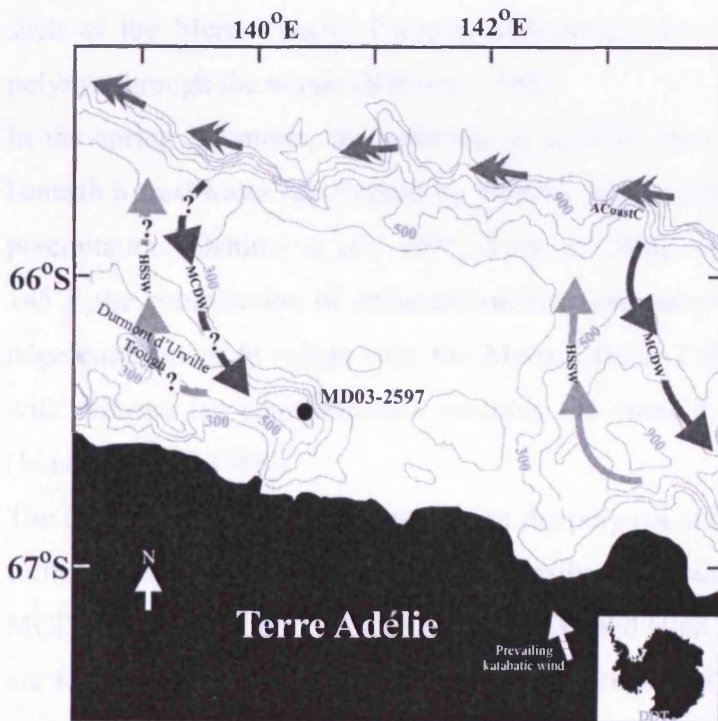


**Figure 2.17**

Oceanographic regime off the George V Coast (modified from Harris *et al.*, 2001). ACoastC = Antarctic Coastal Current. MCDW = Modified Circumpolar Deepwater. HSSW = High Salinity Shelf Water. The position of the core NBP0101 JPC10 is indicated. Inset is the location of the Mertz Ninnis Trough (MNT) on the East Antarctic Margin.



**Figure 2.18**  
Schematic representation of physical processes taking place in deep water and shelf water polynyas. Adapted from Open University Oceanography Course Team (2001) and Maqueda *et al.* (2004).



**Figure 2.19**  
Oceanographic regime off the Terre Adélie Coast. ACoastC = Antarctic Coastal Current. MCDW = Modified Circumpolar Deepwater. HSSW = High Salinity Shelf Water. The position of core MD03 2597 is indicated. Inset is the location of Durmont d'Urville Trough (DDT) on the East Antarctic Margin.

Multi-year special sensor microwave/imager records have shown that the polynya typically attains its largest size fairly consistently in October (20,000 to 60,000 km<sup>2</sup>), at the approximate time of the maximum pack ice extent. The average winter size of the Mertz Glacier Polynya is 23,000 km<sup>2</sup>, extending about 200 km offshore (Massom *et al.*, 1998).

Formation mechanisms are used to classify the two different types of polynya as “latent heat” and “sensible heat” (Figure 2.18). Latent heat polynyas are created by strong winds or oceanic currents, causing divergent ice motion in the region, whereas sensible heat polynyas are created by a continuous flux of ice-melting warm water into the region. Coastal polynyas are often assumed to be strictly latent heat polynyas, but latent and sensible heat fluxes may play a role in maintaining coastal polynyas in areas where significant intrusions of Modified Circumpolar Deep Water (MCDW) occur (Jacobs, 1989). Part of the reason for MCDW upwelling off the George V Coast is the northerly extent of the coastline and the proximity of the warm, saline waters to the shelf break (Orsi *et al.*, 1995). The MCDW appears to enter the Mertz Ninnis Trough through the channel near 143°E (Figure 2.17), connecting the depression to deep water offshore (Rintoul, 1998). The upwelling of warm MCDW (Table 2.2), a source of sensible heat over the continental shelf, may help to maintain a polynya such as the Mertz Glacier Polynya and explain the temporal development of the polynya through the winter (Rintoul, 1998).

In the spring / summer, the reservoir of sensible heat in the MCDW intrusion lies beneath a freshwater cap formed by melting sea ice (increase in solar radiation), and precipitation (Oshima *et al.*, 1998; Rintoul, 1998; Hunke and Ackley, 2001;). At 145°E the combination of enhanced melting and narrow sea ice zone allows an ice edge embayment to merge with the Mertz Glacier Polynya, forming a large region with reduced ice concentrations reaching the coast in austral summer (December) (Massom *et al.*, 1998).

The MCDW cannot reach the surface of the polynya until sufficient cooling and brine formation has occurred to increase the density of the surface layer to equal that of the MCDW (Rintoul, 1998). Winter Water (WW) and High Salinity Shelf Water (HSSW) are formed by brine rejection during sea ice formation (Table 2.2), which contributes to Adélie Land Bottom Water (ALBW). ALBW is a significant source of bottom water and is the second largest source of AABW, contributing 25% of the total AABW volume in the world’s ocean (Rintoul, 1998). A fourth water mass on the

shelf is Ice-Shelf Water (ISW) (Table 2.2). This water mass is much colder than MCDW, WW and HSSW; it is thought to have originated from beneath the Mertz Glacier (Bindoff *et al.*, 2001) (Figure 2.17).

**Table 2.2** Water mass properties (area-averaged) for Mertz Ninnis Trough region. From Williams and Bindoff (2003).

Water mass	Temperature (°C)	Salinity (psu)
Modified Circumpolar Deep Water (MCDW)	-1.83	34.51
Winter water (WW)	-1.90	34.63
Ice shelf water (ISW)	-1.94	34.64
High salinity shelf water (HSSW)	-1.91	34.69

#### 2.5.2.4. Climate

The closest metrological station to the Mertz Ninnis Trough is Durmont d'Urville. Over thirty two years (1957 – 1989) a mean warming temperature of 0.78°C was recorded (Wendler and Prichard, 1991; Periard and Pettré, 1993). Katabatic winds are a major climatic phenomenon in the region; a maximum wind speed of 324 km/h has been recorded at Durmont d'Urville.

### 2.5.3. Durmont d'Urville Trough, East Antarctic Margin

#### 2.5.3.1. Geology

Rocks which outcrop on the coast adjacent to the Durmont d'Urville Trough are Precambrian garnet-rich gneisses and schists of granulite metamorphic facies and charnockites (Stillwell, 1918), a continuation of those found west of the Mertz Ninnis Trough (Figure 2.12).

#### 2.5.3.2. Glaciology

During the LGM Goodwin and Zweck (2000) suggest that a thickness of 1000 m of ice occurred along the EAIS margin between Wilkes Land and Oates Land. Identification of till on the continental shelf has led to the interpretation that the ice sheet grounded on the outer shelf during the LGM (Anderson *et al.*, 1980). Eittrheim *et al.* (1995) established the palaeodrainage of this area (Figure 2.13). The drainage distribution in this area is not convergent and the resulting glaciers are smaller than

the Mertz and Ninnis Glaciers, and are more regularly spaced (Eittrheim *et al.*, 1995). The Dibble Glacier is an exception as it flows from an isolated basinal area of its own (Eittrheim *et al.*, 1995). The Durmont d'Urville Trough was occupied by Zélée and Astrolabe Glacier ice streams during the LGM, which bypassed the outer shelf banks (Eittrheim *et al.*, 1995). The transition from subglacial to glacial-marine sedimentation occurred prior to ~ 9,000 yr BP (corrected date using a reservoir correction of 5,500 yr) (Domack *et al.*, 1989; 1991).

### 2.5.3.3. Regional oceanography

Limited research has been conducted on water mass locations and movements in the Durmont d'Urville Trough region. However it is likely a similar oceanographic setting to Mertz Ninnis Trough exists due to its proximity and similar trough orientation on the shelf (see section 2.5.2.3) (Figure 2.19), influenced by Antarctic Coastal Current, MCDW and HSSW (Rintoul, 1998; Bindoff *et al.*, 2001). MCDW upwells onto the continental shelf and a dense water mass sinks off the shelf region, contributing to AABW (Chiba *et al.*, 2000). The Mertz Glacier Polynya does not extend over Durmont d'Urville Trough (Massom *et al.*, 1998), therefore little HSSW will be produced in this region.

### 2.5.3.4. Climate

As previously discussed in section 2.5.2.4, the area has experienced a warming of 0.78°C between 1957 and 1989 (Wendler and Prichard, 1991; Periard and Pettré, 1993). This region experiences strong katabatic winds, and was described as *The Home of the Blizzard* during Mawson's 1912-1913 expedition (Mawson, 1915).

## 2.6. Summary

This chapter presents background information on Antarctica and the three core sites, Palmer Deep, Mertz Ninnis Trough and Durmont d'Urville Trough. Regional geology, oceanography, glaciology and climate have been discussed and this information will be utilised in context in chapters 6, 7, 8 and 9.

### 3. Diatoms in the Southern Ocean

This chapter presents an introduction to diatoms in Antarctica; environmental and preservation controls on diatom assemblage distribution are described. An account of Antarctic diatom-rich laminated sediment research is also given. In the final section of this chapter the ecology of Antarctic diatoms is presented.

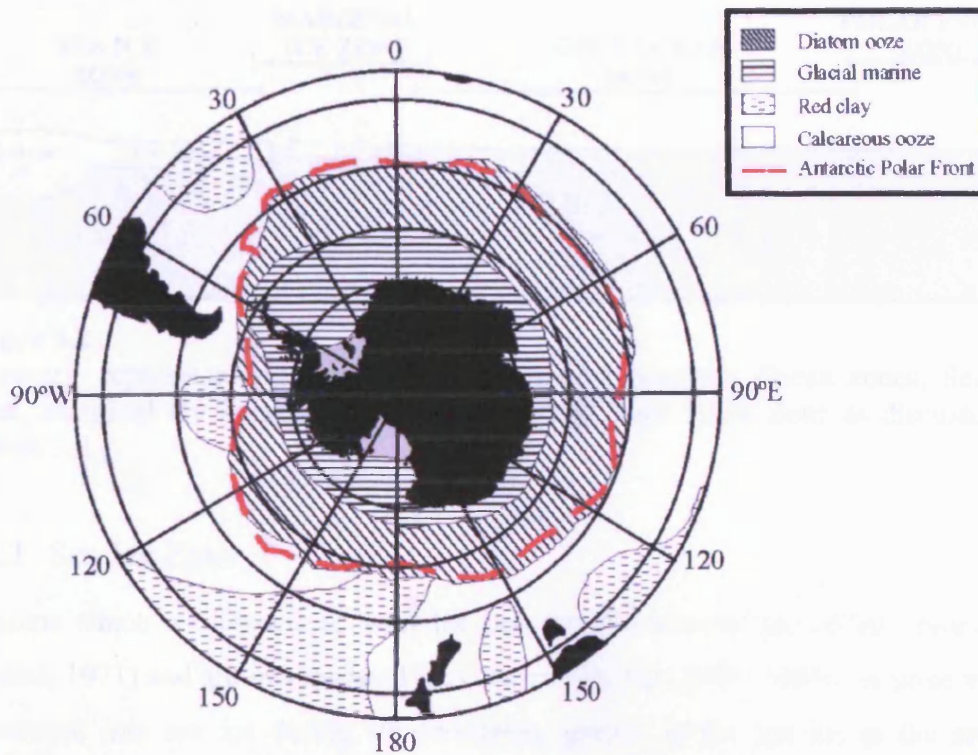
#### 3.1 Introduction

Diatoms are siliceous walled microscopic (1 – 2000 microns) unicellular algae that dominate primary productivity around Antarctica. Diatoms contribute up to 75% of Southern Ocean primary production and, therefore, play an important role in global cycling of silicic acid and carbon (Tréguer *et al.*, 1995). Since the early Neogene, biosiliceous deposition has dominated the sedimentary record of the Southern Ocean (Baldauf and Barron, 1991).

Modern diatom distributions are controlled by interrelated primary processes; light, salinity, sea-surface temperature (Neori and Holm-Hansen, 1982), nutrient availability and proportion (El-Sayad, 1970; Burckle *et al.*, 1987), water-column stability (Leventer, 1991) and sea ice presence (Abelmann and Gersonde, 1991). On the Antarctic continental shelf, sea ice exerts considerable control on environmental variables (Cunningham and Leventer, 1998).

In Antarctica, diatoms are mainly deposited in sediments between the winter sea ice edge and the Polar Front (Lisitzin, 1960; Lozano and Hays, 1976) in a largely continuous belt around Antarctica called the “diatom ooze belt” (Burckle and Cirilli, 1987). This belt is bounded to the north by sediments rich in carbonate and to the south by silty diatomaceous clays (Figure 3.1) (Burckle and Cirilli, 1987). Cooke (1978) and Cooke and Hays (1982) attributed the existence of the siliceous ooze belt to high surface water diatom productivity. Nelson *et al.* (1995) proposed the diatom ooze belt was a result of high preservation efficiency of the diatom frustules, however, this theory has recently been challenged by Pondaven *et al.* (2000). Pondaven *et al.* (2000) believe Southern Ocean diatom rich-sediments are the result of high opal flux rather than high preservation efficiency. A second zone of high biogenic silica deposition (patchier than the diatom ooze belt) occurs on the Antarctic continental shelf (Crosta *et al.*, 2005). Diatom oozes have been encountered on the continental shelf in the Antarctic Peninsula region (e.g. Leventer *et al.*, 2002), in the

Ross Sea (e.g. Truesdale and Kellogg, 1979; Leventer *et al.*, 1993), in Prydz Bay (e.g. Taylor *et al.*, 1997), off Terre Adélie (Leventer *et al.*, 2001), Mertz Ninnis Trough (e.g. Harris *et al.*, 2001; 2003) and MacRobertson shelf (Harris and O'Brien, 1996; Stickley *et al.*, 2005) (Figure 1.1).



**Figure 3.1**

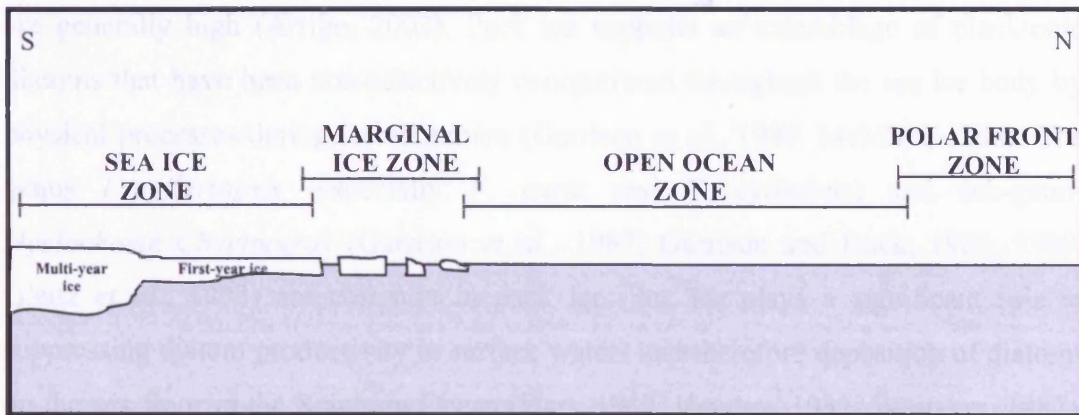
Map of sediment type distribution around Antarctica. Diatoms are mainly deposited in the circumpolar belt of diatomaceous ooze which extends to the Antarctic Polar Front. Adapted from Hays (1967).

### 3.2 Environmental Controls on Diatom Assemblage Distribution

On the Antarctic continental shelf sea ice exerts considerable control over primary productivity (Domack *et al.*, 1993). Distinct diatom assemblages are produced as a result of variation in sea ice formation, sea ice type, sea ice extent and sea ice melt (Grossi and Sullivan, 1985; Smith and Nelson, 1985; Garrison *et al.*, 1986; 1987; Krebs *et al.*, 1987; Garrison and Buck, 1985; 1989; Fryxell, 1989; 1991; Kang and Fryxell, 1991; 1992; 1993; Leventer *et al.*, 1993; Moisan and Fryxell, 1993; McMinn, 1994; Leventer and Dunbar, 1987; 1988; 1996; Bidigare *et al.*, 1996; Gleitz *et al.*, 1996; 1998). Environmental controls on diatom assemblage distribution will be



discussed within the context of four defined zones; Sea Ice Zone, Marginal Ice Zone, Open Ocean Zone and Polar Front Zone (Figure 3.2).



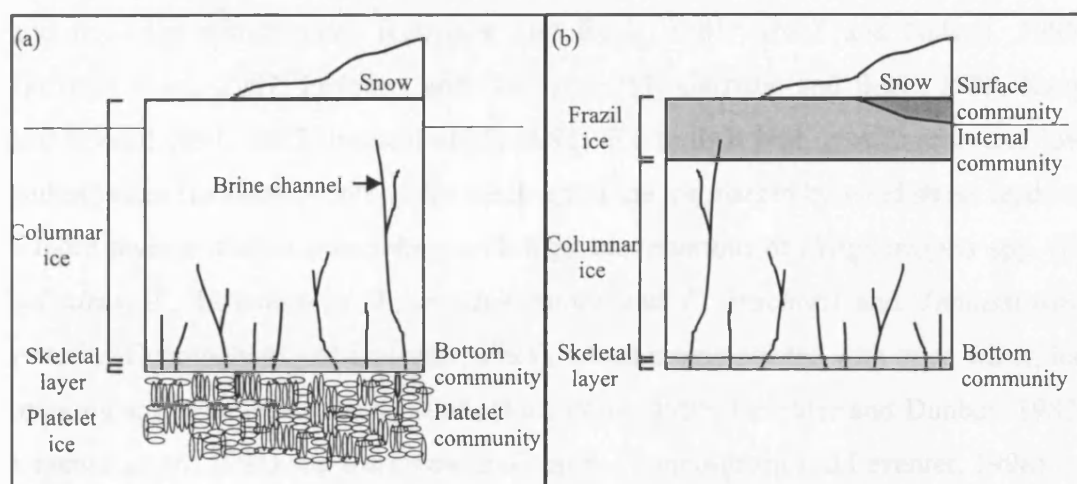
**Figure 3.2**

Schematic representation of the extent of the four Southern Ocean zones; Sea Ice Zone, Marginal Ice Zone, Open Ocean Zone and Polar Front Zone as discussed in section 3.2.

### 3.2.1 Sea Ice Zone

Diatoms which are associated with the sea ice environment are called cryophilic, (Round, 1971) and are incorporated into sea ice (Horner, 1976; 1985a) in three ways; introduced into sea ice during ice formation, growth in the sea ice as the season progresses, and colonisation of the ice matrix after ice has formed (Gleitz *et al.*, 1998). Fifty to 100 diatom species are commonly found in sea ice habitats (Garrison and Buck, 1989; Garrison, 1991; Palmisano and Garrison, 1993). Different forms of sea ice determine the position of diatom growth and the diatom assemblage in sea ice. The position of diatom growth is determined by salinity in sea ice (Arrigo and Sullivan, 1992) and overlaying snow cover thickness (Arrigo *et al.*, 1991). In land-fast ice diatoms occur towards the base of the sea ice (Figure 3.3a; Arrigo, 2003). With the exception of *Fragilariopsis curta* and *F. cylindrus* fast ice diatoms are rare in sediments (Truesdale and Kellogg, 1979; Leventer and Dunbar, 1987; McMinn, 1994). Platelet sea ice forms *in situ* under fast ice (Figure 3.3a) or as a layer of loosely consolidated crystals and is the most porous of all sea ice types (composed of ~20% ice and 80% sea water). *In situ* platelet ice supports a diatom assemblage dominated by pennate diatoms (Smetacek *et al.*, 1992). Loosely consolidated platelet sea ice supports an assemblage dominated by planktonic centric diatoms (*Thalassiosira*

antarctica, *T. tumida*, *Porosira pseudodenticulata*, *P. glacialis* and *Stellarima microtrias*) (El-Sayed, 1971; Smetacek *et al.*, 1992; Gleitz *et al.*, 1996). Pack ice diatoms frequently grow at or near the sea ice surface (Figure 3.3a) where light levels are generally high (Arrigo, 2003). Pack ice supports an assemblage of planktonic diatoms that have been non-selectively concentrated throughout the sea ice body by physical processes during ice formation (Garrison *et al.*, 1989; McMinn, 1994). The genus *Fragilariopsis* (especially *F. curta* and *F. cylindrus*) and sub-genus *Hyalochaete Chaetoceros* (Garrison *et al.*, 1987; Garrison and Buck, 1985; 1989; Gleitz *et al.*, 1998) are common in pack ice. Sea ice plays a significant role in suppressing diatom productivity in surface waters and therefore deposition of diatoms on the sea floor in the Southern Ocean (Hart, 1942; Hendeby, 1937; Whitaker, 1982). Diatom numbers under the sea ice are much lower than at the sea ice edge (Burckle *et al.*, 1987), and the open ocean (Whitaker, 1982).



**Figure 3.3**

Highly idealised schematic illustrations of (a) fast ice and (b) pack ice ecosystems in Antarctica showing the location of the major ice algal communities. Adapted from Arrigo (2003).

### 3.2.2 Marginal Ice Zone

The Marginal Ice Zone is the region where sea ice grades into open ocean. This zone migrates northwards and southwards annually with the seasons. Phytoplankton blooms are commonly associated with this area where the water column is stable and less saline due to sea ice melt-induced stratification (El-Sayed, 1971; Alexander and Niebauer, 1981; Sakshaug and Holm-Hansen, 1984; Smith and Nelson, 1985;

Niebauer and Alexander, 1985; Smith and Nelson, 1986; Nelson *et al.*, 1987; Sullivan *et al.*, 1988; Sakshaug and Skjoldal, 1989; Comiso *et al.*, 1990; Lancelot *et al.*, 1991a; 1991b; Bianchi *et al.*, 1992; Comiso *et al.*, 1993; Schloss and Estrada, 1994) and higher nutrients. These phytoplankton blooms are considered to be responsible for high polar productivity (Smith and Nelson, 1985; Nelson *et al.*, 1987; Leventer, 2003). Marginal ice zone blooms are estimated to produce 50 – 60% of annual primary production in the Southern Ocean (Smith and Nelson, 1986; Legendre *et al.*, 1992), 4-5 times greater than productivity under sea ice (Burckle *et al.*, 1987). The way in which sea ice breaks up in spring, albeit by melting or physical breakout by wind stress, can affect the species living in the water column and deposited in the sediments (Cunningham and Leventer, 1998). Melting of pack and fast ice produces a low salinity lens that stratifies the upper water column and supports a rich algal bloom. The bloom is seeded by diatom species, such as *Fragilariopsis curta* and *F. cylindrus*, which have been released by melting and are common in both the sea ice and ice edge communities (Garrison and Buck, 1985; Smith and Nelson, 1985; Garrison *et al.*, 1987; Leventer and Dunbar, 1987; Garrison and Buck, 1989; Kang and Fryxell 1991; 1992; Bianchi *et al.*, 1992) due to their high growth rates and low sinking rates (Leventer, 1998). The break up of the ice margin by wind stress leads to a more diverse diatom assemblage with high contributions of *Fragilariopsis* spp. (*F. cylindrus*, *F. kerguelensis*, *F. obliquecostata* and *F. ritscheri*) and *Thalassiosira gracilis* (Cunningham and Leventer, 1998), which are associated with open water, ice marginal environments (Hasle, 1965; Buck *et al.*, 1985; Leventer and Dunbar, 1987; Leventer *et al.*, 1993) and a decrease in *F. curta* (Cunningham and Leventer, 1998).

### 3.2.3 Open Ocean Zone

The Open Ocean Zone is a broad region which lies between the Marginal Ice Zone and the Polar Front Zone. The surface waters in this region have relatively low phytoplankton growth compared to the Polar Front Zone and Marginal Ice Zone (Selph, *et al.*, 2001). This is due to growth inhibiting low levels of iron (Martin, 1990) and high grazing pressure (Smetacek *et al.*, 1997). Large centric diatoms dominate the surface mixed layer in the open ocean, but the pennate diatoms *Thalassiothrix* spp. and *Pseudo-nitzschia* spp. are also present (Selph *et al.*, 2001).

### 3.2.4 Polar Front Zone

This zone lies between nutrient-rich Antarctic waters and nutrient-poor Subantarctic waters. Phytoplankton in this region sometimes reach higher concentrations than in the Open Ocean Zone (Moore and Abbott, 2000); de Baar *et al.* (1995) propose that this is due to eddy mixing within the Polar Front (see section 2.3.2.1) increasing the supply of nutrients to surface waters. Centric diatoms dominate this zone, with mixed layer communities tending towards single genera such as *Hyalochaete Chaetoceros* spp. and *Corethron* spp. (Selph *et al.*, 2001). Blooms occur in late spring in the Polar Front Zone initiated by increased light levels and possibly increased water column stratification and decline due to increased nutrient stress (Abbott *et al.*, 2001). In a six week period, in 1992, three species mono-specific blooms of *Fragilariopsis kerguelensis*, *Corethron pennatum* and *Corethron inerme* were observed (Smetacek *et al.*, 1997).

## 3.3 Preservation Controls on Diatom Assemblage Distribution

Aside from the environmental variables that affect diatom assemblage composition in sediments and distribution in surface waters (as discussed in section 3.2), preservation controls such as dissolution, aggregation, grazing and advection alter the diatom assemblage on its journey through the water-column to the sediment. Burckle and Cirilli (1987) propose good preservation is characterised by little frustule breakage, abundant whole valves, high diversity and the presence (although never in high abundance) of delicate weakly silicified forms. Poor preservation is characterised by an abundance of valve fragments, few whole valves, absence of delicate forms and apparent dissolution around broken valve margins (Burckle and Cirilli, 1987).

### 3.3.1 Dissolution

Diatom assemblage composition can be significantly altered by dissolution of frustules in the water-column and at the sediment-water interface (Nelson and Gordon, 1982; Dunbar *et al.*, 1989; Leventer and Dunbar, 1987; Van Bennekom *et al.*, 1988; Leventer and Dunbar, 1996); this accounts for the temporal and spatial variations in sedimentary diatom assemblages observed in Southern Ocean sediments (Shemesh *et al.*, 1989). Seawater and sediment porewaters are usually undersaturated

with respect to biogenic silica (Tréguer *et al.*, 1995), which dissolves diatom frustules rapidly (especially when pH is high, as in calcareous sediments) (Sancetta, 1999). Nelson and Gordon (1982) estimate 18-58% of the biogenic opal produced in the euphotic zone is already dissolved in the upper 100 m of the Southern Ocean. In areas of relatively low silica accumulation (e.g. Weddell Sea), the dissolution of biosiliceous opal can lead to the destruction of accumulated diatoms (Zielinski and Gersonde, 1997). In the Southern Ocean sedimentary diatom assemblages are enriched in the heavily silicified species *Fragilariopsis kerguelensis*, relative to the water column assemblage, due to selective dissolution (DeFelice and Wise, 1981; Abelmann and Gersonde, 1991). This makes *F. kerguelensis* a main opal contributor of the Southern Ocean diatom ooze belt (Figure 3.1) (Kozlova, 1966; DeFelice and Wise, 1981; Zielinski and Gersonde, 1997) and complicates the interpretation of diatom assemblages in sediments (Shemesh *et al.*, 1989). Fragile, lightly silicified diatom species with high surface area to volume ratios, such as *Corethron pennatum*, are more susceptible to mechanical damage and dissolution, (Gersonde and Wefer, 1987; Leventer and Dunbar, 1987; Shemesh *et al.*, 1989; Leventer *et al.*, 1996). Several workers have argued that dissolution contributes less to diatom assemblage alteration than factors such as advection and cell aggregation (Nelson and Gordon, 1982; Dunbar *et al.*, 1985; Ledford-Hoffman *et al.*, 1986; Nelson and Smith, 1986; Leventer and Dunbar, 1987; 1996).

### 3.3.2 Aggregation

Diatoms are effectively exported from surface waters to the sea floor by incorporation into pelagic grazer faecal pellets, millimetre-sized aggregates (marine snow) and *setae* entanglement during super-blooms (Smayda, 1970; Smetacek, 1985; Alldredge and Gottschalk, 1989; Jaeger *et al.*, 1996). Repackaging diatoms in these three ways greatly increases settling rates (Alldredge and Silver, 1988); this increases the likelihood that the diatoms will reach the sea floor and reduces the chance of seeding a new diatom population. Abelmann and Gersonde (1991) calculated that flux pulses, due to faecal pellets and aggregates, in austral summer, accounted for 70-95% of annual flux. Grazing plays a part in controlling the quantity, timing and pattern of vertical transfer of diatoms to the sea floor (Zielinski and Gersonde, 1997). Von Bodungen (1986) observed the production of large faecal pellets in the Bransfeld

Strait (Antarctic Peninsula), and calculated that 45% of the primary productivity in late November to early December was lost via grazing. Many near-monospecific sedimentary laminae, composed of fast growth diatoms in upwelling or spring bloom conditions (e.g. Brodie and Kemp, 1994; Bull and Kemp, 1995), have been formed due to rapid post-bloom flocculation and mass sinking (Smetacek, 1985; Alldredge and Goltschalk, 1989). Diatom coagulation was enhanced by the production of mucus transparent exopolymer particles (Alldredge *et al.*, 1993). Blooms of the buoyant diatom *Rhizosolenia* spp. have been observed to form aggregations (patches) in surface waters at oceanic fronts in the Pacific Ocean (Yoder *et al.*, 1994). The abundance of this species produced a density current, causing the diatoms to rapidly sink through the water column.

### 3.3.3 Advection

Since diatoms are silt-sized, they can be laterally advected by currents; they can be transported large distances during their descent through the water column (Burckle and Stanton, 1975; Leventer, 1991) or can be resuspended from surface sediments and then transported by bottom currents (Leventer and Dunbar, 1987). This redistribution of diatoms can alter the diatom assemblage both in the source region and the deposition site. Bianchi *et al.* (1992) speculated that ice edge blooms of *Thalassiosira gravida* and *Chaetoceros neglectum* in the Weddell Sea were advected into the region from the Bransfield Strait. Displaced diatoms, endemic to the Southern Ocean (e.g. *Fragilariopsis kerguelensis*, *Thalassiosira lentiginosa* and *T. antarctica*) have been used to track transport pathways of Antarctic Bottom Water into mid- and low-latitude areas (Burckle and Stanton, 1975; Burckle, 1981; Schrader and Schütte, 1981; Jones and Johnson, 1984; Pokras and Molfino, 1986; Romero and Hensen, 2002).

## 3.4 Antarctic Laminated Sediments

Laminated sediment research gives an insight into high resolution records of intra- and inter-annual variability in sediment deposition. There are two basic requirements for the formation of laminated sediments; firstly a variation in sedimentary composition via changes in input (chemical or biological) conditions and secondly, environmental conditions that will preserve the laminated sediment fabric from bioturbation (Kemp, 1996; Kemp *et al.*, 2000). Marine laminated diatom ooze from

the Antarctic continental shelf contains a high-resolution record of climatic fluctuations (Domack *et al.*, 1991; Leventer *et al.*, 1996; 2002) and oceanographic variations circum-Antarctica. The resolution of diatom analysis using tooth pick samples is insufficient to resolve seasonal to annual scale records in laminated diatom ooze (Leventer *et al.*, 1996; 2002). To determine inter- and intra-lamina cyclical changes in laminated sequences, high-resolution imaging of resin impregnated thin sections is required. Such analysis has revealed annual cyclical changes of diatom assemblages in deglacial laminated sediments from MacRobertson Shelf, East Antarctic Margin (Stickley *et al.*, 2005) and late Quaternary laminated sediments from western, Antarctic Peninsula (Pike *et al.*, 2001; Bahk *et al.*, 2003).

### 3.5 Species Ecology

This section describes the characteristics of diatom species that occur in the laminated sediments from Palmer Deep, Mertz Ninnis Trough and Durmont d'Urville Trough. Full taxonomic information and photographs of the following species can be found in Appendices 1 and 2, respectively. The ecological information presented here will be used to support interpretations and discussions in chapters 6, 7, 8 and 9.

#### 3.5.1 *Actinocyclus actinochilus* (Ehrenberg) Simonsen

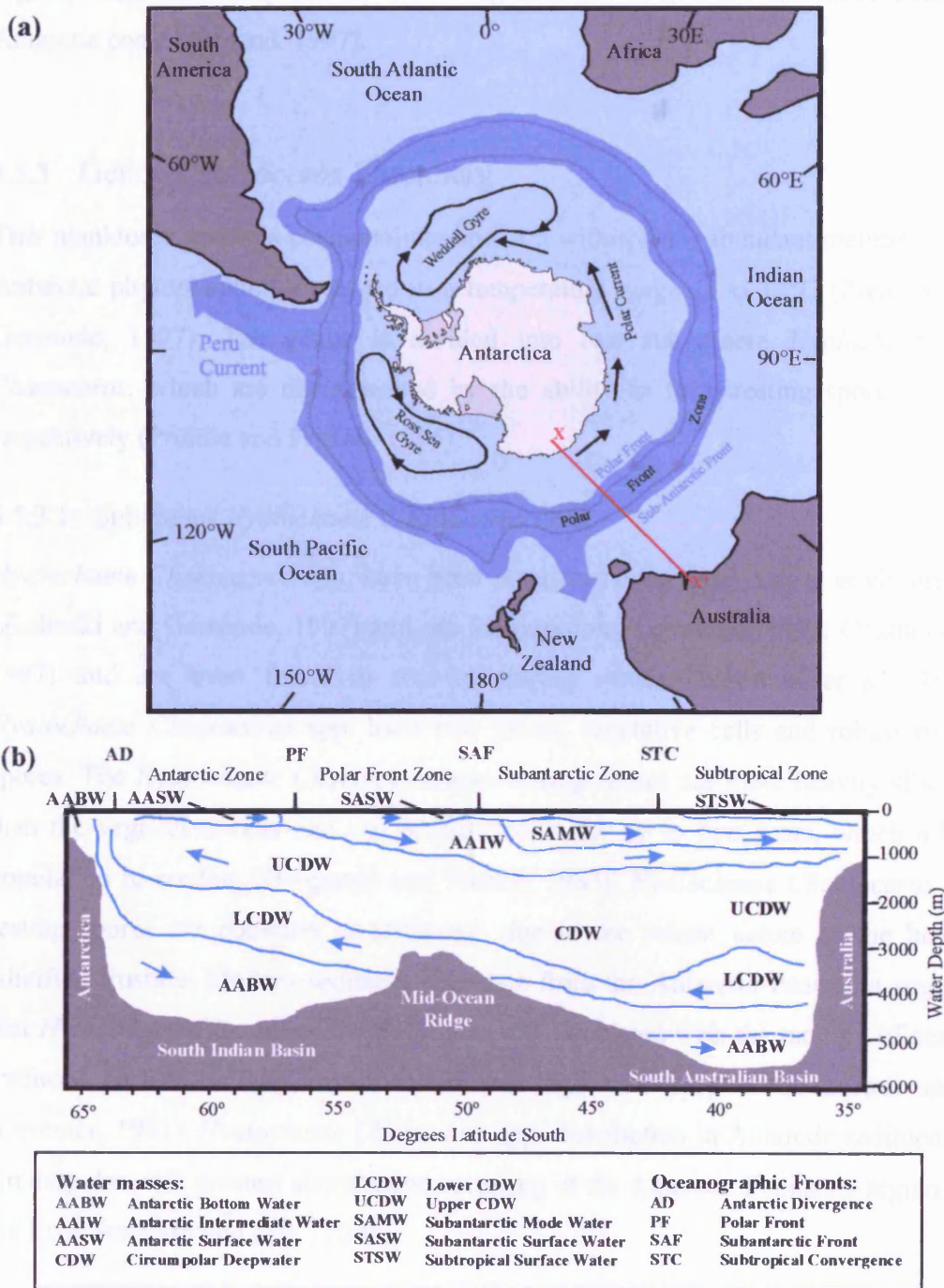
*Actinocyclus actinochilus* is endemic to the Southern Ocean and is a cool water planktonic species associated with water  $-1^{\circ}\text{C}$  to  $0.5^{\circ}\text{C}$  (Zielinski and Gersonde, 1997). *A. actinochilus* has been reported to occur in both open and ice-covered water during the winter (Moisan and Fryxell, 1993), in newly formed spring sea ice (Gersonde, 1984; Garrison *et al.*, 1987; Tanimura *et al.*, 1990; Garrison and Close, 1993) and in both fast and pack-ice (Horner, 1985b; Krebs *et al.*, 1987; Garrison and Buck, 1989; Garrison, 1991). *A. actinochilus* appears to have a higher presence in sea ice than in the adjacent water column (Garrison *et al.*, 1983a; 1987) and is most commonly linked with other sea ice taxa both in the sediments and the sea ice (Armand, 1997). *A. actinochilus* distribution in the sediments has been reported south of the Polar Front (Figure 3.4) (Donahue, 1973; DeFelice and Wise, 1981; Zielinski and Gersonde, 1997; Armand, 1997; Semina, 2003) and has been observed in low to medium abundances along the Antarctic coast (Armand *et al.*, 2005).

#### 3.5.2 Genus *Asteromphalus* Ehrenberg

*Asteromphalus hookeri* Ehrenberg is a planktonic species that has been identified as a minor constituent in both sea ice (Horner, 1985b; Krebs *et al.*, 1987) and in the adjacent water column (Garrison *et al.*, 1983a; 1987) with higher abundances in the adjacent water column (Garrison *et al.*, 1983a; 1987). *A. hookeri* appears to be limited to the north by the Polar Front (Figure 3.4) (Armand, 1997).

High abundances of the planktonic species *Asteromphalus parvulus* Karsten are recorded within the Open Ocean Zone, between the marginal ice zone and the Polar Frontal Zone (Figure 3.2). Abundances of *A. parvulus* decrease north and south of this





**Figure 3.4**

(a) Schematic map showing Southern Ocean circulation. The path of the Antarctic Circumpolar Current is shown by the blue tone; the two dark blue lines represent the average positions of the Polar (Antarctic) Front and the Sub-Antarctic Front. The approximate positions of the gyres in the Weddell Sea and the Ross Sea are shown as is the path of the Polar Current. The Antarctic Divergence lies between the Polar Current and the Antarctic Circumpolar Current. Adapted from Anderson (1999).

(b) Diagrammatic circulation transect through 135°E (X-X' in (a)) in the southeast Indian Ocean. From Armand (1997).

region, with the exception of some regionalised abundance increases near the Antarctic coast (Armand, 1997).

### 3.5.3 Genus *Chaetoceros* Ehrenberg

This planktonic genus is cosmopolitan and is a widespread, abundant member of the Antarctic phytoplankton, observed in a temperature range -2 to 12°C (Zielinski and Gersonde, 1997). The genus is divided into two sub-genera *Hyalochaete* and *Phaeoceros*, which are distinguished by the ability to form resting spores or not, respectively (Priddle and Fryxell, 1985).

#### 3.5.3.1 Sub-genus *Hyalochaete* *Chaetoceros* Gran

*Hyalochaete* *Chaetoceros* spp. have been noted to favour near coastal environments (Zielinski and Gersonde, 1997) and sea ice proximity (Leventer, 1991; Crosta *et al.*, 1997) and are even found in sea ice during winter (Ligowski *et al.*, 1992). *Hyalochaete* *Chaetoceros* spp. have two forms, vegetative cells and robust resting spores. The *Hyalochaete* *Chaetoceros* spp. resting spores are more heavily silicified than the vegetative cells and can remain viable for up to two years, which allows population re-seeding (Hargraves and French, 1983). *Hyalochaete* *Chaetoceros* spp. resting spores are common in sediments due to the robust nature of the heavily silicified frustule. Modern sediment trap data from the Antarctic Peninsula suggests that *Hyalochaete* *Chaetoceros* spp. blooms are associated with the melting of sea ice (reduced surface salinity, stratification and high nutrients) in the austral spring (Leventer, 1991). *Hyalochaete* *Chaetoceros* spp. distribution in Antarctic sediments is circumpolar with greatest abundances occurring in the Antarctic Peninsula region and the Ross Sea (Armand *et al.*, 2005).

#### 3.5.3.2 Sub-genus *Phaeoceros* *Chaetoceros* Gran

*Phaeoceros* *Chaetoceros* spp. do not form resting spores (Priddle and Fryxell, 1985) and presumably survive the winter as vegetative cells. The *Phaeoceros* *Chaetoceros* spp. frustules are larger than *Hyalochaete* *Chaetoceros* spp. and have much more varied, thicker *setae* which are very long (up to 1 mm, Smetacek *et al.*, 2004), striated and possess conspicuous spines. This sub-genus is mostly oceanic in distribution whereas *Hyalochaete* *Chaetoceros* spp. are more coastal (Hasle and Syvertsen, 1997).

### 3.5.4 Genus *Cocconeis* Ehrenberg

*Cocconeis* is a benthic genus that occurs in water depths >9.8 m (Whitehead and McMinn, 1997). *Cocconeis* spp. have been reported to be related to fast-ice consisting of ~90% congelation ice (Scott *et al.*, 1994). In Arthur Harbor (Anvers Island), *Cocconeis* spp. commonly forms spring/summer blooms and benthic diatom mats in the coastal subtidal zone (Krebs, 1983). The mats disintegrate by late spring as wind strength increases and sea ice breaks up (Krebs, 1983). In sediment traps from the northern Antarctic Peninsula, Leventer (1991) recorded an autumn diatom assemblage with increasing amounts of benthos and ice related species, including *Cocconeis*, in near-coastal stations. The assemblages are interpreted to be coastal flora resuspended by autumn storms (Leventer, 1991).

### 3.5.5 *Corethron pennatum* (Grunow) Ostenfeld

*Corethron pennatum* is a planktonic species that occurs in open water with little sea ice (Fryxell and Hasle, 1971; Makarov, 1984; Leventer and Dunbar, 1987), although it has been found in pack ice assemblages (Garrison and Buck, 1989) and reported to be a component of the ice edge phytoplankton (Marra and Boardman, 1984). *C. pennatum* usually reaches its highest concentrations along the Antarctic coast (Sommer, 1991; Ligowski *et al.*, 1992). Sex is considered a causative factor in mass sedimentation of the species and the formation of monospecific sediment layers of *C. pennatum* (Crawford, 1995). The episodic nature of these mass sinking events is thought to explain the generally sporadic record of *C. pennatum* in Antarctic sediments (Crawford *et al.*, 1997).

### 3.5.6 *Coscinodiscus bouvet* Karsten

*Coscinodiscus bouvet* is a large distinctive planktonic Antarctic endemic species. The habitat of *C. bouvet* is primarily coastal and has a circumpolar distribution. Priddle and Thomas (1989) have observed *C. bouvet* in oceanic waters (Scotia Sea) and have attributed this to advection from coastal seed populations in Bransfield Strait.

### 3.5.7 *Eucampia antarctica* (Castracane) Mangin

The occurrence of *Eucampia antarctica* in modern sediments suggests that the distribution of this planktonic species is in surface waters of the Antarctic Zone and the Polar Front Zone (Figure 3.4) (Zielinski and Gersonde, 1997) and that it is not a sea ice-related taxon as proposed by Burckle (1984b) and Burckle *et al.* (1990). *E. antarctica* has been noted to occur in much higher abundances in the adjacent water column than in the sea ice itself (Garrison *et al.*, 1983a; 1987). Two morphologically different varieties of *E. antarctica* with different distribution patterns have been identified (Fryxell and Prasad, 1990; Kaczmarska *et al.* 1993); *E. antarctica* var. *antarctica* and *E. antarctica* var. *recta*. *Eucampia antarctica* var. *antarctica* is a subpolar form associated with open water and *E. antarctica* var. *recta* is a polar form associated with sea ice. In the Prydz Bay region Fryxell (1989) noted that *E. antarctica* var. *antarctica* was abundant far from the sea ice in the open ocean in spring, and that *E. antarctica* var. *recta* was abundant near sea ice during autumn. Both forms produce resting stages which are more heavily silicified than the vegetative valves and are therefore preferentially preserved in the sediments.

### 3.5.8 *Fragilariopsis curta* (Van Heurck) Hustedt

*Fragilariopsis curta* is an endemic planktonic Southern Ocean species and occupies near-shore and open ocean environments. *F. curta* is strongly associated with pack, fast and melting sea ice and surface water stratification (Leventer and Dunbar, 1987; Cunningham and Leventer, 1998; Leventer, 1998). The species is also noted in very high abundances in the water column near the sea ice edge (Fryxell, 1989; Tanimura *et al.*, 1990; Kang and Fryxell, 1992; 1993; Andreoli *et al.*, 1995; Leventer and Dunbar, 1996). *F. curta* is restricted to areas south of the Polar Front Zone (Figure 3.4) with summer surface water temperatures below  $\sim 2^{\circ}\text{C}$  (Zielinski and Gersonde, 1997), with maximum geographical distribution linked to the limit of winter sea ice extent (Armand, 1997). Highest abundances of *F. curta* in sediment samples occur near to the Antarctic coast (Kozlova, 1966; Truesdale and Kellogg, 1979; DeFelice and Wise, 1981; Gersonde, 1984; Gersonde and Wefer, 1987; Kellogg and Kellogg, 1987; Stockwell *et al.*, 1991; Leventer, 1992; Taylor *et al.*, 1997; Zielinski and Gersonde, 1997) e.g. near Prydz Bay, in the Ross Sea region and along the George V

Coast (Armand *et al.*, 2005). It is suggested that the distribution of *F. curta* is bounded by the northern most extent of sea ice (Semina, 2003). The thick silicification of the *F. curta* valves may prevent rapid dissolution of this species compared to other taxa in the same conditions, explaining its concentration in sediments (Tanimura *et al.*, 1990).

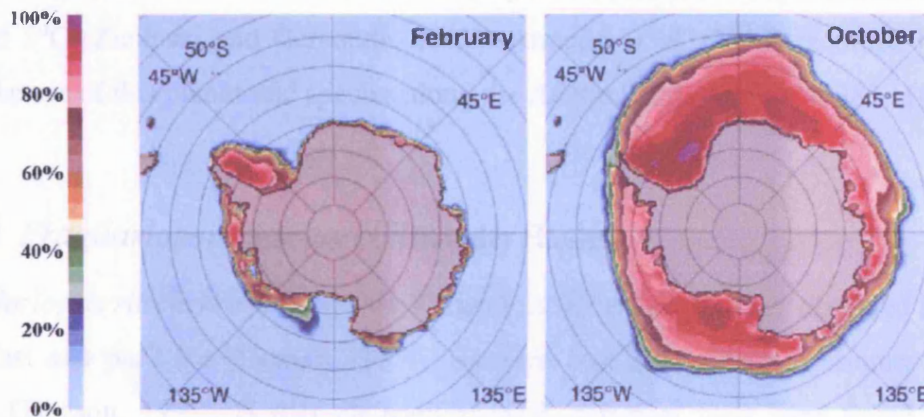
### 3.5.9 *Fragilariopsis cylindrus* (Grunow) Krieger

*Fragilariopsis cylindrus* is a bipolar species and occupies both sea ice habitats (land-fast and pack ice; Garrison, 1991) and well-stratified, stable open water in front of the sea ice edge (Garrison *et al.*, 1987; Garrison and Buck, 1989; Stockwell *et al.*, 1991; Kang and Fryxell, 1992; Leventer *et al.*, 1993; Scott *et al.*, 1994) near the Antarctic coast. *F. cylindrus* has been linked with the process of sea ice formation (Clarke and Ackley, 1983; Garrison and Buck, 1989; Garrison *et al.*, 1989; Garrison, 1991). This planktonic species has been shown to be the most dominant marginal sea ice edge species; with increased seasonal abundance during the summer (Kang and Fryxell, 1992; Kang *et al.*, 1993; Kang and Fryxell, 1993). *F. cylindrus* has been reported to form resting spores (McQuoid and Hobson, 1996) that are likely more dissolution resistant and well preserved in sediments (Jousé *et al.*, 1962; Gersonde, 1984; Tanimura *et al.*, 1990; Leventer, 1992; Zielinski, 1993; Zielinski and Gersonde, 1997). Like *F. curta*, *F. cylindrus* is restricted to areas south of the Antarctic Polar Front (Figure 3.4) with summer surface water temperatures below  $\sim 2^{\circ}\text{C}$  (Zielinski and Gersonde, 1997). Zielinski and Gersonde (1997) propose that *F. curta* and *F. cylindrus* are useful tools for the reconstruction of sea ice distribution in the Southern Ocean.

### 3.5.10 *Fragilariopsis kerguelensis* (O'Meara) Hustedt

*Fragilariopsis kerguelensis* is a heavily silicified planktonic diatom, endemic to the Southern Ocean, which preferentially lives in water with surface water temperatures between 0 and  $10^{\circ}\text{C}$  (Zielinski and Gersonde, 1997). It is considered an indicator of open-water productivity and the abundance of *F. kerguelensis* has been negatively correlated with sea ice concentration (Burckle *et al.*, 1987). Towards neritic, shallow water, near-shore environments the abundance of *F. kerguelensis* in the plankton and the sediment decreases (Kozlova, 1966; Truesdale and Kellogg, 1979; Leventer,

1992; Zielinski and Gersonde, 1997). *F. kerguelensis* dominates the diatom assemblages in pelagic areas of the Antarctic Circumpolar Current (ACC) between the winter sea ice edge (Figure 3.5) and the Subtropical front (Figure 3.4) (Zielinski and Gersonde, 1997). Zielinski and Gersonde (1997) note that close to and north of the Subtropical Front *F. kerguelensis* decreases to less than 20% of the total diatom assemblage.



**Figure 3.5**

Mean monthly sea ice concentrations for February (austral summer) and October (austral winter) averaged over 8.8 years between 1978-1987. From Gloerson *et al.* (1992).

### 3.5.11 *Fragilariopsis obliquecostata* (Van Heurck) Heiden

*Fragilariopsis obliquecostata* has been observed in land-fast and pack ice (McConville and Wetherbee, 1983; Gersonde, 1984; Horner, 1985b; Garrison and Buck, 1989; Tanimura *et al.*, 1990; Garrison, 1991). This planktonic species has been linked to ice surface melt pools and associated with increased abundance in the water column under sea ice (McConville and Wetherbee, 1983; Gersonde, 1984; Garrison *et al.*, 1983a; 1987; Garrison, 1991). *F. obliquecostata* has been found in waters with summer sea surface temperatures (SST) below 2°C. Most studies indicate an increasing abundance of *F. obliquecostata* south of the Antarctic Divergence (Figure 3.4) (Kozlova, 1966; Gersonde, 1984; Gersonde and Wefer, 1987; Kellogg and Kellogg, 1987; Zielinski and Gersonde, 1997). *F. obliquecostata* is confined to the sea ice environment, where winter sea ice concentration may play a greater role in its distribution than summer sea ice concentration (Armand *et al.* 2005).

### 3.5.12 *Fragilariopsis rhombica* (O'Meara) Hustedt

*Fragilariopsis rhombica* has been reported near the Antarctic coast or ice shelves (Kozlova, 1966; Truesdale and Kellogg, 1979; Gersonde and Wefer, 1987; Leventer, 1992; Zielinski and Gersonde 1997; Cunningham and Leventer, 1998) in both fast and pack ice samples (Garrison *et al.*, 1983a; Gersonde, 1984; Horner, 1985b; Krebs *et al.*, 1987; Garrison and Buck, 1989; Garrison, 1991). It is closely related with the Polar Frontal Zone and the Antarctic Zone (Figure 3.4) at water temperatures between -2 and 5°C (Zielinski and Gersonde, 1997). Armand *et al.* (2005) recorded highest abundances of this planktonic species along the Adélie Land coastline (138°– 140°E).

### 3.5.13 *Fragilariopsis ritscheri* (Hustedt) Hasle

*Fragilariopsis ritscheri* is an endemic Antarctic species and has been observed in both land-fast and pack ice (Horner, 1985b, Garrison and Buck, 1989, Tanimura *et al.*, 1990, Garrison, 1991). Higher abundances of *F. ritscheri* have been found in the water column adjacent to sea ice than in sea ice samples (Gersonde, 1984, Garrison *et al.*, 1987) and in ice surface melt pools (McConville and Wetherbee, 1983). This planktonic species has been found in waters with summer SST between -2 and 5°C and at maximum abundances between -2 and 1°C (Zielinski and Gersonde, 1997). Most studies of the species indicate increasing abundances north of the Antarctic divergence (Figure 3.4) (Kozlova, 1966, DeFelice and Wise, 1981, Stockwell *et al.*, 1991, Zielinski and Gersonde, 1997).

### 3.5.14 *Fragilariopsis separanda* Hustedt

Distribution patterns suggest that *Fragilariopsis separanda* prefers open water conditions (Zielinski and Gersonde, 1997). Both Zielinski and Gersonde (1997) and DeFelice and Wise (1981), indicate that in the South Atlantic *F. separanda* is confined to the south by the Polar Front (Figure 3.4) (Kozlova, 1966; Armand, 1997). Observations indicate that the highest maximum abundances of *F. separanda* are slightly increased at offshore locations rather than in-shore coastal environments (Kozlova, 1966; DeFelice and Wise, 1981; Gersonde and Wefer, 1987; Stockwell *et al.*, 1991; Leventer, 1992; Taylor *et al.*, 1997; Cunningham and Leventer, 1998). The SST affinity of this planktonic taxon covers a February range of -1 to 14°C with

maximum abundances at  $-0.5^{\circ}\text{C}$  (Armand, 1997), which is comparable to the temperature range of  $-1$  to  $12^{\circ}\text{C}$  identified by Zielinski and Gersonde (1997).

### 3.5.15 *Fragilariopsis sublinearis* (Van Heurck) Heiden

The distribution of *Fragilariopsis sublinearis* in the Antarctic Zone is reported to be similar to *F. ritscheri* and *F. obliquecostata* (Hasle, 1965; Kozlova, 1966; Hasle, 1976; Zielinski and Gersonde, 1997). *F. sublinearis*, like *F. obliquecostata* is a planktonic species and has an increased abundance in sediments south of the Antarctic Divergence (Kozlova, 1966; Gersonde, 1984; Gersonde and Wefer, 1987; Kellogg and Kellogg, 1987; Taylor *et al.*, 1997; Zielinski and Gersonde, 1997). Leventer (1992) has noted an exception to this; along the George V Coast equal maximum proportions of *F. ritscheri* and *F. sublinearis* have been observed.

### 3.5.16 *Fragilariopsis vanheurckii* (M. Pergallo) Hustedt

The planktonic species *Fragilariopsis vanheurckii* has been recorded near the spring sea ice margin (Garrison *et al.*, 1987) and has been suggested to indicate sea ice, but is not thought to live in sea ice (Taylor and Sjunneskog, 2002).

### 3.5.17 Genus *Navicula* Bory de st-Vincent

*Navicula glaciei* dominates shore ice protected from wave turbulence (Krebs *et al.*, 1987). *N. glaciei* has been observed to constitute a significant component of the spring bloom when shore ice, dominated by this species, is released into the water column upon melting (Krebs, 1983). When the sea ice has disappeared, later in the season, this epipelagic species is not a significant part of the diatom assemblage (Krebs *et al.*, 1987).

### 3.5.18 *Odontella weissflogii* (Janisch) Grunow

*Odontella weissflogii* is characterised as a pack ice species (Garrison and Buck, 1989; Garrison, 1991) and is also located in the adjacent water column sometimes with increasing abundance (Garrison *et al.*, 1983a; Gersonde, 1984). This planktonic



species is found with near year round ice cover (10-11 months), with low September maximum sea ice concentration (30%) and no ice cover in summer (Armand, 1997). The summer SST range of *O. weissflogii* is between -2 and 5°C (Zielinski and Gersonde, 1997) and is closely related with the Polar Front Zone and the Antarctic Zone (Figure 3.1 and 3.4). The highest abundances of *O. weissflogii* have been noted in cool waters of 1°C (Feb SST) and -2.5°C (August SST) (Armand, 1997). These reports indicate that the species is not necessarily confined to the Antarctic coastal regions, but linked with the environmental dynamics of the sea ice zone.

### 3.5.19 Genus *Porosira* Jørgensen

The two Antarctic planktonic species of *Porosira* are *P. glacialis* (Grunow) Jørgensen and *P. pseudodenticulata* (Hustedt) Jousé. *P. glacialis* is a bipolar species associated with waters adjacent to the coast or sea ice (Hasle, 1973). Krebs *et al.* (1987) suggests that *P. glacialis* is associated with slush and wave exposed shore ice, but does not live within the ice (Watanabe, 1988; Scott *et al.*, 1994). *P. pseudodenticulata* is observed in both fast and pack ice samples (e.g. Garrison *et al.*, 1983a; Gersonde, 1984; Krebs *et al.*, 1987) and in the adjacent water column (Garrison *et al.*, 1987; Tanimura *et al.*, 1990). Zielinski and Gersonde (1997) note the summer SST range for *P. glacialis* as -1 to 1.5°C and -2 to 0°C for *P. pseudodenticulata*. The difference in distribution of *P. glacialis* (open water) and *P. pseudodenticulata* (sea ice) is a possible indicator for the proximity of the sea ice margin.

### 3.5.20 Genus *Proboscia* Sunström

*Proboscia* spp. possess elongate frustules, have positive buoyancy (Villareal, 1988) and an ability to form mats (Hart, 1937; Carpenter *et al.*, 1977; Alldredge and Silver, 1982) which allows them to grow relatively abundantly in surface waters (Jordan *et al.*, 1991). Large cells of *Proboscia* spp. frequently dominate summer-autumn communities in warm-temperate to sub-polar regions (Brichta and Nöthig, 2003). Two species observed in Antarctica are *Proboscia truncata* (Karsten) Nöthig & Ligowski and *Proboscia inermis* (Castracane) Jordan & Ligowski. *P. truncata* is only recorded in Antarctic waters (Jordan *et al.*, 1991). *P. inermis* is considered a key planktonic diatom species in Antarctic autumn; during an autumn bloom in the

Bellinghausen Sea this species accounted for 21% of phytoplankton carbon (Brichta and Nöthig, 2003).

### 3.5.21 Genus *Rhizosolenia* Brightwell

*Rhizosolenia* spp. are a common component of the Antarctic phytoplankton and are important as contributors to sea floor sediments (Armand and Zielinski, 2001). *Rhizosolenia* spp. can form large blooms or mats in open water (Harbison *et al.*, 1977; Alldredge and Silver, 1982; Kemp *et al.*, 1999) and have been reported in high abundances from Antarctic waters (Hart, 1934; Holm-Hansen, *et al.*, 1989; Leventer *et al.*, 1996). This planktonic genus is generally absent from sea ice samples (Watanabe, 1982), therefore in the Atlantic sector this genus has been interpreted as an indicator of ice-free Weddell Sea outflow waters (Jordan and Pudsey, 1992). From the Antarctic Peninsula, late Holocene laminae rich in *Rhizosolenia* spp. are thought to have formed by rapid settling following a bloom (Leventer *et al.*, 1996). *R. antennata* f. *semispina* Sundström is the most common *Rhizosolenia* species in the Southern Ocean (Armand, 1997). Ligowski (1993) observed *R. antennata* f. *semispina* in open ocean stations to sublittoral habitats in sea ice. *R. antennata* f. *semispina* has been found to be a dominant species in the open ocean waters of late summer (Froneman *et al.*, 1995). The distribution pattern for this species ranges from the Subantarctic to the Antarctic Zone (Figure 3.4) at temperatures between -1 and 12°C, with highest abundances occurring in the northern Antarctic zone, in waters close to freezing point (-1 and 2°C) (Zielinski and Gersonde 1997). *R. antennata* f. *antennata* is primarily linked to the open ocean water column and not observed in ice conditions (Hendey, 1937; Hart, 1934; Ligowski, 1993). *R. antennata* f. *antennata* is considered to be the resting spore of *R. antennata* f. *semispina* (Sundström, 1986; Priddle *et al.*, 1990; Hasle and Syvertsen, 1997). *R. polydactyla* var. *polydactyla* has been found in melted ice and near coastal environments (Hustedt, 1930; Manguin, 1960), and also observed between Antarctic and Subantarctic waters with a maximum occurrence in the Polar Frontal Zone (Figure 3.4) (Fenner *et al.*, 1976). *R. sima* var. *sima* is reported to thrive in the seasonal sea ice zone (Armand and Zielinski, 2001).

### 3.5.22 *Stellarima microtrias* (Ehrenberg) Hasle & Sims

*Stellarima microtrias* is an Antarctic cool water planktonic species that forms resting spores and is associated with shelf ice and the surrounding shelf waters (Hasle *et al.*, 1988). The highest abundances of *S. microtrias* have been associated with SST <1°C (Zielinski and Gersonde, 1997). *S. microtrias* are observed in sediments along the Antarctic coast and various ice shelves (Jousé *et al.*, 1962; Kozlova, 1966; Truesdale and Kellogg, 1979; Gersonde, 1984; Prasad and Nienow, 1986; Gersonde and Wefer, 1987; Kellogg and Kellogg, 1987; Stockwell *et al.*, 1991; Leventer, 1992; Zielinski and Gersonde, 1997). This species has been reported in both land-fast and pack ice samples (Horner, 1985b; Garrison and Buck, 1989; Garrison, 1991). *S. microtrias* has been observed in many sea ice associated locations. During spring vegetative cells have been found in abundance at depth away from the sea ice edge (Fryxell 1989). In summer, *S. microtrias* has been noted in very high abundance in fast sea ice samples (Watanabe, 1982; Krebs *et al.*, 1987; Tanimura *et al.*, 1990). During autumn, the resting spore is found in high abundance under sea ice and is not present in the open ocean (Fryxell, 1989), and is commonly found in newly forming sea ice (Gersonde, 1984; Garrison and Close, 1993). Zielinski and Gersonde (1997) reported that *S. microtrias* was restricted to the Antarctic Zone south of the Polar Front (Figure 3.4).

### 3.5.23 *Thalassiosira antarctica* Comber

The planktonic genus *Thalassiosira* is widespread in Antarctic waters. *Thalassiosira antarctica* occurs commonly in waters with SST -2°C to 1°C (Zielinski and Gersonde, 1997). In the Weddell Sea spring blooms of this species are observed in newly formed platelet ice in polynyas (Smetacek *et al.*, 1992) and in “crack” pools formed by disintegrating sea ice during summer (Gleitz *et al.*, 1996). *T. antarctica* also occurs in the Bransfield Strait (Gersonde and Wefer, 1987; Leventer, 1991), where its unusually high abundance is thought to be the result of surface water intrusion from the Weddell Sea (Gersonde and Wefer, 1987; Zielinski and Gersonde, 1997). In Ross Sea surface sediment, *T. antarctica* occurs in highest abundances close to the ice shelf front and is associated with the formation of platelet ice from super-cooled water masses that emerge from beneath the ice shelf (Cunningham and Leventer, 1998). It is rare to find *T. antarctica* in sea ice (Leventer and Dunbar, 1987; Fryxell and Kendrick, 1988;

Zielinski and Gersonde, 1997) which is attributed to its inability to survive the low light intensities beneath and within sea ice (Fryxell *et al.*, 1987). However, *T. antarctica* have been observed in some spring sea ice samples (Villareal and Fryxell, 1983) suggesting they over-wintered in the sea ice or were re-suspended from the sediments.

#### 3.5.24 *Thalassiosira gracilis* (Karsten) Hustedt

*Thalassiosira gracilis* occurs in a temperature range between -2 and 13°C, with maximum numbers between -0.5 to 2°C (Zielinski and Gersonde, 1997). This planktonic species has been reported in sea ice samples (Gersonde, 1984; Krebs *et al.*, 1987; Garrison *et al.*, 1983a) and an increase in sea ice cover and cooler SST has been observed to lead to an increase in *T. gracilis* (Armand, 1997). This species has a wide distribution and does not appear to have a northern boundary (Armand, 1997). Fenner *et al.* (1976) reports *T. gracilis* in greater abundance in Antarctic waters than in Subantarctic waters. Zielinski and Gersonde (1997) report the species as uniformly distributed through the South Atlantic with highest abundances found in the sea ice zone and permanently open ocean. There are two morphologically different varieties of *T. gracilis*: *Thalassiosira gracilis* var. *expecta* (Van Landingham) Fryxell & Hasle and *Thalassiosira gracilis* var. *gracilis* (Karsten) Hustedt. Distribution of the two varieties of *T. gracilis* in Prydz Bay and along the George V Coast was noted with higher abundances of *T. gracilis* var. *gracilis* further from the coast, in contrast to a ubiquitous low distribution of *T. gracilis* var. *expecta* (Stockwell *et al.*, 1991; Leventer, 1992). The low distribution of *T. gracilis* var. *expecta* suggests the variety has a lack of relation to sea ice cover and is related to open primary productivity. The heavily silicified *T. gracilis* var. *gracilis* is considered the winter form of the species (Fryxell, 1990).

#### 3.5.25 *Thalassiosira gravida* Cleve

Fryxell and Kendrick (1988) note that *Thalassiosira gravida* Cleve is a common component of the open water assemblage in regions recently uncovered by retreating sea ice. This planktonic species is not common in sea ice (Garrison *et al.*, 1987).

### 3.5.26 *Thalassiosira lentiginosa* (Janisch) Fryxell

*Thalassiosira lentiginosa* has a temperature range of 0 to 7°C (Zielinski and Gersonde, 1997) and is not influenced greatly by sea ice (Armand, 1997). *T. lentiginosa* displays a widespread distribution in the Atlantic sector of the Southern Ocean. The planktonic species is most often reported in highest abundances from sediments under the Open Ocean Zone to the Polar Front Zone (Figure 3.2 and 3.4) (Jousé *et al.*, 1962; Kozlova, 1966; DeFelice and Wise, 1981; Zielinski and Gersonde, 1997). Low abundances or absences of *T. lentiginosa* in coastal abundance records have been noted (Kozlova, 1966; Gersonde and Wefer, 1987; Kellogg and Kellogg, 1987, Stockwell *et al.*, 1991, Zielinski and Gersonde, 1997). This species resistance to dissolution (Kozlova, 1966; Shemesh *et al.*, 1989; Pichon *et al.*, 1992b) increases its presence in sediments, obscuring the true primary signal of distribution (Crosta *et al.*, 2005).

### 3.5.27 *Thalassiosira oliverana* (O'Meara) Makarova & Nikolaev

*Thalassiosira oliverana* is endemic to the Southern Ocean and occurs in a temperature range between -2 and 5°C, the maximum abundances between -1.5 and 1°C (Zielinski and Gersonde, 1997). The concentrations of highest abundances of *T. oliverana* are between the Polar Front and just within the maximum winter sea ice edge (Figure 3.4 and 3.5). The planktonic species has a ubiquitous distribution in sediments of the Southern Ocean with exception to the Antarctic coast where abundances are reduced and are occasionally rare (Armand, 1997).

### 3.5.28 *Thalassiosira oestrupii* (Ostenfeld) Hasle

*Thalassiosira oestrupii*, a planktonic species, has been found in the water column adjacent to the sea ice edge in the Weddell Sea (Garrison *et al.* 1987) but not within the sea ice (Armand, 1997). Within open ocean sediments *T. oestrupii* constitutes 1 to 10% of the diatom assemblage, increasing in abundance northwards (DeFelice and Wise 1981, Zielinski and Gersonde 1997). Leventer (1992) reports trace *T. oestrupii* (up to 0.6%) from Antarctic coastal surface sediments.

### 3.5.29 *Thalassiosira tumida* (Janisch) Hasle

*Thalassiosira tumida* has been classified as a pack ice species (Garrison and Buck, 1989) even though it has been found in fast and pack ice samples from the Weddell Sea and Antarctic Peninsula (Garrison *et al.*, 1983a; Gersonde, 1984; Krebs *et al.*, 1987). *T. tumida* is found in abundance in the water column adjacent to the sea ice edge (Garrison *et al.*, 1987). Past investigations have shown that *T. tumida* is in low to rare abundance (<3%) in sediments around the Antarctic coast (Truesdale and Kellogg, 1979; Gersonde, 1984; Prasad and Nienow, 1986; Stockwell *et al.*, 1991; Leventer, 1992; Cunningham and Leventer, 1998). The planktonic species is very rare in open ocean sediments (Abbott, 1973; DeFelice and Wise, 1981).

### 3.5.30 *Thalassiothrix antarctica* Schimper ex Karsten

*Thalassiothrix antarctica* generally occurs in the warmer waters of the Subantarctic, but in the southern Indian Ocean the Antarctic convergence zone forms the northern distribution limit of this species in the uppermost sediment layer (Kozlova, 1966). *T. antarctica* has been recorded in sediments of the South Atlantic (DeFelice and Wise, 1981; van Iperen *et al.*, 1987; Zielinski, 1993) with maximum abundance within the Polar Front Zone (Figure 3.2 and 3.4) at summer SST between 2.5-6°C (Zielinski and Gersonde, 1997). Low relative abundances of *T. antarctica* are observed in surface sediments from the George V Coast, but this planktonic species is much more abundant in laminated core sections (Leventer, 1992).

### 3.5.31 *Trichotoxon reinboldii* (Van Heurck) Reid & Round

*Trichotoxon reinboldii* is endemic to the Southern Ocean. Maximum occurrences of this planktonic species are in Antarctic waters (Hendey, 1937; Kozlova, 1966) with low abundances in northern Subantarctic waters (Hustedt, 1958). Round *et al.* (1990) describe the species as abundant around Antarctica, yet Stockwell *et al.* (1991) noted low relative abundances of *T. reinboldii* in sediments from Prydz Bay.

### 3.5.32 *Trigonium arcticum* (Brightwell) Cleve

*Trigonium arcticum* has been observed at a water depth of 200-300 m off Cape Crozier, Ross Sea and even in bottom surface samples together with fragments of decaying algae (Thomas, 1966). Both Hendey (1937) and Thomas (1966) believe many specimens of this epiphytic species spend the majority of time as bottom forms and seldom get into the plankton. This species is considered to grow epiphytically on algae (Hendey, 1937; Thomas, 1966) and is saprophytic when not photosynthesising (Thomas, 1966).

## 3.6 Summary

This chapter has presented a brief introduction to diatoms and how diatom assemblages in sediments are influenced by environmental and preservation controls in the Southern Ocean. An account of previous diatom-rich laminated sediment research is given. Environmental preferences of Antarctic diatom species were presented in detail which will be referred to and used in chapters 6, 7, 8 and 9.

## 4. Core site data

This chapter presents a summary of core site locations, bathymetry, lithology and age models for the three core sites: Palmer Deep, Mertz Ninnis Trough and Durmont d'Urville Trough (Table 4.1, Figure 4.1). This information will support chapters 6, 7 and 8 which contain results and interpretations from Palmer Deep, Mertz Ninnis Trough and Durmont d'Urville Trough core analysis, respectively.

**Table 4.1**  
Summary of core data.

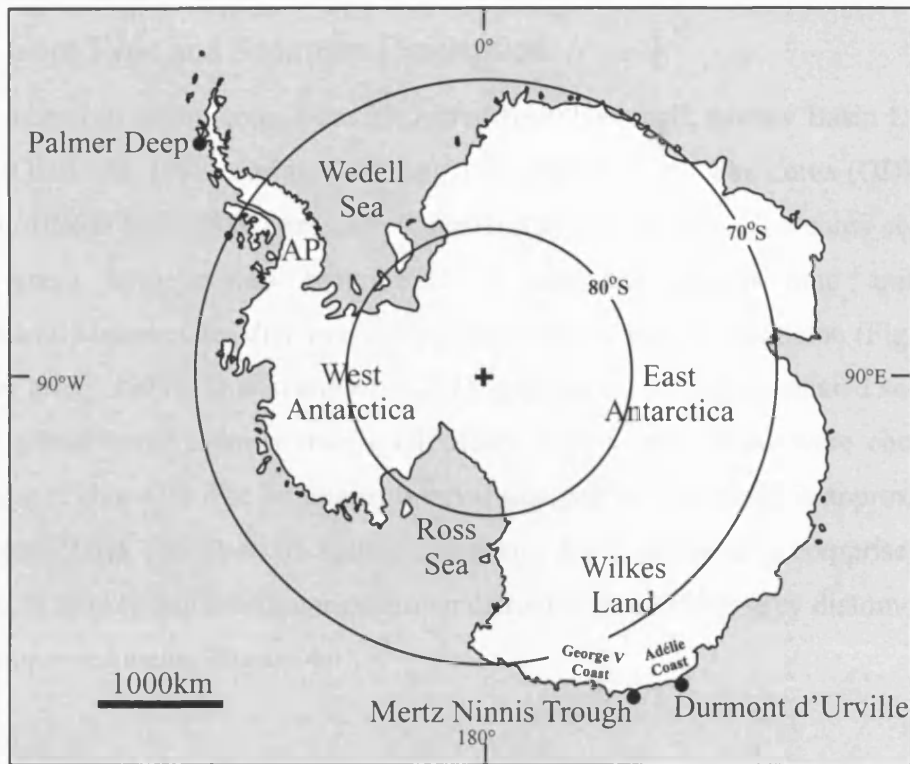
Core site	Core number	Core type	Latitude	Longitude	Water Depth (metres)	Core Length (metres)
Palmer Deep	ODP 178 1098A	Advanced piston	64°51.7235'S	64°12.4712'W	1012	45.9
Palmer Deep	ODP 178 1098C	Advanced piston	64°51.7105'S	64°12.4690'W	1012	46.7
Mertz Ninnis Trough	NBP0101 JPC10	Jumbo piston	66°34.334'S	143°05.168'E	850	21.35
Mertz Ninnis Trough	NBP0101 KC10A	Kasten	66°34.328'S	143°05.249'E	850	2.5
Durmout d'Urville Trough	MD03 2597	Calypso	66°24.74'S	140°25.26'E	1025	57.34

### 4.1. Palmer Deep, Western Antarctic Peninsula

#### 4.1.1 Bathymetry

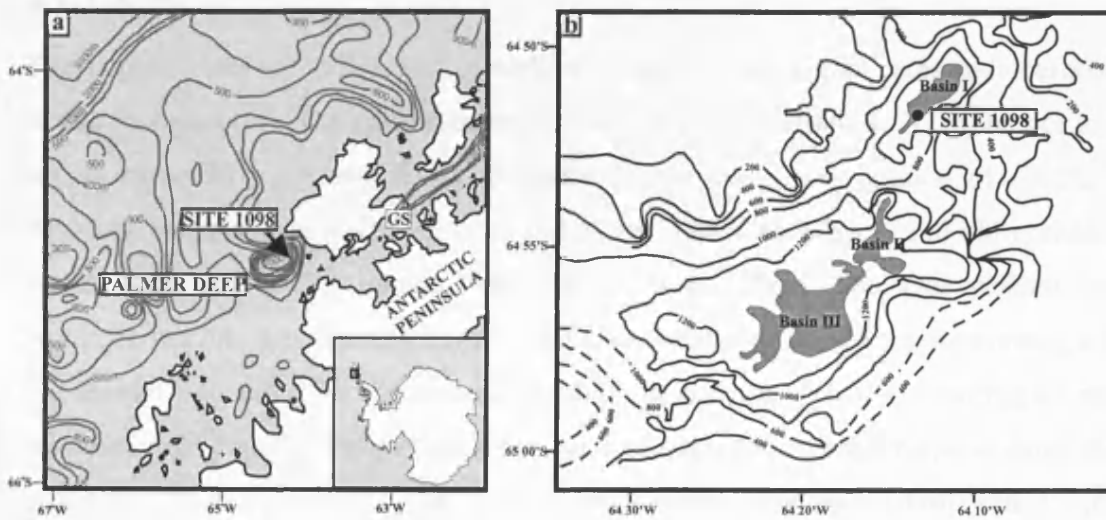
Palmer Deep is an inner shelf bathymetric depression on the western side of the Antarctic Peninsula, approximately 30 km southwest of Anvers Island and approximately 125 km from the shelf break (Figure 4.2a). The shelf on which Palmer Deep is located is broader (~140 km wide) and deeper (average depth 450 m) than low latitude continental shelves (Pudsey *et al.*, 1994) and slopes towards the continent due to previous glacial overburden and its tectonic setting. Palmer Deep is an erosional trough which formed during the most recent period of glaciation; it consists of three steep-sided basins orientated SW-NE, bisected by a fault (Kirby *et al.*, 1998; Rebesco *et al.*, 1998b). The shallowest of the three sub-basins, Basin I, has a 4 km long and 1 km wide basin floor and is surrounded by steep slopes (16-26°).





**Figure 4.1**

Geographic locations of the three core sites: Palmer Deep, Mertz Ninnis Trough and Durmont d'Urville Trough. AP=Antarctic Peninsula



**Figure 4.2**

(a) Location map of ODP Site 1098, Palmer Deep on the Antarctic Peninsula continental margin. Contours in metres. Adapted from Barker *et al.* (1999a).

(b) Map of the three fault bound basins that make up Palmer Deep and the site of Leg 178 Site 1098. Contours in metres. Adapted from Sjunneskog and Taylor (2002).

### 4.1.2 Core Type and Sediment Description

Three advanced piston cores were recovered from the small, narrow Basin I, Palmer Deep (ODP Site 1098) during ODP Leg 178 (Figure 4.2b). The cores (ODP Holes 1098A, 1098B and 1098C) are each approximately 45 m long. The cores consist of olive green homogeneous bioturbated to laminated diatom mud and ooze, rhythmically interbedded diatom ooze, pebbly mud and muddy diamicton (Figure 4.3) (Barker *et al.*, 1999b; Domack *et al.*, 2001). An interval of well-laminated sediments above glaciomarine diamict from ODP Holes 1098A and 1098C were chosen for sampling (Table 4.2). The laminated interval sampled for this study is approximately 4.5 metres thick (45.03-40.63 metres composite depth (mcd)) and comprises thinly bedded to thickly laminated orange-brown diatom ooze and blue-grey diatom-bearing terrigenous sediments (Figure 4.4).

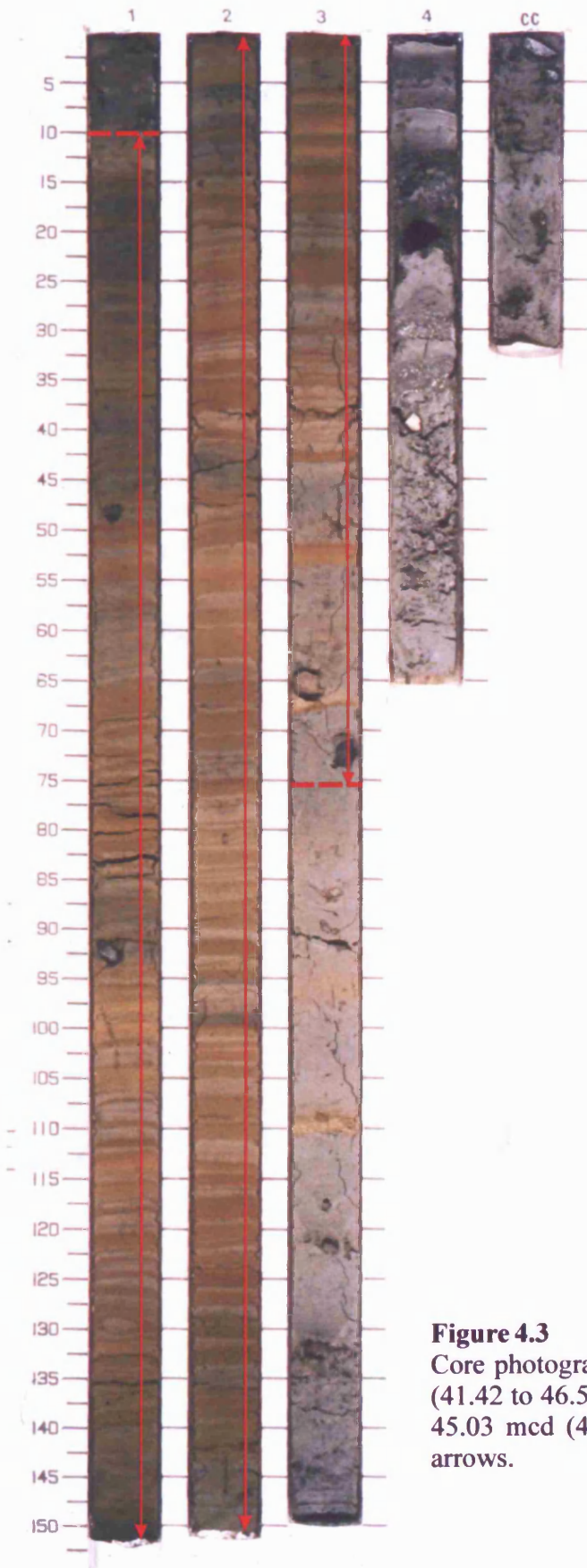
**Table 4.2.**

Palmer Deep core sample depths (to convert metres below sea floor (mbsf) to metres composite depth (mcd), 1.52 m is added to 1098A 6H and 1.82 m to 1098C 5H).

Palmer Deep Core	Depth (mbsf)	Depth (mcd)
ODP Core 178-1098C-5H 2	38.85-39.94	40.67-41.76
ODP Core 178-1098A-6H 1,2 & 3	40.00-43.66	41.52-45.18

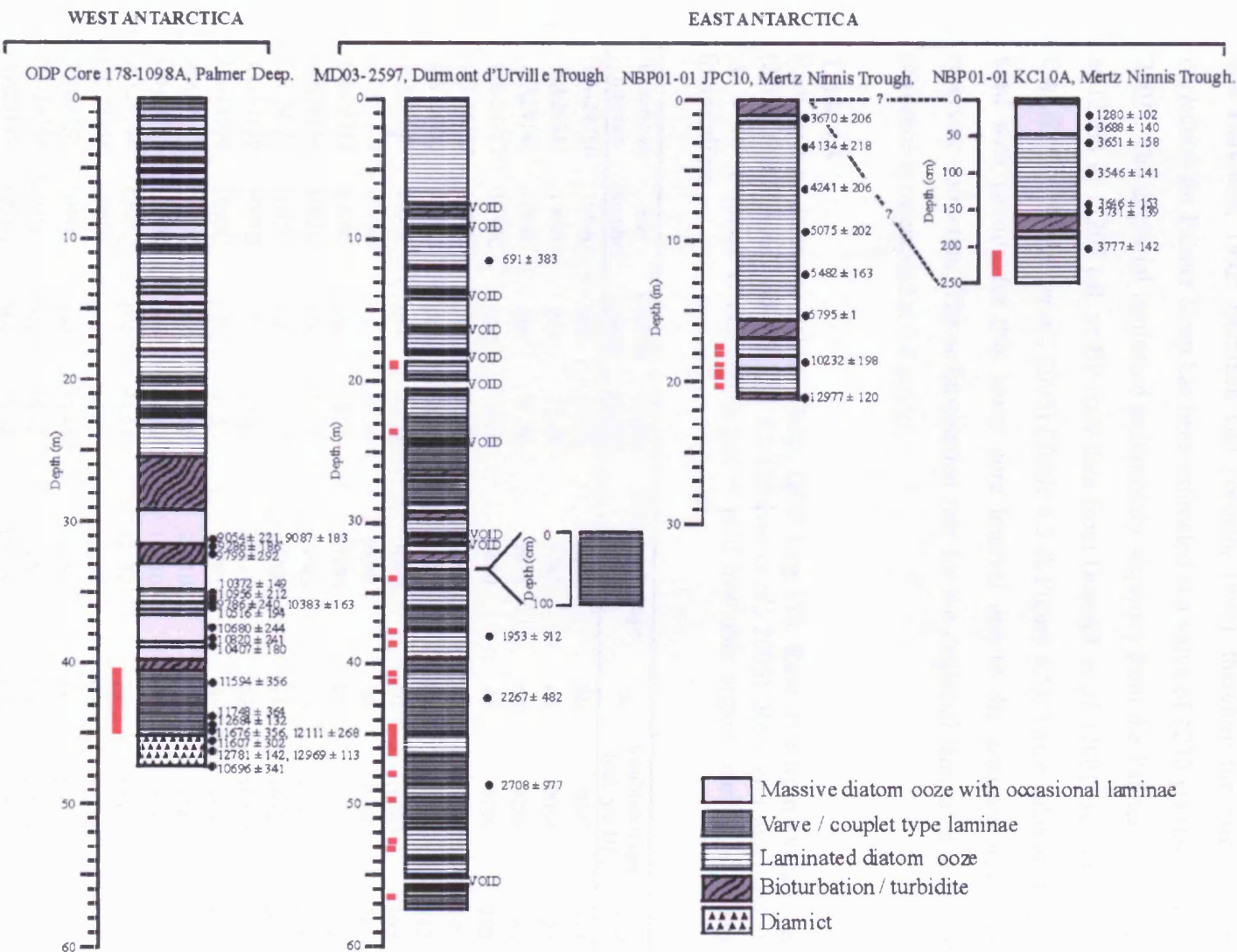
### 4.1.3 Age

The marine reservoir effect and reworking of old carbon complicates radiocarbon dating in Antarctica. The marine reservoir effect is the depletion of  $^{14}\text{C}$  in the ocean, and is particularly elevated in the Southern Ocean due to the dilution of circum-Antarctic water with glacial meltwater and by the upwelling of deep and old oceanic water (Harkness, 1979; Omoto, 1983; Stuiver *et al.*, 1986). The ages yielded by Antarctic samples are anomalously old as a consequence of this effect. Reworking of old carbon into the sediment creates an offset to the true  $^{14}\text{C}$  age, resulting in an artificially old date for seabed sediments. Surface sediment organic matter is dated to calculate a local correction to account for this Antarctic marine reservoir effect and reworking at the site of deposition. Radiocarbon dating of marine sediments is difficult in Antarctica because marine carbonates are scarce (and dates must be obtained from the acid insoluble organic fraction) and marine reservoir effects and local corrections have to be calculated (Domack *et al.*, 1999).



**Figure 4.3**

Core photograph of ODP Core 178-1098A-6H (41.42 to 46.57 mcd). Sampled interval, 41.52-45.03 mcd (40-43.51 mbsf), indicated by red arrows.



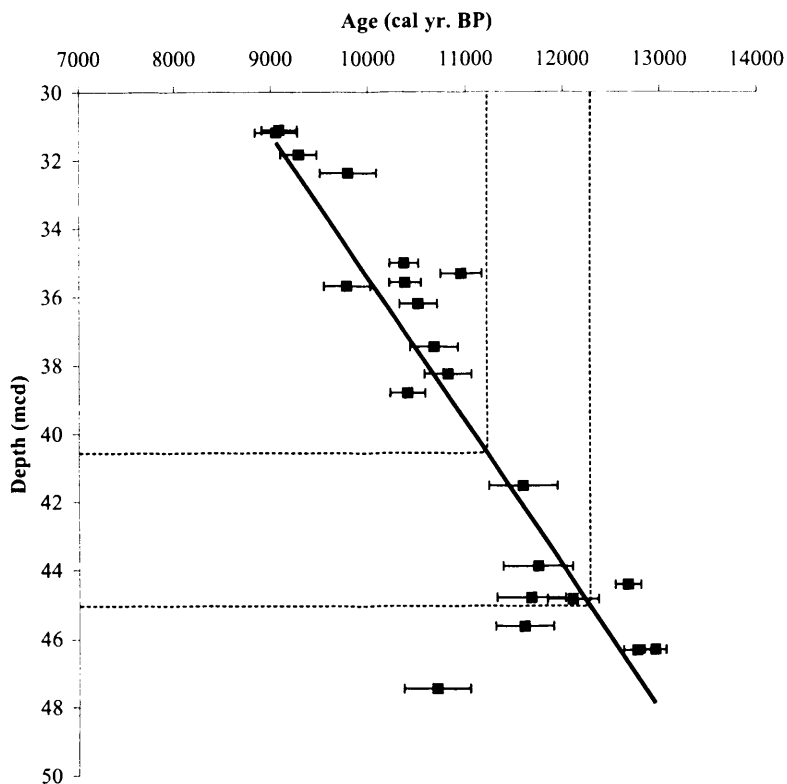
**Figure 4.4**  
 Lithographic logs of ODP 178 1098A, MD03 2597, NBP0101 JPC10 and NBP0101 KC10A. Calibrated ages in calendar years BP (see tables 4.3, 4.5, 4.6 and 4.8). At ~ 33 mbsf on the MD03 2597 lithographic log a 1.0 m thick piece of extruded sediment was also recorded. Red lines indicate sampled intervals.

The surface organic matter at Palmer Deep yields ages of  $1265 \pm 40$  yrs BP and  $1200 \pm 40$  yrs BP (Domack *et al.*, 2001) which are equivalent, or younger than ages derived from biogenic calcite in living marine invertebrates ( $1260 \pm 60$  yrs BP and  $1240 \pm 80$  yrs BP) from the same region (Domack, 1992). Surface organic matter ages are accepted as representing the reservoir age of the shelf waters in the Antarctic (Gordon and Harkness, 1992; Berkman and Forman, 1996), therefore the marine reservoir correction for Palmer Deep has been estimated at a value of 1230 yrs (Domack *et al.*, 2001). The deglacial laminated sedimentary sequence from the Palmer Deep is dated at 12264 to 11207 cal. yr BP (raw data from Domack *et al.* (2001) recalibrated with CALIB 5.0., Stuiver *et al.*, 2005) (Table 4.3 & Figure 4.5). These calibrated ages are used with caution for this lower core interval due to the assumed near modern reservoir correction. The sedimentation rate for the deglacial laminated sedimentary sequence is calculated at 0.4 cm/yr.

**Table 4.3**

Radiocarbon dates for Palmer Deep, ODP Leg 178. Raw data from Domack *et al.* (2001) recalibrated with CALIB 5.0 (Stuiver *et al.*, 2005). Reservoir age used, 1230 yrs  $\pm$  40 (Domack *et al.*, 2001). poc = acid insoluble organic carbon, f = benthic foraminifera.

Laboratory number	Site Number	Carbon source	Depth (mcd)	Uncorrected age (yrs BP)	$\pm$	Calibrated age (cal. yrs BP)	$\pm 2\sigma$
OS-24750	1098C	poc	31.12	9280	50	9087	183
AA29141	1098C	poc	31.19	9265	65	9054	221
AA29142	1098C	poc	31.84	9475	65	9286	186
OS-24751	1098C	poc	32.38	9860	95	9799	292
OS-24752	1098C	poc	35.02	10350	55	10372	149
OS-24753	1098C	poc	35.32	10850	55	10956	212
AA29143	1098C	poc	35.58	10365	70	10383	163
LL-57121	1098B	f	35.69	9890	50	9786	240
OS-24711	1098C	poc	36.2	10500	65	10516	194
AA29144	1098C	poc	37.46	10585	70	10680	244
OS-24754	1098C	poc	38.25	10700	65	10820	241
LL-57122	1098B	f	38.8	10410	80	10407	180
Ua-14999	1098C	f	41.53	11295	90	11594	356
AA29145	1098C	poc	43.89	11410	70	11748	364
OS-24755	1098C	poc	44.43	11850	55	12684	132
AA29146	1098C	poc	44.81	11350	75	11676	356
OS-24756	1098C	poc	44.85	11550	60	12111	268
OS-24757	1098C	poc	45.64	11300	55	11607	302
OS-24758	1098C	poc	46.32	12250	60	12969	113
AA29147	1098C	poc	46.34	12015	80	12781	142
Ua-14998	1098A	f	47.46	10565	105	10696	341



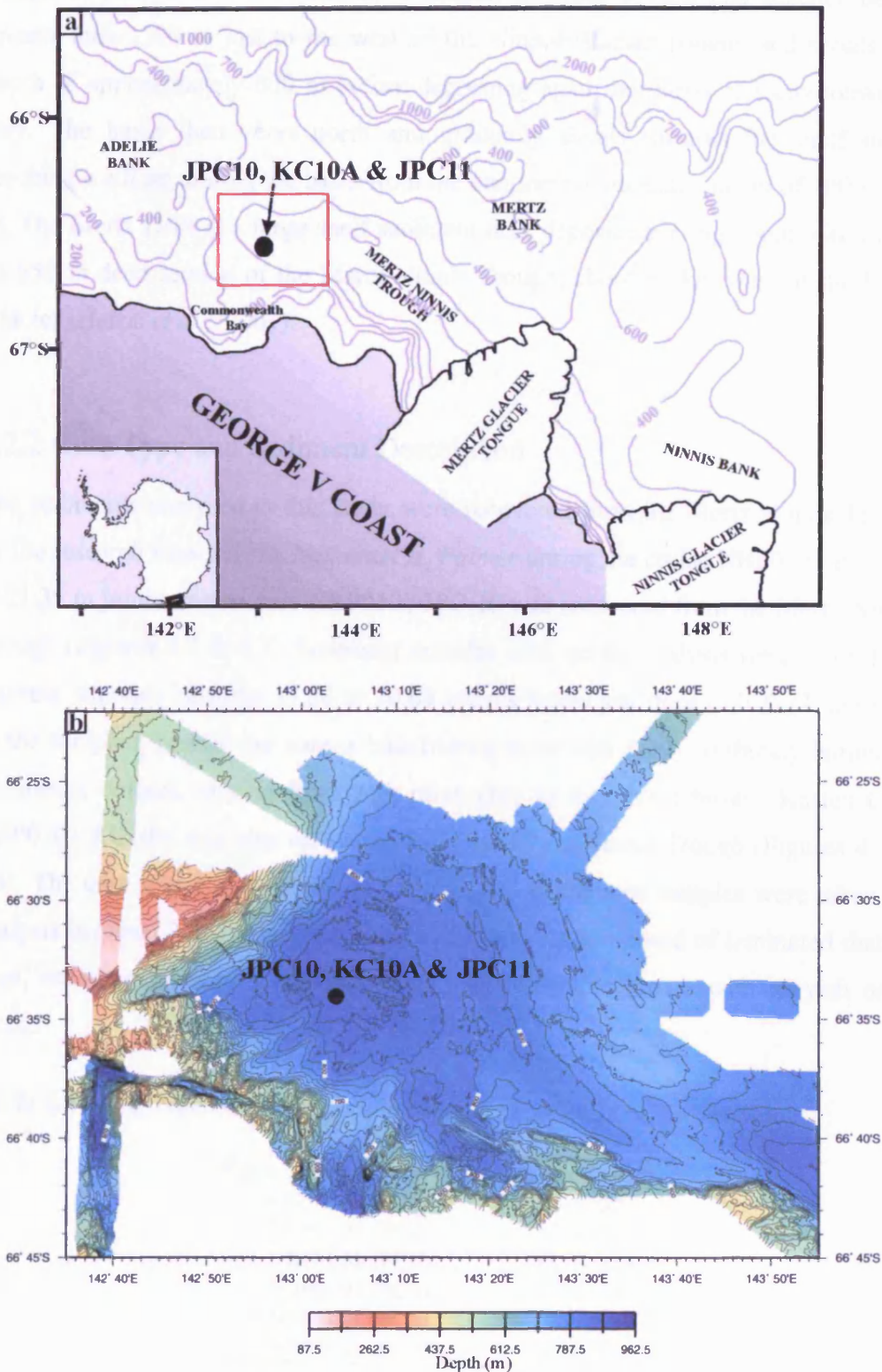
**Figure 4.5**

Age model for the lower 25 m of ODP Core 178-1098, Palmer Deep (Table 4.3.). Dotted lines indicate the sampled interval. Solid line = regression line ( $r^2 = 0.7682$ ). Domack *et al.* (2001) data calibrated with CALIB 5.0 (Stuiver *et al.*, 2005). Reservoir age =  $1230 \pm 40$  yrs (Domack *et al.*, 2001). Error bars = two sigma.

## 4.2. Mertz Ninnis Trough, East Antarctic Margin

### 4.2.1 Bathymetry

George V Land lies between  $142^\circ\text{E}$  and  $146^\circ\text{E}$  of the East Antarctic shelf (Figure 4.6.). Broad linear banks,  $< 200$  to  $400$  m deep are prominent features of the middle and outer portions of the shelf (Domack, 1982). The two largest banks lie directly seaward of the Mertz Glacier Tongue and the Ninnis Glacier Tongues bounding the Mertz Ninnis Trough to the north (Mertz Bank) and east (Ninnis Bank). The George V Coast has a depth of  $500$  m and a width of approximately  $140$  km. The inner shelf is dissected by a deep, linear basin called the Mertz Ninnis Trough [also known as the George V Basin (Domack, 1982; Domack and Anderson, 1983; Leventer, 1992; Harris *et al.*, 2001; Harris and Beaman, 2003; Presti *et al.*, 2003) and the Adélie Depression (Gordon and Tchernia, 1972; Rintoul, 1998)] of glacial origin. The core site in the Mertz Ninnis Trough is approximately  $85$  km from the shelf break. The



**Figure 4.6**

Location maps of NBP0101 JPC10, KC10A and JPC11.

(a) JPC 10, KC10A and JPC11 core locations within the Mertz Ninnis Trough, George V Coast. Contours in metres. Adapted from Leventer (1992).

(b) Seabeam Swath map of highlighted area in (a) of the JPC 10, KC10A and JPC11 core sites (Leventer *et al.*, 2001).

trough is parallel to the coastline, U-shaped in cross section and reaches depths greater than 1300 m just to the west of the Ninnis Glacier Tongue and shoals to a depth of approximately 800 m before deepening again northeast of Commonwealth Bay. The basin then veers north and gradually shoals towards the shelf break, reaching a sill separating the basin from the continental slope at a depth of 400 to 500 m. The Mertz Drift is a large shelf sediment drift deposit covering about 400 km<sup>2</sup> in an 850 m deep section of the Mertz Ninnis Trough, about 80 km west of the Mertz Glacier (Harris *et al.*, 2001).

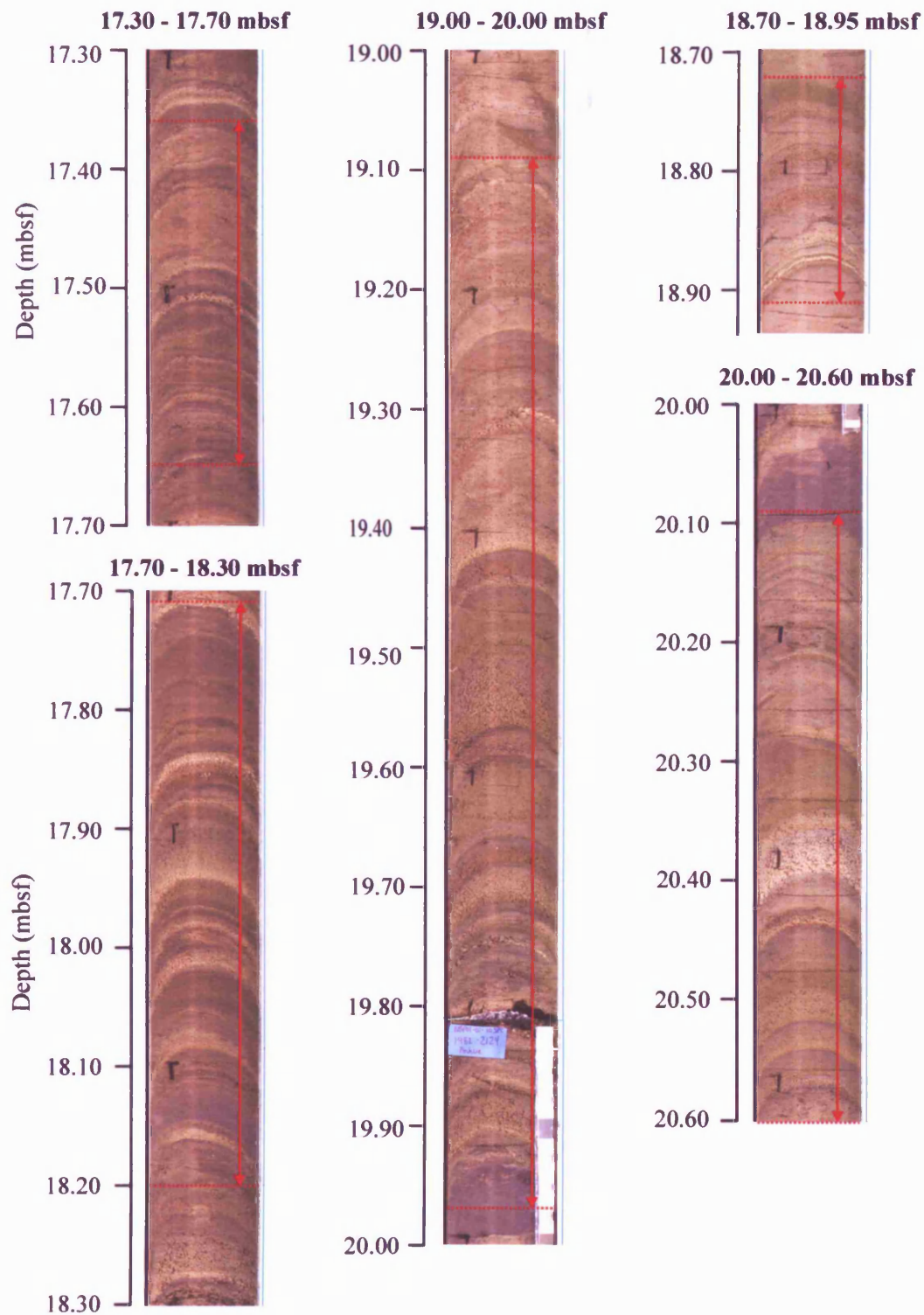
#### 4.2.2 Core Type and Sediment Description

The sediments analysed in this study were recovered from the Mertz Ninnis Trough by the research vessel *RVIB Nathaniel B. Palmer* during the cruise NBP0101 in 2001. A 21.35 m jumbo piston core NBP0101 JPC 10 was recovered from the Mertz Ninnis Trough (Figures 4.4 & 4.7). Sediment samples selected for analysis were taken from discrete intervals between 17.36 to 20.60 metres below sea floor (mbsf) (Table 4.4). In the sampled interval the core is biosiliceous ooze with thinly to thickly laminated sediments, colours varying from dark olive grey to dark olive brown. Kasten Core NBP0101 KC10A was also recovered from the Mertz Ninnis Trough (Figures 4.4 & 4.8). The core was a total length of 250 cm, and continuous samples were taken for analysis between 204.5 and 237.7 cm. This interval is composed of laminated diatom ooze, coloured olive grey (dominant) to moderate olive brown with greyish olive green.

**Table 4.4** Mertz Ninnis Trough sample depths. cmbsf = cm below sea floor.

Mertz Ninnis Trough Core	Depth (cmbsf)
NBP01 01 KC10A	204.5-237.7
NBP01 01 JPC10	1736-1765
NBP01 01 JPC10	1771-1820
NBP01 01 JPC10	1872-1891
NBP01 01 JPC10	1909-1997
NBP01 01 JPC10	2009-2060

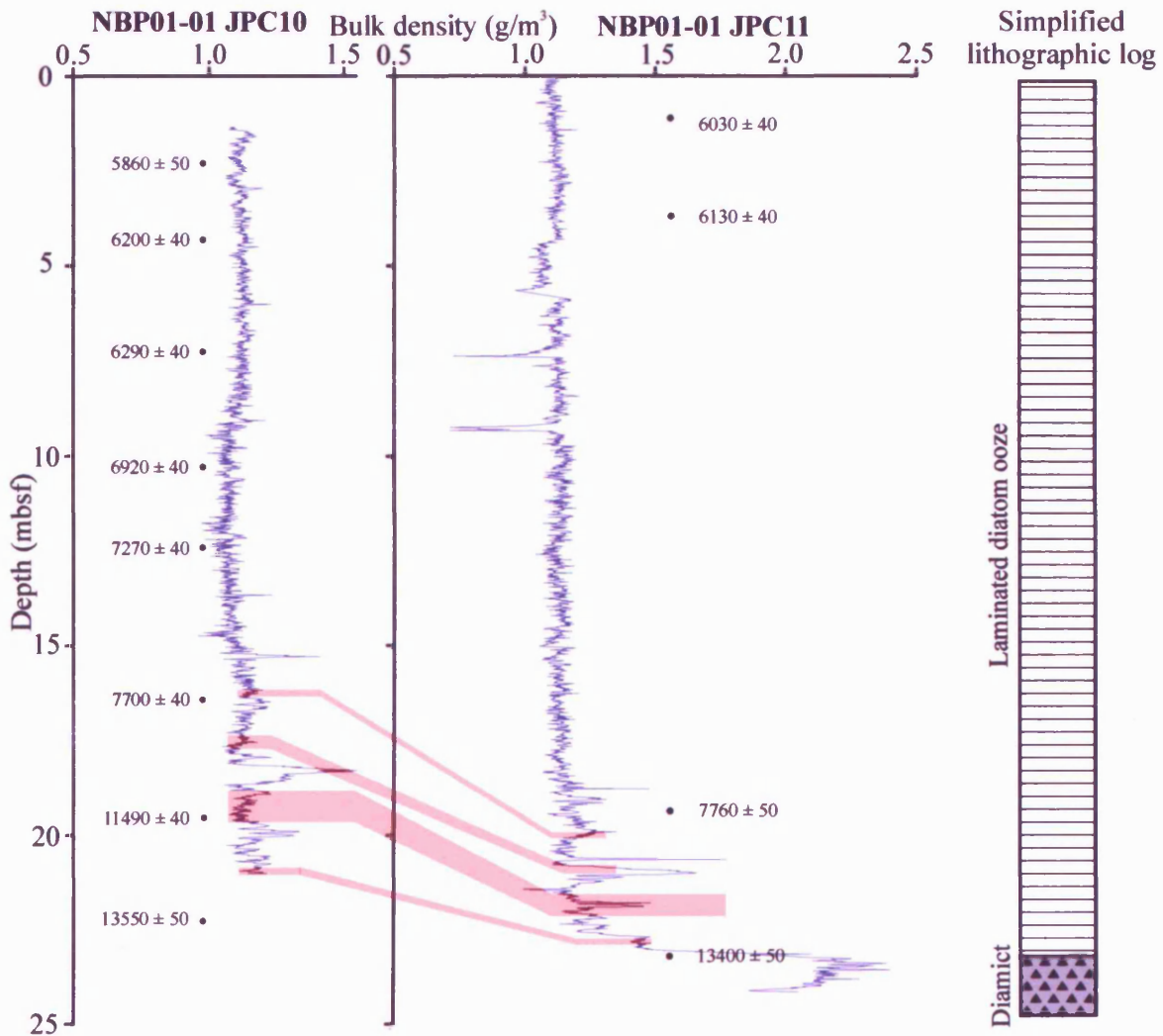




**Figure 4.7**  
Core photographs of NBP0101 JPC10 from the Mertz Ninnis Trough. Sampled intervals between 17.36 - 20.60 metres below sea floor (mbsf), indicated by red arrows.



**Figure 4.8**  
Core photograph of NBP0101 KC10A from the Mertz Ninnis Trough. 2.0-2.5 metres below sea floor (mbsf). Sample interval, 2.04-2.38 mbsf, indicated by red arrow.



**Figure 4.9**  
Comparison of NBP0101 JPC10 and JPC11 bulk density plots. Pink bands are tie points between the bulk density plots (A. Leventer personal communication). Dates plotted are raw uncorrected radiocarbon ages. Simplified lithographic log displayed alongside bulk density plots.

### 4.2.3 Age

Eight radiocarbon ages were obtained from NBP0101 JPC10 to provide a core chronology (Table 4.5). In addition to this, two radiocarbon ages obtained from adjacent core NBP0101 JPC11 (66°33.777 S, 143°03.082 E) (Table 4.5), 1.8 km from JPC10, were used to help construct an age model. The cores were correlated using wet bulk density measurements (Figure 4.9). Reworking of old carbon is an additional concern when interpreting  $^{14}\text{C}$  ages in the Antarctic. To accommodate the reservoir and reworking effects, when developing a chronology for a core, it is common to adjust radiocarbon ages by subtracting local surface ages from sub-surface radiocarbon ages (Andrews *et al.*, 1999; Cunningham *et al.*, 1999; Harris, 2000; Domack *et al.*, 2001). Surface ages measured along the East Antarctic Margin range from 1895 to 7084 yr BP (Domack *et al.*, 1989; Harris *et al.*, 1996; Harris and Beaman, 2003). This age range is older than the accepted reservoir correction for Antarctica (1300 yr BP; Berkman and Forman, 1996), which suggests a combination of reservoir and reworking effects affect this region. A decrease in sedimentation rate at the post-glacial sampled interval was not anticipated for JPC10 since a higher sedimentation rate is inferred from the laminated sediments in chapter 7. This suggests that there may be a change in reservoir and reworking affects downcore. A surface age obtained from NBP0101 KC10A (Table 4.6), 2340  $^{14}\text{C}$  yrs, has been used as a local reservoir correction. At present, there is no way to correct for changing reservoir and reworking effects downcore. The sampled interval, 20.60–17.36 mbsf, has been dated 11,384 – 6,756 cal. yr BP (Figure 4.10). The base of JPC10 has been dated approximately 12,456 cal. yr BP (Figure 4.10).

Eight radiocarbon ages were obtained from NBP0101 KC10A to provide a core chronology (Table 4.6). A surface age of 2340  $^{14}\text{C}$  yrs has been used as a local reservoir correction. The sampled interval, 204.5 – 237.7 cmbsf has been dated 3,820 – 3,892 cal. yr BP (Figure 4.11). The base of KC10A has been dated 3918 cal. yr BP (Figure 4.11). The top of the laminated interval in NBP0101 KC10A (0.49 mbsf) has been dated at approximately 3200  $^{14}\text{C}$  yrs, which is comparable to an average date obtained from several cores from the Mertz Ninnis Trough (3170  $^{14}\text{C}$  yrs; Harris *et al.*, 2001).

**Table 4.5.**

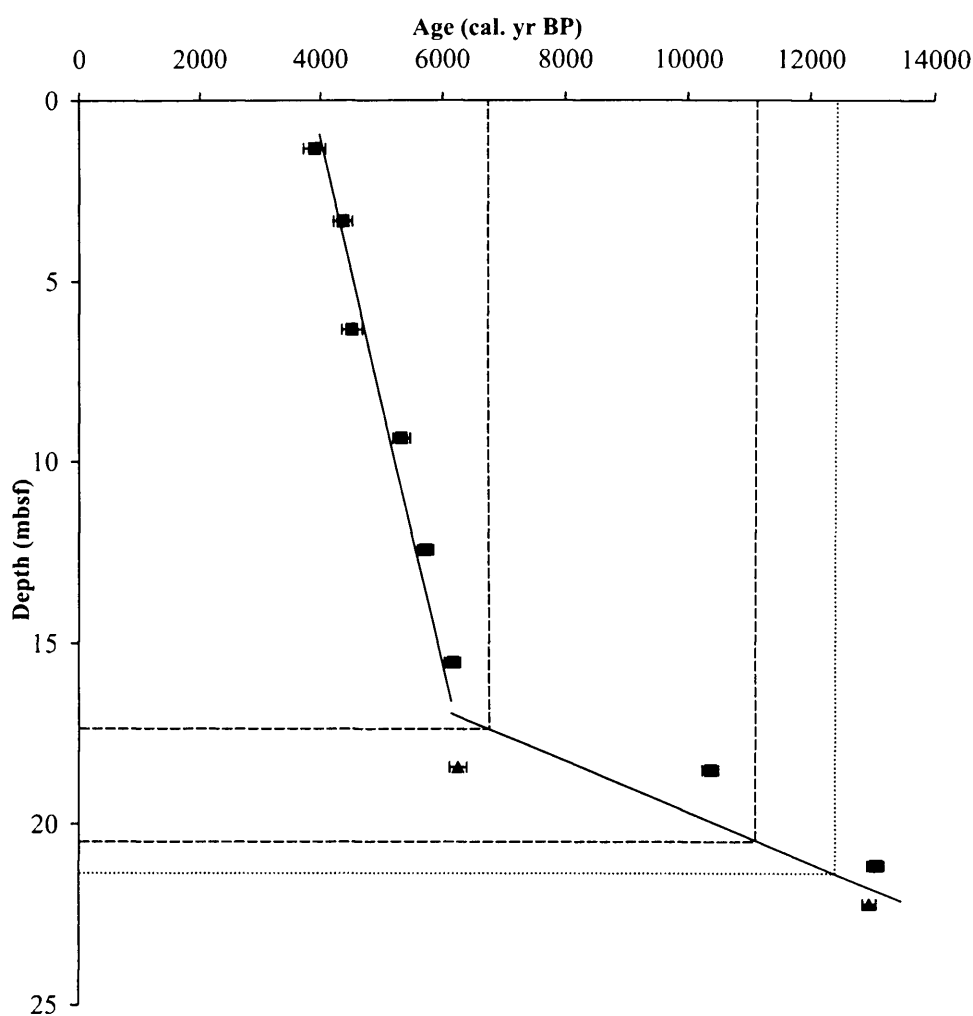
Uncorrected radiocarbon dates (R.Dunbar, personal communication, 2002) for NBP0101 JPC10 and JPC11, Mertz Ninnis Trough, corrected age was derived by subtracting NBP0101 KC10A core top age ( $2340 \pm 35$   $^{14}\text{C}$  yrs; Table 4.6). Ages calibrated with CALIB 5.0. (Stuiver *et al.*, 2005), errors  $2\sigma$ . Decal.  $\text{C}_{\text{org}}$  = decalcified organic carbon.

Laboratory number (CAMS #)	Core source	Depth (cm)	Carbon source	$^{14}\text{C}$ yr	$\pm$	Corrected age ( $^{14}\text{C}$ yr BP)	Calibrated age (cal. yrs BP)	$\pm 2\sigma$
79274	NBP0101 JPC10	132.5	Decal. $\text{C}_{\text{org}}$	5860	50	3520	3898	181
79276	NBP0101 JPC10	332.5	Decal. $\text{C}_{\text{org}}$	6200	40	3860	4364	156
79277	NBP0101 JPC10	632.5	Decal. $\text{C}_{\text{org}}$	6290	40	3950	4511	169
79278	NBP0101 JPC10	934.5	Decal. $\text{C}_{\text{org}}$	6920	40	4580	5333	142
79279	NBP0101 JPC10	1242.5	Decal. $\text{C}_{\text{org}}$	7270	40	4930	5712	129
79280	NBP0101 JPC10	1552.5	Decal. $\text{C}_{\text{org}}$	7700	40	5360	6151	133
79282	NBP0101 JPC10	1852.5	Decal. $\text{C}_{\text{org}}$	11490	40	9150	10394	136
79283	NBP0101 JPC10	2112.5	Decal. $\text{C}_{\text{org}}$	13550	50	11210	13091	131
79281	NBP0101 JPC11	1842.5	Decal. $\text{C}_{\text{org}}$	7760	50	5420	6241	142
79284	NBP0101 JPC11	2218	Decal. $\text{C}_{\text{org}}$	13400	50	11060	12987	106

**Table 4.6.**

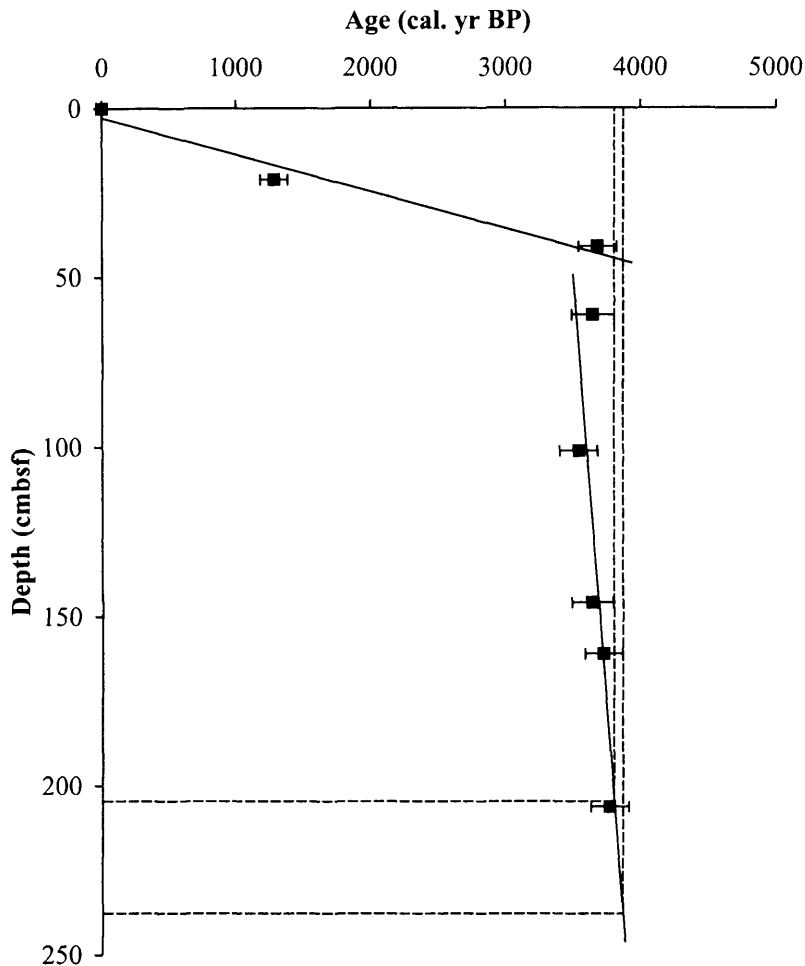
Uncorrected radiocarbon dates (R.Dunbar, personal communication, 2002) for NBP0101 KC10A, Mertz Ninnis Trough, corrected age was derived by subtracting the core top age ( $2340 \pm 35$   $^{14}\text{C}$  yrs). Ages calibrated with CALIB 5.0. (Stuiver *et al.*, 2005), errors  $2\sigma$ . Decal.  $\text{C}_{\text{org}}$  = decalcified organic carbon.

Laboratory number (CAMS #)	Core source	Depth (cm)	Carbon source	$^{14}\text{C}$ yr	$\pm$	Corrected age ( $^{14}\text{C}$ yr BP)	Calibrated age (cal. yrs BP)	$\pm 2\sigma$
85806	NBP0101 KC10A	1	Decal. $\text{C}_{\text{org}}$	2340	35	0	0	-
85807	NBP0101 KC10A	21	Decal. $\text{C}_{\text{org}}$	3675	35	1335	1280	102
85808	NBP0101 KC10A	41	Decal. $\text{C}_{\text{org}}$	5690	35	3350	3688	140
85809	NBP0101 KC10A	61	Decal. $\text{C}_{\text{org}}$	5660	40	3320	3651	158
85810	NBP0101 KC10A	101	Decal. $\text{C}_{\text{org}}$	5585	40	3245	3546	141
85811	NBP0101 KC10A	146	Decal. $\text{C}_{\text{org}}$	5655	35	3315	3646	153
85812	NBP0101 KC10A	161	Decal. $\text{C}_{\text{org}}$	5730	35	3390	3731	139
85813	NBP0101 KC10A	206	Decal. $\text{C}_{\text{org}}$	5770	35	3430	3777	142



**Figure 4.10**

Age model for NBP0101 JPC10 and JPC11, Mertz Ninnis Trough (Table 4.5). Ages supplied by R.Dunbar (2002) and calibrated with CALIB 5.0 (Stuiver *et al.*, 2005) Sampled interval (17.36-20.60 mbsf) indicated by dashed lines. Base of core marked with dotted line. Solid lines = regression lines (upper line  $r^2 = 0.968$ ; lower line  $r^2 = 0.773$ ) Errors = two sigma. Squares = JPC 10. Triangles = JPC11.



**Figure 4.11**

Age model for NBP0101 KC10A, Mertz Ninnis Trough (Table 4.6). Ages supplied by R. Dunbar and calibrated with CALIB 5.0 (Stuiver *et al.*, 2005). Sampled interval (204.5 – 237.7 cmbsf) indicated by dashed lines. Solid lines = regression lines (upper line  $r^2 = 0.9648$ ; lower line  $r^2 = 0.9349$ ). Errors = two sigma.

### 4.3. Durmont d’Urville Trough, East Antarctic Margin

#### 4.3.1 Bathymetry

Adélie Land (136°E to 142°E) lies within the Wilkes Land sector of the East Antarctic shelf. The shelf is approximately 130 km wide with broad, linear flat topped banks occurring at 200 to 400m depth on the middle and outer portions of the continental shelf (Domack, 1982). A broad shallow bank (Adélie Bank) lies to the northeast of the Durmont d’Urville Trough (Eittrheim *et al.*, 1995). The Dumont d’Urville Trough dissects the inner shelf of the Adélie Land coast and trends obliquely across the shelf (Figure 4.12). The trough reaches depths greater than 1300 m, just offshore of the

Astrolabe and Zélée glaciers. These glaciers are the two largest of several outlets that drain into the trough (Domack *et al.*, 1991). The core site in the Durmont d'Urville Trough is approximately 90 km from the shelf break.

### 4.3.2 Core Type and Sediment Description

The sediments analysed for this study from Adélie Land were collected on the *R/V Marion Dufresne* during the MD130 CADO Images X cruise in February 2003. Sediment samples selected for analysis were taken from discrete intervals between 18 to 57 mbsf (Table 4.7). The core consists mainly of black to dark olive grey laminations (Figure 4.13).

**Table 4.7.**

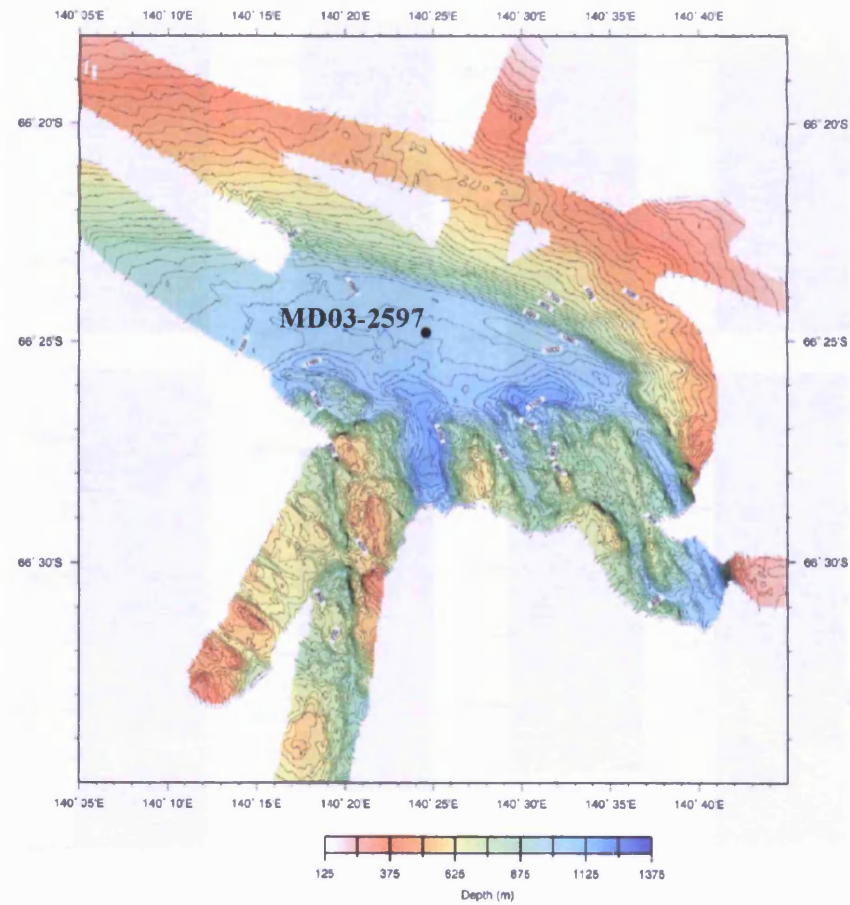
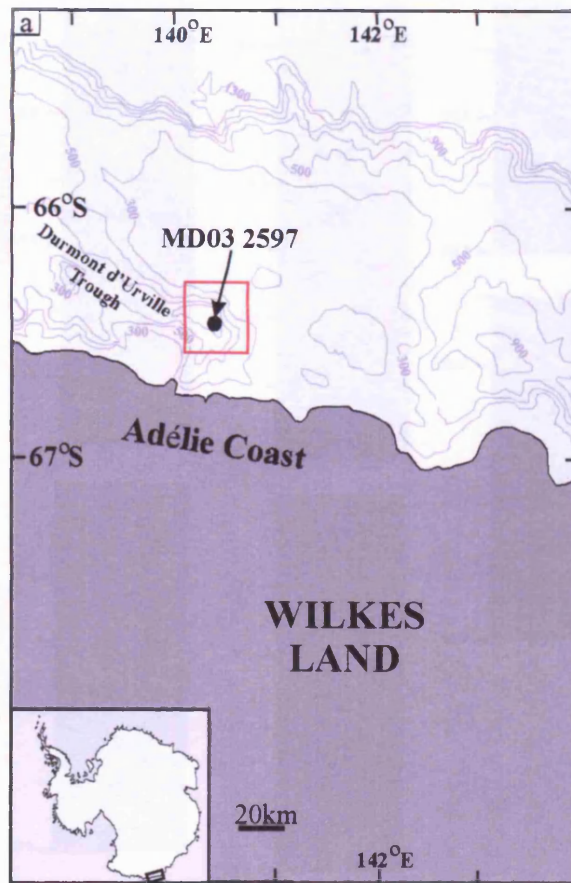
Durmont d'Urville Trough core sample depths. mbsf = metres below sea floor.

Core source	Depth (mbsf)
MD03 2597	18.75-19.00
MD03 2597	23.40-23.55
MD03 2597	33.80-34.05
MD03 2597	37.80-37.95
MD03 2597	38.55-38.70
MD03 2597	40.60-40.75
MD03 2597	41.05-41.20
MD03 2597	44.40-46.77
MD03 2597	47.75-47.90
MD03 2597	49.70-49.90
MD03 2597	52.53-52.68
MD03 2597	53.00-53.15
MD03 2597	56.55-56.83

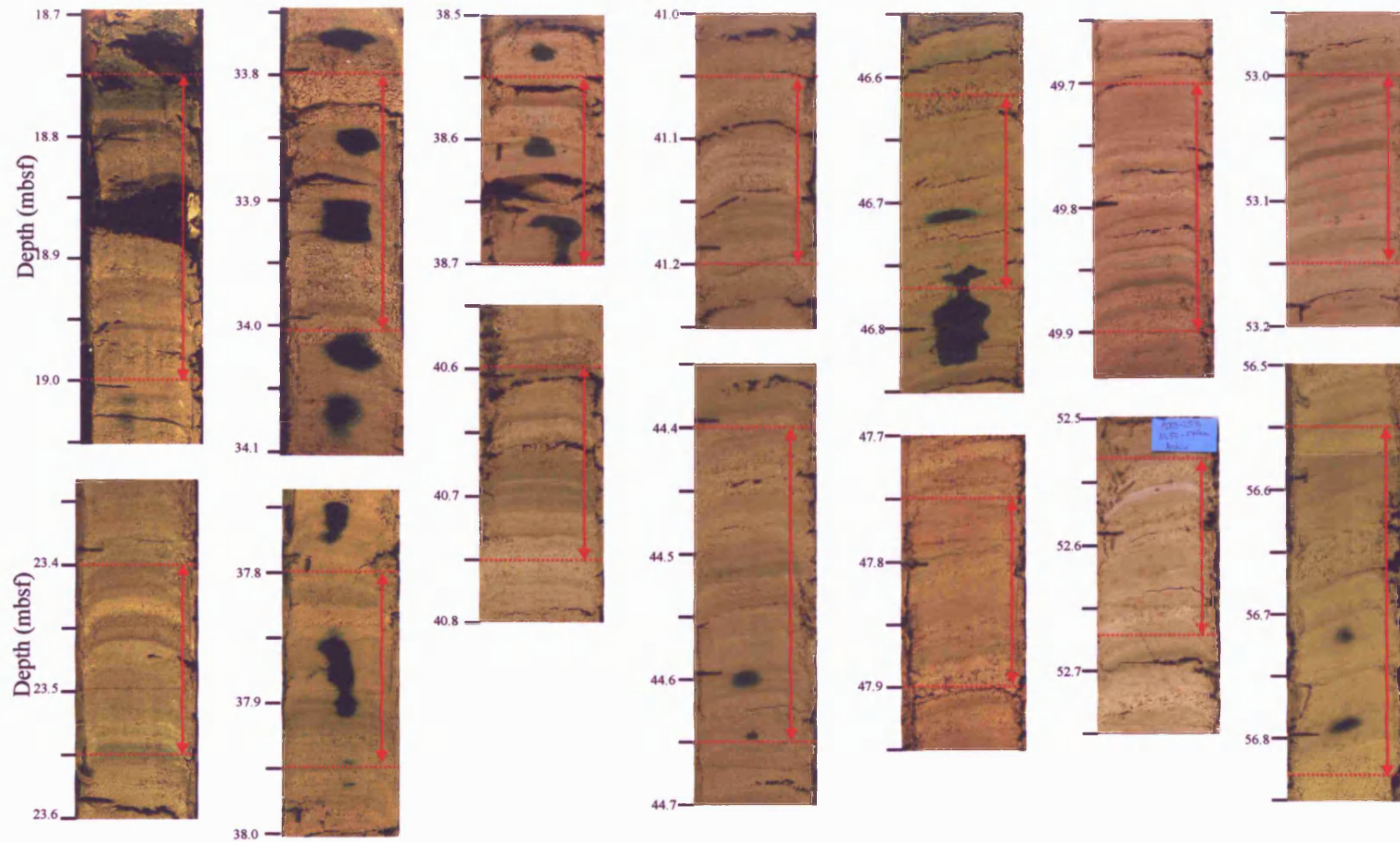
### 4.3.3 Age

Four radiocarbon ages obtained from MD 130 CADO Images X (Table 4.8) have been calibrated with CALIB 5.0 (Stuiver *et al.*, 2005) using a reservoir correction of 1300 years  $\pm$  200 years (Berkman and Forman, 1996) to create an age model for MD03 2597. The sampled interval, 56.83 to 18.75 mbsf has been dated at 2814 to 925 cal. yrs BP (Figure 4.14).





**Figure 4.12.**  
 (a) Bathymetry of the Adélie continental margin. Position of core MD03 2597 indicated. Adapted from Domack *et al.* (1989).  
 (b) Seabeam Swath map of highlighted area in (a) (Leventer, 2001).



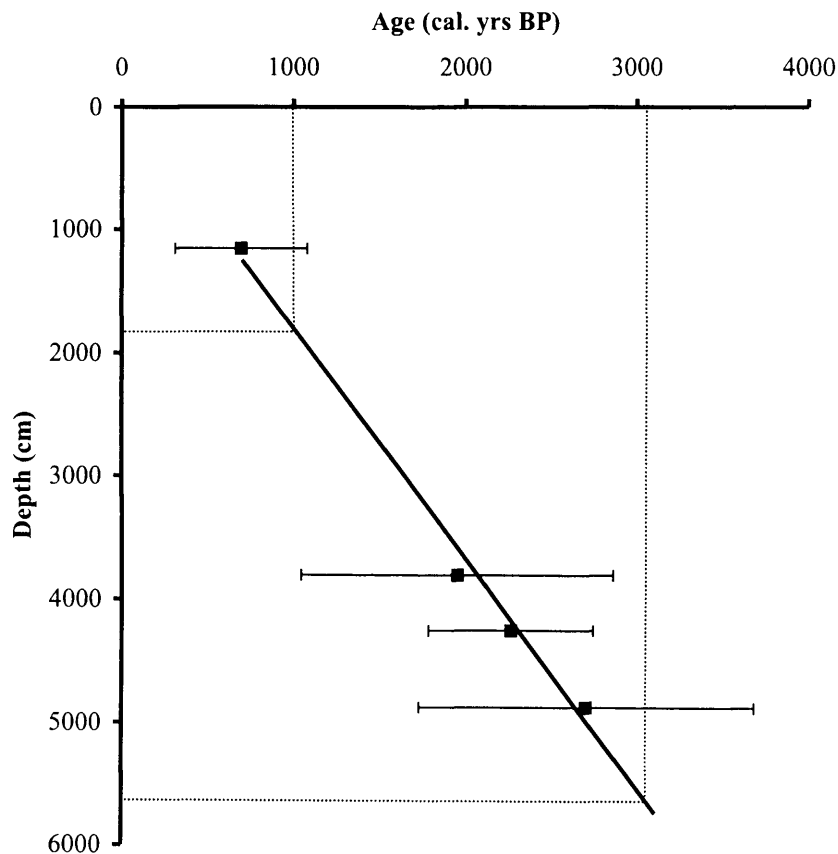
**Figure 4.13**

Core photographs of MD03 2597 from the Durmont d'Urville Trough. Sampled intervals indicated by red arrows. All depths are in metres below sea floor (mbsf).

**Table 4.8**

Uncorrected radiocarbon dates (R.Dunbar, personal communication, 2004) for MD03 2597, Durmont d'Urville Trough, calibrated with CALIB 5.0 (Stuiver *et al.*, 2005). Reservoir age used, 1300 years +/- 200 years (Berkman and Forman, 1996). Uncorrected, calibrated ages and errors rounded to the nearest year.

Laboratory number	Core source	Depth (cm)	Uncorrected age (yrs BP)	±	Calibrated age (cal. yrs BP)	±2σ
107178	MD03 2597	1153	2010	35	691	383
107179	MD03 2597	3803	3195	35	1953	912
107180	MD03 2597	4248	3485	35	2267	482
107181	MD03 2597	4872	3855	35	2708	977

**Figure 4.14**

Age model for MD03 2597, Durmont d'Urville Trough (Table 4.8). Raw data (R.Dunbar, personal communication, 2004) calibrated with CALIB 5.0 (Stuiver *et al.*, 2005). Reservoir age = 1300 years +/- 200 years (Berkman and Forman, 1996). Dotted lines indicate the sampled interval. Solid line = regression lines ( $r^2 = 0.9911$ ). Errors = two sigma.

#### **4.4. Summary**

This chapter has presented core site information, bathymetry, core descriptions and age models for the Palmer Deep, Mertz Ninnis Trough and Durmont d'Urville core sites. This information will be used to support interpretations and discussions in chapters 6, 7 and 8.

## 5. Methods

This chapter presents the methods used to collect diatom assemblage data and determine the sedimentary fabric of laminated sediments from Palmer Deep, Mertz Ninnis Trough and Durmont d'Urville Trough.

### 5.1. Sampling Strategy

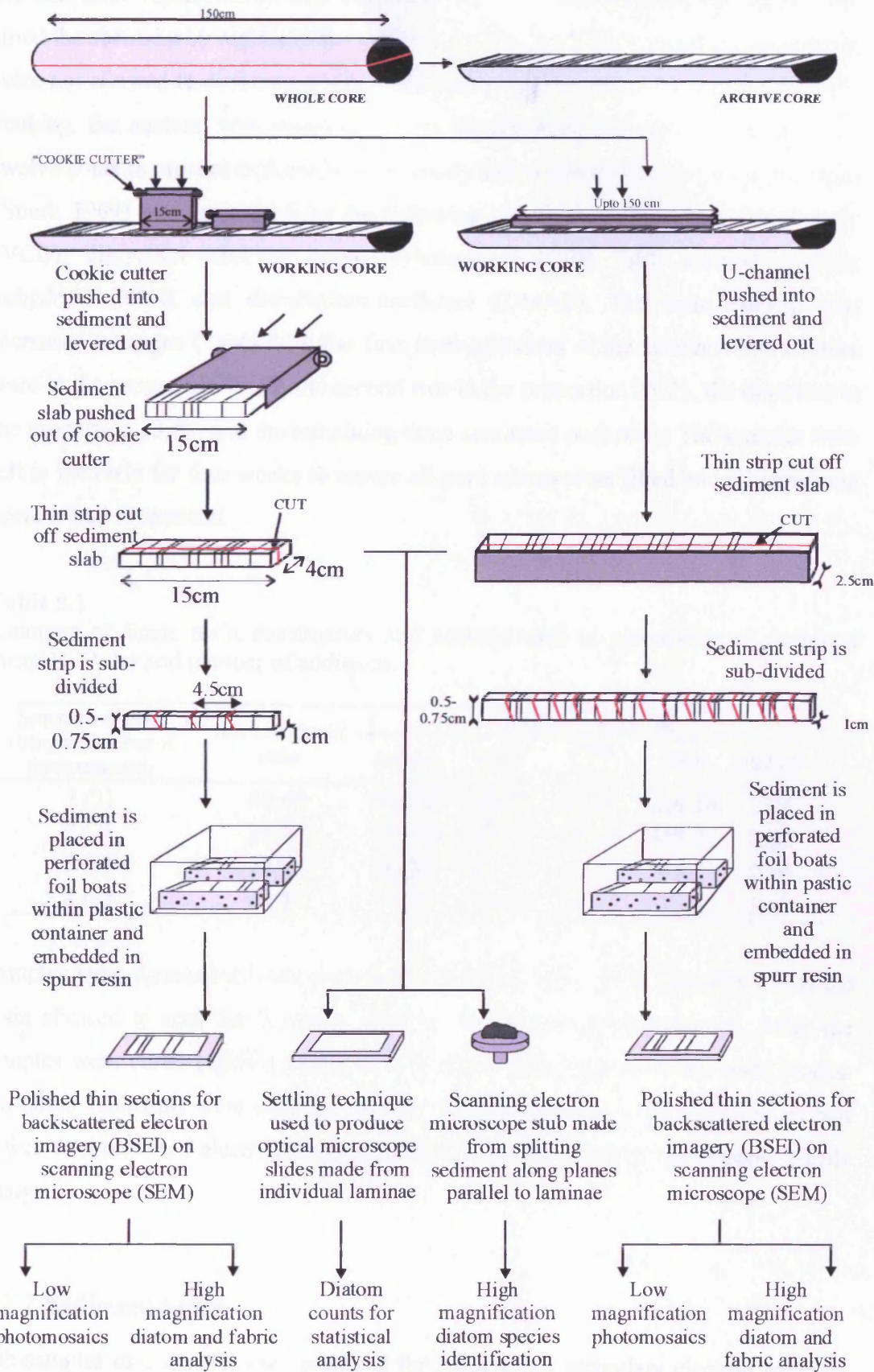
Unconsolidated sediment cores were sampled perpendicular to laminae with a sediment slab cutter, a “cookie cutter” (Schimmelmann *et al.*, 1990) (Figure 5.1), to prevent sedimentary fabric disturbance. To achieve sediment continuity, cookie-cutter sampling was overlapped. The sediment slabs were wrapped in cling film, labelled with core information and upcore direction, placed in air tight plastic containers with moist paper towels and put in to a refrigerator. This procedure kept the samples cold and moist, preventing desiccation and inhibiting the growth of moulds.

### 5.2. Sample Preparation

#### 5.2.1 Polished Thin Sections

Unconsolidated wet sediment samples were prepared for scanning electron microscope (SEM) study. Several methods such as critical point drying (Bouma, 1969), freeze drying (Bouma, 1969) and vacuum drying (Kemp, 1990, Patience *et al.*, 1990) could have been used to produce polished thin sections, however, these three methods remove water prior to resin embedding under vacuum causing partial collapse of the sedimentary fabric. Fluid displacive drying (Jim, 1985; Polysciences Inc., 1986; Lamoureux, 1994; Pike and Kemp, 1996) was selected for sample preparation to ensure the sediment was not left in an unsupported condition. The method used is adapted from the fluid displacive resin embedding techniques detailed in Pike and Kemp (1996), Pearce *et al.*, (1998) and Dean *et al.* (1999).

A 0.5 cm wide block was cut from the longest side of the 15 cm long sedimentary slab and was sub-divided with diagonal cuts (Figure 5.1). These samples were placed in a tight fitting perforated aluminium foil boat and immersed in general laboratory grade acetone (Figure 5.1). Acetone was replaced three times daily for five days,



**Figure 5.1** Summary of core preparation and analysis techniques. Adapted from Dean *et al.* (1999).

the last three replacements with analytical grade acetone. This process chemically dried the sediment by replacing the aqueous pore fluids with the solvent. The samples were not allowed to desiccate at any stage during the process. After the final acetone soaking, the acetone was removed and an acetone/resin mixture was added every twelve hours to prevent an increase in viscosity and to embed the samples. Spurr resin (Spurr, 1969) was prepared from the following chemicals: vinylcyclohexene dioxide (VCD); diglycidol ether of polypropyleneglycol (DER 736); nonenyl succinic anhydride (NSA) and dimethylaminoethanol (DMAE). The resin content was increased in stages (Table 5.1): the first three additions of the acetone/resin mixture were in the proportion 40:60, the second two in the proportion 25:75, the third two in the proportion 13:87, and the remaining three contained pure resin. The samples were left in the resin for four weeks to ensure all pore spaces were filled and all remaining acetone had evaporated.

**Table 5.1**

Amounts of Spurr resin constituents and acetone used in preparation of sediment samples. Order and number of additions.

Sequence of resin changes (number of times repeated)	Acetone: Resin ratio	Reagent quantity (g)				
		Acetone	VCD	DER 736	NSA	DMAE
1 (3)	40:60	288.00	102.37	61.42	266.16	2.05
2 (2)	25:75	192.00	125.12	75.07	325.31	2.50
3 (2)	13:87	96.00	147.87	88.72	384.45	2.96
4 (3)	0:100	0.00	170.62	102.37	443.60	3.41

Samples were then cured in an oven for 24 hours at 35°C, 45°C and 65°C, with the resin allowed to cool for 24 hours between the increasing temperatures. After the samples were cured highly polished thin sections were made from the resin blocks. Oil-based lubricants were used for cutting. The thin sections were coated in carbon before backscattered electron imagery (BSEI) scanning electron microscope (SEM) analysis.

### 5.2.2 Sediment Stubs

Sub-samples of sediment were prepared for topographic secondary electron imagery (SEI) to provide analysis of microfossil components. Blocks of sediments with

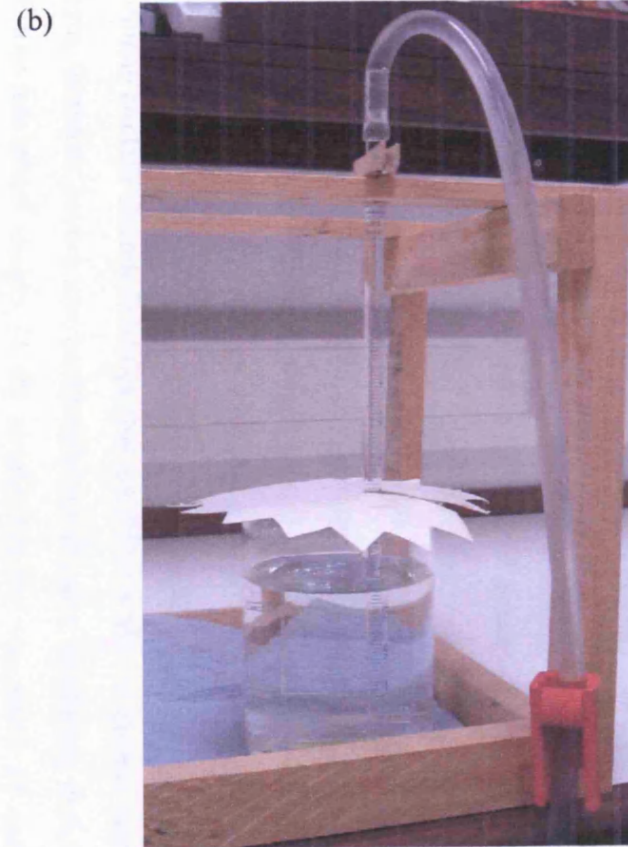
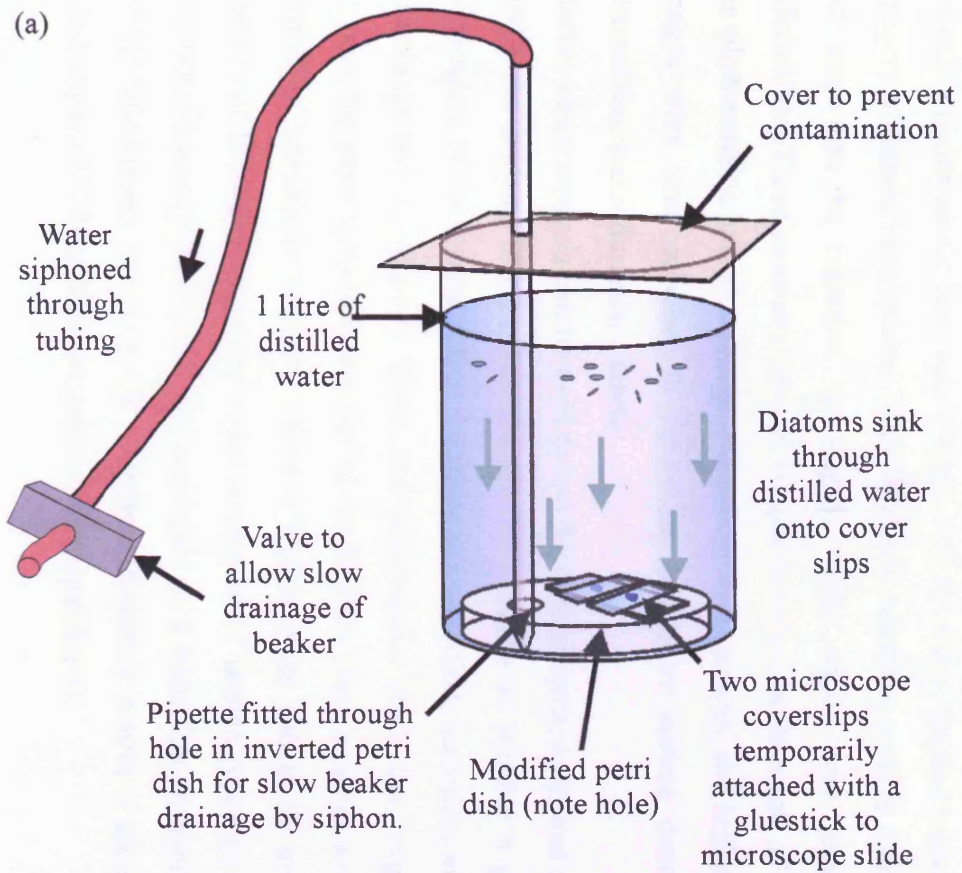
dimensions of less than 0.5 cm were cut from the sediment slabs and fractured to reveal surfaces parallel to the laminated sediment fabric (Pike and Kemp, 1996; Dean *et al.*, 1999). The blocks of sediment were mounted on standard SEM stubs (Figure 5.1), left to dry for 24 hours and then coated in Au-Pd (90:10). The stubs are related to the concomitant lamina in the BSEI thin section to aid diatom species identification.

### 5.2.3 Quantitative Diatom Analysis

Preparation of the sediment for quantitative diatom assemblage analysis followed the settling technique of Scherer (1994), as adapted by C.S. Allen (personal communication, 2003). This method was used to determine absolute diatom concentration (diatoms valves per gramme of dry sediment) and relative abundances of species within the total diatom assemblage. This settling procedure results in slides with an even distribution of valves with minimal clumping.

Samples were taken from selected (following BSEI analysis) lamina or sub laminae. Approximately 0.005-0.01g of oven dried sample was weighed using a Mettler AE240 balance, placed in a glass vial (20 ml) and half filled with distilled water. Approximately 3 ml of hydrogen peroxide (30%) was added to oxidize organics and disaggregate particles and 1 ml of hydrochloric acid (50%) was added to remove any carbonate in the vial. The vials were left on a hotplate on a low setting for 6 hours. After oxidation 10 ml of dispersing agent (e.g. sodium hexametasulphate, prepared from 2 grammes of powder per 500 ml distilled water) was added and left for 1 hour. The vial containing the sample was then placed in an ultrasonic bath for 1-3 seconds to fully disaggregate the sample. The contents of the vial were then emptied into a clean 1 litre flat bottomed beaker filled with distilled water (Figure 5.2). At the bottom of each beaker was a petri dish to which a slide was attached, and two cover slips were attached to this slide with a glue stick. The beaker was covered and after a period of four hours of settling the beaker was slowly drained (over a 12 hour period) from underneath the petri dish by a pipette held in place through a small hole in the petri dish. After allowing the cover slips to air dry, permanent slides were made using Norland Optical Adhesive (Refractive Index 1.56) and were cured with UV light.





**Figure 5.2**

(a) Schematic of apparatus used in the preparation of quantitative light microscope slides. Nine beakers are set up to produce 18 slides (two per sample).

(b) Photograph of apparatus in (a).

## 5.3. Data Collection

### 5.3.1 Backscattered Electron Imagery (BSEI)

The polished thin sections were analysed by backscattered electron imagery (BSEI) using a Cambridge Instruments (LEO) S360 Scanning Electron Microscope (SEM). Backscattered electrons are the result of elastic collisions between energetic beam electrons and atoms within the specimen (Goldstein, *et al.*, 1981). The number of backscattered electrons divided by the number of electrons to strike the sample gives a backscattering coefficient, which varies with the atomic number of the target (Pye and Krinsley, 1984). Terrigenous grains have relatively high average atomic numbers, therefore high backscatter coefficients, producing bright images. Diatom ooze laminae contain diatom frustules that are filled with low atomic number carbon-based resin, therefore have a low backscatter coefficient, producing dark images. A mosaic of low-resolution images (x 20 magnification) was made of each thin section to provide a photomosaic base map (Figure 5.3) for more detailed higher magnification imagery of lamina composition. The BSEI photomosaics provide compositional data, but may also be regarded as porosity maps which give sedimentary fabric information. Three measurements of lamina thickness were made of each lamina on the photomosaics and an average calculated. The mosaics and higher magnification images were used together to determine qualitative lamina diatom assemblage composition and sedimentary fabric.

Markov chain analysis can be used to test for lamina cyclicity (Swan and Sandilands, 1995); the analysis is based on the simple question of whether a given lamina is independent of the lamina below. Laminae are classified, according to lamina diatom assemblage and sedimentary fabric, and designated a letter. The longer the chain of laminae, the more reliable the results of the Markov chain analysis are, therefore, the number of transitions between different lamina types should be greater than  $5 \times (\text{number of laminae categories})^2$ . The succession of lamina types are displayed in a transition frequency matrix and are converted to a transition probability matrix. To test for randomness, the observed transition frequency matrix is compared with the matrix expected if there were no pattern (See appendix 5).



**Figure 5.3**

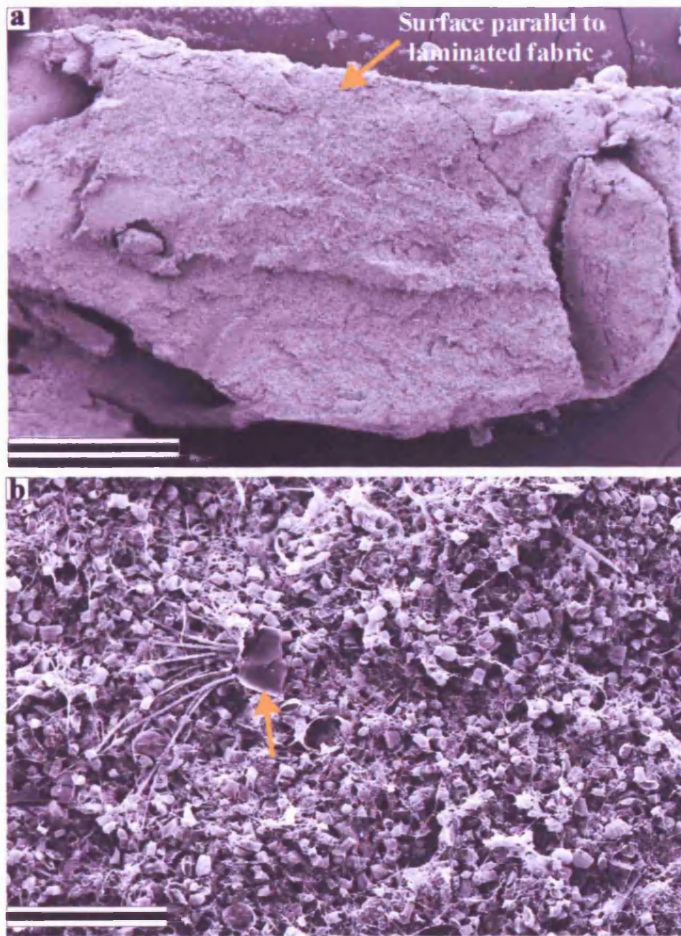
A low magnification backscattered electron imagery (BSEI) photomosaic base map showing alternating laminae of biogenic diatom ooze (dark) and diatom-bearing terrigenous laminae (bright). Scale bar = 3 mm.

### 5.3.2 Secondary Electron Imagery (SEI)

The sediment stubs were analysed by secondary electron imagery (SEI) using a Veeco FEI (Philips) XL30 Environmental Scanning Electron Microscope (ESEM) with FEG (Field Emission Gun). Inelastic collisions of high energy beam electrons and atoms within the sample produce secondary electrons (Pye and Krinsley, 1984). The number of secondary electrons emitted is affected by the topography of the specimen; therefore the images produced are topographic (Pike and Kemp, 1996). This permits the identification of diatoms from three-dimensional images (Figure 5.4).

### 5.3.3 Quantitative Diatom Counts

A minimum of 400 diatom valves were counted per sample using an Olympus BX40 microscope with phase contrast, at x 1000 (Figure 5.5). Four hundred valves per slide were counted to ensure a good representation of diatom species in the sample is presented (Allen, 2003). In coastal Antarctic sediments *Hyalochaete Chaetoceros* spp. resting spores dominate the diatom assemblage therefore two separate counts per slide are made, a total species count and a *Chaetoceros* spp. free count. The *Chaetoceros* spp. free counts allow trends of less common species to be revealed (Leventer *et al.*,

**Figure 5.4**

(a) Secondary electron imagery (SEI) photograph of a sediment block mounted on a standard scanning electron microscope (SEM) stub. Scale bar = 2 mm.

(b) SEI photograph of *Hyalochaete Chaetoceros* spp. resting spores, taken on surface parallel to sedimentary laminated fabric. Gold arrow indicates part of a *Corethron pennatum* frustule. Scale bar = 100 microns.

**Figure 5.5**

Light microscope photograph of *Fragilariopsis curta* (red arrow) and *Hyalochaete Chaetoceros* spp. resting spores (gold arrows). Scale bar = 20 microns.

1996; Allen *et al.*, 2005). Preservation of diatoms in the Palmer Deep, Mertz Ninnis Trough and Durmont d'Urville Trough sediment cores is generally good, but inevitably diatom valves become broken and fragmented. Rules for counting fragmented valves were implemented to ensure valve counts were not overestimated (Figure 5.6). Since both vegetative cells and resting spores of *Hyalochaete* *Chaetoceros* spp. are included in the count a standard way of counting this genera is employed (Figure 5.7) (Cunningham and Leventer, 1998; Armand, 1997). All valves were identified to species or genera level. Where the valves were unidentified to species level they were grouped in a generic group. If still unidentified they were placed in unidentified centric or pennate groups.

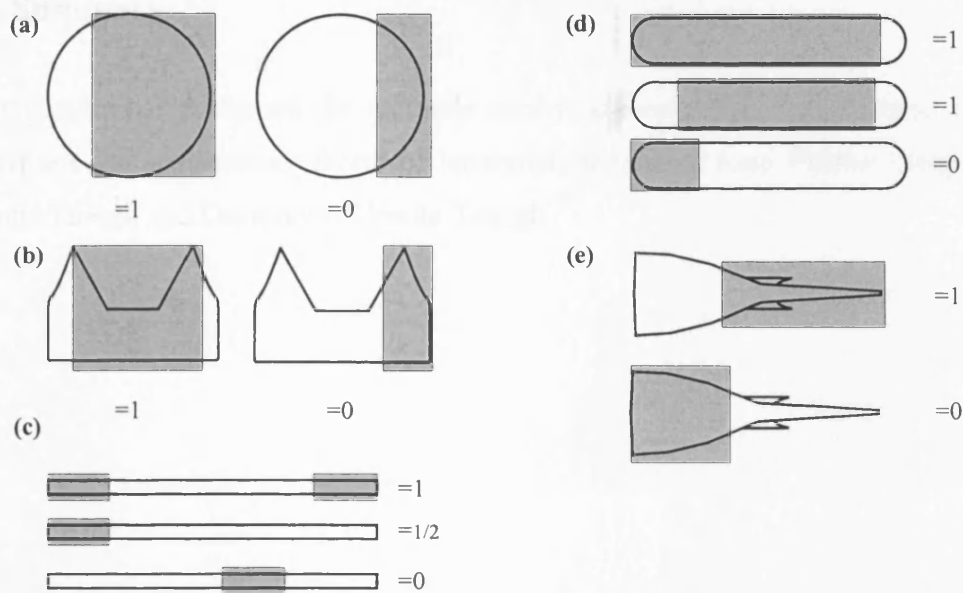
All whole frustules lying within each field of view are counted. Counting was performed along transects from left to right with the edge of the cover slip being avoided. The data collected (number of valves within a number of fields of view) allows the number of diatoms within a known area to be calculated. Using an established calculation (Scherer, 1994), the number of diatom valves in the original sample can be calculated and, therefore, the absolute abundance of diatom valves (number of diatom valves per gramme of dry sediment) can be determined. The absolute abundance of diatom valves per gramme was determined by the expression:

$$T = \frac{(NB / AF)}{M}$$

where

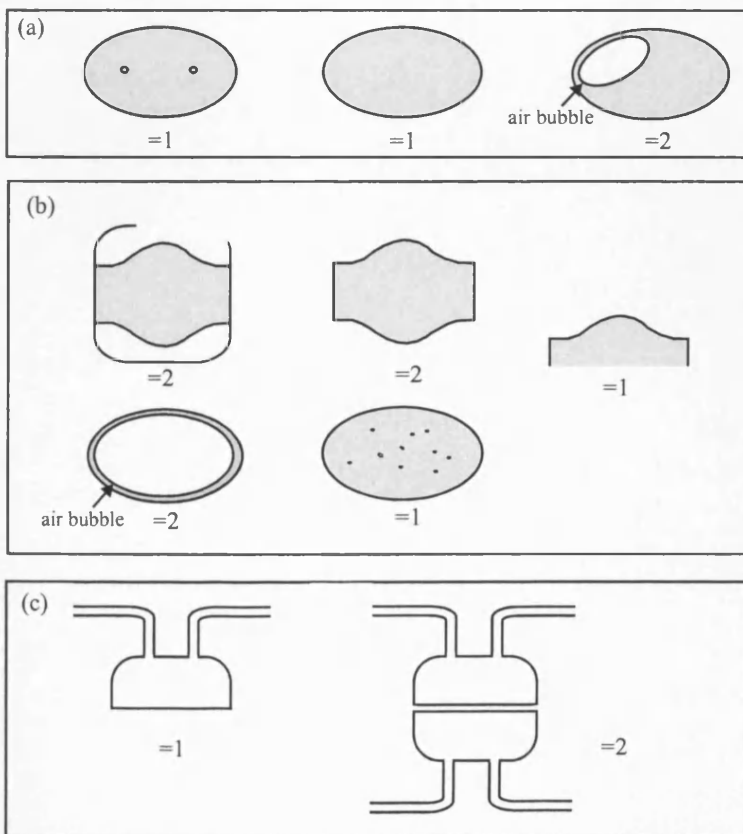
- $T$  = number of diatom valves per gramme
- $N$  = total number of diatom valves counted
- $B$  = area of bottom of beaker (mm<sup>2</sup>)
- $A$  = area per field of view (mm<sup>2</sup>)
- $F$  = number of fields of view counted
- $M$  = mass of sample (g)

Relative abundances of diatom valves were calculated as a percentage of the total diatom assemblage.



**Figure 5.6**

Counting methodology for fragmented valves adapted from Zielinski (1993). The shaded area represents the portion of valve present and the adjacent values indicate the number of valves counted. (a) Centrics e.g. *Thalassiosira* spp., *Actinocyclus* spp.. (b) Bidduphids e.g. *Eucampia* spp.. (c) Araphid pennates e.g. *Thalassiothrix* spp., *Thalassionema* spp.. (d) Raphid pennates e.g. *Fragilariopsis* spp.. (e) Cylindrical e.g. *Rhizosolenia* spp..



**Figure 5.7**

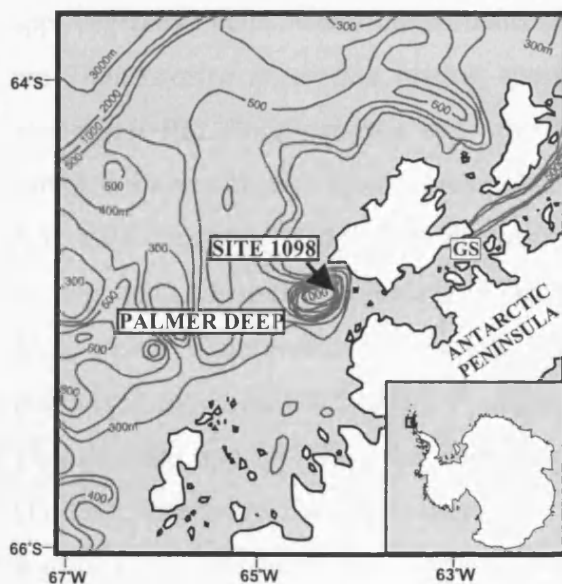
Counting methodology for *Chaetoceros* spp. valves. Values adjacent to valves indicate the number counted. (a) *Hyalochaete Chaetoceros* vegetative cells. (b) *Hyalochaete Chaetoceros* resting spores. (c) *Phaeoceros Chaetoceros* vegetative cells.

## **5.4 Summary**

This chapter has presented the methods used to collect diatom assemblage data and determine the sedimentary fabric of laminated sediments from Palmer Deep, Mertz Ninnis Trough and Durmont d'Urville Trough.

## 6. Palmer Deep

This chapter presents the results and interpretations of backscattered electron imagery (BSEI) analysis, secondary electron imagery (SEI) analysis and quantitative diatom assemblage counts from ODP Core 178-1098A [45.03 to 42.51 metres composite depth (mcd)] Palmer Deep, West Antarctica (Figure 6.1). Additional sections from Palmer Deep, ODP Cores 178-1098A (42.55-41.52 mcd) and 1098C (41.76-40.63 mcd), were used to extend the lamina thickness data range (see appendix 3). Detailed ODP Core 178-1098A and -1098C lithology, sample depths and chronological information are presented in chapter 4 and analytical methods used can be found in chapter 5. Part of this chapter has been published (Maddison *et al.*, 2005).



**Figure 6.1**

Location map of ODP Site 1098, Palmer Deep on the Antarctic Peninsula continental margin. Contours in metres. GS = Gerlache Strait. Adapted from Barker *et al.* (1999a).

### 6.1. Results

In this section lamina types and sub-laminae found in deglacial Palmer Deep sediments are presented and their relationships described. Laminae are classified according to the dominance of terrigenous or biogenic components. All laminae are overwhelmingly composed of *Hyalochaete Chaetoceros* spp. resting spores (95.4-99.8%) therefore minor species of the assemblage, which are visually dominant in BSEI, are used to categorize the laminae. Relative and absolute diatom abundances of each lamina type are averages of several counts conducted on each lamina and sub-lamina type, with the exception of three sub-lamina types (see Tables 6.1 – 6.9). The deglacial laminated sediments, from Palmer Deep, consist of orange-brown diatom



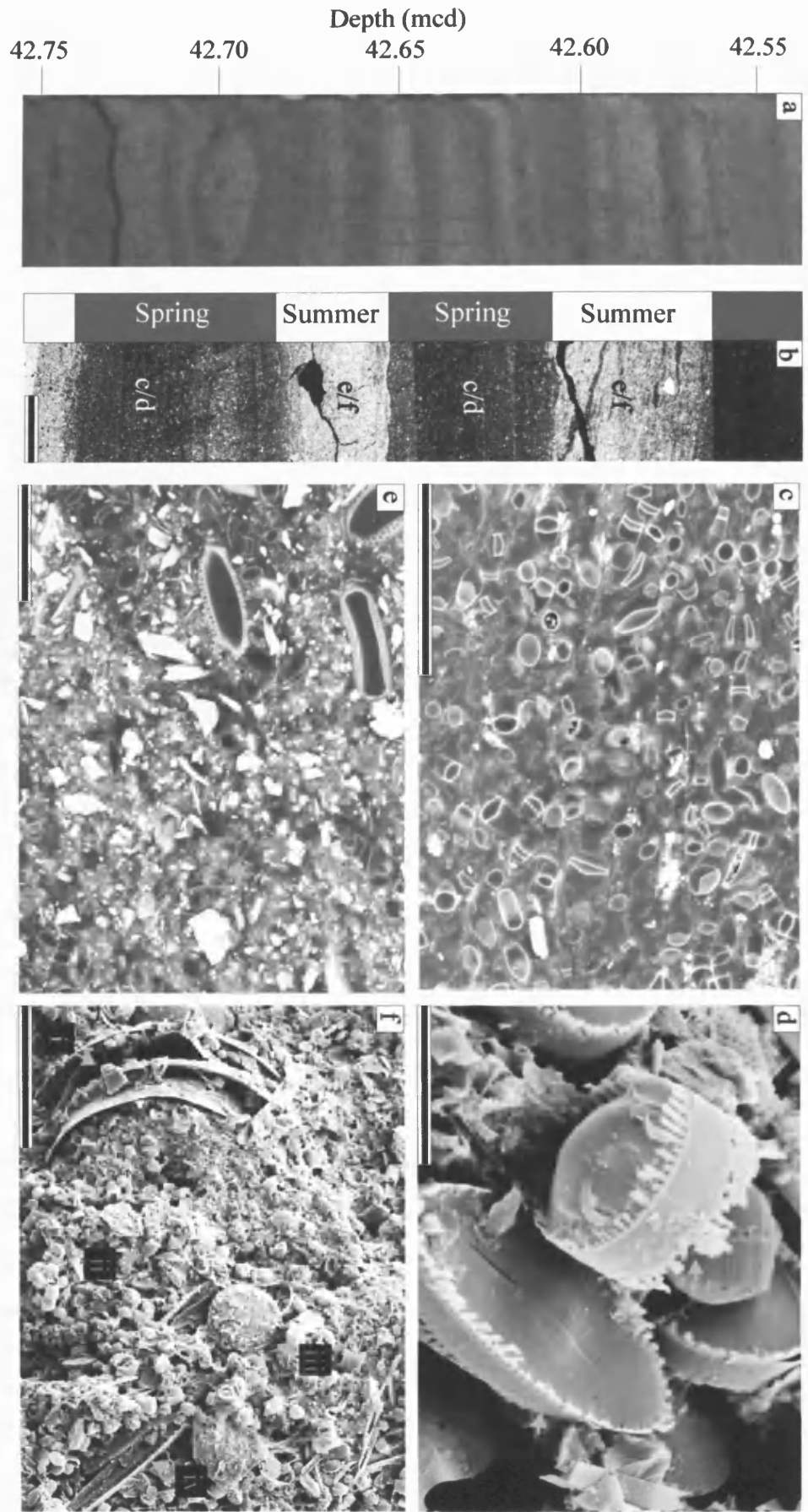
ooze lamina alternating with blue-grey diatom-bearing terrigenous lamina (Figure 6.2 and sections 6.1.1 and 6.1.2). See appendix 4, Tables A4.1.1.1 – A.4.1.1.6 for original counts. One hundred and seventy-two pairs of these laminations make up the deglacial unit.

### 6.1.1. Orange-brown Biogenic Laminae

Laminae of this type are orange-brown in colour and consist of almost pure diatom ooze with very little terrigenous material. BSEI photographs of these laminae are dark owing to the high porosity of the diatom ooze (Figure 6.2b, c and d). BSEI analysis revealed that this biogenic lamina type is overwhelmingly composed of *Hyalochaete Chaetoceros* spp. resting spores (CRS) and, to lesser extent, *Hyalochaete Chaetoceros* spp. vegetative cells. Minor constituents of the diatom assemblage observed in BSEI are *Thalassiosira antarctica* resting spores (RS), *Coscinodiscus bouvet*, *Odontella weissflogii* RS, *Fragilariopsis* spp. and *Corethron pennatum*. Eight laminae were sampled for quantitative diatom counts between 45.03 and 42.51 mcd (see Tables 6.1-6.3). CRS constitute 96.5 – 99.8 % and vegetative cells 0 – 2.8% relative abundance of the total diatom assemblage (Table 6.1). The most dominant species in *Hyalochaete Chaetoceros* free counts (Table 6.2) are *Fragilariopsis* spp. (60.3%; dominated by *F. curta* (22.6%), *F. cylindrus* (18.9%) and *F. vanheurckii* (6.4%)), *Thalassiosira* spp. (17.4%; the dominant species is *T. antarctica* warm RS form (11.6%)), vegetative *Eucampia antarctica* (5.0 %), *Navicula* spp. (4.2 %), *Proboscia inermis* (3.5%), *Corethron pennatum* (2.0%) and *Porosira glacialis* (1.6%). Absolute abundances of biogenic laminae range from 4650 - 9349 x 10<sup>6</sup> valves per gramme of dry sediment (Table 6.3). The highest absolute abundance occurred in the lowest orange-brown biogenic lamina sampled, at 44.97 mcd (log number 4, see appendix 3, table A3.1.1), 12,250 cal. yrs BP (Figure 4.5).

One hundred and seventy-two orange-brown biogenic laminae are present in cores 1098A and 1098C (see appendix 3, table A3.1.1). These laminae are present throughout the interval and constitute 42.5% of the total sediment thickness (Figure 6.3). The laminae range in thickness from 0.9 to 34.0 mm (n = 172,  $\sigma$  = 7.5 mm, mean = 10.0 mm). A linear regression line plotted on Figure 6.4a highlights a decrease in biogenic laminae thickness up-core ( $r^2$  = 0.135).

Figure 6.2



**Figure 6.2** (see previous page)

(a) Photograph of Core 178 1098A 6H, depth ~ 42.55 to 42.75 metres composite depth (mcd), showing alternating orange-brown laminae (biogenic) and blue-grey laminae (terrigenous). Red box indicates location of (b). (b) Backscattered secondary electron imagery (BSEI) photomosaic of alternating diatom ooze biogenic laminae (dark: spring) and diatom-bearing terrigenous laminae (light: summer) from 42.66 to 42.63 mcd; scale bar 3 mm. (c)/(d) and (e)/(f) refer to annotation on (b). (c) BSEI photograph of diatom ooze biogenic laminae composed of *Hyalochaete Chaetoceros* spp. resting spores (gold arrows). Scale bar = 50 microns. (d) Secondary electron imagery (SEI) photograph of *Hyalochaete Chaetoceros* spp. resting spores (gold arrows) from the biogenic laminae. Scale bar = 50 microns. (e) BSEI photograph of terrigenous laminae. *Hyalochaete Chaetoceros* spp. (gold arrow) and *Thalassiosira antarctica* resting spores (red arrows) present. The white fragments are terrigenous grains. Scale bar = 50 microns. (f) SEI photograph of terrigenous laminae with mixed diatom assemblage. Scale bar = 50 microns. Gold arrows: (i) *Coscinodiscus bouvet* girdle bands; (ii) *Hyalochaete Chaetoceros* spp. resting spores; (iii) *Thalassiosira antarctica* resting spore; (iv) *Fragilariopsis* spp..

**Table 6.1**

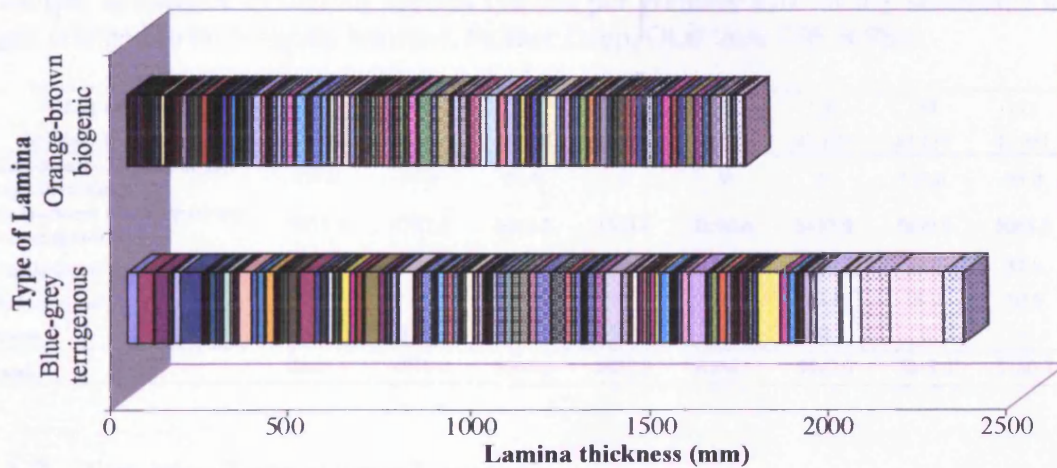
Relative abundance of all diatom species in eight orange-brown biogenic laminae, Palmer Deep, ODP core 178-1098A.

Log number	4	58	60	72	74	130	134	172
Species / Depth (mcd)	44.970	43.996	43.978	43.841	43.825	43.191	43.117	42.651
<i>Hyalochaete Chaetoceros</i> spp. (vegetative) Gran	2.8	1.2	1.2	0	0	0	2.2	1.0
<i>Hyalochaete Chaetoceros</i> spp. (resting spore) Gran	96.5	98.1	98.4	97.5	99.8	99.8	97.3	98.2
<i>Fragilariopsis</i> spp. Hustedt	0.2	0.4	0.2	2.2	0	0	0.2	0.6
<i>Thalassiosira</i> spp. Cleve	0	0	0.2	0	0.2	0.2	0.2	0.2
Others	0.5	0.3	0	0.3	0	0	0.1	0
Total	100.0	100.0	100.0	100.0	100.0	100.0	100.0	100.0

**Table 6.2**

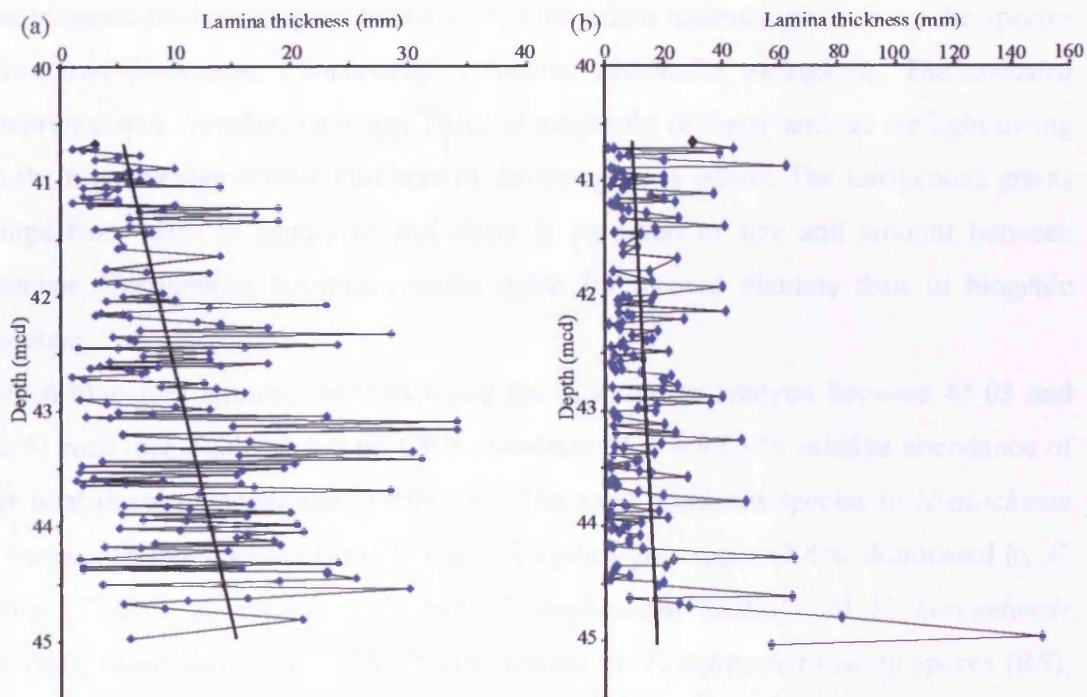
Relative abundance of *Hyalochaete Chaetoceros* spp. free diatom assemblages in eight orange-brown biogenic laminae, Palmer Deep, ODP core 178-1098A.

Log number	4	58	60	72	74	130	134	172
Species / Depth (mcd)	44.970	43.996	43.978	43.841	43.825	43.191	43.117	42.651
<i>Corethron pennatum</i> (Grunow) Ostenfeld	0	0.7	2.2	2.7	0	7.9	0	1.5
<i>Eucampia antarctica</i> (vegetative) (Castracane) Mangin	10.2	16.8	3.7	2	1.7	0.5	4.2	1.0
<i>Fragilariopsis</i> spp. Hustedt	47.2	38.7	58.5	73.7	73.0	46.8	75.5	68.6
<i>Thalassiosira</i> spp. Cleve	20.7	28.4	23.6	13.4	15.8	19.3	4.8	13.0
<i>Navicula</i> spp. Bory de st-Vincent	1.0	1.5	5.6	4.0	4.2	7.9	3.7	5.7
<i>Porosira glacialis</i> (Grunow) Jørgensen	1.5	6.7	0.5	0.5	0.2	0.2	1.5	2.0
<i>Proboscia</i> spp. Sunström	12.4	1.7	1.7	0.9	0.7	11.5	1.5	0.0
Others	7.0	5.5	4.2	2.8	4.4	5.9	8.8	8.2
Total	100.0	100.0	100.0	100.0	100.0	100.0	100.0	100.0



**Figure 6.3**

Graph showing the thicknesses of different types of lamina from Palmer Deep, ODP 178-1098A and -1098C. Individual thicknesses are displayed as coloured bars within the total thickness of each lamina type.



**Figure 6.4**

(a) Graph showing biogenic lamina thicknesses through part of the deglacial interval, 44.967 - 40.664 metres composite depth (mcd). Decrease in thickness indicated by regression line ( $r^2=0.135$ ).

(b) Graph to show terrigenous laminae thickness through part of the deglacial interval, 45.03 - 40.634 mcd. Decrease in thickness indicated by regression line ( $r^2=0.02$ ).

The laminae were plotted according to the depth at the base of the laminae.

**Table 6.3**

Absolute abundance of diatom species (valves per gramme  $\times 10^6$  of dry sediment) in eight orange-brown biogenic laminae, Palmer Deep, ODP core 178-1098A.

Log number	4	58	60	72	74	130	134	172
<b>Species / Depth (mcd)</b>	<b>44.970</b>	<b>43.996</b>	<b>43.978</b>	<b>43.841</b>	<b>43.825</b>	<b>43.191</b>	<b>43.117</b>	<b>42.651</b>
<i>Hyalochaete Chaetoceros</i> spp. (vegetative) Gran	257.2	57.4	65.6	0	0	0	171.0	53.0
<i>Hyalochaete Chaetoceros</i> spp. (resting spore) Gran	9018.6	4787.1	5602.2	4534.0	6090.0	5427.0	7639.0	5065.3
<i>Fragilariopsis</i> spp. Hustedt	18.4	23.0	13.1	106.3	0	0	19.0	31.8
<i>Thalassiosira</i> spp. Cleve	0	0	13.1	0	14.1	13.0	19.0	10.6
Others	55.1	11.5	0	9.7	0	0	0	0
<b>Total:</b>	<b>9349.3</b>	<b>4879.0</b>	<b>5694.0</b>	<b>4650.0</b>	<b>6104.1</b>	<b>5440.0</b>	<b>7848.0</b>	<b>5160.7</b>

### 6.1.2. Blue-grey Terrigenous Laminae

The blue-grey terrigenous laminae have a greater proportion of terrigenous grains such as ice-rafted silt and clay than the biogenic laminae. The diatom assemblage is near-monogeneric *Hyalochaete Chaetoceros* spp. resting spores (CRS) but BSEI analysis indicates that there is a more diverse minor diatom assemblage than seen in the biogenic laminae (Figure 6.2e and f). This minor assemblage includes the species *Corethron pennatum*, *Coscinodiscus bouvet*, *Odontella weissflogii*, *Thalassiosira antarctica* and *Fragilariopsis* spp. BSEI photographs of these laminae are light owing to the high average atomic numbers of the terrigenous grains. The terrigenous grains range from clay- to sand-size and there is variation in size and amount between laminae. Terrigenous laminae contain more fragmented diatoms than in biogenic laminae.

Seven blue-grey laminae were sampled for quantitative analysis between 45.03 and 42.51 mcd (see Tables 6.4-6.6). CRS constitute 95.4 – 99.3 % relative abundance of the total diatom assemblage (Table 6.4). The most dominant species in *Hyalochaete Chaetoceros* free counts (Table 6.5) are *Fragilariopsis* spp. (52.8%; dominated by *F. curta* (27.0%), *F. cylindrus* (8.5%), *F. vanheurckii* (6.0%) and *F. kerguelensis* (4.0%)), *Thalassiosira* spp. (29.8%; dominated by *T. antarctica* resting spores (RS), warm form (21.3%), *T. lentiginosa* (1.7%) and *T. tumida* (1.0%)), *Navicula* spp. (3.3%), *Porosira glacialis* (2.1%), *Corethron pennatum* (1.1%) and *Odontella weissflogii* RS (0.9%). Absolute abundances of terrigenous laminae range from 1135 - 3550  $\times 10^6$  valves per gramme (Table 6.6).

One hundred and seventy-three blue-grey terrigenous laminae are present in ODP core 1098A and 1098C (see appendix 3). Blue-grey terrigenous laminae are present

throughout the interval and constitute 57.5% of the total sediment thickness (Figure 6.3). Lamina thicknesses range from 0.95 to 150.1 mm ( $n = 173$ ,  $\sigma = 17.5$  mm, mean = 13.5 mm). A linear regression line plotted on Figure 6.4b shows a slight decrease in terrigenous laminae thickness up-core ( $r^2 = 0.02$ ). The thickest terrigenous laminae (>50 mm) are at the base of the sequence between 45.03 and 44.28 mcd. From 44.61 to 40.71 mcd, 12,164 to 11,235 cal. yrs BP (Figure 4.5), there appears to be cyclicity in the occurrence of laminae with thicknesses of 40 – 60 mm (Figure 6.4b).

**Table 6.4**

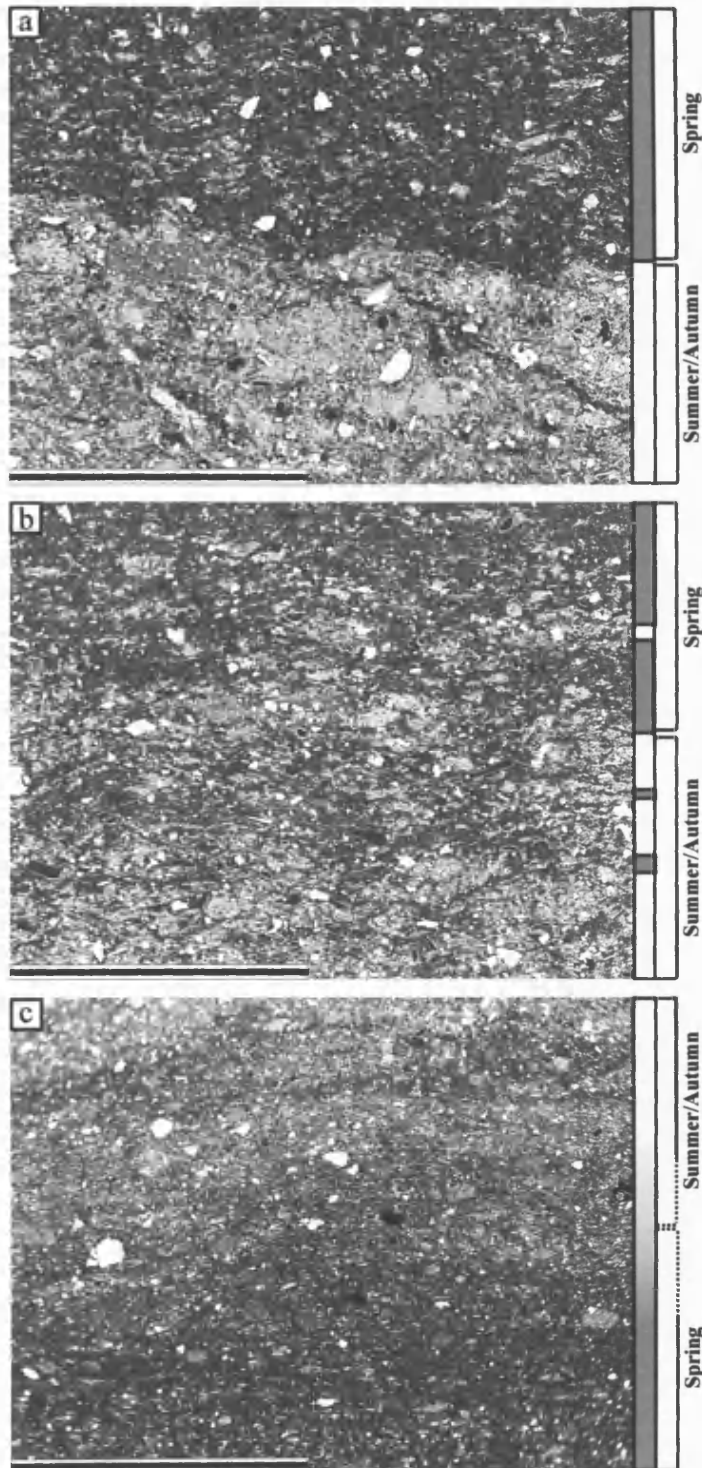
Relative abundance of all diatom species in seven blue-grey terrigenous laminae, Palmer Deep, ODP core 178-1098A.

Log number	5	59	59	61	73	75	135	135	135	173
Species / Depth (mcd)	44.790	43.989	43.987	43.962	43.833	43.819	43.112	43.105	43.100	42.646
<i>Hyalochaete Chaetoceros</i> spp. (vegetative) Gran	0	0	2.7	0	0.2	0.7	0.0	0.0	0.0	1.3
<i>Hyalochaete Chaetoceros</i> spp. (resting spore) Gran	96.3	99.3	95.4	97.5	98.4	98.7	99.0	96.6	97.4	97.8
<i>Fragilariopsis</i> spp. Hustedt	1.6	0.2	0.8	0.7	0.7	0.4	1.0	1.5	1.9	0.7
<i>Thalassiosira</i> spp. Cleve	1.4	0.5	0.6	1.8	0.7	0.2	0.0	0.8	0.2	0.2
Others	0.8	0.0	0.5	0.0	0.0	0.0	0.0	1.1	0.5	0.0
Total	100.0	100.0	100.0	100.0	100.0	100.0	100.0	100.0	100.0	100.0

**Table 6.5**

Relative abundance of *Hyalochaete Chaetoceros* spp. free diatom assemblages in seven blue-grey, terrigenous laminae, Palmer Deep, ODP core 178-1098A. RS = resting spores.

Log number	5	59	59	61	73	75	135	135	135	173
Species / Depth (mcd)	44.790	43.989	43.987	43.962	43.833	43.819	43.112	43.105	43.100	42.646
<i>Corethron pennatum</i> (Grunow) Ostefeld	0.7	0.7	0.0	2.0	0.2	2.2	1.0	0.2	0.2	3.9
<i>Eucampia antarctica</i> (vegetative) (Castracane) Mangin	1.4	2.2	2.2	0.2	0.7	0.2	3.2	0.2	0.5	2.4
<i>Fragilariopsis</i> spp. Hustedt	48.6	57.3	47.0	28.7	63.5	54.8	61.9	54.6	56.5	55.0
<i>Thalassiosira</i> spp. Cleve	32.3	28.9	37.0	62.1	21.8	27.7	17.2	28.8	23.5	17.6
<i>Navicula</i> spp. Bory de st-Vincent	2.1	1.7	3.2	1.2	5.9	2	3.7	3.0	5.7	4.6
<i>Porosira glacialis</i> RS (Grunow) Jørgensen	1.0	2.0	2.5	2.5	1.7	4.2	4.1	1.7	0.7	0.7
<i>Proboscia</i> spp. Sunström	1.7	0.2	0.2	0.2	0.5	0.2	0.4	0.4	6.5	0.0
Others	12.2	7.0	7.9	3.1	5.7	8.7	8.5	11.1	6.4	15.8
Total	100.0	100.0	100.0	100.0	100.0	100.0	100.0	100.0	100.0	100.0



**Figure 6.5**

Types of lamina boundaries observed in ODP 178-1098A Palmer Deep deglacial laminated interval (all scale bars 600 microns).

(a) Backscattered secondary electron imagery (BSEI) photograph of sharp boundary between summer (terrigenous) and spring (biogenic) laminae.

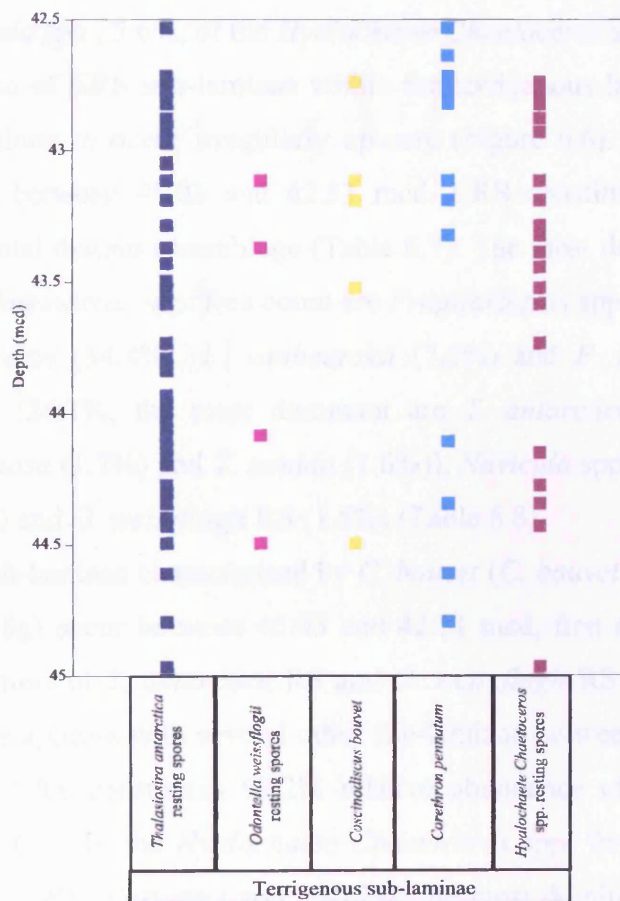
(b) BSEI photograph of bioturbated boundary between summer (terrigenous) and spring (biogenic) laminae.

(c) BSEI photograph of gradational boundary between spring (biogenic) and summer (terrigenous) laminae.



#### 6.1.4. Sub-laminae within Blue-grey Laminae (terrigenous)

Terrigenous laminae in the deglacial laminated interval do not consistently have a homogeneous mixed diatom assemblage. Sub-laminae within the blue-grey terrigenous laminae have an increased abundance of a specific species relative to the rest of the assemblage. These sub-laminae characterised by *Thalassiosira antarctica* resting spores (RS), *Hyalochaete Chaetoceros* spp. resting spores (CRS), *Odontella weissflogii* RS, *Corethron pennatum* and *Coscinodiscus bouvet* occur intermittently between 45.03 and 42.51 mcd (Figure 6.6; see appendix 3, Table A3.1.1), 12,264 – 11,664 cal. yrs BP (Figure 4.5).



**Figure 6.6**

Graph illustrating the distribution of the different terrigenous sub-lamina types, Palmer Deep ODP 178-1098A, between 45.03 and 42.51 metres composite depth (mcd). The sub-laminae are positioned according to the depth of the base of the lamina they are within.



The most commonly observed species forming sub-laminae is *T. antarctica* RS, with 53 appearances between 45.03 and 42.51 mcd (Figure 6.6). These sub-laminae are typically found at the top or just below the top of terrigenous laminae (Figures 6.7 and 6.8c and d). Sometimes more than one sub-laminae of *T. antarctica* RS occurs within a single blue-grey lamina (e.g. *T. antarctica* RS sub-laminae occur three times in lamina log number 33, see appendix 3, Table A3.1.1). Sub-laminae of *T. antarctica* RS within terrigenous laminae start to occur at 44.98 mcd (Figure 6.6). CRS constitute 91.8% relative abundance of the total diatom assemblage (Table 6.7). *T. antarctica* (53.9%; 35.7% of which are the warm RS form) is the most dominant species in the *Hyalochaete Chaetoceros* spp. free count (Table 6.8). *Fragilariopsis* spp. makes up 33.5% (*F. curta* (16.3%) and *F. cylindrus* (10.5%) the most dominant species) and *Navicula* spp., 5.6%, of the *Hyalochaete Chaetoceros* spp. free count.

The first occurrence of CRS sub-laminae within the terrigenous laminae is at 44.97 mcd and they continue to occur irregularly up-core (Figure 6.6). Twenty-five CRS sub-laminae occur between 45.03 and 42.51 mcd. CRS constitute 96.9% relative abundance of the total diatom assemblage (Table 6.7). The most dominant species in the *Hyalochaete Chaetoceros* spp. free count are *Fragilariopsis* spp. (56.6%; the most dominant are *F. curta* (34.4%), *F. vanheurckii* (7.5%) and *F. cylindrus* (7.3%)), *Thalassiosira* spp. (24.1%; the most dominant are *T. antarctica* RS warm form (16.5%), *T. lentiginosa* (1.7%) and *T. tumida* (1.6%)), *Navicula* spp. (5.2%), *Porosira glacialis* RS (1.6%) and *O. weissflogii* RS (1.5%) (Table 6.8).

Five terrigenous sub-laminae characterised by *C. bouvet* (*C. bouvet* visually dominant in BSEI, Figure 6.8g) occur between 45.03 and 42.51 mcd, first appearing at 44.50 mcd with a sub-lamina of *T. antarctica* RS and *O. weissflogii* RS (Figure 6.6). This type of sub-laminae appears with several other sub-laminae between 43.19 and 42.74 mcd (Figure 6.6). CRS constitutes 97.2% relative abundance of the total diatom assemblage (Table 6.7). In the *Hyalochaete Chaetoceros* spp. free counts the most abundant species are *Fragilariopsis* spp. (50.2%; the most dominant species are *F. curta* (35.5%), *F. vanheurckii* (5.4%) and *F. cylindrus* (3.4%)) and *Thalassiosira* spp. (23.8%; *T. antarctica* RS warm form (17.6%) and *T. tumida* (2.0%)), *Actinocyclus actinochilus* (8.6%), *Navicula* spp. (3.4%), *Rhizosolenia* spp. (2.9%; *R. antennata* f. *semispina* (2.2%)), *O. weissflogii* RS (1.2%) and *C. bouvet* (0.7%) (Table 6.8).

There are fifteen occurrences of *C. pennatum* terrigenous sub-laminae (Figure 6.8e and f), the first occurs at 44.80 mcd (Figure 6.6). Sub-laminae of *C. pennatum* occur

with sub-laminae of *T. antarctica* RS, and at 43.11 mcd with *C. bouvet*, *O. weissflogii* RS and *T. antarctica* RS sub-laminae (Figure 6.6). CRS constitute 95.6% relative abundance of the total diatom assemblage (Table 6.7). In the *Hyalochaete Chaetoceros* spp. free counts the most abundant species are *Fragilariopsis* spp. (50.5%; the most dominant species are *F. curta* (24.6%), *F. vanheurckii* (8.5%), *F. cylindrus* (6.2%) and *F. ritscheri* (3.2%)), *Thalassiosira* spp. (31.3%; *T. antarctica* RS warm form (22.4%)), *C. pennatum* (5.0%), *Navicula* spp. (3.7%) and *O. weissflogii* RS (1.2%) (Table 6.8).

*O. weissflogii* RS terrigenous sub-laminae (Figure 6.8a and b) are the least common of the five sub-lamina types, with only four occurrences between 45.03 and 42.51 mcd (Figure 6.6). An *O. weissflogii* RS sub-lamina occurs at 44.50 mcd with sub-lamina of *C. bouvet* and *T. antarctica* RS, at 44.08 mcd with no other sub-laminae, at 43.37 mcd with a sub-lamina of *T. antarctica* RS and at 43.11 mcd with sub-laminae of CRS, *C. bouvet*, *C. pennatum* and *T. antarctica* RS (Figure 6.6). CRS constitute 90.1% relative abundance of the total diatom assemblage (Table 6.7). The most dominant species in the *Hyalochaete Chaetoceros* spp. free count are *Fragilariopsis* spp. (34.7%; the most dominant species are *F. curta* (18.7%), *F. ritscheri* (6.0%) and *F. cylindrus* (3.0%)), *O. weissflogii* RS (11.0%), *Proboscia* spp. (32.2%; *P. inermis* (21.0%) and *P. truncata* (11.2%)) and *Thalassiosira* spp. (12.5%; *T. antarctica* warm form RS (6.2%)) (Table 6.8).

**Table 6.7**

Relative abundance of all diatom species from terrigenous sub-laminae, Palmer Deep, ODP core 178-1098A. CRS = *Hyalochaete Chaetoceros* spp. resting spores. RS = resting spores.

Log number	131	135	135	131	59	131	135	135
Depth ( mcd)	43.177	43.109	43.107	43.171	43.987	43.174	43.098	43.096
Species / Sub-lamina type	CRS		<i>Coscinodiscus bouvet</i>	<i>Corethron pennatum</i>	<i>Thalassiosira antarctica</i> RS			<i>Odontella weissflogii</i> RS
<i>Hyalochaete Chaetoceros</i> spp. (vegetative) Gran	0.0	2.2	0.0	0.2	0.0	0.0	0.0	0.4
<i>Hyalochaete Chaetoceros</i> spp. (RS) Gran	97.1	96.6	97.2	95.6	82.3	96.6	96.4	90.1
<i>Corethron pennatum</i> (Grunow) Ostenfeld	0.2	0.0	0.2	0.2	0.0	0.0	0.0	0.0
<i>Coscinodiscus bouvet</i> Karsten	0.0	0.0	0.2	0.0	0.0	0.0	0.0	0.0
<i>Fragilariopsis</i> spp. Hustedt	1.4	0.7	0.7	2.6	3.1	1.4	1.8	3.1
<i>Thalassiosira antarctica</i> RS Comber	0.0	0.0	1.0	0.2	12.3	1.8	1.4	1.0
<i>Odontella weissflogii</i> RS (Janisch) Grunow	0.0	0.0	0.0	0.0	0.0	0.0	0.0	0.8
Others	1.3	0.5	0.7	1.2	2.3	0.2	0.4	5.0
<b>Total:</b>	100.0	100.0	100.0	100.0	100.0	100.0	100.0	100.0

**Table 6.8**

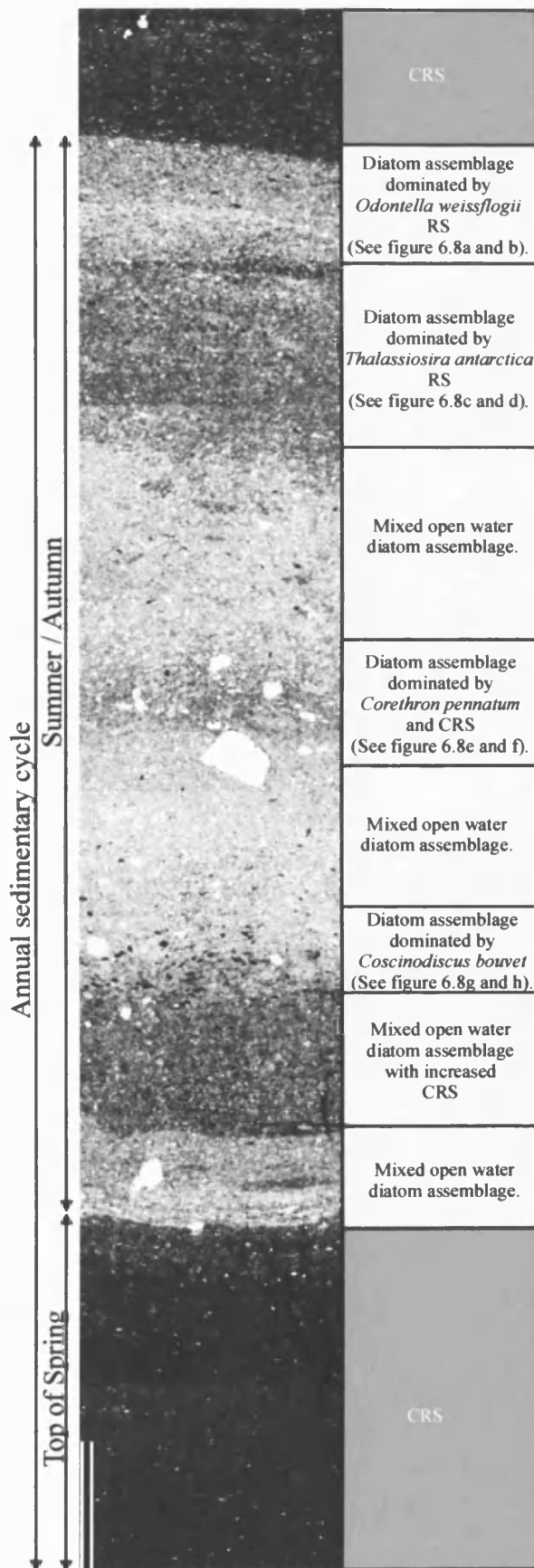
Relative abundance of *Hyalochaete Chaetoceros* spp. free diatom assemblages from terrigenous sub-laminae, Palmer Deep, ODP core 178-1098A. CRS = *Hyalochaete Chaetoceros* spp. resting spores. RS = resting spores.

Log number	131	135	135	131	59	131	135	135
Depth ( mcd)	43.177	43.109	43.107	43.171	43.987	43.174	43.098	43.096
Species / Sub-lamina type	CRS		<i>Coscinodiscus bouvet</i>	<i>Corethron pennatum</i>		<i>Thalassiosira antarctica</i> RS		<i>Odontella weissflogii</i> RS
<i>Corethron pennatum</i> (Grunow) Ostenfeld	4.2	1.2	1.7	5.0	0.7	0.5	0.0	0.2
<i>Coscinodiscus bouvet</i> Karsten	0.0	0.0	0.7	0.0	0.0	0.0	0.0	0.0
<i>Fragilariopsis</i> spp. Hustedt	59.0	54.2	50.2	50.5	22.6	43.3	34.5	34.7
<i>Thalassiosira antarctica</i> RS Comber	16.6	20.0	19.3	24.6	67.1	38.9	55.8	8.2
<i>Odontella weissflogii</i> RS (Janisch) Grunow	1.0	2.0	1.2	1.2	0.0	0.5	0.7	11.0
Others	19.2	22.6	26.9	18.7	9.6	16.8	9.0	45.9
<b>Total:</b>	100.0	100.0	100.0	100.0	100.0	100.0	100.0	100.0

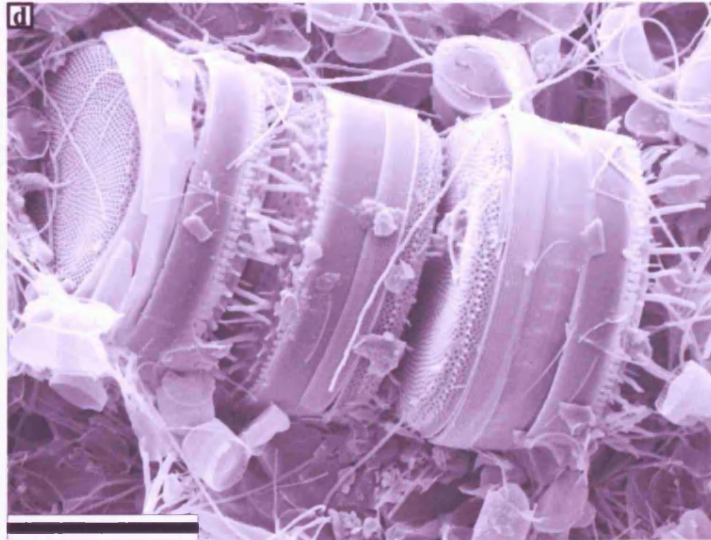
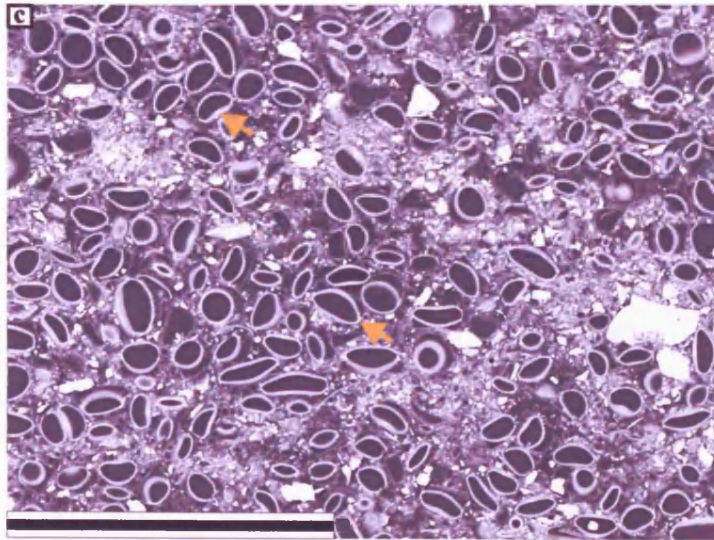
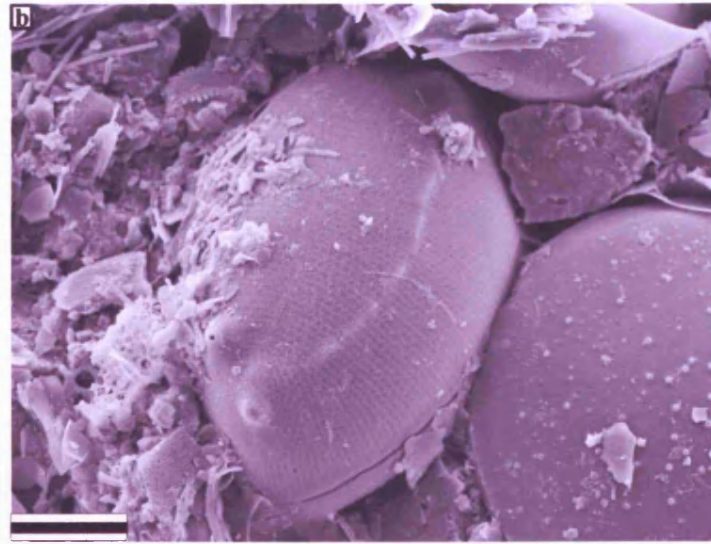
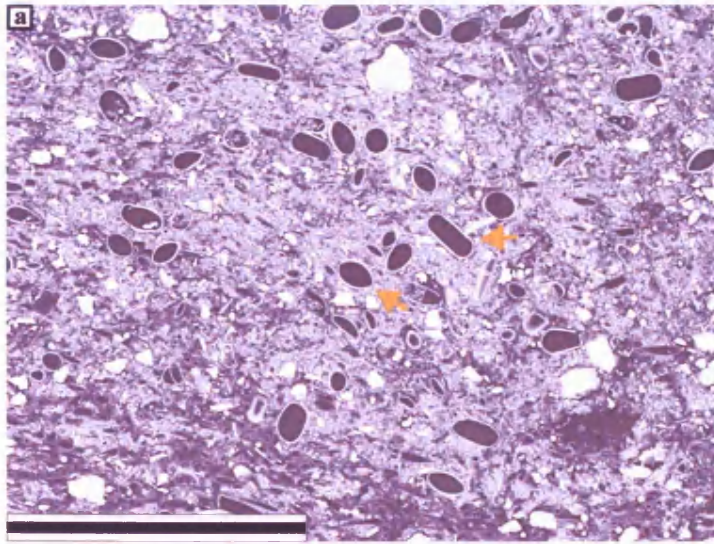
**Table 6.9**

Absolute abundance of diatom species (valves per gramme  $\times 10^6$  of dry sediment) from terrigenous sub-laminae, Palmer Deep, ODP core 178-1098A. CRS = *Hyalochaete Chaetoceros* spp. resting spores. RS = resting spores.

Log number	131	135	135	131	59	131	135	135
Depth ( mcd)	43.177	43.109	43.107	43.171	43.987	43.174	43.098	43.096
Species / Sub-lamina type	CRS		<i>Coscinodiscus bouvet</i>	<i>Corethron pennatum</i>		<i>Thalassiosira antarctica</i> RS		<i>Odontella weissflogii</i> RS
<i>Hyalochaete Chaetoceros</i> spp. (vegetative) Gran	0.0	32.6	0.0	1.7	0.0	0.0	0.0	3.2
<i>Hyalochaete Chaetoceros</i> spp. (resting spore) Gran	1587.1	1426.0	581.1	681.1	827.7	1034.3	2941.2	696.3
<i>Corethron pennatum</i> (Grunow) Ostenfeld	3.9	0.0	1.4	1.7	0.0	0.0	0.0	0.0
<i>Coscinodiscus bouvet</i> Karsten	0.0	0.0	1.4	0.0	0.0	0.0	0.0	0.0
<i>Fragilariopsis</i> spp. Hustedt	23.3	10.9	4.3	18.2	31.5	14.5	55.1	24.0
<i>Thalassiosira antarctica</i> RS Comber	0.0	0.0	5.7	1.7	123.7	19.4	41.3	8.0
<i>Odontella weissflogii</i> RS (Janisch) Grunow	0.0	0.0	0.0	0.0	0.0	0.0	0.0	6.4
Others	19.4	7.2	3.7	8.2	22.5	2.4	13.8	35.2
<b>Total:</b>	1633.7	1476.7	597.6	712.6	1005.4	1070.6	3051.4	773.1

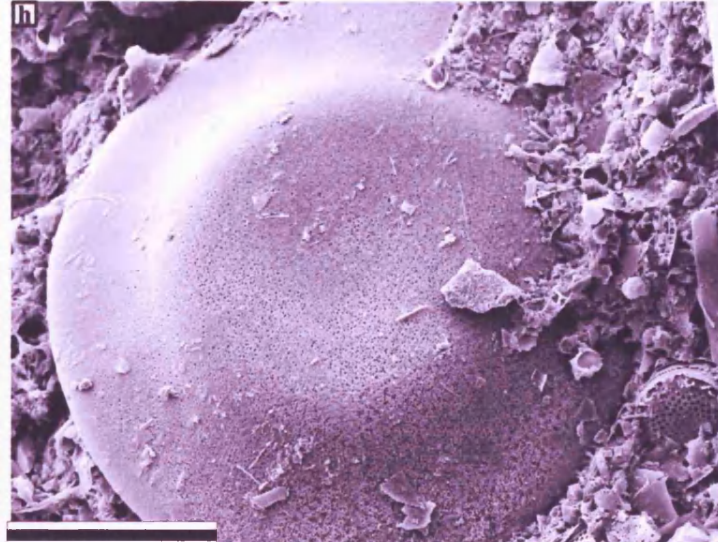
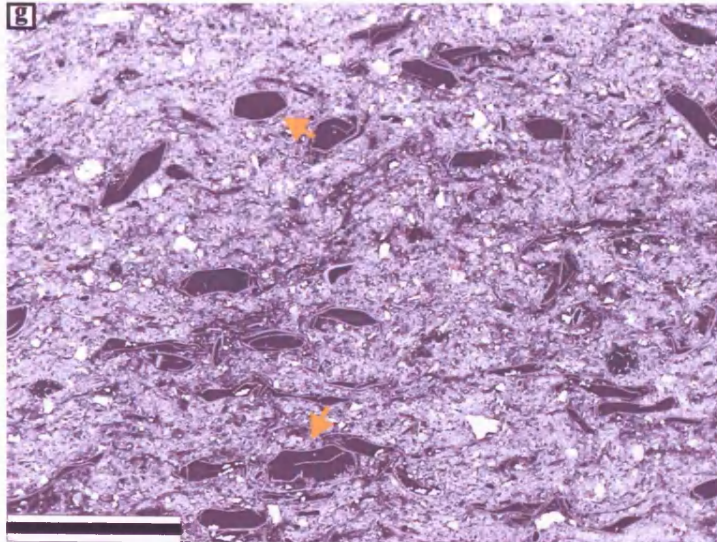
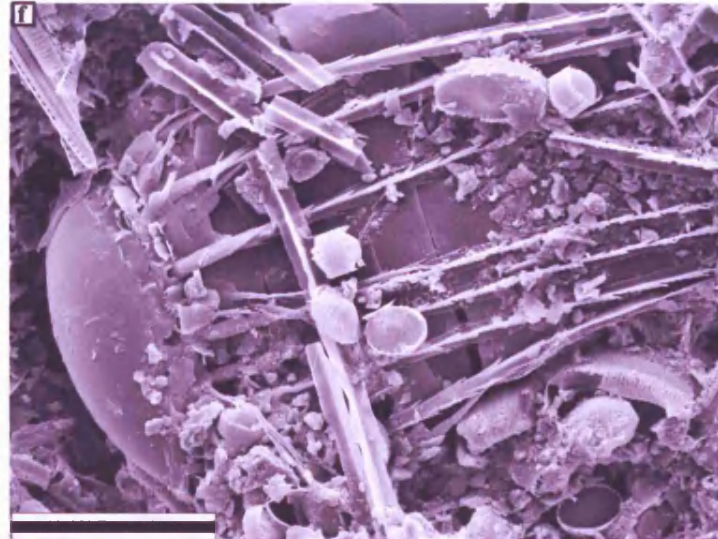
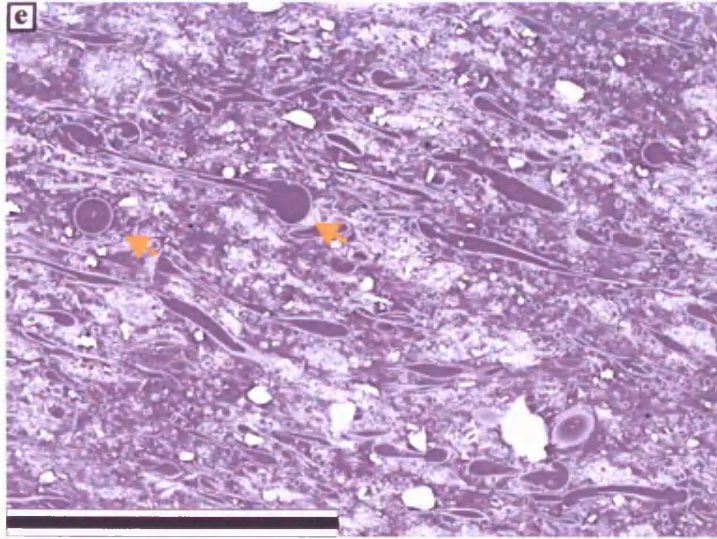
**Figure 6.7**

Backscattered secondary electron imagery (BSEI) photomosaic of multiple sub-laminae within the terrigenous laminae, ODP 178-1098A Palmer Deep (~ 43.12 to 43.09 mcd). Scale bar = 3 mm. CRS = *Hyalochaete Chaetoceros* spp. resting spores. RS = resting spores.



**Figure 6.8**  
Sub-laminae species associated with Figure 6.7.

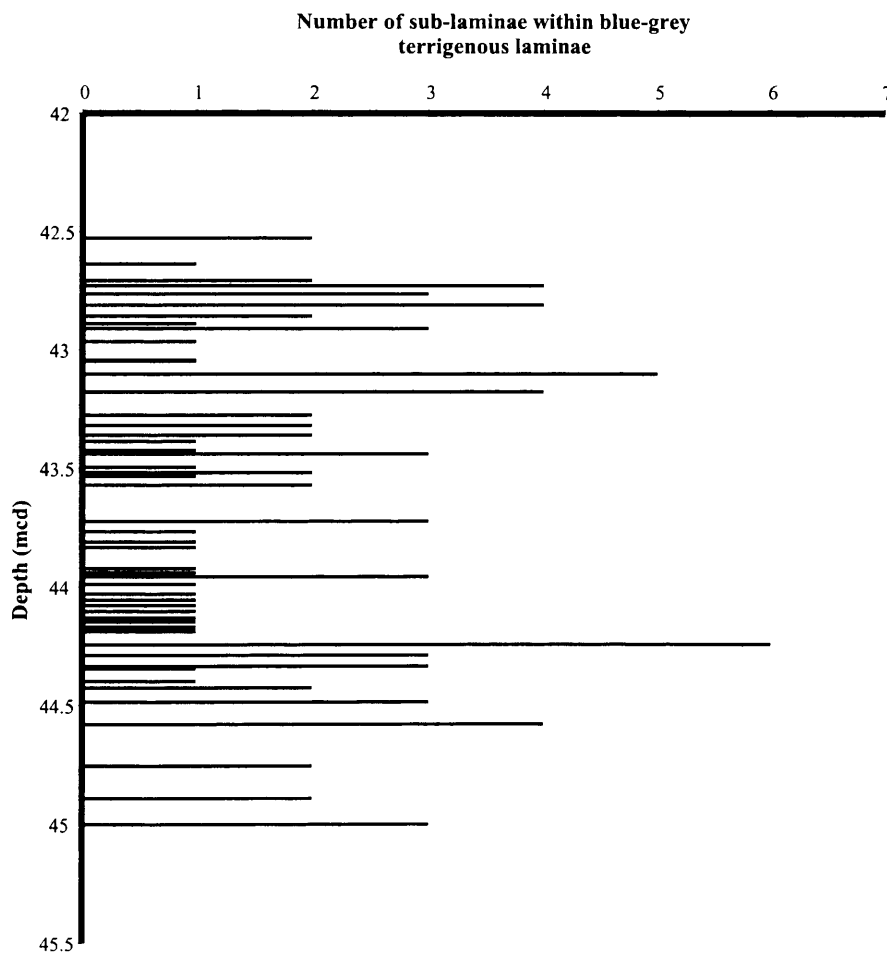
(a) Backscattered electron imagery (BSEI) photograph of *Odontella weissflogii* resting spore (RS) (gold arrows) sub-lamina. Scale bar = 300 microns. (b) Secondary electron imagery (SEI) photograph of *O. weissflogii* RS sub-lamina. Scale bar = 10 microns. (c) BSEI photograph of *Thalassiosira antarctica* RS (gold arrows) sub-lamina. Scale bar = 300 microns. (d) SEI photograph of *T. antarctica* RS sub-lamina. Scale bar = 20 microns.



**Figure 6.8 continued**  
**(e)** BSEI photograph of *Corethron pennatum* (gold arrows) sub-lamina. Scale bar = 200 microns.  
**(f)** SEI photograph of *C. pennatum* sub-lamina. Scale bar = 20 microns.  
**(g)** BSEI photograph of *Coscinodiscus bouvet* (gold arrows) sub-lamina. Scale bar = 300 microns.  
**(h)** SEI photograph of *C. bouvet* (white arrows) sub-lamina. Scale bar = 50 microns.

### 6.1.5. Sub-lamina Relationships

One hundred and two sub-laminae occur between 45.03 and 42.51 mcd (see appendix 3, Table A3.1.1). Out of all the sub-lamina types sub-lamina characterised by *Thalassiosira antarctica* resting spores (RS) have the highest absolute abundance,  $1708 \times 10^6$  valves per gramme of dry sediment (Table 6.9). The lowest absolute abundances occur in the *Coscinodiscus bouvet*, *Odontella weissflogii* RS and *Corethron pennatum* terrigenous sub-laminae (Table 6.9). The first sub-laminae occur at 44.98 mcd (Figure 6.6). Up through the laminated interval multiple sub-laminae occur within a single terrigenous lamina (Figure 6.9), often the sub-laminae assemblages are dominated by the same species. Between 43.19 and 42.72 mcd there are several terrigenous laminae with four or five sub-laminae (Figure 6.6, 6.7 and 6.9).



**Figure 6.9**

Location of sub-laminae (increased abundance of specific species) within the blue-grey terrigenous laminae in the deglacial laminated interval, 45.03-42.51 metres composite depth (mcd), ODP 1098A Palmer Deep.

### 6.1.6. Lamina and Sub-lamina Relationships

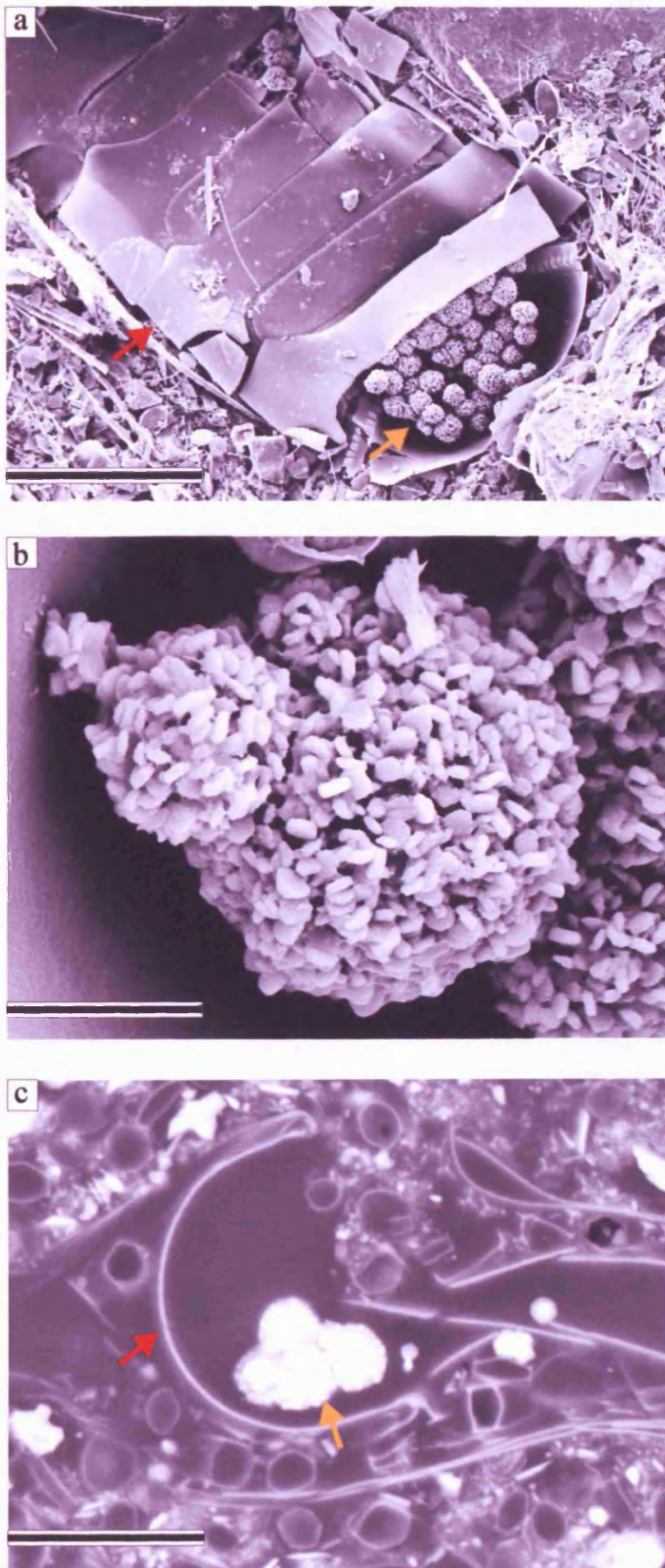
Fifty-three percent of blue-grey terrigenous laminae between 45.03 and 42.51 mcd contain at least one sub-lamina (Figure 6.9). Sub-lamina characterised by *Thalassiosira antarctica* resting spores (RS) are found in 45%, *Hyalochaete Chaetoceros* spp. resting spores (CRS) in 21%, *Corethron pennatum* in 13%, *Coscinodiscus bouvet* in 5% and *Odontella weissflogii* RS in 4% of blue-grey terrigenous laminae.

Two sets of Markov chain analysis were conducted to ascertain if there was a pattern in the record of transitions between a lithology (lamina or sub-lamina) and others (see appendix 5 for calculations). The coding of states in the first set of Markov chain analysis was biogenic laminae, terrigenous laminae and terrigenous laminae with sub-laminae within. Markov chain analysis determined that the cycles: biogenic laminae – terrigenous laminae – biogenic laminae and biogenic laminae – terrigenous lamina with sub-laminae – biogenic laminae were likely to occur and that the occurrence of lithologies was, to an extent, dependent on preceding lithology. Lithologies were redefined in the second Markov chain analysis as; biogenic laminae, terrigenous laminae, terrigenous laminae containing sub-laminae including *Thalassiosira antarctica* resting spores (RS) and terrigenous laminae with sub-laminae not including *T. antarctica* RS. Markov chain analysis determined that the more likely cycles were: biogenic laminae – terrigenous laminae – biogenic laminae and biogenic laminae – terrigenous laminae with sub-laminae including *T. antarctica* RS – biogenic laminae, and the occurrence was to an extent dependent on the preceding lithology.



### 6.1.7. Other Observations

Framboidal pyrite ( $\text{FeS}_2$ ; spheroidal aggregates of discrete pyrite microcrystallites) 5 – 15 microns in diameter, occurred throughout the laminated interval. BSEI analysis showed that framboids were present outside diatom frustules and, more commonly, inside larger diatoms such as *Coscinodiscus bouvet* and *Corethron pennatum*. In SEI analysis many framboids (framboidal aggregates) were observed in *C. pennatum* frustules (Figure 6.10a and b). BSEI analysis of these mineral deposits disclosed two structure types of framboids; a more common homogeneous structure and a less common framboid with a two layered structure (Figure 6.10c). Agglutinated foraminifera were present throughout the laminated interval (Figure 6.11). The foraminifera were not affiliated with any particular laminae or sub-laminae. Very few calcareous foraminifera were present in the laminated interval.



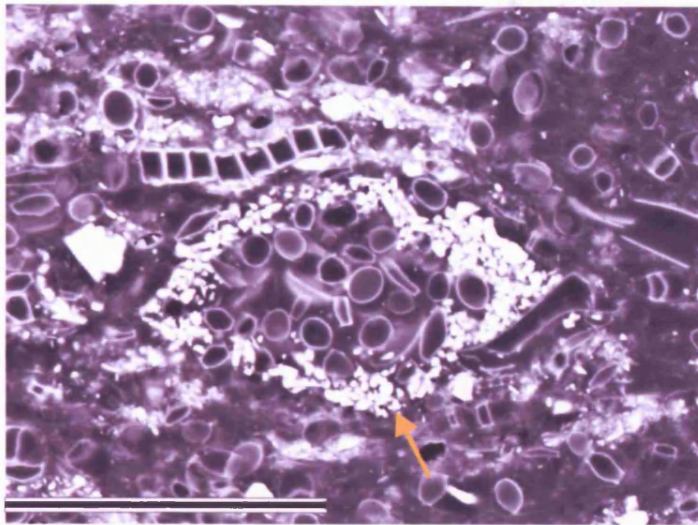
**Figure 6.10**

Secondary electron imagery (SEI) and backscattered electron imagery (BSEI) photographs of pyrite in deglacial laminated sediments, Palmer Deep, ODP site 1098A.

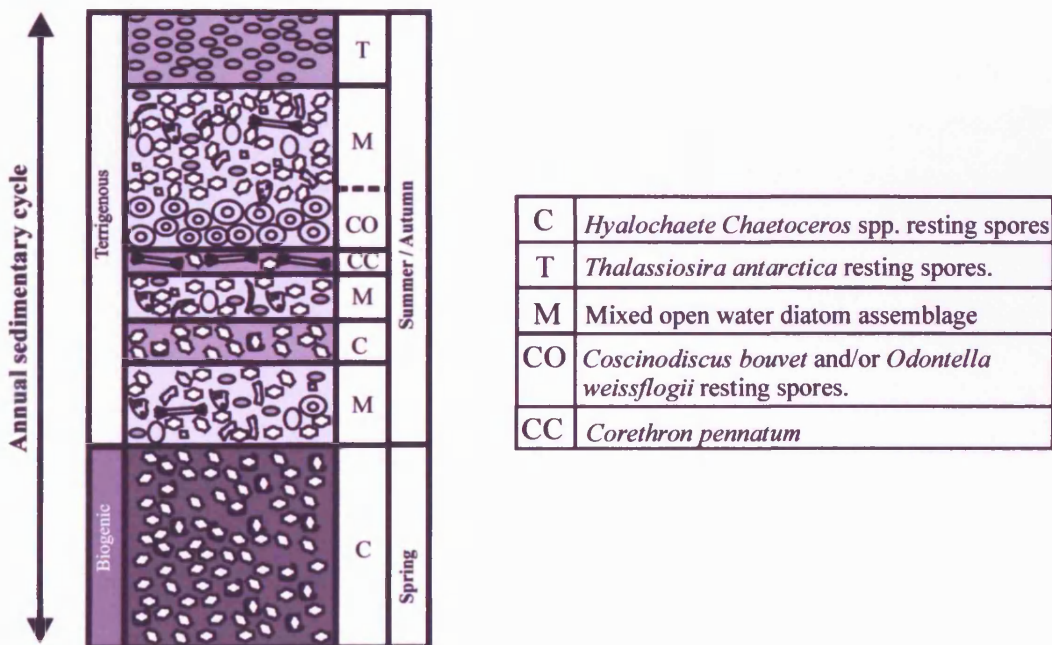
(a) SEI photograph of *Corethron pennatum* (red arrow) filled with balls of pyrite (gold arrow). Scale bar = 50 microns.

(b) SEI photograph of close up of balls of pyrite in (a). Scale bar = 6 microns

(c) BSEI photograph of *C. pennatum* (red arrow) surrounded with *Hyalochaete Chaetoceros* spp. resting spores. Balls of pyrite within the *C. pennatum* frustule (gold arrow). Note the two layered structure of the pyrite balls. Scale bar = 30 microns



**Figure 6.11**  
Backscattered electron imagery (BSEI) photograph of an agglutinated foraminifera (gold arrow) in an orange-brown biogenic laminae. Surrounded by *Hyalochaete Chaetoceros* spp. resting spores. A chain of *Fragilariopsis* spp. is present above the foraminifera. Scale bar = 60 microns.



**Figure 6.12**  
Schematic representation of the sub-seasonal sub-laminae within the terrigenous laminae, Palmer Deep. Compiled from backscattered electron imagery (BSEI) data.

## 6.2. Interpretation

The ecology of the diatom species that are discussed in this section is described in greater detail in chapter 3, section 3.5.

### 6.2.1. Spring: Orange-brown Biogenic Laminae

The dominant diatom genus in the biogenic orange-brown laminae is *Hyalochaete Chaetoceros*. In coastal Antarctica, the *Hyalochaete Chaetoceros* sub-genera favours proximity to sea ice (Leventer, 1991; Crosta *et al.*, 1997) and modern sediment trap data from the Antarctic Peninsula suggests that *Hyalochaete Chaetoceros* spp. blooms are associated with the melting of sea ice in the austral spring (Leventer, 1991). *Fragilariopsis curta* and *F. cylindrus* are also linked with melting sea ice, and resultant surface water column stratification (Leventer and Dunbar, 1987; Garrison, 1991; Cunningham and Leventer, 1998; Leventer, 1998), *F. vanheurckii* associated with the spring sea ice margin (Garrison *et al.*, 1987) and *Navicula* spp. have been noted to be a significant component of the spring bloom when sea ice melts (Krebs, 1983). *Thalassiosira antarctica* has been documented in coastal zones of loose platelet ice crystals floating beneath pack and fast ice (Horner, 1985b; Smetacek *et al.*, 1992; Gleitz *et al.*, 1998). *Corethron pennatum* is a very common lightly silicified Antarctic species which occurs in open water with little sea ice (Fryxell and Hasle, 1971; Makarov, 1984; Leventer and Dunbar, 1987) although it has been reported as a component of the ice-edge phytoplankton (Marra and Boardman, 1984). *C. pennatum* usually reaches its highest concentrations along the Antarctic coast and can dominate the phytoplankton (Sommer, 1991; Ligowski *et al.*, 1992). *Porosira glacialis* is associated with sea ice and has been reported to occur in slush and wave exposed shore ice (Hasle; 1973; Krebs *et al.*, 1987). Hence, the biogenic *Hyalochaete Chaetoceros* spp. resting spores (CRS) orange-brown laminae are interpreted as spring deposition.

During the deglaciation the water column in the vicinity of the Palmer Deep would have been influenced by the adjacent ice sheet. Melting of the sea ice and ice sheet in spring released freshwater, creating a stratified water column. The Gerlache Strait (Figure 6.1) remained largely blocked by ice, preventing the northward flow of surface water, as exists here today (Sjunneskog and Taylor, 2002). This restricted

flow would have further enhanced surface water stratification. These conditions of reduced surface salinity and high nutrients associated with melting ice create ideal conditions for high productivity of *Hyalochaete Chaetoceros* spp.. Environmental stress is likely to occur at the end of spring when nutrients have been used up or when a storm mixes up the water column (breaking down stratification) increasing the salinity and decreasing the temperature of the shelf waters.

I suggest that the thickness of the biogenic laminae (Figure 6.4a) was controlled by the proximity of the West Antarctic Ice Sheet (WAIS) front during the deglacial retreat. As the ice sheet became increasingly distal from Palmer Deep, i.e. nearer to the continent, a decrease in the ice sheet meltwater flux would have led to a less stratified water column and reduced nutrients, which reduced productivity, causing absolute abundance of the orange-brown biogenic laminae to decrease upcore (Table 6.3). Therefore, this reduction in productivity created thinner laminae through time. At the base of the deglacial laminated interval, between 44.973 and 44.967 mcd (see appendix 3, log number 2), there is one biogenic laminae 6 mm thick within 207 mm of terrigenous sediment. This implies that deposition was still dominated by a glacial environment. The biogenic lamina would have been deposited when the sea ice melted in spring; however, the sea ice may not have melted every year during the early part of the deglaciation.

### 6.2.2. Summer: Blue-grey Terrigenous Laminae

As a grounded ice sheet moves, sand, silt and clay are entrained. The sand, silt and clay are transported to the grounded margin by ice streams, the finer fraction becoming suspended in the water column following ice melt and deposited in the sediment (Leventer *et al.*, 2002; Domack *et al.*, 2006). The high proportion of ice-rafted material in the mixed diatom assemblage terrigenous lamina is therefore interpreted as summer/autumn melt and deposition.

The species within the summer laminae such as *Thalassiosira antarctica* resting spores (RS), *Odontella weissflogii* RS, *Corethron pennatum* and *Coscinodiscus bouvet* are considered to be open-water diatoms and are related to ice-free, lower nutrient conditions which would have occurred following total melt of seasonal sea ice (Fryxell and Hasle, 1971; Makarov, 1984; Leventer and Dunbar, 1987; Priddle and Thomas, 1989; Zielinski and Gersonde, 1997). The genus *Thalassiosira* is

widespread in Antarctic waters and commonly occurs in sea temperatures of 2° to 1°C (Zielinski and Gersonde, 1997). It has been considered rare to find *T. antarctica* in sea ice (Fryxell and Kendrick, 1988; Leventer and Dunbar, 1987; Zielinski and Gersonde, 1997), which has been attributed to its inability to survive the low light intensities beneath and within sea ice (Fryxell *et al.*, 1987). There is little documented on the ecology of the *Odontella* genus; however *O. weissflogii* is considered endemic to the Southern Ocean and occurs in Antarctic nearshore regions where water temperatures are between 2° and 5°C (Zielinski and Gersonde, 1997). As previously discussed *C. pennatum* is an open water species (Fryxell and Hasle, 1971; Makarov, 1984; Leventer and Dunbar, 1987). *C. bouvet* is a large distinctive Antarctic endemic species and has a circumpolar distribution. It is found in the neritic environment (coastal habitat) but has been seen in the Scotia Sea (oceanic waters) (Priddle and Thomas, 1989); however, little more is known about the ecology of *C. bouvet*. *Fragilariopsis kerguelensis* is an indicator of open-water productivity and is negatively correlated with sea ice concentration (Burckle *et al.*, 1987). *Navicula* spp. indicate the presence of sea ice in the region (Krebs *et al.*, 1987).

In Figure 6.4b, a general decrease in the thickness of the terrigenous laminae could be explained by the shoreward retreat of the melting glacial ice, the source of the terrigenous component. Up-core there are several repeated peaks of relatively thick terrigenous laminae (40 - 60 mm) (Figure 6.4b) which could indicate summers with much higher melting or longer seasons. These peaks are not regular, they have a periodicity ranging from 6 to 35 couplets (a minimum of 6 to 35 summers) which does not appear to correlate with modern climate cycles known to affect Antarctic Peninsula sea ice distribution such as Antarctic Circumpolar Wave (ACW) or El-Niño (Harangozo, 2000). The terrigenous lamina thicknesses (Figure 6.4b) do not decline smoothly up-core which implies that the ice sheet did not melt at a continuous rate through the deglaciation. Post-deglaciation, the terrigenous laminae become rarer up-core into the Holocene as the glacial margin became land-based (Leventer *et al.*, 2002). Fragmented frustules observed in the terrigenous laminae are produced as a result of grazing zooplankton, which excrete the diatom remains as faecal pellets, and minor frustule dissolution in the surface waters before sedimentation.

### 6.2.3. Winter

An abrupt transition from summer terrigenous laminae to the spring biogenic laminae suggests an abrupt change in sediment regime. The decrease in temperatures in winter would increase sea ice cover causing the input to the sediment to dramatically decrease (Gilbert *et al.*, 2003) - the hiatus between summer and spring could even represent several years, particularly in the early deglacial, owing to sea ice cover not melting during the year.

### 6.2.4. Annual Signal

From the onset of deglaciation the orange-brown diatom ooze laminae are seen to alternate with the blue-grey diatom bearing terrigenous sediment. These discrete laminae are interpreted as spring and summer/autumn respectively. The higher absolute abundance of diatoms in the spring orange-brown biogenic laminae relative to the summer blue-grey diatom bearing terrigenous laminae is a result of different water column conditions and nutrient levels. In the spring higher nutrient levels and water column stability (stratification) are induced by ice melt which allows high productivity to occur. In the summer, nutrient levels will have become depleted and water column stability reduced by mixing, leading to lower productivity. Sea ice cover in winter prevents sediment flux and deposition (Leventer *et al.*, 2002). The rhythmic alternation of two lamina types indicates that the analysed laminated interval is varved. The couplets observed in the deglacial sediment sequence represent an annual cycle with the base of spring laminae marking the start of a year.

### 6.2.5. Sub-seasonal signal

The sub-seasonal diatom blooms (Figures 6.7 and 6.8) seen within some terrigenous laminae suggest an evolution of the environment and/or shelf waters in deglacial summers. The intact nature of the diatoms within the sub-laminae suggests rapid flocculation and consequent mass sinking at bloom termination events. Sub-laminae of *Hyalochaete Chaetoceros* spp. resting spores (CRS) tend to be observed near the base of the terrigenous laminae (Figure 6.7). The sub-laminae are unexpected, since this genus is considered to be associated with spring productivity. The occurrence as

sub-laminae could indicate a brief return to water column stratification caused by the last fragments of sea ice melting or an influx of meltwater from the land allowing this genus to bloom and produce the increase in CRS.

*Coscinodiscus bouvet* sub-laminae (Figures 6.7 and 6.8g and h) are observed in the lower to middle part of the terrigenous laminae. *Rhizosolenia antennata* f. *semispina*, also present in these sub-laminae, indicates open waters in summer (Froneman *et al.*, 1995). The sub-laminae were probably caused by water column mixing (e.g. storms) in the summer. The sub-laminae of *Corethron pennatum* (Figure 6.7 and 6.8e and f) are observed in the middle of terrigenous laminae. The sub-laminae are unusual since high abundances of this species are rarely found in sediments (Taylor and Sjunneskog, 2002). *C. pennatum* has positive buoyancy (Crawford, 1995) which suggests that it may be able to exploit a well-stratified water column, migrating down to take advantage of higher nutrient content at depth and up for higher light levels for photosynthesis (Leventer *et al.*, 2002) to maximise bloom conditions. Deterioration in the water column stability during the summer to autumn transition could potentially trigger a mass sinking of the bloom (Kemp *et al.*, 2000).

The *Odontella weissflogii* resting spore (RS) sub-laminae (Figure 6.7 and 6.8a and b) seen near the top of the terrigenous laminae were most likely to have been deposited owing to a change in water column conditions. Froneman *et al.* (1997) reported *O. weissflogii* to be a temperate neritic species that is transported into Antarctic waters by unusual, southern intrusions of sub-Antarctic surface waters. The end of summer bloom of this species could therefore have been advected into the Palmer Deep region during a period of maximum cyclone activity (King *et al.*, 2003). *Proboscia* spp., which are also present in this sub-laminae, dominate summer-autumn diatom communities (Brichta and Nöthig, 2003).

*Thalassiosira antarctica* RS sub-laminae (Figures 6.7 and 6.8c and d) are seen as one or two bloom events near the top of the terrigenous laminae, acting as a marker for the end of the summer season. Since *T. antarctica* RS sub-laminae are not observed in the biogenic laminae, I believe that *T. antarctica* blooms in the summer/autumn rather than at the beginning of spring. An increase in salinity as sea ice forms retards the species growth (Aletsee and Janhnke, 1992) and this intolerance becomes greater as the temperature decreases (Grant and Horner, 1976; Aletsee and Janhnke, 1992). The annual sea ice advance, decreased light intensities (Taylor, 1999b) and the brine rejection would have caused convective overturning and mixing, decreasing the



nutrients in the water. Therefore, the *T. antarctica* RS probably formed at the end of the summer as a result of environmental stress caused by sea ice formation. Alternatively, high abundances of *T. antarctica* could have been advected into the region, as recorded in the Bransfield Strait, where sporadic incursions of cold Weddell Sea surface water bring *T. antarctica* into the area (Gersonde and Wefer, 1987; Zielinski and Gersonde, 1997).

The sequence of CRS sub-lamina followed by *C. bouvet*, *C. pennatum*, *O. weissflogii* RS and *T. antarctica* RS sub-laminae within one terrigenous lamina has been observed once in the deglacial laminated interval (lamina log number 135, appendix 3, Table A3.1.1), but several times with four of the five types of sub-laminae present. This suggests that there was a repeated evolution of shelf water conditions during the summers which contain the sub-laminae.

#### 6.2.6. Sub-seasonal and Seasonal Relationship

The sub-seasonal laminae which are present in some terrigenous laminae start to occur near the base (44.98 mcd, Figure 6.9) of the deglacial laminated interval. There does not seem to be a periodicity to the occurrence of sub-seasonal blooms in the deglacial interval. Several mechanisms for the multiple sub-seasonal laminae are suggested below, including (1) high tides (2) high cyclone intensity and (3) intrusion of Circumpolar Deep Water (CDW) onto the continental shelf.

(1) A similarity between the alternating laminations and tidal signals and a strong bi-annual control on biogenic and terrigenous laminae deposition has been suggested by Domack *et al.* (2003). A brief period of higher tides in the summer or the increase in autumnal tide amplitude could create conditions which would induce the repeated sub-lamina monospecific blooms seen within some of the terrigenous laminae (Figure 6.7). The high tides could bring coastal diatom blooms up against a frontal zone produced by estuarine (meltwater) flow (Leventer *et al.*, 2002). This oceanographic salinity barrier would cause environmental stress inducing the diatoms to rapidly form resting spores. The high density of the frustules would cause them to sink and be deposited on the sea floor. Repeated high tide pulses throughout the summer/autumn would bring different species blooms against the 'barrier', causing the repeated diatom blooms found within the sediment.

(2) The Antarctic Peninsula is the most northerly part of the continent and is most subject to mid-latitude oceanographic and atmospheric influences. The peninsula

forms the southern boundary to the Drake Passage and is therefore subject to many consequences of this constriction of the Southern Ocean. The Antarctic Peninsula is in close proximity to the Antarctic Circumpolar Current (ACC). The Circumpolar Trough (CPT), a low-pressure system, encircles Antarctica and in the austral summer is found to be extreme off West Antarctica, cutting the Antarctic Peninsula at its halfway point near Marguerite Bay (Simmonds, 2003). High cyclone frequencies have a tendency to be found in the regions of the deeper parts of the CPT. In both summer and winter the number and intensity of cyclones are at a maximum west of the Antarctic Peninsula (King *et al.*, 2003). The presence of large numbers of cyclones to the west of the peninsula means that the region is subject to very high temporal variability on a wide range of timescales from synoptic to interdecadal (Simmonds and Murray, 1999). Consequently a variety of air trajectories reach the Antarctic Peninsula and manipulate surface water masses, pushing diatoms against the meltwater created salinity barrier, causing diatoms to sink and begin resting spore formation. Therefore another possible cause for the multiple sub-laminae could be storms. More storms or a storm of certain intensity or certain direction may cause several blooms to be advected into the Palmer Deep region during the summer, such as *Coscinodiscus bouvet* (Priddle and Thomas, 1989) and *Odontella weissflogii* (Froneman *et al.*, 1997).

(3) A change in oceanographic conditions such as in nutrients, water temperature and salinity could influence the occurrence of different diatom species blooms and/or the form of deposition. Domack *et al.* (1992) observed the intrusion of CDW onto the west Antarctic Peninsula continental shelf to be associated with a major coastward bend in the 3000-m depth contour. This intrusion would introduce a new set of shelf water conditions. Ice melting has been suggested as the driving force behind CDW across-shelf transport (Potter and Paren, 1985). As ice melts, more buoyant, less saline water is released at the surface, this flows outwards drawing the CDW up onto the shelf. This system would have a self-perpetuating circulation because the relatively warm waters of the CDW would melt the ice. A seasonal and interannual variability in the frontal boundary between the ACC and Weddell Sea Transitional Water (more saline water mass from northwestern Weddell Sea) has been observed in the Antarctic Peninsula region (Hofmann and Klinck, 1998b). The boundary ranges from the southern Bransfield Strait into the southern Gerlache Strait. Any impingement of the boundary position onto the continental shelf controls the

upwelling of Upper CDW and resultant changes to shelf waters which could enhance multiple species blooms throughout the summer. It is possible that a threshold in tidal amplitudes, cyclone intensity or intrusion of CDW was reached to produce higher productivity and more multiple sub-seasonal laminae per year. A schematic model of the resulting deposition is presented in Figure 6.12. I believe the *Hyalochaete Chaetoceros* spp. resting spore (CRS), *C. bouvet* and *Corethron pennatum* sub-laminae were caused by a breakdown in the stratification of the water column. The *O. weissflogii* resting spore (RS) sub-lamina was caused by advection of waters into the Palmer Deep region which was followed by a seasonal-change-induced *Thalassiosira antarctica* RS sub-lamina.

#### 6.2.7. Discussion of Other Observations

Pyrite is typically found in anoxic, sulphidic, marine sediments (e.g. Berner, 1970; 1984) and is especially common in sapropels (Love and Amstutz, 1966). The formation of pyrite framboids in sediments or during sedimentation requires an anaerobic environment. This environment could be formed within the sediment as a whole, or it might exist as a microenvironment inside microfossils, such as diatoms (Schallreuter, 1984). Framboidal pyrite is the result of the breakdown of organic matter by decay and sulphate-reducing bacteria. The iron is usually brought into the environment as detritus (Rolfe and Brett, 1969). The organic matter within diatoms does not provide sufficient sulphur or iron to produce a frustule filled with framboidal pyrite. These elements must, therefore, diffuse into the diatom from outside (Schallreuter, 1984). Therefore, the presence of framboidal pyrite throughout the laminated interval, inside and outside diatom frustules, indicates that the depositional environment was anoxic.

Agglutinated foraminifera are common in bathyal environments and are important indicators of palaeoceanographic conditions because they are sensitive to differences in water masses. Temperature, salinity and oxygen content as well as bathymetry and substrate conditions affect the distribution of benthonic foraminifera (Phleger, 1960; Boltovskoy, 1965; Murray, 1973). Unfortunately insufficient detail in the BSEI photographs of the agglutinated foraminifera means that species identification is not possible (I. MacMillan personal communication, 2005) and therefore no environmental inferences can be made.

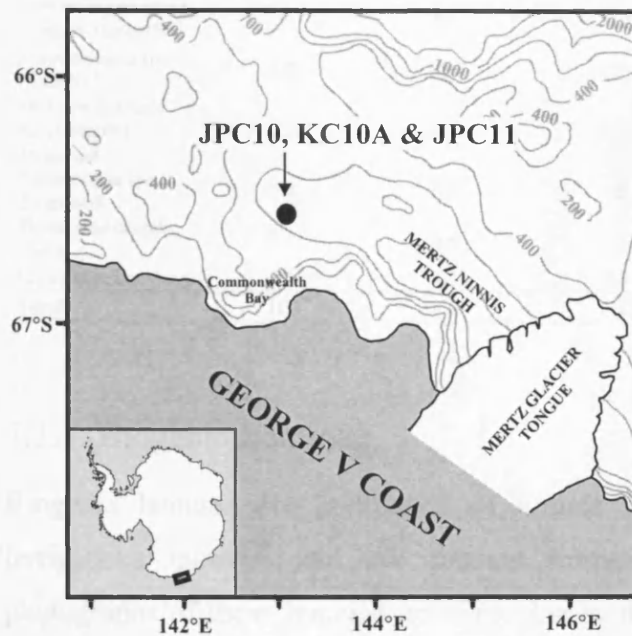
### 6.3. Conclusions

The Palmer Deep deglacial laminated interval has given an insight into seasonal and sub-seasonal variability within a period of rapid climate change, which has implications for understanding the effect of current warming experienced on the Antarctic Peninsula. The deglacial sedimentary interval consists of laminae or thin beds of orange-brown diatom ooze alternating with blue-grey terrigenous sediments. These result from seasonal depositional events. *Hyalochaete Chaetoceros* spp. resting spores (CRS) overwhelmingly dominate the orange-brown laminae and result from early spring sedimentation associated with stratified surface waters and a freshwater cap, trapping nutrients and promoting exceptionally high primary productivity. Productivity decreased during deglaciation as the West Antarctic Ice Sheet (WAIS) retreated. A more open-water Antarctic diatom assemblage (e.g. *Corethron pennatum*, *Coscinodiscus bouvet* and *Thalassiosira antarctica*) characterises the blue-grey terrigenous-rich laminae, which result from summer/autumn sedimentation associated with increased terrigenous input, and relate to ice-free, more open water, lower nutrient conditions following total melt of seasonal sea ice. The terrigenous laminae thickness decreases unevenly up-core, suggesting the melting ice sheet retreated shoreward in pulses during the deglaciation. Sea ice cover in the winter prevents any sedimentation. During the deglaciation, sub-seasonal summer diatom blooms are observed. High abundances of CRS, *C. bouvet*, *C. pennatum*, *Odontella weissflogii* resting spores (RS) and *T. antarctica* RS relative to the remaining assemblage are observed repeatedly through the summer laminae, suggesting changes in shelf waters throughout the summer. Starting from the base of the summer laminae, a sequence of sub-laminae species has been ascertained: CRS, *C. bouvet*, *C. pennatum*, *O. weissflogii* RS and finally *T. antarctica* RS. High tides in austral summer and autumn and high cyclone intensity are proposed as possible causes that could have introduced conditions which enhanced specific species productivity. However, I believe the most likely cause of the multiple sub-seasonal bloom laminae is the upwelling of Circumpolar Deep Water induced by the sub-seasonal variation in the impingement of Antarctic Circumpolar Current onto the continental shelf. After the collapse of the glacial ice sheet, oceanographic and biological systems responded rapidly, early on in the reinstatement of Upper Circumpolar Deep Water upwelling onto the continental shelf. By understanding the responses of diatoms to the retreat of the West Antarctic

Ice Sheet and changing oceanographic conditions during the last deglaciation, a better understanding has been gained of how they may respond to future periods of rapid climate change.

## 7. Mertz Ninnis Trough

This chapter presents the results and interpretations of backscattered electron imagery (BSEI) analysis, secondary electron imagery (SEI) analysis and quantitative diatom assemblage counts from NBP0101 JPC 10 and KC10A, Mertz Ninnis Trough, East Antarctica (Figure 7.1). The diatom count data used to construct Tables 7.1 – 7.6 can be found in appendix 4. Part of this chapter has been submitted for publication (Maddison *et al.*, “Post-glacial seasonal diatom record: an early record of the Mertz Glacier Polynya, East Antarctic Margin”).



**Figure 7.1**

Location map of NBP0101 JPC10 and KC10A, Mertz Ninnis Trough, George V coast. Contours in metres. Adapted from Leventer (1992).

### 7.1. Results NBP0101 JPC10

The post-glacial laminae from NBP0101 JPC10 are classified according to the dominance of terrigenous or biogenic components and diatom assemblages. *Hyalochaete Chaetoceros* spp. (resting spores and vegetative cells) overwhelmingly dominate the laminated sediment (78.8 - 93.8 % of all assemblages, Table 7.1), therefore minor constituents of the assemblage, which are highly visible in the BSEI photographs, are used to categorise the lamina types. The relative and absolute diatom abundances of each lamina type represent an average of five counts conducted on each type of lamina (see appendix 4, Tables A4.2.1.1 – A4.2.1.4 for original counts). Detailed NBP0101 JPC10 core lithology, sample depths and chronological information are presented in chapter 4 and analytical methods used can be found in chapter 5.

**Table 7.1**

Relative abundance of all diatom species by lamina type, Mertz Ninnis Trough, NBP0101 JPC10. CRS = *Hyalochaete Chaetoceros* spp. resting spores. RS = resting spores.

Species / Lamina type	Biogenic			Terrigenous		
	Near-monogeneric CRS laminae	Laminae characterised by <i>Corethron pennatum</i>	Laminae characterised by <i>Rhizosolenia</i> spp.	Mixed diatom assemblage laminae	Mixed diatom assemblage laminae	Sub-laminae characterised by <i>Porosira glacialis</i> RS
<i>Hyalochaete Chaetoceros</i> spp. resting spores Gran	90.5	78.8	80.4	84.8	85.3	93.8
<i>Corethron pennatum</i> (Grunow) Ostenfeld	0	6.9	0.3	0.4	0.2	0.1
<i>Fragilariopsis</i> spp. Hustedt	5.8	10.1	12.7	10.8	10.2	4.4
<i>Porosira glacialis</i> RS (Grunow) Jørgensen	0.2	0.1	0.2	0.3	0.4	0.2
<i>Rhizosolenia</i> spp. Brightwell	0.2	0.2	2	0.2	0.1	0
<i>Thalassiosira</i> spp. Cleve	0.7	0.6	1.1	1	1.2	0.3
Minor species	2.6	3.3	3.3	2.5	2.6	1.2
<b>Total:</b>	100	100	100	100	100	100

### 7.1.1. Biogenic Laminae

Biogenic laminae are composed of almost pure diatom ooze with very little terrigenous material and are present throughout the sampled interval. BSEI photographs of these laminae are dark due to the high porosity of the diatom ooze (Figure 7.2a, c, e and g). Four types of biogenic laminae are identified and described below.

#### 7.1.1.1. Near-monogeneric *Hyalochaete Chaetoceros* spp. Resting Spore Laminae

Laminae of this type are overwhelmingly composed of *Hyalochaete Chaetoceros* spp. resting spores (CRS) (Figure 7.2a and b). The minor constituents of the assemblage observed are *Fragilariopsis* spp., *Corethron pennatum* and *Rhizosolenia* spp.. CRS constitute on average 90.5% relative abundance of the total diatom assemblage (Table 7.1). *Chaetoceros* free counts are dominated by *Fragilariopsis* spp. (78.4%: the most dominant are *F. curta*, *F. rhombica*, *F. kerguelensis*, and *F. separanda*) and *Thalassiosira* spp. (10.9%) (Table 7.2). Sixty-two near-monogeneric CRS laminae are

present in the sampled interval (Figure 7.3). These laminae are present throughout the interval (Figure 7.4), ranging from 0.4 to 46.9 mm thick ( $n = 62$ ,  $\sigma = 6.6$  mm, mean = 5.1 mm), making up 15% of the total sediment thickness. There is no correlation between lamina thickness and core depth.

#### 7.1.1.2. Laminae Characterised by *Corethron pennatum*

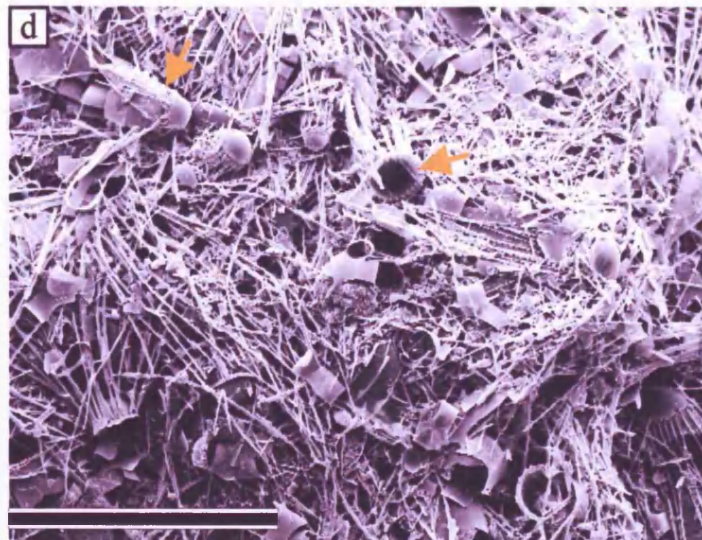
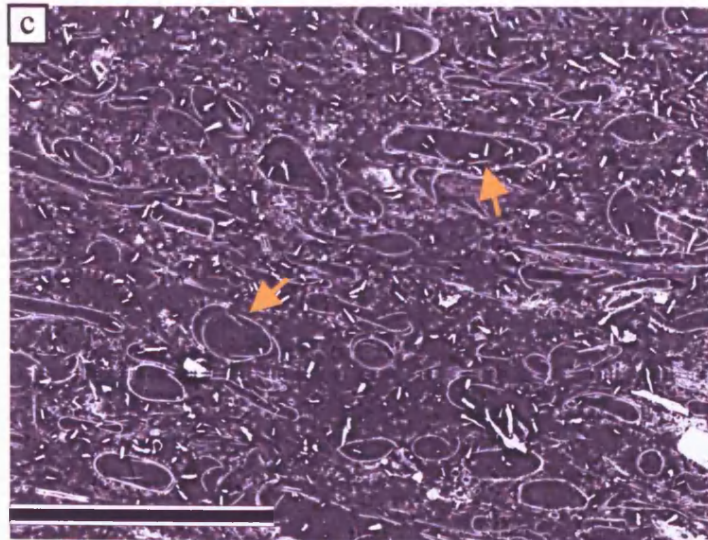
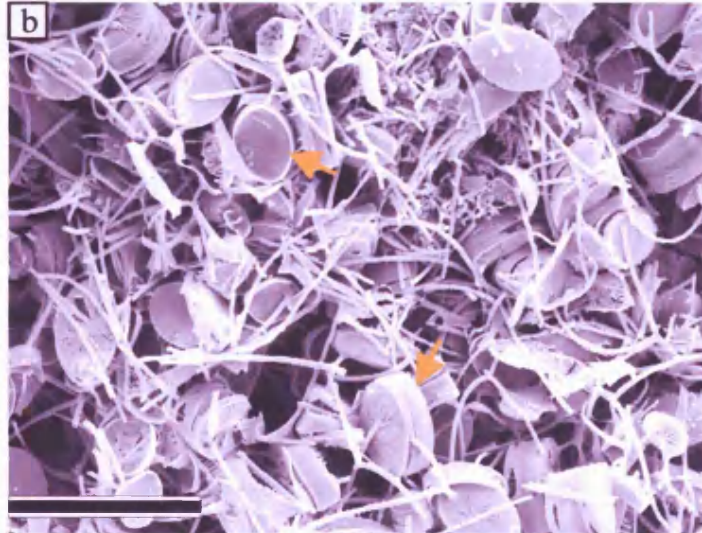
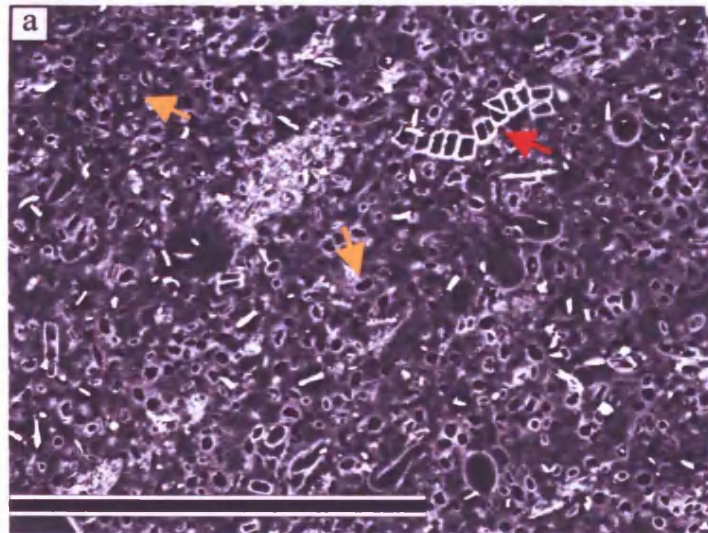
These laminae are characterised by *Corethron pennatum* (Figure 7.2c and d). The other constituents of the assemblage are CRS, *Fragilariopsis* spp. and *Rhizosolenia* spp.. CRS constitute on average 78.8 % relative abundance of the total diatom assemblage (Table 7.1). In the *Chaetoceros* free counts the most abundant species are *C. pennatum* (35.1 %), *Fragilariopsis curta* (23.5 %) and *F. cylindrus* (13.3 %) (Table 7.2). Twenty-eight laminae characterised by *C. pennatum* are distributed throughout the sampled interval (Figure 7.4) making up 25 % of the total sediment thickness (Figure 7.3). These laminae range in thicknesses from 2.1 to 81.0 mm ( $n = 29$ ,  $\sigma = 21.8$  mm, mean = 17.4 mm); half of these laminae have thicknesses over 10.0 mm, three of which are greater than 50.0 mm thick. There is no correlation between lamina thickness and core depth.

**Table 7.2**

Relative abundance of *Chaetoceros* spp. free diatom assemblage by lamina type, Mertz Ninnis Trough, NBP0101 JPC10. CRS = *Hyalochaete Chaetoceros* spp. resting spores. RS = resting spores.

Species / Lamina type	Biogenic			Terrigenous		
	Near-monogeneric CRS laminae	Biogenic laminae characterised by <i>Corethron pennatum</i>	Biogenic laminae characterised by <i>Rhizosolenia</i> spp.	Mixed diatom assemblage laminae	Mixed diatom assemblage laminae	Sub-laminae characterised by <i>Porosira glacialis</i> RS
<i>Corethron pennatum</i> (Grunow) Ostenfeld	0.4	35.1	1.2	3.9	1.5	3.9
<i>Fragilariopsis</i> spp. Hustedt	78.4	54.7	69.1	77.4	80.8	67
<i>Porosira glacialis</i> RS (Grunow) Jørgensen	3.2	1.7	1.8	3.8	2.3	11.4
<i>Rhizosolenia</i> spp. Brightwell	1.6	0.6	10.5	1.7	1.5	1.4
<i>Thalassiosira</i> spp. Cleve	10.9	4	7.5	7	8.8	9.7
Minor species	5.5	3.9	9.9	6.2	5.1	6.6
<b>Total:</b>	100	100	100	100	100	100





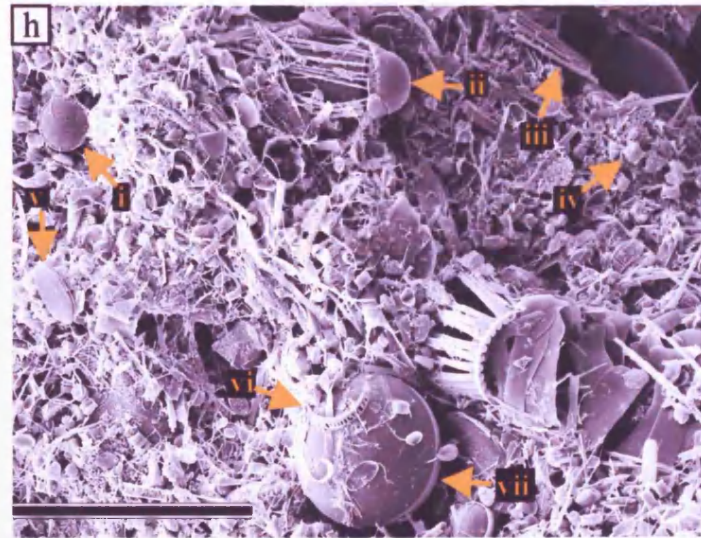
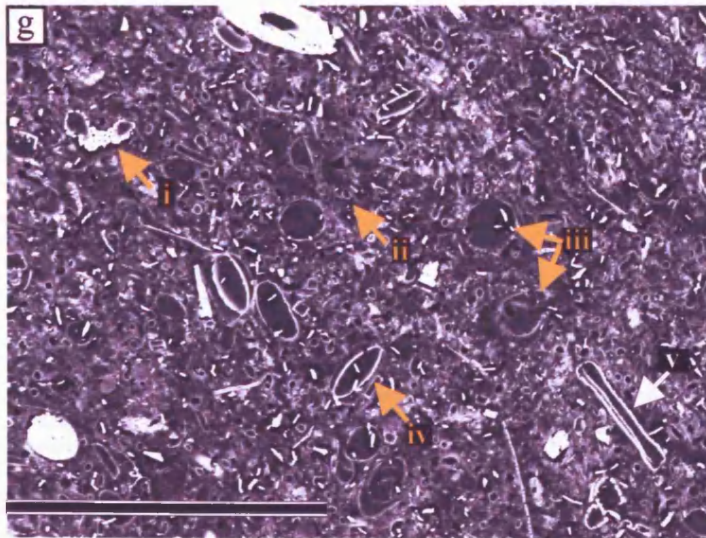
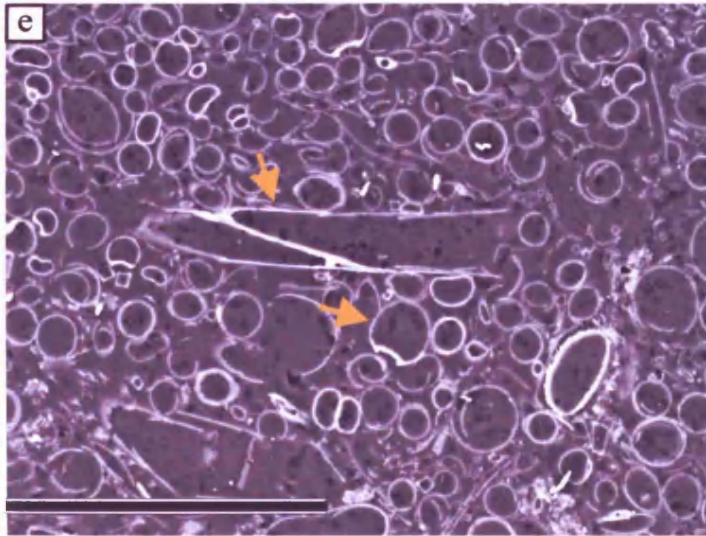
**Figure 7.2**  
Backscattered electron imagery (BSEI) and secondary electron imagery (SEI) photographs of five lamina types and one sub-lamina type, Mertz Ninnis Trough, NBP0101 JPC10.

(a) BSEI photograph of near-monogenic *Hyalochaete Chaetoceros* spp. resting spore (CRS) (gold arrows) laminae. Red arrow indicates a chain of *Fragilariopsis* spp.. Scale bar = 200 microns.

(b) SEI photograph of near-monogenic CRS (gold arrows) laminae. Scale bar = 20 microns.

(c) BSEI photograph of laminae characterised by *Corethron pennatum* (gold arrows). Scale bar = 200 microns.

(d) SEI photograph of laminae characterised by *C. pennatum* (gold arrows). Scale bar = 200 microns.



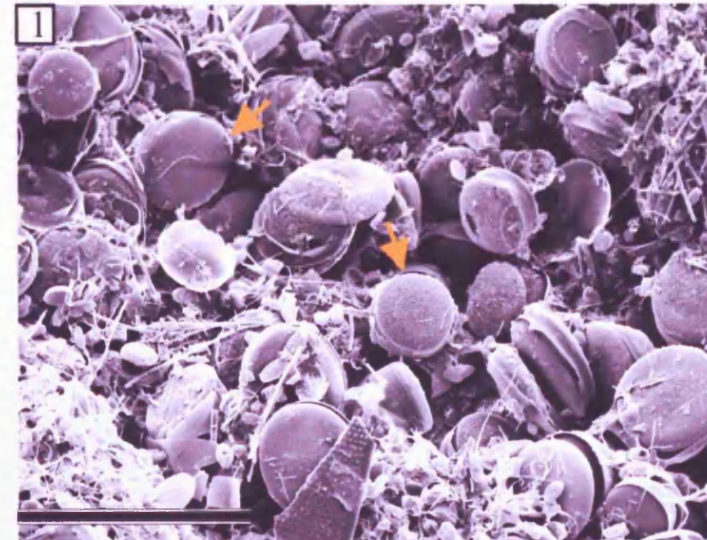
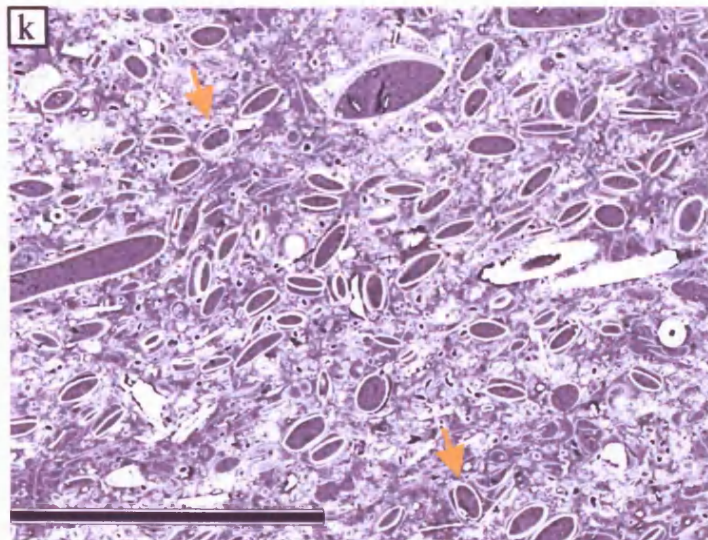
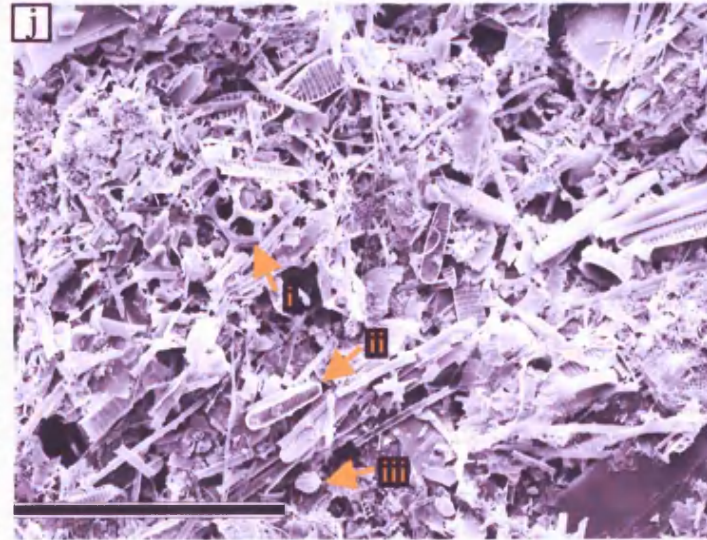
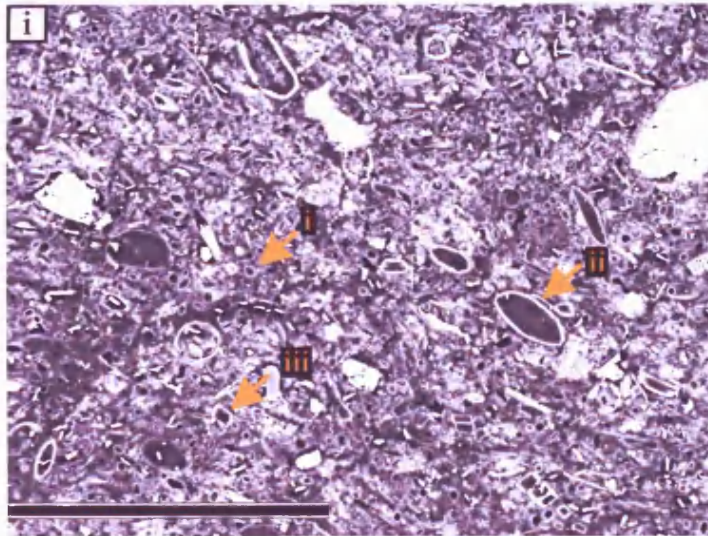
**Figure 7.2 continued**

(e) BSEI photograph of laminae characterised by *Rhizosolenia* spp. (gold arrows). Scale bar = 60 microns.

(f) SEI photograph of laminae characterised by *Rhizosolenia* spp.. Scale bar = 200 microns.

(g) BSEI photograph of mixed diatom assemblage laminae. Gold arrows (i) *Eucampia antarctica*, (ii) CRS, (iii) *C. pennatum*, (iv) *Porosira glacialis* resting spores (RS), (v) *Actinocyclus actinochilus*. Scale bar = 200 microns.

(h) SEI photograph of mixed diatom assemblage laminae. Gold arrows (i) *P. glacialis* RS, (ii) *C. pennatum*, (iii) *Fragilariopsis* spp. colony, (iv) CRS, (v) *F. rhombica*, (vi) *Dactyliosolen* girdle band and (vii) *Stellarima microtrias* RS. Scale bar = 100 microns.



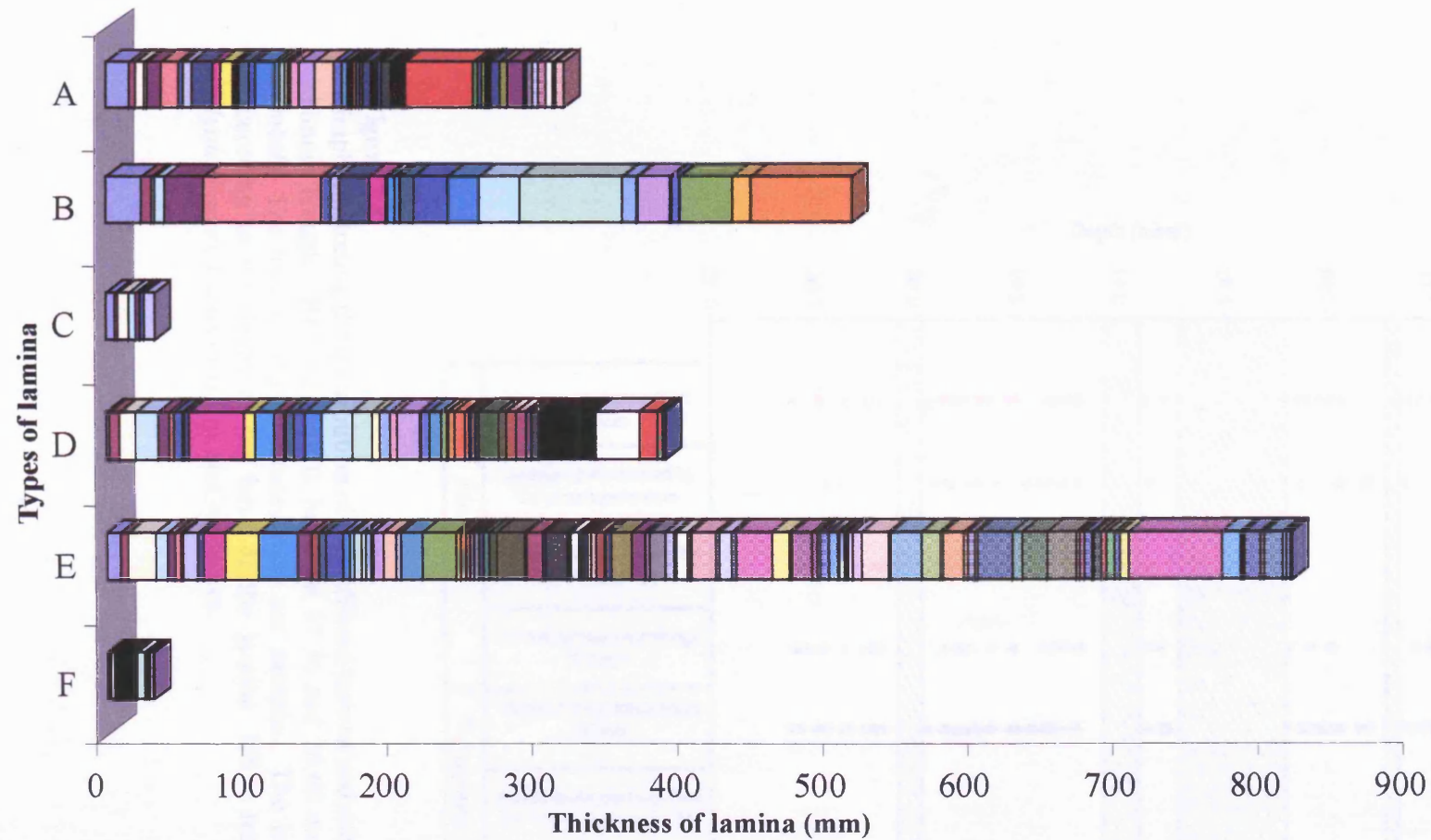
**Figure 7.2 continued**

(i) BSEI photograph of mixed diatom assemblage terrigenous laminae. Gold arrows (i) CRS, (ii) *P. glacialis* RS and (iii) *Fragilariopsis* spp.. Scale bar = 200 microns.

(j) SEI photograph of mixed diatom assemblage terrigenous laminae. Gold arrows (i) Silicoflagellate, (ii) *F. curta* and (iii) CRS. Scale bar = 50 microns.

(k) BSEI photograph of terrigenous sub-laminae characterised by *P. glacialis* RS (gold arrows). Scale bar = 300 microns.

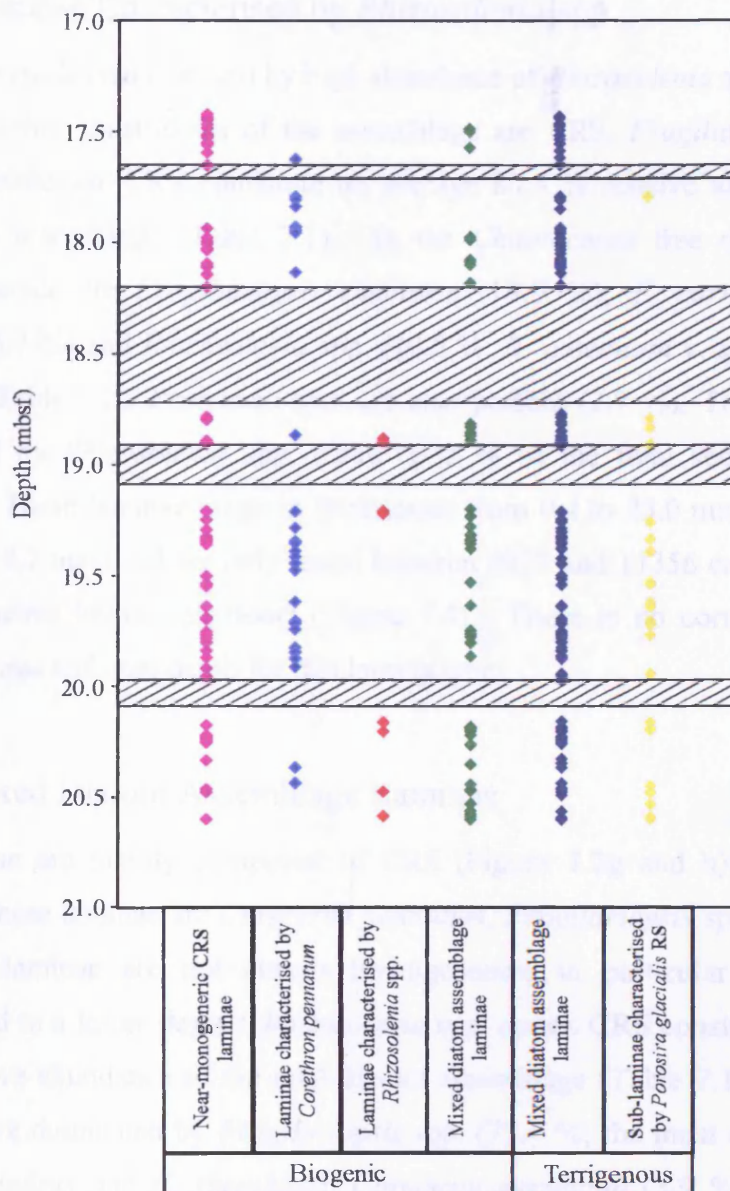
(l) SEI photograph of terrigenous sub-laminae characterised by *P. glacialis* RS (gold arrows). Scale bar = 100 microns.



**Figure 7.3**

Graph showing the thicknesses of different types of lamina and sub-lamina from Mertz Ninnis Trough (NBP0101 JPC10). Individual thicknesses are displayed as coloured bars within the total thickness of each lamina type.

A = Near-monogeneric *Hyalochaete Chaetoceros* spp. resting spore biogenic laminae; B = Biogenic laminae characterised by *Corethron pennatum*; C = Biogenic laminae characterised by *Rhizosolenia* spp.; D = Mixed diatom assemblage biogenic laminae; E = Mixed diatom assemblage terrigenous laminae; F = Terrigenous sub-laminae characterised by *Porosira glacialis* resting spores.



**Figure 7.4**

Graph illustrating the distribution of the different lamina and sub-lamina types, Mertz Ninnis Trough NBP0101 JPC10, between 17.36 and 20.60 metres below sea floor (mbsf). The hashed lines indicates core not sampled. The lamina are positioned according to the depth of the base of the lamina. RS = resting spores. CRS = *Hyalochaete Chaetoceros* spp. resting spores.

### 7.1.1.3. Laminae Characterised by *Rhizosolenia* spp.

This lamina type is characterised by high abundance of *Rhizosolenia* spp. (Figure 7.2e and f). The other constituents of the assemblage are CRS, *Fragilariopsis* spp. and *Corethron pennatum*. CRS constitute on average 80.4 % relative abundance of the total diatom assemblage (Table 7.1). In the *Chaetoceros* free counts the most abundant species are *Fragilariopsis rhombica* (19.9 %), *F. curta* (18.9 %), *F. cylindrus* (15.7 %) and *Rhizosolenia* spp. (10.5 %: *R. antennata* v. *semispina* and *R. species A*) (Table 7.2). *Proboscia* spp. are also present (2.7 %). The eight laminae characterised by *Rhizosolenia* spp. make up 2 % of the total sediment thickness (Figure 7.3). These laminae range in thicknesses from 0.4 to 23.0 mm ( $n = 8$ ,  $\sigma = 2.6$  mm, mean = 4.2 mm) and are only found between 8927 and 11356 cal. yrs BP (18.88 and 20.58 metres below sea floor) (Figure 7.4). There is no correlation between lamina thickness and core depth for this lamina type.

### 7.1.1.4. Mixed Diatom Assemblage Laminae

These laminae are mainly composed of CRS (Figure 7.2g and h). Minor species observed in these laminae are *Corethron pennatum*, *Fragilariopsis* spp., *Rhizosolenia* spp.. These laminae are not always homogeneous; in particular patches of *C. pennatum* and to a lesser degree, *Rhizosolenia* spp. occur. CRS constitute on average 84.8 % relative abundance of the total diatom assemblage (Table 7.1). *Chaetoceros* free counts are dominated by *Fragilariopsis* spp. (77.4 %; the most dominant are *F. curta*, *F. cylindrus* and *F. rhombica*), *Corethron pennatum* (3.9 %) and *Porosira glacialis* resting spores (RS) (3.8 %) (Table 7.2). Overall, diatoms are much less abundant in the mixed diatom assemblage lamina type than in the near-monogeneric CRS laminae. When compared to the near-monogeneric CRS laminae, the mixed diatom assemblage lamina type has a lower absolute abundance of *Hyalochaete* *Chaetoceros* spp. and *Rhizosolenia* spp., similar abundance of *Fragilariopsis* spp. and *P. glacialis* RS, but more abundant *C. pennatum* and *Thalassiosira* spp. (Table 7.3). The forty-five mixed diatom assemblage laminae present in the interval make up 18 % of the total sediment thickness (Figure 7.3). These laminae range in thicknesses from 0.5 to 38.0 mm ( $n = 45$ ,  $\sigma = 8.7$  mm, mean = 8.5 mm) and are present

throughout the sampled interval (Figure 7.4). There is no correlation between lamina thickness and core depth for this lamina type.

**Table 7.3**

Absolute abundance of diatom species (valves per gramme of dry sediment  $\times 10^6$ ) by lamina type, Mertz Ninnis Trough, NBP0101 JPC10. CRS = *Hyalochaete Chaetoceros* spp. resting spores. RS = resting spores.

Species / Lamina type	Biogenic			Terrigenous		
	Near-monogeneric CRS laminae	Biogenic laminae characterised by <i>Corethron pennatum</i>	Biogenic laminae characterised by <i>Rhizosolenia</i> spp.	Mixed diatom assemblage laminae	Mixed diatom assemblage laminae	Sub-laminae characterised by <i>Porosira glacialis</i> RS
<i>Hyalochaete Chaetoceros</i> spp. resting spore Gran	4198.5	1238	1642.7	2639.7	1659.1	3629.8
<i>Corethron pennatum</i> (Grunow) Ostenfeld	2.5	98.4	3.3	11.3	3.3	3.4
<i>Fragilariopsis</i> spp. Hustedt	192.7	146.2	179	231.9	201.6	103.8
<i>Porosira glacialis</i> RS (Grunow) Jørgensen	10.4	1.3	2.5	9.9	6.9	5.7
<i>Rhizosolenia</i> spp. Brightwell	8.7	3.1	23.1	3.1	1.4	0
<i>Thalassiosira</i> spp. Cleve	17.1	6.3	15.2	27	21	8.3
Minor species	75.3	44.2	49.5	69.3	39.8	41.3
<b>Total:</b>	<b>4505.2</b>	<b>1537.5</b>	<b>1915.3</b>	<b>2992.2</b>	<b>1933.1</b>	<b>3792.3</b>

### 7.1.2. Terrigenous Laminae

Diatom-bearing terrigenous laminae have a greater number of terrigenous grains such as ice-rafted silt and clay relative to the biogenic laminae. There is variation in size (clay to sand) and amount of terrigenous grains between laminae. The BSEI photographs of these laminae are light due to the high average atomic number of the grains (Figure 7.2i and k).

#### 7.1.2.1. Mixed Diatom Assemblage Terrigenous Laminae

Laminae of this type are characterised by a diatom assemblage that is near-monogeneric CRS (Figure 7.2i and j), however a more diverse minor diatom assemblage (includes the species: *Corethron pennatum*, *Coscinodiscus bouvet*, *Fragilariopsis* spp., *Porosira glacialis* resting spores (RS), *Stellarima microtrias* RS, and to an even more minor extent *Eucampia antarctica*, *Rhizosolenia* spp., *Trigonium arcticum*) is present than is seen in the biogenic mixed diatom assemblage laminae.

CRS constitute on average 85.3% relative abundance of the total diatom assemblage (Table 7.1). *Chaetoceros* free counts show the minor assemblage is dominated by *Fragilariopsis* spp. (80.8 %: the most dominant are *F. curta*, *F. kerguelensis* and *F. rhombica*) and *Thalassiosira* spp. (8.8 %). Both *C. pennatum* and *Rhizosolenia* spp. have relative abundances of 1.5 % (Table 7.2). The one hundred and twelve mixed diatom assemblage terrigenous laminae present in the interval make up 39 % of the total sediment thickness (Figure 7.3). These laminae are present throughout the sampled interval (Figure 7.4) and range in thicknesses from 0.4 to 64.3 mm ( $n = 112$ ,  $\sigma = 8.3$  mm, mean = 7.3 mm). There is no correlation between lamina type and core depth.

#### 7.1.2.2. Terrigenous Sub-laminae Characterised by *Porosira glacialis* Resting Spores

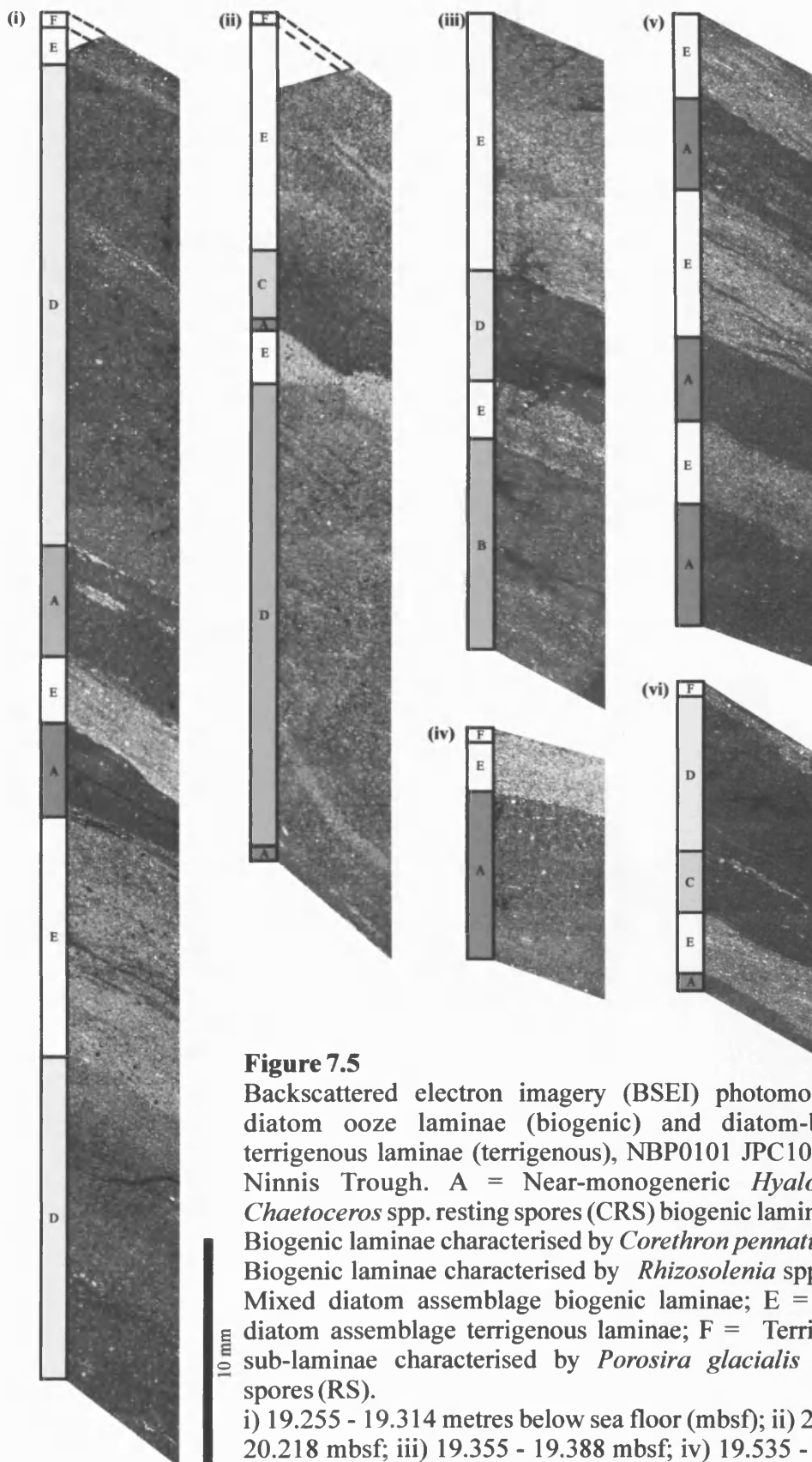
BSEI and SEI reveal this sub-lamina type is characterised by *Porosira glacialis* resting spores (RS) (often observed within vegetative remains) (Figure 7.2k and l). These sub-laminae are found within, and mostly at the top of, the mixed diatom assemblage terrigenous laminae. Occasionally *P. glacialis* RS dominate the assemblage of thin terrigenous laminae (1.0 - 2.0 mm thick). CRS constitute on average 93.8 % relative abundance of the total diatom assemblage (Table 7.1). In the *Chaetoceros* free counts the most abundant species are *Fragilariopsis curta* (32.8 %), *F. rhombica* (18.3 %) and *P. glacialis* RS (11.4 %) (Table 7.2). The twenty-three terrigenous sub-laminae characterised by *P. glacialis* RS present in the interval make up 2 % of the total sediment thickness sampled (Figure 7.3). These sub-laminae range in thickness from 0.5 to 5.5 mm ( $n = 23$ ,  $\sigma = 1.1$  mm, mean = 1.4 mm) and become less common after 7370 cal. yrs BP (above 17.79 mbsf) (Figure 7.4). There is no correlation between sub-lamina type and core depth.

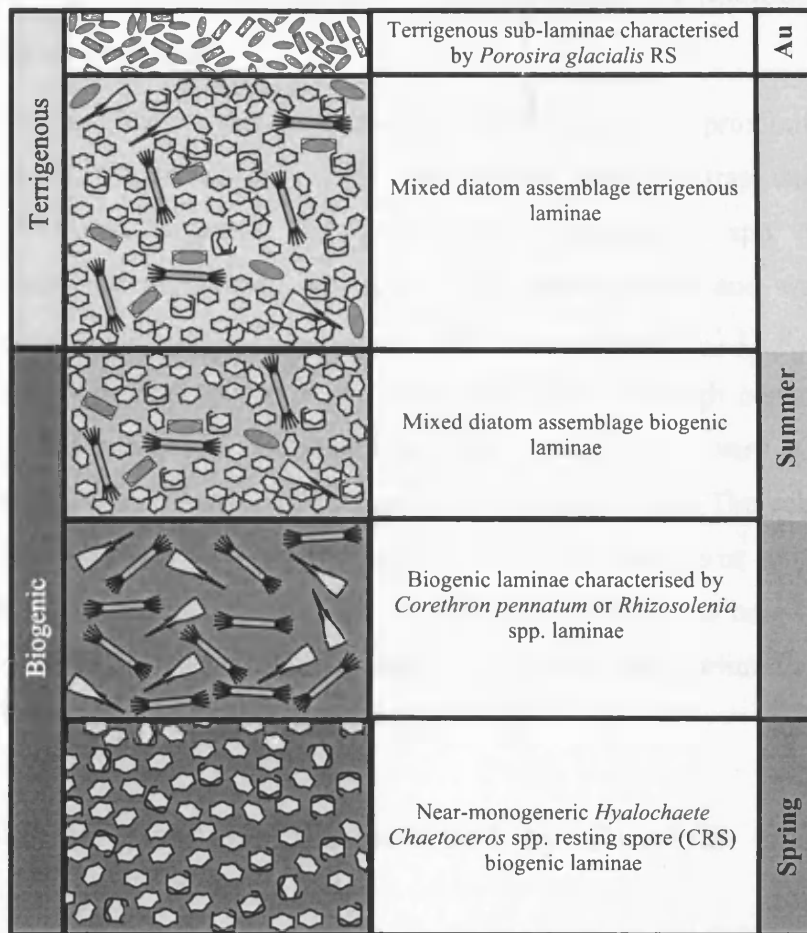


### 7.1.3. Lamina Relationships

Two hundred and fifty-six laminae and twenty-three sub-laminae are present in the laminated intervals analysed (Appendix 3, Table A3.2.1). Out of all the lamina and sub-lamina types, the near-monogeneric CRS laminae show the greatest absolute abundance,  $4505 \times 10^6$  valves per gramme (Table 7.3). Laminae characterised by *Corethron pennatum* and *Rhizosolenia* spp. and the mixed diatom assemblage terrigenous laminae show the lowest abundance, ranging from  $1538 - 1933 \times 10^6$  valves per gramme dry sediment (Table 7.3). The terrigenous sub-laminae characterised by *Porosira glacialis* resting spores (RS) has the second highest abundance,  $3792 \times 10^6$  valves per gramme. There is no correlation between the thickness of any of the lamina and sub-lamina types with core depth. Lamina boundaries in this post-glacial interval are gradational, with occasionally minor bioturbation.

Variable combinations of the different types of lamina have been observed (Figure 7.5), however, a typical succession of the lamina types upcore can be defined as: (i) near-monogeneric *Hyalochaete Chaetoceros* spp. resting spore (CRS) laminae, (ii) laminae characterised by *Corethron pennatum*, (iii) laminae characterised by *Rhizosolenia* spp., (iv) mixed diatom assemblage laminae, (v) mixed diatom assemblage terrigenous laminae, and finally (vi) terrigenous sub-laminae characterised by *Porosira glacialis* RS (Figure 7.6).





**Figure 7.6**

Schematic representation of the biogenic and terrigenous laminae and terrigenous sub-laminae succession in laminated interval, Mertz Ninnis Trough, NBP0101 JPC10. RS = resting spores.

## 7.2. Interpretation and Discussion NBP0101 JPC10

### 7.2.1. Seasonal Signal

The high values of absolute abundances in all of the lamina types indicate that primary productivity was high throughout the growing season. The overwhelming dominance of *Hyalochaete Chaetoceros* spp., in all of the lamina types, shows that conditions for this sub-genus were favourable during the entire growing season. The ecology of diatom species discussed in the following sections are described in greater detail in chapter 3, section 3.5.

### 7.2.1.1. Spring: Near-monogeneric *Hyalochaete Chaetoceros* spp. Resting Spore Laminae

In Antarctica, the *Hyalochaete Chaetoceros* sub-genus favours proximity to sea ice (Leventer, 1991; Crosta *et al.*, 1997) and modern sediment trap data from the Antarctic Peninsula suggests that *Hyalochaete Chaetoceros* spp. blooms are associated with the melting of sea ice in the austral spring and water column stratification (Leventer, 1991; Crosta *et al.*, 1997) (see section 3.5.3.1). Resting spores are a survival strategy response to environmental stress and high concentrations of CRS in the sediments are interpreted as being indicative of very high primary productivity in surface waters (Donegan and Schrader, 1982). The relatively high numbers of *Fragilariopsis curta* and *F. cylindrus* in the *Chaetoceros* spp. free diatom assemblage also indicate the existence of sea ice, therefore, the near-monogeneric *Hyalochaete* CRS laminae are interpreted as reflecting high primary productivity associated with water column stratification in spring.

### 7.2.1.2. Summer: Laminae Characterised by *Corethron pennatum* or *Rhizosolenia* spp.

The diatom assemblages of these two biogenic laminae are characterised by different genera. However, they are associated with similar water column conditions (see sections 3.5.5 and 3.5.21) and, therefore, will be discussed together for the rest of the chapter.

*Corethron pennatum* occurs in open water (Fryxell and Hasle, 1971) and has positive buoyancy (Crawford, 1995) which suggests that it may be able to exploit a well-stratified water column, migrating down to take advantage of higher nutrient content at depth and up for higher light levels for photosynthesis (Leventer *et al.*, 2002) to maximise bloom conditions. Deterioration in the water column stability during the summer to autumn transition could potentially trigger a mass sinking of the bloom (Kemp *et al.*, 2000). Relatively high numbers of *Fragilariopsis curta* and *F. cylindrus* in the *Chaetoceros* spp. free diatom assemblage implies that sea ice was still present in the area. Therefore, laminae characterised by *C. pennatum* are interpreted as being deposited in summer when more stable open water conditions prevail in front of the sea ice edge.

*Rhizosolenia* spp. bloom and form mats in open water conditions (Harbison *et al.*, 1977; Alldredge and Silver, 1982; Kemp *et al.*, 1999). Leventer *et al.* (2002) have suggested the presence of *Rhizosolenia* spp. and *Proboscia* spp. below the thermocline is associated with strong summer surface water stratification and the mass sedimentation of the blooms as a result of strong mixing of the water column in autumn. Villareal *et al.* (1993; 1996) have shown that *Rhizosolenia* spp. migrate up and down in the water column, to increased depths to acquire nutrients and return to the nutrient poor surface waters to photosynthesise. Sea ice is present as suggested by *Fragilariopsis curta* and *F. cylindrus* in the *Chaetoceros* spp. free diatom assemblage. Therefore, laminae characterised by *Rhizosolenia* spp. are interpreted as summer blooms when stable open oligotrophic water conditions prevail in front of the sea ice edge.

#### 7.2.1.3. Summer: Mixed Diatom Assemblage Biogenic Laminae

The more mixed assemblage of these laminae (less *Hyalochaete Chaetoceros* spp. and more *Corethron pennatum*, *Thalassiosira* spp. and *Porosira glacialis*) suggests a less stratified, more mixed water column. The presence of *Corethron pennatum* and, to a lesser degree, *Rhizosolenia* spp. patches within the laminae suggest that stable open water conditions lasted for relatively short periods of time during this season. Mixing and the resultant destabilisation of the water column would cause mass sedimentation of the colonial diatoms and allow a more mixed assemblage to return.

#### 7.2.1.4. Summer / Autumn: Mixed Diatom Assemblage Terrigenous Laminae

The terrigenous component of these mixed diatom assemblage laminae represents the input of ice rafted material from the Mertz Glacier Tongue, sediments from “dirty” sea ice and / or Modified Circumpolar Deep Water (MCDW) entrained fine grained sediments (Dunbar *et al.*, 1985; Domack, 1988; Rintoul, 1998; Bindoff *et al.*, 2001).

The species within this summer / autumn laminae such as *Corethron pennatum* and *Rhizosolenia* spp. are considered to be indicative of open water conditions with little influence of sea ice (Fryxell and Hasle, 1971; Harbison *et al.*, 1977; Alldredge and Silver, 1982; Watanabe, 1982; Makarov, 1984; Leventer and Dunbar, 1987). However

Marra and Boardman (1984) found *C. pennatum* to be part of ice edge phytoplankton and *R. antennata* f. *semispina*, the most dominant *Rhizosolenia* spp. present in this laminae diatom assemblage (see appendix 4, table A4.2.1.4), has been reported in open ocean to sublittoral sea ice habitats (Ligowski, 1993). *Porosira glacialis* is associated with waters adjacent to the coast or sea ice, in particular, slush and wave exposed shore ice (Krebs *et al.*, 1987), but does not live within the ice (Watanabe, 1988; Scott *et al.*, 1994). *Coscinodiscus bouvet* is a neritic species and *Stellarima microtrias* is associated with shelf ice and the surrounding shelf waters (Hasle *et al.*, 1988). High abundances of *S. microtrias* have been observed in summer fast sea ice (Watanabe, 1982; Krebs *et al.*, 1987; Tanimura *et al.*, 1990) and during autumn, the resting spore is found in high abundances under sea ice and is not present in the open ocean (Fryxell, 1989). *Trigonium arcticum* lives epiphytically on algae (possibly saprophytic) at a depth of 200-300 m in the water column (Hendey, 1937; Thomas, 1966). Therefore, it is likely that this species is swept into the Mertz Ninnis Trough from the broad, relatively shallow Adélie and Mertz Banks by High Salinity Shelf Water (HSSW) (Figure 2.13 and 2.17). The terrigenous component and the diatom assemblage suggests that this lamina type was deposited in summer / autumn when open water conditions were impinged upon by the growth of sea ice and there was an increase in bottom water currents.

#### 7.2.1.5. Autumn: Terrigenous Sub-laminae Characterised by *Porosira glacialis* Resting Spores

This sub-seasonal *Porosira glacialis* bloom and consequent resting spore formation implies that a specific environmental condition repeatedly occurred during the autumn. The relationship of this species with sea ice (Krebs *et al.*, 1987; Watanabe, 1988; Scott *et al.*, 1994) suggests that sea ice formation overwhelmed aspects of circulation and associated biogenic productivity in the area resulting in resting spore formation.

### 7.2.2. Lamina Relationships

The difference in absolute abundance of diatoms between the different types of lamina results from changes in the water column stability and surface water nutrient levels. As the sea ice melts in the spring, stratification of the water column traps nutrients derived from the sea ice itself, MCDW (water mass reaches surface waters in winter) and atmospheric particles (particle concentrations reach a maximum in late spring and early summer (Tuncel *et al.*, 1989; Wagenbach, 1996)). These elevated nutrient levels and stratified waters in spring would have been conducive to high primary productivity and the formation of near-monogeneric CRS laminae. The rapid growth of *Hyalochaete Chaetoceros* spp. blooms (Grimm *et al.*, 1996; 1997; Alldredge and Gotschalk, 1989) would have depleted the nutrients in the water column; this along with more stable open water conditions would have allowed the laminae characterised by *Corethron pennatum* and *Rhizosolenia* spp. to be produced in summer. Water column mixing due to storms elevates surface water nutrient levels increasing productivity to levels recorded in the mixed diatom assemblage laminae. A further bio-depletion of these nutrients and an introduction of terrigenous material would induce a decrease in productivity to levels observed in the mixed diatom assemblage terrigenous laminae. In autumn the cooling of surface waters enables upwelling of nutrient rich-MCDW to re-supply surface waters, replenishing the waters depleted by phytoplankton growth. The proximity of sea ice and increased nutrients promote high productivity, resulting in the formation of the terrigenous sub-laminae characterised by *Porosira glacialis* resting spores (RS) at the end of the growing season, before light levels are too low to prevent growth.

A transition from summer/autumn terrigenous laminae to spring /summer biogenic laminae suggests that there was little or no deposition in the winter. Although the different types of laminae always occur in same sequence relative to each other in the laminated interval (Figure 7.6), not every annual sedimentary increment contains each of the six types of laminae (Figure 7.5). I suggest that this is the result of annual variability in the dynamics of the Mertz Glacier Polynya. The analysed laminated interval is not varved because annual deposition consists of sequences of laminae which are not rhythmically repeated. The average accumulation rate calculated from annual laminae deposition is 1.7 cm/yr. Markov chain analysis was not conducted on

this laminated interval since there were insufficient lamina transitions between laminae and sub-lamina to ensure reliable results.

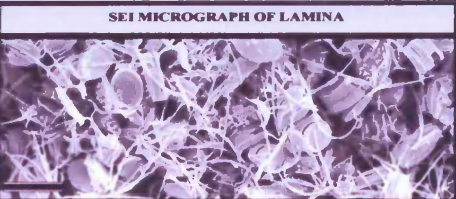

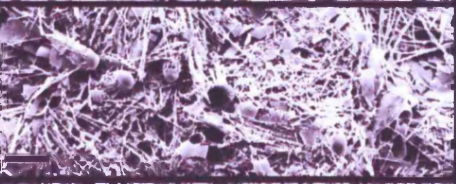
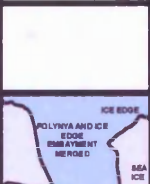
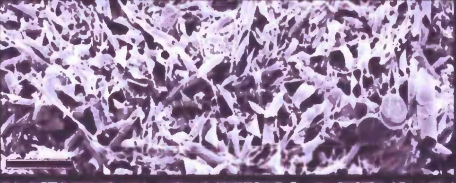



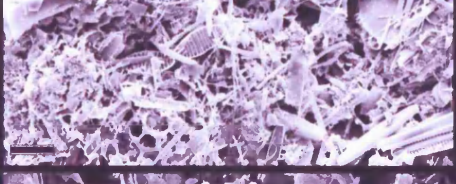

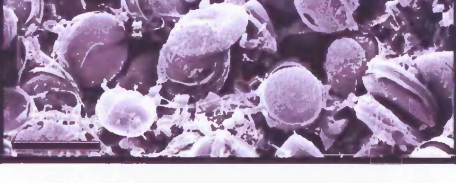

### 7.2.3. Polynya Model for Mertz Ninnis Trough Laminated Sediments

The East Antarctic Ice Sheet (EAIS) grounding line reached the edge of the continental shelf at the last glacial maximum (Figure 2.13) (Domack, 1982; Barnes, 1987; Eitrem *et al.*, 1995) and the transition from subglacial to glacial-marine sedimentation occurred prior to ~9000 yrs BP (Domack *et al.*, 1991). Open water conditions and sea ice would therefore have prevailed in the region following ice sheet retreat, when the laminated sediments were deposited. Today the Mertz Glacier Polynya is active above the NBP0101 JPC10 core site and is considered likely to play a part in the intensity and distribution of plankton growth (Sambrotto *et al.*, 2003). I believe post-glacial polynya dynamics increased diatom productivity and the length of growing season uniquely enhancing seasonal diatom deposition relative to other continental shelf conditions.

#### 7.2.3.1. Spring

In the spring solar radiation levels start to rise, melting the polynya sea ice margins and increasing open water area. A change in heat regime from latent heat to a sensible heat polynya occurs. Nutrient-rich MCDW is prevented from reaching surface waters by sea ice melt-induced water column stratification. However, a finite amount of nutrients, already supplied to surface waters during winter upwelling of MCDW, is trapped by the stratification. The reduced sea ice cover would allow elevated phytoplankton production to occur early in the growing season, just after the spring equinox (Sambrotto *et al.*, 2003). These stratified, nutrient-rich waters promote *Hyalochaete Chaetoceros* spp. blooms. Katabatic winds in Adélie Land have been shown to be intense and frequent through the growing season (Périard and Pettré, 1993) which can cause intermittent mixing of the stratified surface waters. Environmental stress created by this disruption would cause resting spore formation and the resultant deposition of near-monogeneric CRS laminae (Figure 7.2a and b & Figure 7.7a).



SEASON	LAMINA	LAMINA SPECIES ASSEMBLAGE	SEI MICROGRAPH OF LAMINA	POLYNYA HEAT STATUS	WATER CONDITIONS	POLYNYA AREAL EXTENT
A SPRING	BIOGENIC LAMINAE	NEAR-MONOGENERIC <i>HYALOCHATE</i> <i>CHAETOCEROS</i> SPP RESTING SPORE		LATENT ↓ SENSIBLE HEAT POLYNYA	SEA ICE MELT AROUND THE MARGINS OF THE POLYNYA STRATIFIED WATER COLUMN.	
B SPRING / SUMMER	BIOGENIC LAMINAE	CHARACTERISED BY <i>CORETHRON PENNATUM</i>		SENSIBLE HEAT POLYNYA	ICE EDGE MARGIN MELTS FORMING AN EMBAYMENT WHICH MERGES WITH POLYNYA BY OCTOBER. STABLE OPEN WATER.	
C SPRING / SUMMER	BIOGENIC LAMINAE	CHARACTERISED BY <i>RHIZOSOLENIA</i> SPP.		SENSIBLE HEAT POLYNYA	ICE EDGE MARGIN MELTS FORMING AN EMBAYMENT WHICH MERGES WITH POLYNYA BY NOVEMBER. MIXED WATER COLUMN.	
D SUMMER	BIOGENIC LAMINAE	MIXED DIATOM ASSEMBLAGE (SEE SECTION 7.1.1.4).		SENSIBLE HEAT POLYNYA	REDUCED SEA ICE MELT AND INCREASED WATER DENSITY. MIXED WATER COLUMN. ENTRAINED FINE GRAINED SEDIMENT TERRIGENOUS SOURCE	
E SUMMER	TERRIGENOUS LAMINAE	MIXED DIATOM ASSEMBLAGE (SEE SECTION 7.1.2.1).		SENSIBLE HEAT POLYNYA	SEA ICE FORMS AND POLYNYA REDUCES IN SIZE. HOMOGENEOUS WATER COLUMN. ENTRAINED FINE GRAINED SEDIMENT TERRIGENOUS SOURCE	
F SUMMER / AUTUMN	TERRIGENOUS SUB-LAMINAE	CHARACTERISED BY <i>POROSIRA GLACIALIS</i> RESTING SPORES		SENSIBLE ↓ LATENT HEAT POLYNYA		

**Figure 7.7** Summary table displaying polynya model and seasonal information responsible for the formation of multiple types of laminae through the deglaciation. (A) Scale bar = 10 microns; (B, C, D, F) Scale bar = 50 microns; and (E) Scale bar = 20 microns. MGT=Mertz Glacier Tongue

### 7.2.3.2. Summer

The continued high solar radiation in the region provides a continuous flux of heat further melting the sensible heat polynya margins. The sea ice edge at the shelf break also melts. Two scenarios can occur, which control the type of laminae deposited:

1. Occasionally an embayment in the sea ice edge encroaches far enough to join the polynya by October. This has been observed to occur in 16% of winter months between 1987 and 1994 (Massom *et al.* 1998).
2. The sea ice edge embayment retreats later in the season, reaching the polynya by November and the coast by December. This has been observed to be an annual occurrence (Massom *et al.* 2003).

Both of these scenarios produce open water conditions with little sea ice influence. Weak katabatic winds permit a stable water column to be created throughout the summer (Périard and Pettré, 1993). The open water conditions, created by October in scenario one, would allow open water adapted species such as *Corethron pennatum* and *Rhizosolenia* spp. to become established early in the season. The ability of these particular species to take advantage of nutrients trapped lower in the water column would allow large prolonged blooms to occur. This would result in thick biogenic laminae characterised by *C. pennatum* or *Rhizosolenia* spp. (Figure 7.2c, d, e and f & Figure 7.7b and c).

A greater number of mixed diatom assemblage laminae than laminae characterised by *C. pennatum* or *Rhizosolenia* spp. indicates that open water conditions created later in the season is the more common scenario. The reduced growing season time with open water conditions means that *C. pennatum* and *Rhizosolenia* spp. are unable to establish a dominant bloom; therefore other diatom species are able to flourish. This results in a mixed diatom biogenic laminae being deposited, occasionally with patches characterised by *C. pennatum* and *Rhizosolenia* spp. (Figure 7.2g & Figure 7.6d).

### 7.2.3.3. Summer / Autumn

A reduction in sea ice melting around the polynya margin creates denser surface waters, allowing upwelling MCDW to reach surface waters. Water column stratification is discontinued, creating conditions suitable for a mixed diatom assemblage. The upwelling of MCDW onto the continental shelf entrains fine grained

terrigenous sediments, which are transported landwards and deposited in the Mertz Ninnis Trough. The terrigenous input into the laminae dilutes the biogenic component (Figure 7.2i and j & Figure 7.7e) forming the mixed diatom assemblage terrigenous laminae.

#### 7.2.3.4. Autumn

Solar radiation levels decrease which results in a return to latent heat conditions, where heat loss to the atmosphere is balanced by the latent heat of fusion of ice that continuously forms (Mysak and Huang, 1992). The reduction of polynya areal extent results in increased proximity of sea ice and marginally elevated seawater salinities, coincidental with the strongest annual average winds (Périard and Pettré, 1993) which in combination, would create conditions ideal for the growth and subsequent deposition of the terrigenous sub-laminae characterised by *Porosira glacialis* resting spores (Figure 7.2k and l & Figure 7.6f).

#### 7.2.3.5. Winter

The latent heat polynya has reduced in size as an increase in ice production is associated with colder temperatures, along with a relatively constant rate of ice advection (Pease, 1987; Darby *et al.*, 1995). Light levels are too low for productivity (from May to August); therefore biogenic input to the sediment dramatically decreases, resulting in a hiatus between autumn and spring. MCDW is unrestricted by stratification and is able to reach surface waters, replenishing them with nutrients for the following growing season.

### 7.3. Conclusions NBP0101 JPC10

The presence of laminae at the base of NBP0101 JPC10 suggests that seasonal sea ice formation was active when the laminated sediments at the base of the core were deposited. The different types of lamina observed throughout NBP0101 JPC10, as set within the context of the polynya model, indicate that the Mertz Glacier Polynya was active during early post-glacial times and, therefore, the Mertz Glacier Tongue also must have existed at this time to act as an obstacle for sea ice drift. It has been proposed that if the Mertz Glacier Tongue were to break off, then the Mertz Glacier Polynya would be much reduced in size, which would lead to a decrease or a cessation of Adélie Land Bottom Water (ALBW) formation (Williams and Bindoff, 2003) which presently contributes to annual Antarctic Bottom Water (AABW) production.

Pinning down the timing of the onset of polynya and deepwater formation is critical. Neodymium (Nd) isotope ratios are used as a proxy to determine the balance between North Atlantic Deep Water (NADW) and southern-sourced waters in the South Atlantic (Piotrowski *et al.*, 2004; 2005). Piotrowski *et al.* (2004) examined Nd isotope ratios in the authigenic ferromanganese oxide component of a southeastern Atlantic core, to determine the history of global overturning circulation intensity through the last deglaciation. A prominent peak in Nd isotopes at ~ 15,300 cal. yrs BP was interpreted as a weakening of the NADW mass component (Trough II; Piotrowski *et al.*, 2004; 2005). However, the peak could, in fact, be caused by an increase in southern sourced waters, Antarctic Bottom Water (AABW), a result of ice sheet melt and the resultant polynya controlled bottom water formation in the George V Land region. At this stage, however, the core chronology is not robust enough to explore this hypothesis.

## 7.4. Results NBP0101 KC10A

The mid-Holocene laminae from NBP0101 KC10A are classified according to the dominance of terrigenous or biogenic components and diatom assemblages. Lamina types are categorised using the same approach for NBP0101 JPC10 laminated sediments (sections 7.1 - 7.3). Detailed NBP0101 KC10A core lithology, sample depths and chronological information are presented in chapter 4 and analytical methods used can be found in chapter 5.

### 7.4.1. Biogenic Laminae

Two of the biogenic laminae types present in the post-glacial laminated sediments of NBP0101 JPC10 (20.60 to 17.36 mbsf; 11384 – 6756 cal. yr BP), near-monogeneric *Hyalochaete Chaetoceros* spp. resting spore (CRS) and mixed diatom assemblage laminae, are also present in the mid-Holocene laminated sediments of NBP0101 KC10A (2.38 to 2.05 mbsf; 3892-3820 cal. yr BP). Two near-monogeneric CRS laminae are present in the sampled interval (Figure 7.8). These lamina range in thickness from 6.0 to 14.0 mm ( $n = 2$ ,  $\sigma = 5.7$  mm, mean = 10.0 mm), making up 7 % of the total sediment thickness (Figure 7.9). Eleven mixed diatom assemblage laminae are present throughout the sampled interval (Figure 7.8). Mixed diatom assemblage laminae consist of CRS, *Fragilariopsis* spp., *Eucampia antarctica* and *Corethron pennatum*. These lamina range from 0.7 to 15.1 mm thick ( $n = 11$ ,  $\sigma = 5.4$  mm, mean = 7.3 mm) and makes up 28 % of the total sediment thickness (Figure 7.9). Laminae characterised by *Corethron pennatum* and *Rhizosolenia* spp. did not occur in the NBP0101 KC10A laminated interval. A third biogenic lamina type characterised by *Fragilariopsis* spp. occurs in the NBP0101 KC10A, but is not present in NBP0101 JPC10 post-glacial interval.

#### 7.4.1.1. Biogenic Laminae Characterised by *Fragilariopsis* spp.

Laminae of this type are characterised by *Fragilariopsis* spp. (Figure 7.10a and b). The other constituents of the assemblage are CRS, *Phaeoceros Chaetoceros* spp., *Corethron pennatum* and *Thalassiosira* spp.. CRS constitute 62.9 % relative abundance of the total diatom assemblage (Table 7.4). *Fragilariopsis* spp. dominate the *Chaetoceros* free counts (88.3%; *F. rhombica* (30.5 %), *F. curta* (25.9 %) and *F.*

*keruelensis* (17.4 %)). *Thalassiosira gracilis* v. *gracilis* (4.1%) is the most dominant *Thalassiosira* spp. (Table 7.5). These biogenic laminae have an absolute abundance of  $886 \times 10^6$  valves per gramme (Table 7.6). Five laminae characterised by *Fragilariopsis* spp. are present in the sampled interval (Figure 7.8). These laminae range from 1.0 to 24.5 mm thick ( $n = 5$ ,  $\sigma = 9.8$  mm, mean = 8.1 mm), making up 14 % of the total sediment thickness (Figure 7.9).

**Table 7.4**

Relative abundance of all diatom species by lamina type, Mertz Ninnis Trough, NBP0101 KC10A. One lamina sampled per lamina type due to low numbers of occurrences in laminated interval. RS = resting spore.

Species / Lamina type	Biogenic laminae characterised by <i>Fragilariopsis</i> .spp	Terrigenous laminae characterised by <i>Fragilariopsis</i> spp.
<i>Hyalochaete Chaetoceros</i> spp. (resting spore) Gran	62.9	78.8
<i>Corethron pennatum</i> (Grunow) Ostenfeld	0.0	0.0
<i>Fragilariopsis</i> spp. Hustedt	32.6	15.0
<i>Porosira glacialis</i> RS (Grunow) Jørgensen	0.0	0.0
<i>Rhizosolenia</i> spp. Brightwell	0.0	0.0
<i>Thalassiosira</i> spp. Cleve	2.2	1.7
Minor species	2.3	4.5
<b>Total:</b>	100	100

**Table 7.5**

Relative abundance of *Chaetoceros* spp. free diatom assemblage by lamina type, Mertz Ninnis Trough, NBP0101 KC10A. One lamina sampled per lamina type due to low numbers of occurrences in laminated interval. RS = resting spore

Species	Biogenic laminae characterised by <i>Fragilariopsis</i> .spp	Terrigenous laminae characterised by <i>Fragilariopsis</i> spp.
<i>Corethron pennatum</i> (Grunow) Ostenfeld	0.2	2.8
<i>Fragilariopsis</i> spp. Hustedt	88.3	81.6
<i>Porosira glacialis</i> RS (Grunow) Jørgensen	0.7	7.4
<i>Rhizosolenia</i> spp. Brightwell	0.0	0.9
<i>Thalassiosira</i> spp. Cleve	8.2	7.4
Minor species	2.6	6.6
<b>Total:</b>	100	100

**Table 7.6**

Absolute abundance of diatom species (valves per gramme of dry sediment  $\times 10^6$ ) by lamina type, Mertz Ninnis Trough, NBP0101 KC10A. One lamina sampled per lamina type due to low numbers of occurrences in laminated interval. RS = resting spore.

Species	Biogenic laminae characterised by <i>Fragilariopsis</i> .spp	Terrigenous laminae characterised by <i>Fragilariopsis</i> spp.
<i>Hyalochaete Chaetoceros</i> spp. (resting spore) Gran	558	1599
<i>Corethron pennatum</i> (Grunow) Ostenfeld	0	0
<i>Fragilariopsis</i> spp. Hustedt	288	305
<i>Porosira glacialis</i> RS (Grunow) Jørgensen	0	0
<i>Rhizosolenia</i> spp. Brightwell	0	0
<i>Thalassiosira</i> spp. Cleve	20	34
Minor species	20	92
<b>Total:</b>	<b>886</b>	<b>2030</b>

#### 7.4.2. Terrigenous Laminae

The terrigenous laminae present in the post-glacial laminated sediments of NBP0101 JPC10, mixed diatom assemblage laminae, are also present in the mid-Holocene laminated sediments of NBP0101 KC10A (2.38 to 2.05 mbsf; 3892-3820 cal. yr BP). Thirteen of these laminae were present throughout the sampled interval (Figure 7.8). These lamina range in thickness from 1.2 to 29.0 mm ( $n = 13$ ,  $\sigma = 6.9$  mm, mean = 7.0 mm) and constitutes 37% of the total sediment thickness (Figure 7.9). Terrigenous sub-laminae characterised by *Porosira glacialis* resting spores (RS) were not present in NBP0101 KC10A, but a second type of terrigenous laminae occurs, characterised by *Fragilariopsis* spp., that is not present in the NBP0101 JPC10 post-glacial interval.

##### 7.4.2.1. Terrigenous Laminae Characterised by *Fragilariopsis* spp.

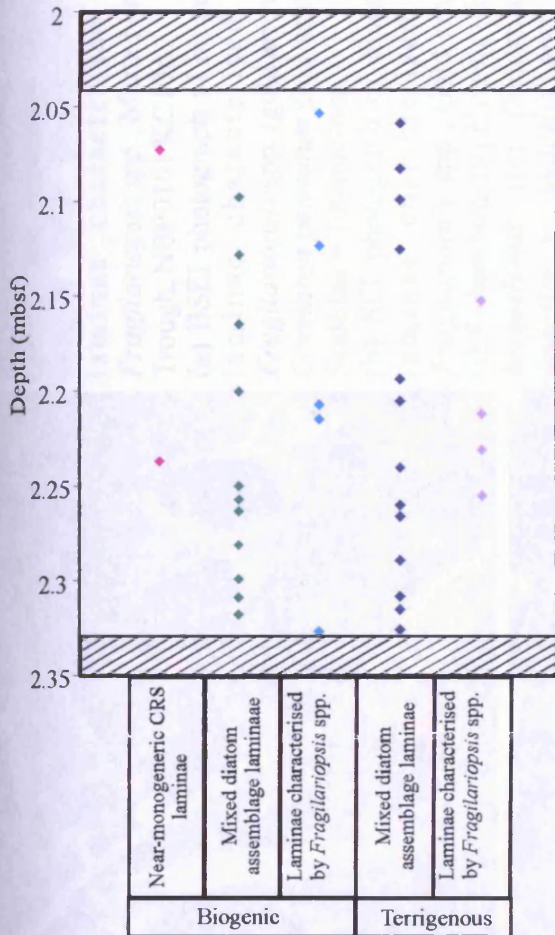
Laminae of this type are characterised by *Fragilariopsis* spp. (Figure 7.10c and d). The other constituents of the assemblage are CRS, *Corethron pennatum*, *Odontella weissflogii* RS, *Porosira glacialis* RS, *Eucampia antarctica* (vegetative), *Stellarima microtrias* RS and *Thalassiosira* spp.. CRS constitute 78.8 % relative abundance of the total diatom assemblage (Table 7.4). *Fragilariopsis* spp. (81.6 %) dominate the *Chaetoceros* free counts; the most dominant *Fragilariopsis* species are *F. rhombica* (26.6 %), *F. curta* (24.0 %), *F. ritscheri* (10.2%) and *F. kerguelensis* (8.3 %) (Table 7.5). These terrigenous laminae have an absolute abundance of  $2030 \times 10^6$  valves per gramme (Table 7.6). Four laminae characterised by *Fragilariopsis* spp. are present in

the sampled interval (Figure 7.9). These laminae range from 4.7 to 24.0 mm thick ( $n = 4$ ,  $\sigma = 9.3$  mm, mean = 12.4 mm), making up 11% of the total sediment thickness (Figure 7.8).

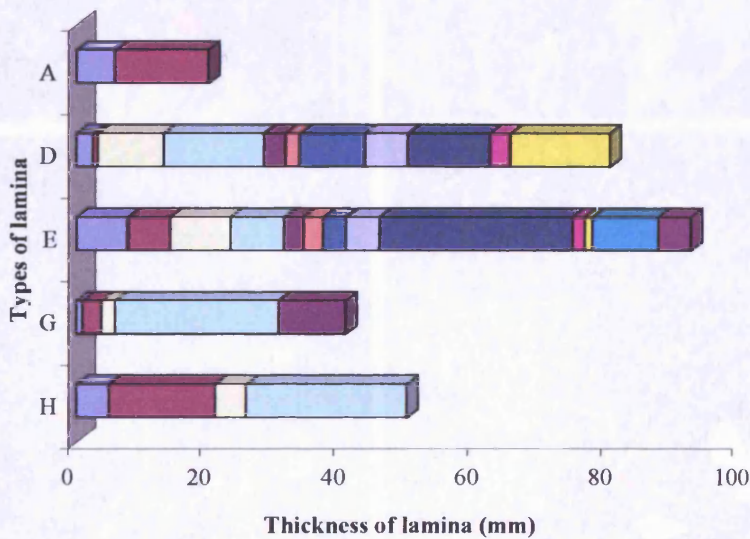
### 7.4.3. Lamina Relationships

Thirty-five laminae are present in the laminated interval. The most common succession of lamina types is mixed diatom assemblage biogenic followed by mixed diatom assemblage terrigenous laminae and less commonly, biogenic laminae characterised by *Fragilariopsis* spp. followed by mixed diatom assemblage terrigenous laminae. Laminae are not very well defined in NBP0101 KC10A and are occasionally disturbed (Figure 7.11). Lamina boundaries in the interval are all gradational, some with a small degree of bioturbated.

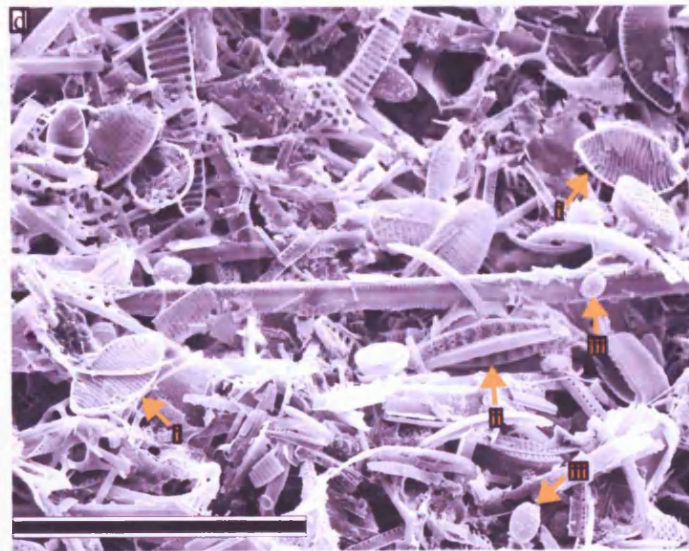
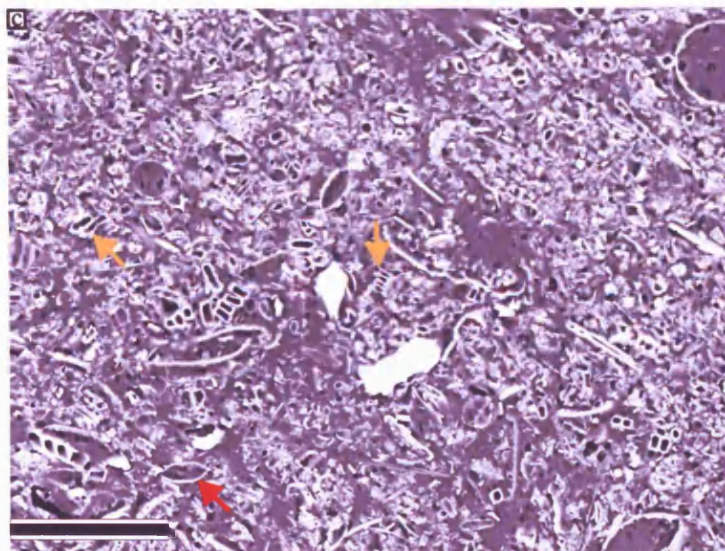
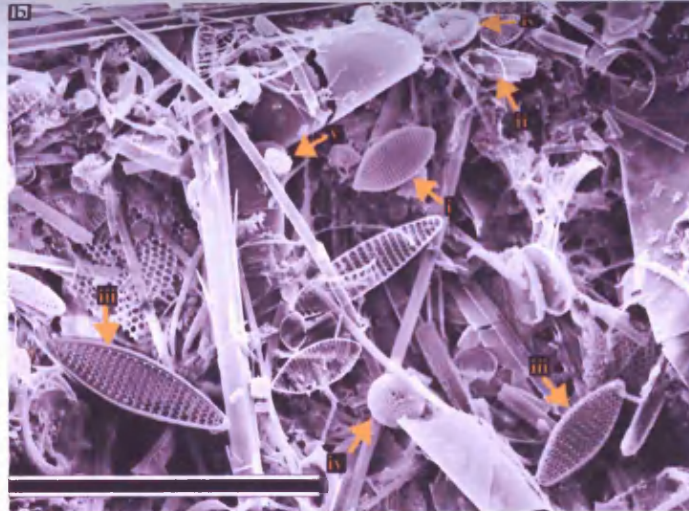
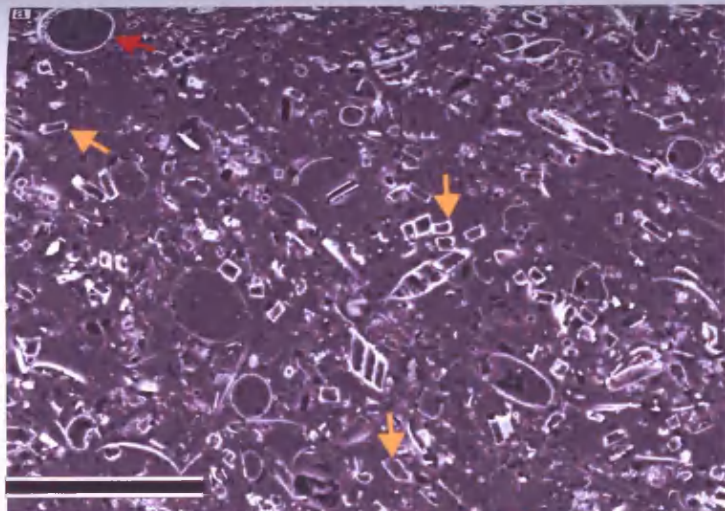




**Figure 7.8**  
 Graph illustrating the distribution of the different lamina types, Mertz Ninnis Trough NBP0101 KC10A, between 2.05 and 2.38 metres below sea floor (mbsf). The hashed lines indicates core not sampled. The lamina are positioned according to the depth of the base of the lamina. CRS = *Hyalochaete Chaetoceros* spp. resting spores.



**Figure 7.9**  
 Graph showing the thicknesses of different types of lamina from Mertz Ninnis Trough (NBP0101 KC10A). Individual thicknesses are displayed as coloured bars within the total thicknesses of each lamina type. A = Near-monogeneric *Hyalochaete Chaetoceros* spp. resting spore (CRS) biogenic laminae; D = Mixed diatom assemblage biogenic laminae; E = Mixed diatom assemblage terrigenous laminae; G = Biogenic laminae dominated by *Fragilariopsis* spp.; H = Terrigenous laminae dominated by *Fragilariopsis* spp..



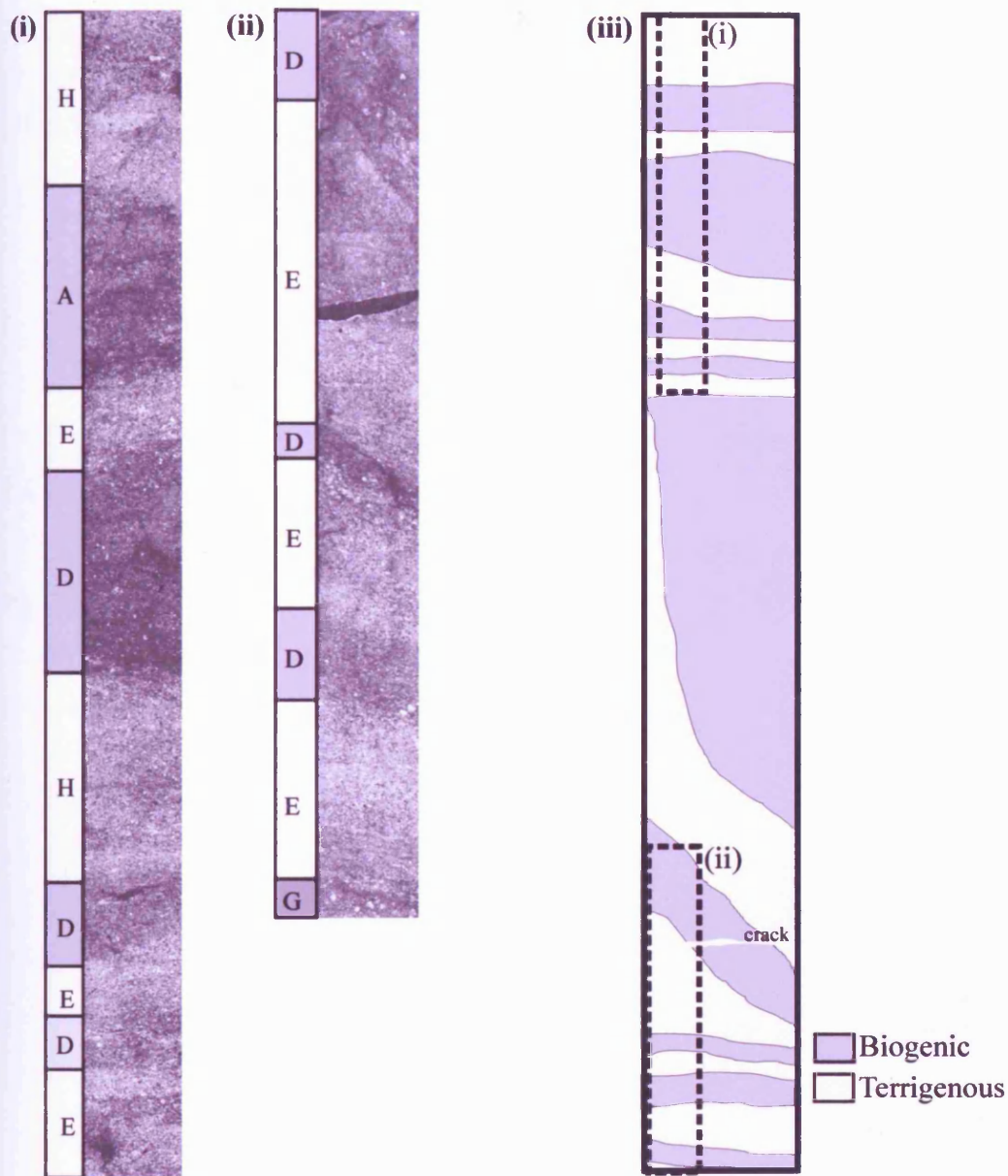
**Figure 7.10**  
Backscattered electron imagery (BSEI) and secondary electron imagery (SEI) photographs of laminae characterised by *Fragilariopsis* spp., Mertz Ninnis Trough, NBP0101 KC10A.

(a) BSEI photograph of biogenic laminae characterised by *Fragilariopsis* spp. (gold arrows). *Corethron pennatum* (red arrow). Scale bar = 100 microns.

(b) SEI photograph of biogenic laminae characterised by *Fragilariopsis* spp.. Gold arrows (i) *F. rhombica*, (ii) *F. curta*, (iii) *F. kerguelensis*, (iv) *Thalassiosira gracilis* v. *gracilis* and (v) *Hyalochaete Chaetoceros* spp. resting spores (CRS). Scale bar = 70 microns.

(c) BSEI photograph of terrigenous laminae characterised by *Fragilariopsis* spp. (gold arrows). *Porosira glacialis* resting spore (RS) (red arrow). Scale bar = 100 microns

(d) SEI photograph of terrigenous laminae characterised by *Fragilariopsis* spp.. Gold arrows (i) *F. rhombica*, (ii) *F. kerguelensis* and (iii) CRS. Scale bar = 50 microns.



**Figure 7.11**

Backscattered electron imagery (BSEI) photomosaics of biogenic laminae and terrigenous laminae, NBP0101 KC10A. A = Near-monogenic *Hyalochaete Chaetoceros* spp. resting spore (CRS) biogenic laminae; D = Mixed diatom assemblage biogenic laminae; E = Mixed diatom assemblage terrigenous laminae; G = Biogenic laminae characterised by *Fragilariopsis* spp.; H = Terrigenous laminae characterised by *Fragilariopsis* spp..

(i) 2.2161 - 2.2673 metres below sea floor (mbsf); (ii) 2.2903 - 2.3279 mbsf.

(iii) Cartoon of NBP0101 KC10A thin sections indicating the position of (i) and (ii) photomosaics. Note the lamina disturbance.

## 7.5. Interpretation and Discussion NBP0101 KC10A

The ecology of diatom species discussed in the following sections is described in greater detail in chapter 3, section 3.5.

### 7.5.1. Seasonal Signal

#### 7.5.1.1. Spring / Summer: Biogenic Laminae

As discussed in section 7.2.1.1, near-monogeneric CRS laminae are interpreted as high productivity associated with water column stratification in spring. Mixed diatom assemblage laminae, as discussed in section 7.2.1.3., suggest a less stratified more mixed water column in summer. The lack of laminae characterised by *Rhizosolenia* spp. and *Corethron pennatum* indicate that water column conditions were not stable enough for large blooms of these species to occur.

In the laminae characterised by *Fragilariopsis* spp., *F. rhombica* and *F. kerguelensis*, suggests relatively warm open waters (Burckle *et al.*, 1987; Zielinski and Gersonde, 1997). *Thalassiosira gracilis* v. *gracilis* is an open water species which has been used to indicate early seasonal sea ice reduction from wind stress and deep mixing (Cunningham and Leventer, 1998) and *T. gravida* indicates open water with no sea ice (Garrison *et al.*, 1987; Fryxell and Kendrick, 1988). Therefore, laminae characterised by *Fragilariopsis* spp. are interpreted as spring/summer productivity associated with warm open waters free from sea ice.

#### 7.5.1.2. Summer / Autumn: Terrigenous Laminae

As discussed in section 7.2.1.4, the mixed diatom assemblage lamina type indicates open water conditions increasing, melt of ice and increase in bottom water dynamics in summer. Sub-laminae characterised by *Porosira glacialis* resting spores are not present probably due to later sea ice formation in autumn.

In the laminae characterised by *Fragilariopsis* spp, *Fragilariopsis rhombica* and *F. ritscheri* suggest warm open waters (Gersonde, 1984, Garrison *et al.*, 1987; Zielinski and Gersonde, 1997). *Thalassiosira gracilis* v. *gracilis* and *T. lentiginosa* are associated with warm open waters (Zielinski and Gersonde, 1997). *T. tumida* and *Eucampia antarctica* are associated with the water column adjacent to sea ice

(Garrison *et al.*, 1983b; 1987). The terrigenous component, as in NBP0101 JPC10, originates from the Mertz Glacier Tongue, sea ice melting and / or MCDW entrained sediments, as discussed previously in section 7.2.1.4.

### 7.5.2. Lamina Relationships

The presence of biogenic and terrigenous laminae characterised by *Fragilariopsis* spp., near-monogeneric *Hyalochaete Chaetoceros* spp. resting spore laminae, mixed diatom assemblage biogenic laminae and mixed diatom assemblage terrigenous laminae and the absence of laminae and sub-laminae characterised by *Corethron pennatum*, *Rhizosolenia* spp. and *Porosira glacialis* resting spores, indicates that relatively warm mixed open water conditions prevailed whilst the mid-Holocene laminated sediments were deposited. This analysed laminated interval has been dated 3,892 – 3,820 cal. yr BP, which has been interpreted as deposition during an Antarctic warm interval, the mid-Holocene Climatic Optimum (Harris *et al.*, 2001). This warmer period is characterised by increased primary productivity, less sea ice than at present (Cunningham *et al.*, 1999; Leventer *et al.*, 1996; Shevenell *et al.*, 1996) and a more energetic coastal wave regime (Ingólfsson *et al.*, 1998). The Mertz Glacier Polynya would most likely still be present due to katabatic winds, but sea ice formation and periods of stable surface waters would be reduced relative to those encountered during post-glacial sediment deposition (NBP0101 JPC10). The reduced sea ice regime would lead to a decrease in HSSW production and, therefore, a decrease in bottom water circulation on the shelf (Harris *et al.*, 2001). Using the sequence of diatom assemblages seventeen annual cycles are identified in the laminated interval and the accumulation rate determined as 1.6 cm/yr. Even though annual deposit is made up of two laminae, the analysed interval is not varved because there is no rhythmic repetition of the same two lamina types.

## 7.6. Conclusions NBP0101 KC10A

The five lamina types identified in NBP0101 KC10A were deposited during a period of relatively warm climate, the mid-Holocene Climatic Optimum, when sea ice conditions were less persistent than today. It has previously been suggested that the mid-Holocene climatic optimum can be used as an analogy to determine responses to possible future climatic warming (Harris and Beaman, 2003). Bi *et al.* (2001) present an ocean-atmospheric model which predicts changes in rates of AABW production during global warming (when atmospheric CO<sub>2</sub> is triple current levels). They predict that increased precipitation along Antarctic coast and increased meltwater outflow freshens surface waters reducing AABW formation. In addition Bi *et al.* (2001) predict that sea ice formation would reduce over the continental shelf. The results and interpretations presented in sections 7.4 and 7.5 support these predictions.

## 7.7. Summary

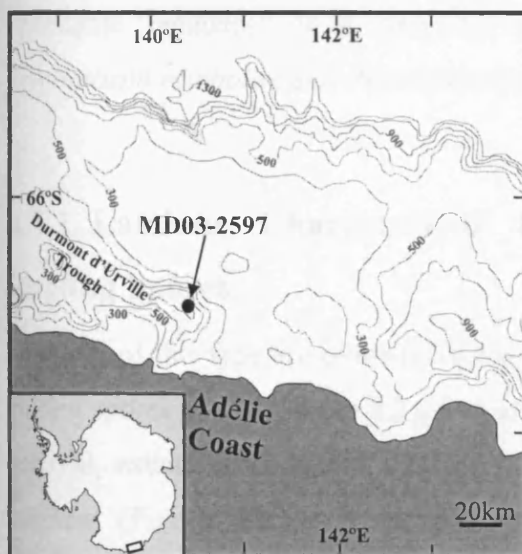
Diatom species blooms and the resultant deposition of diatom-rich post-glacial laminae and sub-laminae in the Mertz Ninnis Trough, East Antarctica are seasonally controlled (light levels, sea ice extent and nutrient levels). The fluctuations in the size and heat regime of the Mertz Glacier Polynya (caused by variations in upwelling; katabatic wind strength and direction; areal extent and orientation of the Mertz Glacier Tongue) also play a role in controlling the type of laminae deposited. Four biogenic diatom ooze laminae types, one diatom-bearing terrigenous laminae type and one diatom-bearing terrigenous sub-laminae type have been identified in the early Holocene laminated sequence. The biogenic laminae are deposited in spring and summer, and terrigenous laminae and sub-laminae in summer and autumn. The different laminae types consistently occur in the same order throughout the early Holocene laminated interval. This high-resolution record demonstrates that the Mertz Glacier Polynya was active in early post-glacial times.

The diatom blooms and subsequent lamina deposition of diatom-rich mid-Holocene laminae in the Mertz Ninnis Trough, East Antarctica are also controlled by seasons. The Mertz Glacier Polynya is still active during the mid-Holocene Climatic Optimum, but warmer conditions led to reduced sea ice. Three biogenic diatom ooze lamina types and two diatom-bearing terrigenous laminae types have been identified in the mid-Holocene laminated sequence, two of which did not occur in the postglacial laminated sequence. Spring/summer deposition is characterised by biogenic laminae deposition and summer/autumn by terrigenous laminae. The polynya was less active in the mid-Holocene, producing less HSSW (Harris *et al.*, 2001) and ultimately less AABW.

The behaviour of the Mertz Glacier Polynya controls the rate of bottom water formation on the Adélie Coast. Future climate change would probably have an impact on the extent and rate of sea ice formation in the polynya and therefore, global thermohaline circulation.

## 8. Durmont d'Urville Trough

This chapter presents the results and interpretations of backscattered electron imagery (BSEI) analysis, secondary electron imagery (SEI) analysis and quantitative diatom assemblage counts from core MD03 2597, Durmont d'Urville Trough, East Antarctica (Figure 8.1). The diatom count data used to construct tables 8.1 – 8.3 can be found in appendix 4. Detailed MD03 2597 core lithology, sample depths and chronological information are presented in chapter 4 and analytical methods used can be found in chapter 5.



**Figure 8.1**  
Location map of MD03-2597, Durmont d'Urville Trough on the Adélie Coast continental margin. Contours in metres. Adapted from Domack *et al.* (1989).

### 8.1. Results

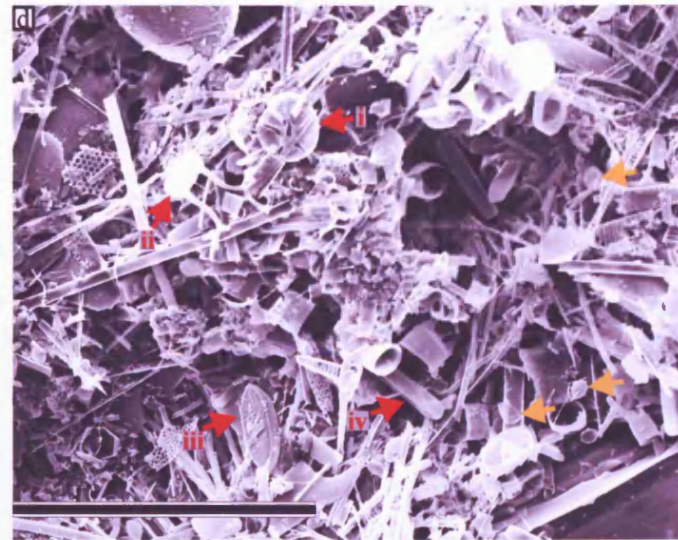
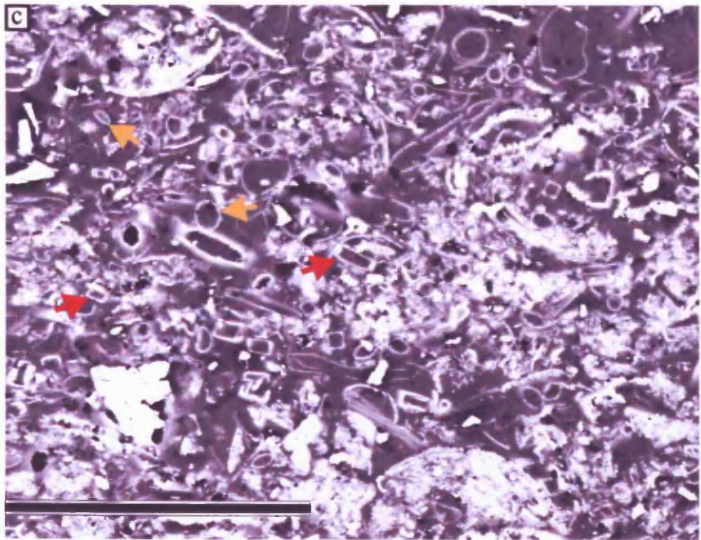
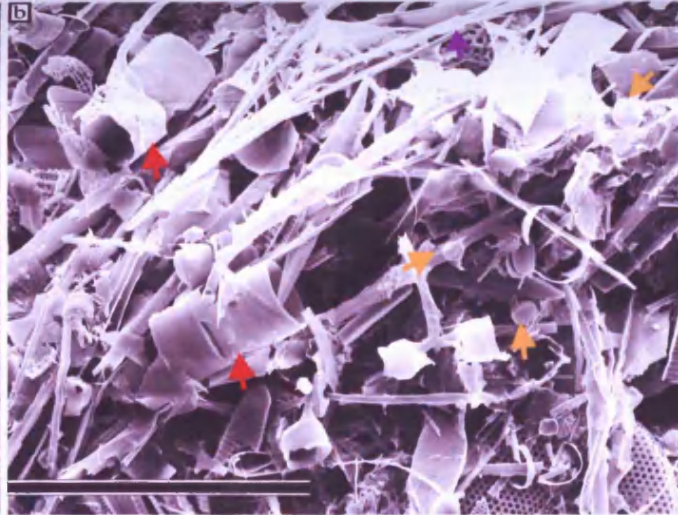
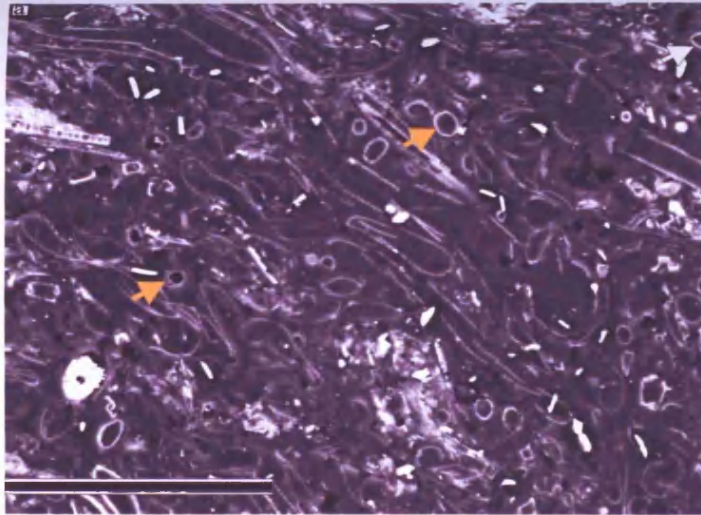
The late-Holocene laminae and sub-laminae found in Durmont d'Urville Trough sediments are presented and their relationships described. Laminae and sub-laminae are classified principally according to diatom assemblages; the dominance of terrigenous or biogenic components is also utilised. Biogenic laminae are composed of diatom ooze with very little terrigenous material and are present throughout the sampled intervals. Terrigenous laminae have a greater proportion of terrigenous grains (silt and clay) relative to the biogenic laminae. Terrigenous grain sizes vary between laminae. *Hyalochaete Chaetoceros* spp. (resting spores and vegetative cells) and *Fragilariopsis* spp. overwhelmingly dominate the laminated sediment, together representing 78.9 – 90.0 % of the diatom assemblage (Table 8.1), therefore more minor constituents of the assemblage, which are highly visible in the BSEI



photographs, are used to categorise the laminae types. Eight types of lamina and one sub-lamina type have been identified in the analysed intervals. Biogenic and terrigenous forms of the lamina/sub-lamina types occur in this late-Holocene laminated interval and are discussed together in this chapter. The discussion of biogenic and terrigenous laminae therefore differs from the laminae descriptions in the previous two chapters (deglacial laminated sediments, Palmer Deep; and post-glacial and mid-Holocene laminated sediments from Mertz Ninnis Trough, respectively). An average of at least three diatom species counts per lamina and sub-lamina type is used to calculate relative and absolute diatom abundances in this chapter (see appendix 4, Table A.4.3.1.1 and A.4.3.1.2 for original diatom counts). “Elongate pennates” is a grouping of the species *Thalassiothrix antarctica*, *Trichotoxon reinboldii* and *Pseudonitzschia turgidula* used in this chapter.

### 8.1.1. Laminae Characterised by *Hyalochaete Chaetoceros* spp. Resting Spores

Laminae of this type are overwhelmingly composed of *Hyalochaete Chaetoceros* spp. resting spores (CRS) (Figure 8.2). Out of twenty-three occurrences within the analysed interval, twenty are biogenic laminae (Figure 8.2a and b) and three are terrigenous laminae (Figure 8.2c and d). The minor constituents of the assemblage are *Fragilariopsis* spp., *Corethron pennatum* and *Porosira glacialis* resting spores (RS). CRS constitute 50.6% and *Fragilariopsis* spp. constitute 38.4% of the total diatom assemblage (Table 8.1). *Hyalochaete Chaetoceros* free counts (Table 8.2) are dominated by *Fragilariopsis* spp. (75.7%; most dominant species *F. curta* (35.1%), *F. rhombica* (11.7%), *F. kerguelensis* (8.8%), *F. cylindrus* (7.8%) and *F. ritscheri* (3.7%)) and *Phaeoceros Chaetoceros* spp. (9.6%), *Thalassiosira* spp. (6.2%; most dominant species are *T. poroseriata* (1.7%), *T. lentiginosa* (1.6%) and *T. gracilis* v. *gracilis* (1.5%)) and *P. glacialis* RS (3.3%). This lamina type has an absolute abundance of  $874 \times 10^6$  valves per gramme of dry sediment (Table 8.3). The biogenic laminae are present in the analysed intervals in two depth ranges, 18 – 24 and 40-57 mbsf (~ 990-1310 cal. yrs BP and 2160 – 2814 cal. yrs BP) (Figure 8.3). The terrigenous laminae occur between 47 and 50 metres below sea floor (mbsf) in the



**Figure 8.2**

Backscattered electron imagery (BSEI) and secondary electron imagery (SEI) photographs of biogenic and terrigenous laminae characterised by *Hyalochaete Chaetoceros* spp. resting spores (CRS), Durmont d'Urville Trough.

(a) BSEI photograph of biogenic laminae. CRS (gold arrows). Scale bar = 100 microns.

(b) SEI photograph of biogenic laminae. CRS (gold arrows). *Phaeoceros Chaetoceros* spp. (red arrows) and *Corethron pennatum setae* (purple arrow). Scale bar = 70 microns.

(c) BSEI photograph of terrigenous laminae. CRS (gold arrows) and *Fragilariopsis* spp. (red arrows). Scale bar = 100 microns.

(d) SEI photograph of terrigenous laminae. CRS (gold arrows). (i) *Astermophalus* spp.; (ii) *Phaeoceros Chaetoceros*; (iii) *Fragilariopsis rhombica*; (iv) *F. curta*. (red arrows). Scale bar = 50 microns.

**Table 8.1**  
Relative abundance of all diatom species (percentage) by lamina type, Durmont d'Urville Trough, MD03 2597. RS = resting spores.

Species / Lamina type	Laminae characterised by <i>Stellarima microtrias</i> RS, <i>Porosira glacialis</i> RS and / or <i>Coccolithus bouveti</i>	Sub-laminae characterised by <i>Porosira glacialis</i> RS	Mixed diatom assemblage terrigenous laminae	Mixed diatom assemblage biogenic laminae	Laminae characterised by <i>Rhizosolenia</i> spp.	Laminae characterised by <i>Corethron pennatum</i>	Laminae characterised by <i>Corethron pennatum</i> and <i>Rhizosolenia</i> spp.	Laminae characterised by <i>Fragilariopsis</i> spp.	Laminae characterised by <i>Hyalochaete Chaetoceros</i> spp. RS and <i>Fragilariopsis</i> spp.	Laminae characterised by <i>Hyalochaete Chaetoceros</i> spp. RS
<i>Hyalochaete Chaetoceros</i> spp. RS Gran	40.1	59.6	36.7	43.0	21.1	29.9	40.5	22.5	43.2	50.6
<i>Hyalochaete Chaetoceros</i> spp. (vegetative) Gran	0.5	1.0	1.5	0.6	1.7	0.2	2.0	0.0	0.2	0.3
<i>Phaeoceros Chaetoceros</i> spp. Gran	3.5	1.5	2.4	2.1	1.3	2.4	6.5	6.2	7.1	3.2
<i>Corethron pennatum</i> (Grunow) Ostenfeld	0.7	0.2	0.5	0.3	0.1	0.9	0.7	0.3	0.6	0.2
<i>Eucampia antarctica</i> (Castracane) Mangin	0.7	0.7	0.7	0.7	0.6	0.6	2.5	1.4	0.5	0.6
<i>Fragilariopsis</i> spp. Hustedt	39.8	20.3	48.6	46.4	56.1	56.2	37.3	63.4	42.3	38.4
<i>Porosira glacialis</i> RS (Grunow) Jørgensen	2.9	7.1	2.4	0.6	0.7	1.0	0.9	1.0	1.2	1.5
<i>Proboscia</i> spp. Jørgensen	0.9	0.1	0.5	0.3	10.1	0.7	0.6	0.3	0.1	0.2
<i>Rhizosolenia</i> spp. Brightwell	0.3	0.5	0.8	0.6	2.3	1.3	3.3	0.2	0.4	0.0
<i>Stellarima microtrias</i> RS (Ehrenberg) Hasle & Sims	1.1	0.2	0.1	0.4	0.2	0.1	0.0	0.0	0.1	0.2
<i>Thalassiosira</i> spp. Cleve	7.6	8.0	4.2	2.9	2.4	4.1	3.2	2.9	2.8	3.0
Elongate pennates	0.7	0.2	0.8	1.1	2.2	1.5	1.5	0.6	0.8	0.6
Others	1.2	0.6	0.8	1.0	1.2	1.1	1.0	1.2	0.7	1.2
<b>Total:</b>	100	100	100	100	100	100	100	100	100	100

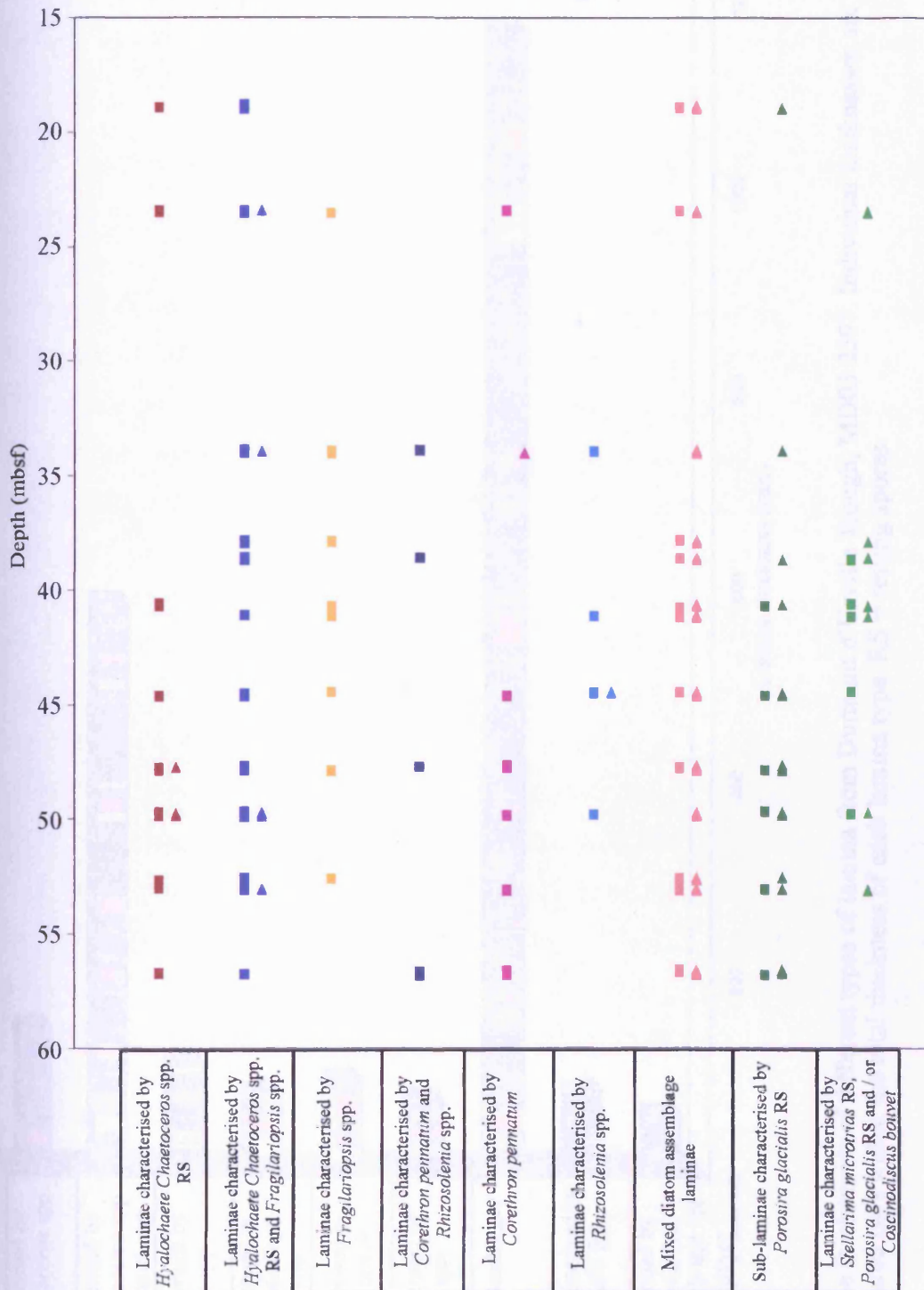
**Table 8.2**  
Relative abundance of *Hyalochaete Chaetcoeros* spp. free counts (percentage) by lamina type, Durmont d'Urville Trough, MD03 2597. RS = resting spores.

Species / Lamina type	Laminae characterised by <i>Stellarima microtrias</i> resting spores, <i>Porosira glacialis</i> resting spores and / or <i>Coscinodiscus bouveti</i>	Sub-laminae characterised by <i>Porosira glacialis</i> RS	Mixed diatom assemblage terrigenous laminae	Mixed diatom assemblage biogenic laminae	Laminae characterised by <i>Rhizosolenia</i> spp.	Laminae characterised by <i>Corethron pennatum</i>	Laminae characterised by <i>Corethron pennatum</i> and <i>Rhizosolenia</i> spp.	Laminae characterised by <i>Fragilariopsis</i> spp.	Laminae characterised by <i>Hyalochaete Chaetcoeros</i> spp. RS and <i>Fragilariopsis</i> spp.	Laminae characterised by <i>Hyalochaete Chaetcoeros</i> spp. RS
<i>Phaeoceros Chaetcoeros</i> spp. Gran	6.5	3.4	4.6	4.8	1.7	3.2	9.8	8.6	10.8	9.6
<i>Corethron pennatum</i> (Grunow) Ostenfeld	1.1	0.3	0.9	0.6	0.3	1.4	1.2	0.6	1.1	0.3
<i>Eucampia antarctica</i> (Castracane) Mangin	1.4	1.9	1.7	1.2	0.7	0.7	5.3	1.9	0.9	1.2
<i>Fragilariopsis</i> spp. Hustedt	67.3	54.2	75.9	82.4	73.7	81.8	66.4	80.3	75.7	75.7
<i>Porosira glacialis</i> RS (Grunow) Jørgensen	5.1	15.5	4.5	0.9	0.8	1.5	1.6	1.3	2.5	3.3
<i>Proboscia</i> spp. Jørgensen	1.4	0.1	1.0	0.4	1.1	1.1	0.6	1.3	0.1	0.3
<i>Rhizosolenia</i> spp. Brightwell	0.9	2.0	1.3	0.8	1.2	1.2	5.3	0.3	0.7	0.4
<i>Stellarima microtrias</i> RS (Ehrenberg) Hasle & Sims	1.6	0.9	0.1	0.4	0.2	0.1	0.0	0.1	0.1	0.2
<i>Thalassiosira</i> spp. Cleve	12.3	18.7	7.1	5.2	2.7	5.1	5.9	4.3	5.4	6.2
Elongate pennates	1.0	1.2	1.1	1.6	2.3	1.6	2.3	0.7	1.4	0.9
Others	1.4	1.8	1.8	1.7	2.0	2.3	1.6	0.6	1.3	1.9
<b>Total:</b>	100	100	100	100	100	100	100	100	100	100

**Table 8.3**

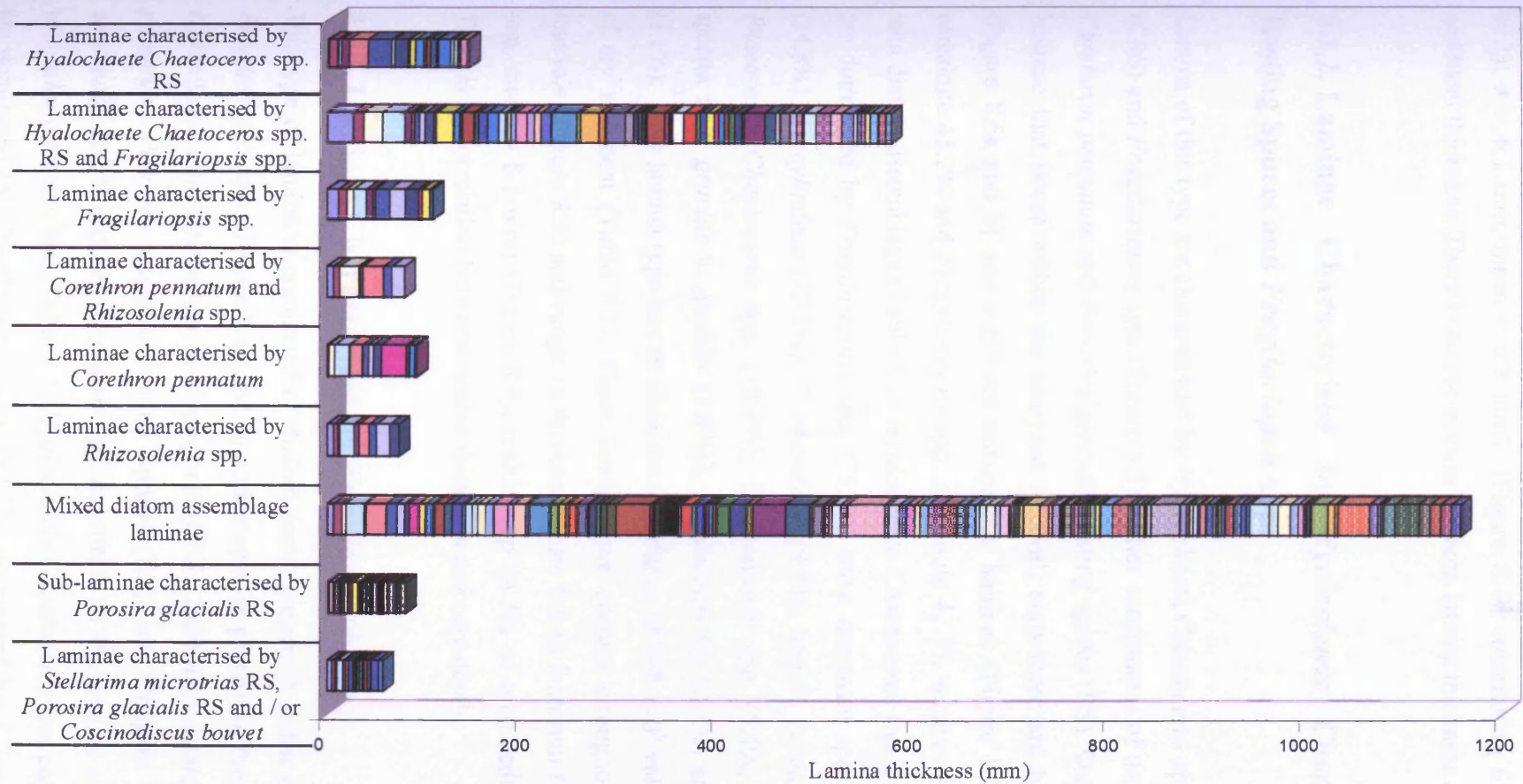
Absolute abundance of all diatom species ( $\times 10^6$  valves per gramme of dry sediment) by lamina type, Durmont d'Urville Trough, MD03 2597. RS = resting spores.

Species / Lamina type	Laminae characterised by <i>Hyalochaete</i> spp. RS and <i>Fragilariopsis</i> spp.	Laminae characterised by <i>Hyalochaete</i> spp. RS and <i>Fragilariopsis</i> spp.	Laminae characterised by <i>Fragilariopsis</i> spp.	Laminae characterised by <i>Corethron pennatum</i> and <i>Rhizosolenia</i> spp.	Laminae characterised by <i>Corethron pennatum</i>	Laminae characterised by <i>Rhizosolenia</i> spp.	Mixed diatom assemblage biogenic laminae	Mixed diatom assemblage terrigenous laminae	Sub-laminae characterised by <i>Porosira glacialis</i> RS	Laminae characterised by <i>Stellarima microtrias</i> RS, <i>Porosira glacialis</i> RS and / or <i>Coscinodiscus bowyeri</i>
<i>Hyalochaete</i> <i>Chaetoceros</i> spp. RS Gran	499.5	330.4	194.2	309.5	187.1	155.1	331.3	227.9	831.9	276.3
<i>Phaeoceros</i> <i>Chaetoceros</i> spp. Gran	37.4	54.3	55.8	33.9	14.1	9.6	18.9	14.7	12.6	26.4
<i>Corethron pennatum</i> (Grunow) Ostenfeld	1.5	4.2	3.3	3.3	4.5	1.1	3.2	3.0	1.5	5.5
<i>Eucampia antarctica</i> (Castracane) Mangin	4.1	3.7	11.7	22.1	2.7	4.3	6.5	4.8	6.9	5.1
<i>Fragilariopsis</i> spp. Hustedt	286.3	304.0	614.1	226.3	300.2	417.2	325.3	241.8	164.0	261.4
<i>Porosira glacialis</i> RS (Grunow) Jørgensen	8.7	9.5	7.5	5.6	5.1	4.9	3.2	14.3	53.9	20.3
<i>Proboscia</i> spp. Jørgensen	2.3	0.9	2.7	4.2	3.7	74.9	2.0	2.9	1.6	6.0
<i>Rhizosolenia</i> spp. Brightwell	0.0	3.2	1.7	15.7	7.6	16.9	4.3	3.6	4.2	3.0
<i>Stellarima microtrias</i> RS (Ehrenberg) Hasle & Sims	0.6	0.4	0.0	0.0	0.4	1.7	2.4	0.5	2.2	6.7
<i>Thalassiosira</i> spp. Cleve	18.7	18.8	27.8	19.7	23.9	17.9	19.3	21.2	65.4	45.3
Elongate pennates	4.9	6.1	6.2	6.9	9.1	16.3	6.7	4.2	4.0	4.5
Others	10.3	7.5	11.2	19.6	9.2	22.5	10.9	17.2	16.7	9.8
<b>Total:</b>	874.3	743.0	936.2	666.8	567.6	742.4	734.0	556.1	1164.9	670.3



**Figure 8.3**

Graph illustrating the distribution of different lamina types, Durmont d'Urville Trough MD03 2597, in discrete intervals between 18.75 and 56.80 metres below sea floor (mbsf) (see table 4.7). The lamina are positioned according to the depth of the base of the lamina. Squares indicate the position of biogenic laminae and sub-laminae. Triangles indicate the position of terrigenous laminae and sub-laminae. RS = resting spores.



**Figure 8.4**  
 Graph showing the thicknesses of different types of lamina from Durmont d'Urville Trough, MD03 2597. Individual thicknesses are displayed as coloured bars within the total thickness of each lamina type. RS = resting spores.

sampled intervals (Figure 8.3). The laminae range in thickness from 1.0 to 24.0 mm ( $n = 23$ ,  $\sigma = 6.1$  mm, mean = 6.3 mm) (Figure 8.4), constituting 6.1% of the total sediment thickness. There is no correlation between lamina thickness and core depth.

### 8.1.2. Laminae Characterised by *Hyalochaete Chaetoceros* spp. Resting Spores and *Fragilariopsis* spp.

Lamina of this type are characterised by *Hyalochaete Chaetoceros* spp. resting spores (CRS) and *Fragilariopsis* spp. (Figure 8.5). Other constituents of the assemblage are *Corethron pennatum* and *Porosira glacialis* resting spores (RS). Out of seventy-one laminae that occur within the analysed interval, sixty-three are biogenic laminae (Figure 8.5a and b) and eight are terrigenous laminae (Figure 8.5c and d). CRS constitute 43.2% and *Fragilariopsis* spp. constitute 42.3% relative abundance of the total diatom assemblage (Table 8.1). *Hyalochaete Chaetoceros* free counts (Table 8.2) are dominated by *Fragilariopsis* spp. (75.7%; most dominant species are *F. curta* (34.8%), *F. cylindrus* (12.3%), *F. rhombica* (9.5%) and *F. kerguelensis* (7.4%)), *Phaeoceros Chaetoceros* spp. (10.8%), *Thalassiosira* spp. (5.4%; most dominant species is *T. gracilis* v. *gracilis* (1.6%)), *P. glacialis* RS (2.5%) and *C. pennatum* (1.1%). This lamina type has an absolute abundance of  $743 \times 10^6$  valves per gramme of dry sediment (Table 8.3). These laminae are present throughout the analysed intervals (Figure 8.3) and range in thickness from 0.8 to 26.6 mm ( $n = 71$ ,  $\sigma = 6.1$  mm, mean = 8.1 mm) (Figure 8.4), making up 24.3% of total sediment thickness. There is no correlation between lamina thickness and core depth.

### 8.1.3. Laminae Characterised by *Fragilariopsis* spp.

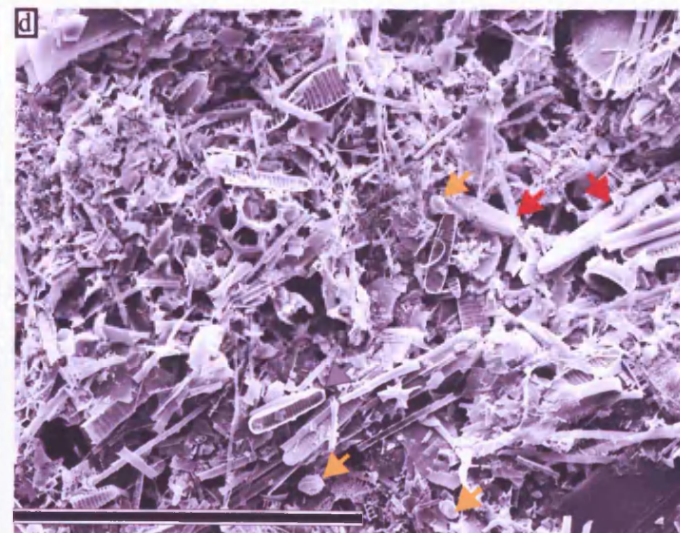
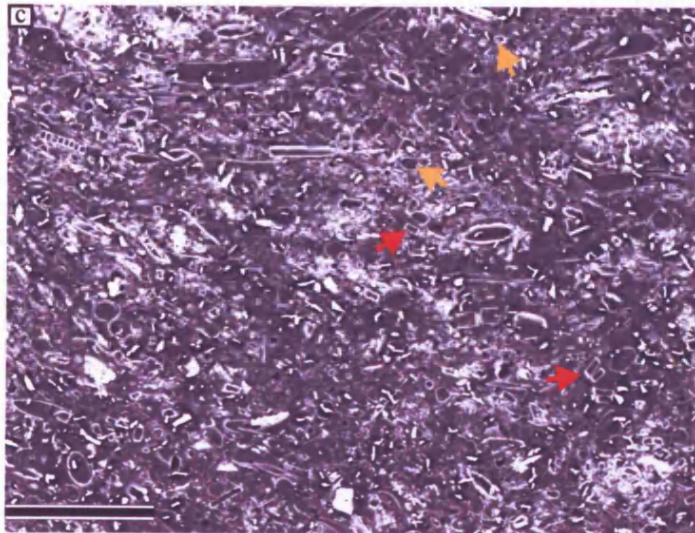
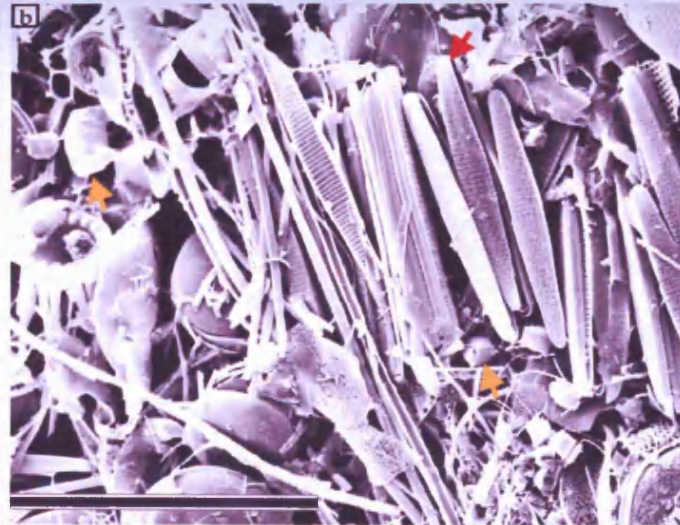
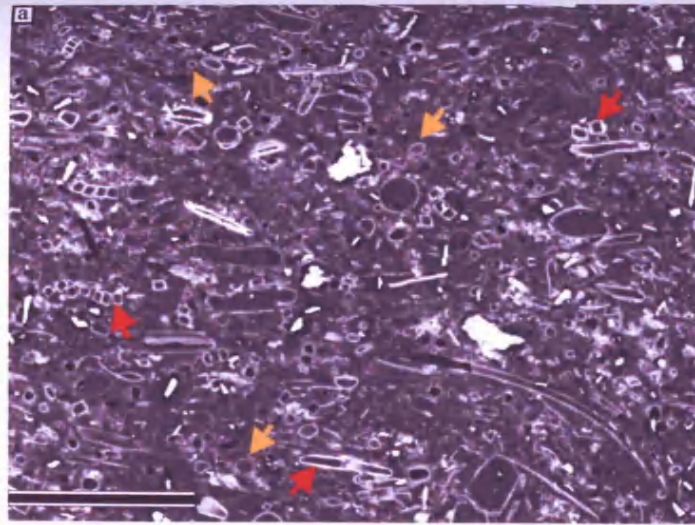
This type of lamina is composed of diatom ooze (biogenic) and is characterised by *Fragilariopsis* spp. (Figure 8.6a and b). Other species present in the assemblage are *Hyalochaete Chaetoceros* spp. resting spores (CRS), *Eucampia antarctica*, *Corethron pennatum*, *Porosira glacialis* resting spores (RS) and elongate pennates. CRS constitutes 22.5% and *Fragilariopsis* spp. constitute 63.4% relative abundance of the total diatom assemblage (Table 8.1) *Hyalochaete Chaetoceros* free counts (Table 8.2) are dominated by *Fragilariopsis* spp. (80.3%; dominated by *F. curta* (29.4%), *F.*



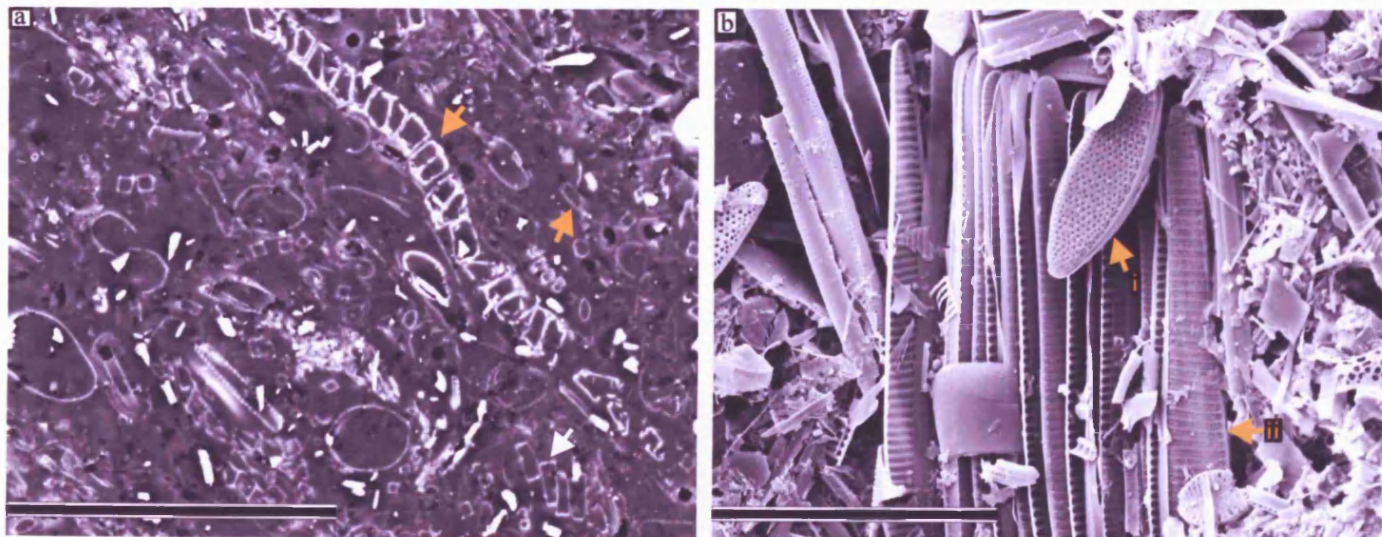
*cylindrus* (26.2%), *F. rhombica* (12.8%) and *F. kerguelensis* (3.9%), *Phaeoceros Chaetoceros* spp. (8.6%), *Thalassiosira* spp. (4.3%; dominated by *T. gracilis* v. *gracilis* (1.0%)), *E. antarctica* (1.9%), elongate pennates (0.7%) and *C. pennatum* (0.6%). This lamina type has an absolute abundance of  $936 \times 10^6$  valves per gramme of dry sediment (Table 8.3). Twelve laminae characterised by *Fragilariopsis* spp. are present throughout the core but not in every analysed interval (Figure 8.3). These lamina range in thickness from 2.4 to 16.1 mm ( $n = 12$ ,  $\sigma = 4.7$  mm, mean = 9.0 mm) (Figure 8.4) and make up 4.6% of the total sediment thickness. There is no correlation between lamina thickness and core depth.

#### **8.1.4. Laminae Characterised by *Corethron pennatum* and *Rhizosolenia* spp.**

Laminae of this type are composed of diatom ooze (biogenic) and are characterised by *Corethron pennatum* and *Rhizosolenia* spp. (Figure 8.7a and b). The other constituents of the assemblage are *Hyalochaete Chaetoceros* spp. resting spores (CRS), *Fragilariopsis* spp., *Phaeoceros Chaetoceros* spp., *Eucampia antarctica*, elongate pennates and *Porosira glacialis* resting spores (RS). CRS constitutes 40.5% and *Fragilariopsis* spp. constitute 37.3% relative abundance of the total diatom assemblage (Table 8.1). *Hyalochaete Chaetoceros* free counts (Table 8.2) are dominated by *Fragilariopsis* spp. (66.4%; dominated by *F. curta* (19.1%), *F. cylindrus* (13.5%), *F. rhombica* (12.9%), *F. ritscheri* (7.7%), *F. kerguelensis* (5.5%) and *F. sublinearis* (2.8%)), *Phaeoceros Chaetoceros* spp. (9.8%), *Thalassiosira* spp. (5.9%; dominated by *T. lentiginosa* (1.9%)), *E. antarctica* (5.3%), *Rhizosolenia* spp. (5.3%), *C. pennatum* (1.2%), *P. glacialis* RS (1.6%) and elongate pennates (2.3%). This lamina type has an absolute abundance of  $667 \times 10^6$  valves per gramme of dry sediment (Table 8.3). Eight laminae characterised by *C. pennatum* and *Rhizosolenia* spp. are present in the sampled intervals below 33.9 mbsf (before ~1840 cal. yr BP) (Figure 8.3). These laminae range from 1.4 to 21.0 mm thick ( $n = 8$ ,  $\sigma = 7.4$  mm, mean = 9.9 mm) (Figure 8.4) and make up 3.3% of the total sediment thickness. There is no correlation between lamina thickness and core depth.



**Figure 8.5** Backscattered electron imagery (BSEI) and secondary electron imagery (SEI) photographs of laminae characterised by *Hyalochaete Chaetoceros* spp. resting spores (CRS) and *Fragilariopsis* spp. biogenic and terrigenous laminae, Durmont d'Urville Trough. (a) BSEI photograph of biogenic laminae. CRS (gold arrows) and *Fragilariopsis* spp. (red arrows). (b) SEI photograph of biogenic laminae. CRS (gold arrows) and *Fragilariopsis* spp. (red arrow). Scale bar = 100 microns. (c) BSEI photograph of terrigenous laminae. CRS (gold arrows) and *Fragilariopsis* spp. (red arrow). Scale bar = 100 microns. (d) SEI photograph of terrigenous laminae. CRS (gold arrows) and *Fragilariopsis* spp. (red arrows). Scale bar = 50 microns.

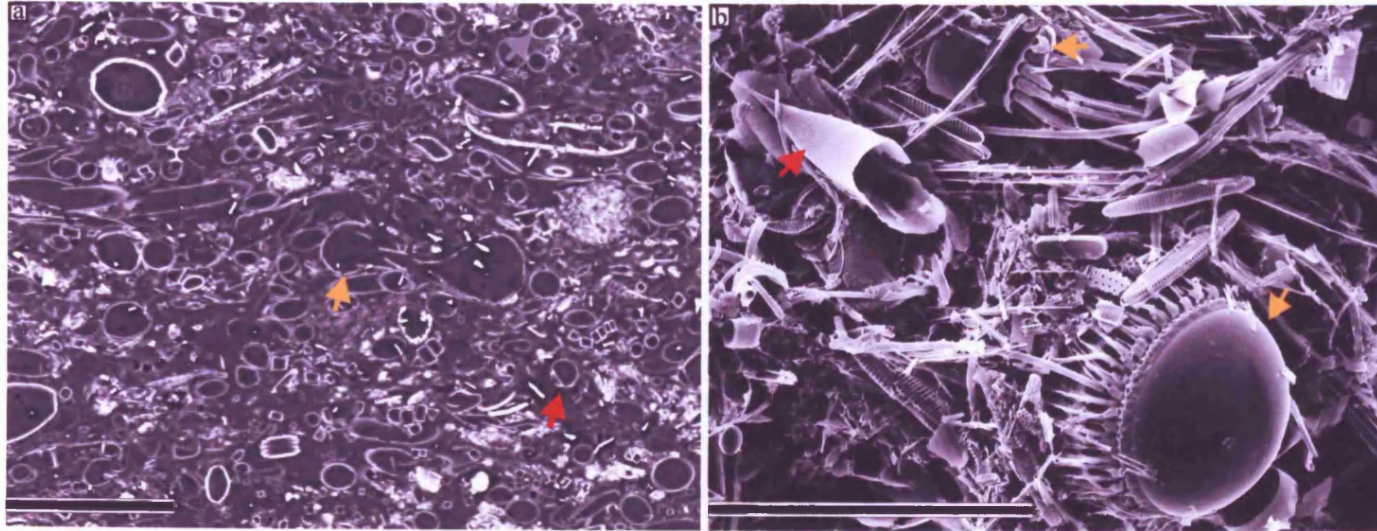


**Figure 8.6**

Backscattered electron imagery (BSEI) and secondary electron imagery (SEI) photographs of biogenic and terrigenous laminae characterised by *Fragilariopsis* spp., Dumont d'Urville Trough.

(a) BSEI photograph of biogenic laminae. *Fragilariopsis* spp. (gold arrows). Scale bar = 60 microns.

(b) SEI photograph of biogenic laminae. Gold arrows (i) *F. kerguelensis*; (ii) *F. obliquecostata*. Scale bar = 40 microns.



**Figure 8.7**

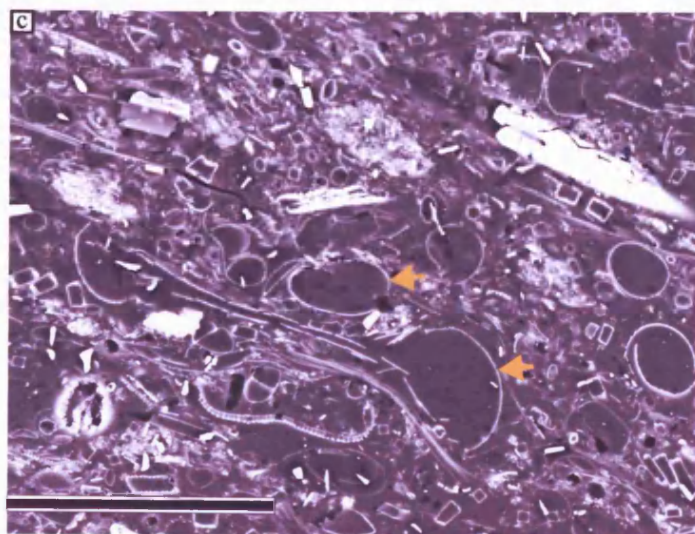
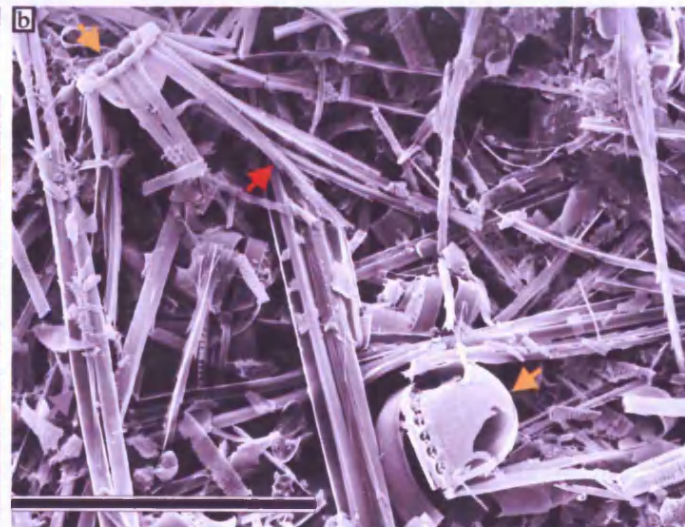
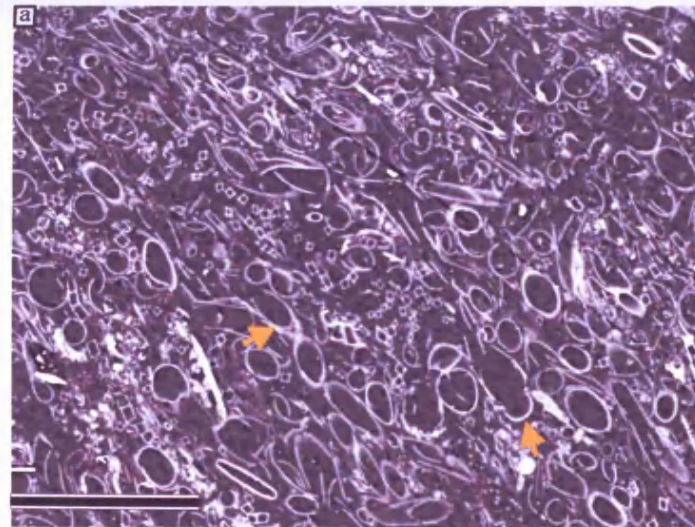
Backscattered electron imagery (BSEI) and secondary electron imagery (SEI) photographs of biogenic laminae characterised by *Corethron pennatum* and *Rhizosolenia* spp., Durmont d'Urville Trough.

(a) BSEI photograph of biogenic laminae. *C. pennatum* (gold arrow) and *Rhizosolenia* spp. (red arrow). Scale bar = 100 microns.

(b) SEI photograph of laminae characterised by *C. pennatum* (gold arrows) and *Rhizosolenia* spp. (red arrow). Scale bar = 90 microns.

### 8.1.5. Laminae Characterised by *Corethron pennatum*

This lamina type is characterised by high abundance of *Corethron pennatum* (Figure 8.8). Thirteen laminae are present within the analysed intervals, twelve of which are biogenic laminae (Figure 8.8a and b) and one a terrigenous lamina (Figure 8.8c and d). The other constituents of the assemblage are *Hyalochaete Chaetoceros* spp. resting spores (CRS), *Fragilariopsis* spp., *Porosira glacialis* resting spores (RS), *Phaeoceros Chaetoceros* spp., *Rhizosolenia* spp. and elongate pennates. CRS constitute 29.9% and *Fragilariopsis* spp. constitute 56.2% of the total diatom assemblage (Table 8.1). *Hyalochaete Chaetoceros* free counts (Table 8.2) are dominated by *Fragilariopsis* spp. (81.8%; dominated by *F. curta* (28.3%), *F. cylindrus* (28.1%), *F. rhombica* (10.9%), *F. kerguelensis* (5.0%) and *F. ritscheri* (3.6%)), *Thalassiosira* spp. (5.1%; dominated by *T. lentiginosa* (2.3%) and *T. gracilis* v. *gracilis* (1.2%)), *Rhizosolenia* spp. (1.2%), *Phaeoceros Chaetoceros* spp. (3.2%), *P. glacialis* RS (1.5%), *C. pennatum* (1.4%) and elongate pennates (1.6%). This lamina type has an absolute abundance of  $568 \times 10^6$  valves per gramme of dry sediment (Table 8.3). Most of the biogenic laminae occur in the analysed intervals below 44 mbsf (~ 2370 to 2814 cal. yrs BP) (Figure 8.3). One lamina with increased terrigenous content occurs at approx 34.0 mbsf. The laminae range in thickness from 0.8 to 25.7 mm ( $n = 13$ ,  $\sigma = 7.0$  mm, mean 7.1 mm) (Figure 8.4), making up 3.9% of the total sediment thickness. There is no correlation between lamina thickness and core depth.



**Figure 8.8**

Backscattered electron imagery (BSEI) and secondary electron imagery (SEI) photographs of biogenic and terrigenous laminae characterised by *Corethron pennatum*, Durmont d'Urville Trough.

(a) BSEI photograph of biogenic laminae. *C. pennatum* (gold arrows). Scale bar = 100 microns.

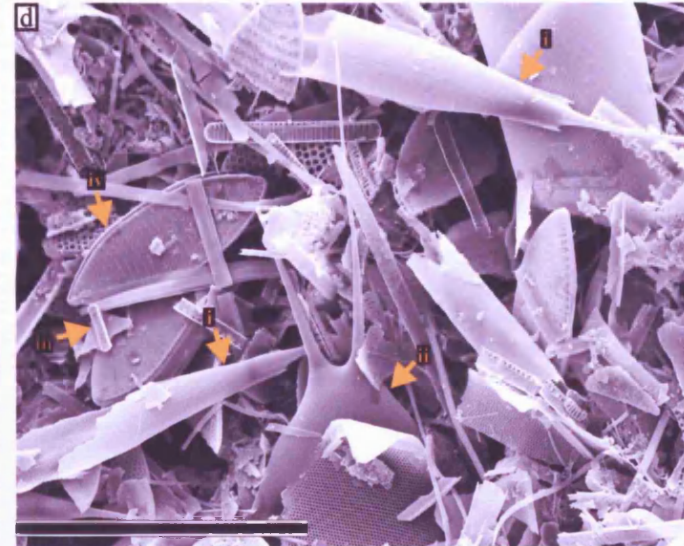
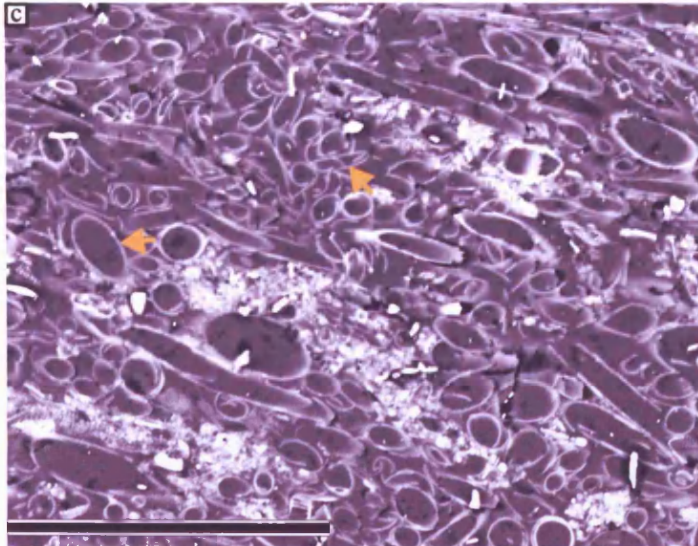
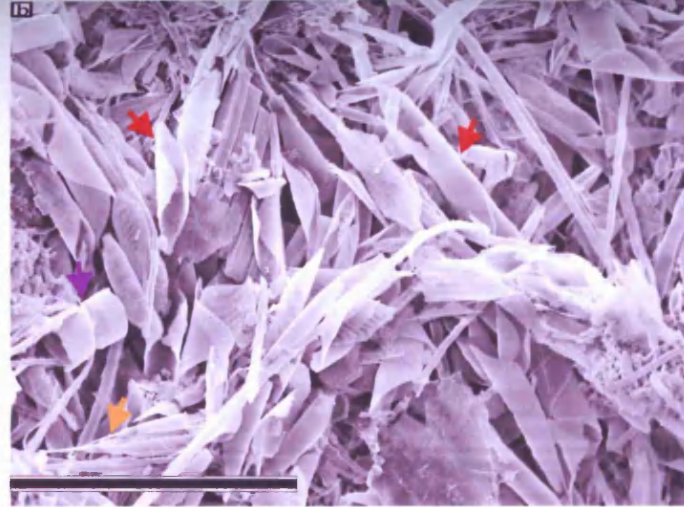
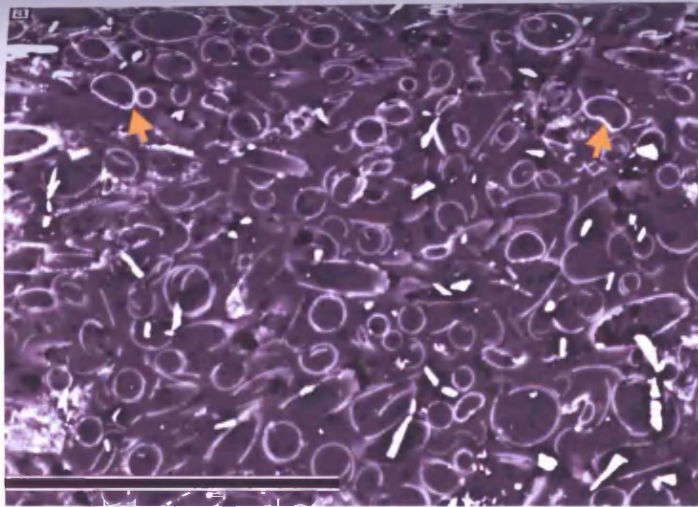
(b) SEI photograph of biogenic laminae. *C. pennatum* (gold arrows) and *C. pennatum* setae (red arrow). Scale bar = 70 microns.

(c) BSEI photograph of terrigenous laminae. *C. pennatum* (gold arrows). Scale bar = 100 microns.

(d) SEI photograph of terrigenous laminae. *C. pennatum* (gold arrows). Scale bar = 70 microns.

### 8.1.6. Laminae characterised by *Rhizosolenia* spp.

Laminae of this type are characterised by high abundance of *Rhizosolenia* spp. (Figure 8.9). Nine laminae are present in the analysed interval; seven are biogenic laminae (Figure 8.9a and b) and two terrigenous laminae (Figure 8.9c and d). Other constituents of the assemblage are *Hyalochaete Chaetoceros* spp. resting spores (CRS), *Fragilariopsis* spp., *Corethron pennatum* and elongate pennates. CRS constitute 21.1% and *Fragilariopsis* spp. constitute 56.1% of the total diatom assemblage (Table 8.1). *Hyalochaete Chaetoceros* free counts (Table 8.2) are dominated by *Fragilariopsis* spp. (73.7%; dominated by *F. cylindrus* (33.8%), *F. curta* (20.7%), *F. rhombica* (9.9%) and *F. kerguelensis* (3.2%)), *Proboscia* spp. (12.4%), *Rhizosolenia* spp. (3.2%; dominated by *R. antennata* f. *semispina*), *Thalassiosira* spp. (2.7%; dominated by *T. gracilis* v. *gracilis* (1.0%)), elongate pennates (2.3%), *Phaeoceros Chaetoceros* spp. (1.7%) and *C. pennatum* (0.3%). This lamina type has an absolute abundance of  $742 \times 10^6$  valves per gramme of dry sediment (Table 8.3). The laminae occur between 33 and 50 mbsf (~ 1790 – 2680 cal. yrs BP) (Figure 8.3) and range in thickness from 1.8 to 14.4 mm ( $n = 9$ ,  $\sigma = 4.3$  mm, mean = 8.2 mm) (Figure 8.4), making up 3.1% of total sediment thickness. There is no correlation between lamina thickness and core depth.



**Figure 8.9**

Backscattered electron imagery (BSEI) and secondary electron imagery (SEI) photographs of biogenic and terrigenous laminae characterised by *Rhizosolenia* spp., Durmont d'Urville Trough.

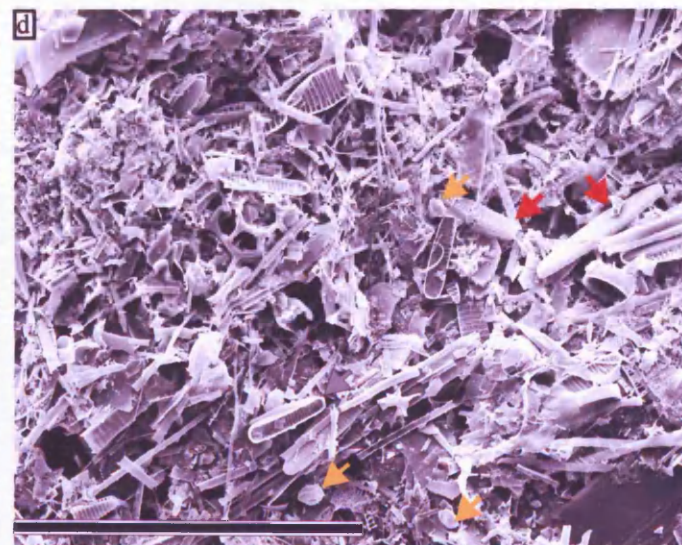
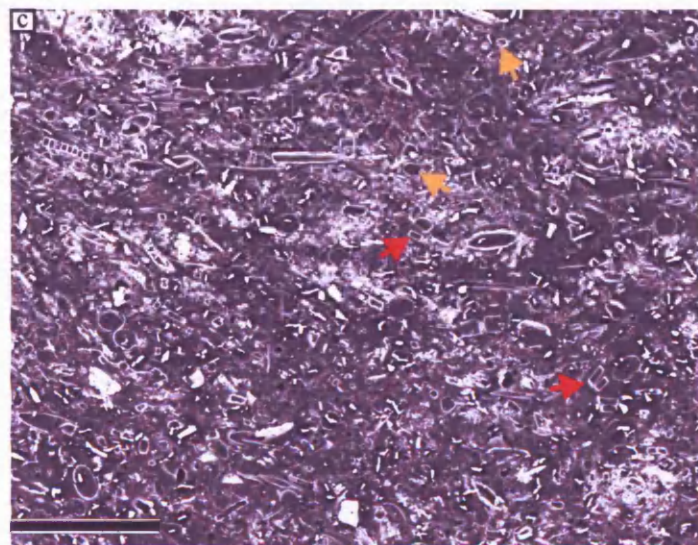
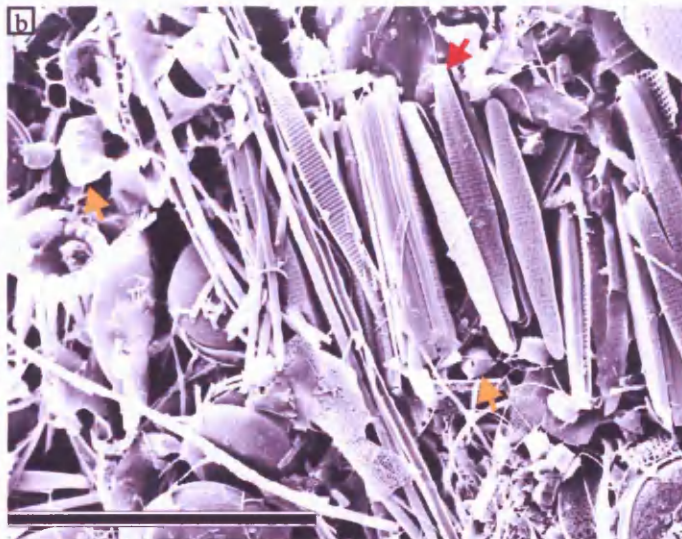
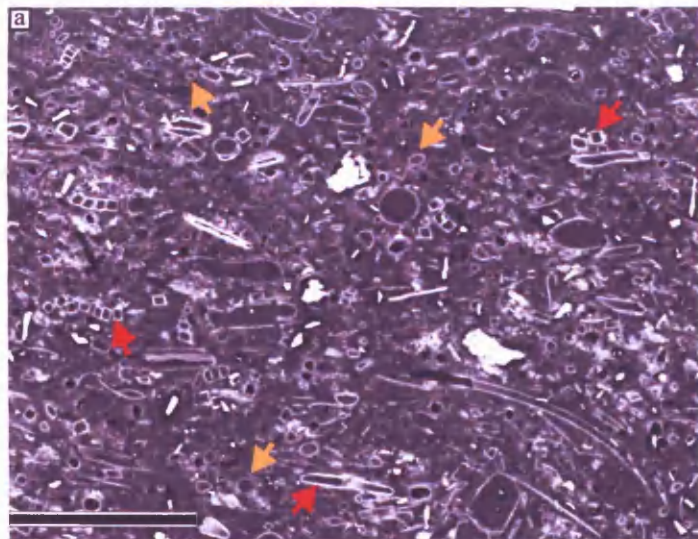
(a) BSEI photograph of biogenic laminae. *Rhizosolenia* spp. (gold arrows). Scale bar = 100 microns.

(b) SEI photograph of biogenic laminae. *R. antennata* f. *semispina* (gold arrow), *Rhizosolenia* spp. girdle bands (red arrows) and *Phaeoceros Chaetoceros* spp. (purple arrow). Scale bar = 100 microns.

(c) BSEI photograph of terrigenous laminae. *Rhizosolenia* spp. (gold arrows). Scale bar = 100 microns.

(d) SEI photograph of terrigenous laminae. (i) *R. antennata* f. *semispina*, (ii) *R. antennata* f. *antennata*, (iii) *Fragilariopsis cylindrus* and (iv) *F. rhombica* (gold arrows). Scale bar = 40 microns.





**Figure 8.5**

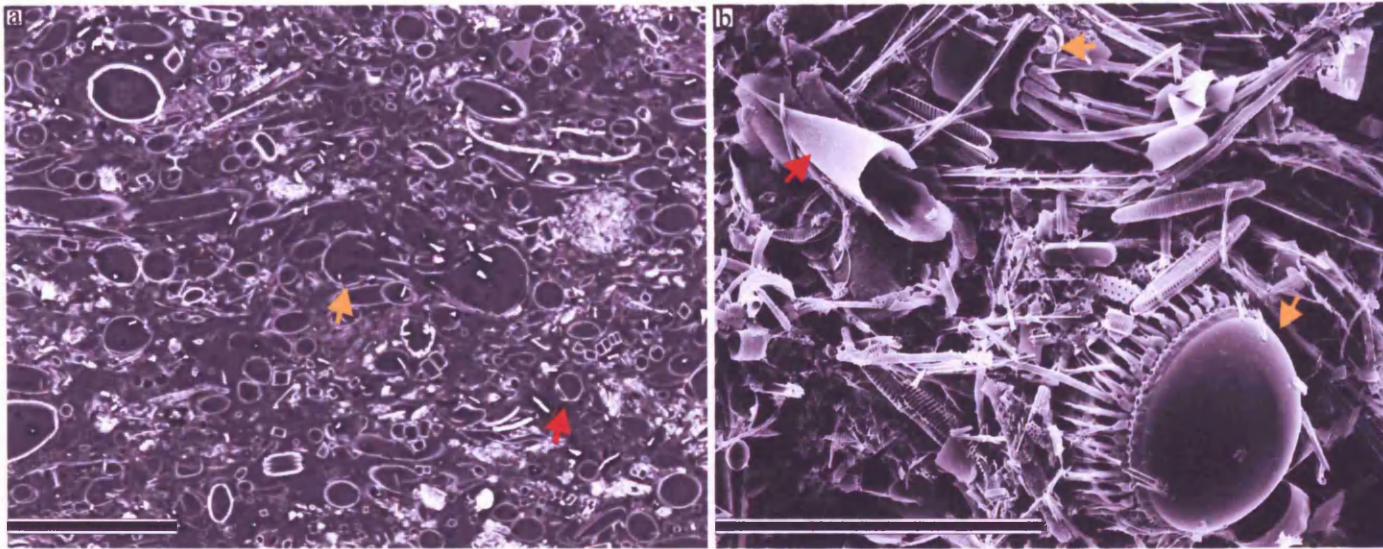
Backscattered electron imagery (BSEI) and secondary electron imagery (SEI) photographs of laminae characterised by *Hyalochaete Chaetoceros* spp. resting spores (CRS) and *Fragilariopsis* spp. biogenic and terrigenous laminae, Durmont d'Urville Trough.

(a) BSEI photograph of biogenic laminae. CRS (gold arrows) and *Fragilariopsis* spp. (red arrows).

(b) SEI photograph of biogenic laminae. CRS (gold arrows) and *Fragilariopsis* spp. (red arrow). Scale bar = 100 microns.

(c) BSEI photograph of terrigenous laminae. CRS (gold arrows) and *Fragilariopsis* spp. (red arrow). Scale bar = 100 microns.

(d) SEI photograph of terrigenous laminae. CRS (gold arrows) and *Fragilariopsis* spp. (red arrows). Scale bar = 50 microns.



**Figure 8.7**

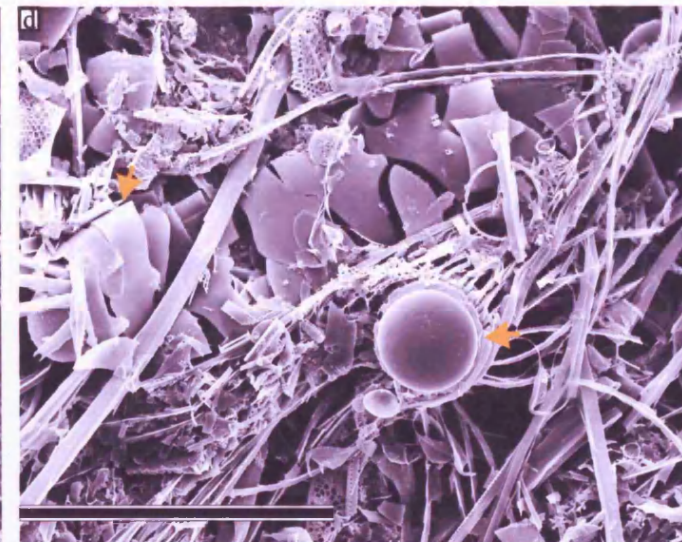
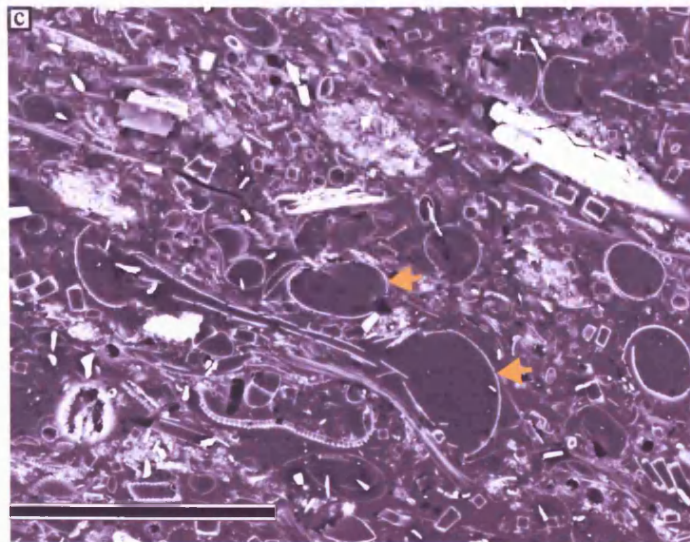
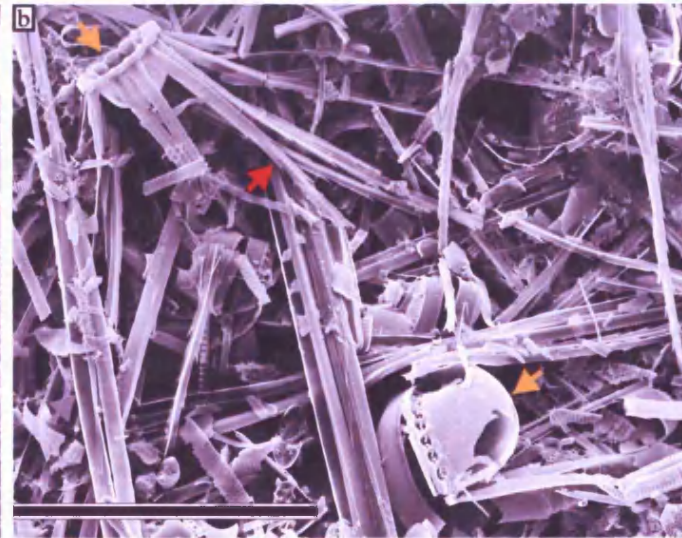
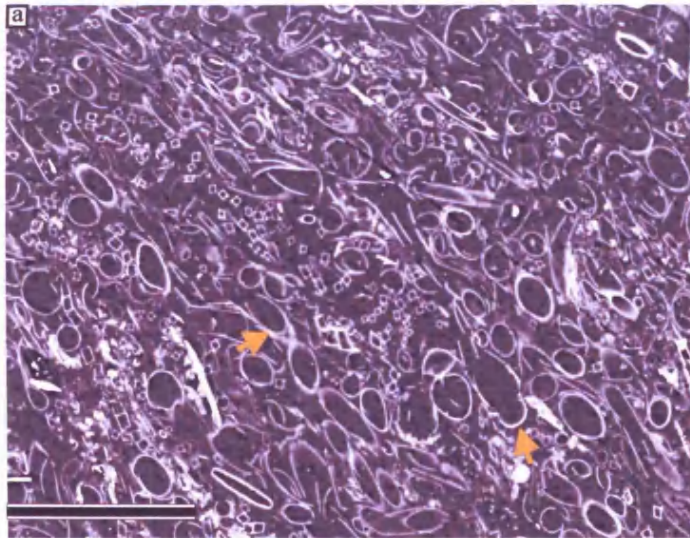
Backscattered electron imagery (BSEI) and secondary electron imagery (SEI) photographs of biogenic laminae characterised by *Corethron pennatum* and *Rhizosolenia* spp., Durmont d'Urville Trough.

**(a)** BSEI photograph of biogenic laminae. *C. pennatum* (gold arrow) and *Rhizosolenia* spp. (red arrow). Scale bar = 100 microns.

**(b)** SEI photograph of laminae characterised by *C. pennatum* (gold arrows) and *Rhizosolenia* spp. (red arrow). Scale bar = 90 microns.

### 8.1.5. Laminae Characterised by *Corethron pennatum*

This lamina type is characterised by high abundance of *Corethron pennatum* (Figure 8.8). Thirteen laminae are present within the analysed intervals, twelve of which are biogenic laminae (Figure 8.8a and b) and one a terrigenous lamina (Figure 8.8c and d). The other constituents of the assemblage are *Hyalochaete Chaetoceros* spp. resting spores (CRS), *Fragilariopsis* spp., *Porosira glacialis* resting spores (RS), *Phaeoceros Chaetoceros* spp., *Rhizosolenia* spp. and elongate pennates. CRS constitute 29.9% and *Fragilariopsis* spp. constitute 56.2% of the total diatom assemblage (Table 8.1). *Hyalochaete Chaetoceros* free counts (Table 8.2) are dominated by *Fragilariopsis* spp. (81.8%; dominated by *F. curta* (28.3%), *F. cylindrus* (28.1%), *F. rhombica* (10.9%), *F. kerguelensis* (5.0%) and *F. ritscheri* (3.6%)), *Thalassiosira* spp. (5.1%; dominated by *T. lentiginosa* (2.3%) and *T. gracilis* v. *gracilis* (1.2%)), *Rhizosolenia* spp. (1.2%), *Phaeoceros Chaetoceros* spp. (3.2%), *P. glacialis* RS (1.5%), *C. pennatum* (1.4%) and elongate pennates (1.6%). This lamina type has an absolute abundance of  $568 \times 10^6$  valves per gramme of dry sediment (Table 8.3). Most of the biogenic laminae occur in the analysed intervals below 44 mbsf (~ 2370 to 2814 cal. yrs BP) (Figure 8.3). One lamina with increased terrigenous content occurs at approx 34.0 mbsf. The laminae range in thickness from 0.8 to 25.7 mm ( $n = 13$ ,  $\sigma = 7.0$  mm, mean 7.1 mm) (Figure 8.4), making up 3.9% of the total sediment thickness. There is no correlation between lamina thickness and core depth.



**Figure 8.8**

Backscattered electron imagery (BSEI) and secondary electron imagery (SEI) photographs of biogenic and terrigenous laminae characterised by *Corethron pennatum*, Durmont d'Urville Trough.

(a) BSEI photograph of biogenic laminae. *C. pennatum* (gold arrows). Scale bar = 100 microns.

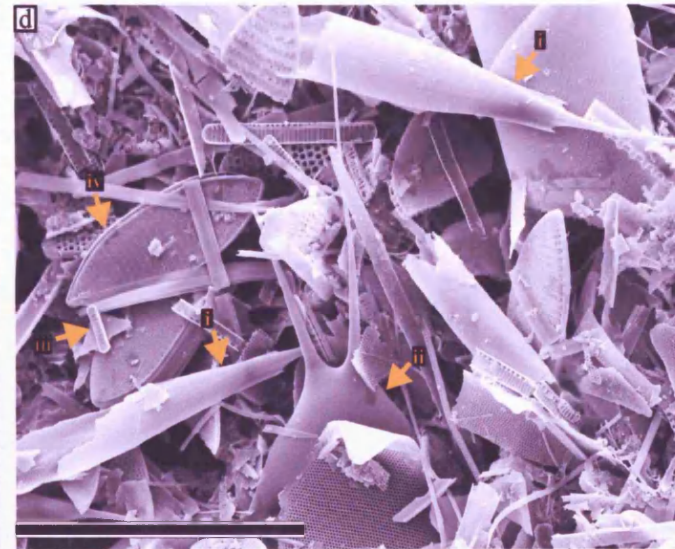
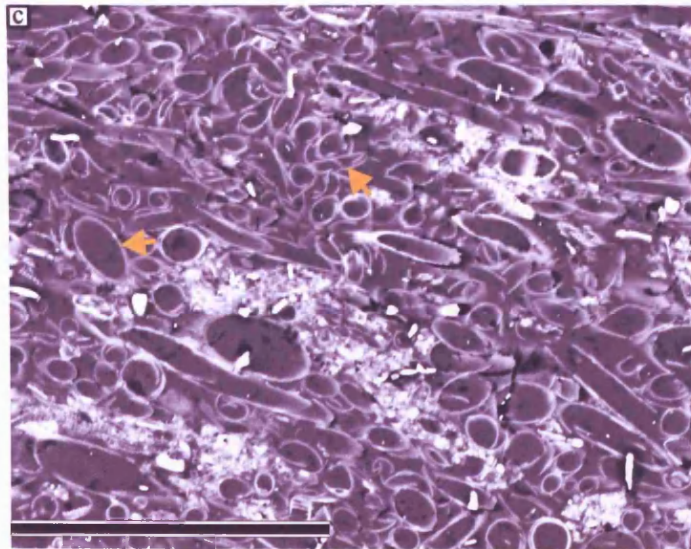
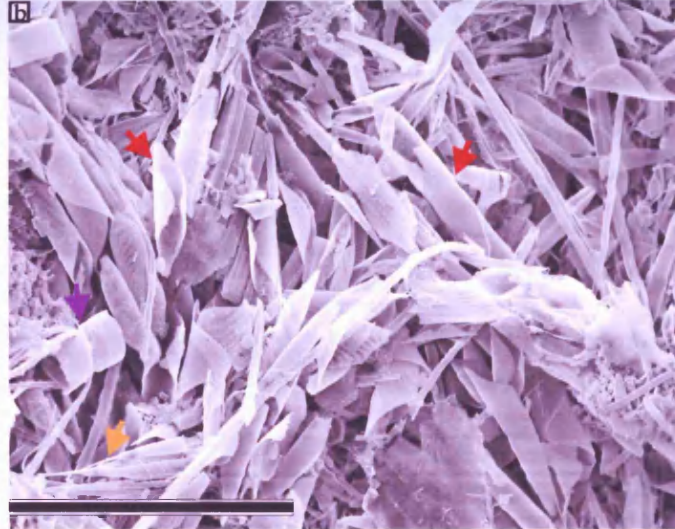
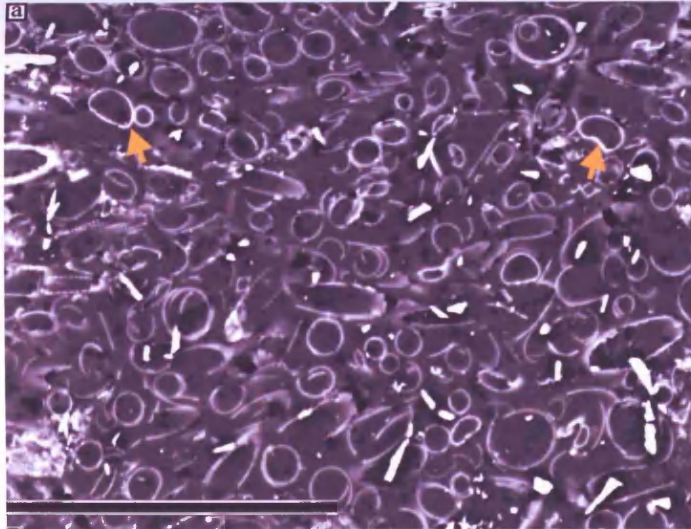
(b) SEI photograph of biogenic laminae. *C. pennatum* (gold arrows) and *C. pennatum* setae (red arrow). Scale bar = 70 microns.

(c) BSEI photograph of terrigenous laminae. *C. pennatum* (gold arrows). Scale bar = 100 microns.

(d) SEI photograph of terrigenous laminae. *C. pennatum* (gold arrows). Scale bar = 70 microns.

### 8.1.6. Laminae characterised by *Rhizosolenia* spp.

Laminae of this type are characterised by high abundance of *Rhizosolenia* spp. (Figure 8.9). Nine laminae are present in the analysed interval; seven are biogenic laminae (Figure 8.9a and b) and two terrigenous laminae (Figure 8.9c and d). Other constituents of the assemblage are *Hyalochaete Chaetoceros* spp. resting spores (CRS), *Fragilariopsis* spp., *Corethron pennatum* and elongate pennates. CRS constitute 21.1% and *Fragilariopsis* spp. constitute 56.1% of the total diatom assemblage (Table 8.1). *Hyalochaete Chaetoceros* free counts (Table 8.2) are dominated by *Fragilariopsis* spp. (73.7%; dominated by *F. cylindrus* (33.8%), *F. curta* (20.7%), *F. rhombica* (9.9%) and *F. kerguelensis* (3.2%)), *Proboscia* spp. (12.4%), *Rhizosolenia* spp. (3.2%; dominated by *R. antennata* f. *semispina*), *Thalassiosira* spp. (2.7%; dominated by *T. gracilis* v. *gracilis* (1.0%)), elongate pennates (2.3%), *Phaeoceros Chaetoceros* spp. (1.7%) and *C. pennatum* (0.3%). This lamina type has an absolute abundance of  $742 \times 10^6$  valves per gramme of dry sediment (Table 8.3). The laminae occur between 33 and 50 mbsf (~ 1790 – 2680 cal. yrs BP) (Figure 8.3) and range in thickness from 1.8 to 14.4 mm ( $n = 9$ ,  $\sigma = 4.3$  mm, mean = 8.2 mm) (Figure 8.4), making up 3.1% of total sediment thickness. There is no correlation between lamina thickness and core depth.



**Figure 8.9**

Backscattered electron imagery (BSEI) and secondary electron imagery (SEI) photographs of biogenic and terrigenous laminae characterised by *Rhizosolenia* spp., Durmont d'Urville Trough.

(a) BSEI photograph of biogenic laminae. *Rhizosolenia* spp. (gold arrows). Scale bar = 100 microns.

(b) SEI photograph of biogenic laminae. *R. antennata* f. *semispina* (gold arrow), *Rhizosolenia* spp. girdle bands (red arrows) and *Phaeoceros Chaetoceros* spp. (purple arrow). Scale bar = 100 microns.

(c) BSEI photograph of terrigenous laminae. *Rhizosolenia* spp. (gold arrows). Scale bar = 100 microns.

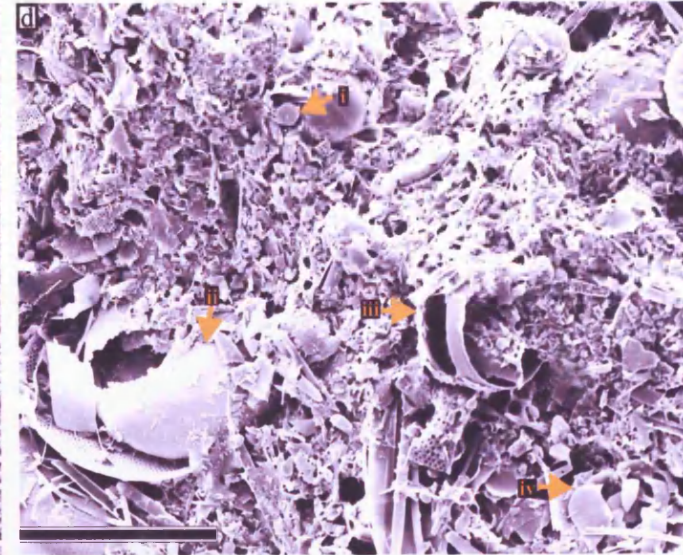
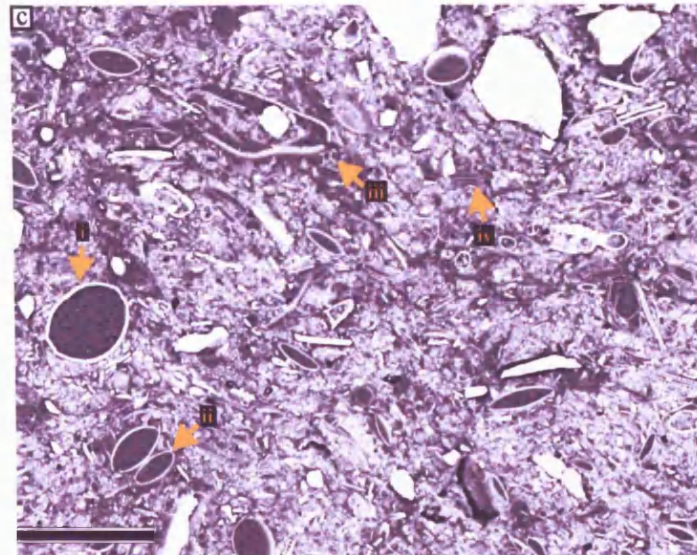
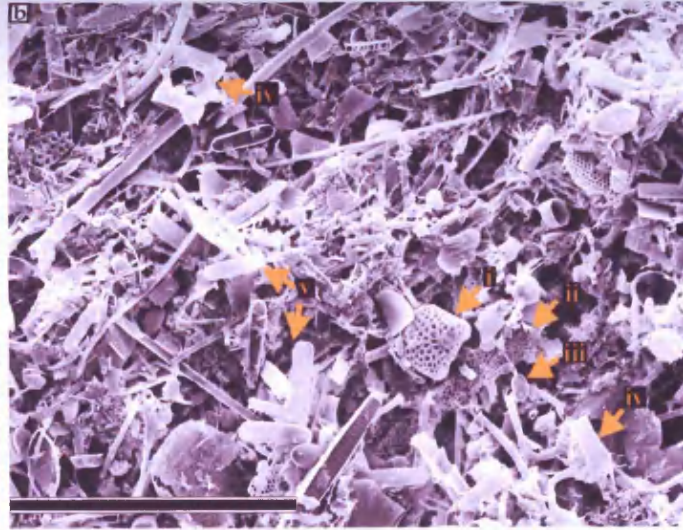
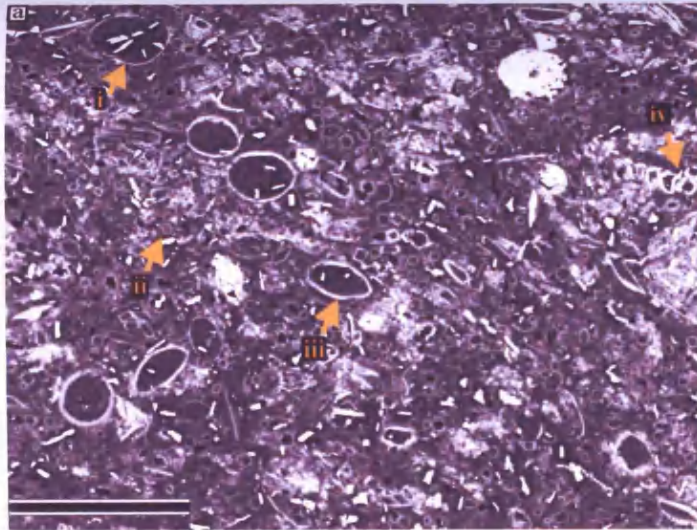
(d) SEI photograph of terrigenous laminae. (i) *R. antennata* f. *semispina*, (ii) *R. antennata* f. *antennata*, (iii) *Fragilariopsis cylindrus* and (iv) *F. rhombica* (gold arrows). Scale bar = 40 microns.

### 8.1.7. Mixed Diatom Assemblage Laminae

Laminae with this mixed diatom assemblage have been sub-divided into those with a higher biogenic content and a higher terrigenous content. The laminae with the higher biogenic content will be presented first.

The mixed diatom assemblage biogenic laminae are mainly composed of *Fragilariopsis* spp. and *Hyalochaete Chaetoceros* spp. resting spores (CRS) (Figure 8.10a and b). More minor species observed in this lamina type are *Corethron pennatum*, *Porosira glacialis* resting spores (RS) and *Stellarima microtrias* RS. CRS constitute 43.0% and *Fragilariopsis* spp. constitute 46.4% of the total diatom assemblage (Table 8.1). *Hyalochaete Chaetoceros* free counts (Table 8.2) are dominated by *Fragilariopsis* spp. (82.4%; dominated by *F. curta* (41.6%), *F. cylindrus* (14.3%), *F. rhombica* (11.7%) and *F. kerguelensis* (6.0%)), *Thalassiosira* spp. (5.2%; dominated by *T. lentiginosa* (1.4%) and *T. gracilis* v. *gracilis* (1.3%)), *Phaeoceros Chaetoceros* spp. (4.8%), *P. glacialis* RS (0.9%), *Rhizosolenia* spp. (0.8%), *C. pennatum* (0.6%) and elongate pennates (1.6%). This lamina type has an absolute abundance of  $734 \times 10^6$  valves per gramme of dry sediment (Table 8.3). The biogenic laminae are present throughout the analysed intervals (Figure 8.3) and range in thickness from 1.6 to 19.1 mm ( $n = 20$ ,  $\sigma = 4.9$  mm, mean = 8.1 mm) (Figure 8.4). This lamina type makes up 6.8% of total sediment thickness and there is no correlation between lamina thickness and core depth.

The mixed diatom assemblage terrigenous laminae are also mainly composed of *Fragilariopsis* spp. and CRS (Figure 8.10c and d). More minor species that make up the assemblage are *P. glacialis* RS, *S. microtrias* RS, *C. pennatum*, *Thalassiosira* spp., *Coscinodiscus bouvet* and *Trigonium arcticum*. CRS constitute 36.7% and *Fragilariopsis* spp. constitute 48.6% of the total diatom assemblage (Table 8.1). *Hyalochaete Chaetoceros* free counts (Table 8.2) are dominated by *Fragilariopsis* spp. (75.9%; dominated by *F. curta* (30.1%), *F. cylindrus* (15.8%), *F. rhombica* (13.0%), *F. kerguelensis* (7.2%) and *F. ritscheri* (3.6%)), *Thalassiosira* spp. (7.1%; dominated by *T. poroseriata* and *T. lentiginosa*), *Phaeoceros Chaetoceros* spp. (4.6%), *P. glacialis* RS (4.5%), *Rhizosolenia* spp. (1.3%) and *C. pennatum* (0.9%). This lamina type has an absolute abundance of  $556 \times 10^6$  valves per gramme of dry sediment (Table 8.3). The mixed diatom assemblage terrigenous laminae occur



**Figure 8.10**  
Backscattered electron imagery (BSEI) and secondary electron imagery (SEI) photographs of mixed diatom assemblage biogenic and terrigenous laminae, Durmont d'Urville Trough.

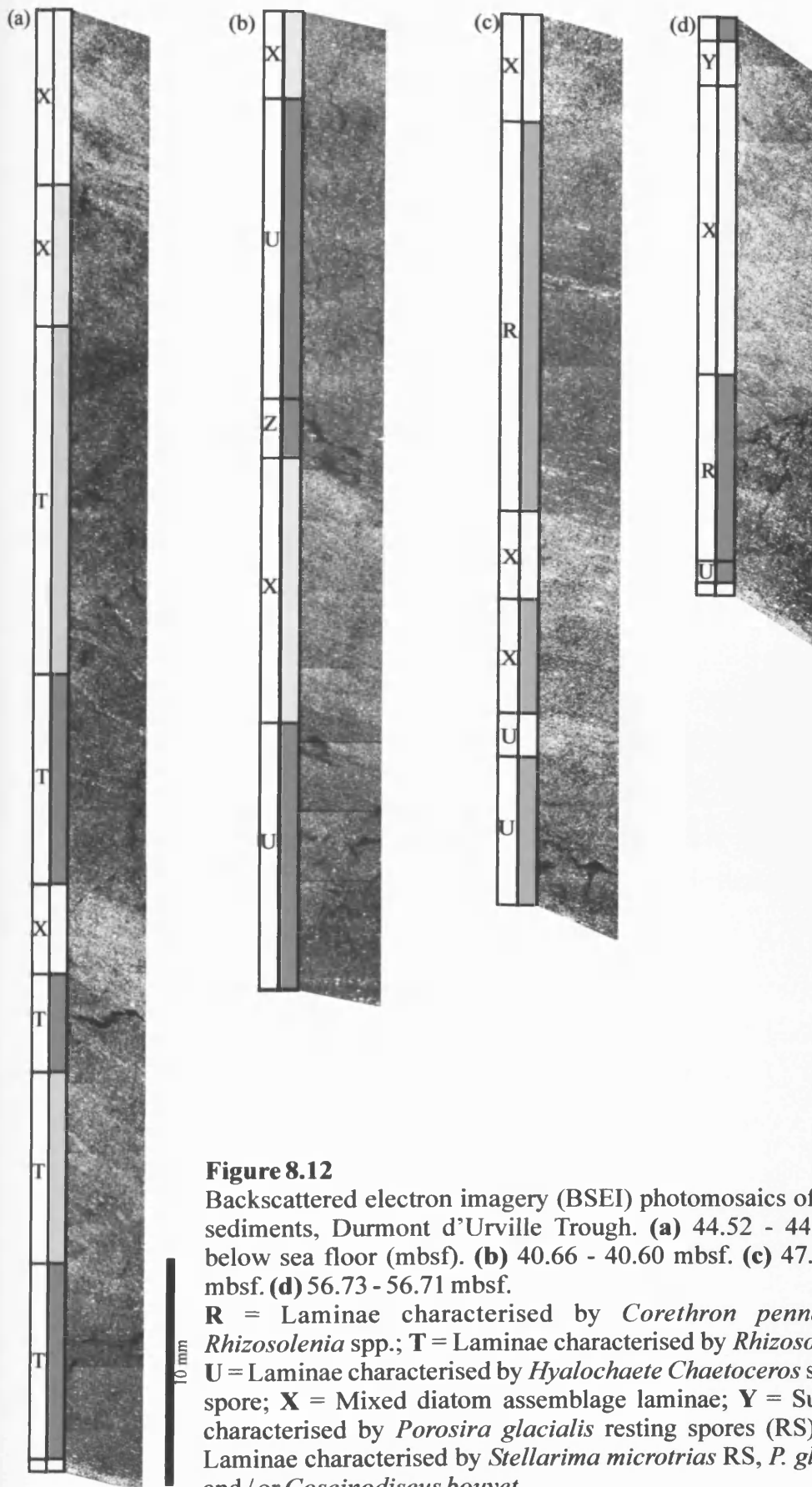
(a) BSEI photograph of biogenic laminae. Gold arrows (i) *Corethron pennatum* (ii) *Hyalochaete Chaetoceros* spp. resting spore (CRS) (iii) *Porosira glacialis* resting spores (RS) (iv) *Fragilariopsis* spp.. Scale bar = 100 microns.

(b) SEI photograph of biogenic laminae. Gold arrows *Eucampia antarctica* (i) resting spore and (ii) vegetative cell; (iii) CRS; (iv) *Phaeoceros Chaetoceros* spp.; (v) *Fragilariopsis curta*. Scale bar = 100 microns.

(c) BSEI photograph of terrigenous laminae. Gold arrows (i) *Stellarima microtrias* RS; (ii) *Porosira glacialis* RS; (iii) CRS; (iv) *Fragilariopsis* spp.. Scale bar = 100 microns.

(d) SEI photograph of terrigenous laminae. Gold arrows (i) CRS; (ii) *Coscinodiscus bouvet*; (iii) girdle bands; (iv) *Corethron pennatum* oirdle hands. Scale bar = 100





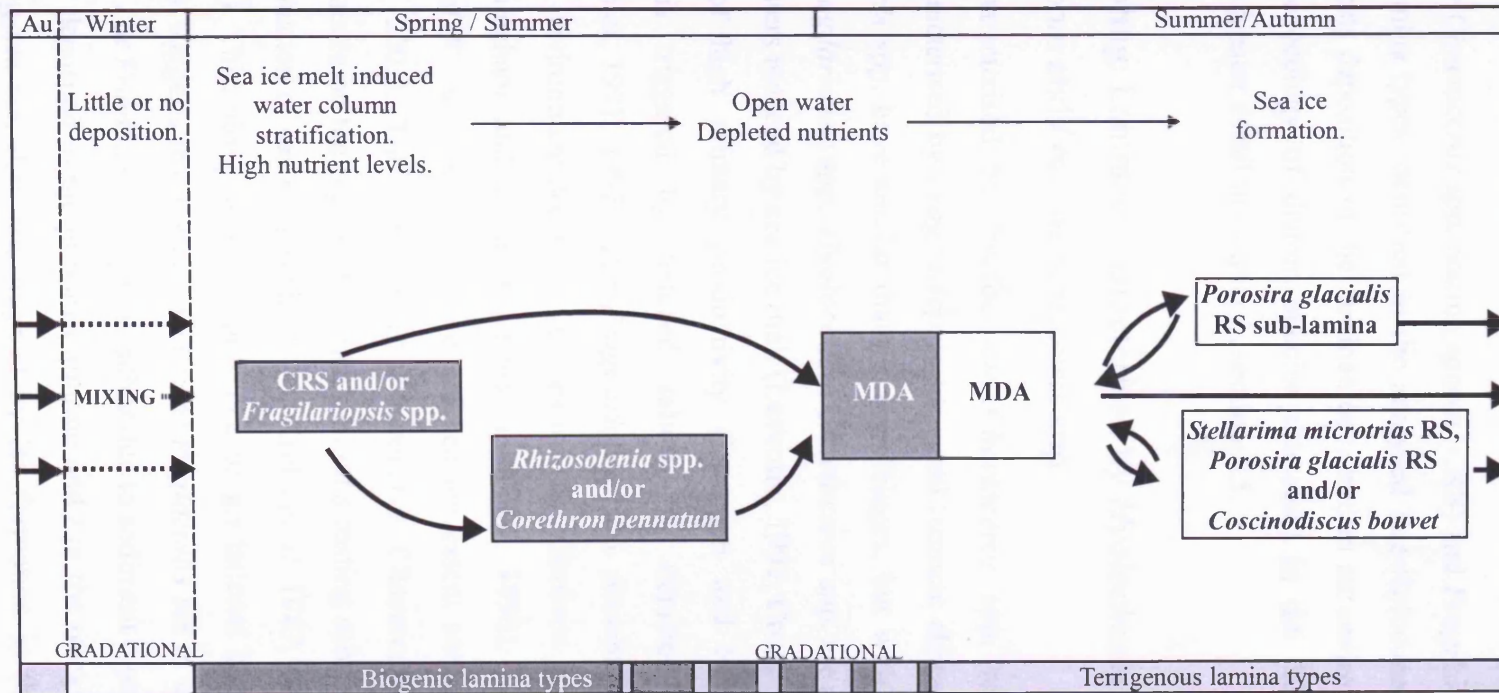
**Figure 8.12**

Backscattered electron imagery (BSEI) photomosaics of laminated sediments, Durmont d'Urville Trough. **(a)** 44.52 - 44.45 metre: below sea floor (mbsf). **(b)** 40.66 - 40.60 mbsf. **(c)** 47.76 - 47.71 mbsf. **(d)** 56.73 - 56.71 mbsf.

**R** = Laminae characterised by *Corethron pennatum* and *Rhizosolenia* spp.; **T** = Laminae characterised by *Rhizosolenia* spp. **U** = Laminae characterised by *Hyalochaete Chaetoceros* spp. resting spore; **X** = Mixed diatom assemblage laminae; **Y** = Sub-laminae characterised by *Porosira glacialis* resting spores (RS); and **Z** = Laminae characterised by *Stellarima microtrias* RS, *P. glacialis* RS and / or *Coscinodiscus bouvet*.

### 8.1.10. Lamina Relationships

Three hundred and three laminae and thirty-six sub-laminae are present in the analysed intervals (Appendix 3, Table A3.3.1). Absolute abundances of the biogenic and terrigenous laminae and sub-lamina types range from 556 – 1165 x10<sup>6</sup> valves per gramme of dry sediment (Table 8.3). Sub-laminae characterised by *Porosira glacialis* resting spores (RS) have the greatest absolute abundance of diatoms and mixed diatom assemblage terrigenous laminae have the smallest absolute abundance of diatoms (Table 8.3). There is no correlation between lamina thickness and core depth for any of the lamina and sub-lamina types. The majority of boundaries throughout the analysed intervals are gradational (Figure 8.12); very occasionally boundaries are slightly disturbed by bioturbation. Typical sequences of lamina types have been identified in the laminated intervals and are schematically represented in Figure 8.14, however, not every lamina type occurs in every sequence. Lamina in the lower part of the lamina sequence have a high biogenic content and are characterised by *Hyalochaete Chaetoceros* spp. resting spores (CRS) and / or *Fragilariopsis* spp.. These are mostly succeeded by mixed diatom assemblage; however, intermittently through the analysed intervals, laminae characterised by *Corethron pennatum* and / or *Rhizosolenia* spp. may occur between CRS and / or *Fragilariopsis* spp. and mixed diatom assemblage laminae. In the upper part of the sequence, laminae have a higher terrigenous content with a mixed diatom assemblage. The sequence can end with terrigenous laminae characterised by *Stellarima microtrias* RS, *P. glacialis* RS and / or *Coscinodiscus bouvet* or sub-lamina (terrigenous or biogenic) characterised by *P. glacialis* RS. Biogenic sub-laminae characterised by *P. glacialis* RS also occur at the beginning of the following sequence. Pulses of terrigenous material occasionally occur in the lower part of the sequence creating laminae characterised by CRS, *Fragilariopsis* spp., *C. pennatum* or *Rhizosolenia* spp. with increased terrigenous content.



**Figure 8.14**

Schematic diagram showing the sequence of lamina type deposition, Durmont d'Urville Trough. CRS = *Hyalochaete Chaetoceros* spp. resting spore. RS = resting spore. MDA = Mixed diatom assemblage. Au = Autumn.

## 8.2. Interpretation and Discussion

### 8.2.1. Seasonal Signal

*Hyalochaete Chaetoceros* spp. resting spores (CRS) and *Fragilariopsis* spp. dominate all of the lamina types identified in the analysed late-Holocene laminated intervals, which suggests deposition of the laminae occurred in an environment dominated by sea ice. The ecology of diatom species discussed in the following sections are described in greater detail in chapter 3, section 3.5.

#### 8.2.1.1. Spring: Laminae Characterised by *Hyalochaete Chaetoceros* spp. Resting Spore and / or *Fragilariopsis* spp.

Laminae characterised by *Hyalochaete Chaetoceros* spp. resting spore (CRS), laminae characterised by *Fragilariopsis* spp., and laminae characterised by CRS and *Fragilariopsis* spp. have similar diatom assemblages, but with varying amounts of CRS and *Fragilariopsis* spp.. *Hyalochaete Chaetoceros* spp. are associated with well-stratified waters induced by sea ice melt (Leventer, 1991; Crosta *et al.*, 1997), and are indicative of high primary productivity (Donegan and Schrader, 1982). CRS formation is triggered by reduced salinity or depleted nitrogen near the edge (Leventer, 1991; 1992). The *Fragilariopsis* spp. present in these lamina types bloom in an environment dominated by sea ice (e.g. Garrison *et al.*, 1983a; Garrison, 1991; Cunningham and Leventer, 1998; Leventer, 1998). In particular, a high abundance of *F. curta* indicates increased sea ice extent and duration (Taylor and Sjunneskog, 2002). The presence of *Phaeoceros Chaetoceros* spp. suggests an oceanic influence on the region. *Porosira glacialis* resting spores (RS) are associated with the formation of sea ice (Hasle, 1973; Krebs *et al.* 1987; Watanabe, 1988; Scott *et al.*, 1994). This, along with the presence of gradational boundaries between all lamina types, suggests that the occurrence of *P. glacialis* RS in laminae characterised by CRS and / or *Fragilariopsis* spp. is either due to sediment bioturbation of laminae / sub-laminae deposited in the previous autumn and / or the release of *P. glacialis* RS from melting sea ice, that was trapped by ice formation in the previous growing season. The dominance of CRS or *Fragilariopsis* spp. over one another in these lamina types is probably controlled by varied sea ice cover and sea ice persistence in

the growing season. Blooms of *Hyalochaete Chaetoceros* spp. and *Fragilariopsis* spp. recorded in these three lamina types (terrigenous and biogenic laminae forms) indicate stratified, low salinity and nutrient-rich waters associated with sea ice melt in spring. The less common terrigenous lamina forms are a result of terrigenous material released by sporadic, accelerated sea ice and / or iceberg melt in spring.

#### 8.2.1.2. Summer: Laminae Characterised by *Corethron pennatum* and / or *Rhizosolenia* spp.

Laminae characterised by *Corethron pennatum*, laminae characterised by *Rhizosolenia* spp., and laminae characterised by *C. pennatum* and *Rhizosolenia* spp. have similar diatom assemblages, but with varying abundances of *Corethron pennatum* and / or *Rhizosolenia* spp. These species and genera are associated with comparable water column conditions. The lamina type characterised by *C. pennatum* occurs most often, out of these three types, in the analysed intervals and has the highest sediment thickness percentage out of these three types.

*C. pennatum* is a cosmopolitan and widespread species (e.g. Fryxell and Hasle, 1971; Fenner *et al.*, 1976; Leventer *et al.*, 1993) that has a preference for open water, ice free conditions (Fryxell and Hasle, 1971; Makarov, 1984). Stickley *et al.* (2005) suggested that *C. pennatum* bloom when an influx of warmer open water (under stratified conditions) occurs after, or at the end of spring sea ice melt. *C. pennatum* can take advantage of higher light levels in surface waters for photosynthesis and nutrients at depth by migrating up and down in the water column (Leventer *et al.*, 2002). Mass sedimentation of *C. pennatum* blooms is thought to occur when the water column is destabilised (Crawford *et al.*, 1997; Kemp *et al.*, 2000) by mixing events such as storms. *C. pennatum* blooms have been associated with periods of unusual warmth during the unstable transition between the mid-Holocene Climatic Optimum and subsequent cooling in Palmer Deep, Antarctic Peninsula (Taylor and Sjunneskog, 2002). *Rhizosolenia* spp. also have the ability to migrate up and down the water column in search of higher nutrients and light levels. This genus blooms in open water conditions which has little sea ice influence (Harbison *et al.*, 1977; Alldredge and Silver, 1982; Kemp *et al.*, 1999). *Rhizosolenia* spp. are dominated by *R. antennata* f. *semispina*; this species has been observed in a range of environments, between open

water and sublittoral sea ice environments (Ligowski, 1993) and dominates open waters in late summer (Froneman *et al.*, 1995). The closely related genus *Proboscia* occurs with *Rhizosolenia* spp. and is a buoyant mat former which can play a major part in summer – autumn diatom assemblages (Brichta and Nöthig, 2003). Stickley *et al.* (2005) suggest that *Rhizosolenia* spp. and *Proboscia* spp. blooms indicate increasingly oligotrophic warmer waters. *Fragilariopsis curta* and *F. cylindrus* are co-dominant species of the *Fragilariopsis* genus present in these lamina types. Both of these species have a wide distribution from offshore to nearshore environments (Zielinski and Gersonde, 1997), with highest abundances occurring in coastal regions influenced by sea ice (Truesdale and Kellogg, 1979; Leventer and Dunbar, 1988; Leventer, 1992; 1998; Zielinski and Gersonde, 1997; McMinn *et al.*, 2001). Both *Fragilariopsis* species can live within or beneath sea ice (e.g. Armand, 2000; Fryxell *et al.*, 1987). Blooms of *C. pennatum* and / or *Rhizosolenia* spp. recorded in these three lamina types (biogenic and terrigenous laminae forms) indicate stable relatively warm open waters which occur in late spring/early summer, which have minimal sea ice influence. The less common terrigenous lamina forms are a result of terrigenous material released from sea ice and/or iceberg melt.

### 8.2.1.3. Summer: Mixed Diatom Assemblage

The species within the mixed diatom assemblage laminae such as *Thalassiosira lentiginosa*, *T. gracilis* v. *gracilis*, *T. poroseriata*, *Porosira glacialis* resting spores (RS) and *Phaeoceros Chaetoceros* spp. suggest less stratified, more mixed open water conditions (Jousé *et al.*, 1962; Kozlova, 1966; DeFelice and Wise, 1981; Hasle and Syvertsen, 1997; Zielinski and Gersonde, 1997). The high abundance of *Fragilariopsis* spp. within these laminae also suggests that sea ice is still present in the vicinity. Mixed diatom assemblage biogenic laminae are associated with summer deposition when sea ice has reduced a little and the water column becomes mixed by storms. Mixed diatom assemblage terrigenous laminae are associated with later summer deposition; the input of ice rafted debris from local glaciers, sediment from sea ice and entrained fine grained sediments (as occurs in Mertz Ninnis Trough; Dunbar *et al.*, 1985; Domack, 1988; Rintoul, 1998; Bindoff *et al.*, 2001) increases the terrigenous component of the laminae. *Trigonium arcticum* occurs in the mixed diatom assemblage terrigenous laminae. This species epiphytically lives on algae

between 200 and 300 metres depth in the water column (Thomas, 1966; Hendeby, 1937); therefore it is possible that it is swept into the trough by bottom currents.

#### 8.2.1.4. Autumn/Spring Transition: Sub-lamina Characterised by *Porosira glacialis* Resting Spores

*Porosira glacialis* blooms in the area adjacent to sea ice (Hasle, 1973) but not within sea ice (Watanabe, 1988; Scott *et al.*, 1994). Resting spores are produced when sea ice formation overwhelms the environment in autumn. The relatively thin sub-laminae of *P. glacialis* resting spores (RS) suggest a single, relatively short episode of resting spore formation. These sub-laminae are not always present in the sediment after late summer laminae; this indicates that the resting spores were either not preserved in the sediments or environmental conditions were not favourable for blooms and / or resting spore formation of *P. glacialis*. This sub-lamina type therefore, is associated with autumn sea ice formation. The majority of the sub-laminae are terrigenous, which is due to the influx of terrigenous material from local glaciers (ice rafted debris), melting sea ice and advection of fine-grained material into the region (see section 8.2.1.3). The biogenic sub-laminae result from biogenic flux overwhelming terrigenous material flux to the trough floor.

#### 8.2.1.5. Autumn/Spring Transition: Laminae Characterised by *Stellarima microtrias* Resting Spores, *Porosira glacialis* Resting Spores and / or *Coscinodiscus bouvet*

*Stellarima microtrias* is associated with shelf ice and surrounding waters (Hasle *et al.*, 1988). In summer high abundances of the species have been observed in fast ice (Watanabe, 1982; Krebs *et al.*, 1987; Tanimura *et al.*, 1990) and in autumn the resting spore is found in high abundances under sea ice (Fryxell, 1989). *Porosira glacialis* RS are produced during sea ice formation in autumn (as discussed in section 8.2.1.4). *Coscinodiscus bouvet* is a neritic species which may have been advected into the region (Priddle and Thomas, 1989). Both the terrigenous and biogenic forms of this lamina type are associated with autumn sea ice formation; the biogenic form (as with biogenic *P. glacialis* RS sub-laminae) is likely to be a result of biogenic material overwhelming terrigenous flux to the sediment.

### 8.2.2. Lamina Relationships

The difference in absolute abundance of diatoms between the laminae characterised by *Hyalochaete Chaetoceros* spp. resting spore (CRS) and the remaining lamina types is due to differences in water column stratification and nutrient levels. The dominance of sea ice taxa (*Fragilariopsis* spp.; *F. curta* and *F. cylindrus*) in all the lamina types suggests that persistent sea ice was present in the late-Holocene, between 2814 and 925 cal. yrs BP; the time period encompassed by the laminated sediment analysed here. In several East Antarctic and Antarctic Peninsula sites (e.g. Bunge Oasis, Prydz Bay, Terra Nova Bay, Lallemand Fjord, Palmer Deep) this time period has been defined as post mid-Holocene Climatic Optimum cooling (see section 2.4.3), which corroborates the predicted presence of persistent sea ice.

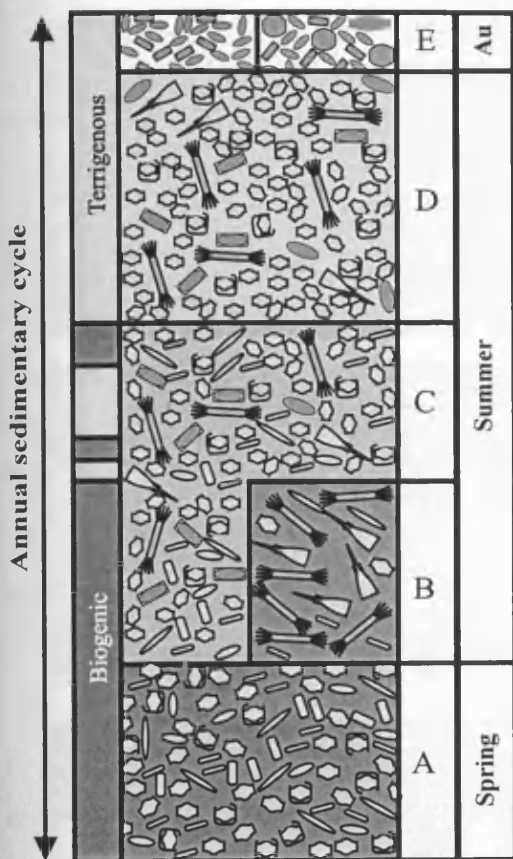
An annual cyclicality in lamina types is ascertained from diatom assemblages (Figure 8.15). In spring, sea ice melt induces water column stratification which traps nutrients released from the sea ice and atmospheric particles (Tuncel *et al.*, 1989; Wagenbach, 1996). Highly stratified surface waters with high nutrient levels are conducive for *Hyalochaete Chaetoceros* spp. blooms and, therefore, the deposition of laminae characterised by CRS. If, in spring, the sea ice does not melt rapidly and there is a substantial quantity of sea ice remaining in the environment as the growing season commences, *Fragilariopsis* spp. (sea ice taxa) will bloom and be deposited as laminae characterised by *Fragilariopsis* spp.. Currently, the earliest sea ice retreat from over the core site is December; therefore this site has a shorter growing season than over the Mertz Ninnis Trough (see chapter 7) where the Mertz Glacier Polynya is in operation (Figure 8.16). When the environment in spring is an average of these two environmental conditions (highly stratified surface waters, trapped nutrients and a moderate amount of sea ice) *Hyalochaete Chaetoceros* spp. and *Fragilariopsis* spp. will bloom, co-dominating the diatom assemblage; resulting in the deposition of laminae characterised by CRS and *Fragilariopsis* spp..

In late spring / early summer two possible scenarios may occur which result in the deposition of different lamina types. Firstly, uncharacteristically early seasonal warmth and stable stratified waters would allow *Corethron pennatum* and / or *Rhizosolenia* spp. to bloom (*Rhizosolenia* spp. more dominant in more oligotrophic conditions). Deposition of laminae characterised by *C. pennatum* and / or *Rhizosolenia* spp. would result. The laminae characterised by *C. pennatum* and / or



*Rhizosolenia* spp. are present before 1840 cal. yrs BP which may indicate that the environment fluctuated between relatively warmer and cooler conditions during the transition from the mid-Holocene Climatic Optimum before stabilising, as is observed in Lallemand Fjord (Taylor *et al.*, 2001). Secondly, more commonly in summer, surface waters bio-depleted in nutrients become mixed by storm activity redistributing nutrients throughout the water column, allowing a more mixed diatom assemblage to thrive; resulting in the deposition of mixed diatom assemblage laminae. As summer progresses terrigenous material derived from local glaciers, sea ice and bottom water currents increases, which augments the terrigenous content of lamina. In autumn, sea ice formation commences and blooms of *Stellarima microtrias*, *Porosira glacialis* and / or *Coscinodiscus bouvet* occur. Environmental stress, such as increased salinity and reduced light levels, causes resting spore formation, producing sub-lamina characterised by *P. glacialis* RS and lamina characterised by *S. microtrias* RS, *P. glacialis* RS and / or *C. bouvet*. The terrigenous content of the sub-lamina and laminae will be controlled by the biogenic flux to the trough floor. A transition from late summer / autumn laminae to spring/summer laminae suggests that there was little or no deposition during the winter.

The laminations in the analysed intervals can not be described as varves. The annual cycle consists of two or more laminae per annual deposit but there is no rhythmic repetition of the same two lamina types. Using the sequence of diatom assemblages, one hundred and twenty-one complete years have been identified in the analysed intervals (see Appendix 3, Table A3.3.1). Not every lamina or sub-lamina type is present in every annual deposit as similar environmental conditions are not repeated every year. Markov chain analysis was not conducted on the sequence of lamina types since there was an insufficient number of lamina in each analysed interval.



**Figure 8.15**

Schematic representation of an annual succession of lamina types, Durmont d'Urville Trough. Compiled from backscattered electron imagery (BSEI) data.

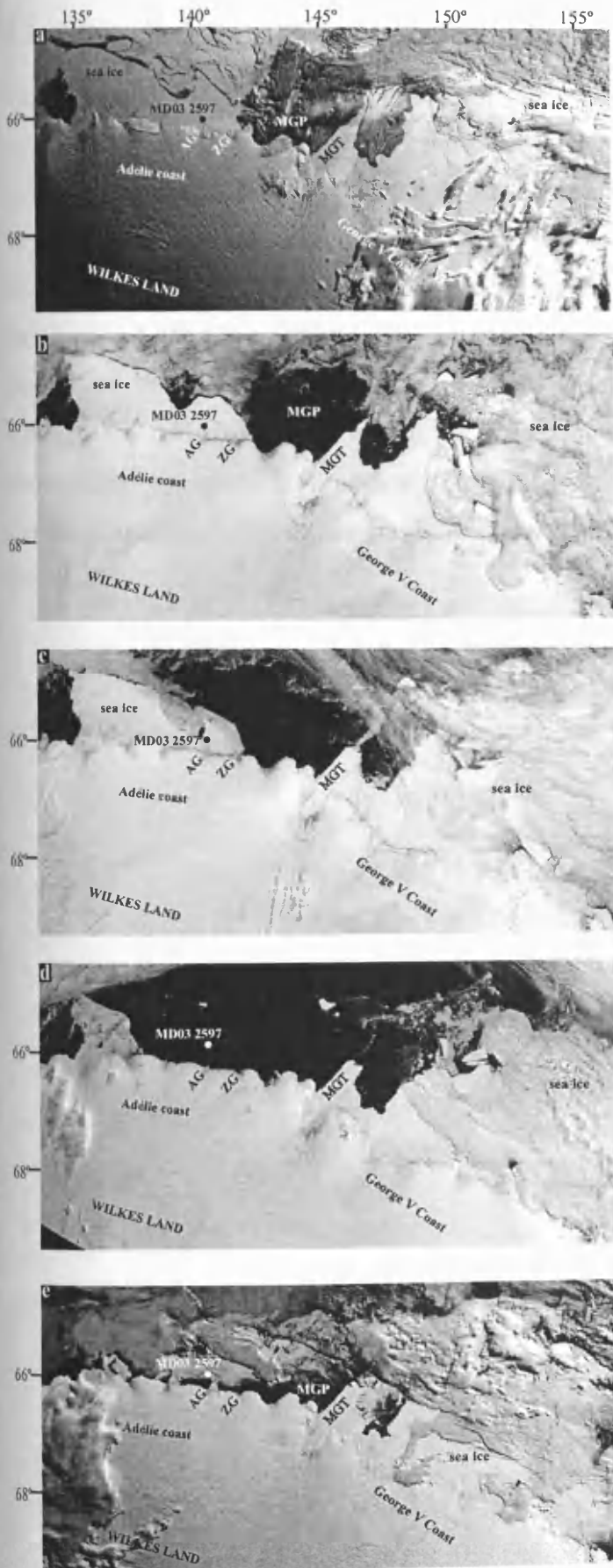
A = Laminae characterised by *Hyalochaete*, *Chaetoceros* spp. resting spores and/or *Fragilariopsis* spp.

B = Laminae characterised by *Corethron pennatum* and/or *Rhizosolenia* spp.

C = Mixed diatom assemblage biogenic laminae

D = Mixed diatom assemblage terrigenous laminae

E = Sub-laminae characterised by *Porosira glacialis* resting spores and/or laminae characterised by *Stellarima microtrias* resting spores, *P. glacialis* resting spores and/or *Coscinodiscus bouvet*



**Figure 8.16**

Polar stereographic satellite MODIS (Moderate Resolution Imaging Spectroradiometer) images of Adélie and George V coast, East Antarctica, from spring to autumn.

(a) 2nd September 2003

(b) 26th November 2003

(c) 5th December 2003

(d) 9th February 2004

(e) 31st March 2004

Durmont d'Urville Trough core site, MD03 2597 is marked.

MGT = Mertz Glacier Tongue

AG = Astrolabe Glacier

ZG = Zélée Glacier

MGP = Mertz Glacier

Polynya.

Scambos *et al.* (2001).

[Http://nsidc.org/data/iceshelves\\_images/mertz.html](http://nsidc.org/data/iceshelves_images/mertz.html)

(07/09/05).

### 8.3. Conclusions

Three hundred and three laminae and thirty-six sub-laminae are preserved in the analysed laminated intervals which have been interpreted as one hundred and twenty complete years of deposition. These laminae provide a high resolution archive of climate and palaeoceanography between 2814 and 925 cal. yrs BP during the post mid-Holocene Climatic Optimum cooling. Several lamina and sub-lamina types were identified and interpreted as resulting from a particular season of deposition. Lamina types were influenced by extensive sea ice, associated with the cooling which followed the mid-Holocene Climatic Optimum. Before 1840 cal. yr BP, laminae characterised by open, ice-free-water loving species indicate a possible unstable climatic transition between the mid-Holocene Climatic Optimum and subsequent cooling.

## 9. Core Site Comparison

This chapter compares the western Antarctic Peninsula laminated intervals from ODP 178 1098A (Palmer Deep) and the East Antarctic Margin laminated intervals from NBP0101 JPC10 and NBP0101 KC10A (Mertz Ninnis Trough) and MD03 2597 (Durmont d'Urville Trough). The laminated intervals are composed of several lamina and sub-lamina types. Each type of lamina and sub-lamina is classified according to diatom species identified in backscattered electron imagery (BSEI) analysis. Lamina and sub-lamina types from all of the laminated intervals analysed during this study are associated with seasonal productivity. The number of lamina types, diatom assemblages within lamina types and style of laminations from the four laminated intervals are compared and implications discussed in this chapter. The individual results and interpretations of the four laminated intervals can be found in chapters 6, 7 and 8.

### 9.1. Deglacial and Post-glacial Laminated Sediment Comparison

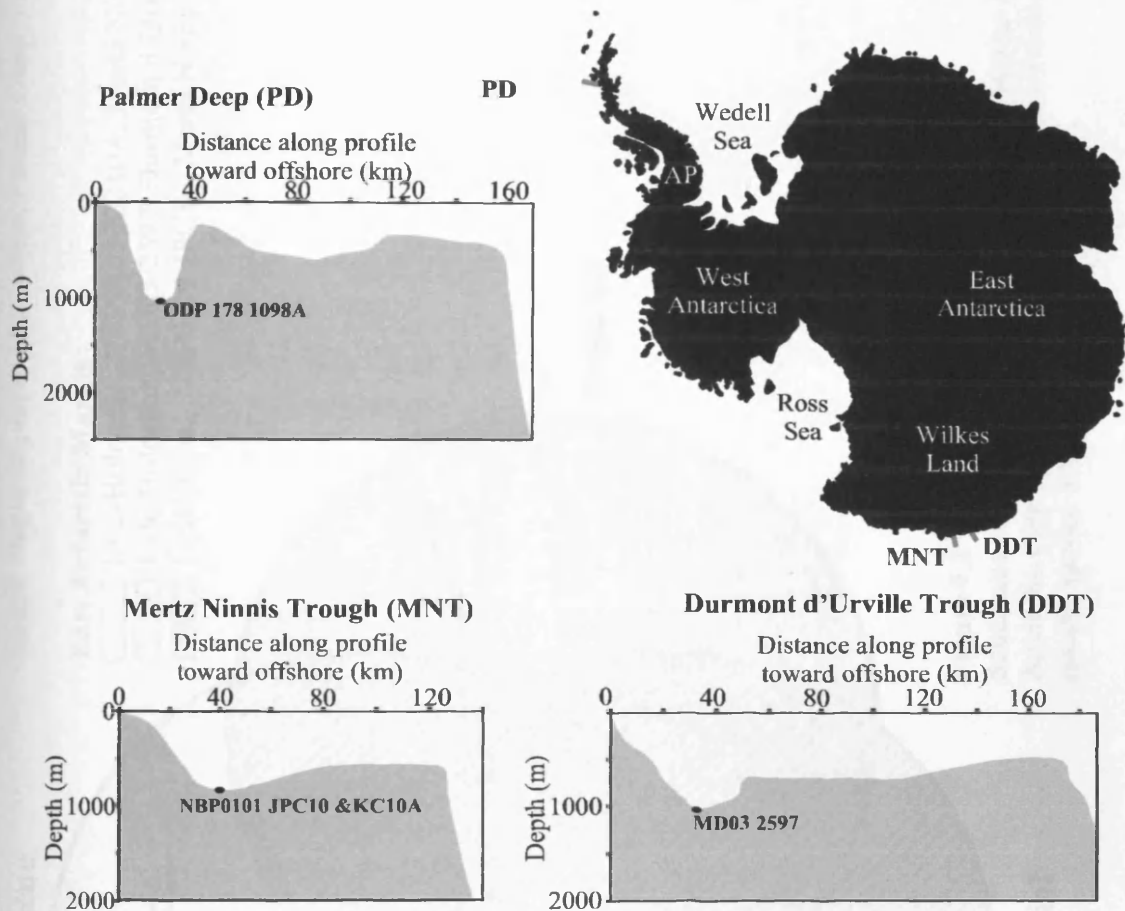
In this section the deglacial, 12264 – 11207 cal. yr BP, laminated interval from Palmer Deep, Western Antarctic Peninsula is compared with the post-glacial, 11384 – 6756 cal. yr BP, laminated interval from the Mertz Ninnis Trough on the East Antarctic Margin (Figure 9.1). Implications of the comparisons are then discussed.

#### 9.1.1. Comparison

##### 9.1.1.1. Position of Core Sites

The deglacial Palmer Deep (PD) and post-glacial Mertz Ninnis Trough (MNT) laminated intervals were deposited in depressions on the Antarctic continental shelf at 1012 m and 850 m water depths, respectively. The geomorphology of the PD basin and the MNT are different (Figure 9.1). PD is an approximately circular enclosed depression (Figure 4.2), whereas, MNT is an elongate depression that extends from the coast to the shelf break in a north-westerly direction (Figure 4.6). PD and MNT are both influenced by the upwelling of Circumpolar Deepwater onto the continental shelf. The MNT has a more complex oceanographic regime than PD; Adélie Land

Bottom Water is formed from High Salinity Shelf Waters and Winter Water in the Mertz Glacier Polynya (see section 2.5.2.3). PD has lower latitude than the MNT, being 190 km further north.

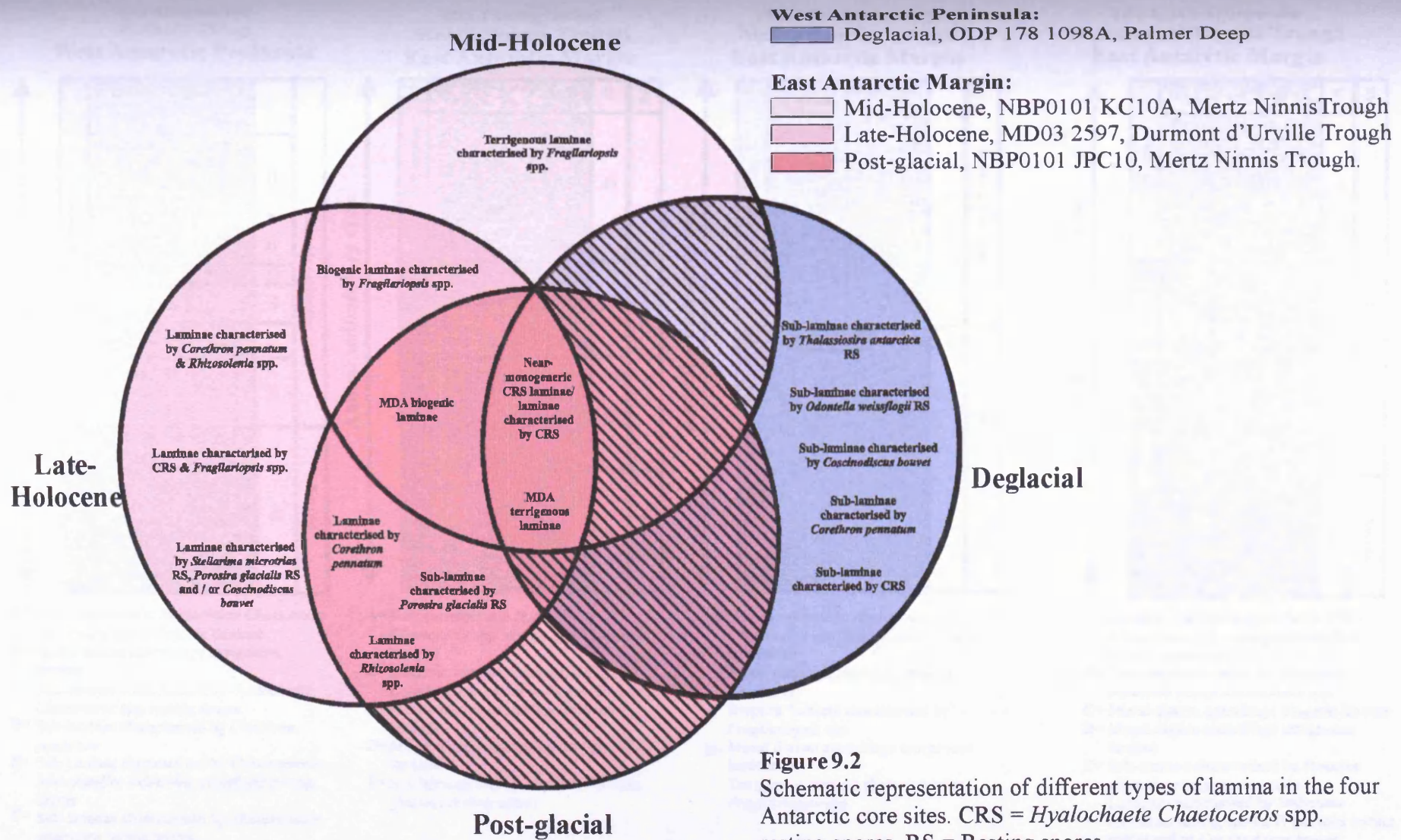


**Figure 9.1**

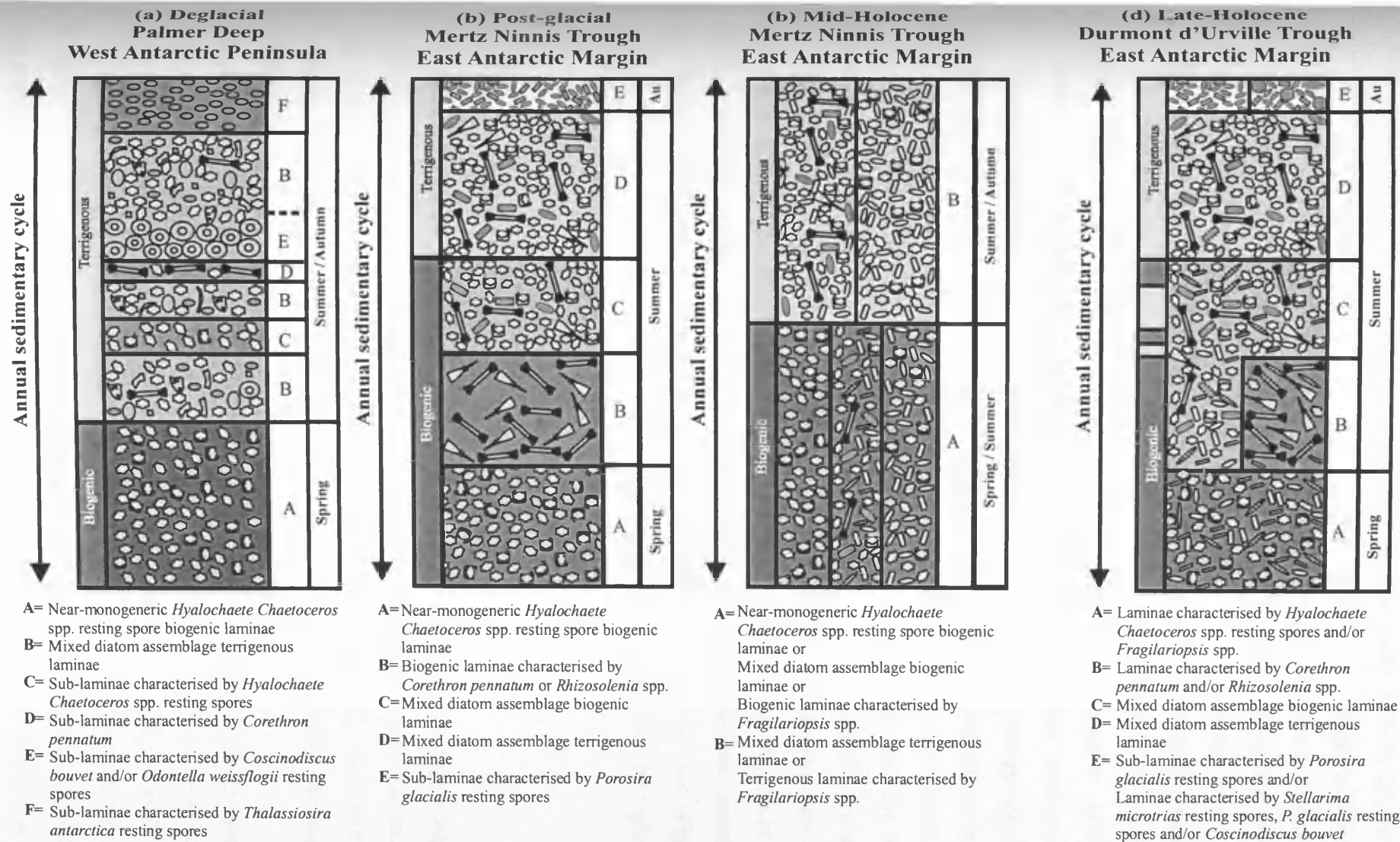
Continental shelf bathymetric profiles crossing through Palmer Deep (PD), West Antarctica (north-west profile), Mertz Ninnis Trough (MNT) (north profile) and Durmont d'Urville Trough (DUT) (following line of trough to shelf break), East Antarctica. Lines of bathymetric profiles are shown as red lines on the map of Antarctica. AP = Antarctic Peninsula. Core sites indicated on continental shelf profiles. Profiles constructed from bathymetric maps in Domack *et al.* (1989), Barker *et al.* (1999a) and Harris *et al.* (2001).

#### 9.1.1.2. Annual Cycle of Lamina and Sub-lamina Deposition

The Palmer Deep (PD) deglacial laminated interval is varved. Rhythmic alternation of near-monogeneric *Hyalochaete Chaetoceros* spp. resting spore (CRS) biogenic laminae and mixed diatom assemblage terrigenous laminae make up an annual cycle of deposition (Figure 9.2 and 9.3a). One hundred and seventy two annual cycles are present in the PD deglacial laminated interval. The comparison of this number of



**Figure 9.2**  
 Schematic representation of different types of lamina in the four Antarctic core sites. CRS = *Hyalochaete Chaetoceros* spp. resting spores. RS = Resting spores.



**Figure 9.3**

Schematic representation of annual diatom-rich laminated sediment deposited in (a) ODP 178 1098A Palmer Deep, (b) NBP0101 JPC10 Mertz Ninnis Trough (c) NBP0101 KC10A Mertz Ninnis Trough and (d) MD03 2597 Durmont d'Urville Trough. Compiled from backscattered electron imagery (BSEI) data. Au = Autumn.



annual cycles with 1057 radiocarbon years suggests that only 16.3 % of the PD sedimentary record is present. Some of the mixed diatom assemblage terrigenous laminae contain multiple species-specific sub-laminae. Five sub-laminae characterised by CRS, *Coscinodiscus bouvet*, *Corethron pennatum*, *Odontella weissflogii* resting spores (RS) and *Thalassiosira antarctica* RS (Figure 9.2) are present in the PD deglacial laminated interval. The Mertz Ninnis Trough (MNT) post-glacial laminated interval is composed of five lamina types (near-monogeneric CRS biogenic laminae; biogenic laminae characterised by *Corethron pennatum*; biogenic laminae characterised by *Rhizosolenia* spp.; mixed diatom assemblage biogenic laminae; and mixed diatom assemblage terrigenous laminae) and one sub-lamina (terrigenous sub-lamina characterised by *Porosira glacialis* RS). An annual cycle of deposition in the MNT post-glacial laminated interval is composed of two or more laminae (Figure 9.2 and 9.3b) but is not varved because laminae are not rhythmically repeated. One hundred and sixteen annual cycles occur in the studied post-glacial MNT laminated intervals. Comparison of 2801 radiocarbon years with 116 annual cycles indicates that only 4.2 % of the MNT sedimentary record is present. Close to or at the top of the annual cycle a sub-lamina characterised by *Porosira glacialis* RS sometimes occurs. The terrigenous content of laminae in the PD deglacial laminated interval (Figure 6.2b) is more well-confined in the terrigenous laminae than in the MNT post-glacial laminated interval (Figure 7.5).

### 9.1.1.3. Lamina Types

The deglacial Palmer Deep (PD) and post-glacial Mertz Ninnis Trough (MNT) laminated intervals both contain near-monogeneric CRS biogenic laminae and mixed diatom assemblage terrigenous laminae (Figure 9.2 and 9.3a and b); these will be compared first. Lamina types which only occur in the post-glacial MNT laminated interval will then be considered.

The deglacial PD and post-glacial MNT near-monogeneric CRS biogenic lamina types (Figure 9.2 and 9.3a and b) have high diatom absolute abundances,  $6141 \times 10^6$  and  $4505 \times 10^6$  valves per gramme of dry sediment, respectively (Table 6.3 and 7.3). The deglacial PD and post-glacial MNT laminae of this type are interpreted as blooms of *Hyalochaete Chaetoceros* spp. taking advantage of well-stratified waters in spring (see sections 6.2.1 and 7.2.1.1). The PD deglacial near-monogeneric CRS biogenic

laminae diatom assemblage is dominated by CRS (Table 6.3), whereas the MNT post-glacial diatom assemblage is dominated primarily by CRS and secondarily by *Fragilariopsis* spp. (Table 7.3).

The deglacial PD and post-glacial MNT mixed diatom assemblage terrigenous laminae types (Figure 9.2 and 9.3a and b) have approximately the same diatom absolute abundances,  $1846 \times 10^6$  and  $1933 \times 10^6$  valves per gramme of dry sediment, respectively (Table 6.6 and 7.3). This lamina type is interpreted as diverse diatom assemblages taking advantage of well-mixed open waters in summer / autumn (see sections 6.2.2 and 7.2.1.4). The deglacial PD mixed diatom assemblage terrigenous laminae are dominated by CRS, whereas the post-glacial MNT mixed diatom assemblage terrigenous laminae are dominated primarily by CRS and secondarily by *Fragilariopsis* spp..

The post-glacial MNT laminated interval contains three lamina types that do not occur in the deglacial PD laminated interval: biogenic laminae characterised by *Corethron pennatum*; biogenic laminae characterised by *Rhizosolenia* spp.; and mixed diatom assemblage biogenic laminae. The post-glacial MNT biogenic laminae characterised by *C. pennatum* and *Rhizosolenia* spp. are a result of stable open waters forming early in the growing season in the Mertz Glacier Polynya, which allow *C. pennatum* and *Rhizosolenia* spp. to bloom (see section 7.2.3.2). The post-glacial MNT mixed diatom assemblage biogenic laminae are interpreted as mixed water column conditions occurring in summer.

#### 9.1.1.4. Sub-lamina Types

Five terrigenous sub-laminae occur in the PD deglacial laminated interval and one sub-lamina occurs in the MNT post-glacial laminated interval (Figure 9.2). The species which characterise these sub-laminae are exclusive to each site.

The PD deglacial sub-laminae occur within the mixed diatom assemblage terrigenous laminae intermittently through the laminated interval. An upcore sequence of sub-laminae was observed: sub-laminae characterised by CRS, *Coscinodiscus bouvet*, *Corethron pennatum*, *Odontella weissflogii* RS and *Thalassiosira antarctica* RS (Figure 9.3a). The sub-lamina order of occurrence is discussed in section 6.2.6 and is interpreted as a result of changing continental shelf waters caused either by high tides,

high cyclone intensity or intermittent Circumpolar Deepwater upwelling onto the continental shelf.

The post-glacial MNT sub-lamina is characterised *Porosira glacialis* RS and is a result of environmental stress induced by sea ice formation in autumn (see section 7.2.1.5).

Deglacial PD sub-laminae characterised by *T. antarctica* RS and post-glacial MNT sub-laminae characterised by *P. glacialis* RS both occur at or near the top of the annual deposition cycle and are both interpreted as autumn deposition.

### 9.1.2. Implications

The differences in annual laminae and sub-laminae deposition in the western Antarctic Peninsula deglacial Palmer Deep (PD) and the East Antarctic Margin post-glacial Mertz Ninnis Trough (MNT) laminated intervals are due to different times of deposition, geomorphology, latitudes, glaciological and oceanographic conditions on the continental shelf. All of these factors are interlinked.

The differences in the geomorphology of PD and MNT have meant that these continental shelf depressions have experienced differing degrees of sediment focusing. A higher degree of sediment focusing occurs in PD due to its funnel like shape whereas the elongate MNT is connected to the shelf edge and is influenced by MCDW upwelling which redistributes sediment. Sediment focusing therefore has affected how confined the terrigenous material is to the terrigenous laminae, i.e. more so in PD.

In spring, surface waters were well-stratified and nutrient-rich in the vicinity of both core sites. This allowed *Hyalochaete Chaetoceros* spp. to bloom, resulting in the deposition of near-monogeneric *Hyalochaete Chaetoceros* spp. resting spore biogenic laminae. The lower latitude of the western Antarctic Peninsula PD site ensures that it experiences a warmer climate than MNT on the East Antarctic Margin. Therefore, sea ice and ice sheet melt occurs earlier in the year on the western Antarctic Peninsula than on the East Antarctic Margin. The prolonged well-stratified waters around PD allowed higher diatom productivity to occur.

The different glaciological conditions played a part in producing different laminae and sub-laminae. During deglacial times, deposition in PD was influenced by a retreating ice sheet and seasonal sea ice, which resulted in varved laminations. During post-

glacial times, deposition in the MNT was not only influenced by seasonal sea ice and the Mertz Glacier Tongue, but the Mertz Glacier Polynya as well. The Mertz Glacier Polynya influences sea ice melting and formation, and, therefore primary productivity and subsequent lamina deposition. The more complex, dominant nature of sea ice in the vicinity of the MNT led to a higher absolute abundance of *Fragilariopsis* spp. in all lamina types compared to the deglacial PD laminae.

*Porosira glacialis* is more abundant in the MNT post-glacial laminated interval and *Thalassiosira antarctica* is more abundant in the PD deglacial laminated interval. I propose the occurrence of these species are related to temperature, with *P. glacialis* preferring cooler conditions than *T. antarctica*. This interpretation has recently been supported by unpublished data from Durmont d'Urville Trough (X. Crosta, personal communication, 2005).

The presence of deglacial sub-laminae characterised by *Corethron pennatum* in the PD laminated interval and post-glacial laminae characterised by *C. pennatum* in the MNT laminated interval suggests that both core sites experienced stable open waters, but at different times in the year and for varying lengths of time, i.e. in mid summer in PD and late spring/early summer in MNT.

The comparison of radiocarbon years with the number of annual cycles that occur in the laminated intervals gives an insight into how complete the sedimentary record is. According to this calculation, deglacial PD and post-glacial MNT laminated intervals have 83.7 % and 95.7 % of the sedimentary record missing, respectively. There are four possible reasons for the disparity between the number of annual cycles present in the laminated intervals and radiocarbon years. Firstly, difficulties involved in radiocarbon dating of Antarctic marine sediments, such as spatial variation in reservoir ages and unknown changes in reworking of old carbon down core (discussed in more detail in sections 4.1.3 and 4.2.3) may affect the accuracy of radiocarbon dating of these laminated intervals. Secondly, errors may have been made in the seasonal interpretation of laminae, altering the number of annual cycles. Thirdly, sea ice may have been persistent over the core sites throughout a year or for multiple years. The low light levels would have prevented diatom productivity in the region, resulting in a hiatus in sedimentation. Fourthly, laminae and sub-laminae may have been eroded / re-suspended by bottom water currents, removing sediment from the sea floor. I do not consider the incomplete sedimentary records to be a result of errors in seasonal interpretation of laminae, as ecological preferences of many species were

utilised to determine seasonal lamina deposition. I believe that the incomplete sedimentary records are a result of errors associated with radiocarbon dating and / or environmental conditions during deposition.

The MNT post-glacial laminated interval has a less complete sedimentary record than the PD deglacial laminated interval, this is probably because of stronger bottom currents (associated with bottom water formation in the Mertz Glacier Polynya) eroding annual cycles of sedimentation from the sea floor. Radiocarbon dating is also more problematic on the East Antarctic Margin (see section 4.2.3) than on the Antarctic Peninsula, which may have affected the accuracy of radiocarbon dating of MNT sediments. Even though PD has a more complete sedimentary record than the MNT post-glacial sediments, there is less than 20 % of the PD sedimentary record present in the studied interval. This is probably due to multiple year sea ice and / or greater ice sheet influence at the beginning of deglaciation.

In summary, the western Antarctic Peninsula and East Antarctic Margin laminated intervals contain different annual cycles of deposition and absolute abundances of diatoms due to different times of deposition and different depositional environments.

## **9.2. Post-glacial and Mid-Holocene Laminated Sediment Comparison**

Post-glacial, 11384 – 6755 cal. yr BP, laminated sediments and mid-Holocene, 3892 – 3820 cal. yr BP, laminated sediments from Mertz Ninnis Trough, East Antarctic Margin, are compared in this section (Figure 9.1). The mid-Holocene laminated interval analysed is stratigraphically restricted and places limits on the comparison of these two laminated intervals.

### **9.2.1. Comparison**

#### **9.2.1.1. Position of core sites**

The post-glacial and mid-Holocene sediments were both taken from the same continental shelf depression, the Mertz Ninnis Trough (MNT). The core sites are 0.06 km apart and are at the same water depth (850 m; Figure 9.1). This allows a direct comparison of the two laminated intervals.

### 9.2.1.2. Annual Cycle of Lamina and Sub-lamina Deposition

Five types of lamina and one sub-lamina type occur in the post-glacial laminated interval (near-monogeneric CRS biogenic laminae; biogenic laminae characterised by *Corethron pennatum*; biogenic laminae characterised by *Rhizosolenia* spp.; mixed diatom assemblage biogenic laminae; and mixed diatom assemblage terrigenous laminae; terrigenous sub-lamina characterised by *Porosira glacialis* RS). The post-glacial annual cycle is composed of two or more laminae (Figure 9.2 and 9.3b). One hundred and sixteen annual cycles are present in the post-glacial laminated intervals. The number of annual cycles compared to 2801 radiocarbon years indicates that only 4.2 % the post-glacial sedimentary record is present. Five lamina types also occur in the mid-Holocene laminated interval (near-monogeneric CRS biogenic laminae; mixed diatom assemblage biogenic laminae; biogenic laminae characterised by *Fragilariopsis* spp.; terrigenous laminae characterised by *Fragilariopsis* spp.; and mixed diatom assemblage terrigenous laminae). The mid-Holocene annual cycle is composed of two laminae. Seventeen annual cycles occur in the mid-Holocene laminated interval. The comparison of 72 radiocarbon years with 17 annual cycles indicates that 23.6 % of the mid-Holocene sedimentary record is present in the studied interval. Neither the post-glacial nor the mid-Holocene laminated intervals are varved because neither have annual rhythmic repetition of laminae.

Terrigenous content in the laminated intervals is more well-confined in the post-glacial terrigenous laminae (Figure 7.5) than in the mid-Holocene terrigenous laminae (Figure 7.11). Even though the boundaries of laminae in both intervals are gradational, the terrigenous content of the sediment appears to be more dispersed in the mid-Holocene.

### 9.2.1.3. Lamina Types

The MNT post-glacial and mid-Holocene laminated intervals both contain near-monogeneric CRS biogenic laminae, mixed diatom assemblage biogenic laminae and mixed diatom assemblage terrigenous laminae (Figure 9.2). Both the post-glacial and mid-Holocene near-monogeneric CRS biogenic laminae are a result of spring blooms of *Hyalochaete Chaetoceros* spp. in well-stratified, nutrient-rich surface waters. The post-glacial and mid-Holocene mixed diatom assemblage biogenic laminae are a

result of well-mixed surface waters allowing a mixed diatom assemblage to bloom in the summer. The post-glacial and mid-Holocene mixed diatom assemblage terrigenous laminae are a result of well-mixed surface waters allowing a mixed diatom assemblage to bloom in the late summer with increased terrigenous flux to the sea floor, from ice rafted material from the Mertz Glacier Tongue, sea ice and / or Modified Circumpolar Deepwater entrained fine grained sediments, as the growing season progressed.

Two biogenic laminae characterised by *Corethron pennatum* and *Rhizosolenia* spp. are present in the post-glacial laminated interval but not in the mid-Holocene laminated interval (Figure 9.2). These post-glacial laminae are formed as a result of *C. pennatum* and *Rhizosolenia* spp. blooms taking advantage of early stable open water conditions (with nutrients at depth in the water column) created within the Mertz Glacier Polynya (see section 7.2.3.2).

A biogenic laminae characterised by *Fragilariopsis* spp. and a terrigenous laminae characterised by *Fragilariopsis* spp. are present in the mid-Holocene laminated interval but not in the post-glacial laminated interval (Figure 9.2). *Fragilariopsis rhombica* and *F. kerguelensis* are the dominant *Fragilariopsis* spp. in the biogenic laminae and are a result of open water conditions with little sea ice (see section 7.5.1.1). *Fragilariopsis rhombica*, *F. ritscheri* and *F. kerguelensis* are dominant in the terrigenous laminae characterised by *Fragilariopsis* spp. and are also a result of open water conditions with little sea ice, but accompanied by an increase in terrigenous flux to the sea bed (see section 7.5.1.2).

#### 9.2.1.4. Sub-lamina Types

Sub-laminae only occur in the post-glacial laminated interval (Figure 9.2 and 9.3b). The post-glacial sub-lamina is characterised by *P. glacialis* RS and is a result of sea ice formation-induced environmental stress in autumn.

#### 9.2.2. Implications

The three lamina types that occur in both the post-glacial and mid-Holocene MNT laminated intervals suggests that there were similar conditions occurring in both time periods. The post-glacial lamina types and sequence of these laminae are interpreted

as being formed in an environment influenced by the Mertz Glacier Polynya (see section 7.2.3). The presence of biogenic and terrigenous laminae characterised by open water *Fragilariopsis* spp. and the absence of sub-laminae characterised by *P. glacialis* RS in the mid-Holocene laminated interval suggests that sea ice formation in the Mertz Glacier Polynya was reduced relative to the post-glacial. Reduced sea ice formation in the polynya suggests that Adélie Land Bottom Water (ALBW) production was lower in the mid-Holocene than in the post-glacial.

The mid-Holocene MNT laminated interval has a more complete sedimentary record than the post-glacial MNT laminated interval. Since these two laminated intervals are from the same site the differences in sedimentary record completeness is probably not related to errors in radiocarbon dating. The reduced sea ice cover and decrease in bottom water formation (and therefore bottom currents) in the mid-Holocene would have allowed a more complete sedimentary record to occur in the mid-Holocene laminated interval.

### **9.3. Post-glacial and Late-Holocene Laminated Sediment Comparison**

The post-glacial, 11384 – 6756 cal. yr BP, laminated sediments from Mertz Ninnis Trough and late Holocene, 2814 – 925 cal. yr BP, laminated sediments from Durmont d'Urville Trough, East Antarctic Margin are compared in this section due to similarities in lamina types (Figure 9.1).

#### **9.3.1. Comparison**

##### **9.3.1.1. Position of Core Sites**

The post-glacial Mertz Ninnis Trough (MNT) and late-Holocene Durmont d'Urville Trough (DUT) sediments were taken from core sites positioned in the bottom of deep continental shelf troughs on the East Antarctic Margin. The MNT and the DUT are of a similar size, depth and orientation (Figures 2.17, 2.19 and 9.1). The two troughs are influenced by upwelling Modified Circumpolar Deepwater (MCDW). Oceanography in the MNT region is more complex due to sea ice formation associated with the Mertz Glacier Polynya and resultant ALBW formation. The polynya does not extend



over the DUT (Figure 8.16). MNT is adjacent to the large Mertz Glacier Tongue and DUT is adjacent to two smaller glaciers, Astrolabe and Zelée.

### 9.3.1.2. Annual Cycle of Lamina and Sub-lamina Deposition

The post-glacial Mertz Ninnis Trough (MNT) laminated interval can not be described as varves. The annual cycle deposit consists of two or more laminae but no rhythmic repetition of the same two laminae occurs. One hundred and sixteen annual cycles occur in the post-glacial laminated intervals. The number of annual cycles compared to 2801 radiocarbon years indicates that only 4.2 % of the post-glacial sedimentary record is present. The laminated interval consists of five types of lamina and one sub-lamina. Annual deposition in the late-Holocene Durmont d'Urville Trough (DUT) laminated interval is composed of two or more laminae and can not be described as varves since there is no rhythmic repetition of the same two laminae. One hundred and twenty one annual cycles occur in the DUT late-Holocene laminated intervals. Comparison of 116 radiocarbon years with 121 annual cycles suggests that 104 % of the sedimentary record is present. Eight lamina types and one sub-lamina type occur in the late-Holocene laminated interval.

Terrigenous material is better confined to the post-glacial MNT terrigenous laminae (Figure 7.5) than it is to the late-Holocene DUT terrigenous laminae (Figure 8.12). Even though the boundaries of laminae in both East Antarctic Margin laminated intervals are gradational, the terrigenous content of lamina appears to be more dispersed in the late-Holocene DUT laminated interval. Increased terrigenous content in laminae is not always confined to the upper part of the late-Holocene DUT annual cycle, as it is in the post-glacial MNT annual cycle.

### 9.3.1.3. Lamina Types

The post-glacial Mertz Ninnis Trough (MNT) and late-Holocene Durmont d'Urville Trough (DUT) annual sequence of laminae are similar (Figure 9.3b and c), but when diatom assemblages of the individual laminae are compared differences are observed. The laminae which occur in both the post-glacial MNT and late-Holocene DUT laminated intervals are: laminae characterised by *Corethron pennatum*; laminae

characterised by *Rhizosolenia* spp.; mixed diatom assemblage biogenic laminae and mixed diatom assemblage terrigenous laminae.

The post-glacial MNT and late-Holocene DUT laminated intervals both contain laminae characterised by *Corethron pennatum* and laminae characterised by *Rhizosolenia* spp. (Figure 9.2). The post-glacial MNT laminae characterised by *C. pennatum* contributes to a greater percentage of sediment thickness, a higher absolute diatom abundance (Figure 9.4a) and higher absolute abundance of *C. pennatum* (Figure 9.4b) than in the late-Holocene DUT laminated interval. The late-Holocene DUT laminae characterised by *C. pennatum* has a higher absolute abundance of *Fragilariopsis* spp. and *Thalassiosira* spp. than in the post-glacial laminae (Figure 9.4b). The laminae characterised by *Rhizosolenia* spp. have approximately the same percentage thickness in both the post-glacial MNT and late-Holocene DUT laminated intervals. The late-Holocene DUT lamina type has a greater absolute abundance of *Fragilariopsis* spp. and a slightly smaller absolute abundance of *Rhizosolenia* spp. than in the post-glacial MNT laminae (Figure 9.4c).

The post-glacial MNT and late-Holocene DUT laminated intervals both contain mixed diatom assemblage biogenic and terrigenous laminae (Figure 9.2) which are a result of mixed open surface waters occurring in summer and late summer respectively. The post-glacial MNT mixed diatom assemblage biogenic and terrigenous laminae have greater total absolute diatom abundances than the late-Holocene DUT laminae (Figure 9.4a). The late-Holocene DUT mixed diatom assemblage lamina types have higher *Fragilariopsis* spp. and lower CRS absolute abundances than in the post-glacial MNT laminae (Figure 9.4d and e).

Both laminated intervals contain laminae dominated by *Hyalochaete Chaetoceros* spp. resting spores (CRS). However, the relative abundance of CRS of the post-glacial MNT laminae is much greater than the late-Holocene DUT laminae, 90.5% and 50.6% respectively (See section 7.1.1.1. and 8.1.1).

Laminae characterised by *Fragilariopsis* spp., laminae characterised by CRS and *Fragilariopsis* spp., laminae characterised by *C. pennatum* and *Rhizosolenia* spp. and laminae characterised by *Stellarima microtrias* RS, *Porosira glacialis* RS and / or *Coscinodiscus bouvet* all occur in the late-Holocene DUT laminated interval but not in the post-glacial MNT laminated interval (Figure 9.2).

#### 9.3.1.4. Sub-lamina Types

Post-glacial Mertz Ninnis Trough (MNT) and late-Holocene Durmont d'Urville Trough (DUT) laminated intervals both contain sub-laminae characterised by *Porosira glacialis* RS (Figure 9.2) and are interpreted as autumn deposition, a result of environmental stress induced by sea ice formation. The post-glacial MNT sub-laminae total diatom assemblage absolute abundance is greater than the late-Holocene DUT total diatom assemblage absolute abundance (Figure 9.4a). The late-Holocene DUT absolute abundance of *P. glacialis* RS in the sub-laminae is ten times greater than the post-glacial MNT absolute abundance of *P. glacialis* RS in the sub-laminae (Figure 9.4f). The absolute abundance of *Fragilariopsis* spp. and *Thalassiosira* spp. is also higher in the late-Holocene sub-lamina.

#### 9.3.2. Implications

The similar geomorphologic features of the East Antarctic Margin Mertz Ninnis Trough (MNT) and Durmont d'Urville Trough (DUT) suggest that sediment focusing will be comparable between these two sites. The size of glaciers close to the two troughs (Mertz Glacier Tongue east of the MNT is much larger and drains a larger area of the East Antarctic Ice Sheet than the Astrolabe and Zelée Glaciers which are near the DUT) means that there is possibly a greater amount of terrigenous material brought into the MNT region. However, I do not believe that this is the reason for differences in terrigenous content distribution in the annual cycles of laminae. The higher absolute abundance of diatoms in the MNT laminae indicates that productivity was higher in the post-glacial than in the late-Holocene. Therefore, biogenic flux to the sea bed was more diluted by terrigenous flux in the late-Holocene due to lower productivity levels.

The higher abundance of *Fragilariopsis* spp., lower CRS and lower productivity in late-Holocene DUT laminae indicates that spring conditions were characterised by less well-stratified waters with low nutrient levels. The presence of laminae characterised by *Fragilariopsis* spp., laminae characterised by *Stellarima microtrias* RS, *Porosira glacialis* RS and / or *Coscinodiscus bouvet* and the higher absolute abundance of *P. glacialis* RS in the sub-laminae in the late-Holocene DUT laminated interval indicates that sea ice was present for longer in the growing season in the late-Holocene than in the post-glacial. This is also confirmed by the lower absolute

**Figure 9.4**

Comparison of absolute abundances of lamina types from post-glacial (NBP0101 JPC10 Mertz Ninnis Trough) and late-Holocene (MD03 2597 Durmont d'Urville Trough) laminated interval. Absolute abundance data from tables 7.3 and 8.3 and original count data in appendix 4.

(a) Comparison of post-glacial and late-Holocene lamina types absolute abundance totals.

(b) Comparison of post-glacial and late-Holocene absolute abundances (all species) of laminae characterised by *Corethron pennatum* diatom assemblage.

(c) Comparison of post-glacial and late-Holocene absolute abundances (all species) of laminae characterised by *Rhizosolenia* spp. diatom assemblage.

(d) Comparison of post-glacial and late-Holocene absolute abundances (all species) of mixed diatom assemblage (MDA) biogenic laminae diatom assemblage.

(e) Comparison of post-glacial and late-Holocene absolute abundances (all species) of MDA terrigenous laminae diatom assemblage.

(f) Comparison of post-glacial and late-Holocene absolute abundances (all species) of sub-laminae characterised by *Porosira glacialis* resting spores (RS) diatom assemblage.

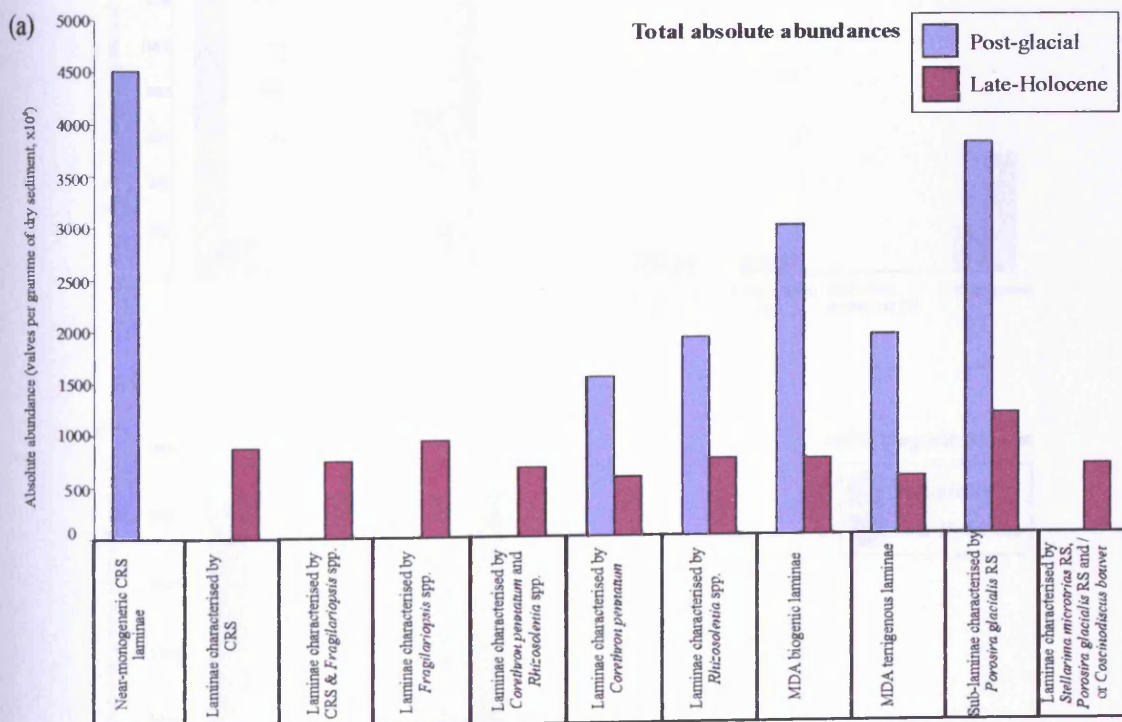


Figure 9.4 continued

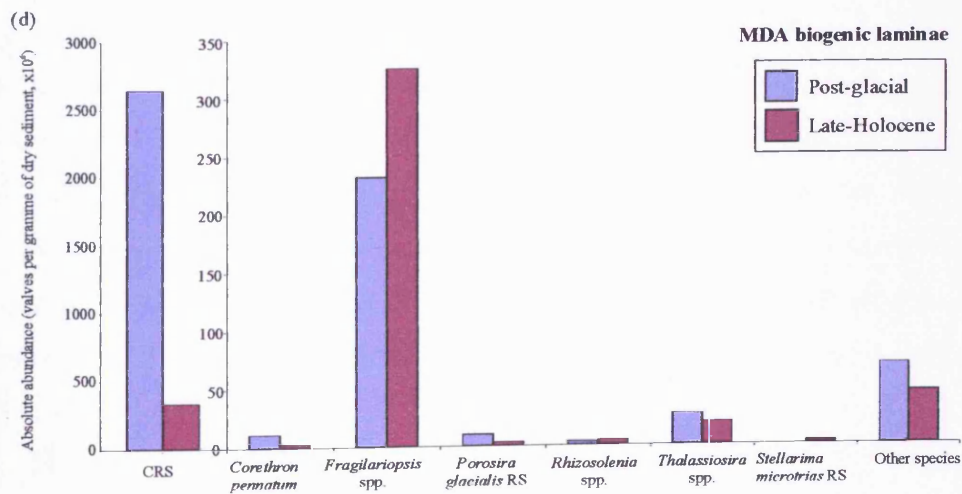
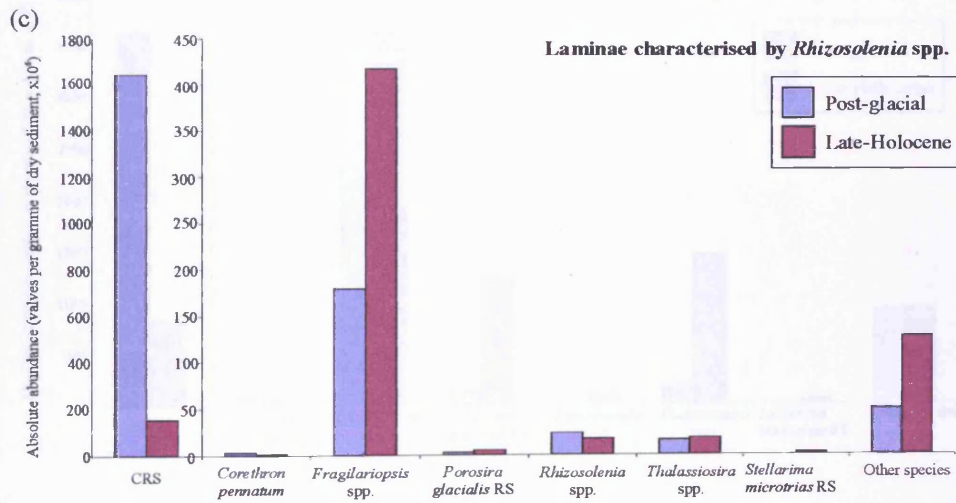
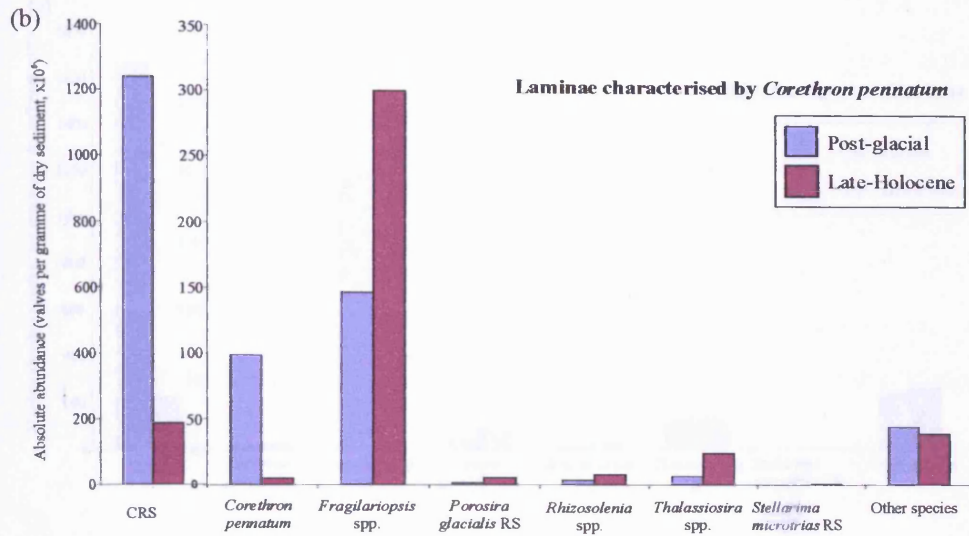
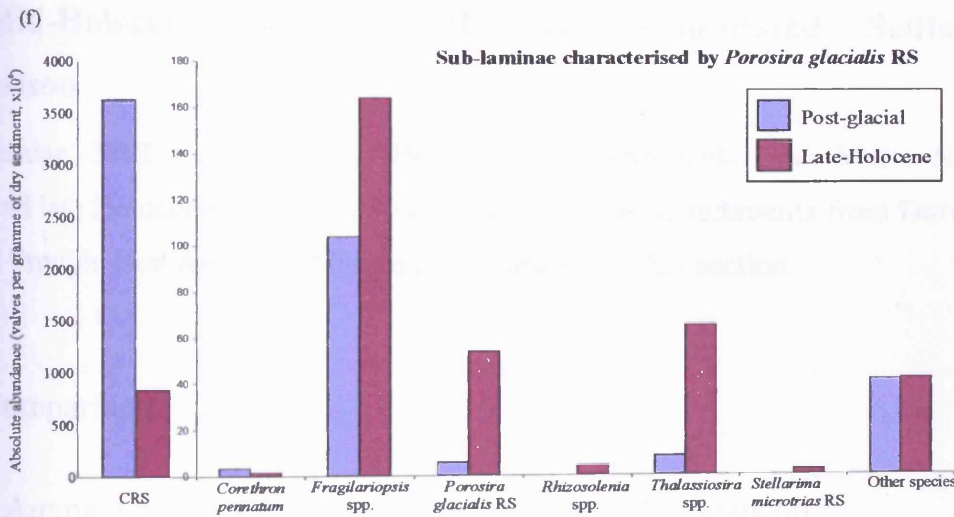
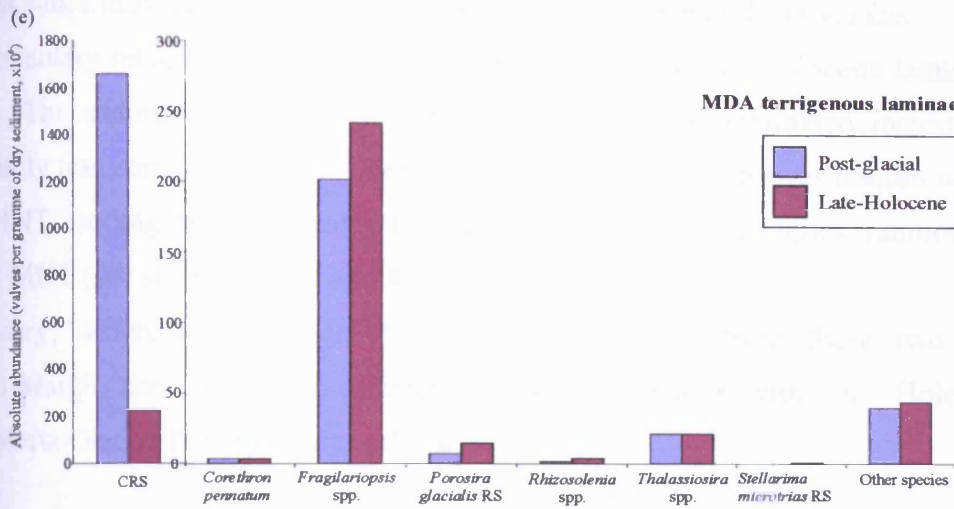


Figure 9.4 continued



undance of *C. pennatum* in the late-Holocene DUT laminae characterised by *C. pennatum*, since in Antarctica this species likes open waters with little sea ice.

The sedimentary record appears to be complete in the DUT late-Holocene laminated intervals. The sedimentary record in the MNT post-glacial laminated intervals is considerably less complete. This difference is probably due to stronger bottom waters in the MNT eroding sediment from the sea floor and more complex radiocarbon dating in MNT (see sections 4.2.3 and 4.3.3).

In summary, differences between the laminated intervals from these two East Antarctic Margin sites are due to different times of deposition within the Holocene and the Mertz Glacier Polynya only influencing the MNT.

#### 4.4. Mid-Holocene and Late-Holocene Laminated Sediment Comparison

Mid-Holocene, 3892 – 3820 cal. yr BP, laminated sediments from Mertz Ninnis Trough and late Holocene, 2814 – 925 cal. yr BP, laminated sediments from Durmont d'Urville Trough, East Antarctic Margin are compared in this section.

##### 4.4.1. Comparison

###### 4.4.1.1. Annual Cycle of Lamina and Sub-lamina Deposition

Five lamina types occur in the mid-Holocene Mertz Ninnis Trough (MNT) laminated interval. A mid-Holocene MNT annual cycle is composed of two laminae but since there is no rhythmic repetition of the lamina types the sediments are not varved. Seventeen annual cycles occur in the mid-Holocene laminated interval. Comparison of 72 radiocarbon years with 17 annual cycles suggests that 23.6 % of the mid-Holocene sedimentary record is present. Annual deposition in the late-Holocene Durmont d'Urville Trough (DUT) laminated interval consists of two or more laminae but also can not be described as being varved since there is no rhythmic repetition of the same two laminae. One hundred and twenty one annual cycles occur in the DUT late-Holocene laminated intervals. Comparison of 116 radiocarbon years with 121 annual cycles indicates that 104 % of the sedimentary record is present. Eight laminae and one sub-lamina occur in the late-Holocene DUT laminated interval.

The terrigenous content of both laminated intervals is not well confined to the terrigenous laminae (Figure 7.11 and 8.12). Lamina boundaries are gradational and the biogenic laminae have a little terrigenous material. postulate

#### 9.4.1.2. Lamina Types

Four laminae occur in both the mid-Holocene Mertz Ninnis Trough (MNT) and late-Holocene Durmont d'Urville Trough (DUT) laminated intervals: laminae characterised by *Fragilariopsis* spp.; biogenic laminae characterised by *Hyalochaete Chaetoceros* spp. resting spores / near-monogeneric *Hyalochaete Chaetoceros* spp. resting spores biogenic laminae, mixed diatom assemblage biogenic laminae and mixed diatom assemblage terrigenous laminae

Mid-Holocene MNT and late-Holocene DUT laminated intervals both contain biogenic laminae characterised by *Fragilariopsis* spp., both of which have approximately the same absolute abundances of diatom species (Tables 7.6 and 8.3).

Mid-Holocene MNT and late-Holocene DUT laminated intervals both contain biogenic laminae characterised by *Hyalochaete Chaetoceros* spp. resting spores / near-monogeneric *Hyalochaete Chaetoceros* spp. resting spores biogenic laminae. Mixed diatom assemblage biogenic and terrigenous laminae also occur in both mid-Holocene MNT and late-Holocene DUT laminated intervals.

The mid-Holocene MNT laminated interval contains terrigenous laminae characterised by *Fragilariopsis* spp.. This lamina type is not present in the late-Holocene DUT laminated interval. The lamina types which only occur in the late-Holocene DUT laminated intervals are laminae characterised by *Corethron pennatum* and / or *Rhizosolenia* spp. and laminae characterised by *Stellarima microtrias* resting spores, *Porosira glacialis* resting spores and / or *Coscinodiscus bouvet*.

#### 9.4.1.3. Sub-lamina Types

Sub-laminae characterised by *Porosira glacialis* RS occur in the late-Holocene laminated interval, but not in the mid-Holocene MNT laminated interval.



### 9.4.2. Implications

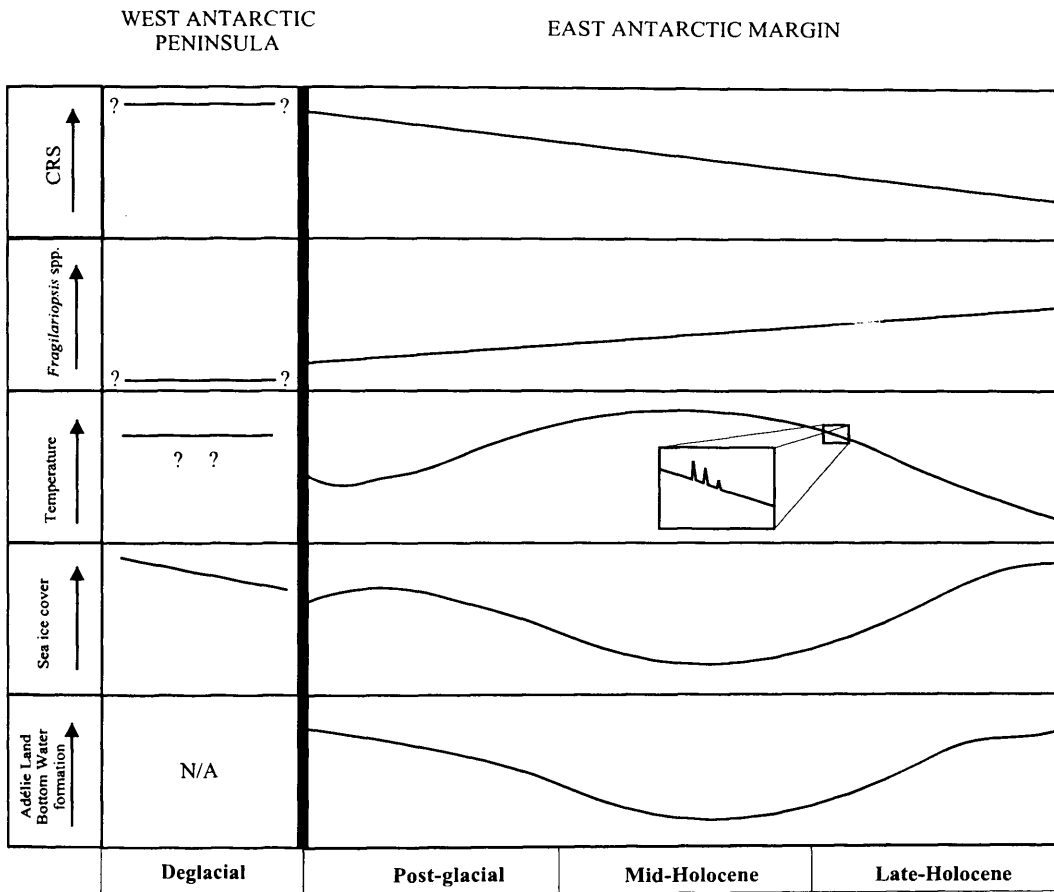
The similar distribution of terrigenous material in the laminated intervals suggests that biogenic deposition in the mid- and late-Holocene were both, to an extent, diluted by terrigenous flux to the sea floor. The laminae characterised by *Stellarima microtrias* RS, *Porosira glacialis* RS and / or *Coscinodiscus bouvet* and sub-laminae characterised by *P. glacialis* RS suggests that there was more extensive sea ice cover in the late-Holocene in the vicinity of the DUT than in the mid-Holocene MNT region influenced by the polynya. The DUT late-Holocene laminated intervals have a complete sedimentary record whereas the mid-Holocene MNT laminated interval has approximately a quarter of the sedimentary record present. The MNT experienced less persistent sea ice in the mid-Holocene than the DUT did in the late-Holocene, therefore the less complete sedimentary record is not due to multiple year sea ice. This implies that stronger bottom currents must have been the cause of a less complete sedimentary record in the mid-Holocene MNT laminated interval.

## 9.5. Comparison of the Four Laminated Sediments

### 9.5.1. Temporal Change in Absolute Abundance of Diatoms

Biogenic laminae in the deglacial Palmer Deep (PD) laminated interval have the highest absolute diatom abundances out of all four laminated intervals, therefore, the highest primary productivity. There is a decrease in absolute abundance of diatoms with time, from the deglacial PD laminated interval to the late-Holocene Durmont d'Urville Trough (DUT) laminated interval. The small amount of diatom abundance data for the mid-Holocene laminated interval means that further work is required to identify whether this laminated interval truly fits into the trend. Absolute abundance of *Hyalochaete Chaetoceros* spp. resting spores in laminae also decreases with time (Figure 9.5). In the Western Antarctic Peninsula deglacial laminated interval, the absolute abundance of *Fragilariopsis* spp. in the laminae and sub-laminae was very low. All three East Antarctic Margin laminated intervals have much higher absolute abundances of *Fragilariopsis* spp. which increases from the post-glacial to the late-Holocene (Figure 9.5). These patterns suggest that Western Antarctic Peninsula

surface waters were more well-stratified in the deglacial than during and after the post-glacial on the East Antarctic Margin, and sea ice played a larger role in determining diatom assemblages on the East Antarctic Margin through the Holocene than in the deglacial on the western Antarctic Peninsula (Figure 9.5).



**Figure 9.5** Schematic displaying absolute abundance changes in *Fragilariopsis* spp. and *Hyalochaete Chaetoceros* spp. resting spores from the deglacial to the late-Holocene. Temperature, sea ice cover and inferred Adélie Bottom Water formation are also displayed.

### 9.5.2. Species Distribution Circum-Antarctica

The full range of diatom species in the laminae are found in all four laminated intervals, however the abundance of some species varies between these laminated intervals. *Thalassiosira antarctica* RS and *Porosira glacialis* RS are found in all the laminated intervals, but in varying degrees of abundance. *Thalassiosira antarctica* resting spores are only found in abundance in the deglacial Palmer Deep (PD)

laminated interval whereas *P. glacialis* RS are only found in abundance in the post-glacial Mertz Ninnis Trough (MNT) and late-Holocene Durmont d'Urville Trough (DUT) laminated intervals of the East Antarctic Margin. Neither species occur in abundance in the mid-Holocene MNT laminated interval. The high abundance of *T. antarctica* RS in the deglacial PD laminated interval and high abundance of *P. glacialis* RS in the MNT post-glacial laminated interval has already been discussed in section 9.1.2 and has been attributed to warmer and cooler climatic preferences respectively. This agrees with *P. glacialis* RS being found in the late-Holocene DUT laminated interval. The mid-Holocene was relatively warmer than the post-glacial and late-Holocene (Figure 9.5) so *T. antarctica* RS would be expected to occur in abundance in MNT, however, this does not occur. Either it was not warm enough for *T. antarctica* to dominate at this time, or not enough laminated sediment was examined from the mid-Holocene.

*Corethron pennatum* and *Rhizosolenia* spp. are observed in all the laminated intervals but high abundances only occur in the post-glacial MNT and late-Holocene DUT laminated intervals. This species and genus occur in abundance in the post-glacial MNT laminated interval due to stable water column conditions, with nutrients trapped at depth, created by the Mertz Glacier Polynya. *C. pennatum* and *Rhizosolenia* spp. also occur in abundance in the late-Holocene DUT laminated interval (not as high as in the post-glacial MNT) due to sporadic warmer years in the transition from mid-Holocene Climatic Optimum to cooler conditions, which induced stable water column conditions (with nutrients trapped at depth) (Figure 9.5). In the PD deglacial laminated interval sub-laminae of *C. pennatum* occurred occasionally in the terrigenous laminae, a result of Circumpolar Deepwater upwelling, which suggests that stable water column conditions were only temporary and short lived. High abundances of *C. pennatum* and *Rhizosolenia* spp. did not occur in the mid-Holocene MNT laminated interval because an energetic wave regime prevailed (Ingólfsson *et al.*, 1998) disrupting any water column stability.

*Trigonium arcticum* only occurs in the post-glacial MNT and late-Holocene DUT East Antarctic Margin laminated intervals. *T. arcticum* lives at 200-300 m water depth (Thomas, 1966), most likely on the East Antarctic Margin shallow banks (e.g. Mertz Bank, Ninnis Bank and Adélie Bank, Figure 4.6a) on the continental shelf, and is swept into the Mertz Ninnis Trough and Durmont d'Urville Trough by MDCW. I suggest *T. arcticum* is not present in the mid-Holocene laminated interval due to

weaker bottom water currents (a result of reduced sea ice cover). This species is not present in the western Antarctic Peninsula deglacial laminated interval from PD because the shelf is too deep (average depth 450 m, section 4.1.1) for *T. arcticum*.

### 9.5.3. Temporal Oceanographic Changes

The species specific sub-laminae in the Palmer Deep laminated interval from the Western Antarctic Peninsula indicates that Circumpolar Deepwater intermittently upwelled onto the continental shelf during the deglacial.

The Mertz Ninnis Trough (MNT) and the Durmont d'Urville Trough (DUT) laminated intervals from the East Antarctic Margin have given an insight into how ALBW formation may have varied through the Holocene. The sequence of post-glacial lamina types from the MNT indicates that the polynya was active and bottom water was formed during the post-glacial. The mid-Holocene MNT laminated interval indicates that seasonal sea ice cover was reduced, hence bottom water production was lower than in the post-glacial (Figure 9.5). The late-Holocene laminated interval from DUT (~120 km west of MNT), has an increase in sea ice cover relative to the mid-Holocene. Extrapolating this finding to the Mertz Glacier Polynya site, it suggests that bottom water formation may have re-strengthened following the mid-Holocene Climatic Optimum (Figure 9.5).

### 9.5.4. Temporal Sedimentary Record Changes

Comparison of the number of annual cycles that occur in the laminated intervals with radiocarbon years reveals some marked differences in how complete the laminated sedimentary records are both spatially and temporally in Antarctica.

The laminated sedimentary records from the East Antarctic Margin sites become more complete with decreasing age. The Mertz Ninnis Trough (MNT) post-glacial laminated intervals have the most incomplete sedimentary record of the East Antarctic Margin sites with only 4.2 % present. The MNT mid-Holocene laminated interval has 23.6 % and the Durmont d'Urville Trough (DUT) late-Holocene laminated intervals has 104 % of the sedimentary record present. This temporal trend may be a consequence of changing climate, variation in oceanography regimes and variation in radiocarbon affects. The incomplete sedimentary record in the MNT post-glacial

laminated intervals is a result of this site at this time having the strongest bottom currents due to active bottom water formation in the Mertz Glacier Polynya (Figure 9.5). In the mid-Holocene there were weaker bottom currents than in the post-glacial in the MNT due to a warmer mid-Holocene climate (reduced bottom water formation). However, bottom currents were stronger in the mid-Holocene in the MNT than in the late-Holocene in the DUT because bottom waters do not form in the DUT. Since there is a full sedimentary record present in the late-Holocene DUT sediments, multiple year sea ice must not have occurred even though the late-Holocene was cooler than the mid-Holocene. Palmer Deep (PD) has 16.3 % of the sedimentary record present, which is greater than the MNT post-glacial laminated interval and less than the MNT mid-Holocene laminated interval. Since PD is not a site of bottom water formation, it is unlikely that bottom currents are the cause of missing annual cycles. PD laminated sediments were deposited during deglaciation, and as discussed in section 9.1.2, multiple year sea ice may have been more prevalent at this time on the Antarctic Peninsula than on the East Antarctic Margin later in the Holocene.

#### 9.5.5. Temporal Climate Changes

The four laminated intervals examined in this study have given an insight into how climate changed from the Late Pleistocene through the Holocene in Antarctica. Deglacial diatom-rich laminated sediments in Palmer Deep (PD) indicates that seasonal sea ice formation occurred between 12,264 and 11,207 cal. yrs BP. Below the laminated interval in PD the sediment is composed of glaciomarine diamict (Figure 4.3). This suggests prior to 12,264 cal. yrs BP the area above PD was covered by an ice sheet. The transition from glaciomarine diamict to laminated sediments implies that the ice sheet retreated away from PD. The laminated interval in PD therefore, was deposited during a period of climate warming. Post-glacial diatom-rich laminated sediments from Mertz Ninnis Trough (MNT) also indicates that seasonal sea ice formation was active between 11,384 and 6,756 cal. yrs BP. Diatom assemblages in the mid-Holocene MNT laminated sediments indicates that sea ice cover was not as extensive and persistent as in post-glacial times and therefore a warmer climate prevailed between 3,892 and 3,820 cal. yrs BP (Figure 9.5). Diatom assemblages in the Durmont d'Urville Trough late-Holocene laminated sediments suggests that sea ice was extensive between 2,814 and 925 cal. yrs BP, which implies

that the climate had cooled since the mid-Holocene (with an unstable transition from warm to cooler conditions; Figure 9.5).

## **9.6. Summary**

This chapter has compared the lamina types, number of lamina types, absolute abundances and diatom assemblages of the four laminated intervals analysed. All the laminated intervals were recovered from similar depositional settings, deep depressions on the continental shelf. Examination of laminated intervals from the western Antarctic Peninsula and the East Antarctic Margin has given an insight into oceanographic and climatic changes both through the Holocene and between west and east Antarctic sites. Diatom assemblages and biogenic/terrigenous content of laminae has allowed all the laminae to be interpreted as deposition from seasonally controlled primary productivity.

## 10. Conclusions and Future Research

This chapter summarises the main conclusions from investigations of the four laminated intervals (discussed in chapters 6, 7, 8 and 9) and presents ideas for future research into Antarctic diatom-rich laminated sediments.

### 10.1. Main Conclusions

High resolution analyses of four diatom-rich laminated intervals have given an insight into climatic and oceanographic changes on the Antarctic continental shelf.

#### 10.1.1. Deglacial Laminated Sediments, Palmer Deep, Western Antarctic Peninsula

A total of one hundred and seventy-two annual cycles of lamina deposition (couplets) have been identified in the Palmer Deep deglacial laminated interval. Annual deposition is varved and consists of near-monogeneric *Hyalochaete Chaetoceros* spp. resting spore biogenic laminae and mixed diatom assemblage terrigenous laminae which are interpreted as spring and summer deposition, respectively. Negligible winter deposition occurred. Species specific sub-laminae are found repeatedly in the summer laminae and are interpreted as a result of changes in shelf waters induced by tidal cycles, high storm intensities and / or Circumpolar Deep Water intrusion onto the continental shelf. Absolute abundance of diatoms was high during deposition which suggests high productivity. *Hyalochaete Chaetoceros* spp. resting spores dominated all lamina and sub-lamina types.

#### 10.1.2. Post-glacial Laminated Sediments, Mertz Ninnis Trough, East Antarctic Margin

One hundred and sixteen annual cycles of lamina deposition have been identified in the Mertz Ninnis Trough laminated interval investigated here. Annual deposition consists of two or more laminae, however, the laminated interval is not varved because there is no rhythmic repetition of the same two lamina types. Near-monogeneric *Hyalochaete Chaetoceros* spp. resting spore biogenic laminae are a

result of spring water column stratification; biogenic laminae characterised by *Corethron pennatum* or *Rhizosolenia* spp. are a result of stable open water in front of the sea ice edge in summer; mixed diatom assemblage biogenic laminae are a result of mixed surface waters in summer; mixed diatom assemblage terrigenous laminae are a result of mixed surface waters impinged upon by sea ice growth in summer/autumn with increases in terrigenous flux to the sea floor; and terrigenous sub-laminae characterised by *Porosira glacialis* resting spores are a result of sea ice formation-induced environmental stress in autumn. Negligible deposition occurred in the winter. Sea ice formation was active during deposition of the post-glacial laminated interval. The sequence of annual lamina deposition and the types of laminae in the interval indicate that the Mertz Glacier Polynya was active, Adélie Land Bottom Water formation was strong and the Mertz Glacier Tongue was present during lamina formation. Lamina and sub-lamina diatom assemblages were dominated primarily by *Hyalochaete Chaetoceros* spp. resting spores and secondarily by *Fragilariopsis* spp..

### 10.1.3. Mid-Holocene Laminated Sediments, Mertz Ninnis Trough, East Antarctic Margin

Seventeen annual cycles of lamina deposition have been identified in the mid-Holocene laminated interval. The laminated interval is not varved because annual deposition consists of sequences of laminae which are not rhythmically repeated. Near-monogeneric *Hyalochaete Chaetoceros* spp. resting spore biogenic laminae are a result of highly stratified nutrient rich surface waters in spring; biogenic and terrigenous laminae characterised by *Fragilariopsis* spp. (specifically *Fragilariopsis rhombica*, *F. ritscheri* and *F. kerguelensis*) are a result of mixed surface waters free from sea ice in spring/summer and mixed surface waters with an increase in terrigenous input to the sediment from sea ice and Modified Circumpolar Deepwater (MCDW) entrained fine-grained sediment in summer, respectively; mixed diatom assemblage biogenic and terrigenous laminae are a result of mixed open water conditions in summer and mixed open water conditions with an increase in terrigenous input to the sediment from sea ice and MCDW entrained fine-grained sediment in late summer. During the deposition of this laminated interval, sea ice cover and sea ice formation were reduced relative to post-glacial times. The Mertz



Glacier Polynya was therefore, not as active as in the post-glacial and therefore High Salinity Shelf Water, Winter Water and ultimately Adélie Land Bottom Water production would have been lower.

#### 10.1.4. Late-Holocene Laminated Sediments, Durmont d'Urville Trough, East Antarctic Margin

One hundred and twenty cycles of lamina deposition have been identified in the late-Holocene laminated interval. The laminated interval is not varved as an annual cycle does not consist of rhythmically repeated sequences of laminae. Near-monogeneric *Hyalochaete Chaetoceros* spp. resting spore laminae, laminae characterised by *Hyalochaete Chaetoceros* spp. resting spores and *Fragilariopsis* spp. and laminae characterised by *Fragilariopsis* spp. (specifically *F. curta* and *F. cylindrus*) are a result of stratified, low salinity surface waters, high in nutrients with wide-ranging sea ice cover in spring; laminae characterised by *Corethron pennatum* and *Rhizosolenia* spp., laminae characterised by *C. pennatum* and laminae characterised by *Rhizosolenia* spp. are a result of stable, relatively warm open waters with minimal sea ice cover in spring / summer; mixed diatom assemblage biogenic and terrigenous laminae are a result of mixed surface waters in summer with increased terrigenous input to the sediment from sea ice and MCDW entrained fine grained sediments in late summer; laminae characterised by *Stellarima microtrias* resting spores (RS), *Porosira glacialis* RS and / or *Coscinodiscus bouvet*, and sub-laminae characterised by *P. glacialis* RS are a result of sea ice formation-induced environmental stress in autumn. Negligible deposition occurred in winter. Persistent and dense sea ice cover was present during the deposition of the late-Holocene laminated interval. The presence of laminae characterised by *Corethron pennatum* and *Rhizosolenia* spp. in the lower portion of the interval indicated that warmer years / periods occurred during the transition from mid-Holocene Climatic Optimum to cooler climatic conditions.

### 10.1.5. Wider Implications

The Antarctic Peninsula is one of the most sensitive sites in Antarctica where ecological and cryospheric systems respond rapidly to climate fluctuations. High-resolution examination of deglacial diatom-rich laminated sediments from Palmer Deep on the western Antarctic Peninsula continental shelf has allowed intra- and inter-annual changes in diatom productivity to be ascertained during a period of rapid climate change. This study of deglacial sediments has given an invaluable insight into environmental responses to climate warming and can therefore be used to help understand future responses to climate warming on the Antarctic Peninsula.

To date, the East Antarctic Margin has received much less attention than the West Antarctic Margin (e.g. Antarctic Peninsula) therefore, the study of diatom-rich laminated sediments from the Mertz Ninnis Trough and Durmont d'Urville Trough has provided important information on environmental, climatic and oceanographic changes in the George V Coast and Adélie Land region through the Holocene.

The examination of laminated sediments from the MNT has provided a high-resolution study of variation in the Mertz Glacier Polynya and Adélie Land Bottom Water formation from post-glacial times to the mid-Holocene. Since Adélie Land Bottom Water is a major source of Antarctic Bottom Water (a key water mass in the thermohaline circulation), it is imperative to understand the environment in this region, especially environmental responses to climate change. Postulated future climate warming may decrease the salinity of waters above the Mertz Ninnis Trough and therefore, reduce bottom water input into the Southern Ocean. This potential change in Antarctic Bottom Water volume could affect the equilibrium of the thermohaline circulation and cause further global climate change.

### 10.1.6. Summary

Annual cycles of lamina deposition have been identified in all four laminated intervals from the west Antarctic Peninsula and the East Antarctic Margin. Lamina deposition is seasonally controlled by light levels, nutrients and degree of sea ice cover. These factors are influenced by climate and oceanography. The lamina types and diatom assemblages of laminae vary temporally and spatially circum-Antarctica. These laminated Antarctic sediments have revealed information about the extent of sea ice

cover and the presence, strength and formation of water masses on the continental shelf. In particular, the East Antarctic Margin laminated sediments have given an insight into formation rates of Adélie Bottom Water and its potential contribution to Antarctic Bottom Water through the Holocene. These water masses are key players in the global thermohaline circulation. The laminated sediments therefore, give an insight into oceanographic responses to climatic change and variation through the Holocene around the Antarctic margin.

## 10.2. Future Research

This study of Antarctic laminated sediments has raised further questions to be answered in future work.

- Analysis of the mid-Holocene laminated interval from Mertz Ninnis Trough, East Antarctic Margin has given an insight into oceanographic and environmental responses to a warmer climate. It has been suggested that this period is analogous to possible future climate warming. By analysing a greater length of core, a fuller, more complete picture of sea ice cover and oceanographic conditions in the mid-Holocene and determine responses to possible future climatic warming. The observation made in this study that *Porosira glacialis* prefers relatively cooler climatic conditions and *Thalassiosira antarctica* prefers relatively warmer conditions could also be tested, by seeing if there are any sub-laminae characterised by *Thalassiosira antarctica* RS in the warmer mid-Holocene.
- In this study a decrease in absolute abundance of diatoms and an increase in the absolute abundance of *Fragilariopsis* spp. has been observed with time from the four different core sites. By conducting further diatom assemblage counts of specific laminae through the Holocene from one core taken from a continental shelf depression, changes in absolute abundances of diatoms could be determined for one site, so any variation caused by geomorphology (sediment focusing) and local oceanography will be eradicated.
- The analysis of laminated intervals from beneath the Mertz Glacier Polynya, in the Mertz Ninnis Trough has given an insight into how sea ice and bottom water formation has varied through the Holocene off the George Vth Coast. By investigating diatom assemblages and sedimentary fabrics of laminated sediments

from under other polynyas (e.g. Ross Sea Polynya, Terra Nova Bay Polynya), the interpretations of the laminated intervals from the Mertz Ninnis Trough could be compared and tested.

- In this study diatom assemblages and terrigenous content of laminae have been used to determine seasonal deposition in the laminated intervals. By collecting surface water samples throughout the growing season in the vicinity of the core sites and conducting diatom counts, seasonal changes in surface water diatom assemblages can be recorded and compared to the appropriate seasonal laminae. All but one of the studied sites are inaccessible until late spring/early summer. The Mertz Glacier Polynya has open waters early in the growing season and would therefore be ideal for this kind of study. The surface water diatom assemblages associated with each season can therefore, be compared to the annual cycle of laminae deduced from this study.
- In this study the four different aged laminated intervals have been compared in chapter nine. To make a more meaningful comparison of these diatom-rich laminated sediments, better age control is required than is obtained with radiocarbon dating. Two new techniques could be used in the future to establish a more accurate core chronology of Antarctic marine sediments. Geomagnetic field palaeointensity dating provides a chronological control on sediment sequences that do not contain sufficient material for radiocarbon dating (Brachfeld *et al.*, 2003). This method eliminates the complications associated with radiocarbon dating (discussed in chapter four). Compound-specific radiocarbon dating of organic compounds in diatom frustules may be useful for improving the reliability of radiocarbon dating within Antarctic margin sediments. This technique is currently under development (E.Domack, personal communication, 2005).

## A.1 Diatom Taxonomy

This appendix lists the taxonomic classification of diatoms identified in laminated sediments from Palmer Deep, Mertz Ninnis Trough and Durmont d'Urville Trough and supports chapter 3, section 3.5 and chapters 6, 7 and 8. Images (light microscope and secondary electron imagery) of these species are presented in appendix 2.

**Genus:** *Actinocyclus*

**Ref:** Ehrenberg, C.G. (1837) Ber. Bekanntm. Verh. Königl. Preuss. Akad. Wiss. Berlin. 2: 61.

**Species:** *A. actinochilus* (Ehrenberg) Simonsen

**Ref:** Simonsen, R. (1982) Bacillaria. 2: 9-71.

**Species:** *A. curvatulus* Janisch in Schmidt

**Ref:** Schmidt, A. (1878) "Atlas der Diatomaceenkunde" Reisland, Leipzig.

**Genus:** *Asteromphalus*

**Ref:** Ehrenberg, C.G. (1844) Ber. Bekanntm. Verh. Königl. Preuss. Akad. Wiss. Berlin. 1844: 198.

**Species:** *A. hookeri* Ehrenberg

**Ref:** Ehrenberg, C.G. (1844) Deutsche Akademie der Wissenschaften zu Berlin, Berichte: Mai 1844: 182-207 & Juni 1844: 252-275.

**Species:** *A. parvalus* Karsten

**Ref:** Karsten, G. (1905) Deutsche Tiefsee-Expedition 1889-99. 2(2): 221-538.

**Genus:** *Chaetoceros*

**Ref:** Ehrenberg, C.G. (1844) Ber. Bekanntm. Verh. Königl. Preuss. Akad. Wiss. Berlin. 1844: 198.

**Sub-genera:** *Hyalochaete* *Chaetoceros* Gran

**Ref:** Gran, H.H. (1897) Botanik. Protophyta: Diatomaceae, Silicoflagellata og Cilioflagellata. Den Norske Nordhavs-Expedition 1876. 1878 7(4): 1-36.

**Sub-genera:** *Phaeoceros* *Chaetoceros* Gran

**Ref:** Gran, H.H. (1897) Botanik. Protophyta: Diatomaceae, Silicoflagellata og Cilioflagellata. Den Norske Nordhavs-Expedition 1876. 1878 7(4): 1-36.

**Genus:** *Cocconeis*

**Ref:** C.G. Ehrenberg 1837  
Abh. Königl. Acad. Wiss. Berlin. 1835: 173.

**Genus:** *Gomphonema*

**Ref:** Ehrenberg, C.G. (1832) Abh. Königl. Akad. Wiss. Berlin, 1831: 87, 1832.

**Genus:** *Navicula*

**Ref:** Bory de st-Vincent (1822) Dict. Class. Hist. Nat. 2: 128.

**Genus:** *Nitzschia*

**Ref:** Hassall, (1845) Hist. Brit. Freshwater Algae1: 435.

**Genus:** *Odontella*

**Ref:** Agardh, C.A. (1832) Consp. Crit. Diat.: 56.

**Species:** *O. weissflogii* (Janisch) Grunow

**Ref:** In van Heurck, H. (1882) Synopsis des diatomées de Belgique Pl 78-103. Ducaju et cie., Anvers. J.R. Dieltjens, Anvers. 128 pp.

**Genus:** *Porosira*

**Ref:** Jørgensen, E. (1905) Bergens Mus. Skr. 7: 97.

**Species:** *P. glacialis* (Grunow) Jørgensen

**Ref:** Jørgensen, E. (1905). Bergens Mus. Skr. Hydrological and Biological investigations of Norwegian fjords: 47-145.

**Species:** *P. pseudodenticulata* (Hustedt) Jousé

**Ref:** Jousé, A.P., Koroleva, G.S. & Nagaeva, G.A. (1962) Trudy Inst. Okeanol. 61: 19-92.

**Genus:** *Proboscia*

**Ref:** Sunström, B.G. (1986) The marine diatom genus *Rhizosolenia*. A new approach to the taxonomy, p 99. Lund. 117 pp.

**Species:** *P. inermis* (Castracane) Jordan & Ligowski

**Ref:** Jordan, R.W., Ligowski, R., Nöthig, E.-M. & Priddle, J. (1991) Diat. Res. 6(1): 63-78.

**Species:** *P. truncata* (Karsten) Nöthig & Ligowski

**Ref:** Jordan, R.W., Ligowski, R., Nöthig, E.-M. & Priddle, J. (1991) Diat. Res. 6(1): 63-78.

**Genus:** *Pseudo-nitzschia* H. Peragallo in H. & M. Peragallo

**Ref:** Peragallo, H. & M. (1897-1908) "Diatomées marines de France" (M.J. Tempère, ed), pp 1-35.

**Species:** *Pseudo-nitzschia turgidula* (Hustedt) Hasle

**Ref:** Hasle, G.R. (1993) Beiheft zur Nova Hedwigia. 106: 315-321.

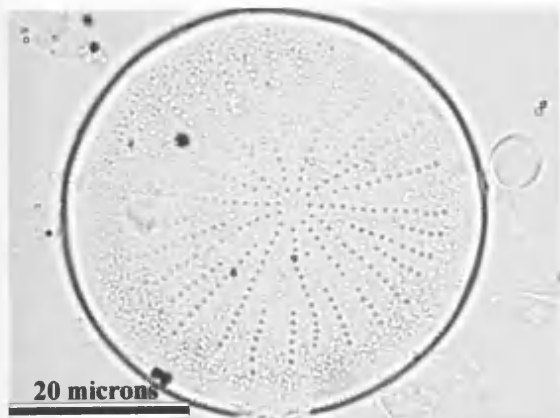
- Genus:** *Rhizosolenia*  
**Ref:** T. Brightwell 1858  
 Quart. J. Microsoc. Sci. 6: 94 (nom. Cons.)
- Species:** *R. antennata* f. *antennata* (Ehrenberg) Brown  
**Ref:** Brown, N.E. (1920) English Mechanic and World of Science. 111: 210-211, 219-220, 232-233.
- Species:** *R. antennata* f. *semispina* Sundström  
**Ref:** Sundström, B.G. (1986) Doctoral dissertation. Lund University, Lund, Sweden.
- Species:** *R. polydactyla* f. *polydactyla* Castracane  
**Ref:** Castracane, F. (1886) Report on the scientific Results of the voyage of H.M.S. Challenger during the Years 1873-76. Botany 2(4): I-III: 1-178.
- Species:** *R. species* Armand & Zielinski  
**Ref:** Armand, L. and Zielinski, U. (2001) Diatom Research. 16(2): 259-294.
- Genus:** *Stellarima*  
**Ref:** Hasle, G.R. & Sims, P.A. (1986) Br. Phycol. J. 21: 111.
- Species:** *S. microtrias* (Ehrenberg) Hasle & Sims  
**Ref:** Hasle, G.R. & Sims P.A. (1986) Br. Phycol. J. 21: 97-114.
- Genus:** *Stephanodiscus*  
**Ref:** Ehrenberg, C.G. (1845) Ber. Bekanntm. Verh. Königl. Preuss. Akad. Wiss. Berlin: 80.
- Genus:** *Thalassiosira*  
**Ref:** Cleve, P.T. (1873) Bih. Kongl. Svenska. Vetensk-Akad. Handl. 1: 6.
- Species:** *T. ambigua*  
**Ref:** Kozlova, O.G. (1967) Novit. Syst. Palnt. Non. Vas. 54-62.
- Species:** *T. anatarctica* Comber  
**Ref:** Comber, T. (1896). J. R. micr. Soc. 9: 489-491.
- Species:** *T. australis*  
**Ref:** Peragallo (1921) Deux. Expéd. Antarct. Française 1908-1910. Botanique: 1-98.
- Species:** *T. gracilis* (Karsten) Hustedt  
**Ref:** Hustedt, F. (1958). Dt. Antarkt. Exped. 1938/39 (2):103-191.
- Species:** *T. gracilis* var. *expecta* (Van Landingham) Fryxell & Hasle  
**Ref:** Fryxell, G.A. & Hasle, G.R. (1979) Phycologia. 18: 378-393.
- Species:** *T. gravida* Cleve  
**Ref:** Cleve, P.T. (1896) Bihang till Kongliga Svenska Vetenskaps-Akademiens Handlingar. 22(3-4): 1-22.
- Species:** *T. lentiginosa* (Janisch) Fryxell  
**Ref:** Fryxell, G.A. (1977) Phycologia. 16: 95-104.
- Species:** *T. lineate* Jousé  
**Ref:** Jousé, A.P. (1968) Novitas Systematicae Plantarum non Vascularium. 1968: 12-21.

- Species:** *T. oestrupii* (Ostenfield) Hasle  
**Ref:** Hasle, G.R. (1972) *Taxon*. 21: 543-544.
- Species:** *T. oliverana* (O'Meara) Makarova & Nikolaev  
**Ref:** Makarov, I.L. & Nikolaev, B.K. (1983).
- Species:** *T. poroseriata* (Ramsfjell) Hasle  
**Ref:** Hasle, G.R. (1972) *Taxon*. 21: 543-544.
- Species:** *T. ritscheri* (Hustedt) Hasle in Hasle & Heimdal  
**Ref:** Hasle, G.R. & Heimdal, B.R. (1970) *Beiheft zur Nova Hedwigia*
- Species:** *T. tumida* (Janisch) Hasle in Hasle *et al.*,  
**Ref:** Hasle, G.R., *et al.*, (1971) *Antarctic Research Series*. 17: 313-333.
- Genus:** *Thalassionema*  
**Ref:** A.Grunow ex F. Hustedt (1932) *In Rabenhorst Krypt.-Flora*. 7 (2): 244.
- Genus:** *Thalassiothrix*  
**Ref:** Cleve, P.T. & Grunow, A. (1880) *Kongl. Svenska Vetenskap. Akad. Handl., Ser 2*. 17(2): 108.
- Species:** *T. antarctica* Schimper ex Karsten  
**Ref:** Karsten, G. (1905) *Deutsche Tiefsee-Expedition 1898-1899*. 2(2): 1-136.
- Genus:** *Trachyneis*  
**Ref:** Cleve, P.T. (1894)
- Species:** *T. aspera* (Ehrenberg) Cleve  
**Ref:** = *Navicula aspera*. Lectotype selected by Boyer (1928) *Proc. Acad. Nat. Sci. Philad.* 79 *Suppl.*: 428.
- Genus:** *Trichotoxon*  
**Ref:** Reid, F.M. H. & Round, F.E. (1987) *Diat. Res.* 2: 224.
- Species:** *T. reinboldii* (Van Heurck) Reid & Round  
**Ref:** Reid, F.M.H. & Round, F.E. (1987) *Diat. Res.* 2(2): 219-227.
- Genus:** *Trigonium*  
**Ref:** Cleve, P.T. (1868) *Ofvers Kongl. Vetensk-Akad. Forhandl.* 1867: 663.
- Species:** *T. arcticum* (Brightwell) Cleve (= *Triceratium arcticum*)  
**Ref:** Cleve, P.T. (1868). *Öfversigt af Kongliga Vetenskaps-Akademiens Förhandlingar*. 25(3): 213-240.

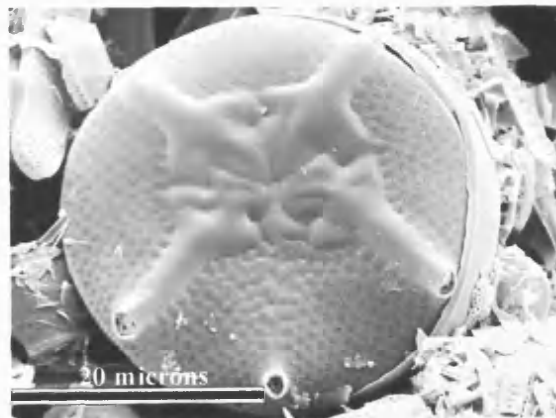
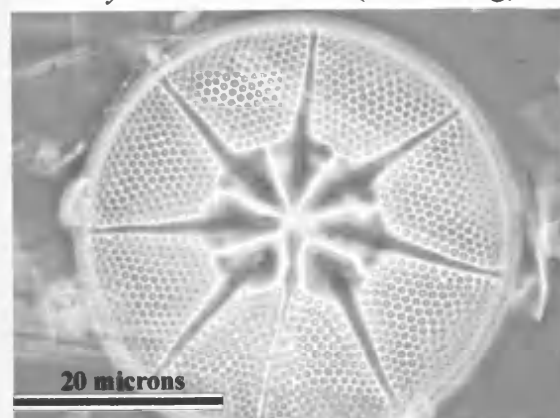


## **A.2 Diatom Images**

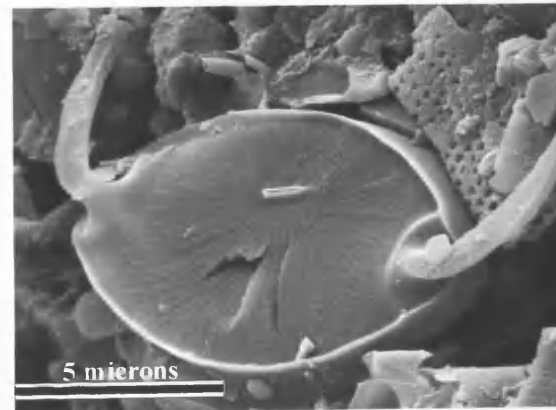
This appendix contains images of diatoms identified in laminated sediments from Palmer Deep, Mertz Ninnis Trough and Durmont d'Urville Trough and supports chapter 3, section 3.5 and chapters 6, 7 and 8. Appendix 1 lists the taxonomic classification for these diatoms.



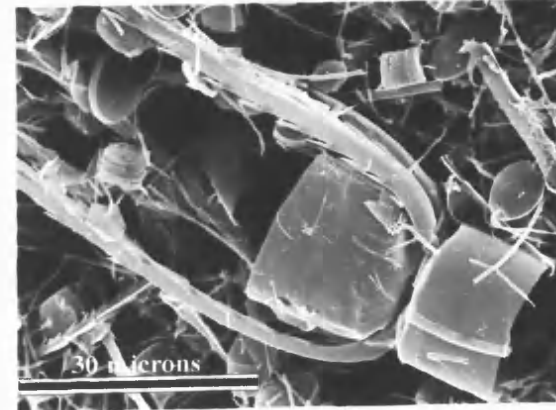
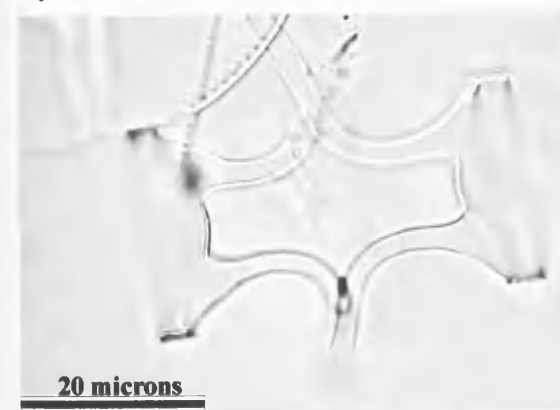
*Actinocyclus actinochilus* (Ehrenberg) Simonsen



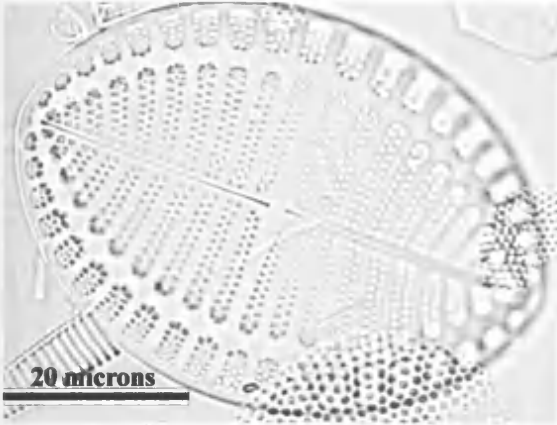
*Astermophalus* spp. Ehrenberg



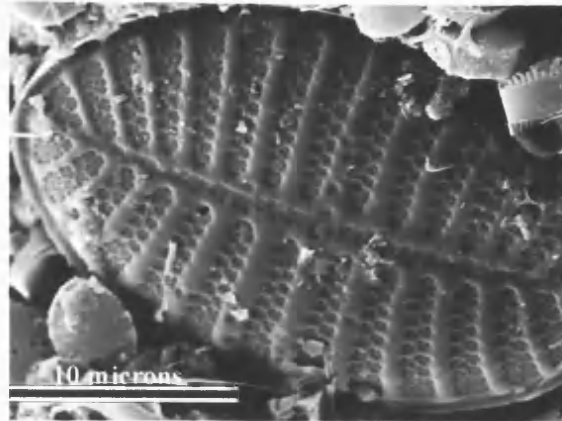
*Hyalochaete Chaetoceros* spp. Gran



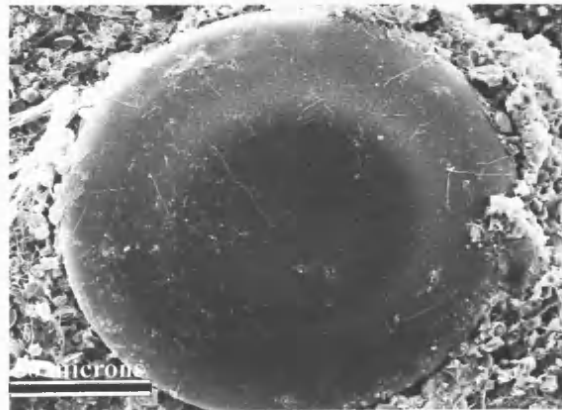
*Phaeoceros Chaetoceros* spp. Gran



*Cocconeis* spp. Ehrenberg



*Corethron pennatum* (Grunow) Ostenfeld

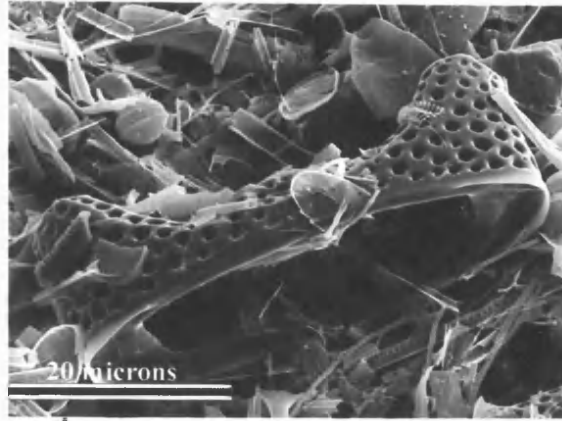
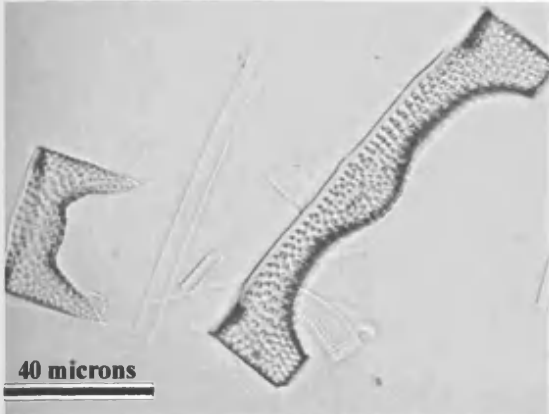


*Coscinodiscus bouvet* Karsten

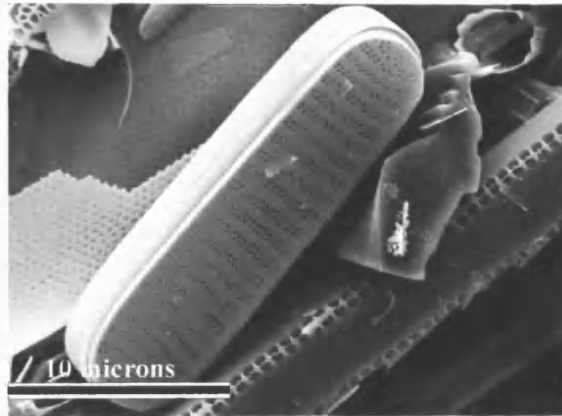
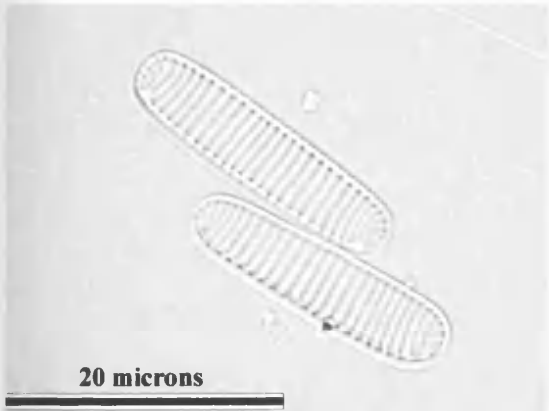


*Eucampia antarctica* (Castracane) Mangin - vegetative

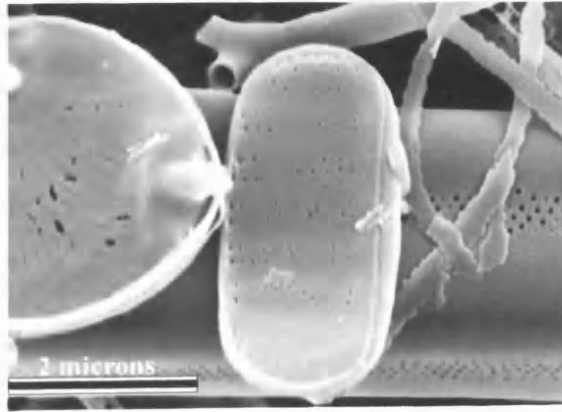




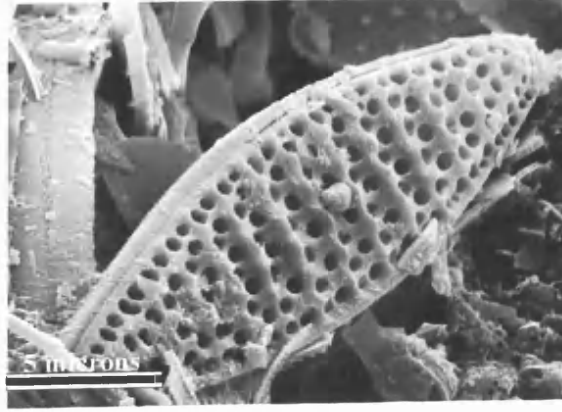
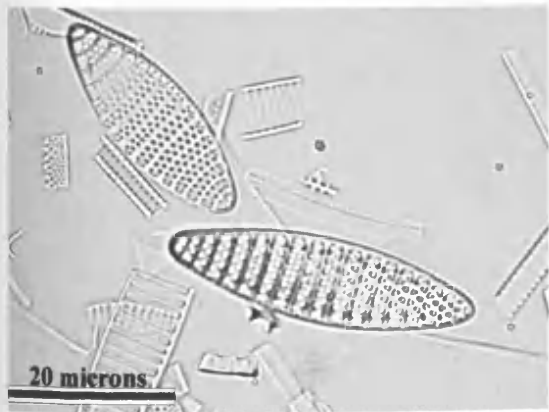
*Eucampia antarctica* (Castracane) Mangin - resting spore



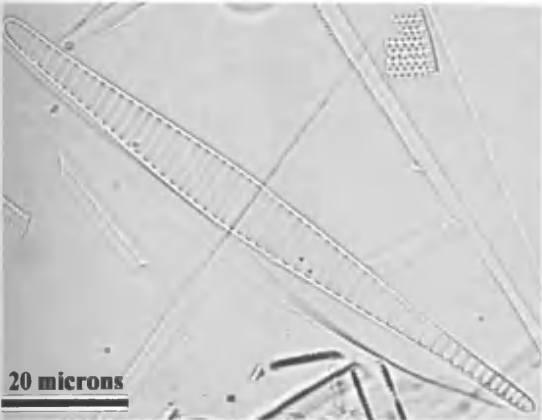
*Fragilariopsis curta* (Van Heurck) Hustedt



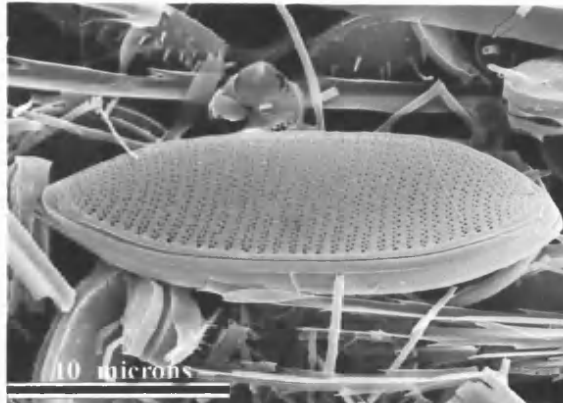
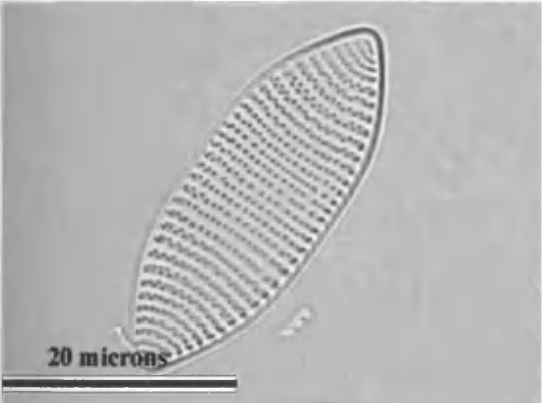
*Fragilariopsis cylindrus* (Grunow) Krieger



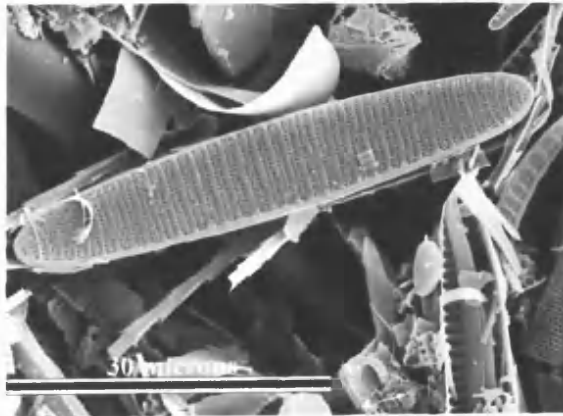
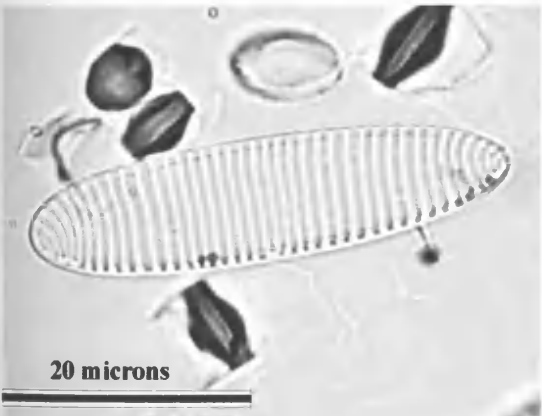
*Fragilariopsis kerguelensis* (O'Meara) Hustedt



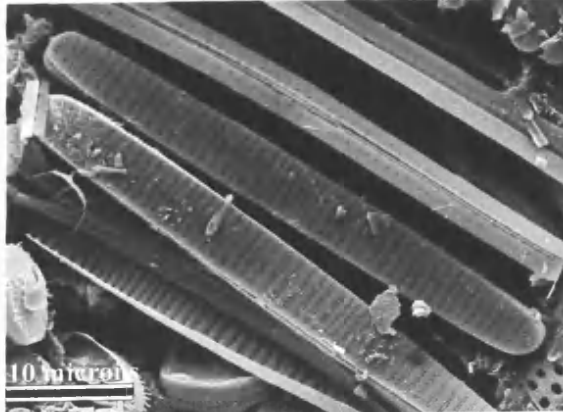
*Fragilariopsis obliquecostata* (Van Heurck) Heiden



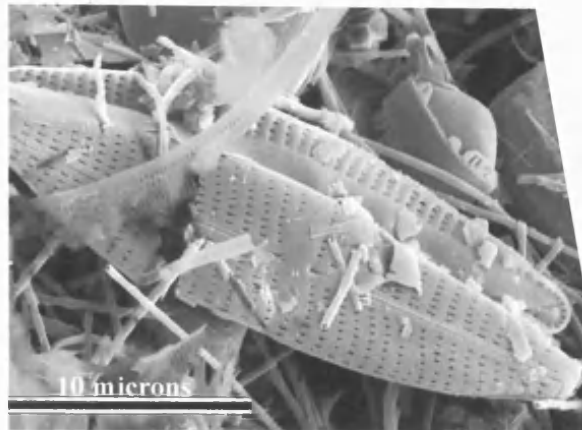
*Fragilariopsis rhombica* (O'Meara) Hustedt



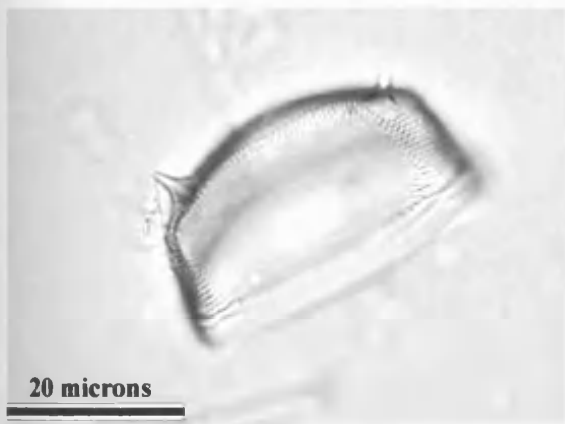
*Fragilariopsis ritscheri* (Hustedt) Hasle



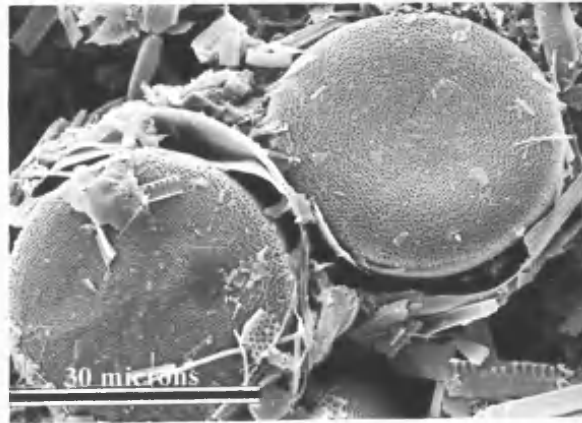
*Fragilariopsis vanheurckii* (Pergallo) Hustedt



*Navicula* spp. Bory de st-Vincent



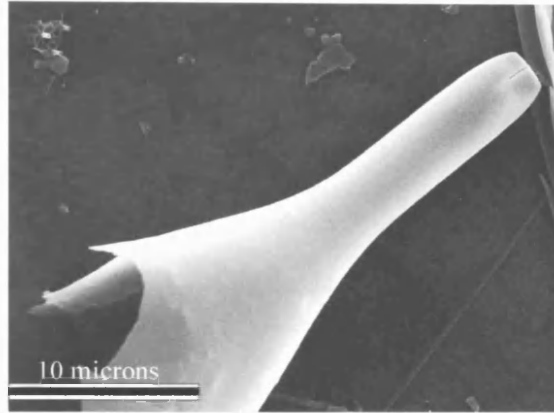
*Odontella weissflogii* (Janisch) Grunow



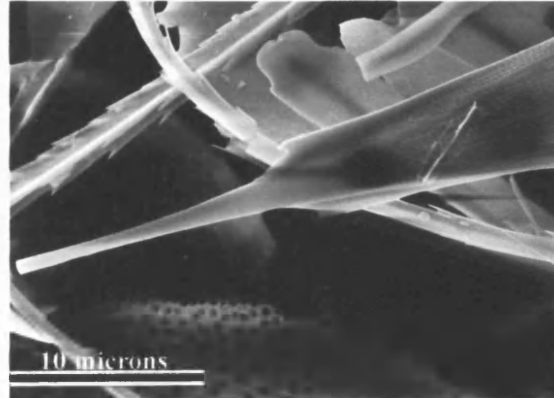
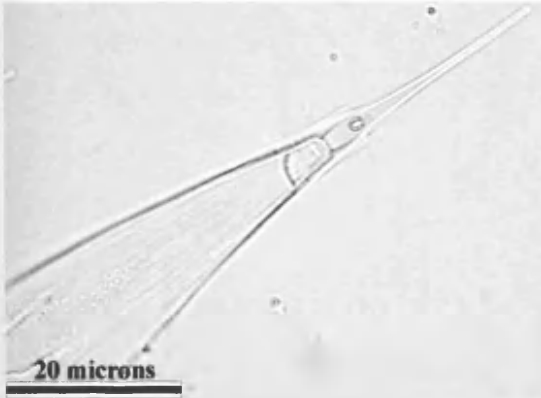
*Coscinodiscus glacialis* (Grunow) Jørgensen



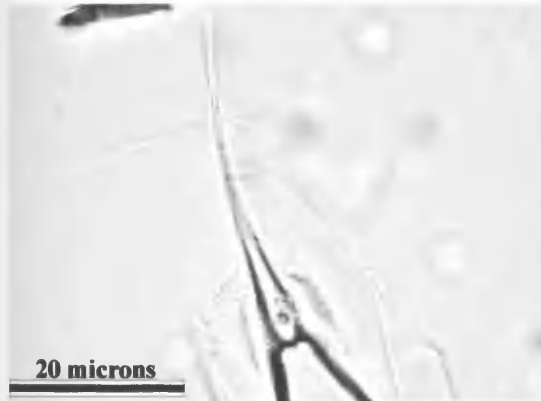
*Thalassiosira inermis* (Castracane) Jordan & Ligowski



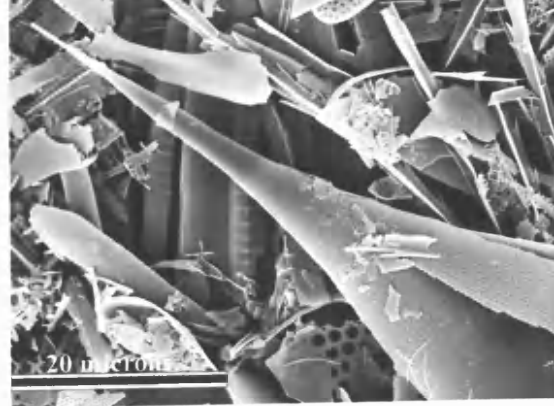
*Proboscia truncata* (Karsten) Nöthig & Ligowski



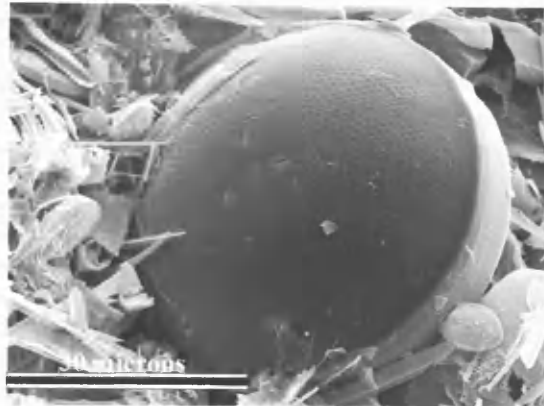
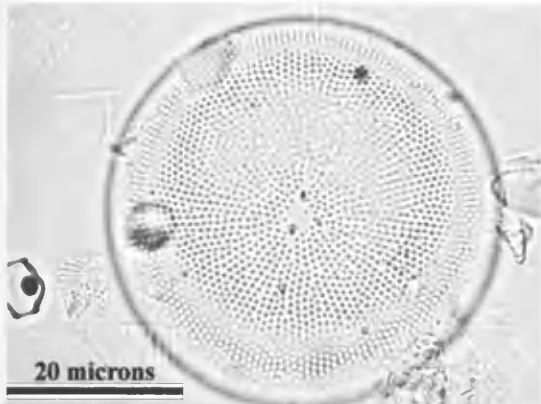
*Rhizosolenia antennata* f. *semispina* Sundström



*Rhizosolenia polydactyla* f. *polydactyla* Castracane



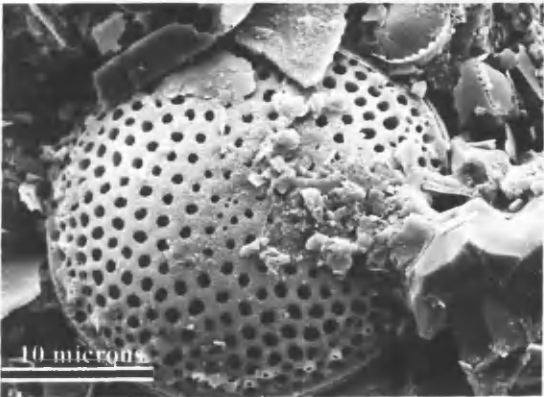
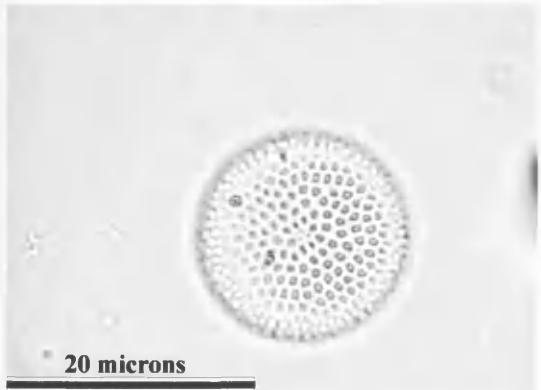
*Rhizosolenia* species A



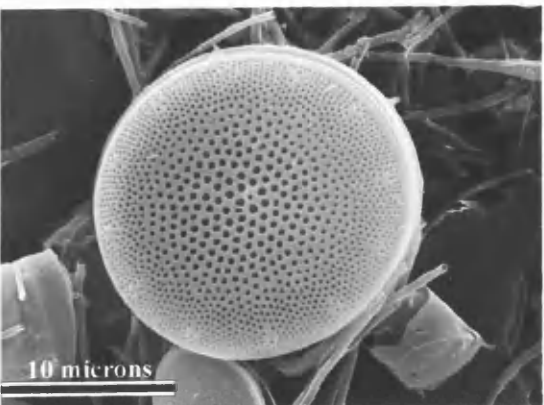
*Stellarima microtrias* (Ehrenberg) Hasle & Sims



*Thalassiosira antarctica* Comber - warm

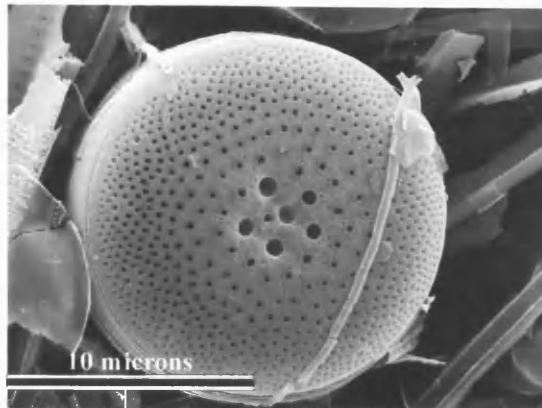
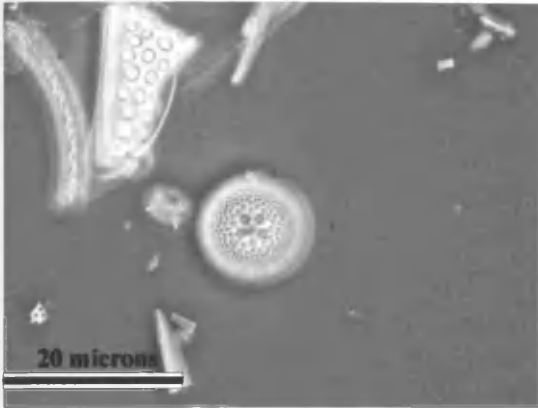


*Thalassiosira antarctica* Comber - cold

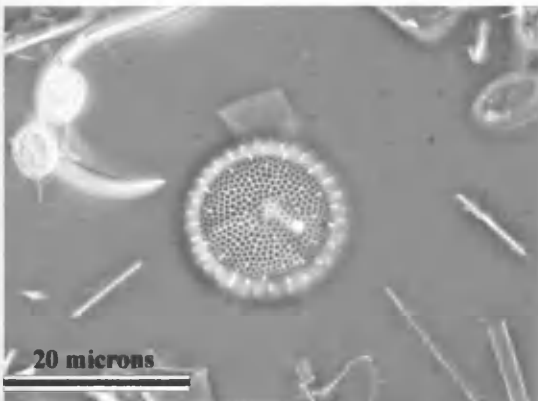


*Thalassiosira gracilis* var. *expecta* (Van Landringham) Fryxell & Hasle

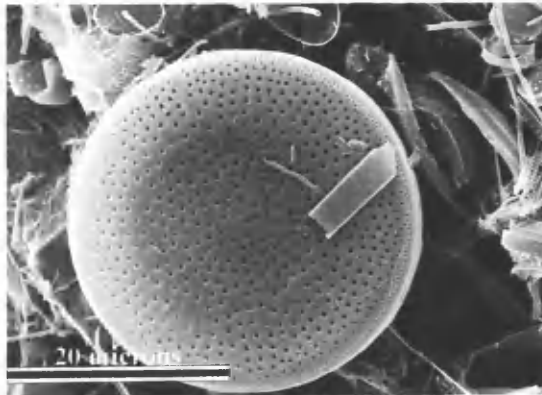
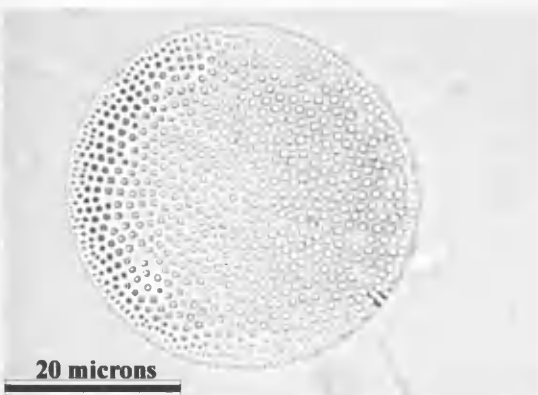




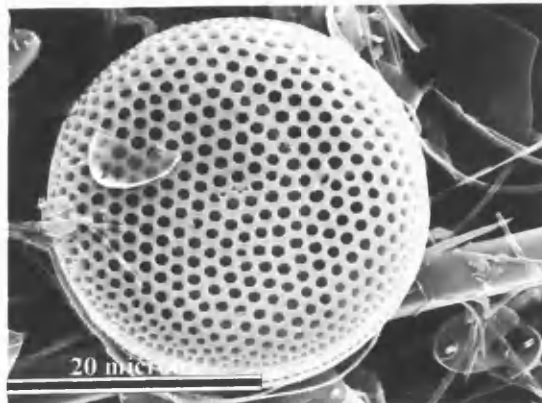
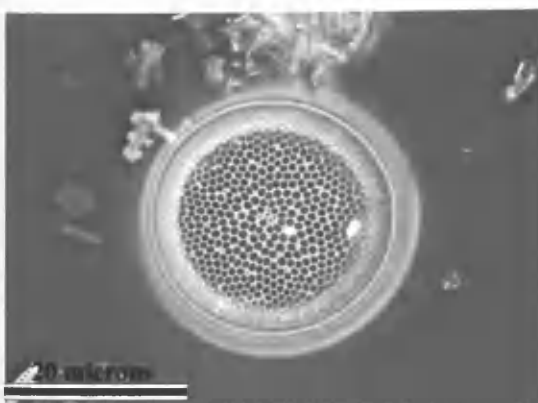
*Thalassiosira gracilis* var. *gracilis* (Karsten) Hustedt



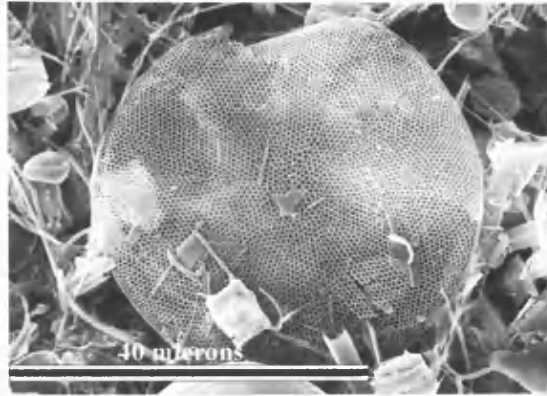
*Thalassiosira gravida* Cleve



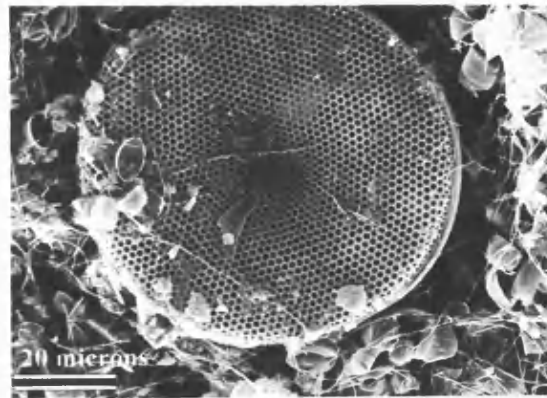
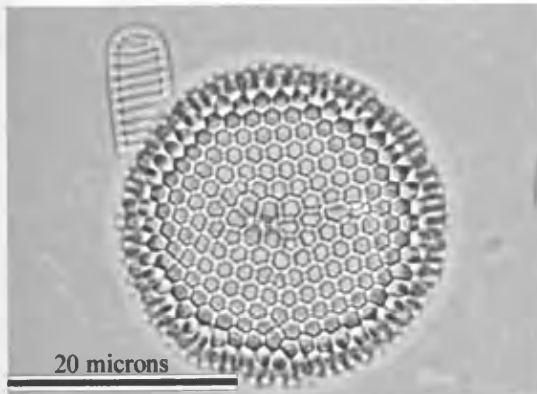
*Thalassiosira lentiginosa* (Janisch) Fryxell



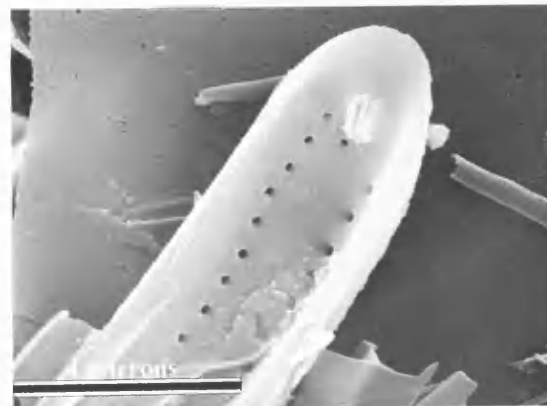
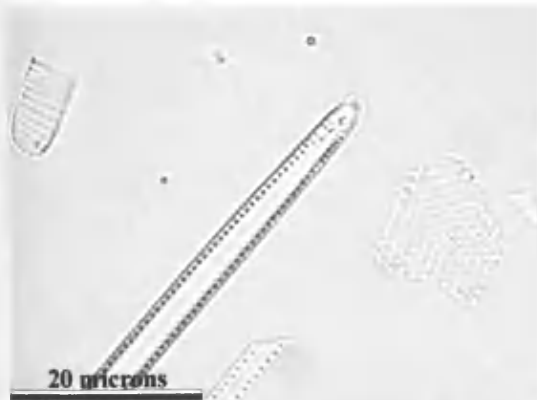
*Thalassiosira poroseriata* (Ramsfjell) Hasle



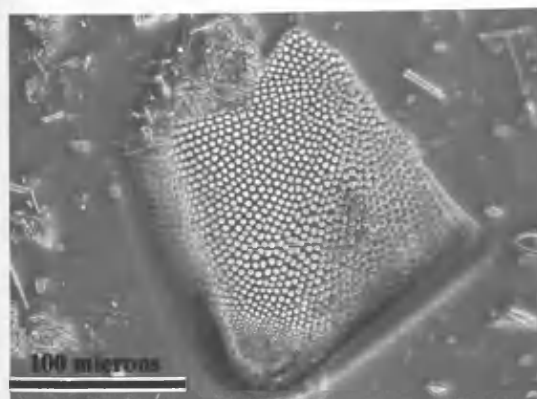
*Thalassiosira ritsheri* (Hustedt) Hasle



*Thalassiosira tumida* (Janisch) Hasle



*Thalassiothrix antarctica* Schimper ex Karsten



*Trigonium arcticum* (Brightwell) Cleve

### A.3.1 Palmer Deep, Western Antarctic Peninsula

Two tables are presented in this section. The first (ODP Core 178-1098A-6H) gives details of the lamina diatom assemblages. The second (ODP Core 178-1098A-6H & -1098C-5H) was not examined in the SEM; therefore, lamina thicknesses were measured on the thin sections, to extend the lamina thickness data range. The lamina log number 192, ODP Core 178-1098A-6H is equivalent to lamina 2 in ODP Core 178-1098A-6H&-1098C-5H.

#### Abbreviations used in the Palmer Deep (ODP Core 178-1098A-6H) table:

##### Terrigenous or biogenic content

B	Biogenic laminae
T	Terrigenous laminae

##### Diatom assemblage of laminae or sub-laminae

M	Mixed diatom assemblage, includes some or all of the following species: <i>Hyalochaete Chaetoceros</i> spp. resting spores, <i>Thalassiosira antarctica</i> , <i>Coscinodiscus bouvet</i> , <i>Odontella weissflogii</i> , <i>Corethron pennatum</i> , <i>Fragilariopsis</i> spp.
C	Near-monogeneric <i>Hyalochaete Chaetoceros</i> spp. resting spore
CB	Characterised by <i>Coscinodiscus bouvet</i>
CP	Characterised by <i>Criophilum pennatum</i>
OW	Characterised by <i>Odontella weissflogii</i> resting spores
TA	Characterised by <i>Thalassiosira antarctica</i> resting spores

##### Other features

Bioturb	Bioturbation
Gyp	Grains of gypsum
TP	Terrigenous pulse
FP	Faecal pellets

Double lines within the table indicate a break in the laminated interval.

APPENDIX 3

A.3.1.1 ODP Core 178-1098A-6H

Log no.	Depth (mcd)		Laminae thickness (mm)	Biogenic / terrigenous laminae	Diatom species assemblage	Sub-laminae	Other information	Year thickness (mm)	No. years
	Base of laminae	Top of laminae							
193	42.5154	42.5124	3	T	M			10.3	96
192	42.5227	42.5154	7.3	B	C		FP		
191	42.532	42.5227	9.3	T	M	CP,TA		22.3	95
190	42.545	42.532	13	B	C				
189	42.558	42.545	13	T	M		Bioturb	17.2	94
188	42.5622	42.558	4.2	B	C		FP		
187	42.5673	42.5622	5.1	T	OW			23.1	93
186	42.5853	42.5673	18	B	C		FP		
185	42.5871	42.5853	1.8	T	M			15.8	92
184	42.6011	42.5871	14	B	C				
183	42.6036	42.6011	2.5	T	C		Bioturb	5.9	91
182	42.607	42.6036	3.4	B	CP				
181	42.6098	42.607	2.8	T	C			11.3	90
180	42.6183	42.6098	8.5	B	C		FP		
179	42.6213	42.6183	3	T	M			5.5	89
178	42.6238	42.6213	2.5	B	C				
177	42.6263	42.6238	2.5	T	M			8.35	88
176	42.63215	42.6263	5.85	B	M				
175	42.6379	42.63215	5.75	T	M	CP	Bioturb	12	87
174	42.64415	42.6379	6.25	B	C				
173	42.6475	42.64415	3.35	T	M			10.8	86
172	42.65495	42.6475	7.45	B	C				
171	42.66695	42.65495	12	T	M			19.1	85
170	42.67405	42.66695	7.1	B	C				
169	42.69655	42.67405	22.5	T	M		Bioturb	23.4	84
168	42.69745	42.69655	0.9	B	C				
167	42.71665	42.69745	19.2	T	M	CP,TA		21.2	83
166	42.71865	42.71665	2	B	C				
165	42.73865	42.71865	20	T	M	C,CB,CP,TA		32.5	82
164	42.75115	42.73865	12.5	B	C				
163	42.77595	42.75115	24.8	T	M	C,CP,TA	TP	33.6	81
162	42.78475	42.77595	8.8	B	C		FP		
161	42.78715	42.78475	2.4	T	M			16	80
160	42.80075	42.78715	13.6	B	C		FP		
159	42.81995	42.80075	19.2	T	M	C,CP,CP,TA		35.2	79
158	42.83595	42.81995	16	B	C		FP		
157	42.87595	42.83595	40	T	CB	C,TA		50.6	78
156	42.88655	42.87595	10.6	B	C				
155	42.89055	42.88655	4	T	M	TA		5.6	77
154	42.89215	42.89055	1.6	B	C				
153	42.92815	42.89215	36	T	M	C,C,TA	Bioturb, FP	39.95	76
152	42.9321	42.92815	3.95	B	C		Bioturb		
151	42.9496	42.9321	17.5	T	M		Bioturb	27.5	75
150	42.9596	42.9496	10	B	C				
149	42.9706	42.9596	11	T	M	TA		24	74
148	42.9836	42.9706	13	B	C				
147	43.0006	42.9836	17	T	M			22	73
146	43.0056	43.0006	5	B	CP				

APPENDIX 3

Log no.	Depth (mcd)		Laminae thickness (mm)	Biogenic / terrigenous laminae	Diatom species assemblage	Sub-laminae	Other information	Year thickness (mm)	No. years
	Base of laminae	Top of laminae							
145	43.0082	43.0056	2.6	T	M		FP	10.6	72
144	43.0162	43.0082	8	B	C				
143	43.0187	43.0162	2.5	T	M			25.5	71
142	43.0417	43.0187	23	B	C		FP		
141	43.0447	43.0417	3	T	M	TA		5.2	70
140	43.0469	43.0447	2.2	B	C				
139	43.0511	43.0469	4.2	T	M	TA		8.4	69
138	43.0553	43.0511	4.2	B	C				
137	43.0598	43.0553	4.5	T	M		Bioturb	38.5	68
136	43.0938	43.0598	34	B	C		FP		
135	43.1138	43.0938	20	T	M	C,CB,CP,TA,OW		35	67
134	43.1288	43.1138	15	B	C				
133	43.1314	43.1288	2.6	T	M			36.6	66
132	43.1654	43.1314	34	B	C				
131	43.1894	43.1654	24	T	M	CB, C, CP, TA		29.4	65
130	43.1948	43.1894	5.4	B	C				
129	43.1984	43.1948	3.6	T	M			9	64
128	43.2038	43.1984	5.4	B	C		FP		
127	43.2503	43.2038	46.5	T	M		Bioturb	62.9	63
126	43.2667	43.2503	16.4	B	C				
125	43.2857	43.2667	19	T	M	TA,C		39	62
124	43.3057	43.2857	20	B	C				
123	43.3089	43.3057	3.2	T	M			10.25	61
122	43.31595	43.3089	7.05	B	C,CP				
121	43.3222	43.31595	6.25	T	M	C,CP		36.55	60
120	43.3525	43.3222	30.3	B	C				
119	43.3693	43.3525	16.8	T	M	OW,TA		32.4	59
118	43.3849	43.3693	15.6	B	C				
117	43.3876	43.3849	2.7	T	M	C		33.7	58
116	43.4186	43.3876	31	B	C				
115	43.4301	43.4186	11.5	T	M	TA		15.1	57
114	43.4337	43.4301	3.6	B	C		Bioturb		
113	43.4441	43.4337	10.4	T	M	C,C,C,		30.7	56
112	43.4644	43.4441	20.3	B	C				
111	43.4661	43.4644	1.7	T	M			3.5	55
110	43.4679	43.4661	1.8	B	C				
109	43.475	43.4679	7.1	T	M			26.4	54
108	43.4943	43.475	19.3	B	C				
107	43.4962	43.4943	1.9	T	M	TA		17.7	53
106	43.512	43.4962	15.8	B	C				
105	43.5234	43.512	11.4	T	M	CB,C		13	52
104	43.525	43.5234	1.6	B	C				
103	43.5406	43.525	15.6	T	M	TA		30.9	51
102	43.5559	43.5406	15.3	B	C				
101	43.5839	43.5559	28	T	M	TA, C		30.8	50
100	43.5867	43.5839	2.8	B	C				
99	43.5891	43.5867	2.4	T	CP			11.3	49
98	43.598	43.5891	8.9	B	C				
97	43.5998	43.598	1.8	T	M			3.1	48
96	43.6011	43.5998	1.3	B	C				

APPENDIX 3

Log no.	Depth (mcd)		Laminae thickness (mm)	Biogenic / terrigenous laminae	Diatom species assemblage	Sub-laminae	Other information	Year thickness (mm)	No. years
	Base of laminae	Top of laminae							
95	43.6042	43.6011	3.1	T	M				
94	43.6082	43.6042	4	B	C			7.1	47
93	43.6108	43.6082	2.6	T	M				
92	43.6265	43.6108	15.7	B	C			18.3	46
91	43.6278	43.6265	1.3	T	M				
90	43.6335	43.6278	5.7	B	C			7	45
89	43.6355	43.6335	2	T	M				
88	43.6374	43.6355	1.9	B	C			3.9	44
87	43.6417	43.6374	4.3	T	M				
86	43.6585	43.6417	16.8	B	C			21.1	43
85	43.6621	43.6585	3.6	T	M				
84	43.6905	43.6621	28.4	B	C			32	42
83	43.7015	43.6905	11	T	M				
82	43.7136	43.7015	12.1	B	C			23.1	41
81	43.7335	43.7136	19.9	T	M	C,C,TA			
80	43.7421	43.7335	8.6	B	C			28.5	40
79	43.7903	43.7421	48.2	T	M	TA			
78	43.8068	43.7903	16.5	B	C			64.7	39
77	43.8131	43.8068	6.3	T	M	TA			
76	43.8186	43.8131	5.5	B	C			11.8	38
75	43.8208	43.8186	2.2	T	M				
74	43.83	43.8208	9.2	B	C			11.4	37
73	43.837	43.83	7	T	M	TA			
72	43.84825	43.837	11.25	B	C			18.25	36
71	43.86645	43.84825	18.2	T	M		TP		
70	43.88635	43.86645	19.9	B	C			38.1	35
69	43.88755	43.88635	1.2	T	M				
68	43.89285	43.88755	5.3	B	C			6.5	34
67	43.89465	43.89285	1.8	T	M				
66	43.91075	43.89465	16.1	B	C			17.9	33
65	43.93195	43.91075	21.2	T	M	TA	TP		
64	43.93915	43.93195	7.2	B	C			28.4	32
63	43.94065	43.93915	1.5	T	M	TA			
62	43.95155	43.94065	10.9	B	C			12.4	31
61	43.96385	43.95155	12.3	T	M	TA,TA,TA			
60	43.98435	43.96385	20.5	B	C			32.8	30
59	43.99195	43.98435	7.6	T	M	TA			
58	44.00495	43.99195	13	B	C			20.6	29
57	44.00765	44.00495	2.7	T	M				
56	44.01275	44.00765	5.1	B	C			7.8	28
55	44.01885	44.01275	6.1	T	M				
54	44.02925	44.01885	10.4	B	C			16.5	27
53	44.03105	44.02925	1.8	T	M	TA			
52	44.05205	44.03105	21	B	C			22.8	26
51	44.05645	44.05205	4.4	T	M	TA			
50	44.07265	44.05645	16.2	B	C			20.6	25
49	44.08445	44.07265	11.8	T	M	OW			
48	44.0997	44.08445	15.25	B	C	TA		27.05	24
47	44.1076	44.0997	7.9	T	M	CP			
46	44.1261	44.1076	18.5	B	C			26.4	23

APPENDIX 3

Log no.	Depth (mcd)		Laminae thickness (mm)	Biogenic / terrigenous laminae	Diatom species assemblage	Sub-laminae	Other information	Year thickness (mm)	No. years
	Base of laminae	Top of laminae							
45	44.1341	44.1261	8	T	M	TA	Bioturb	16.2	22
44	44.1423	44.1341	8.2	B	CP				
43	44.1502	44.1423	7.9	T	M	C		26.95	21
42	44.16925	44.1502	19.05	B	C				
41	44.1702	44.16925	0.95	T	M	TA		4.75	20
40	44.174	44.1702	3.8	B	C				
39	44.17615	44.174	2.15	T	M	TA		9.15	19
38	44.18315	44.17615	7	B	C				
37	44.1955	44.18315	12.35	T	M	TA		26.85	18
36	44.21	44.1955	14.5	B	C		Bioturb		
35	44.275	44.21	65	T	M	C,C,C,TA,TA,TA	Bioturb	66.6	17
34	44.2766	44.275	1.6	B	C				
33	44.2998	44.2766	23.2	T	M	TA,TA,TA		47.2	16
32	44.3238	44.2998	24	B	C				
31	44.3443	44.3238	20.5	T	M	C, CP, TA	TP	22.4	15
30	44.3462	44.3443	1.9	B	C	CP			
29	44.3501	44.3462	3.9	T	M			19.6	14
28	44.3658	44.3501	15.7	B	C				
27	44.3687	44.3658	2.9	T	M			4.8	13
26	44.3706	44.3687	1.9	B	C				
25	44.3735	44.3706	2.9	T	M			25.9	12
24	44.3965	44.3735	23	B	C				
23	44.3989	44.3965	2.4	T	M	TA		25.4	11
22	44.4219	44.3989	23	B	C				
21	44.43	44.4219	8.1	T	M	C, TA	Gypsum	33.6	10
20	44.4555	44.43	25.5	B	C				
19	44.457	44.4555	1.5	T	M		Gypsum	20.5	9
18	44.476	44.457	19	B	C				
17	44.4958	44.476	19.8	T	M	CB, TA, OW		23.4	8
16	44.4994	44.4958	3.6	B	C				
15	44.5174	44.4994	18	T	M			48	7
14	44.5474	44.5174	30	B	C				
13	44.6116	44.5474	64.2	T	M	CP, TA, TA, TA	TP	80.4	6
12	44.6278	44.6116	16.2	B	C		Bioturb		
11	44.6358	44.6278	8	T	M			19	5
10	44.6468	44.6358	11	B	C				
9	44.6718	44.6468	25	T	M			30.5	4
8	44.6773	44.6718	5.5	B	C		Bioturb		
7	44.7056	44.6773	28.3	T	M		Bioturb	37.4	3
6	44.7147	44.7056	9.1	B	C				
5	44.796	44.7147	81.3	T	M	CP, TA	Bioturb	102.2	2
4	44.8169	44.796	20.9	B	C		Bioturb		
3	44.967	44.8169	150.1	T	M	TA, C	Gypsum	156.1	1
2	44.973	44.967	6	B	C		Bioturb		
1	45.03	44.973	57	T	M	TA, TA, C			

## A.3.1.2 ODP Core 178-1098A-6H &amp; -1098C-5H (combined)

Log no.	Depth (mcd)		Lamina thickness (mm)	Biogenic / terrigenous laminae	Number of years
	Base of laminae	Top of laminae			
155	40.6638	40.6338	30	T	77
154	40.6668	40.6638	3	B	
153	40.7108	40.6668	44	T	76
152	40.7118	40.7108	1	B	
151	40.7148	40.7118	3	T	75
150	40.7178	40.7148	3	B	
149	40.7188	40.7178	1	T	74
148	40.7208	40.7188	2	B	
147	40.7598	40.7208	39	T	73
146	40.7668	40.7598	7	B	
145	40.7748	40.7668	8	T	72
144	40.7798	40.7748	5	B	
143	40.7848	40.7798	5	T	71
142	40.7898	40.7848	5	B	
141	40.8098	40.7898	20	T	70
140	40.8128	40.8098	3	B	
139	40.8748	40.8128	62	T	69
138	40.8848	40.8748	10	B	
137	40.8868	40.8848	2	T	68
136	40.8938	40.8868	7	B	
135	40.8968	40.8938	3	T	67
134	40.9028	40.8968	6	B	
133	40.9073	40.9028	4.5	T	66
132	40.9133	40.9073	6	B	
131	40.9193	40.9133	6	T	65
130	40.9223	40.9193	3	B	
129	40.9263	40.9223	4	T	64
128	40.9323	40.9263	6	B	
127	40.9523	40.9323	20	T	63
126	40.9573	40.9523	5	B	
125	40.9673	40.9573	10	T	62
124	40.9743	40.9673	7	B	
123	40.9808	40.9743	6.5	T	61
122	40.9823	40.9808	1.5	B	
121	40.9853	40.9823	3	T	60
120	40.9933	40.9853	8	B	
119	41.0133	40.9933	20	T	59
118	41.0193	41.0133	6	B	
117	41.0273	41.0193	8	T	58
116	41.0413	41.0273	14	B	
115	41.0433	41.0413	2	T	57
114	41.0473	41.0433	4	B	
113	41.0533	41.0473	6	T	56
112	41.0553	41.0533	2	B	
111	41.0613	41.0553	6	T	55
110	41.0663	41.0613	5	B	



Log no.	Depth (mcd)		Lamina thickness (mm)	Biogenic / terrigenous laminae	Number of years
	Base of laminae	Top of laminae			
109	41.1033	41.0663	37	T	54
108	41.1073	41.1033	4	B	
107	41.1228	41.1073	15.5	T	53
106	41.1248	41.1228	2	B	
105	41.1448	41.1248	20	T	52
104	41.1473	41.1448	2.5	B	
103	41.1513	41.1473	4	T	51
102	41.1563	41.1513	5	B	
101	41.1803	41.1563	24	T	50
100	41.1853	41.1803	5	B	
99	41.1873	41.1853	2	T	49
98	41.1883	41.1873	1	B	
97	41.1903	41.1883	2	T	48
96	41.2003	41.1903	10	B	
95	41.2033	41.2003	3	T	47
94	41.2058	41.2033	2.5	B	
93	41.2098	41.2058	4	T	46
92	41.2288	41.2098	19	B	
91	41.2343	41.2288	5.5	T	45
90	41.2433	41.2343	9	B	
89	41.2513	41.2433	8	T	44
88	41.2583	41.2513	7	B	
87	41.2723	41.2583	14	T	43
86	41.2893	41.2723	17	B	
85	41.3143	41.2893	25	T	42
84	41.3203	41.3143	6	B	
83	41.3263	41.3203	6	T	41
82	41.3453	41.3263	19	B	
81	41.3862	41.3453	40.9	T	40
80	41.3922	41.3862	6	B	
79	41.4092	41.3922	17	T	39
78	41.4122	41.4092	3	B	
77	41.4295	41.4122	17.3	T	38
76	41.4375	41.4295	8	B	
75	41.4405	41.4375	3	T	37
74	41.448	41.4405	7.5	B	
73	41.46	41.448	12	T	36
72	41.465	41.46	5	B	
71	41.5575	41.5515	6	T	35
70	41.563	41.5575	5.5	B	
69	41.574	41.563	11	T	34
68	41.579	41.574	5	B	
67	41.6305	41.6245	6	T	33
66	41.6445	41.6305	14	B	
65	41.669	41.6445	24.5	T	32
64	41.762	41.758	4	B	
63	41.777	41.762	15	T	31
62	41.7845	41.777	7.5	B	

APPENDIX 3

Log no.	Depth (mcd)		Lamina thickness (mm)	Biogenic / terrigenous laminae	Number of years
	Base of laminae	Top of laminae			
61	41.787	41.7845	2.5	T	30
60	41.8	41.787	13	B	
59	41.87	41.854	16	T	29
58	41.8735	41.87	3.5	B	
57	41.8785	41.8735	5	T	28
56	41.8815	41.8785	3	B	
55	41.883	41.8815	1.5	T	27
54	41.888	41.883	5	B	
53	41.928	41.888	40	T	26
52	41.977	41.968	9	B	
51	41.9935	41.977	16.5	T	25
50	41.999	41.9935	5.5	B	
49	42.005	41.999	6	T	24
48	42.0125	42.005	7.5	B	
47	42.0205	42.0125	8	T	23
46	42.0305	42.0205	10	B	
45	42.0345	42.0305	4	T	22
44	42.0385	42.0345	4	B	
43	42.054	42.0385	15.5	T	21
42	42.077	42.054	23	B	
41	42.0815	42.077	4.5	T	20
40	42.0945	42.0815	13	B	
39	42.136	42.0945	41.5	T	19
38	42.1395	42.136	3.5	B	
37	42.144	42.1395	4.5	T	18
36	42.1495	42.144	5.5	B	
35	42.157	42.1495	7.5	T	17
34	42.16	42.157	3	B	
33	42.1758	42.1668	9	T	16
32	42.1818	42.1758	6	B	
31	42.2088	42.1818	27	T	15
30	42.2208	42.2088	12	B	
29	42.2263	42.2208	5.5	T	14
28	42.2403	42.2263	14	B	
27	42.2415	42.2403	1.2	T	13
26	42.2555	42.2415	14	B	
25	42.2595	42.2555	4	T	12
24	42.2775	42.2595	18	B	
23	42.2825	42.2775	5	T	11
22	42.2895	42.2825	7	B	
21	42.3075	42.2895	18	T	10
20	42.336	42.3075	28.5	B	
19	42.345	42.336	9	T	9
18	42.3495	42.345	4.5	B	
17	42.3655	42.3495	16	T	8
16	42.3715	42.3655	6	B	
15	42.3855	42.3715	14	T	7
14	42.392	42.3855	6.5	B	

Log no.	Depth (mcd)		Lamina thickness (mm)	Biogenic / terrigenous laminae	Number of years
	Base of laminae	Top of laminae			
13	42.398	42.392	6	T	6
12	42.422	42.398	24	B	
11	42.427	42.422	5	T	5
10	42.443	42.427	16	B	
9	42.445	42.443	2	T	4
8	42.4465	42.445	1.5	B	
7	42.4535	42.4465	7	T	3
6	42.4585	42.4535	5	B	
5	42.48	42.4585	21.5	T	2
4	42.493	42.48	13	B	
3	42.528	42.515	13	T	1
2	42.537	42.528	9	B	
1	42.55	42.537	13	T	

### A.3.2 Mertz Ninnis Trough, East Antarctic Margin

Two tables are presented in this section, NBP0101 JPC10 and KC10A.

#### Abbreviations used in NBP0101 JPC10 and KC10A tables:

##### Lamina types

- A Near-monogeneric *Hyalochaete Chaetoceros* spp. resting spore biogenic laminae
- B Biogenic laminae characterised by *Corethron pennatum*
- C Biogenic laminae characterised by *Rhizosolenia* spp.
- D Mixed diatom assemblage biogenic laminae, includes some or all of the following species: *Hyalochaete Chaetoceros* spp. resting spores, *Phaeoceros Chaetoceros* spp., *Fragilariopsis* spp., *Porosira glacialis* resting spores, *Stellarima microtrias* resting spores, *Rhizosolenia* spp., *Eucampia antarctica*, *Corethron pennatum*, *Odontella weissflogii* resting spores
- E Mixed diatom assemblage terrigenous laminae, includes some or all of the following species: *Hyalochaete Chaetoceros* spp. resting spores, *Phaeoceros Chaetoceros* spp., *Fragilariopsis* spp., *Porosira glacialis* resting spores, *Stellarima microtrias* resting spores, *Rhizosolenia* spp., *Eucampia antarctica*, *Corethron pennatum*, *Odontella weissflogii* resting spores, *Trigonium arcticum*
- F Terrigenous sub-laminae characterised by *Porosira glacialis* resting spores
- G Biogenic laminae characterised by *Fragilariopsis* spp.
- H Terrigenous laminae characterised by *Fragilariopsis* spp.

##### Other features

Bioturb	Bioturbated
Gyp	Grains of gypsum
TP	Terrigenous pulse
FP	Faecal pellets

Double lines within the table indicate a break in the laminated interval.

## A.3.2.1 NBP0101 JPC10

Log no.	Depth (mbsf)		Laminae thickness (mm)	Diatom species assemblage	Year thickness (mm)	Number of years	Other information
	Base of laminae	Top of laminae					
279	17.41828	17.40208	16.2	A			
278	17.42738	17.41828	9.1	E	13.4	116	
277	17.43168	17.42738	4.3	A			
276	17.43688	17.43168	5.2	E	11.3	115	
275	17.44298	17.43688	6.1	A			
274	17.46228	17.44298	19.3	E	21.3	114	
273	17.46428	17.46228	2.0	A			
272	17.47228	17.46428	8.0	E	19.6	113	
271	17.48168	17.47228	9.4	A			
270	17.4839	17.48168	2.2	D			
269	17.4892	17.4839	5.3	E	24.1	112	TP
268	17.496	17.4892	6.8	D			
267	17.508	17.496	12.0	A			FP
266	17.5121	17.508	4.1	E	7.1	111	
265	17.5151	17.5121	3.0	A			
264	17.5163	17.5151	1.2	E	7.3	110	
263	17.5224	17.5163	6.1	A			
262	17.5324	17.5224	10.0	E	24.3	109	
261	17.5467	17.5324	14.3	A			
260	17.5508	17.5467	4.1	E	9.8	108	
259	17.5565	17.5508	5.7	A			
258	17.5676	17.5565	11.1	D	11.1	107	Bioturb
257	17.5828	17.5676	15.2	E	23.7	106	
256	17.5913	17.5828	8.5	A			
255	17.6141	17.5913	22.8	E	29.8	105	
254	17.6211	17.6141	7.0	B			
253	17.6484	17.6211	27.3	E	28.9	104	Bioturb
252	17.65	17.6484	1.6	A			
251	17.788	17.7788	9.2	E	11.3	103	
250	17.7901	17.788	2.1	B			
249	17.7908	17.7901	0.7	F	12.3	102	
248	17.7957	17.7908	4.9	E			
247	17.8024	17.7957	6.7	B			
246	17.8074	17.8024	5.0	E	32.0	101	
245	17.8344	17.8074	27.0	B			
244	17.8459	17.8344	11.5	E	92.5	100	
243	17.9269	17.8459	81.0	B			FP
242	17.9317	17.9269	4.8	E	6.3	99	
241	17.9332	17.9317	1.5	A			
240	17.9361	17.9332	2.9	E	9.6	98	
239	17.9428	17.9361	6.7	B			
238	17.948	17.9428	5.2	E	10.7	97	
237	17.9535	17.948	5.5	B			
236	17.9564	17.9535	2.9	E	18.3	96	
235	17.9718	17.9564	15.4	D			
234	17.9754	17.9718	3.6	E	4.5	95	
233	17.9763	17.9754	0.9	A			
232	17.9776	17.9763	1.3	E	16.1	94	
231	17.9851	17.9776	7.5	D			FP

APPENDIX 3

Log no.	Depth (mbsf)		Laminae thickness (mm)	Diatom species assemblage	Year thickness (mm)	Number of years	Other information
	Base of laminae	Top of laminae					
230	17.9924	17.9851	7.3	A			FP
229	17.9996	17.9924	7.2	E			
228	18.0036	17.9996	4.0	A	11.2	93	
227	18.0119	18.0036	8.3	E			
226	18.0251	18.0119	13.2	A	21.5	92	
225	18.0288	18.0251	3.7	E			
224	18.0323	18.0288	3.5	A	7.2	91	
223	18.0473	18.0323	15.0	E			
222	18.0703	18.0473	23.0	E	41.5	90	
221	18.0738	18.0703	3.5	D			
220	18.077	18.0738	3.2	E			
219	18.083	18.077	6.0	D	10.3	89	
218	18.0841	18.083	1.1	D			
217	18.0876	18.0841	3.5	E			
216	18.0911	18.0876	3.5	A	7.0	88	
215	18.0938	18.0911	2.7	E			
214	18.0969	18.0938	3.1	D	5.8	87	
213	18.1	18.0969	3.1	E			
212	18.1022	18.1	2.2	A	5.3	86	
211	18.1053	18.1022	3.1	E			
210	18.1073	18.1053	2.0	A	5.1	85	
209	18.1104	18.1073	3.1	E			
208	18.1313	18.1104	20.9	B	24.0	84	
207	18.1353	18.1313	4.0	E			
206	18.1411	18.1353	5.8	A	9.8	83	FP
205	18.1791	18.1411	38.0	E	42.9	82	
204	18.184	18.1791	4.9	A			
203	18.1893	18.184	5.3	E			
202	18.2	18.1893	10.7	A	16.0	81	
201	18.7689	18.7498	19.1	E			
200	18.7821	18.7689	13.2	A	32.3	80	
199	18.7835	18.7821	1.4	E			
198	18.7888	18.7835	5.3	A	6.7	79	
197	18.7902	18.7888	1.4	F			
196	18.7942	18.7902	4.0	A	5.4	78	
195	18.8051	18.7942	10.9	E			
194	18.8129	18.8051	7.8	D	18.7	77	
193	18.8149	18.8129	2.0	E			
192	18.8278	18.8149	12.9	D	14.9	76	
191	18.8304	18.8278	2.6	F			
190	18.8453	18.8304	14.9	E			
189	18.8522	18.8453	6.9	D	35.5	75	
188	18.8633	18.8522	11.1	B			
187	18.8659	18.8633	2.6	E			
186	18.8671	18.8659	1.2	D	3.8	74	
185	18.8723	18.8671	5.2	E			
184	18.8782	18.8723	5.9	C	11.1	73	
183	18.88	18.8782	1.8	E			
182	18.8855	18.88	5.5	D	7.3	72	
181	18.8875	18.8855	2.0	E			
180	18.8885	18.8875	1.0	A	3.0	71	

APPENDIX 3

Log no.	Depth (mbsf)		Laminae thickness (mm)	Diatom species assemblage	Year thickness (mm)	Number of years	Other information
	Base of laminae	Top of laminae					
179	18.891	18.8885	2.5	E	6.5	70	
178	18.8931	18.891	2.1	C			
177	18.895	18.8931	1.9	A			
176	18.8973	18.895	2.3	E	3.1	69	
175	18.8981	18.8973	0.8	A			
174	18.9015	18.8981	3.4	E	5.5	68	
173	18.9036	18.9015	2.1	A			
172	18.9039	18.9036	0.3	E	5.5		
171	18.9045	18.9039	0.6	F			
170	18.91	18.9045	5.5	E			
169	19.1972	19.1897	7.5	D	17.7	67	
168	19.2047	19.1972	7.5	C			
167	19.2074	19.2047	2.7	A			
166	19.2082	19.2074	0.8	E	2.0	66	
165	19.2094	19.2082	1.2	B			
164	19.2133	19.2094	3.9	E	20.5	65	Bioturb
163	19.2183	19.2133	5.0	C			
162	19.2299	19.2183	11.6	D			
161	19.2441	19.2299	14.2	E	15.9	64	
160	19.2458	19.2441	1.7	A			
159	19.2548	19.2458	9.0	E	35.8	63	
158	19.2556	19.2548	0.8	F			
157	19.256	19.2556	0.4	E			
156	19.2769	19.256	20.9	D			
155	19.2816	19.2769	4.7	B			
154	19.2843	19.2816	2.7	E	8.2	62	
153	19.2898	19.2843	5.5	A			
152	19.3005	19.2898	10.7	E	24.2	61	
151	19.314	19.3005	13.5	D			
150	19.32	19.314	6.0	E	7.2	60	
149	19.3212	19.32	1.2	A			
148	19.3231	19.3212	1.9	E	9.9	59	
147	19.3307	19.3231	7.6	E			
146	19.3311	19.3307	0.4	A			
145	19.332	19.3311	0.9	F	12.2	58	
144	19.3374	19.332	5.4	D			
143	19.339	19.3374	1.6	A			
142	19.3426	19.339	3.6	B			
141	19.3433	19.3426	0.7	A			
140	19.345	19.3433	1.7	E			
139	19.3521	19.345	7.1	D	9.5	57	
138	19.3528	19.3521	0.7	B			
137	19.3537	19.3528	0.9	E	1.9	56	
136	19.3547	19.3537	1.0	A			
135	19.3715	19.3547	16.8	E	21.4	55	
134	19.3761	19.3715	4.6	D			
133	19.3787	19.3761	2.6	E	11.5	54	
132	19.3876	19.3787	8.9	B			
131	19.3885	19.3876	0.9	F	24.4	53	Bioturb
130	19.412	19.3885	23.5	B			

APPENDIX 3

Log no.	Depth (mbsf)		Laminae thickness (mm)	Diatom species assemblage	Year thickness (mm)	Number of years	Other information
	Base of laminae	Top of laminae					
129	19.4203	19.412	8.3	E			Bioturb
128	19.4418	19.4203	21.5	B	29.8	52	
127	19.4449	19.4418	3.1	E			
126	19.4729	19.4449	28.0	B	31.1	51	
125	19.4976	19.4729	24.7	E			
124	19.5	19.4976	2.4	A	27.1	50	
123	19.512	19.5	12.0	E			
122	19.5278	19.512	15.8	D	27.8	49	
121	19.5285	19.5278	0.7	F			
120	19.5352	19.5285	6.7	A	7.4	48	
119	19.5363	19.5352	1.1	F			
118	19.5381	19.5363	1.8	E	11.0	47	
117	19.5462	19.5381	8.1	A			
116	19.6162	19.5462	70.0	B	70.0	46	
115	19.6178	19.6162	1.6	F			
114	19.6313	19.6178	13.5	E	15.7	45	
113	19.6319	19.6313	0.6	D			
112	19.6353	19.6319	3.4	E			
111	19.6369	19.6353	1.6	A	5.0	44	
110	19.6374	19.6369	0.5	F			
109	19.6396	19.6374	2.2	E	49.6	43	
108	19.6865	19.6396	46.9	A			
107	19.6925	19.6865	6.0	E			
106	19.6957	19.6925	3.2	A	9.2	42	
105	19.702	19.6957	6.3	E			
104	19.7022	19.702	0.2	B	6.5	41	
103	19.7035	19.7022	1.3	F			
102	19.7133	19.7035	9.8	B	11.1	40	
101	19.7143	19.7133	1.0	E			
100	19.7151	19.7143	0.8	B	1.8	39	
99	19.7169	19.7151	1.8	F			
98	19.7391	19.7169	22.2	B	30.0	38	
97	19.7451	19.7391	6.0	D			
96	19.7485	19.7451	3.4	E			
95	19.7513	19.7485	2.8	A	6.2	37	
94	19.7528	19.7513	1.5	E			
93	19.7608	19.7528	8.0	D	9.5	36	
92	19.7616	19.7608	0.8	E			
91	19.764	19.7616	2.4	A	3.2	35	
90	19.7648	19.764	0.8	F			
89	19.7684	19.7648	3.6	E	8.6	34	
88	19.7726	19.7684	4.2	D			
87	19.7789	19.7726	6.3	E			
86	19.7794	19.7789	0.5	A	6.8	33	
85	19.7976	19.7794	18.2	E			
84	19.798	19.7976	0.4	A	18.6	32	
83	19.7999	19.798	1.9	E			
82	19.8006	19.7999	0.7	D	2.6	31	
81	19.8216	19.8006	21.0	E			
80	19.8227	19.8216	1.1	B	22.1	30	



APPENDIX 3

Log no.	Depth (mbsf)		Laminae thickness (mm)	Diatom species assemblage	Year thickness (mm)	Number of years	Other information
	Base of laminae	Top of laminae					
79	19.8355	19.8227	12.8	E	13.7	29	
78	19.8364	19.8355	0.9	A			
77	19.8384	19.8364	2.0	E	7.0	28	
76	19.8434	19.8384	5.0	B			
75	19.858	19.8434	14.6	E	18.9	27	
74	19.8623	19.858	4.3	D			
73	19.8647	19.8623	2.4	E	4.0	26	
72	19.8663	19.8647	1.6	A			
71	19.8714	19.8663	5.1	E	5.7	25	
70	19.872	19.8714	0.6	B			
69	19.8737	19.872	1.7	E	44.0	24	
68	19.9097	19.8737	36.0	B			
67	19.916	19.9097	6.3	A			Bioturb
66	19.94	19.916	24.0	E			Bioturb
65	19.9408	19.94	0.8	F	37.0	23	Bioturb
64	19.9478	19.9408	7.0	E			Bioturb
63	19.953	19.9478	5.2	A			Bioturb
62	19.97	19.953	17.0	E			
61	20.1565	20.1366	19.9	E	22.7	22	TP
60	20.1593	20.1565	2.8	C			
59	20.1611	20.1593	1.8	F	20.3	21	
58	20.1723	20.1611	11.2	A			
57	20.1796	20.1723	7.3	D			
56	20.182	20.1796	2.4	E	5.8	20	
55	20.1849	20.182	2.9	D			
54	20.1854	20.1849	0.5	D			
53	20.1861	20.1854	0.7	F	7.8	19	
52	20.1893	20.1861	3.2	E			
51	20.1932	20.1893	3.9	D			
50	20.1943	20.1932	1.1	F	8.7	18	
49	20.1995	20.1943	5.2	E			
48	20.2015	20.1995	2.0	D			
47	20.2019	20.2015	0.4	C			
46	20.2034	20.2019	1.5	E	16.2	17	
45	20.2173	20.2034	13.9	D			
44	20.2181	20.2173	0.8	A			
43	20.2231	20.2181	5.0	E	6.4	16	
42	20.2245	20.2231	1.4	A			
41	20.2283	20.2245	3.8	E	7.6	15	
40	20.2321	20.2283	3.8	A			
39	20.2377	20.2321	5.6	E	9.7	14	
38	20.2418	20.2377	4.1	A			
37	20.2451	20.2418	3.3	E	8.4	13	
36	20.2502	20.2451	5.1	A			
35	20.2562	20.2502	6.0	E	11.2	12	
34	20.2614	20.2562	5.2	D			
33	20.3257	20.2614	64.3	E	69.4	11	Bioturb
32	20.3308	20.3257	5.1	A			
31	20.3439	20.3308	13.1	E	103.2	10	Bioturb
30	20.3508	20.3439	6.9	D			
29	20.3636	20.3508	12.8	B			

APPENDIX 3

Log no.	Depth (mbsf)		Laminae thickness (mm)	Diatom species assemblage	Year thickness (mm)	Number of years	Other information
	Base of laminae	Top of laminae					
28	20.3645	20.3636	0.9	E			
27	20.434	20.3645	69.5	B			
26	20.4356	20.434	1.6	E			TP
25	20.4421	20.4356	6.5	D	8.1	9	
24	20.4476	20.4421	5.5	F			TP
23	20.4584	20.4476	10.8	E			
22	20.4597	20.4584	1.3	A	21.3	8	
21	20.4634	20.4597	3.7	D			
20	20.4638	20.4634	0.4	E			
19	20.4691	20.4638	5.3	D	8.4	7	
18	20.4718	20.4691	2.7	C			
17	20.4741	20.4718	2.3	E			
16	20.4748	20.4741	0.7	A	3.0	6	
15	20.4764	20.4748	1.6	F			
14	20.4891	20.4764	12.7	E	53.3	5	TP
13	20.5281	20.4891	39.0	D			
12	20.5297	20.5281	1.6	F			
11	20.5597	20.5297	30.0	D	31.6	4	
10	20.5619	20.5597	2.2	E			
9	20.5742	20.5619	12.3	D			
8	20.5814	20.5742	7.2	C	25.2	3	
7	20.5849	20.5814	3.5	D			
6	20.5873	20.5849	2.4	F			
5	20.5902	20.5873	2.9	E	10.8	2	
4	20.5957	20.5902	5.5	A			
3	20.5967	20.5957	1.0	F			
2	20.5987	20.5967	2.0	D	3.0	1	
1	20.6	20.5987	1.3	E			

## A.3.2.1 NBP0101 KC10A

Log no.	Depth (mbsf)		Laminae thickness (mm)	Diatom species assemblage	Year thickness (mm)	Number of years	Other information
	Base of laminae	Top of laminae					
35	2.055	2.045	10.0	G			
34	2.06	2.055	5.0	E			
33	2.074	2.06	14.0	A	19.0	17	
32	2.084	2.074	10.0	E			
31	2.0991	2.084	15.1	D	25.1	16	
30	2.1003	2.0991	1.2	E			
29	2.1248	2.1003	24.5	G	25.7	15	
28	2.1266	2.1248	1.8	E			
27	2.1296	2.1266	3.0	D	4.8	14	
26	2.1536	2.1296	24.0	H			
25	2.1659	2.1536	12.3	D	36.3	13	
24	2.1949	2.1659	29.0	E			
23	2.2014	2.1949	6.5	D	35.5	12	Bioturb
22	2.2064	2.2014	5.0	E			
21	2.2085	2.2064	2.1	G	7.1	11	
20	2.2132	2.2085	4.7	H			
19	2.2161	2.2132	2.9	G	7.6	10	
18	2.2321	2.2161	16.0	H			
17	2.2381	2.2321	6.0	A	22.0	9	Bioturb
16	2.2415	2.2381	3.4	E			
15	2.2512	2.2415	9.7	D	13.1	8	
14	2.2562	2.2512	5.0	H			
13	2.2583	2.2562	2.1	D	7.1	7	
12	2.2613	2.2583	3.0	E			
11	2.2645	2.2613	3.2	D	6.2	6	
10	2.2673	2.2645	2.8	E			
9	2.2823	2.2673	15.0	D	17.8	5	Bioturb
8	2.2903	2.2823	8.0	E			
7	2.3003	2.2903	10.0	D	18.0	4	Bioturb Bioturb
6	2.3093	2.3003	9.0	E			
5	2.31	2.3093	0.7	D	9.7	3	
4	2.3164	2.31	6.4	E			
3	2.319	2.3164	2.6	D	9.0	2	
2	2.3269	2.319	7.9	E			
1	2.3279	2.3269	1.0	G	8.9	1	

A.3.3.1 MD03 2597

Log no.	Depth (mbsf)		Laminae thickness (mm)	Biogenic / terrigenous laminae	Lamina type	Year thickness (mm)	Number of years	Other information
	Base of laminae	Top of laminae						
339	18.8032	18.7766	26.6	B	V			
338	18.8111	18.8032	7.9	T	X	18.1	121	
337	18.8213	18.8111	10.2	B	V			
336	18.8363	18.8213	15.0	T	X	34.4	120	
335	18.8557	18.8363	19.4	B	V			
334	18.8617	18.8557	6.0	T	X	28.6	119	
333	18.8843	18.8617	22.6	B	V			
332	18.8963	18.8843	12.0	T	X			
331	18.9028	18.8963	6.5	B	X	25.7	118	
330	18.91	18.9028	7.2	B	V			
329	18.913	18.91	3.0	T	X	4.2	117	
328	18.9142	18.913	1.2	B	U			
327	18.9362	18.9142	22.0	T	X	30.1	116	
326	18.9443	18.9362	8.1	B	X			
325	18.9534	18.9443	9.1	T	X	12.0	115	
324	18.9563	18.9534	2.9	B	V			
323	18.9633	18.9563	7.0	T	X	11.8	114	
322	18.9681	18.9633	4.8	B	V			
321	18.9711	18.9681	3.0	T	Y			
320	18.9741	18.9711	3.0	T	X	12.0	113	
319	18.9801	18.9741	6.0	B	V			
318	18.9828	18.9801	2.7	T	Y			
317	18.9912	18.9828	8.4	T	X	19.9	112	
316	19	18.9912	8.8	B	V			
315	23.4132	23.4046	8.6	B	U			
314	23.424	23.4132	10.8	T	X			
313	23.425	23.424	1.0	B	U	16.5	111	
312	23.4289	23.425	3.9	B	X			
311	23.4297	23.4289	0.8	B	S			
310	23.4317	23.4297	2.0	T	X	2.9	110	
309	23.4326	23.4317	0.9	B	S			
308	23.4398	23.4326	7.2	T	X			
307	23.4441	23.4398	4.3	T	X	14.0	109	
306	23.4466	23.4441	2.5	B	V			
305	23.4506	23.4466	4.0	T	V	21.9	108	
304	23.4685	23.4506	17.9	B	V			
303	23.4748	23.4685	6.3	T	X	12.1	107	Bioturb
302	23.4806	23.4748	5.8	B	V			
301	23.4825	23.4806	1.9	T	Z			
300	23.492	23.4825	9.5	T	X	14.1	106	Bioturb
299	23.4947	23.492	2.7	B	U			
298	23.5292	23.4947	34.5	T	X	37.3	105	
297	23.532	23.5292	2.8	B	V			
296	23.5352	23.532	3.2	T	X			
295	23.5363	23.5352	1.1	T	Z	18.0	104	TP
294	23.5384	23.5363	2.1	T	X			
293	23.55	23.5384	11.6	B	W			
292	33.8754	33.8629	12.5	B	V			
291	33.8797	33.8754	4.3	B	V			
290	33.8835	33.8797	3.8	T	X	12.6	103	
289	33.8923	33.8835	8.8	B	V			
288	33.9123	33.8923	20.0	T	X	26.4	102	
287	33.9187	33.9123	6.4	B	R			

### A.3.3 Dumont d'Urville Trough, East Antarctic Margin

One table is presented in this section, MD03 2597.

#### Abbreviations used in MD03 2597 table:

##### Terrigenous or biogenic content

B	Biogenic laminae
T	Terrigenous laminae

##### Lamina types

R	Laminae characterised by <i>Corethron pennatum</i> and <i>Rhizosolenia</i> spp.
S	Laminae characterised by <i>Corethron pennatum</i>
T	Laminae characterised by <i>Rhizosolenia</i> spp.
U	Laminae characterised by <i>Hyalochaete Chaetoceros</i> spp. resting spores
V	Laminae characterised by <i>Hyalochaete Chaetoceros</i> spp. resting spores and <i>Fragilariopsis</i> spp.
W	Laminae characterised by <i>Fragilariopsis</i> spp.
X	Mixed diatom assemblage laminae
Y	Sub-laminae characterised by <i>Porosira glacialis</i> resting spores
Z	Laminae characterised by <i>Stellarima microtrias</i> resting spores, <i>Porosira glacialis</i> resting spores and / or <i>Coscinodiscus bouvet</i>

##### Other features

Bioturb	Bioturbated
Gyp	Grains of gypsum
TP	Terrigenous pulse
FP	Faecal pellets

Double lines within the table indicate a break in the laminated interval.

## A.3.3.1 MD03 2597

Log no.	Depth (mbsf)		Laminae thickness (mm)	Biogenic / terrigenous laminae	Lamina type	Year thickness (mm)	Number of years	Other information
	Base of laminae	Top of laminae						
339	18.8032	18.7766	26.6	B	V			
338	18.8111	18.8032	7.9	T	X	18.1	121	
337	18.8213	18.8111	10.2	B	V			
336	18.8363	18.8213	15.0	T	X	34.4	120	
335	18.8557	18.8363	19.4	B	V			
334	18.8617	18.8557	6.0	T	X	28.6	119	
333	18.8843	18.8617	22.6	B	V			
332	18.8963	18.8843	12.0	T	X			
331	18.9028	18.8963	6.5	B	X	25.7	118	
330	18.91	18.9028	7.2	B	V			
329	18.913	18.91	3.0	T	X	4.2	117	
328	18.9142	18.913	1.2	B	U			
327	18.9362	18.9142	22.0	T	X	30.1	116	
326	18.9443	18.9362	8.1	B	X			
325	18.9534	18.9443	9.1	T	X	12.0	115	
324	18.9563	18.9534	2.9	B	V			
323	18.9633	18.9563	7.0	T	X	11.8	114	
322	18.9681	18.9633	4.8	B	V			
321	18.9711	18.9681	3.0	T	Y			
320	18.9741	18.9711	3.0	T	X	12.0	113	
319	18.9801	18.9741	6.0	B	V			
318	18.9828	18.9801	2.7	T	Y			
317	18.9912	18.9828	8.4	T	X	19.9	112	
316	19	18.9912	8.8	B	V			
315	23.4132	23.4046	8.6	B	U			
314	23.424	23.4132	10.8	T	X			
313	23.425	23.424	1.0	B	U	16.5	111	
312	23.4289	23.425	3.9	B	X			
311	23.4297	23.4289	0.8	B	S			
310	23.4317	23.4297	2.0	T	X	2.9	110	
309	23.4326	23.4317	0.9	B	S			
308	23.4398	23.4326	7.2	T	X			
307	23.4441	23.4398	4.3	T	X	14.0	109	
306	23.4466	23.4441	2.5	B	V			
305	23.4506	23.4466	4.0	T	V	21.9	108	
304	23.4685	23.4506	17.9	B	V			
303	23.4748	23.4685	6.3	T	X	12.1	107	Bioturb
302	23.4806	23.4748	5.8	B	V			
301	23.4825	23.4806	1.9	T	Z			
300	23.492	23.4825	9.5	T	X	14.1	106	Bioturb
299	23.4947	23.492	2.7	B	U			
298	23.5292	23.4947	34.5	T	X	37.3	105	
297	23.532	23.5292	2.8	B	V			
296	23.5352	23.532	3.2	T	X			
295	23.5363	23.5352	1.1	T	Z	18.0	104	TP
294	23.5384	23.5363	2.1	T	X			
293	23.55	23.5384	11.6	B	W			
292	33.8754	33.8629	12.5	B	V			
291	33.8797	33.8754	4.3	B	V			
290	33.8835	33.8797	3.8	T	X	12.6	103	
289	33.8923	33.8835	8.8	B	V			
288	33.9123	33.8923	20.0	T	X	26.4	102	
287	33.9187	33.9123	6.4	B	R			

APPENDIX 3

Log no.	Depth (mbsf)		Laminae thickness (mm)	Biogenic / terrigenous laminae	Lamina type	Year thickness (mm)	Number of years	Other information
	Base of laminae	Top of laminae						
286	33.9209	33.9187	2.2	T	X	10.2	101	
285	33.9289	33.9209	8.0	B	W			
284	33.9402	33.9289	11.3	T	X	22.7	100	
283	33.9516	33.9402	11.4	B	V			
282	33.9543	33.9516	2.7	T	Y	19.5	99	
281	33.9583	33.9543	4.0	T	X			
280	33.965	33.9583	6.7	B	V			
279	33.9711	33.965	6.1	B	T			Bioturb
278	33.9748	33.9711	3.7	T	V	6.5	98	
277	33.9776	33.9748	2.8	B	V			
276	33.9862	33.9776	8.6	T	X	15.8	97	
275	33.9934	33.9862	7.2	B	W			
274	33.9949	33.9934	1.5	T	X	14.7	96	
273	34.0081	33.9949	13.2	B	W			
272	34.0114	34.0081	3.3	T	X	6.4	95	
271	34.0145	34.0114	3.1	B	V			
270	34.0181	34.0145	3.6	T	X	8.6	94	
269	34.0231	34.0181	5.0	B	V			
268	34.0265	34.0231	3.4	T	X	10.0	93	Bioturb
267	34.0331	34.0265	6.6	B	W			
266	34.0357	34.0331	2.6	T	S			
265	34.05	34.0357	14.3	T	X			
264	37.8166	37.8	16.6	T	X	35.7	92	
263	37.8357	37.8166	19.1	B	X			
262	37.8427	37.8357	7.0	T	X	18.6	91	
261	37.8543	37.8427	11.6	B	V			FP, Bioturb
260	37.8639	37.8543	9.6	T	W	12.0	90	
259	37.8663	37.8639	2.4	B	W			
258	37.8995	37.8663	33.2	T	X		89	
257	37.9142	37.8995	14.7	B	W			
256	37.9156	37.9142	1.4	T	Z	33.4	88	
255	37.9405	37.9156	24.9	T	X			
254	37.9476	37.9405	7.1	B	V			
253	37.95	37.9476	2.4	T	X			
252	38.5689	38.5616	7.3	B	V			
251	38.5801	38.5689	11.2	T	X	21.4	87	
250	38.5903	38.5801	10.2	B	V			
249	38.5918	38.5903	1.5	T	X	7.5	86	
248	38.5978	38.5918	6.0	B	R			FP
247	38.6021	38.5978	4.3	T	X	20.1	85	
246	38.6051	38.6021	3.0	T	X			
245	38.6075	38.6051	2.4	T	Z			
244	38.6163	38.6075	8.8	T	X			
243	38.6179	38.6163	1.6	B	X			
242	38.6249	38.6179	7.0	T	X	33.0	84	
241	38.6509	38.6249	26.0	B	V			
240	38.689	38.6509	38.1	T	X	46.7	83	Bioturb
239	38.6928	38.689	3.8	B	V			
238	38.6976	38.6928	4.8	B	Z			
237	38.7	38.6976	2.4	T	Y			
236	40.6	40.592	8.0	B	U			
235	40.6044	40.6	4.4	T	X	26.8	82	
234	40.6237	40.6044	19.3	B	U			
233	40.6268	40.6237	3.1	B	Z			

APPENDIX 3

Log no.	Depth (mbsf)		Laminae thickness (mm)	Biogenic / terrigenous laminae	Lamina type	Year thickness (mm)	Number of years	Other information
	Base of laminae	Top of laminae						
232	40.6373	40.6268	10.5	T	X	34.5	81	
231	40.6613	40.6373	24.0	B	U			
230	40.6672	40.6613	5.9	T	Y	9.2	80	
229	40.6705	40.6672	3.3	B	U			
228	40.6781	40.6705	7.6	T	X	22.9	79	
227	40.6922	40.6781	14.1	B	U			
226	40.6934	40.6922	1.2	B	U			
225	40.7016	40.6934	8.2	T	X			
224	40.703	40.7016	1.4	B	Y	28.7	78	
223	40.706	40.703	3.0	T	Z			
222	40.7221	40.706	16.1	B	W			
221	40.7237	40.7221	1.6	T	Z			
220	40.729	40.7237	5.3	T	X	27.9	77	
219	40.75	40.729	21.0	B	X			
218	41.0629	40.8449	10.7	B	X			
217	41.0713	41.0629	8.4	T	X	41.9	76	Bioturb
216	41.0856	41.0713	14.3	T	X			Bioturb
215	41.1048	41.0856	19.2	B	V			
214	41.12	41.1048	15.2	T	X			
213	41.1334	41.12	13.4	B	W	28.6	75	
212	41.142	41.1334	8.6	T	X			
211	41.15	41.142	8.0	B	X	23.2	74	
210	41.1548	41.15	4.8	B	T			
209	41.1566	41.1548	1.8	B	T			
208	41.16	41.1566	3.4	T	Z			
207	41.162	41.16	2.0	B	Z	14.2	73	
206	41.168	41.162	6.0	B	Z			
205	41.1708	41.168	2.8	B	Z			
204	41.1731	41.1708	2.3	T	X			
203	41.1772	41.1731	4.1	B	X	6.4	72	
202	41.1854	41.1772	8.2	T	X			
201	41.1961	41.1854	10.7	B	X	18.9	71	
200	41.2	41.1961	3.9	T	X			
199	44.4396	44.4326	7.0	T	X			
198	44.4432	44.4396	3.6	B	W			
197	44.4464	44.4432	3.2	B	Z	18.5	70	
196	44.4551	44.4464	8.7	T	X			
195	44.4617	44.4551	6.6	B	X			
194	44.4758	44.4617	14.1	T	T			
193	44.4902	44.4758	14.4	B	T	28.5	69	
192	44.4952	44.4902	5.0	T	X			
191	44.5002	44.4952	5.0	B	T	10.0	68	
190	44.5095	44.5002	9.3	T	T			
189	44.5202	44.5095	10.7	B	T	20.0	67	
188	44.5299	44.5202	9.7	T	X			
187	44.5317	44.5299	1.8	T	Y	24.2	65	
186	44.5339	44.5317	2.2	T	X			
185	44.5359	44.5339	2.0	T	Y			
184	44.5384	44.5359	2.5	T	X			
183	44.5444	44.5384	6.0	B	V			
182	44.5467	44.5444	2.3	T	X			
181	44.5477	44.5467	1.0	B	V	3.3	64	
180	44.5503	44.5477	2.6	T	X			
179	44.57	44.5503	19.7	B	V	22.3	63	



APPENDIX 3

Log no.	Depth (mbsf)		Laminae thickness (mm)	Biogenic / terrigenous laminae	Lamina type	Year thickness (mm)	Number of years	Other information
	Base of laminae	Top of laminae						
178	44.5712	44.57	1.2	T	Y			
177	44.5763	44.5712	5.1	T	X	14.4	62	
176	44.5844	44.5763	8.1	B	V			
175	44.6008	44.5844	16.4	T	X	21.4	61	Bioturb
174	44.6058	44.6008	5.0	B	V			
173	44.6086	44.6058	2.8	T	Y			
172	44.6176	44.6086	9.0	T	X			
171	44.6228	44.6176	5.2	B	Y			
170	44.6268	44.6228	4.0	T	X	36.6	60	
169	44.6328	44.6268	6.0	B	U			
168	44.6388	44.6328	6.0	B	S			
167	44.6424	44.6388	3.6	B	V			
166	44.65	44.6424	7.6	T	X			
165	47.6679	47.6536	14.3	B	S			
164	47.6699	47.6679	2.0	T	X			
163	47.6712	47.6699	1.3	T	Y			
162	47.6717	47.6712	0.5	T	X	7.9	59	
161	47.6722	47.6717	0.5	T	Y			
160	47.6758	47.6722	3.6	B	V			
159	47.6766	47.6758	0.8	T	X			
158	47.6789	47.6766	2.3	T	Y			
157	47.6802	47.6789	1.3	T	X	14.0	58	
156	47.6812	47.6802	1.0	T	Y			
155	47.688	47.6812	6.8	T	X			
154	47.6898	47.688	1.8	B	V			
153	47.6931	47.6898	3.3	T	X	20.7	57	
152	47.7105	47.6931	17.4	B	V			FP
151	47.7147	47.7105	4.2	T	X	24.0	56	
150	47.7345	47.7147	19.8	B	R			FP
149	47.7382	47.7345	3.7	T	X	11.1	55	
148	47.7456	47.7382	7.4	B	X			
147	47.7478	47.7456	2.2	T	U	10.7	54	
146	47.7563	47.7478	8.5	B	U			FP
145	47.7599	47.7563	3.6	T	X	4.8	53	
144	47.7611	47.7599	1.2	B	S			
143	47.7629	47.7611	1.8	T	X	14.7	52	
142	47.7758	47.7629	12.9	B	S			
141	47.779	47.7758	3.2	T	X	5.4	51	
140	47.7812	47.779	2.2	B	X			
139	47.7861	47.7812	4.9	T	X	10.7	50	
138	47.7909	47.7861	4.8	B	V			
137	47.7919	47.7909	1.0	B	V			
136	47.7922	47.7919	0.3	T	X	1.1	49	
135	47.793	47.7922	0.8	B	V			
134	47.7971	47.793	4.1	T	X	8.0	48	
133	47.7978	47.7971	0.7	T	Y			
132	47.7994	47.7978	1.6	T	X			
131	47.801	47.7994	1.6	B	V			
130	47.8127	47.801	11.7	T	X	23.0	47	
129	47.824	47.8127	11.3	B	V			
128	47.8402	47.824	16.2	T	X	33.4	46	TP
127	47.8534	47.8402	13.2	B	V			
126	47.8574	47.8534	4.0	B	V			
125	47.8624	47.8574	5.0	T	X	7.8	45	
124	47.8652	47.8624	2.8	B	U			

APPENDIX 3

Log no.	Depth (mbsf)		Laminae thickness (mm)	Biogenic / terrigenous laminae	Lamina type	Year thickness (mm)	Number of years	Other information
	Base of laminae	Top of laminae						
69	52.5535	52.5488	4.7	B	V			
68	52.5549	52.5535	1.4	T	Y			
67	52.5633	52.5549	8.4	T	X	20.0	26	
66	52.5735	52.5633	10.2	B	V			FP
65	52.5748	52.5735	1.3	T	Y			
64	52.5824	52.5748	7.6	T	X			TP
63	52.5921	52.5824	9.7	B	X	25.2	25	
62	52.5987	52.5921	6.6	B	V			
61	52.6045	52.5987	5.8	T	X	9.1	24	
60	52.6078	52.6045	3.3	B	W			
59	52.6112	52.6078	3.4	T	X	11.1	23	
58	52.6189	52.6112	7.7	B	X			Bioturb
57	52.6389	52.6189	20.0	T	X	25.6	22	
56	52.6445	52.6389	5.6	B	V			
55	52.6533	52.6445	8.8	T	X	19.1	21	
54	52.6636	52.6533	10.3	B	X			
53	52.6764	52.6636	12.8	T	X	16.4	20	
52	52.68	52.6764	3.6	B	U			
51	53.0215	53.0175	4.0	B	U			
50	53.0294	53.0215	7.9	T	X	9.5	19	
49	53.031	53.0294	1.6	B	V			
48	53.0368	53.031	5.8	T	X	18.5	18	
47	53.0495	53.0368	12.7	B	V			
46	53.0516	53.0495	2.1	T	X	16.8	17	
45	53.0663	53.0516	14.7	B	V			
44	53.0689	53.0663	2.6	T	Y			FP
43	53.0699	53.0689	1.0	T	X	9.2	16	
42	53.0755	53.0699	5.6	T	V			
41	53.0781	53.0755	2.6	B	Y			
40	53.0811	53.0781	3.0	T	X	17.0	15	
39	53.0925	53.0811	11.4	B	V			
38	53.095	53.0925	2.5	T	Y			
37	53.0965	53.095	1.5	T	X	9.3	14	
36	53.1018	53.0965	5.3	B	S			FP
35	53.1093	53.1018	7.5	T	Z	11.1	13	
34	53.1129	53.1093	3.6	B	X			Bioturb
33	53.1301	53.1129	17.2	T	X	25.2	12	
32	53.1381	53.1301	8.0	B	S			FP
31	53.1429	53.1381	4.8	T	Z	11.9	11	
30	53.15	53.1429	7.1	T	X			
29	56.585	56.5781	6.9	B	X			
28	56.5893	56.585	4.3	T	Y			
27	56.5926	56.5893	3.3	T	X	33.3	10	
26	56.6183	56.5926	25.7	B	S			Bioturb
25	56.6211	56.6183	2.8	T	Y			
24	56.6533	56.6211	32.2	T	X	40.6	9	Bioturb
23	56.6589	56.6533	5.6	B	X			
22	56.6599	56.6589	1.0	T	Y			
21	56.6688	56.6599	8.9	T	X	19.0	8	
20	56.6765	56.6688	7.7	B	X			
19	56.6779	56.6765	1.4	B	R			
18	56.6806	56.6779	2.7	T	X	5.7	7	
17	56.6836	56.6806	3.0	B	R			
16	56.6861	56.6836	2.5	T	X	23.5	6	FP
15	56.7071	56.6861	21.0	B	R			FP

**APPENDIX 3**

Log no.	Depth (mbsf)		Laminae thickness (mm)	Biogenic / terrigenous laminae	Lamina type	Year thickness (mm)	Number of years	Other information
	Base of laminae	Top of laminae						
14	56.7102	56.7071	3.1	T	Y	25.0	5	
13	56.7226	56.7102	12.4	T	X			
12	56.7311	56.7226	8.5	B	R			
11	56.7321	56.7311	1.0	B	U			
10	56.7561	56.7321	24.0	T	X			
9	56.7683	56.7561	12.2	B	V	36.2	4	FP
8	56.7739	56.7683	5.6	T	Y	20.2	3	
7	56.7855	56.7739	11.6	T	X			
6	56.7885	56.7855	3.0	B	S			
5	56.7994	56.7885	10.9	T	X	16.2	2	
4	56.8047	56.7994	5.3	B	S			
3	56.806	56.8047	1.3	B	Y	25.3	1	
2	56.8169	56.806	10.9	T	X			
1	56.83	56.8169	13.1	B	R			

## A.4 Quantitative diatom abundance data

This appendix lists the diatom valve count data for Palmer Deep (ODP Core 178-1098A-6H), Mertz Ninnis Trough (NBP0101 JPC10 and KC10A) and Durmont d'Urville Trough (MD03 2597). *Hyalochaete Chaetoceros* spp. resting spores dominate the diatom assemblages of all three core sites, therefore, two separate counts per sample are made; a total species count and a *Chaetoceros* spp. free count. The *Chaetoceros* free counts allow trends of less common species to be revealed (Leventer *et al.*, 1996). All slides were prepared in a beaker with a diameter of 10 cm and the area of the microscope field of view used during counting was 0.00143 cm<sup>2</sup>. The log numbers in the tables refers to the number allocated to individual laminae in Appendix 3.

### A.4.1 Palmer Deep, Western Antarctic Peninsula

#### A.4.1.1 ODP Core 178-1098A-6H

Quantitative diatom analysis samples were taken from biogenic laminae, terrigenous laminae and terrigenous sub-laminae identified during backscattered electron imagery (BSEI) analysis. This data is used to support results and discussions in chapter 6.

**Table A4.1.1.1** Palmer Deep, ODP Core 178-1098A-6H, biogenic laminae quantitative diatom abundance counts, all species.

Log number	4	58	60	72	74	130	134	172
Depth (mcd)	44.970	43.996	43.978	43.841	43.825	43.191	43.117	42.651
Number of FOV	2	3	3	4	3	3	2	4
Mass (g)	0.006	0.006	0.006	0.006	0.005	0.006	0.006	0.005
Species								
<i>Hyalochaete Chaetoceros</i> spp. (vegetative) Gran	14	5	5	0	0	0	9	5
<i>Hyalochaete Chaetoceros</i> spp. (resting spore) Gran	491	417	427	469	431	421	402	478
<i>Eucampia antarctica</i> (vegetative) (Castracane) Mangin	0	1	0	1	0	0	0	0
<i>Fragilariopsis curta</i> (Van Heurck) Hustedt	0	0	1	5	0	0	1	0
<i>Fragilariopsis cylindrus</i> (Grunow) Krieger	1	0	0	4	0	0	0	1
<i>Fragilariopsis cylindriciformis</i> (Hasle) Hasle	0	1	0	0	0	0	0	0
<i>Fragilariopsis rhombica</i> (O'Meara) Hustedt	0	0	0	0	0	0	0	1
<i>Fragilariopsis ritscheri</i> (Hustedt) Hasle	0	1	0	0	0	0	0	0
<i>Fragilariopsis vanheurckii</i> (M. Pergallo) Hustedt	0	0	0	2	0	0	0	1
<i>Porosira glacialis</i> (Grunow) Jørgensen	1	0	0	0	0	0	0	0
<i>Proboscia</i> spp. Sunström	1	0	0	0	0	0	0	0
<i>Thalassiosira antarctica</i> (resting spore - warm) Comber	0	0	1	0	1	0	0	1
<i>Thalassiosira lentiginosa</i> (Janisch) Fryxell	0	0	0	0	0	1	0	0
Unidentified pennates	1	0	0	0	0	0	0	0
<b>Total:</b>	<b>509</b>	<b>425</b>	<b>434</b>	<b>481</b>	<b>432</b>	<b>422</b>	<b>412</b>	<b>487</b>

**Table A4.1.1.2** Palmer Deep, ODP Core 178-1098A-6H, biogenic laminae quantitative diatom abundance counts, *Hyalochaete Chaetoceros* spp. free.

	Log number	4	58	60	72	74	130	134	172
	Depth (mcd)	44.970	43.996	43.978	43.841	43.825	43.191	43.117	42.651
	Number of FOV	348	393	434	317	723	859	362	465
	Mass (g)	0.006	0.006	0.006	0.006	0.005	0.006	0.006	0.005
Species									
<i>Actinocyclus actinochilus</i> (Ehrenberg) Simonsen	6	7	4	3	3	0	5	2	
<i>Actinocyclus curvatus</i> Janisch in Schmidt	0	0	0	0	0	2	0	0	
<i>Actinocyclus</i> spp. Ehrenberg	0	0	0	0	0	1	0	0	
<i>Asteromphalus</i> spp. Ehrenberg	0	0	0	0	0	0	1	1	
<i>Phaeoceros Chaetoceros</i> spp. Gran	1	0	0	0	0	0	0	3	
<i>Cocconeis</i> spp. Ehrenberg	0	0	0	0	0	6	0	1	
<i>Corethron pennatum</i> (Grunow) Ostenfeld	0	3	9	11	0	32	5	6	
<i>Eucampia antarctica</i> (resting spore) (Castracane) Mangin	0	0	0	1	0	1	1	0	
<i>Eucampia antarctica</i> (vegetative) (Castracane) Mangin	41	68	15	8	7	2	17	4	
<i>Fragilariopsis curta</i> (Van Heurck) Hustedt	37	63	112	128	84	65	161	81	
<i>Fragilariopsis cylindrus</i> (Grunow) Krieger	86	15	73	66	145	72	77	77	
<i>Fragilariopsis cylindriiformis</i> (Hasle) Hasle	0	1	1	1	0	1	1	0	
<i>Fragilariopsis kerguelensis</i> (O'Meara) Hustedt	10	23	2	0	6	5	1	27	
<i>Fragilariopsis obliquecostata</i> (Van Heurck) Heiden	0	1	0	0	1	2	0	0	
<i>Fragilariopsis rhombica</i> (O'Meara) Hustedt	25	17	3	0	2	8	3	38	
<i>Fragilariopsis ritscheri</i> (Hustedt) Hasle	10	10	3	6	1	8	13	5	
<i>Fragilariopsis separanda</i> Hustedt	3	1	0	0	0	0	2	5	
<i>Fragilariopsis sublinearis</i> (Van Heurck) Heiden	0	2	1	4	1	4	12	4	
<i>Fragilariopsis vanheurckii</i> (M. Pergallo) Hustedt	9	14	19	71	39	19	18	19	
<i>Fragilariopsis</i> spp. Hustedt	10	10	25	20	16	6	20	22	
<i>Gomphonema</i> spp. Ehrenberg	0	0	0	0	0	5	0	0	
<i>Navicula</i> spp. Bory de St-Vincent	4	6	23	16	17	32	15	23	
<i>Nitzschia</i> spp. Hassall	0.5	1	0.5	0	0	0.5	0	0	
<i>Odontella weissflogii</i> (Janisch) Grunow	0	2	1	0	1	0	0	3	
<i>Porosira glacialis</i> (Grunow) Jørgensen	6	27	2	2	1	1	6	8	
<i>Porosira pseudodenticula</i> (Hustedt) Jousé	0	0	0	0	0	0	0	1	
<i>Proboscia</i> spp. Sunström	6	0	0	0	0	0	0	0	
<i>Proboscia inermis</i> (Castracane) Jordan & Ligowski	47	4	6	3	2	46	6	0	
<i>Proboscia truncata</i> (Karsten) Nöthig & Ligowski	3	3	1	1	1	1	0	0	
<i>Pseudonitzschia turgidula</i> (Hustedt) Hasle	1.5	4.5	3.5	4	3.5	1	4	5.5	
<i>Rhizosolenia antennata</i> f. <i>antennata</i> (Ehrenberg) Brown	3	0	0	0	0	0	0	1	
<i>Rhizosolenia antennata</i> f. <i>semispina</i> Sundström	4	0	0	0	0	0	0	3	
<i>Rhizosolenia</i> species A Armand	0	1	0	0	0	0	0	0	
<i>Rhizosolenia</i> spp. Brightwell	2	1	0	0	0	0	0	0	
<i>Stellarima microtrias</i> (resting spore) (Ehrenberg) Hasle & Sims	0	5	1	1	0	2	0	1	
<i>Stephanodiscus</i> spp. Ehrenberg	0	0	0	0	0	1	17	0	
<i>Thalassiosira ambigua</i> Kozlova	0	2	0	0	0	0	1	0	
<i>Thalassiosira antarctica</i> (resting spore - cold) Comber	3	19	11	12	1	6	1	0	
<i>Thalassiosira antarctica</i> (resting spore - warm) Comber	52	66	69	30	60	57	17	24	
<i>Thalassiosira antarctica</i> (vegetative) Comber	9	2	4	3	0	3	0	5	
<i>Thalassiosira australis</i> Peragallo	0	0	1	0	0	0	0	0	
<i>Thalassiosira gracilis</i> v. <i>expecta</i> (Van Landingham) Fryxell & Hasle	3	0	3	2	0	1	0	1	
<i>Thalassiosira gracilis</i> v. <i>gracilis</i> (Karsten) Hustedt	0	0	0	2	0	0	0	4	
<i>Thalassiosira gravida</i> Cleve	1	3	0	0	1	0	0	2	
<i>Thalassiosira lentiginosa</i> (Janisch) Fryxell	7	0	1	0	0	6	0	10	
<i>Thalassiosira ritscheri</i> (Hustedt) Hasle	0	12	5	3	0	1	0	1	
<i>Thalassiosira tumida</i> (Janisch) Hasle	3	4	1	2	2	1	0	4	
<i>Thalassiosira</i> spp. Cleve	6	7	2	0	0	4	1	2	
<i>Thalassiothrix antarctica</i> Schimper ex Karsten	0	0	0	0.5	0	0	0	0.5	
<i>Trichotoxon reinboldii</i> (Van Heurck) Reid & Round	0	1	0	0	0	0	0	0.5	
<i>Trachyneis aspera</i> (Ehrenberg) Cleve	0	0	0	0	0	0	0	1.5	
Unidentified centrics	1	0	3	0	6	2	2	2	
Unidentified pennates	1	0	3	1	3	2	0	8	
<b>Total:</b>	<b>401</b>	<b>405.5</b>	<b>408</b>	<b>401.5</b>	<b>403.5</b>	<b>406.5</b>	<b>407</b>	<b>406</b>	

**Table A4.1.1.3** Palmer Deep, ODP Core 178-1098A-6H, terrigenous laminae quantitative diatom abundance counts, all species.

Log number	5	59	59	61	73	75	135	135	135	173
Depth (mcd)	44.790	43.989	43.987	43.962	43.833	43.819	43.112	43.105	43.100	42.646
Number of POV	9	3	6	9	6	5	7	10	8	8
Mass (g)	0.0093	0.0083	0.0089	0.0071	0.0072	0.0092	0.0079	0.0078	0.0083	0.0074
<b>Species</b>										
<i>Hyalochacte Chaetoceros</i> spp. (vegetative) Gran	0	0	13	0	1	3	0	0	0	6
<i>Hyalochaete Chaetoceros</i> spp. (resting spore) Gran	420	398	466	421	427	449	404	388	408	449
<i>Phaeoceros Chaetoceros</i> spp. Gran	0	0	0	0	0	0	0	0	0	0
<i>Eucampia antarctica</i> (vegetative) (Castracane) Mangin	0	0	1	0	0	0	0	0	0	0
<i>Fragilariopsis curta</i> (Van Heurck) Hustedt	5	0	1	3	2	1	2	3	4	2
<i>Fragilariopsis cylindrus</i> (Grunow) Krieger	0	0	2	0	1	0	2	3	3	0
<i>Fragilariopsis kerguelensis</i> (O'Meara) Hustedt	1	1	0	0	0	0	0	0	0	0
<i>Fragilariopsis rhombica</i> (O'Meara) Hustedt	0	0	0	0	0	1	0	0	0	0
<i>Fragilariopsis rischeri</i> (Hustedt) Hasle	1	0	1	0	0	0	0	0	0	1
<i>Fragilariopsis vanheurckii</i> (M. Pergallo) Hustedt	0	0	0	0	0	0	0	0	1	0
<i>Navicula</i> spp. Bory de St-Vincent	2	0	0	0	0	0	0	0	1	0
<i>Odontella weissflogii</i> (Janisch) Grunow	0	0	1	0	0	0	0	1	0	0
<i>Proboscia truncata</i> (Karsten) Nöthig & Ligowski	1	0	0	0	0	0	0	0	0	0
<i>Pseudonitzschia turgidula</i> (Hustedt) Hasle	0	0	0.5	0	0	0	0	0.5	0	0
<i>Rhizosolenia antennata</i> f. <i>semispina</i> Sundström	0	0	0	0	0	0	0	0	1	0
<i>Thalassiosira antarctica</i> (resting spore - warm) Conber	6	2	3	6	2	1	0	1	1	0
<i>Thalassiosira gracilis</i> v. <i>gracilis</i> (Karsten) Hustedt	0	0	0	1	0	0	0	0	0	0
<i>Thalassiosira lentiginosa</i> (Janisch) Fryxell	0	0	0	0	0	0	0	2	0	1
<i>Thalassiosira</i> spp. Cleve	0	0	0	1	1	0	0	0	0	0
<i>Stephanodiscus</i> spp. Ehnberg	0	0	0	0	0	0	0	3	0	0
<b>Total:</b>	<b>436</b>	<b>401</b>	<b>488.5</b>	<b>432</b>	<b>434</b>	<b>455</b>	<b>408</b>	<b>401.5</b>	<b>419</b>	<b>459</b>

**Table A4.1.1.4** Palmer Deep, ODP Core 178-1098A-6H terrigenous laminae quantitative diatom abundance counts, *Hyalochaete Chaetoceros* spp. free.

	Log number	5	59	59	61	73	75	135	135	135	173
	Depth (mcd)	44.790	43.989	43.987	43.962	43.833	43.819	43.112	43.105	43.100	42.646
	Number of FOV	378	430	473	439	367	376	444	684	422	514
	Mass (g)	0.0093	0.0083	0.0089	0.0071	0.0072	0.0092	0.0079	0.0078	0.0083	0.0074
Species											
<i>Achnanthes</i> spp. Bory de St.-Vincent	0	1	0	0	0	0	0	0	0	0	0
<i>Actinocyclus actinochilus</i> (Ehrenberg) Simonsen	3	5	8	3	3	3	3	3	13	1	3
<i>Actinocyclus curvatus</i> Janisch in Schmidt	0	0	0	0	0	0	0	1	1	0	0
<i>Asteromphalus</i> spp. Ehrenberg	0	0	0	0	1	1	1	1	0	0	0
<i>Chaetoceros Chaetoceros</i> spp. Gran	0	0	0	0	0	0	0	0	0	0	9
<i>Cocconeis</i> spp. Ehrenberg	2	1	0	0	2	1	3	2	1	1	0
<i>Corethron pennatum</i> (Grunow) Ostenfeld	3	3	0	8	1	9	4	1	1	1	16
<i>Eucampia antarctica</i> (resting spore) (Castracane) Mangin	0	3	2	1	0	6	1	6	1	1	11
<i>Eucampia antarctica</i> (vegetative) (Castracane) Mangin	6	9	9	1	3	1	13	1	2	1	10
<i>Fragilariopsis curta</i> (Van Heurck) Hustedt	102	110	112	77	108	93	164	130	107	102	102
<i>Fragilariopsis cylindrus</i> (Grunow) Krieger	38	20	17	11	80	31	25	38	61	23	23
<i>Fragilariopsis cylindriciformis</i> (Hasle) Hasle	0	0	0	0	0	0	1	1	1	0	0
<i>Fragilariopsis kerguelensis</i> (O'Meara) Hustedt	20	35	23	4	7	29	9	9	4	4	21
<i>Fragilariopsis obliquecostata</i> (Van Heurck) Heiden	0	2	0	0	0	3	2	0	0	0	0
<i>Fragilariopsis pseudonana</i> (Hasle) Hasle	0	0	1	0	0	0	0	0	0	0	0
<i>Fragilariopsis rhombica</i> (O'Meara) Hustedt	6	9	7	5	3	21	11	4	0	0	29
<i>Fragilariopsis ritscheri</i> (Hustedt) Hasle	8	17	8	2	4	5	13	4	3	8	8
<i>Fragilariopsis separanda</i> Hustedt	1	6	0	0	3	1	0	0	0	0	2
<i>Fragilariopsis sublinearis</i> (Van Heurck) Heiden	1	3	1	0	0	0	5	3	1	3	3
<i>Fragilariopsis vanheurckii</i> (M. Pergallo) Hustedt	8	22	16	17	43	24	14	31	39	29	29
<i>Fragilariopsis</i> spp. Hustedt	20	9	6	1	10	14	10	1	12	9	9
<i>Gomphonema</i> spp. Ehrenberg	1	0	0	0	0	0	0	0	0	0	0
<i>Navicula</i> spp. Bory de St.-Vincent	9	7	13	5	24	8	15	12	23	19	19
<i>Nitzschia</i> spp. Hassall	8	0.5	1	0	4	0	0	1.5	1	0	0
<i>Odontella weissflogii</i> (Janisch) Grunow	1	1	5	3	1	3	1	5	2	14	14
<i>Porosira glacialis</i> (Grunow) Jørgensen	4	8	10	10	7	17	17	7	3	3	3
<i>Porosira pseudodenticula</i> (Hustedt) Jousé	0	0	0	0	0	0	0	0	0	1	1
<i>Proboscia inermis</i> (Castracane) Jordan & Ligowski	3	1	0	0	0	0	1	1	4	2	2
<i>Proboscia truncata</i> (Karsten) Nøthig & Ligowski	4	0	1	1	2	1	1	1	22	0	0
<i>Pseudonitzschia turgidula</i> (Hustedt) Hasle	17	12.5	4	1	5.5	14	4	2.5	6	14	14
<i>Rhizosolenia antennata</i> f. <i>sempina</i> Sundström	13	3	1	2	0	0	0	1	3	4	4
<i>Rhizosolenia</i> spp. Brightwell	1	0	1	0	0	1	0	0	0	1	1
<i>Stellarima microtrias</i> (resting spore) (Ehrenberg) Hasle & Sims	1	0	0	0	1	1	0	0	1	0	0
<i>Stephanodiscus</i> spp. Ehrenberg	0	0	0	0	0	0	18	7	6	0	0
<i>Thalassiosira antarctica</i> (resting spore) Comber	1	23	13	18	1	0	6	3	0	8	8
<i>Thalassiosira antarctica</i> (resting spore - warm) Comber	104	80	106	214	66	82	39	72	76	30	30
<i>Thalassiosira antarctica</i> (vegetative) Comber	1	1	10	2	8	1	9	10	4	1	1
<i>Thalassiosira gracilis</i> v. <i>expecta</i> (Van Landingham) Fryxell & Hasle	1	2	4	2	0	0	3	3	2	1	1
<i>Thalassiosira gracilis</i> v. <i>gracilis</i> (Karsten) Hustedt	1	1	4	2	0	3	1	1	1	4	4
<i>Thalassiosira gravida</i> Cleve	5	0	0	0	0	7	0	0	0	0	0
<i>Thalassiosira lentiginosa</i> (Janisch) Fryxell	15	3	0	1	8	7	2	11	4	19	19
<i>Thalassiosira poroseriata</i> (Ramsfjell) Hasle	1	0	1	0	0	2	0	1	1	0	0
<i>Thalassiosira ritscheri</i> (Hustedt) Hasle	0	0	6	1	0	2	1	4	1	1	1
<i>Thalassiosira tumida</i> (Janisch) Hasle	0	5	0	10	1	0	8	10	4	4	4
<i>Thalassiosira</i> spp. Cleve	7	3	6	3	5	8	2	2	2	5	5
<i>Thalassiothrix antarctica</i> Schimper ex Karsten	0.5	0	0	0	0	0.5	0.5	0	0	0.5	0.5
<i>Thalassiothrix</i> spp. Cleve & Grunow	0	0	0.5	0	0	0	0	0	0	0	0
<i>Trichotoxon reinholdii</i> (Van Heurck) Reid & Round	0	0	0	0	0	0	0	0	0	0.5	0.5
Unidentified centrics	2	0	1	1	1	1	1	2	1	1	1
Unidentified pennates	1	0	9	1	4	2	1	2	2	3	3
<b>Total:</b>	<b>419.5</b>	<b>406</b>	<b>406.5</b>	<b>407</b>	<b>406.5</b>	<b>402.5</b>	<b>410.5</b>	<b>404</b>	<b>403</b>	<b>411</b>	<b>411</b>

**Table A4.1.1.5** Palmer Deep, ODP Core 178-1098A-6H, terrigenous sub-laminae quantitative diatom abundance counts, all species.

	<i>Hyalochaete</i> spp. RS	<i>Chaetoceros</i> spp. RS	<i>Coscinodiscus</i> <i>bouvet</i>	<i>Corethron</i> <i>pennatum</i>	<i>Thalassiosira antarctica</i> RS			<i>Odontella</i> <i>weissflogii</i> RS
<b>Log number</b>	131	135	135	131	59	131	135	135
<b>Depth (mcd)</b>	43.177	43.109	43.107	43.171	43.987	43.174	43.098	43.096
<b>Number of FOV</b>	8	7	20	19	14	13	4	17
<b>Mass (g)</b>	0.0071	0.0087	0.0077	0.007	0.007	0.007	0.008	0.0081
<b>Species</b>								
<i>Actinocyclus actinochilus</i> (Ehrenberg) Simonsen	0	0	1	1	1	0	0	0
<i>Hyalochaete Chaetoceros</i> spp. (vegetative) Gran	0	9	0	1	0	0	0	2
<i>Hyalochaete Chaetoceros</i> spp. (resting spore) Gran	409	394	406	411	368	427	427	435
<i>Phaeoceros Chaetoceros</i> spp. Gran	0	0	0	1	0	0	0	0
<i>Corethron pennatum</i> (Grunow) Ostenfeld	1	0	1	1	0	0	0	0
<i>Coscinodiscus bouvet</i> Karsten	0	0	1	0	0	0	0	0
<i>Eucampia antarctica</i> (resting spore) (Castracane) Mangin	0	0	0	0	0	0	0	1
<i>Eucampia antarctica</i> (vegetative) (Castracane) Mangin	0	0	0	0	0	0	0	3
<i>Fragilariopsis curta</i> (Van Heurck) Hustedt	3	2	0	6	0	2	8	7
<i>Fragilariopsis cylindrus</i> (Grunow) Krieger	2	0	3	2	11	4	0	2
<i>Fragilariopsis kerguelensis</i> (O'Meara) Hustedt	0	0	0	0	1	0	0	0
<i>Fragilariopsis pseudonana</i> (Hasle) Hasle	0	0	0	0	0	0	0	2
<i>Fragilariopsis rhombica</i> (O'Meara) Hustedt	0	0	0	0	1	0	0	0
<i>Fragilariopsis ritscheri</i> (Hustedt) Hasle	1	0	0	3	0	0	0	2
<i>Fragilariopsis vanheurckii</i> (M. Pergallo) Hustedt	0	1	0	0	0	0	0	0
<i>Fragilariopsis</i> spp. Hustedt	0	0	0	0	1	0	0	2
<i>Navicula</i> spp. Bory de St-Vincent	1	0	1	1	5	0	0	1
<i>Odontella weissflogii</i> (Janisch) Grunow	0	0	0	0	0	0	0	4
<i>Proboscia inermis</i> (Castracane) Jordan & Ligowski	1	0	0	0	0	1	1	9
<i>Proboscia truncata</i> (Karsten) Nöthig & Ligowski	0	0	0	1	0	0	0	5
<i>Pseudonitzschia turgidula</i> (Hustedt) Hasle	0	0	0.5	0	0	0	0	2
<i>Rhizosolenia</i> spp. Brightwell	0	1	0	0	0	0	0	0
<i>Rhizosolenia antennata</i> f. <i>semispina</i> Sundström	0	0	0	0	0	0	1	0
<i>Thalassiosira antarctica</i> (resting spore) Comber	0	0	0	0	16	0	0	1
<i>Thalassiosira antarctica</i> (resting spore – warm) Comber	0	0	4	1	19	4	5	3
<i>Thalassiosira antarctica</i> (vegetative) Comber	0	0	0	0	20	4	1	1
<i>Thalassiosira lentiginosa</i> (Janisch) Fryxell	0	0	0	1	0	0	0	0
<i>Thalassiosira ritscheri</i> (Hustedt) Hasle	0	0	0	0	0	0	0	1
<i>Thalassiosira tumida</i> (Janisch) Hasle	2	0	0	0	1	0	0	0
<i>Thalassiosira</i> spp. Cleve	1	1	0	0	2	0	0	0
Unidentified centric	0	0	0	0	1	0	0	0
<b>Total:</b>	<b>421</b>	<b>408</b>	<b>417.5</b>	<b>430</b>	<b>447</b>	<b>442</b>	<b>443</b>	<b>483</b>



**Table A4.1.1.6** Palmer Deep, ODP Core 178-1098A-6H, terrigenous sub-laminae quantitative diatom abundance counts, *Hyalochaete Chaetoceros* spp. free.

	<i>Hyalochaete Chaetoceros</i> spp. RS		<i>Coscinodiscus bouvet</i>	<i>Corethron pennatum</i>	<i>Thalassiosira antarctica</i> RS			<i>Odontella weissflogii</i> RS
Log number	131	135	135	131	59	131	135	135
Depth (mcd)	43.177	43.109	43.107	43.171	43.987	43.174	43.098	43.096
Number of FOV	400	736	681	931	87	368	137	214
Mass(g)	0.0071	0.0087	0.0077	0.007	0.007	0.007	0.008	0.0081
<b>Species</b>								
<i>Actinocyclus actinochilus</i> (Ehrenberg) Simonsen	11	10	35	7	4	4	5	6
<i>Actinocyclus curvatulus</i> Janisch in Schmidt	0	0	0	0	0	0	0	0
<i>Amphora</i> spp. (Ehrenberg) Kükzing	0	1	0	0	0	0	0	0
<i>Asteromphalus</i> spp. (Ehrenberg)	0	0	0	0	0	0	0	0
<i>Phaeoceros Chaetoceros</i> spp. Gran	0	0	0	1	0	0	0	0
<i>Cocconeis</i> spp. Ehrenberg	2	1	3	4	0	0	0	0
<i>Corethron pennatum</i> (Grunow) Ostenfeld	17	5	7	20	3	2	0	1
<i>Coscinodiscus bouvet</i> Karsten	0	0	3	0	0	0	0	0
<i>Coscinodiscus</i> spp. Ehrenberg	1	0	0	0	0	0	0	0
<i>Denticulopsis</i> spp. (Simonsen) Akiba & Yanagisawa	0	0	1	0	0	0	0	0
<i>Eucampia antarctica</i> (resting spore) (Castracane) Mangin	1	1	5	4	0	2	0	6
<i>Eucampia antarctica</i> (vegetative) (Castracane) Mangin	3	11	1	1	0	1	0	11
<i>Fragilariopsis curta</i> (Van Heurck) Hustedt	149	130	145	99	36	66	96	75
<i>Fragilariopsis cylindrus</i> (Grunow) Krieger	25	34	14	25	51	70	7	12
<i>Fragilariopsis cylindriciformis</i> (Hasle) Hasle	0	0	0	0	0	0	0	0
<i>Fragilariopsis kerguelensis</i> (O'Meara) Hustedt	7	2	4	2	1	1	4	6
<i>Fragilariopsis obliquecostata</i> (Van Heurck) Heiden	1	0	1	2	0	3	0	0
<i>Fragilariopsis pseudonana</i> (Hasle) Hasle	0	0	0	0	0	0	0	2
<i>Fragilariopsis rhombica</i> (O'Meara) Hustedt	2	3	2	7	1	3	1	2
<i>Fragilariopsis ritscheri</i> (Hustedt) Hasle	10	14	7	13	0	3	20	24
<i>Fragilariopsis separanda</i> Hustedt	0	1	2	3	1	1	0	0
<i>Fragilariopsis sublinearis</i> (Van Heurck) Heiden	3	3	3	2	0	1	2	0
<i>Fragilariopsis vanheurckii</i> (M. Pergallo) Hustedt	36	25	22	34	0	17	10	9
<i>Fragilariopsis</i> spp. Hustedt	8	5	5	16	2	11	1	9
<i>Gomphonema</i> spp. Ehrenberg	0	0	0	0	0	0	0	1
<i>Navicula</i> spp. Bory de St-Vincent	25	17	14	15	27	39	2	3
<i>Nitzschia</i> spp. Hassall	0	1.5	1.5	3	0	2	0	0
<i>Odontella weissflogii</i> (Janisch) Grunow	4	8	5	5	0	2	3	44
<i>Porosira glacialis</i> (Grunow) Jørgensen	6	7	2	3	0	2	7	2
<i>Proboscia inermis</i> (Castracane) Jordan & Ligowski	3	1	2	3	0	2	5	84
<i>Proboscia truncata</i> (Karsten) Nöthig & Ligowski	1	2	1	2	0	0	6	45
<i>Pseudonitzschia turgidula</i> (Hustedt) Hasle	1.5	1	4	2	1	1.5	0.5	6.5
<i>Rhizosolenia antennata</i> f. <i>semispina</i> Sundström	0	3	9	1	0	0	2	0
<i>Rhizosolenia</i> species A Armand	0	0	1	0	0	0	0	0
<i>Rhizosolenia</i> spp. Brightwell	0	3	2	0	0	0	0	0
<i>Stellarima microtrias</i> (resting spore) (Ehrenberg) Hasle & Sims	0	0	0	0	1	0	5	1
<i>Stephanodiscus</i> spp. Ehrenberg	2	0	6	0	0	0	0	0
<i>Thalassiosira antarctica</i> (resting spore - cold) Comber	4	1	2	1	66	4	32	5
<i>Thalassiosira antarctica</i> (resting spore - warm) Comber	60	73	72	90	135	107	194	25
<i>Thalassiosira antarctica</i> (vegetative) Comber	4	6	5	8	72	47	2	3
<i>Thalassiosira gracilis</i> v. <i>expecta</i> (Van Landingham) Fryxell & Hasle	1	0	1	5	0	0	0	0
<i>Thalassiosira gracilis</i> v. <i>gracilis</i> (Karsten) Hustedt	1	2	3	3	0	0	0	1
<i>Thalassiosira gravida</i> Cleve	0	0	0	0	1	0	0	0
<i>Thalassiosira lentiginosa</i> (Janisch) Fryxell	3	11	2	14	0	11	0	2
<i>Thalassiosira ritscheri</i> (Hustedt) Hasle	2	1	3	0	0	0	1	2
<i>Thalassiosira tumida</i> (Janisch) Hasle	8	5	8	1	1	1	3	4
<i>Thalassiosira</i> spp. Cleve	5	8	1	4	3	1	0	8
<i>Thalassiothrix antarctica</i> Schimper ex Karsten	0.5	0	0	0	0	0	0	0
<i>Trichotoxon reinboldii</i> (Van Heurck) Reid & Round	0	0	0	0	0	0	0	0.5
Unidentified centrics	1	3	1	0	1	0	0	1
Unidentified pennates	1	1	3	2	0	2	0	0
<b>Total:</b>	<b>409</b>	<b>400.5</b>	<b>408.5</b>	<b>402</b>	<b>407</b>	<b>406.5</b>	<b>408.5</b>	<b>401</b>

## **A.4.2 Mertz Ninnis Trough, East Antarctic Margin**

### **A.4.2.1 NBP0101 JPC10**

Quantitative diatom analysis samples were taken from the six types of laminae/sub-lamina identified during BSEI analysis. This data is used to support results and discussions in chapter 7. Five counts were made per lamina type and the average used in chapter 7.

Table A4.2.1.1 Mertz Ninnis Trough, NBP0101 JPC10, biogenic laminae quantitative counts, all species

Log number	200	38	177	173	175	98	243	243	116	27	60	184	163	18	168	110	19	97	122	151
Depth (mbsf)	18.770	20.230	18.894	18.903	18.898	19.720	17.880	17.900	19.580	20.390	20.157	18.875	19.215	20.470	19.200	20.540	20.466	19.740	19.521	19.310
Number of FOV	4	7	3.5	2	7.5	8	9	10	7	30	7	5	20	14.5	8	5	16	8	3	6
Mass (g)	0.006	0.0067	0.005	0.0053	0.0066	0.0069	0.006	0.0059	0.006	0.0066	0.0055	0.007	0.0061	0.0056	0.0058	0.0059	0.0056	0.0051	0.0068	0.0051
Species / Lamina type	Near-monogeneric <i>Chaetoceros</i> spp. resting spore biogenic laminae					Biogenic laminae characterised by <i>Corethron pennatum</i>					Biogenic laminae characterised by <i>Rhizosolenia</i> spp.					Mixed Diatom Assemblage biogenic laminae				
<i>Actinocyclus actinocylus</i> (Ehrenberg) Simonsen	1	0	0	0	0	2	0	0	0	0	0	0	0	0	1	0	0	0	0	0
<i>Actinocyclus curvatus</i> Janisch in Schmidt	0	0	0	0	0	0	0	0	0	0	0	0	0	1	0	0	0	0	0	0
<i>Asteromphalus</i> spp. Ehrenberg	0	0	0	0	0	0	0	0	0	2	1	0	1	0	0	0	0	1	0	0
<i>Hyalochaete Chaetoceros</i> spp. (vegetative) Gran	15	10	4	0	8	7	4	3	4	19	2	6	14	5	1	4	9	6	8	8
<i>Hyalochaete Chaetoceros</i> spp. (resting spore) Gran	435	402	364	438	318	329	332	326	375	301	442	407	256	251	416	432	289	358	450	342
<i>Phaeoceros Chaetoceros</i> spp. Gran	0	0	1	6	4	3	6	4	0	0	2	2	3	1	4	0	2	8	0	0
<i>Corethron pennatum</i> (Grunow) Ostenfeld	0	0	1	0	0	21	35	46	11	32	0	0	0	6	0	1	4	1	3	0
<i>Coscinodiscus</i> spp. Ehrenberg	0	0	0	0	0	0	0	0	0	0	0	0	0	0	0	0	0	0	0	0
<i>Eucampia antarctica</i> (Castracane) Mangin	0	2	0	0	1	1	0	0	1	0	0	0	6	1	0	0	0	2	1	1
<i>Fragilariopsis curta</i> (Van Heurck) Hustedt	7	7	8	4	20	15	19	14	10	29	2	8	24	29	4	16	29	20	3	33
<i>Fragilariopsis cylindrica</i> (Grunow) Krieger	4	0	5	0	1	7	27	24	10	2	4	11	34	33	0	4	45	3	1	14
<i>Fragilariopsis cylindrica</i> (Hasle) Hasle	0	0	1	0	0	0	0	0	0	0	1	0	10	0	0	1	0	0	0	0
<i>Fragilariopsis kerguelensis</i> (O'Meara) Hustedt	5	2	3	0	11	2	0	3	1	5	4	2	1	5	8	4	1	2	2	1
<i>Fragilariopsis obliquecostata</i> (Van Heurck) Heiden	0	2	1	1	0	0	0	0	0	0	0	1	0	1	0	0	1	0	0	0
<i>Fragilariopsis pseudonana</i> (Hasle) Hasle	0	0	0	0	0	0	0	1	2	0	0	0	0	3	0	0	5	0	0	0
<i>Fragilariopsis rhombica</i> (O'Meara) Hustedt	1	3	2	1	12	14	2	6	2	9	6	8	21	19	9	4	31	2	3	5
<i>Fragilariopsis ritscheri</i> (Hustedt) Hasle	0	0	0	0	0	2	0	0	0	2	1	0	1	0	2	1	0	3	0	0
<i>Fragilariopsis separanda</i> Hustedt	1	0	4	0	9	0	1	0	0	3	1	1	2	23	0	1	2	0	0	0
<i>Fragilariopsis sublinearis</i> (Van Heurck) Heiden	0	1	0	0	0	1	0	0	0	0	0	0	0	0	0	0	0	0	0	0
<i>Fragilariopsis vanheurckii</i> (M. Pergallo) Hustedt	0	0	1	0	0	0	0	0	0	0	0	0	0	0	1	0	0	0	0	0
<i>Fragilariopsis</i> spp. Hustedt	0	0	2	0	6	0	0	0	0	1	0	0	0	0	0	0	0	0	0	0
<i>Navicula</i> spp. Bory de St-Vincent	0	0	1	0	1	0	0	0	1	0	0	0	1	0	0	0	0	0	0	1
<i>Porosira glacialis</i> (Grunow) Jørgensen	1	2	1	1	0	0	0	0	1	1	0	1	2	1	0	1	1	0	3	1
<i>Proboscia inermis</i> (Castracane) Jordan & Ligowski	0	0	0	0	0	0	1	0	0	0	1	0	5	1	1	0	0	0	0	0
<i>Proboscia truncata</i> (Karsten) Nöthig & Ligowski	0	0	0	0	0	0	0	0	0	0	0	0	1	0	0	0	0	0	0	0
<i>Pseudonitzschia turgidula</i> (Hustedt) Hasle	0.5	0	1	0	1	3	0	3	2	0	0	4	4.5	3	0.5	0.5	3.5	0	0	1
<i>Rhizosolenia antennata</i> f. <i>semispina</i> Sundström	1	1	2	0	0	0	0	0	2	1	1	3	23	1	2	0	2	1	0	0
<i>Rhizosolenia polydaetyla</i> Castracane f. <i>polydaetyla</i>	0	0	0	0	0	0	0	0	0	0	0	1	1	0	0	0	0	0	0	0
<i>Rhizosolenia</i> species A Armand	0	0	0	0	1	1	0	0	0	0	1	0	8	1	2	0	0	0	0	0
<i>Rhizosolenia</i> spp. Brightwell	0	0	0	0	0	0	0	0	0	0	0	0	0	0	0	0	1	0	0	0
<i>Thalassiosira antarctica</i> (resting spore) Comber	0	0	0	0	2	0	0	0	0	0	0	0	0	0	0	0	0	0	0	0
<i>Thalassiosira gracilis</i> v. <i>expecta</i> (Van Landingham) Fryxell & Hasle	0	1	0	0	0	0	0	0	0	1	0	1	0	1	0	2	0	0	0	1
<i>Thalassiosira gracilis</i> v. <i>gracilis</i> (Karsten) Hustedt	0	3	0	0	1	0	1	0	1	3	0	1	0	3	1	0	1	2	0	3
<i>Thalassiosira gravida</i> Cleve	0	0	0	0	1	0	0	0	0	0	2	0	0	0	1	0	0	0	0	0
<i>Thalassiosira lentiginosa</i> (Janisch) Fryxell	0	0	1	0	1	0	0	1	2	0	1	6	0	0	1	0	1	0	2	3
<i>Thalassiosira lineata</i> Jousé	0	0	0	0	0	0	0	0	0	0	0	1	0	0	0	0	0	0	0	0
<i>Thalassiosira oestrupii</i> (Ostenfeld) Hasle	0	0	0	0	0	0	0	0	0	0	0	0	1	0	0	0	0	0	0	0
<i>Thalassiosira poroseriata</i> (Ramsfjell) Hasle	0	5	0	0	0	0	0	0	1	0	0	0	0	0	0	0	1	0	0	0
<i>Thalassiosira ritscheri</i> (Hustedt) Hasle	0	1	0	0	0	0	0	0	0	1	0	0	2	0	0	0	0	0	0	0
<i>Thalassiosira tumida</i> (Janisch) Hasle	0	0	0	0	0	0	0	0	0	1	0	0	2	0	1	0	1	0	0	2
<i>Thalassiosira</i> spp. Cleve	0	0	0	0	0	0	0	0	0	0	0	1	0	0	0	0	0	0	0	0
<i>Thalassiothrix antarctica</i> Schimper ex Karsten	0	0	0	0	0.5	0	0.5	0.5	0	1	0	0	0	0	0	0.5	0	0	0.5	0
<i>Trichotoxon reinboldii</i> (Van Heurck) Reid & Round	0	0	0	0	2.5	0	0	0	0.5	1	0	0	0.5	0	0.5	0	0	0	0	0
Unidentified centrics	0	0	0	0	0	0	0	0	0	1	0	0	0	0	0	0	0	0	0	0
Unidentified pennates	0	0	0	0	0	0	0	0	0	0	0	1	0	0	0	0	0	0	0	0
<b>Total:</b>	<b>471.5</b>	<b>442</b>	<b>402</b>	<b>446</b>	<b>400</b>	<b>409</b>	<b>428.5</b>	<b>430.5</b>	<b>425.5</b>	<b>417</b>	<b>468</b>	<b>459</b>	<b>423</b>	<b>400</b>	<b>454</b>	<b>471</b>	<b>424.5</b>	<b>417</b>	<b>474.5</b>	<b>419</b>



Table A4.2.1.3 Mertz Ninnis Trough, NBP0101 JPC10, terrigenous lamina and sub-lamina quantitative counts all species

	62	135	181	179	174	6	119	99	119	121
Log number	62	135	181	179	174	6	119	99	119	121
Depth (mbsf)	19.960	19.360	18.887	18.889	18.900	20.586	19.536	19.716	19.536	19.528
Number of FOV	12	6	5	5	4	6	2	7	3	2.5
Mass (g)	0.0081	0.0095	0.0093	0.0093	0.008	0.0085	0.0067	0.0097	0.007	0.0083
Species / Lamina type	Mixed Diatom Assemblage terrigenous laminae					Terrigenous sub-laminae characterised by <i>Porosira glacialis</i> resting spores				
<i>Actinocyclus actinochilus</i> (Ehrenberg) Simonsen	0	1	0	0	1	0	0	0	0	0
<i>Actinocyclus curvatus</i> Janisch in Schmidt	0	0	0	0	0	0	0	0	0	0
<i>Asteromphalus</i> spp. Ehrenberg	0	0	1	0	0	0	1	0	0	0
<i>Hyalochaete Chaetoceros</i> spp. (vegetative) Gran	21	11	6	1	0	1	5	8	3	0
<i>Hyalochaete Chaetoceros</i> spp. (resting spore) Gran	353	367	403	315	388	399	414	373	407	389
<i>Phaeoceros Chaetoceros</i> spp. Gran	1	0	0	1	0	0	0	1	0	0
<i>Corethron pennatum</i> (Grunow) Ostenfeld	0	3	1	0	0	0	0	2	1	0
<i>Coscinodiscus</i> spp. Ehrenberg	0	0	0	0	0	0	0	0	1	0
<i>Eucampia antarctica</i> (Castracane) Mangin	0	2	0	0	1	1	0	0	1	0
<i>Fragilariopsis curta</i> (Van Heurck) Hustedt	13	13	10	33	21	9	0	15	1	2
<i>Fragilariopsis cylindrus</i> (Grunow) Krieger	11	5	5	4	3	2	1	11	0	0
<i>Fragilariopsis cylindriformis</i> (Hasle) Hasle	0	0	0	1	0	0	0	0	0	0
<i>Fragilariopsis kerguelensis</i> (O'Meara) Hustedt	6	5	4	9	6	7	1	1	1	2
<i>Fragilariopsis obliquecostata</i> (Van Heurck) Heiden	0	1	0	0	0	0	0	1	1	0
<i>Fragilariopsis pseudonana</i> (Hasle) Hasle	0	0	0	0	0	0	0	0	0	0
<i>Fragilariopsis rhombica</i> (O'Meara) Hustedt	9	3	14	13	11	7	1	10	2	1
<i>Fragilariopsis riischeri</i> (Hustedt) Hasle	0	3	0	0	0	0	0	1	0	0
<i>Fragilariopsis separanda</i> Hustedt	0	0	1	4	1	3	1	1	1	3
<i>Fragilariopsis sublinearis</i> (Van Heurck) Heiden	0	0	0	0	0	1	0	0	0	0
<i>Fragilariopsis vanheurckii</i> (M. Pergallo) Hustedt	0	2	1	0	0	0	0	0	0	0
<i>Fragilariopsis</i> spp. Hustedt	0	0	2	3	2	0	2	2	1	0
<i>Navicula</i> spp. Bory de St-Vincent	0	0	1	1	0	0	0	0	0	0
<i>Porosira glacialis</i> (Grunow) Jørgensen	2	1	2	2	1	1	0	1	1	1
<i>Proboscia inermis</i> (Castracane) Jordan & Ligowski	0	0	1	0	0	0	0	0	0	0
<i>Proboscia truncata</i> (Karsten) Nöthig & Ligowski	0	0	0	0	0	0	0	0	0	0
<i>Pseudonitzschia turgidula</i> (Hustedt) Hasle	2	1	1	1	0	1	0	4	0	0
<i>Rhizosolenia antennata</i> f. <i>semispina</i> Sundström	1	0	0	0	0	0	0	0	0	0
<i>Rhizosolenia polydactyla</i> Castracane f. <i>polydactyla</i>	0	0	0	0	0	0	0	0	0	0
<i>Rhizosolenia</i> species A Armand	0	0	0	1	0	0	0	0	0	0
<i>Rhizosolenia</i> spp. Brightwell	0	0	0	0	0	0	0	0	0	0
<i>Thalassiosira antarctica</i> (resting spore) Comber	0	0	0	0	0	0	0	0	0	0
<i>Thalassiosira gracilis</i> v. <i>expecta</i> (Van Ledingham) Fryxell & Hasle	0	2	0	0	0	0	0	0	0	0
<i>Thalassiosira gracilis</i> v. <i>gracilis</i> (Karsten) Hustedt	1	1	1	1	0	0	0	1	0	0
<i>Thalassiosira gravida</i> Cleve	0	2	0	0	0	0	0	0	0	0
<i>Thalassiosira lentiginosa</i> (Janisch) Fryxell	0	0	2	5	0	0	0	2	1	2
<i>Thalassiosira lineata</i> Jousé	0	0	0	0	0	0	0	0	0	0
<i>Thalassiosira oestrupii</i> (Ostenfeld) Hasle	0	0	0	0	0	0	0	0	0	0
<i>Thalassiosira poroseriata</i> (Ramsfjell) Hasle	0	0	0	0	0	0	0	0	0	0
<i>Thalassiosira riischeri</i> (Hustedt) Hasle	0	0	0	0	0	0	0	0	0	0
<i>Thalassiosira tumida</i> (Janisch) Hasle	1	2	1	5	0	0	0	0	0	0
<i>Thalassiosira</i> spp. Cleve	1	0	0	0	0	0	0	0	0	0
<i>Thalassiothrix antarctica</i> Schimper ex Karsten	0	0.5	0	0	0	0	0	0	0	0
<i>Trichotoxon reinboldii</i> (Van Heurck) Reid & Round	0	0	0	0	0	0	0	0	0	0
Unidentified centrics	0	0	0	0	0	0	0	0	0	0
Unidentified pennates	0	0	1	0	0	0	0	0	0	0
<b>Total:</b>	<b>422</b>	<b>425.5</b>	<b>458</b>	<b>400</b>	<b>435</b>	<b>432</b>	<b>426</b>	<b>434</b>	<b>422</b>	<b>400</b>

	62	135	181	179	174	6	119	99	119	121
Log number	19.960	19.360	18.887	18.889	18.900	20.586	19.536	19.716	19.536	19.528
Depth (mbsf)	79	56	49	37	45	78	106	57	104	71
Number of FOV	0.0081	0.0095	0.0093	0.0093	0.008	0.0085	0.0067	0.0097	0.007	0.0083
Mass (g)										
Species / Sample number	Mixed Diatom Assemblage terrigenous laminae					Terrigenous sub-laminae characterised by <i>Porosira glacialis</i> resting spores				
<i>Actinocyclus actinocilius</i> (Ehrenberg) Simonsen	0	4	0	3	0	1	1	4	5	2
<i>Actinocyclus curvatulus</i> Janisch in Schmidt	0	0	1	1	0	0	0	0	0	0
<i>Asteromphalus</i> spp. Ehrenberg	7	0	3	0	3	2	1	2	3	3
<i>Azpeitia tabularis</i> (Grunow) Fryxell & Sims	0	0	0	0	0	0	0	0	0	3
<i>Cocconeis</i> spp. Ehrenberg	0	0	0	0	0	0	0	0	0	1
<i>Corethron pennatum</i> (Grunow) Ostenfeld	3	23	4	1	1	6	34	25	7	9
<i>Coscinodiscus</i> spp. Ehrenberg	0	0	0	0	0	0	0	0	0	0
<i>Cyclotella</i> spp. (Kützing) Brébisson	0	0	0	0	0	0	0	0	0	3
<i>Eucampia antarctica</i> (Castracane) Mangin	2	19	9	1	2	5	20	9	9	9
<i>Fragilariopsis curta</i> (Van Heurck) Hustedt	98	95	179	132	184	106	67	130	83	81
<i>Fragilariopsis cylindrus</i> (Grunow) Krieger	52	26	4	15	12	15	3	22	4	23
<i>Fragilariopsis cylindriciformis</i> (Hasle) Hasle	0	1	1	0	0	0	0	0	0	0
<i>Fragilariopsis kerguelensis</i> (O'Meara) Hustedt	38	54	73	61	43	50	36	43	46	29
<i>Fragilariopsis obliquocostata</i> (Van Heurck) Heiden	5	7	5	1	1	4	1	5	4	25
<i>Fragilariopsis pseudonana</i> (Hasle) Hasle	4	0	1	2	0	1	0	0	1	0
<i>Fragilariopsis rhombica</i> (O'Meara) Hustedt	79	58	67	85	95	96	91	68	62	14
<i>Fragilariopsis ritscheri</i> (Hustedt) Hasle	5	22	12	6	7	17	10	10	6	11
<i>Fragilariopsis separanda</i> Hustedt	25	13	34	22	8	19	16	11	48	69
<i>Fragilariopsis sublinearis</i> (Van Heurck) Heiden	0	1	0	0	0	16	6	1	0	0
<i>Fragilariopsis vanheurckii</i> (M. Perçallo) Hustedt	4	7	0	3	1	0	3	1	0	2
<i>Fragilariopsis</i> spp. Hustedt	10	4	13	4	14	0	7	4	3	7
<i>Navicula</i> spp. Bory de St-Vincent	3	1	1	3	3	2	2	4	0	2
<i>Odontella weissflogii</i> (Janisch) Grunow	0	0	0	0	0	0	0	0	0	0
<i>Porosira glacialis</i> (Grunow) Jørgensen	13	11	10	8	6	25	50	38	56	66
<i>Porosira pseudodenticula</i> (Hustedt) Jousé	0	0	0	0	0	0	0	0	0	1
<i>Proboscia inermis</i> (Castracane) Jordan & Ligowski	1	1	2	0	0	2	0	0	1	2
<i>Proboscia truncata</i> (Karsten) Nöthig & Ligowski	0	0	1	0	1	0	0	0	0	0
<i>Pseudonitzschia turgidula</i> (Hustedt) Hasle	13	4	2.5	2	5	10	5	7.5	3	2.5
<i>Rhizosolenia antennata</i> f. <i>antennata</i> (Ehrenberg) Brown	0	0	0	0	0	1	2	1	0	0
<i>Rhizosolenia antennata</i> f. <i>sempina</i> Sundström	6	1	4	5	0	4	7	4	1	0
<i>Rhizosolenia polydactyla</i> Castracane f. <i>polydactyla</i>	1	1	0	0	0	0	0	0	0	0
<i>Rhizosolenia</i> species A Armand	1	0	1	9	1	0	1	0	3	4
<i>Rhizosolenia</i> spp. Brightwell	1	0	0	0	0	0	0	0	0	0
<i>Stellarima microtrias</i> (resting spore) (Ehrenberg) Hasle &	0	1	0	0	0	0	0	0	3	0
<i>Thalassiosira antarctica</i> (resting spore) Comber	0	2	2	3	0	0	0	0	0	0
<i>Thalassiosira antarctica</i> (vegetative) Comber	0	2	0	0	0	0	0	0	0	0
<i>Thalassiosira gracilis</i> v. <i>expecta</i> (Van Landingham) Fryxell	4	3	3	1	1	10	5	2	6	2
<i>Thalassiosira gracilis</i> v. <i>gracilis</i> (Karsten) Hustedt	8	12	12	3	3	10	1	6	5	4
<i>Thalassiosira gravida</i> Cleve	2	1	0	2	0	3	1	1	1	1
<i>Thalassiosira lentiginosa</i> (Janisch) Fryxell	15	17	13	11	5	10	13	6	12	8
<i>Thalassiosira lineata</i> Jousé	1	0	0	2	1	0	0	0	2	0
<i>Thalassiosira oestrupii</i> (Ostenfeld) Hasle	0	0	0	0	1	0	0	0	0	0
<i>Thalassiosira oliverana</i> (O'Meara) Makarova & Nikolaev	0	0	0	0	0	0	0	0	0	0
<i>Thalassiosira poroseriata</i> (Ramsfjell) Hasle	3	8	3	2	4	0	6	2	4	1
<i>Thalassiosira ritscheri</i> (Hustedt) Hasle	2	1	0	0	0	1	9	3	2	1
<i>Thalassiosira tumida</i> (Janisch) Hasle	3	6	3	8	1	11	8	4	15	9
<i>Thalassiosira scottia</i> Fryxell & Hoban	0	0	0	0	0	0	0	0	1	0
<i>Thalassiosira</i> spp. Cleve	3	3	3	2	0	1	4	0	6	2
<i>Thalassiothrix/nema/toxon</i>	0	0	0	0	0	0	0	0	0	0
<i>Thalassiothrix antarctica</i> Schimper ex Karsten	0	1.5	0.5	0.5	0	0.5	0	0	0	0
<i>Trichotoxon reinboldii</i> (Van Heurck) Reid & Round	0.5	0	1.5	0.5	0.5	0.5	0	0.5	0	0
<i>Trachyneis aspera</i> (Ehrenberg) Cleve	0	0	0.5	0	0	0	0	0	0	0.5
Unidentified centrics	0	0	0	1	0	0	0	0	0	3
Unidentified pennates	0	1	0	0	0	0	0	0	0	0
<b>TOTAL:</b>	<b>412.5</b>	<b>411.5</b>	<b>469</b>	<b>400</b>	<b>403.5</b>	<b>429</b>	<b>410</b>	<b>415</b>	<b>402</b>	<b>400</b>

Table A4.2.1.4 Mertz Ninnis Trough, NBP0101 JPC10, terrigenous lamina and sub-lamina quantitative counts, *Chaetoceros* spp. free.

## A.4.2.2 NBP0101 KC10A

Quantitative diatom analysis samples from the two lamina types identified during BSEI analysis that are restricted in occurrence to KC10A. These data are used to support results and discussions in chapter 7.

**Table A4.2.2.1** Mertz Ninnis Trough, NBP0101 KC10A, quantitative diatom abundance counts, all species.

	Log number	35	26
	Depth (mbsf)	2.050	2.140
	Number of FOV	18	5
	Mass (g)	0.0056	0.0091
Species / Lamina type	Biogenic laminae characterised by <i>Fragilariopsis</i> spp.	Terrigenous laminae characterised by <i>Fragilariopsis</i> spp.	
<i>Hyalochaete Chaetoceros</i> spp. (vegetative) Gran	30	5	
<i>Hyalochaete Chaetoceros</i> spp. (resting spore) Gran	225	325	
<i>Phaeoceros Chaetoceros</i> spp. Gran	3	12	
<i>Cocconeis</i> spp. Ehrenberg	2	0	
<i>Eucampia antarctica</i> (resting spore) (Castracane) Mangin	1	0	
<i>Eucampia antarctica</i> (vegetative) (Castracane) Mangin	0	6	
<i>Fragilariopsis curta</i> (Van Heurck) Hustedt	30	16	
<i>Fragilariopsis cylindrus</i> (Grunow) Krieger	14	8	
<i>Fragilariopsis cylindriciformis</i> (Hasle) Hasle	2	0	
<i>Fragilariopsis kerguelensis</i> (O'Meara) Hustedt	24	8	
<i>Fragilariopsis obliquocostata</i> (Van Heurck) Heiden	1	0	
<i>Fragilariopsis rhombica</i> (O'Meara) Hustedt	49	17	
<i>Fragilariopsis ritscheri</i> (Hustedt) Hasle	2	8	
<i>Fragilariopsis separanda</i> Hustedt	7	0	
<i>Fragilariopsis vanheurckii</i> (M. Pergallo) Hustedt	1	2	
<i>Fragilariopsis</i> spp. Hustedt	2	4	
<i>Navicula</i> spp. Bory de St-Vincent	1	0	
<i>Proboscia inermis</i> (Castracane) Jordan & Ligowski	0	1	
<i>Pseudonitzschia turgidula</i> (Hustedt) Hasle	1.5	0	
<i>Stellarima microtrias</i> (Ehrenberg) Hasle & Sims	1	0	
<i>Thalassiosira gracilis</i> v. <i>gracilis</i> (Karsten) Hustedt	3	2	
<i>Thalassiosira gravida</i> Cleve	2	0	
<i>Thalassiosira lentiginosa</i> (Janisch) Fryxell	2	2	
<i>Thalassiosira poroseriata</i> (Ramsfjell) Hasle	2	2	
<i>Thalassiosira tumida</i> (Janisch) Hasle	0	1	
<b>TOTAL:</b>	<b>405.5</b>	<b>419</b>	

**Table A4.2.2.2** Mertz Ninnis Trough, NBP0101 KC10A, quantitative diatom abundance counts, *Chaetoceros* spp. free,.

	Log number	35	26
	Depth (mbsf)	2.050	2.140
	Number of FOV	47	32
	Mass (g)	0.0056	0.0091
Species / Lamina type	Biogenic laminae characterised by <i>Fragilariopsis</i> spp.		Terrigenous laminae characterised by <i>Fragilariopsis</i> spp.
<i>Asteromphalus</i> spp. (Ehrenberg)	0		2
<i>Cocconeis</i> spp. Ehrenberg	2		0
<i>Corethron pennatum</i> (Grunow) Ostenfeld	1		12
<i>Eucampia antarctica</i> (Castracane) Mangin resting spore	1		1
<i>Eucampia antarctica</i> (Castracane) Mangin vegetative	0		15
<i>Fragilariopsis curta</i> (Van Heurck) Hustedt	107		101
<i>Fragilariopsis cylindrus</i> (Grunow) Krieger	20		23
<i>Fragilariopsis cylindriciformis</i> (Hasle) Hasle	2		0
<i>Fragilariopsis kerguelensis</i> (O'Meara) Hustedt	72		35
<i>Fragilariopsis obliquecostata</i> (Van Heurck) Heiden	2		0
<i>Fragilariopsis pseudonana</i> (Hasle) Hasle	1		0
<i>Fragilariopsis rhombica</i> (O'Meara) Hustedt	126		112
<i>Fragilariopsis ritscheri</i> (Hustedt) Hasle	14		43
<i>Fragilariopsis separanda</i> Hustedt	10		4
<i>Fragilariopsis vanheurckii</i> (M. Pergallo) Hustedt	3		8
<i>Fragilariopsis</i> spp. Hustedt	8		18
<i>Navicula</i> spp. Bory de St-Vincent	1		1
<i>Porosira glacialis</i> (Grunow) Jørgensen	3		3
<i>Proboscia inermis</i> (Castracane) Jordan & Ligowski	0		3
<i>Pseudonitzschia turgidula</i> (Hustedt) Hasle	3.5		1.5
<i>Rhizosolenia antennata</i> f. <i>semispina</i> Sundström	0		1
<i>Rhizosolenia polydactyla</i> Castracane f. <i>polydactyla</i>	0		2
<i>Rhizosolenia</i> species A Armand	0		1
<i>Stellarima microtrias</i> (Ehrenberg) Hasle & Sims	2		4
<i>Thalassiosira gracilis</i> v. <i>expecta</i> (Van Landingham) Fryxell & Hasle	0		1
<i>Thalassiosira gracilis</i> v. <i>gracilis</i> (Karsten) Hustedt	17		7
<i>Thalassiosira gravida</i> Cleve	6		2
<i>Thalassiosira lentiginosa</i> (Janisch) Fryxell	4		7
<i>Thalassiosira poroseriata</i> (Ramsfjell) Hasle	5		5
<i>Thalassiosira tumida</i> (Janisch) Hasle	1		6
<i>Thalassiosira</i> spp. Cleve	1		3
<i>Thalassiothrix antarctica</i> Schimper ex Karsten	1		0
<b>TOTAL:</b>	<b>413.5</b>		<b>421.5</b>



### **A. 4.3 Durmont d'Urville Trough, East Antarctic Margin**

#### A.4.3.1 MD03 2597

Quantitative diatom analysis samples were taken from the nine types of laminae/sub-lamina identified during BSEI analysis. This data is used to support the results and discussions in chapter 8. At least three counts were made per lamina/sub-lamina type and the average used in chapter 8.

**Table A4.3.1.1** Durmont d'Urville Trough, MD03 2597, quantitative diatom abundance counts of all species, lamina types: laminae characterised by *Hyalochaete Chaetoceros* spp. resting spore; and laminae characterised by *Hyalochaete Chaetoceros* spp. resting spores and *Fragilariopsis* spp.; and *Fragilariopsis* spp..

Lamina log number	11	96	231	9	39	280	335	222	257	273
Depth (mbsf)	56.732	49.772	40.65	56.762	53.087	33.962	18.846	40.714	37.907	34.002
Number of FOV	39	19	9	28	13	20	16	21	13	13
Mass (g)	0.0062	0.0063	0.0071	0.0056	0.0084	0.007	0.0064	0.0064	0.0062	0.0068
Species / Lamina type	Laminae characterised by <i>Hyalochaete Chaetoceros</i> spp. resting spore s			Laminae characterised by <i>Hyalochaete Chaetoceros</i> spp. resting spores and <i>Fragilariopsis</i> spp.				Laminae characterised by <i>Fragilariopsis</i> spp.		
<i>Actinocyclus actinochilus</i> (Ehrenberg) Simonsen	1	0	1	0	1	0	0	1	0	3
<i>Asteromphalus</i> spp. Ehrenberg	0	1	0	0	1	0	0	2	0	1
<i>Hyalochaete Chaetoceros</i> spp. (vegetative) Gran	3	0	1	0	4	0	0	0	0	0
<i>Hyalochaete Chaetoceros</i> spp. (resting spore) Gran	153	193	291	188	263	102	170	157	77	46
<i>Phaeoceros Chaetoceros</i> spp. Gran	9	4	28	6	16	45	49	31	18	27
<i>Cocconeis</i> spp. Ehrenberg	0	0	0	0	0	1	0	0	1	1
<i>Corethron pennatum</i> (Grunow) Ostenfeld	1	0	1	1	1	3	4	0	0	4
<i>Eucampia antarctica</i> (resting spore) (Castracane) Mangin	2	0	0	0	2	3	0	1	1	2
<i>Eucampia antarctica</i> (vegetative) (Castracane) Mangin	4	0	2	0	3	0	0	11	1	2
<i>Fragilariopsis curta</i> (Van Heurck) Hustedt	99	82	35	99	57	111	61	69	90	130
<i>Fragilariopsis cylindrus</i> (Grunow) Krieger	12	24	19	22	21	15	46	32	145	82
<i>Fragilariopsis cylindriciformis</i> (Hasle) Hasle	0	0	0	0	0	0	0	0	1	0
<i>Fragilariopsis kerguelensis</i> (O'Meara) Hustedt	25	17	12	24	10	12	14	16	15	6
<i>Fragilariopsis obliquecostata</i> (Van Heurck) Heiden	1	0	0	1	1	2	1	2	1	4
<i>Fragilariopsis pseudonanna</i> (Hasle) Hasle	0	0	0	0	0	0	0	0	6	1
<i>Fragilariopsis rhombica</i> (O'Meara) Hustedt	29	30	23	34	10	33	17	48	16	54
<i>Fragilariopsis ritscheri</i> (Hustedt) Hasle	14	5	5	8	5	15	3	13	7	8
<i>Fragilariopsis separanda</i> Hustedt	0	0	0	0	1	0	0	0	0	0
<i>Fragilariopsis sublinearis</i> (Van Heurck) Heiden	5	21	2	6	8	13	2	3	1	1
<i>Fragilariopsis vanheurckii</i> (M. Pergallo) Hustedt	2	0	2	1	2	2	1	4	0	0
<i>Fragilariopsis</i> spp. Hustedt	3	6	2	3	1	21	18	8	3	12
<i>Navicula</i> spp. Bory de St-Vincent	5	1	1	2	2	4	0	0	1	1
<i>Porosira glacialis</i> (Grunow) Jørgensen	13	4	2	4	8	2	6	9	1	2
<i>Porosira pseudodenticula</i> (Hustedt) Jousé	3	0	0	0	0	0	0	0	0	0
<i>Proboscia inermis</i> (Castracane) Jordan & Ligowski	0	0	2	0	0	0	1	0	2	0
<i>Proboscia truncata</i> (Karsten) Nøthig & Ligowski	0	0	0	0	0	1	0	0	1	0
<i>Pseudonitzschia turgidula</i> (Hustedt) Hasle	0	1	1	2	1.5	0	4	0.5	2.5	2.5
<i>Rhizosolenia antennata</i> f. <i>semispina</i> Sundström	0	0	0	0	0	2	2	0	0	2
<i>Rhizosolenia</i> species A Armand	0	0	0	0	0	2	0	0	0	0
<i>Rhizosolenia</i> spp. Brightwell	0	0	0	0	1	0	0	0	0	0
<i>Stellarima microtrias</i> (resting spore) (Ehrenberg) Hasle & Sims	2	0	0	1	0	0	0	0	0	0
<i>Thalassiosira antarctica</i> (resting spore - warm) Comber	0	0	0	0	0	0	0	0	1	0
<i>Thalassiosira antarctica</i> (vegetative) Comber	1	0	0	0	0	0	0	0	0	0
<i>Thalassiosira gracilis</i> v. <i>expecta</i> (Van Landingham) Fryxell & Hasle	0	2	1	1	0	1	0	1	3	1
<i>Thalassiosira gracilis</i> v. <i>gracilis</i> (Karsten) Hustedt	2	2	1	6	3	2	2	1	5	3
<i>Thalassiosira gravida</i> Cleve	0	0	0	0	0	0	1	1	1	0
<i>Thalassiosira lentiginosa</i> (Janisch) Fryxell	5	6	0	3	3	3	1	1	2	0
<i>Thalassiosira poroseriata</i> (Ramsfjell) Hasle	9	2	0	4	1	3	0	1	2	3
<i>Thalassiosira ritscheri</i> (Hustedt) Hasle	0	0	0	0	0	1	0	2	0	0
<i>Thalassiosira tumida</i> (Janisch) Hasle	1	0	0	0	0	3	0	4	0	0
<i>Thalassiosira</i> spp. Cleve	2	1	2	4	1	3	0	1	2	1
<i>Thalassiothrix/nema/toxon</i>	1	0	0	0.5	0	0.5	0	0	0	0
<i>Thalassiothrix antarctica</i> Schimper ex Karsten	0	2	1	0.5	1	1	0.5	0.5	0	0
<i>Trichotoxon reinboldii</i> (Van Heurck) Reid & Round	0.5	0.5	0	1.5	0.5	0	0	0	0.5	1
Unidentified centrics	1	1	1	0	0	1	0	4	0	0
Unidentified pennates	0	0	0	0	1	0	0	1	0	0
<b>Total:</b>	<b>408.5</b>	<b>405.5</b>	<b>436</b>	<b>422.5</b>	<b>430</b>	<b>407.5</b>	<b>403.5</b>	<b>425</b>	<b>407</b>	<b>400.5</b>

**Table A4.3.1.1 continued** Durmont d'Urville Trough, MD03 2597, quantitative diatom abundance counts of all species, lamina types: laminae characterised by *Corethron pennatum* and *Rhizosolenia* spp.; laminae characterised by *C. pennatum*; and laminae characterised by *Rhizosolenia* spp..

Lamina log number	12	15	15	77	142	144	189	190	191	193	194
Depth (mbsf)	56.723	56.693	56.700	49.851	47.769	47.760	44.515	44.505	44.498	44.483	44.469
Number of FOV	12	32	31	19	30	29	21	21	17	18	20
Mass (g)	0.0068	0.0062	0.0064	0.006	0.0061	0.0076	0.0053	0.0062	0.0081	0.0067	0.0058
Species / Lamina type	Laminae characterised by <i>Corethron pennatum</i> and <i>Rhizosolenia</i> spp.			Laminae characterised by <i>Corethron pennatum</i>			Laminae characterised by <i>Rhizosolenia</i> spp.				
<i>Actinocyclus actinocylus</i> (Ehrenberg) Simonsen	0	0	2	1	0	0	0	0	0	0	0
<i>Asteromphalus</i> spp. Ehrenberg	0	0	1	2	1	2	2	2	1	2	1
<i>Hyalochaete Chaetoceros</i> spp. (vegetative) Gran	10	15	0	2	0	0	4	7	6	13	5
<i>Hyalochaete Chaetoceros</i> spp. (resting spore) Gran	238	133	124	190	73	106	36	77	113	107	104
<i>Phaeoceros Chaetoceros</i> spp. Gran	8	16	56	12	10	7	4	2	9	9	3
<i>Cocconeis</i> spp. Ehrenberg	0	0	0	0	0	0	0	1	0	0	1
<i>Corethron pennatum</i> (Grunow) Ostenfeld	0	6	3	1	7	3	0	1	0	2	0
<i>Eucampia antarctica</i> (resting spore) (Castracane) Mangin	1	1	1	0	0	2	0	1	1	0	0
<i>Eucampia antarctica</i> (vegetative) (Castracane) Mangin	19	8	1	0	5	0	1	1	1	3	4
<i>Fragilariopsis curta</i> (Van Heurck) Hustedt	19	60	60	42	102	92	33	79	93	57	59
<i>Fragilariopsis cylindrus</i> (Grunow) Krieger	27	38	36	51	130	65	173	90	67	119	108
<i>Fragilariopsis cylindriciformis</i> (Hasle) Hasle	1	0	0	0	1	0	1	0	0	0	0
<i>Fragilariopsis kerguelensis</i> (O'Meara) Hustedt	4	6	19	14	9	13	4	13	7	12	9
<i>Fragilariopsis obliquecostata</i> (Van Heurck) Heiden	3	2	1	0	4	2	0	1	2	0	0
<i>Fragilariopsis pseudonana</i> (Hasle) Hasle	0	0	0	1	1	3	1	1	2	3	5
<i>Fragilariopsis rhombica</i> (O'Meara) Hustedt	29	21	38	27	22	40	14	26	36	30	43
<i>Fragilariopsis riischeri</i> (Hustedt) Hasle	14	31	9	18	6	9	2	4	3	3	4
<i>Fragilariopsis separanda</i> Hustedt	5	1	1	0	0	0	1	2	1	0	0
<i>Fragilariopsis sublinearis</i> (Van Heurck) Heiden	2	12	6	2	9	9	5	5	5	1	5
<i>Fragilariopsis vanheurckii</i> (M. Pergallo) Hustedt	0	0	0	0	1	0	1	1	1	0	1
<i>Fragilariopsis</i> spp. Hustedt	3	8	2	5	4	10	2	4	10	5	3
<i>Gomphonema</i> spp. Ehrenberg	0	0	0	0	0	0	0	0	1	0	0
<i>Navicula</i> spp. Bory de St-Vincent	0	2	0	1	1	0	2	1	1	2	0
<i>Odontella litigiosa</i> (van Heurck) Hoban	0	0	0	0	0	1	0	0	0	0	0
<i>Odontella weissflogii</i> (Janisch) Grunow	1	0	0	0	0	0	0	1	0	0	0
<i>Porosira glacialis</i> (Grunow) Jørgensen	3	3	5	3	2	7	0	5	2	3	4
<i>Porosira pseudodenticula</i> (Hustedt) Jouse	0	1	1	0	1	0	0	0	0	0	0
<i>Proboscia inermis</i> (Castracane) Jordan & Ligowski	3	3	1	2	1	4	89	61	40	7	5
<i>Proboscia truncata</i> (Karsten) Nöthig & Ligowski	0	0	0	1	0	0	0	3	1	1	0
<i>Pseudonitzschia turgidula</i> (Hustedt) Hasle	0.5	7	8.5	9	2	4.5	6.5	4	6	13	12
<i>Rhizosolenia antennata</i> f. <i>antennata</i> (Ehrenberg) Brown	0	0	0	0	0	0	0	1	0	0	0
<i>Rhizosolenia antennata</i> f. <i>semispina</i> Sundström	1	18	10	4	2	3	9	3	13	7	11
<i>Rhizosolenia sima</i> Castracane f. <i>sima</i>	0	0	0	0	0	0	0	0	0	1	1
<i>Rhizosolenia simplex</i> Karsten	0	0	0	2	0	0	0	0	0	0	0
<i>Rhizosolenia species</i> A Armand	0	3	0	0	0	1	0	0	0	0	0
<i>Rhizosolenia</i> spp. Brightwell	0	7	2	1	0	3	0	0	0	1	0
<i>Stellarima microtrias</i> (resting spore) (Ehrenberg) Hasle & Sims	0	0	0	0	1	0	0	2	1	2	0
<i>Thalassiosira antarctica</i> (resting spore - cold) Comber	1	2	3	0	0	0	1	0	0	0	0
<i>Thalassiosira antarctica</i> (resting spore - warm) Comber	0	0	0	0	0	0	0	0	0	0	6
<i>Thalassiosira antarctica</i> (vegetative) Comber	2	2	1	0	0	0	0	0	0	0	0
<i>Thalassiosira gracilis</i> v. <i>expecta</i> (Van Landingham) Fryxell & Hasle	0	2	1	0	2	2	0	0	1	4	3
<i>Thalassiosira gracilis</i> v. <i>gracilis</i> (Karsten) Hustedt	3	2	1	4	5	4	3	3	4	5	1
<i>Thalassiosira gravida</i> Cleve	0	0	0	1	0	0	0	0	0	3	2
<i>Thalassiosira lentiginosa</i> (Janisch) Fryxell	2	4	5	13	4	6	2	1	1	1	1
<i>Thalassiosira poroseriata</i> (Ramsfjell) Hasle	0	0	1	0	2	0	0	1	0	0	0
<i>Thalassiosira riischeri</i> (Hustedt) Hasle	0	0	0	0	0	0	0	0	0	2	1
<i>Thalassiosira tumida</i> (Janisch) Hasle	1	0	1	1	1	1	0	0	0	0	0
<i>Thalassiosira</i> spp. Cleve	1	2	2	1	1	2	1	1	0	0	1
<i>Thalassiothrix antarctica</i> Schimper ex Karsten	0	0.5	1.5	0	0	0.5	0	0.5	0	0	0.5
<i>Trachyneis aspera</i> (Ehrenberg) Cleve	0	0	0	0	0.5	0	1	0	0	0	0
<i>Trichotoxon reinboldii</i> (Van Heurck) Reid & Round	0	0	0	0	0	2.5	0.5	0	0	1	0.5
Unidentified centrics	0	0	4	2	1	4	2	1	0	1	3
Unidentified pennates	0	0	0	0	0	0	1	0	0	0	0
<b>Total:</b>	<b>401.5</b>	<b>416.5</b>	<b>408</b>	<b>413</b>	<b>411.5</b>	<b>408.5</b>	<b>402</b>	<b>406.5</b>	<b>429</b>	<b>420</b>	<b>407</b>

**Table A4.3.1.1 continued** Durmont d'Urville Trough, MD03 2597, quantitative diatom abundance counts of all species, lamina types: mixed diatom assemblage biogenic laminae; and mixed diatom assemblage terrigenous laminae.

	Lamina log number	54	195	263	10	13	143	145	192	196	232	281	336
	Depth (mbsf)	52.658	44.458	37.826	56.744	56.7164	47.762	47.7581	44.493	44.451	40.632	33.9563	18.829
	Number of FOV	21	20	11	26	21	28	26	17	25	10	31	17
	Mass (g)	0.0088	0.0075	0.0074	0.0082	0.0094	0.0081	0.0094	0.0081	0.0078	0.0079	0.0088	0.0089
Species / Lamina type		Mixed diatom assemblage biogenic laminae						Mixed diatom assemblage terrigenous laminae					
<i>Actinocyclus actinocylus</i> (Ehrenberg) Simonsen		0	1	0	0	0	2	0	0	0	2	0	0
<i>Asteromphalus</i> spp. Ehrenberg		1	1	0	2	0	2	1	2	2	1	1	0
<i>Hyalochaete Chaetoceros</i> spp. (vegetative) Gran		3	3	2	3	18	0	0	6	2	25	2	3
<i>Hyalochaete Chaetoceros</i> spp. (resting spore) Gran		219	95	219	153	228	115	111	116	133	281	93	159
<i>Phaeoceros Chaetoceros</i> spp. Gran		5	5	16	1	1	15	4	6	4	15	15	30
<i>Cocconeis</i> spp. Ehrenberg		0	1	0	0	0	0	1	2	0	0	0	1
<i>Corethron pennatum</i> (Grunow) Ostenfeld		0	1	3	1	2	4	0	0	0	2	1	9
<i>Eucampia antarctica</i> (resting spore) (Castracane) Mangin		0	4	0	1	0	1	4	1	1	0	1	2
<i>Eucampia antarctica</i> (vegetative) (Castracane) Mangin		0	0	5	2	0	0	1	2	1	7	2	2
<i>Fragilariopsis curta</i> (Van Heurck) Hustedt		105	69	93	107	31	102	106	59	74	23	127	80
<i>Fragilariopsis cylindrus</i> (Grunow) Krieger		15	99	15	17	25	57	27	120	63	41	25	34
<i>Fragilariopsis kerguelensis</i> (O'Meara) Hustedt		18	19	4	20	16	14	22	14	19	9	30	17
<i>Fragilariopsis obliquecostata</i> (Van Heurck) Heiden		0	0	1	4	4	2	2	2	0	0	1	2
<i>Fragilariopsis pseudonana</i> (Hasle) Hasle		0	0	0	0	0	0	1	3	2	0	0	1
<i>Fragilariopsis rhombica</i> (O'Meara) Hustedt		24	42	11	37	34	40	45	23	37	9	37	23
<i>Fragilariopsis ritscheri</i> (Hustedt) Hasle		5	8	2	20	8	6	9	4	10	3	16	5
<i>Fragilariopsis separanda</i> Hustedt		2	0	0	0	0	0	0	2	0	0	0	0
<i>Fragilariopsis sublinearis</i> (Van Heurck) Heiden		3	5	6	1	1	3	11	9	5	5	6	4
<i>Fragilariopsis vanheurckii</i> (M. Pergallo) Hustedt		0	1	2	3	1	5	3	0	1	1	3	3
<i>Fragilariopsis</i> spp. Hustedt		5	14	9	2	7	7	11	2	14	2	14	16
<i>Navicula</i> spp. Bory de St-Vincent		1	1	2	1	0	2	1	0	1	0	2	1
<i>Odontella litigiosa</i> (van Heurck) Hoban		0	0	0	0	0	0	0	0	1	0	0	0
<i>Odontella weissflogii</i> (Janisch) Grunow		0	0	0	0	0	1	0	0	0	0	0	0
<i>Porosira glacialis</i> (Grunow) Jørgensen		2	5	0	14	12	5	6	7	11	15	6	14
<i>Proboscia inermis</i> (Castracane) Jordan & Ligowski		0	3	0	0	0	4	2	6	1	2	0	1
<i>Proboscia truncata</i> (Karsten) Nöthig & Ligowski		0	1	0	0	0	0	0	0	0	0	0	2
<i>Pseudonitzschia turgidula</i> (Hustedt) Hasle		2	7	0.5	0	1	2.5	0.5	4.5	3.5	2	0.5	2.5
<i>Rhizosolenia antennata</i> f. <i>semispina</i> Sundström		0	5	1	0	3	4	3	6	2	0	3	0
<i>Rhizosolenia</i> spp. Brightwell		0	0	1	0	0	1	5	0	2	0	0	0
<i>Stellarima microtrias</i> (resting spore) (Ehrenberg) Hasle & Sims		0	5	0	0	0	0	0	1	0	1	0	0
<i>Thalassiosira antarctica</i> (resting spore - cold) Comber		1	0	0	0	0	0	2	0	0	0	0	0
<i>Thalassiosira antarctica</i> (vegetative) Comber		0	1	0	0	1	1	0	0	0	1	0	0
<i>Thalassiosira gracilis</i> v. <i>expecta</i> (Van Landingham) Fryxell & Hasle		1	1	1	2	0	0	3	1	0	0	0	0
<i>Thalassiosira gracilis</i> v. <i>gracilis</i> (Karsten) Hustedt		2	4	2	13	2	5	7	2	0	4	4	2
<i>Thalassiosira gravida</i> Cleve		0	3	0	0	0	0	0	6	2	3	1	0
<i>Thalassiosira lentiginosa</i> (Janisch) Fryxell		4	3	1	0	2	6	4	5	6	2	5	0
<i>Thalassiosira oliveriana</i> (O'Meara) Makarova & Nikolaev		0	0	0	0	0	0	1	0	0	0	0	0
<i>Thalassiosira poroseriata</i> (Ramsfjell) Hasle		0	2	2	13	8	0	2	3	3	0	9	1
<i>Thalassiosira ritscheri</i> (Hustedt) Hasle		0	0	0	1	0	0	0	1	0	0	1	2
<i>Thalassiosira tumida</i> (Janisch) Hasle		1	1	0	0	1	0	4	0	0	2	1	3
<i>Thalassiosira</i> spp. Cleve		4	1	1	1	0	0	6	0	1	0	0	1
<i>Thalassiothrix/nema/toxon</i>		0.5	0	0	0	0	0	0	0	0	0	0	0
<i>Thalassiothrix antarctica</i> Schimper ex Karsten		0.5	1.5	0	0	0	1.5	1	0	1.5	0	1	1
<i>Trachyneis aspera</i> (Ehrenberg) Cleve		0	0	0	0	1	0.5	0.5	0.5	0.5	0	0	0
<i>Trichoaxton reinholdii</i> (Van Heurck) Reid & Round		0.5	0.5	0.5	0	0	0	1	1.5	1.5	0	0	1
Unidentified centrics		0	1	0	0	0	1	0	0	1	0	0	0
Unidentified pennates		0	1	1	0	0	2	0	0	0	0	0	0
<b>Total:</b>		<b>424.5</b>	<b>415</b>	<b>401</b>	<b>419</b>	<b>407</b>	<b>411.5</b>	<b>408</b>	<b>417.5</b>	<b>406</b>	<b>458</b>	<b>407.5</b>	<b>422.5</b>

**Table A4.3.1.1 continued** Durmont d'Urville Trough, MD03 2597, quantitative diatom abundance counts of all species, lamina types: sub-laminae characterised by *Porosira glacialis* resting spores; and laminae characterised by *Stellarima microtrias* resting spores, *P. glacialis* resting spores and / or *Coscinodiscus bouvet*.

	Lamina log number	14	224	282	35	205	206	207	233
	Depth (mbsf)	56.709	40.702	33.953	53.106	41.169	41.165	41.161	40.625
	Number of FOV	13	7	26	11	21	18	25	15
	Mass (g)	0.0076	0.0065	0.0064	0.0098	0.0073	0.0079	0.0081	0.0073
Species / Lamina type		Sub-laminae characterised by <i>Porosira glacialis</i> resting spores			Laminae characterised by <i>Stellarima microtrias</i> resting spores, <i>Porosira glacialis</i> resting spore and / or <i>Coscinodiscus bouvet</i>				
<i>Actinocyclus actinocilius</i> (Ehrenberg) Simonsen		0	0	1	1	0	0	4	1
<i>Asteromphalus</i> spp. Ehrenberg		0	2	1	0	2	0	1	3
<i>Hyalochaete Chaetoceros</i> spp. (vegetative) Gran		12	0	0	3	0	4	2	2
<i>Hyalochaete Chaetoceros</i> spp. (resting spore) Gran		297	353	93	203	97	176	165	186
<i>Phaeoceros Chaetoceros</i> spp. Gran		0	4	14	11	11	7	2	40
<i>Cocconeis</i> spp. Ehrenberg		0	0	1	0	1	0	0	0
<i>Corethron pennatum</i> (Grunow) Ostenfeld		2	0	0	3	2	0	2	8
<i>Eucampia antarctica</i> (resting spore) (Castracane) Mangin		1	0	4	0	0	0	0	0
<i>Eucampia antarctica</i> (vegetative) (Castracane) Mangin		1	2	1	2	5	2	1	5
<i>Fragilariopsis curta</i> (Van Heurck) Hustedt		19	11	89	72	59	61	56	31
<i>Fragilariopsis cylindrus</i> (Grunow) Krieger		3	1	11	25	94	51	30	48
<i>Fragilariopsis cylindriformis</i> (Hasle) Hasle		7	0	14	11	10	13	21	21
<i>Fragilariopsis kerguelensis</i> (O'Meara) Hustedt		0	3	3	3	2	1	1	1
<i>Fragilariopsis obliquecostata</i> (Van Heurck) Heiden		0	0	1	0	3	0	1	0
<i>Fragilariopsis pseudonanna</i> (Hasle) Hasle		0	1	0	0	0	0	0	0
<i>Fragilariopsis rhombica</i> (O'Meara) Hustedt		11	8	24	20	19	18	27	13
<i>Fragilariopsis ritscheri</i> (Hustedt) Hasle		10	2	7	4	8	11	13	7
<i>Fragilariopsis separanda</i> Hustedt		1	0	2	5	0	2	0	0
<i>Fragilariopsis sublinearis</i> (Van Heurck) Heiden		4	0	6	6	11	6	4	1
<i>Fragilariopsis vanheurckii</i> (M. Pergallo) Hustedt		0	3	1	0	5	1	2	1
<i>Fragilariopsis</i> spp. Hustedt		3	1	6	5	6	4	3	3
<i>Navicula</i> spp. Bory de St-Vincent		0	0	0	1	3	0	0	0
<i>Porosira glacialis</i> (Grunow) Jørgensen		15	9	64	17	11	9	10	13
<i>Proboscia inermis</i> (Castracane) Jordan & Ligowski		0	1	0	0	5	4	3	6
<i>Proboscia truncata</i> (Karsten) Nøthig & Ligowski		0	0	0	0	0	0	1	0
<i>Pseudonitzschia turgidula</i> (Hustedt) Hasle		0.5	2	0	2	3	3	0.5	2
<i>Rhizosolenia antennata</i> f. <i>semispina</i> Sundström		1	0	1	1	2	0	1	2
<i>Rhizosolenia</i> species A Armand		0	0	0	1	0	0	0	0
<i>Rhizosolenia</i> spp. Brightwell		4	0	0	1	0	0	1	0
<i>Stellarima microtrias</i> (resting spore) (Ehrenberg) Hasle & Sims		3	0	0	2	6	8	6	1
<i>Thalassiosira antarctica</i> (resting spore - cold) Comber		4	0	0	0	1	0	0	0
<i>Thalassiosira antarctica</i> (vegetative) Comber		2	0	5	1	5	0	1	0
<i>Thalassiosira gracilis</i> v. <i>expecta</i> (Van Landingham) Fryxell & Hasle		1	1	0	0	5	4	0	1
<i>Thalassiosira gracilis</i> v. <i>gracilis</i> (Karsten) Hustedt		1	2	7	2	0	1	4	3
<i>Thalassiosira gravida</i> Cleve		0	2	0	0	0	3	1	0
<i>Thalassiosira lentiginosa</i> (Janisch) Fryxell		2	1	5	5	3	0	5	2
<i>Thalassiosira perpusilla</i> Kozlova		0	0	1	0	0	0	0	0
<i>Thalassiosira poroveriata</i> (Ramsfjell) Hasle		0	5	41	0	20	22	35	2
<i>Thalassiosira ritscheri</i> (Hustedt) Hasle		0	3	3	0	3	2	1	0
<i>Thalassiosira tumida</i> (Janisch) Hasle		2	0	2	1	3	2	0	1
<i>Thalassiosira</i> spp. Cleve		4	0	6	7	2	4	3	1
<i>Thalassiothrix antarctica</i> Schimper ex Karsten		0.5	0	0	0	0.5	0	1	0.5
<i>Trachyneis aspera</i> (Ehrenberg) Cleve		1	0	0	0	0	0	0	0
<i>Trichotoxon reinboldii</i> (Van Heurck) Reid & Round		0	0	0	0.5	0	0	0	0.5
Unidentified centrics		1	1	0	1	1	0	1	0
<b>Total:</b>		<b>413</b>	<b>418</b>	<b>414</b>	<b>416.5</b>	<b>408.5</b>	<b>419</b>	<b>409.5</b>	<b>406</b>

**Table A4.3.1.2** Durmont d'Urville Trough, MD03 2597, quantitative diatom abundance *Hyalochaete Chaetoceros* spp. free counts, lamina types: laminae characterised by *Hyalochaete Chaetoceros* spp. resting spore; laminae characterised by *Hyalochaete Chaetoceros* spp. resting spores and *Fragilariopsis* spp.; and laminae characterised by *Fragilariopsis* spp..

Lamina log number	11	231	96	9	39	280	335	222	257	273
Depth (mbsf)	56.732	40.65	49.772	56.762	53.087	33.962	18.846	40.71	37.907	34.002
Number of FOV	58	26	33	48	29	30	27	34	17	15
Mass (g)	0.0062	0.0071	0.0063	0.0056	0.0084	0.007	0.0064	0.006	0.0062	0.0068
Species / Lamina type	Laminae characterised by <i>Hyalochaete Chaetoceros</i> spp. resting spore			Laminae characterised by <i>Hyalochaete Chaetoceros</i> spp. resting spores and <i>Fragilariopsis</i> spp.				Laminae characterised by <i>Fragilariopsis</i> spp.		
<i>Actinocyclus actinochilus</i> (Ehrenberg) Simonsen	1	1	1	1	1	1	0	1	0	3
<i>Asteromphalus</i> spp. Ehrenberg	0	1	2	1	1	0	0	3	2	1
<i>Phaeoceros Chaetoceros</i> spp. Gran	9	95	13	11	29	61	77	48	29	30
<i>Cocconeis</i> spp. Ehrenberg	1	0	0	0	0	1	0	1	1	1
<i>Corethron pennatum</i> (Grunow) Ostenfeld	3	1	0	1	3	4	10	2	0	5
<i>Eucampia antarctica</i> (resting spore) (Castracane) Mangin	3	1	0	0	2	4	1	1	1	2
<i>Eucampia antarctica</i> (vegetative) (Castracane) Mangin	6	5	0	0	7	0	0	14	3	2
<i>Fragilariopsis curta</i> (Van Heurck) Hustedt	159	104	170	171	145	152	101	101	118	147
<i>Fragilariopsis cylindrus</i> (Grunow) Krieger	15	42	39	33	57	18	94	47	190	95
<i>Fragilariopsis cylindriciformis</i> (Hasle, in Hasle & Booth) Hasle	0	0	0	0	0	0	0	0	1	0
<i>Fragilariopsis kerguelensis</i> (O'Meara) Hustedt	44	32	32	44	38	16	22	22	20	7
<i>Fragilariopsis obliquecostata</i> (Van Heurck) Heiden	3	2	0	3	5	3	3	2	1	5
<i>Fragilariopsis pseudonanna</i> (Hasle) Hasle	0	0	0	0	0	0	0	0	6	1
<i>Fragilariopsis rhombica</i> (O'Meara) Hustedt	53	44	47	53	26	48	28	72	21	64
<i>Fragilariopsis ritscheri</i> (Hustedt) Hasle	20	11	14	12	14	22	9	21	7	8
<i>Fragilariopsis separanda</i> Hustedt	0	1	0	0	3	0	0	0	0	0
<i>Fragilariopsis sublinearis</i> (Van Heurck) Heiden	6	6	38	7	17	9	5	7	1	3
<i>Fragilariopsis vanheurckii</i> (M. Pergallo) Hustedt	2	6	0	3	2	5	2	6	0	1
<i>Fragilariopsis</i> spp. Hustedt	8	20	15	6	9	28	28	11	5	12
<i>Navicula</i> spp. Bory de St-Vincent	5	1	2	2	5	4	1	0	1	1
<i>Odontella weissflogii</i> (Janisch) Grunow	0	0	0	1	0	0	0	0	0	0
<i>Parosira glacialis</i> (Grunow) Jørgensen	26	5	10	13	14	2	12	12	2	2
<i>Parosira pseudodenticula</i> (Hustedt) Jousé	4	0	0	0	0	0	0	0	0	0
<i>Proboscia inermis</i> (Castracane) Jordan & Ligowski	1	3	0	0	0	0	1	0	2	0
<i>Proboscia truncata</i> (Karsten) Nöthig & Ligowski	0	0	0	0	0	1	0	0	1	0
<i>Pseudonitzschia turgidula</i> (Hustedt) Hasle	0.5	3	1	3	3.5	1.5	6.5	1	3	2.5
<i>Rhizosolenia antennata</i> f. <i>semispina</i> Sundström	2	0	1	1	0	3	3	0	0	3
<i>Rhizosolenia</i> spp. Brightwell	1	0	1	0	2	2	0	0	0	0
<i>Stellarima microtrias</i> (resting spore) (Ehrenberg) Hasle & Sims	2	1	0	1	0	0	0	1	0	0
<i>Thalassiosira antarctica</i> (resting spore - cold) Comber	0	0	0	0	3	0	0	0	0	0
<i>Thalassiosira antarctica</i> (resting spore - warm) Comber	0	0	0	0	0	0	0	0	1	0
<i>Thalassiosira antarctica</i> (vegetative) Comber	1	0	0	0	0	0	0	0	0	0
<i>Thalassiosira gracilis</i> v. <i>expecta</i> (Van Landingham) Fryxell & Hasle	0	1	4	4	1	1	0	1	3	1
<i>Thalassiosira gracilis</i> v. <i>gracilis</i> (Karsten) Hustedt	6	7	5	12	6	4	4	2	6	4
<i>Thalassiosira gravida</i> Cleve	0	0	0	0	0	0	2	3	1	0
<i>Thalassiosira lentiginosa</i> (Janisch) Fryxell	7	4	9	5	3	6	2	2	3	1
<i>Thalassiosira oliverana</i> (O'Meara) Makarova & Nikolaev	1	0	0	0	0	0	0	0	0	0
<i>Thalassiosira poroseriata</i> (Ramsfjell) Hasle	15	2	4	8	3	5	0	3	2	3
<i>Thalassiosira ritscheri</i> (Hustedt) Hasle	0	0	0	0	0	1	1	3	1	1
<i>Thalassiosira tumida</i> (Janisch) Hasle	2	0	1	0	1	4	1	8	0	0
<i>Thalassiosira</i> spp. Cleve	5	2	1	5	2	4	0	1	2	1
<i>Thalassiothrix/nema/toxon</i>	1	0	0	1	0	0.5	0	0	0	0
<i>Thalassiothrix antarctica</i> Schimper ex Karsten	0.5	1	2.5	0.5	1	1.5	0.5	0.5	0	0
<i>Trichotoxon reinholdii</i> (Van Heurck) Reid & Round	0.5	0	0.5	1.5	1	0	0.5	0	0.5	1
<i>Trigonium arcticum</i> (Brightwell) Cleve	0	0	0	0	0	1	0	0	0	0
Unidentified centrics	1	1	1	0	0	1	0	6	0	0
Unidentified pennates	0	0	0	0	2	0	0	1	1	0
<b>Total:</b>	<b>414.5</b>	<b>403</b>	<b>414</b>	<b>404</b>	<b>406.5</b>	<b>414.5</b>	<b>414.5</b>	<b>403.5</b>	<b>435.5</b>	<b>407.5</b>

**Table A4.3.1.2 continued** Durmont d'Urville Trough, MD03 2597, quantitative diatom abundance *Hyalochaete Chaetoceros* spp. free counts, lamina types: laminae characterised by *Corethron pennatum* and *Rhizosolenia* spp.; laminae characterised by *C. pennatum*; and laminae characterised by *Rhizosolenia* spp..

Lamina log number	12	15	15	77	142	144	189	190	191	193	194
Depth (mbsf)	56.723	56.693	56.700	49.851	47.769	47.760	44.515	44.505	44.498	44.483	44.469
Number of FOV	33	48	46	40	36	41	24	28	25	24	25
Mass (g)	0.0068	0.0062	0.0064	0.006	0.0061	0.0076	0.0053	0.0062	0.0081	0.0067	0.0058
Species / Lamina type	Laminae characterised by <i>Corethron pennatum</i> and / or <i>Rhizosolenia</i> spp.			Laminae characterised by <i>Corethron pennatum</i>			Laminae characterised by <i>Rhizosolenia</i> spp.				
<i>Actinocyclus actinochilus</i> (Ehrenberg) Simonsen	1	0	2	2	0	1	0	0	0	0	0
<i>Asteromphalus</i> spp. Ehrenberg	1	0	1	2	1	3	2	2	1	2	2
<i>Phaeoceros Chaetoceros</i> spp. Gran	16	22	82	20	10	9	4	4	13	10	4
<i>Cocconeis</i> spp. Ehrenberg	1	0	0	2	0	0	0	2	0	0	1
<i>Corethron pennatum</i> (Grunow) Ostenfeld	2	10	3	3	11	3	0	1	0	4	1
<i>Eucampia antarctica</i> resting spores (Castracane) Mangin	1	1	1	0	0	2	0	1	1	0	0
<i>Eucampia antarctica</i> vegetative (Castracane) Mangin	50	12	1	1	6	0	1	1	1	6	4
<i>Fragilariopsis curta</i> (Van Heurck) Hustedt	55	92	88	85	130	131	37	105	136	75	77
<i>Fragilariopsis cylindrus</i> (Grunow) Krieger	65	52	50	102	154	88	197	112	97	152	138
<i>Fragilariopsis cylindriciformis</i> (Hasle) Hasle	4	0	0	0	1	0	2	0	0	0	1
<i>Fragilariopsis kerguelensis</i> (O'Meara) Hustedt	15	16	36	28	13	20	5	16	11	20	14
<i>Fragilariopsis obliquecostata</i> (Van Heurck) Heiden	7	4	2	3	5	2	0	1	3	1	0
<i>Fragilariopsis pseudonana</i> (Hasle) Hasle	1	1	0	3	1	3	1	1	2	4	6
<i>Fragilariopsis rhombica</i> (O'Meara) Hustedt	70	36	53	52	28	53	19	36	51	43	55
<i>Fragilariopsis ritscheri</i> (Hustedt) Hasle	40	40	15	23	11	10	2	5	4	5	9
<i>Fragilariopsis separanda</i> Hustedt	14	2	1	0	0	0	1	2	1	0	0
<i>Fragilariopsis sublinearis</i> (Van Heurck) Heiden	6	22	6	8	9	10	5	6	7	2	7
<i>Fragilariopsis vanheurckii</i> (M. Pergallo) Hustedt	0	1	2	1	1	0	1	1	2	0	1
<i>Fragilariopsis</i> spp. Hustedt	11	11	3	10	4	11	3	4	14	14	6
<i>Gomphonema</i> spp. Ehrenberg	0	0	0	0	0	1	0	0	1	0	0
<i>Navicula</i> spp. Bory de St-Vincent	0	4	1	3	1	0	2	1	2	3	9
<i>Odontella litigiosa</i> (van Heurck) Hoban	0	0	0	0	0	1	0	0	0	0	0
<i>Odontella weissflogii</i> (Janisch) Grunow	1	0	0	1	0	0	0	1	0	0	0
<i>Porosira glacialis</i> (Grunow) Jørgensen	9	5	6	5	2	11	0	7	2	3	4
<i>Porosira pseudodenticula</i> (Hustedt) Jousé	0	2	1	0	1	0	0	0	0	0	0
<i>Proboscia inermis</i> (Castracane) Jordan & Ligowski	4	3	1	4	2	5	103	71	57	9	9
<i>Proboscia truncata</i> (Karsten) Nöthig & Ligowski	0	0	0	1	0	1	1	4	1	2	0
<i>Pseudonitzschia turgidula</i> (Hustedt) Hasle	4.5	10.5	10	6.5	3	6	7	1.5	5	14	16
<i>Rhizosolenia antennata</i> f. <i>antennata</i> (Ehrenberg) Brown	0	0	0	0	0	0	0	1	0	1	0
<i>Rhizosolenia antennata</i> f. <i>semispina</i> Sundström	6	32	10	5	2	0	11	5	16	10	16
<i>Rhizosolenia sima</i> Castracane f. <i>sima</i>	0	0	0	0	0	0	0	0	0	1	2
<i>Rhizosolenia simplex</i> Karsten	0	0	0	2	0	0	0	0	0	0	0
<i>Rhizosolenia</i> species A Armand	1	3	2	0	0	1	0	0	0	0	1
<i>Rhizosolenia</i> spp. Brightwell	2	7	2	1	0	3	0	0	0	2	0
<i>Stellarima microtrias</i> (resting spore) (Ehrenberg) Hasle & Sims	0	0	0	0	1	0	0	2	1	2	0
<i>Thalassiosira antarctica</i> (resting spore - cold) Comber	3	3	4	0	0	0	1	0	0	0	0
<i>Thalassiosira antarctica</i> (vegetative) Comber	2	3	1	0	0	0	0	0	0	0	0
<i>Thalassiosira gracilis</i> v. <i>expecta</i> (Van Landingham) Fryxell & Hasle	0	2	1	1	2	2	0	0	2	4	3
<i>Thalassiosira gracilis</i> v. <i>gracilis</i> (Karsten) Hustedt	4	2	2	6	5	4	3	3	6	5	3
<i>Thalassiosira gravida</i> Cleve	1	0	0	1	0	0	0	0	0	3	2
<i>Thalassiosira lentiginosa</i> (Janisch) Fryxell	8	8	7	15	4	9	2	2	1	2	2
<i>Thalassiosira lineata</i> Jousé	0	0	0	0	0	0	0	0	0	0	0
<i>Thalassiosira poroseriata</i> (Ramsfjell) Hasle	4	1	2	3	2	0	0	2	0	0	0
<i>Thalassiosira ritscheri</i> (Hustedt) Hasle	0	0	0	1	0	0	0	0	0	2	1
<i>Thalassiosira tumida</i> (Janisch) Hasle	2	0	1	1	1	1	0	1	0	0	0
<i>Thalassiosira</i> spp. Cleve	5	4	3	1	1	2	1	1	1	1	1
<i>Thalassiothrix antarctica</i> Schimper ex Karsten	0.5	1	1.5	1	0.5	0.5	0	1	0	0	0.5
<i>Trachyneis aspera</i> (Ehrenberg) Cleve	0	0	0	0	0.5	0	1	0	0	0	0
<i>Trichotoxon reinboldii</i> (Van Heurck) Reid & Round	0	0	0	0	0	2.5	0.5	0	0	1.5	0.5
Unidentified centrics	1	0	4	3	1	4	2	1	0	2	4
Unidentified pennates	0	0	0	0	0	1	1	0	0	0	0
<b>Total:</b>	<b>418</b>	<b>412.5</b>	<b>405.5</b>	<b>406.5</b>	<b>414</b>	<b>401</b>	<b>415.5</b>	<b>404.5</b>	<b>439</b>	<b>405.5</b>	<b>400</b>

**Table A4.3.1.2 continued** Durmont d'Urville Trough, MD03 2597, quantitative diatom abundance *Hyalochaete Chaetoceros* spp. free counts, lamina types: mixed diatom assemblage biogenic laminae; and mixed diatom assemblage terrigenous laminae.

	Lamina log number	54	263	195	10	13	143	145	192	196	232	281	336
	Depth (mbsf)	52.658	37.826	44.458	56.744	56.7164	47.762	47.7581	44.493	44.451	40.632	33.9563	18.829
	Number of FOV	37	22	25	42	54	39	37	24	46	33	40	29
	Mass (g)	0.0088	0.0074	0.0075	0.0082	0.0094	0.0081	0.0094	0.0081	0.0078	0.0079	0.0088	0.0089
Species / Lamina type		Mixed diatom assemblage biogenic laminae						Mixed diatom assemblage terrigenous laminae					
<i>Actinocyclus actinocylus</i> (Ehrenberg) Simonsen		0	0	1	0	2	2	0	0	0	2	0	1
<i>Asteromphalus</i> spp. Ehrenberg		1	3	1	2	2	4	1	3	2	7	1	0
<i>Phaeoceros Chaetoceros</i> spp. Gran		7	46	6	1	3	18	4	9	8	49	20	57
<i>Cocconeis</i> spp. Ehrenberg		0	0	1	1	0	0	1	2	1	0	0	2
<i>Corethron pennatum</i> (Grunow) Ostenfeld		0	5	2	2	5	4	1	1	0	7	1	12
<i>Coscinodiscus bouveti</i> Karsten		0	0	0	0	1	0	0	0	0	0	0	0
<i>Eucampia antarctica</i> (resting spore) (Castracane) Mangin		1	0	4	1	3	2	5	2	3	0	3	3
<i>Eucampia antarctica</i> (vegetative) (Castracane) Mangin		0	9	1	4	2	1	2	4	1	20	3	4
<i>Fragilariopsis curta</i> (Van Heurck) Hustedt		210	209	95	177	96	150	147	77	130	54	167	129
<i>Fragilariopsis cylindrus</i> (Grunow) Krieger		20	30	126	21	41	80	36	161	88	76	28	59
<i>Fragilariopsis cylindriciformis</i> (Hasle) Hasle		0	0	0	0	0	0	0	0	0	0	0	0
<i>Fragilariopsis kerguelensis</i> (O'Meara) Hustedt		38	15	21	32	37	14	34	16	44	31	37	26
<i>Fragilariopsis obliquecostata</i> (Van Heurck) Heiden		1	1	0	8	5	3	3	2	1	1	1	2
<i>Fragilariopsis pseudonana</i> (Hasle) Hasle		0	0	1	0	0	1	1	4	2	1	0	1
<i>Fragilariopsis rhombica</i> (O'Meara) Hustedt		51	36	57	70	92	50	60	34	64	25	53	39
<i>Fragilariopsis ritscheri</i> (Hustedt) Hasle		13	8	11	27	31	7	14	9	12	6	23	7
<i>Fragilariopsis separanda</i> Hustedt		4	0	0	0	0	0	0	2	0	0	0	0
<i>Fragilariopsis sublinearis</i> (Van Heurck) Heiden		7	16	7	4	1	4	13	10	11	11	6	6
<i>Fragilariopsis vanheurckii</i> (M. Pergallo) Hustedt		0	2	1	3	2	6	4	0	4	2	3	3
<i>Fragilariopsis</i> spp. Hustedt		11	11	15	3	11	11	13	4	21	4	16	18
<i>Gomphonema</i> spp. Ehrenberg		1	0	0	0	0	0	0	0	1	0	0	0
<i>Navicula</i> spp. Bory de St-Vincent		1	4	4	2	1	3	1	2	4	0	2	2
<i>Odontella weissflogii</i> (Janisch) Grunow		0	1	0	0	0	1	0	0	0	0	0	0
<i>Odontella litigiosa</i> (van Heurck) Hoban		0	0	0	0	0	0	0	0	1	0	0	0
<i>Porosira glacialis</i> (Grunow) Jørgensen		5	0	6	28	24	7	11	8	16	51	7	18
<i>Porosira pseudodenticula</i> (Hustedt) Jousé		0	0	0	0	0	0	0	1	0	0	0	0
<i>Proboscia inermis</i> (Castracane) Jordan & Ligowski		0	0	4	0	2	4	2	11	4	8	0	1
<i>Proboscia truncata</i> (Karsten) Nöthig & Ligowski		0	0	1	0	0	0	0	0	1	0	0	3
<i>Pseudonitzschia turgidula</i> (Hustedt) Hasle		3.5	1.5	8	0	2	2.5	1.5	6	6	7	1	2.5
<i>Rhizosolenia antennata</i> f. <i>antennata</i> (Ehrenberg) Brown		0	0	0	0	0	0	0	1	0	0	0	0
<i>Rhizosolenia antennata</i> f. <i>semispina</i> Sundström		1	1	6	1	6	5	3	11	6	0	5	0
<i>Rhizosolenia</i> spp. Brightwell		1	1	0	1	0	1	5	0	4	0	0	0
<i>Stellarima microtrias</i> (resting spore) (Ehrenberg) Hasle & Sims		0	0	5	1	0	0	0	0	0	2	0	0
<i>Stephanodiscus</i> spp. Ehrenberg		0	0	0	0	0	0	0	1	0	0	0	0
<i>Thalassiosira antarctica</i> (resting spore - cold) Comber		3	0	0	0	0	0	3	0	0	0	0	0
<i>Thalassiosira antarctica</i> (vegetative) Comber		0	0	1	0	3	1	0	0	0	2	0	0
<i>Thalassiosira gracilis</i> v. <i>expecta</i> (Van Ledingham) Fryxell & Hasle		1	3	2	4	0	0	3	3	0	4	1	0
<i>Thalassiosira gracilis</i> v. <i>gracilis</i> (Karsten) Hustedt		7	4	5	9	4	5	8	2	2	12	5	2
<i>Thalassiosira gravula</i> Cleve		0	0	3	0	1	0	0	6	3	4	1	1
<i>Thalassiosira lentiginosa</i> (Janisch) Fryxell		11	1	5	9	6	8	7	8	8	7	7	0
<i>Thalassiosira oliverana</i> (O'Meara) Makarova & Nikolaev		1	0	0	0	0	0	1	0	0	0	0	0
<i>Thalassiosira poroseriata</i> (Ramsfjell) Hasle		1	3	2	16	15	2	4	3	3	0	15	3
<i>Thalassiosira ritscheri</i> (Hustedt) Hasle		1	0	0	1	0	0	0	1	2	4	1	2
<i>Thalassiosira tumida</i> (Janisch) Hasle		2	0	1	3	4	0	4	0	1	9	1	4
<i>Thalassiosira</i> spp. Cleve		5	1	1	1	1	2	7	0	1	3	0	1
<i>Thalassiothrix/nema/toxon</i>		0.5	0	0	0	0	0	0	0	0	0	0	0
<i>Thalassiothrix antarctica</i> Schinper ex Karsten		2	0.5	1.5	0	0	1.5	1.5	0	2	0	1	1
<i>Trachymeis aspera</i> (Ehrenberg) Cleve		0	0	0	0	1	1	0.5	0.5	0.5	0	0	0
<i>Trichotoxon reinboldii</i> (Van Heurck) Reid & Round		1.5	0.5	0.5	0	0	0.5	1	2	1.5	0.5	0	1
Unidentified centrics		0	0	2	0	0	1	0	0	3	0	0	0
Unidentified pennates		0	1	1	0	0	3	0	0	0	0	0	0
<b>Total:</b>		<b>412.5</b>	<b>413.5</b>	<b>409</b>	<b>432</b>	<b>404</b>	<b>405.5</b>	<b>402.5</b>	<b>405.5</b>	<b>463</b>	<b>409.5</b>	<b>409</b>	<b>410.5</b>



**Table A4.3.1.2 continued** Durmont d'Urville Trough, MD03 2597, quantitative diatom abundance *Hyalochaete Chaetoceros* spp. free counts, lamina types: sub-laminae characterised by *Porosira glacialis* resting spores; and laminae characterised by *Stellarima microtrias* resting spores, *P. glacialis* resting spores and / or *Coscinodiscus bouvet*.

Lamina log number	14	224	282	35	205	206	207	233
Depth (mbsf)	56.709	40.702	33.953	53.106	41.169	41.165	41.161	40.625
Number of FOV	48	44	36	21	28	30	42	28
Mass (g)	0.0076	0.0065	0.0064	0.0098	0.0073	0.0079	0.0081	0.0073
Species / Lamina type	Sub-laminae characterised by <i>Porosira glacialis</i> resting spores			Laminae characterised by <i>Stellarima microtrias</i> resting spores, <i>Porosira glacialis</i> resting spore and / or <i>Coscinodiscus bouvet</i>				
<i>Actinocyclus actinochilus</i> (Ehrenberg) Simonsen	1	1	1	1	0	1	4	1
<i>Asteromphalus</i> spp. Ehrenberg	1	3	3	1	2	0	1	3
<i>Phaeoceros Chaetoceros</i> spp. Gran	2	23	16	23	11	16	10	74
<i>Cocconeis</i> spp. Ehrenberg	1	1	1	0	1	0	1	0
<i>Corethron pennatum</i> (Grunow) Ostenfeld	4	0	0	3	3	1	3	13
<i>Eucampia antarctica</i> (resting spores) (Castracane) Mangin	1	0	7	0	0	1	0	0
<i>Eucampia antarctica</i> (vegetative) (Castracane) Mangin	5	9	1	5	5	5	2	10
<i>Fragilariopsis curta</i> (Van Heurck) Hustedt	76	82	108	153	76	106	90	64
<i>Fragilariopsis cylindrus</i> (Grunow) Krieger	24	7	13	46	130	85	49	89
<i>Fragilariopsis cylindriciformis</i> (Hasle) Hasle	1	0	0	0	0	0	0	0
<i>Fragilariopsis kerguelensis</i> (O'Meara) Hustedt	18	57	20	25	16	18	39	37
<i>Fragilariopsis obliquecostata</i> (Van Heurck) Heiden	4	1	4	6	3	1	4	1
<i>Fragilariopsis pseudonana</i> (Hasle) Hasle	1	1	1	0	4	0	1	0
<i>Fragilariopsis rhombica</i> (O'Meara) Hustedt	46	43	30	42	27	33	46	27
<i>Fragilariopsis ritscheri</i> (Hustedt) Hasle	39	14	9	10	9	19	16	12
<i>Fragilariopsis separanda</i> Hustedt	4	0	2	6	0	2	0	0
<i>Fragilariopsis sublinearis</i> (Van Heurck) Heiden	14	8	8	13	17	6	8	2
<i>Fragilariopsis vanheurckii</i> (M. Pergallo) Hustedt	0	6	1	0	5	3	3	1
<i>Fragilariopsis</i> spp. Hustedt	7	8	8	13	8	10	4	7
<i>Gomphonema</i> spp. Ehrenberg	0	1	0	0	0	0	0	0
<i>Navicula</i> spp. Bory de St-Vincent	1	2	1	1	4	1	3	1
<i>Odontella weisflogii</i> (Janisch) Grunow	0	0	1	0	0	0	0	0
<i>Porosira glacialis</i> (Grunow) Jørgensen	57	51	82	37	12	14	21	22
<i>Porosira pseudodenticula</i> (Hustedt) Jousé	1	0	0	0	0	0	0	0
<i>Proboscia inermis</i> (Castracane) Jordan & Ligowski	0	1	0	1	6	8	3	9
<i>Proboscia truncata</i> (Karsten) Nöthig & Ligowski	0	0	0	0	0	0	1	0
<i>Pseudonitzschia turgidula</i> (Hustedt) Hasle	2	9	0.5	3	4	4	1	3.5
<i>Rhizosolenia antennata</i> f. <i>semispina</i> Sundström	14	2	1	2	2	1	4	4
<i>Rhizosolenia</i> species A Armand	2	0	0	1	0	0	0	0
<i>Rhizosolenia</i> spp. Brightwell	6	0	0	2	0	1	1	0
<i>Stellarima microtrias</i> (resting spore) (Ehrenberg) Hasle & Sims	11	0	0	5	7	8	11	2
<i>Thalassiosira antarctica</i> (resting spore - cold) Comber	19	3	0	4	1	0	0	0
<i>Thalassiosira antarctica</i> (resting spore - warm) Comber	1	0	0	0	0	0	0	0
<i>Thalassiosira antarctica</i> (vegetative) Comber	4	0	12	1	8	2	1	0
<i>Thalassiosira ambigua</i> Kozlova	1	0	0	0	0	0	0	0
<i>Thalassiosira gracilis</i> v. <i>expecta</i> (Van Landingham) Fryxell & Hasle	3	7	0	1	7	2	1	1
<i>Thalassiosira gracilis</i> v. <i>gracilis</i> (Karsten) Hustedt	9	8	8	4	1	7	7	5
<i>Thalassiosira gravida</i> Cleve	13	17	0	0	2	1	1	1
<i>Thalassiosira lentiginosa</i> (Janisch) Fryxell	0	11	5	7	3	6	5	3
<i>Thalassiosira oestrupii</i> (Ostenfeld) Hasle	1	0	0	0	0	0	0	0
<i>Thalassiosira perpusilla</i> Kozlova	0	0	1	0	0	0	0	0
<i>Thalassiosira poroseriata</i> (Ramsfjell) Hasle	3	19	51	1	30	32	61	3
<i>Thalassiosira ritscheri</i> (Hustedt) Hasle	1	7	3	1	4	3	5	0
<i>Thalassiosira tumida</i> (Janisch) Hasle	2	0	2	1	3	2	1	2
<i>Thalassiosira</i> spp. Cleve	10	0	8	7	2	6	5	4
<i>Thalassiothrix antarctica</i> Schimper ex Karsten	0.5	1.5	0	0	0.5	0.5	1	0.5
<i>Trachyneis aspera</i> (Ehrenberg) Cleve	1	0	0	0	0	0	0	0
<i>Trichotoxon reinboldii</i> (Van Heurck) Reid & Round	0	1.5	0	1	0	0	0	0.5
Unidentified centrics	1	1	0	1	1	0	1	1
Unidentified pennates	0	0	0	0	0	0	1	0
<b>Total:</b>	<b>412.5</b>	<b>406</b>	<b>408.5</b>	<b>428</b>	<b>414.5</b>	<b>405.5</b>	<b>416</b>	<b>403.5</b>

## A.5 Markov chain analysis

This appendix contains Markov chain analysis of lithology transitions within ODP site 1098A Palmer Deep. Lithology transition information can be found in appendix 3.

- Three lithologies (m) are defined: Biogenic laminae (BL), Terrigenous laminae (TL), Terrigenous laminae with sub-laminae (SL).

Markov chain results are reliable if:

$$\text{number of observed transitions} > 5 \times (\text{number of lithological categories})^2$$

$$192 > 5 \times (3)^2$$

$$192 > 45$$

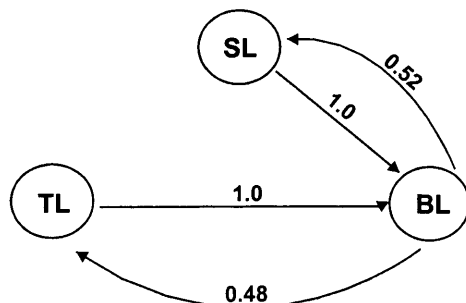
Observed transition frequency matrix

		<i>To</i>			<b>Total</b>
		BL	TL	SL	
<i>From</i>	BL	0	46	50	96
	TL	45	0	0	45
	SL	51	0	0	51
	<b>Total</b>	96	46	50	192

Observed transition probability matrix (elements of the matrix divided by row totals)

		<i>To</i>		
		BL	TL	SL
<i>From</i>	BL	0	0.48	0.52
	TL	1	0	0
	SL	1	0	0

This matrix allows a flow diagram to be constructed which may elucidate the nature of the pattern.



This flow diagram shows that there are two cycles that are more likely to occur:

BL → SL → BL

BL → TL → BL

This appears to have a cyclic pattern, but it is necessary to test whether this succession is significantly different from random.

Fixed probability vector (probability of going to each lithology):

BL	0.5
TL	0.24
SL	0.26

Expected random probability matrix

		<i>To</i>		
		BL	TL	SL
<i>From</i>	BL	0.5	0.24	0.26
	TL	0.5	0.24	0.26
	SL	0.5	0.24	0.26

Expected random transition frequency matrix (probabilities converted into expected counts: row totals from the transition frequency matrix multiplied with probabilities)

		<i>To</i>		
		BL	TL	SL
<i>From</i>	BL	48	23.04	24.96
	TL	22.5	10.8	11.7
	SL	22.5	12.24	13.26

The observed transition frequency matrix and expected random transition frequency matrix are compared using  $\chi^2$ .

$$\text{Where } \chi^2 = \sum_{j=1}^{m_2} (O_j - E_j)^2 / E_j$$

with  $(m-1)^2$  degrees of freedom

where

$O_j$  = observed transition frequency in the  $j^{\text{th}}$  class.

$E_j$  = frequency from the expected random transition frequency matrix

$H_0$ : the data came from a population of transitions that are random; the probability of encountering a lithology is not dependent on the underlying lithology

$H_1$ : the data came from a population of transitions that are non-random

Class	$O_j$	$E_j$	$(O_j - E_j)^2 / E_j$
BL-BL	0	48	48
BL-TL	46	23.04	22.88
BL-SL	50	24.96	25.12
TL-BL	45	22.5	22.5
TL-TL	0	10.8	10.8
TL-SL	0	11.7	11.7
SL-BL	5.1	25.5	25.5
SL-TL	0	12.24	12.24
SL-SL	0	13.26	13.26
			$\Sigma = 172$

The degrees of freedom

$$\nu = ((\text{number of lithologies}) - 1)^2$$

$$\nu = (3 - 1)^2 = 4$$

The critical value is

$$\chi_{0.05,4}^2 = 9.49$$

(using Appendix 2.6 in Swan and Sandilands (1995))

The calculated value exceeds the critical value, so the null hypothesis is rejected and conclude that there is a significant Markov property. That the occurrence of lithologies is, to an extent, dependent on preceding lithology.

2. Four lithologies are defined: Biogenic laminae (BL), Terrigenous laminae (TL), Terrigenous laminae with sub-laminae including *T. antarctica* (TAL) and terrigenous laminae with sub-laminae not including *T. antarctica* (NTAL).

$$192 > 5 \times (4)^2$$

$$192 > 80$$

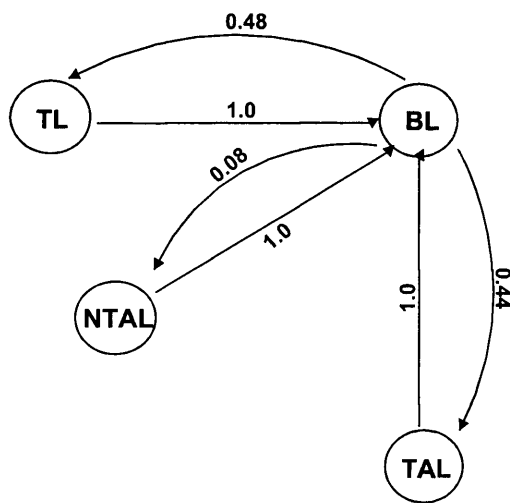
Transition frequency matrix

		<i>To</i>				<b>Total</b>
		BL	TL	NTAL	TAL	
<i>From</i>	BL	0	46	8	42	96
	TL	45	0	0	0	45
	NTAL	8	0	0	0	8
	TAL	43	0	0	0	43
	<b>Total</b>	96	46	8	42	192

Observed transition probability matrix

		<i>To</i>			
		BL	TL	NTAL	TAL
<i>From</i>	BL	0	0.48	0.08	0.44
	TL	1	0	0	0
	NTAL	1	0	0	0
	TAL	1	0	0	0

Flow diagram



BL → TL → BL

BL → TAL → BL

Fixed probability vector:

- BL 0.5
- TL 0.24
- TAL 0.22
- NTAL 0.04

Expected random probability matrix

		<i>To</i>			
		BL	TL	NTAL	TAL
<i>From</i>	BL	0.5	0.24	0.04	0.22
	TL	0.5	0.24	0.04	0.22
	NTAL	0.5	0.24	0.04	0.22
	TAL	0.5	0.24	0.04	0.22

Expected random transition frequency matrix (probabilities converted into expected counts)

		<i>To</i>			
		BL	TL	NTAL	TAL
<i>From</i>	BL	0	23.04	3.84	21.12
	TL	22.5	0	0	0
	NTAL	4	0	0	0
	TAL	21.5	0	0	0

Class	$O_j$	$E_j$	$(O_j - E_j)^2 / E_j$
BL-BL	0	0	0
BL-TL	46	23.04	22.88
BL-NTAL	8	3.84	4.51
BL-TAL	42	21.12	20.64
TL-BL	45	22.5	22.5
TL-TL	0	0	0
TL-NTAL	0	0	0
TL-TAL	0	0	0
NTAL-BL	8	4	4
NTAL-TL	0	0	0
NTAL-NTAL	0	0	0
NTAL-TAL	0	0	0
TAL-BL	43	21.5	21.5
TAL-TL	0	0	0
TAL-NTAL	0	0	0
TAL-TAL	0	0	0
			$\Sigma = 92.03$

$$\nu = (4 - 1)^2 = 9$$

The critical value is

$$\chi_{0.05,9}^2 = 16.92$$

using Appendix 2.6  $\chi^2$  distribution in Swan and Sandilands (1995).

The calculated value exceeds the critical value, so the null hypothesis is rejected and conclude that there is a significant Markov property. That the occurrence of lithologies is, to an extent, dependent on preceeding lithology.

## A

- Abbott Jr., W.H. (1973). Vertical and lateral patterns of diatomaceous ooze found between Australia and Antarctica. PhD Thesis. Department of Geology, University of South Carolina, USA.
- Abbott, M.R., Richman, J.G., Nahorniak, J.S., Barksdale, B.S. (2001). Meanders in the Antarctic polar frontal zone and their impact on phytoplankton. *Deep-Sea Research Part II-Topical Studies in Oceanography*. **48** (19-20): 3891-3912.
- Abelmann, A., Gersonde, R. (1991). Biosiliceous particle-flux in the Southern-Ocean. *Marine Chemistry*. **35** (1-4): 503-536.
- Adolphs, U. Wendler, G. (1995). A Pilot-Study on the interactions between katabatic winds and polynyas at the Adélie Coast, Eastern Antarctica. *Antarctic Science*. **7** (3): 307-314.
- Aletsee, L., Jahnke, J. (1992). Growth and productivity of the psychrophilic marine diatoms *Thalassiosira antarctica* Comber and *Nitzschia Frigida* Grunow in batch cultures at temperatures below the freezing point of sea-water. *Polar Biology*. **11**: 643-647.
- Alexander, V., Niebauer, H.J. (1981). Oceanography at the eastern Bering Sea ice edge zone in spring. *Limnology and Oceanography*. **26**: 1111-1125.
- Allredge, A.L., Silver, M.W. (1982). Abundance and production rates of floating diatom mats (*Rhizosolenia castracanei* and *R. imbricata* va. *shrubsolei*) in the eastern Pacific Ocean. *Marine Biology*. **66**: 83-88.
- Allredge, A.L., Silver, M.W. (1988). Characteristics, dynamics and significance of marine snow. *Progress in Oceanography*. **20**: 42-82.
- Allredge, A.L., Gotschalk C.C. (1989). Direct observations of the mass flocculation of diatom blooms - characteristics, settling velocities and formation of diatom aggregates. *Deep-Sea Research Part A - Oceanographic Research Papers*. **36** (2): 159-171.
- Allredge, A.L., Passow, U., Logan, B. (1993). The abundance and significance of a class of large, transparent organic particles in the ocean. *Deep-Sea Research Part I - Oceanographic Research Papers*. **40**: 1131-1140.
- Allen, C.S. (2003). Late quaternary palaeoceanography of the Scotia Sea, Southwest Atlantic: evidence from the diatom record. PhD Thesis. University of Wales, Cardiff. pp. 1-228.
- Allen, C.S., Pike, J., Pudsey, C.J., Leventer, A. (2005). Submillennial variations in ocean conditions during deglaciation based on diatom assemblages from the southwest Atlantic. *Paleoceanography*. **20** (2). PA2012, doi:10.1029/2004PA001055.



- Anderson, J.B. (1999). Antarctic Marine Geology. Cambridge, Cambridge University Press. pp. 1-289.
- Anderson, J.B., Shipp S.S. (2001). Evolution of the West Antarctic Ice Sheet. In: Alley, R.B., Bindshadler, R.A. (Eds.). The West Antarctic Ice Sheet: behaviour and environment. Antarctic Research Series. **77**: 45-57.
- Anderson, J.B., Kurtz, D.D., Domack, E.W., Balshaw, K.M. (1980). Glacial and glacial-marine sediments of the Antarctic continental shelves. *Journal of Geology*. **88**: 399-414.
- Anderson, J.B., Shipp, S.S., Lowe, A.L., Wellner, J.S., Mosola, A.B. (2002). The Antarctic Ice Sheet during the Last Glacial Maximum and its subsequent retreat history: a review. *Quaternary Science Reviews*. **21** (1-3): 49-70.
- Andreoli, C., Tolomio, C., Moror, I., Radice, M., Moschin, E., Bellato, S. (1995). Diatoms and dinoflagellates in Terra Nova Bay (Ross Sea - Antarctica) during austral summer 1990. *Polar Biology*. **15**: 465-475.
- Andrews, J.T., Domack, E.W., Cunningham, W.L., Leventer, A., Licht, K.J., Jull, A.J.T., DeMaster, D.J., Jennings, A.E. (1999). Problems and possible solutions concerning radiocarbon dating of surface marine sediments, Ross Sea, Antarctica. *Quaternary Research*. **52** (2): 206-216.
- Armand, L.K. (1997). The use of diatom transfer functions in estimating sea-surface temperature and sea-ice in cores from the southeast Indian Ocean. PhD Thesis. Australian National University, Canberra, Australia.
- Armand, L.K. (2000). An ocean of ice - advances in the estimation of past sea ice in the Southern Ocean. *GSA Today*. **10**: 1-7.
- Armand, L.K., Zielinski U. (2001). Diatom species of the genus *Rhizosolenia* from Southern Ocean sediments: distribution and taxonomic notes. *Diatom Research*. **16**: 259-294.
- Armand, L.K., Crosta, X. Romero, O., Pichon, J.J. (2005). The biogeography of major diatom taxa in Southern Ocean sediments: 1. Sea ice related species. *Palaeogeography Palaeoclimatology Palaeoecology*. **223** (1-2): 93-126.
- Arrigo, K.R. (2003). Primary production in sea ice. In: Thomas, D.N., Dieckmann, G.S. (Eds.). *Sea Ice: An introduction to its physics, chemistry, biology and geology*. Oxford, Blackwell Science Ltd. pp. 143-183.
- Arrigo, K.R., Sullivan, C.W. (1992). The influence of salinity and temperature covariation on the photophysiological characteristics of Antarctic sea ice microalgae. *Journal of Phycology*. **28** (6): 746-756.
- Arrigo, K.R., Sullivan, C.W., Kremer, J.N. (1991). A bio-optical model of Antarctic sea ice. *Journal of Geophysical Research – Oceans*. **96** (C6):10581-10592.

**B**

- Bahk, J.J., Yoon, H.I., Kim, Y.D., Kang, C.Y., Bae, S.H. (2003). Microfabric analysis of laminated diatom ooze (Holocene) from the eastern Bransfield Strait, Antarctic Peninsula. *Geosciences Journal*. **7** (2): 135-142.
- Baldauf, J.G., Barron, J.A. (1991). Diatom biostratigraphy: Kerguelen Plateau and Prydz bay regions of the Southern Ocean. *Proceedings of the Ocean Drilling Program, Scientific Results*. **119**: 547-598.
- Barker P.F. (2001) Scotia Sea regional tectonic evolution: implications for mantle flow and palaeocirculation. *Earth-Science Reviews*. **55** (1-2):1-39.
- Barker, P.F., Carmelenghi, A., Acton, G.D. (1999a). Leg 178 summary: Antarctic glacial history and sea level change. *Proceedings of the Ocean Drilling Program Initial Report*. **178**: 1-58.
- Barker, P.F., Camerlenghi, A., Acton, G.D., Brachfeld, S.A., Cowan, E.A., Daniels, J., Domack, E.W., Escutia, C., Evans, A.J., Eyles, N., Guyodo, Y.J.B., Iorio, M., Iwai, M., Kyte, F.T., Lauer, C., Maldonado, A., Moerz, T., Osterman, L.E., Pudsey, C.J., Schuffert, J.D., Sjunneskog, C.M., Vigar, K.L., Weinheimer, A.L., Williams, T., Winter, D.M., Wolf-Welling, T.C.W. (1999b). *Proceedings of the Ocean Drilling Program, Initial Reports*. **178**. [http://www-odp.tamu.edu/publications/178\\_IR/front.htm](http://www-odp.tamu.edu/publications/178_IR/front.htm)
- Barnes, P.W. (1987). Morphologic studies of the Wilkes Land, continental shelf, Antarctica - glacial and iceberg effects. In: Eittrem, S.L., Hampton, M.A. (Eds.). *The Antarctic Continental Margin: Geology and Geophysics of Offshore Wilkes Land*. Houston, TX, Circum-Pacific Council for Energy and Mineral resources. pp. 175-194.
- Bart, P.J., Anderson, J.B. (1996). Seismic expression of depositional sequences associated with expansion and contraction of ice sheets on the Northwestern Antarctic Peninsula, Continental Shelf. *Geological Society Special Publication*. **117**: 171-186.
- Beaman, R.J., Harris, P.T. (2003). Seafloor morphology and acoustic facies of the George V Land shelf. *Deep-Sea Research Part II-Topical Studies in Oceanography*. **50** (8-9): 1343-1355.
- Bentley, M.J., Hodgson, D.A., Sugden, D.E., Roberts, S.J., Smith, J.A., Leng, M.J., Bryant, C. (2005). Early Holocene retreat of the George VI Ice Shelf, Antarctic Peninsula. *Geology*. **33**: 173-176.
- Berkman, P.A., Forman, S.L. (1996). Pre-bomb radiocarbon and the reservoir correction for calcareous marine species in the Southern Ocean. *Geophysical Research Letters*. **23** (4): 363-366.
- Berkman, P., Andrews, J.T., Bjorck, S., Colhoun, E.A., Emslie, S.D., Goodwin, I.D., Hall, B.L., Hart, C.P., Hirakawa, K., Igarashi, A., Ingólfsson, O., Lopez-Martinez, J., Lyons, W.B., Mabin, M.C.G., Quilty, P.G., Tavianni, M., Yoshida, Y. (1998). Circum-Antarctic coastal environmental shifts during the late Quaternary reflected by emerged marine deposits. *Antarctic Science*. **10**: 345-362.

- Berner, R.A. (1970). Sedimentary pyrite formation. *American Journal of Science*. **268**: 1-23.
- Berner, R.A. (1984). Sedimentary pyrite formation: an update. *Geochimica et Cosmochimica Acta*. **48**: 605-615.
- Bi, D.H., Budd, W.F., Hirst, A.C., Wu, X.R. (2001). Collapse and reorganisation of the Southern Ocean overturning under global warming in a coupled model. *Geophysical Research Letters*. **28** (20): 3927-3930.
- Bianchi, F., Boldrin, A., Cioce, F., Dieckmann, G., Kuosa, H., Larsson, A.-M., Nöthig, E.-M., Sehlstedt, P.-I., Socal, G., Syvertsen, E.E. (1992). Phytoplankton distribution in relation to sea ice, hydrography and nutrients in the northwestern Weddell Sea in early spring 1988 during EPOS. *Polar Biology*. **12**: 225-235.
- Bidigare, R.R., Iriarte, J.L. Kang, S.-H., Karentz, D., Ondrusek, M.E., Fryxell, G.A. (1996). Phytoplankton: quantitative and qualitative assessments. In: Ross, R.M., Hofmann, E.E., Quetin, L.B. (Eds.) *Phytoplankton: Quantitative and qualitative assessments. Foundations for Ecological Research West of the Antarctic Peninsula*. Antarctic Research Series. **70**: 173-198.
- Bigg, G.R. (2001). *The Oceans and Climate*. Cambridge, Cambridge University Press. pp. 1-266.
- Bindoff, N.L., Williams, G.D., Allison, I. (2001). Sea-ice growth and water-mass modification in the Mertz Glacier polynya, East Antarctica, during winter. *Annals of Glaciology*. **33**: 399-406.
- Blunier, T., Brook, E.J. (2001). Timing of millennial-scale climate change in Antarctica and Greenland during the last glacial period. *Science*. **291**: 109-112.
- Blunier, T., Schwander, J., Stauffer, B., Stocker, T., Dällenbach, A., Indermühle, A., Tschumi, J., Chappellaz, J., Raynaud, D., Barnola, J.-M. (1997). Timing of the Antarctic Cold Reversal and the atmospheric CO<sub>2</sub> increase with respect to the Younger Dryas event. *Geophysical Research Letters*. **24** (21): 2683-2686.
- Blunier, T., Chappellaz, J., Schwander, J., Dällenbach, A., Stauffer, B., Stocker, T.F., Raynaud, D., Jouzel, J., Clausen, H.B., Hammer, C.U., Johnsen, S.J. (1998). Asynchrony of Antarctic and Greenland climate change during the last glacial period. *Nature*. **394**: 739-743.
- Boltovskoy, E. (1965). *Los Foraminiferos Recientes*. Editorial Universitaria de Buenos Aires, Buenos Aires.
- Bouma, A.G. (1969). *Methods for the Study of Sedimentary Structures*. New York, Wiley-Interscience, John Wiley and Sons.
- Bowler, J.M. (1976). Aridity in Australia - age, origins and expression in aeolian landforms and sediments. *Earth-Science Reviews*. **12** (2-3): 279-310.

- Boyle, E.A. (1986). Paired carbon isotope and cadmium data from benthic foraminifera - implications for changes in oceanic phosphorus, oceanic circulation, and atmospheric carbon-dioxide. *Geochimica et Cosmochimica Acta*. **50** (2): 265-276.
- Brachfeld, S., Domack, E., Kissel, C., Laj, C., Leventer, A., Ishman, S., Gilbert, R., Camerlenghi, A., Eglinton, L.B. (2003). Holocene history of the Larsen-A Ice Shelf constrained by geomagnetic paleointensity dating. *Geology*. **31** (9): 749-752.
- Brancolini, G., Harris, P. (2000). Post cruise report AGSO Survey 217: Joint Italian/Australian marine geoscience expedition aboard the R.V. *Tangaroa* to the George Vth Land region of East Antarctica, during February-March. AGSO Rec. 2000/38.
- Brathauer, U., Abelmann, U. (1999). Late Quaternary variations in sea surface temperatures and their relationship to orbital forcing recorded in the Southern Ocean (Atlantic sector). *Paleoceanography*. **14** (2): 135-148.
- Brennecke, W. (1921). Die ozeanographischen Arbeiten der Deutschen Antarktischen Expedition 1911-1912. Aus dem Archiv der Deutschen Seewarte. **39**: 216.
- Brichta, M., Nöthig, E.-M. (2003). *Proboscia inermis*: A key diatom species in Antarctic autumn. Abstract AGU Chapman conference: The role of Diatom Production and Si flux and Burial in the Regulation of Global Cycles.
- Brodie, I., Kemp, A.E.S. (1994). Variation in biogenic and detrital fluxes and formation of laminae in Late Quaternary sediments from the Peruvian coastal upwelling zone. *Marine Geology*. **116** (3-4): 385-398.
- Broecker, W.S. (1998). Paleoocean circulation during the last deglaciation: A bipolar seesaw. *Paleoceanography*. **13** (2): 119-121.
- Buck, K.R., Garrison, D.L., Fryxell, G.A. (1985). Algal assemblages in sea ice and in the ice-edge zone of the Weddell Sea: An AMERIEZ study. AGU Fall Meeting. *Eos*. **66**: 1287.
- Bull, D., Kemp, A.E.S. (1995). Composition and origins of laminae in late Quaternary and Holocene sediments from the Santa Barbara Basin. Proceedings of the Ocean Drilling Program, Scientific Results. **146**: 77-87.
- Burckle, L.H. (1972). Diatom evidence bearing on the Holocene in the South Atlantic. *Quaternary Research*. **2**: 323-326.
- Burckle, L.H. (1981). Displaced Antarctic diatoms in the Amiranter passage. *Marine Geology*. **39**: M39-M43.
- Burckle, L.H. (1984a). Diatom distribution and paleoceanographic reconstruction in the Southern-Ocean - present and Last Glacial Maximum. *Marine Micropaleontology*. **9** (3): 241-261.

- Burckle, L.H. (1984b). Ecology and paleoecology of the marine diatom *Eucampia antarctica* (Castracane) Mangin. *Marine micropalaeontology*. **9**: 77-86.
- Burckle, L.H., Stanton, D. (1975). Distribution of displaced Antarctic diatoms in the Argentine Basin. *Nova Hedwigia*. **53**: 283-292.
- Burckle, L.H., Cirilli, J. (1987). Origin of diatom ooze belt in the Southern-Ocean - implications for Late Quaternary paleoceanography. *Micropaleontology*. **33** (1): 82-86.
- Burckle, L.H., Robinson, D., Cooke, D., (1982). Reappraisal of sea-ice distribution in Atlantic and Pacific sectors of the Southern-Ocean at 18,000 yr BP. *Nature*. **299**: 435-437.
- Burckle, L.H., Jacobs, S.S., McLaughlin, R.B. (1987). Late austral spring diatom distribution between New Zealand and the Ross Ice Shelf, Antarctica: hydrographic and sediment correlations. *Micropaleontology*. **33** (1): 74-81.
- Burckle, L.H., Gersonde, R. Abrams, N. (1990). Late Pliocene-Pleistocene paleoclimate in the Jane Basin region: ODP Site 697. *Proceedings of the Ocean Drilling Program, Scientific Results*. **113**: 803-809.
- C**
- Carmack, E.C., Foster, T.D. (1975). Circulation and distribution of oceanographic properties near the Filchner Ice Shelf. *Deep-Sea Research and Oceanographic Abstracts*. **22** (2): 77-90.
- Carpenter, E.J., Harbison, G.R. Madin, L.P., Swanberg, N.R., Biggs, D.C., Hulbert, E.M., McAlister, V.L., McCarthy, J.J. (1977). *Rhizosolenia* mats. *Limnology and Oceanography*. **22**: 739-741.
- Cavaliere, D.J., Martin, S. (1985). A passive microwave study of polynyas along the Antarctic Wilkes Land Coast. In: Jacobs, S.S. (Ed.). *Oceanology of the Antarctic Continental Shelf*. *Antarctic Research Series*. **43**: 227-252.
- Chase, T.E., Seekins, B.A., Young, J.D., Eittrheim, S.L., (1987). Marine topography of offshore Antarctica. In: Eittrheim S.L., Hampton, M.A. (Eds.). *The Antarctic Continental Margin: Geology and Geophysics of Offshore Wilkes Land*. Houston, TX, Circum-Pacific Council for Energy and Mineral resources. pp. 147-150.
- Chiba, S., Hirakawa, K., Ushio, S., Horimoto, N., Satoh, R., Nakajima, Y., Ishimaru, T., Yamaguchi, Y. (2000). An overview of the biological/oceanographic survey by the RTV Umitaka-Marui III off Adélie Land, Antarctica in January-February 1996. *Deep-Sea Research Part II – Topical Studies in Oceanography*. **47**: 2589-2613.
- Clark, J.A., Lingle, C.S. (1979). Predicted relative sea-level changes (18,000-years BP to present) caused by Late-Glacial retreat of the Antarctic Ice Sheet. *Quaternary Research*. **11** (3): 279-298.

- Clarke, D.B., Ackley, S.F. (1983). Relative abundance of diatoms in Weddell Sea pack ice. *Antarctic Journal of the United States*. **18**: 181-182.
- Claussen, M., Kubatzki, C., Brovkin, V., Ganopolski, A., Hoelzmann, P., Pachur, H.-J. (1999). Simulation of an abrupt change in Saharan vegetation in the mid-Holocene. *Geophysical Research Letters*. **14**: 2037-2040.
- CLIMAP (1981). Seasonal reconstructions of the earth's surface at the last glacial maximum. Geological Society of America Map and Chart Series. MC-36.
- Cooke, D.W. (1978). Variations in the seasonal extent of sea ice in the Antarctic during the last 140, 000 years. PhD thesis. Columbia University, USA. pp. 1-123.
- Cooke, D.W., Hays, J.D. (1982). Estimates of Antarctic seasonal ice cover during glacial intervals. In: Craddock, C. (Ed.) *Proceedings of the Third Symposium on Antarctic Geology and Geophysics*. pp. 1017-1026.
- Comiso, J.C., Maynard, N.G., Smith, W.O., Sullivan, C.W. (1990). Satellite ocean color studies of Antarctic ice edges in summer and autumn. *Journal of Geophysical Research – Oceans*. **95** (C6): 9481 – 9496.
- Comiso, J.C., McClain, C.R., Sullivan, C.W., Ryan, J.P., Leonard, C.L. (1993). Coastal zone color scanner pigment concentrations in the Southern Ocean and relationships to geophysical surface-features. *Journal of Geophysical Research – Oceans*. **98** (C2): 2419-2451.
- Coxall, H.K., Wilson, P.A., Palike, H., Lear, C.H., Backman, J. (2005). Rapid stepwise onset of Antarctic glaciation and deeper calcite compensation in the Pacific Ocean. *Nature*. **433**: 53-57.
- Craddock, C. (1972). *Geologic Map of Antarctica*, 1:5.000.000. American Geographical Society. New York.
- Crawford, R.M. (1995). The role of sex in the sedimentation of a marine diatom bloom. *Limnology and Oceanography*. **40** (1): 200-204.
- Crawford, R.M., Hinz, F., Ryneerson, T. (1997). Spatial and temporal distribution of assemblages of the diatom *Corethron criophilum* in the Polar Frontal region of the South Atlantic. *Deep-Sea Research Part II – Topical Studies in Oceanography*. **44** (1-2): 479-496.
- Cremer, H., Gore, D., Melles, M., Roberts, D. (2003) Palaeoclimatic significance of late Quaternary diatom assemblages from southern Windmill Islands, East Antarctica. *Palaeogeography, Palaeoclimatology, Palaeoecology*. **195**: 261-280.
- Crosta, X., Pichon, J.-J., Labracherie, M. (1997). Distribution of *Chaetoceros* resting spores in modern peri-Antarctic sediments. *Marine Micropaleontology*. **29**: 283-299.

- Crosta, X., Pichon, J.-J., Burckle, L.H. (1998). Application of modern analog technique to marine Antarctic diatoms: Reconstruction of maximum sea-ice extent at the Last Glacial Maximum. *Paleoceanography*. **13** (3): 284-297.
- Crosta, X., Romero, O., Armand, L.K., Pichon, J.-J. (2005). The biogeography of major diatom taxa in Southern Ocean sediments: 2. Open ocean related species. *Palaeogeography Palaeoclimatology Palaeoecology*. **223** (1-2): 66-92.
- Cuffey, K.M., Clow G.D. (1997). Temperature, accumulation, and ice sheet elevation in central Greenland through the last deglacial transition. *Journal of Geophysical Research-Oceans*. **102** (C12): 26383-26396.
- Cunningham, W.L., Leventer A. (1998). Diatom assemblages in surface sediments of the Ross Sea: relationship to present oceanographic conditions. *Antarctic Science*. **10** (2): 134-146.
- Cunningham, W.L., Leventer, A., Andrews, J.T., Jennings, A.E., Licht, K.J. (1999). Late Pleistocene-Holocene marine conditions in the Ross Sea, Antarctica: evidence from the diatom record. *The Holocene*. **9** (2): 129-139.
- D**
- Damuth, J.E., Fairbridge, R.W. (1970). Equatorial Atlantic deep-sea arkosic sands and ice-age aridity in tropical South-America. *Geological Society of America Bulletin*. **81** (1): 189-206.
- Darby, M.S., Wilmott, A.J., Somerville, T.A. (1995). On the influence of coastline orientation on the steady state width of latent heat polynya. *Journal of Geophysical Research*. **100** (C7): 13625-13633.
- Davis, C.H., Li, Y.H., McConnell, J.R., Frey, M.M., Hanna, E. (2005). Snowfall-driven growth in East Antarctic ice sheet mitigates recent sea-level rise. *Science*. **308**: 1898-1901.
- Deacon, G.E.R. (1937). The hydrology of the southern ocean. *Discovery Reports*. **15**: 1-124.
- Dean, J.M., Kemp, A.E.S., Bull, D., Pike, J., Patterson, G., Zolitschka, B. (1999). Taking varves to bits: scanning electron microscopy in the study of laminated sediments and varves. *Journal of Paleolimnology*. **22**: 121-136.
- De Baar, H.J.W., de Jong, J.T.M., Bakker, D.C.E., Löscher, B.M., Veth, C., Bathmann, U., Smetacek, V. (1995) Importance of iron for plankton blooms and carbon dioxide drawdown in the Southern Ocean. *Nature*. **373**: 412-415.
- DeConto, R.M., Pollard, D. (2003). A coupled climate-ice sheet modeling approach to the Early Cenozoic history of the Antarctic ice sheet. *Palaeogeography, palaeoclimatology, palaeoecology*. **198** (1-2): 39-52.

- DeFelice, D.R., Wise S.W.J.R. (1981). Surface lithofacies, biofacies, and diatom diversity patterns as models for delineation of climatic change in the Southeast Atlantic Ocean. *Marine Micropaleontology*. **6**: 29-70.
- Denton, G.H., Prentice, M.L., Burckle, L.H. (1991). Cainozoic history of the Antarctic Ice Sheet. In: Tingey, R.J. (Ed.). *The Geology of Antarctica*. Oxford, Clarendon Press. pp. 365-433.
- Doake, C.S.M., Vaughan D.G. (1991). Rapid disintegration of the Wordie Ice Shelf in response to atmospheric warming. *Nature*. **350**: 328-330.
- Doake, C.S.M., Corr, H.F.J., Rott, H., Skvarca, P., Young, N.W. (1998). Breakup and conditions for stability of the northern Larsen Ice Shelf. *Nature*. **391**: 778-779.
- Domack, E.W. (1982). Sedimentology of Glacial and Glacial Marine Deposits on the George-V - Adélie Continental-Shelf, East Antarctica. *Boreas*. **11** (1): 79-97.
- Domack, E.W. (1988). Biogenic facies in the Antarctic glacimarine environment: basis for a polar glacimarine summary. *Palaeogeography, Palaeoclimatology, Palaeoecology*. **63**: 357-372.
- Domack, E.W. (1992).  $^{14}\text{C}$  ages and reservoir corrections for the Antarctic Peninsula and Gerlache Strait area. *Antarctic Journal of the United States*. **27**: 63-63.
- Domack, E.W., Anderson, J.B. (1983). Marine geology of the George V continental margin; combined results of Deep Freeze 79 and the 1911-14 Australasian expedition. In: Oliver R.L., James P.R., Jago, J.B. (Eds.). *Antarctic earth science; fourth international symposium*. Cambridge, Cambridge University. pp. 402-406.
- Domack, E.W., Mayewski, P.A. (1999). Bi-polar ocean linkages: evidence from late-Holocene Antarctic marine and Greenland ice-core records. *The Holocene*. **9** (2): 247-251.
- Domack, E.W., Jull, A.J.T., Anderson, J.B., Linick, T.W., Williams, C.R. (1989). Application of tandem accelerator mass-spectrometer dating to Late Pleistocene Holocene sediments of the East Antarctic continental-shelf. *Quaternary Research*. **31** (2): 277-287.
- Domack, E.W., Jull, A.J.T., Anderson, J.B., Linick, T.W. (1991). Mid-Holocene glacial recession from the Wilkes Land continental shelf, East Antarctica. In: Thomson, M.R.A., Crame, J.A., Thomson, J.W. (Eds.) *Geological Evolution of Antarctica*. Cambridge, UK, Cambridge University Press. pp. 693-698.
- Domack, E.W., Schere, E., McClennen, C., Anderson, J. (1992). Intrusion of circumpolar deep water along the Bellingshausen Sea continental shelf. *Antarctic Journal of the United States*. **27**: 71.
- Domack, E., Mashiotto, T.A., Burkley, L.A., Ishman, S.E. (1993). 300-Year cyclicality in organic matter preservation in Antarctic fjord sediments. In: Kennett, J.P., Warnke,



- D.A. (Ed.) The Antarctic paleoenvironment: A perspective on global change. Antarctic Research Series. **60**: 265-272.
- Domack, E.W., Ishman, S.E., Stein, A.B., McClennen, C.E., Jull, A.J.T. (1995). Late Holocene advance of the Müller ice shelf, Antarctic Peninsula: sedimentological, geochemical and palaeontological evidence. *Antarctic Science*. **7** (2): 159-170.
- Domack, E.W., Jacobson, E.A., Shipp, S., Anderson, J.B. (1999). Late Pleistocene-Holocene retreat of the West Antarctic Ice-Sheet system in the Ross Sea: Part 2 - sedimentologic and stratigraphic signature. *Geological Society of America Bulletin*. **111**: 1517-1536.
- Domack, E., Leventer, A., Dunbar, R.B., Taylor, F., Brachfeld, S., Sjunneskog, C. (2001). Chronology of the Palmer Deep site, Antarctic Peninsula: a Holocene palaeoenvironmental reference for the circum-Antarctic. *The Holocene*. **11** (1): 1-9.
- Domack, E.W., Burnett, A., Leventer, A. (2003). Environmental setting of the Antarctic Peninsula. In: Domack, E.W., Burnett, A., Leventer, A. (Eds.). *Antarctic Peninsula Climate Variability*. Antarctic Research Series. **79**: 1-13.
- Domack, E.W., Leventer, A., Root, S., Ring, J., Williams, E., Carlson, D., Hirshorn, E., Wright, W., Gilbert, R., Burr, G. (2003). Marine sedimentary record of natural environmental variability and recent warming in the Antarctic Peninsula. In: Domack, E., Leventer, A., Burnett, A., Bindshadler, R., Convey, P., Kirby, M. (Eds.). *Antarctic Peninsula Climate Variability*. Antarctic Research Series. **79**: 205-224.
- Domack, E., Duran, D., Leventer, A., Ishman, S., Doane, S., McCallum, S., Amblas, D., Ring, J., Gilbert, R., Prentice, M. (2005). Stability of the Larsen B ice shelf on the Antarctic Peninsula during the Holocene epoch. *Nature*. **436**: 681-685.
- Domack, E., Amblas, D., Gilbert, R., Brachfeld, S., Camerlenghi, A., Rebesco, M., Canals, M., Urgeles, R. (2006). Subglacial morphology and glacial evolution of the Palmer Deep outlet system, Antarctic Peninsula. *Geomorphology*.
- Donahue, J.G. (1973). Distribution of planktonic diatoms in surface sediments of the Southern South Pacific. In: Goodhall, H.G. (Ed.). *Marine Sediments of the Southern Ocean*, American Geophysical Union. **17**: 18.
- Donegan, D., Schrader, H. (1982). Biogenic and abiogenic components of laminated hemipelagic sediments in the central Gulf of California. *Marine Geology*. **48**: 215-237.
- Drewry, D.J., Morris, E.M. (1992). The response of large ice sheets to climate change. *Philosophical Transactions of the Royal Society of London. Series B. Biological Sciences*. **338**: 235-242.
- Dunbar, R.B., Anderson, J.B., Domack, E.W., Jacobs, S.S. (1985). Oceanographic influences on sedimentation along the Antarctic Continental Shelf. In: Jacobs, S.S. (Ed.). *Oceanology of the Antarctic Continental Shelf*. Antarctic Research Series. **43**: 291-312.

Dunbar, R.B., Leventer, A.R., Stockton, W.L. (1989). Biogenic sedimentation in McMurdo Sound, Antarctica. *Marine Geology*. **85** (2-4): 155-179.

Duplessy, J.C., Shackleton, N.J., Matthews, R.K., Prell, W., Ruddiman, W.F., Caralp, M., Hendy, C.H. (1984). C-13 Record of benthic foraminifera in the Last Interglacial ocean - implications for the carbon-cycle and the global deep-water circulation. *Quaternary Research*. **21** (2): 225-243.

## E

El-Sayed, S.Z. (1970). On the productivity of the Southern Ocean (Atlantic and Pacific sectors). In: Holdgate, M.W. (Ed.). *Antarctic Ecology*. London and New York, Academic Press. pp. 119-135.

El-Sayed, S.Z., (1971). Observations on phytoplankton bloom in the Weddell Sea. In: Llano, G.A., Wallen, I.E. (Eds.). *Biology of the Antarctic Seas IV*. Antarctic Research Series. **17**: 301-312.

Eittrheim, S.L., Cooper, A.K., Wannesson, J. (1995). Seismic stratigraphic evidence of ice-sheet advances on the Wilkes Land margin of Antarctica. *Sedimentary Geology*. **96** (1-2): 131-156.

## F

Fairbanks, R.G. (1989). A 17,000-year glacio-eustatic sea-level record - influence of glacial melting rates on the Younger Dryas event and deep-ocean circulation. *Nature*. **342**: 637-642.

Fenner, J., Schrader, H.J., Wienigk, H. (1976). Diatom phytoplankton studies in the Southern Pacific Ocean, composition and correlation to the Antarctic Convergence and its paleoecological significance. Initial Reports of the Deep-Sea Drilling Project. **35**: 757- 813.

Flower, B.P., Kennett, J.P. (1994). The middle Miocene climatic transition – East Antarctic ice-sheet development, deep-ocean circulation and global carbon cycling. *Palaeogeography, Palaeoclimatology, Palaeoecology*. **108** (3-4): 537-555.

Froneman, P.W., Perissinotto, R., McQuaid, C.D., Laubscher, R.K. (1995). Summer distribution of net phytoplankton in the Atlantic sector of the Southern Ocean. *Polar Biology*. **15**: 77- 84.

Froneman, P.W., Pakhomov, E.A., Laubscher, R.K. (1997). Microphytoplankton assemblages in the waters surrounding South Georgia, Antarctica during austral summer 1994. *Polar Biology*. **17**: 515-522.

Fryxell, G.A. (1989). Marine-phytoplankton at the Weddell Sea ice edge - seasonal-changes at the specific level. *Polar Biology*. **10** (1): 1-18.

Fryxell, G.A. (1990). Planktonic marine diatom winter stages: Antarctic alternatives to resting spores. Proceedings of the 11th International Diatom Symposium. Memoirs of the Californian Academy of Sciences. **17**: 437-448.

Fryxell, G.A. (1991). Comparison of winter and summer growth stages of the diatom *Eucampia antarctica* from the Kerguelen Plateau and south of the Antarctic Convergence Zone. Proceedings of the Ocean Drilling Program, Scientific Results. **119**: 675-685.

Fryxell, G.A., Hasle, G.R. (1971). *Corethron criophilum* Castracane: Its distribution and structure. In: Llano, G.A., Wallen, I.E. (Eds.). Biology of the Antarctic Seas IV. Antarctic Research Series. **17**: 335-346.

Fryxell, G.A., Kendrick, G.A. (1988). Austral spring microalgae across the Weddell Sea ice edge; spatial relationships found along a northward transect during AMERIEZ 83. Deep-Sea Research Part A. Oceanographic Research Papers. **35**: 1-20.

Fryxell, G.A., Prasad, A.K.S.K. (1990). *Eucampia antarctica* var. *recta* (Mangin) stat. nov. (Biddulphiaceae, Bacillariophyceae): Life stages at the Weddell Sea ice edge. Phycologia. **29**: 27-38.

Fryxell, G.A., Kang, S.-H., Reap, M.E. (1987). AMERIEZ 1986: phytoplankton at the Weddell Sea ice edge. Antarctic Journal of the United States. **22**: 173-175.

## G

Ganopolski, A., Kubatzki, C., Claussen, M., Brovkin, V., Petoukhov V. (1998). The influence of vegetation-atmosphere-ocean interactions on climate during the mid-Holocene. Science. **220**: 1916-1919.

Garrison, D.L. (1991). Antarctic sea ice biota. American Zoologist. **31** (1):17-33.

Garrison, D.L., Buck, K.R. (1985). Sea-ice algal communities in the Weddell Sea: species composition in ice and plankton assemblages. In: Gray, J.S., Christiansen, M.E. (Eds.). Marine Biology of Polar Regions and Effects of Stress on Marine Organisms. John Wiley and sons Ltd. pp. 103-122.

Garrison, D.L. Buck, K.R. (1989). The biota of Antarctic pack ice in the Weddell Sea and Antarctic Peninsula regions. Polar Biology. **10** (3): 211-219.

Garrison, D.L. Close, A.R. (1993). Winter ecology of the sea-ice biota in Weddell Sea pack ice. Marine Ecology-Progress Series. **96** (1): 17-31.

Garrison, D.L., Buck, K.R. Silver, M.W. (1983a). Studies of ice-algal communities in the Weddell Sea. Antarctic Journal of the United States. **18**: 179-181.

Garrison, D.L., Ackley, S.F., Buck, K.R. (1983b). A physical mechanism for establishing algal populations in frazil ice. Nature. **306**: 363-365.

- Garrison, D.L., Sullivan, C.W., Ackley, S.F. (1986). Sea ice microbial communities in Antarctica. *Bioscience*. **36**: 243-250.
- Garrison, D.L., Buck, K.R., Fryxell, G.A. (1987). Algal assemblages in Antarctic pack ice and in ice-edge plankton. *Journal of Phycology*. **23**: 564-572.
- Garrison, D.L., Close, A.R., Reimnitz, E. (1989). Algae concentrated by frazil ice – evidence from laboratory experiments and field-measurements. *Antarctic Science*. **1** (4): 313-316.
- Gersonde, R. (1984). Siliceous microorganisms in sea ice and their record in sediments in the Southern Weddell Sea (Antarctica). 8th Diatom-Symposium. pp. 549-566.
- Gersonde, R., Wefer, G. (1987). Sedimentation of biogenic siliceous particles in Antarctic waters from the Atlantic Sector. *Marine Micropalaeontology*. **11**: 311-332.
- Gilbert, R., Chong, A., Dunbar, R.B., Domack, E.W. (2003). Sediment trap records of glacial marine sedimentation at Müller Ice Shelf, Lallemand Fjord, Antarctic Peninsula. *Arctic, Antarctic, and Alpine Research*. **35**: 24–33.
- Gleitz, M., Grossmann, S., Scharek, R., Smetacek, V. (1996). Ecology of diatom and bacterial assemblages in water associated with melting summer sea ice in the Weddell Sea, Antarctica. *Antarctic Science*. **8** (2): 135-146.
- Gleitz, M., Bartsch, A., Dieckmann, G.S., Eicken, H. (1998). Composition and succession of sea ice diatom assemblages in the eastern and southern Weddell Sea, Antarctica. In: Lizotte M.P., Arrigo K.R. (Eds.) *Antarctic sea ice biological processes, interactions, and variability*. *Antarctic Research Series*. **73**: 107-120.
- Gloersen, P., Campbell, W.J., Cavalieri, D.J., Comiso, J.C., Parkinson, C.L., Zwally, H.J. (1992). *Arctic and Antarctic sea ice, 1978-1987: satellite passive-microwave observations and analysis*. National Aeronautics and Space Administration. Special Publication 511. Washington, D.C. pp.1-290.
- Goldstein, J.I., Newbury, D.E., Echlin, P., Joy, D.C., Fiori, C., Lifshin, E. (1981). *Scanning electron microscopy and X-ray microanalysis*. New York, Plenum Press. pp. 1-673.
- Goodwin, I.D. (1993). Holocene deglaciation, sea-level change, and the emergence of the Windmill Islands, Budd Coast, Antarctica. *Quaternary Research*. **40** (1): 70-80.
- Goodwin, I.D. (1996). A mid to late Holocene readvance of the Law Dome ice margin, Budd Coast, East Antarctica. *Antarctic Science*. **8**: 395-406.
- Goodwin, I.D., Zweck, C. (2000). Glacio-isostasy and glacial ice load at Law Dome, Wilkes Land, East Antarctica. *Quaternary Research*. **53**: 285-293.

Gordon, A.L. Tchernia, P. (1972). Waters of the continental margin of Adélie Coast, Antarctica. In: Hayes, D.E. (Ed.). Antarctic Oceanology II: The Australian-New Zealand sector. Antarctic Research Series. **19**: 59-70.

Gordon, J.E., Harkness D.D., (1992). Magnitude and geographic-variation of the radiocarbon content in Antarctic marine life - implications for reservoir corrections in radiocarbon dating. Quaternary Science Reviews. **11** (7-8): 697-708.

Grant, W.S., Horner, R.A. (1976). Growth responses to salinity variation in four Arctic ice diatoms. Journal of Phycology. **12**: 180-185.

Grimm, K.A., Lange, C.B., Gill, A.S. (1996). Biological forcing of hemipelagic laminae: Evidence from ODP site 893, Santa Barbara Basin, California. Journal of Sedimentary Research. **66**: 613-624.

Grimm, K.A., Lange, C.B., Gill, A.S., (1997). Self-sedimentation of phytoplankton blooms in the geological record. Sedimentary Geology. **110**: 151-161.

Grotes, P.M., Stuiver, M., White, J.W.C., Johnsen, S., Jouzel, J. (1993). Comparison of oxygen-isotope records from the GISP2 and GRIP Greenland ice cores. Nature. **366**: 552-554.

Grossi, S.M., Sullivan, C.W. (1985). Sea ice microbial communities V. The vertical zonation of diatoms in an Antarctic fast ice community. Journal of Phycology. **21** (3): 401-409.

Grove, J.M. (1988). The Little Ice Age. Methuen, London. pp. 1-498.

## H

Harangozo, S.A. (2000). A search for the ENSO teleconnections in the west Antarctic Peninsula climate in austral winter. International Journal of Climatology. **20**: 1660-1673.

Harbison, G.R., Madin, L.P., Swanberg, N.R., Biggs, D.C., Hulburt, E.M., McAlister, V.L. (1977). *Rhizosolenia* mats. Limnology and Oceanography. **22**: 739-741.

Harden, S.L., DeMaster, D.J. Nittrouer, C.A. (1992). Developing sediment geochronologies for high-latitude continental shelf deposits: a radiochemical approach. Marine Geology. **103**: 69-97.

Hargraves, P.E., French F.W. (1983). Diatom resting spores; significance and strategies. In: Fryxell, G.A. (Ed.). Survival strategies of the algae. Cambridge University Press. pp. 49-68.

Harkness, D.D. (1979). Radiocarbon dates from Antarctica. British Antarctic Survey Bulletin. **47**: 43-59.

- Harris, P.T. (2000). Ripple cross-laminated sediments on the East Antarctic Shelf: evidence for episodic bottom water production during the Holocene? *Marine Geology*. **170**: 317-330.
- Harris, P.T., O'Brien, P.E. (1996). Geomorphology and sedimentology of the continental shelf adjacent to Mac. Robertson Land, East Antarctica: A scalped shelf. *Geo-Marine Letters*. **16**: 287-296.
- Harris, P.T., Beaman, R.J. (2003). Processes controlling the formation of the Mertz Drift, George Vth continental shelf, East Antarctica: evidence from 3.5 kHz sub-bottom profiling and sediment cores. *Deep-Sea Research Part II-Topical Studies in Oceanography*. **50** (8-9): 1463-1480.
- Harris, P.T., O'Brien, P.E., Sedwick, P., Truswell, A.M. (1996). Late Quaternary history of sedimentation on the Mac.Robertson shelf, East of Antarctica: problems with <sup>14</sup>C-dating of marine sediment cores. *Papers and Proceedings of the Royal Society of Tasmania*. **130** (2): 47-53.
- Harris, P.T., Brodie, P., Connell, R., Phillips, B., Radley, A., Reeve, S., Robertson, L., Stephenson, R., Thomas, S. (1997). Vincennes Bay, Prydz Bay and Mac.Robertson Shelf: Post-cruise Report. AGSO Rec. 1997/51.
- Harris, P.T., Brancolini, G., Armand, L., Busetti, M., Beaman, R.J., Giorgetti, G., Presti, M., Trincardi, F. (2001). Continental shelf drift deposit indicates non-steady state Antarctic bottom water production in the Holocene. *Marine Geology*. **179** (1-2): 1-8.
- Harris, P.T., Brancolini, G., Bindoff, N., De Santis, L. (2003). Recent investigations of the Mertz Polynya and George Vth Land continental margin, East Antarctica - Preface. *Deep-Sea Research Part II-Topical Studies in Oceanography*. **50** (8-9): 1335-1336.
- Hart, T.J. (1934). On the phytoplankton of the south-west Atlantic and the Bellingshausen Sea. *Discovery reports*. **8**: 1-268.
- Hart, T.J. (1937). *Rhizosolenia curvata* Zacharias, an indicator species in the Southern Ocean. *Discovery reports*. **16**: 413-446.
- Hart, T.J. (1942). Phytoplankton periodicity in Antarctic surface waters. *Discovery Reports*. **11**: 261-356.
- Hasle, G.R. (1965). *Nitzschia* and *Fragilariopsis* species studied in the light and electron microscopes, III, The genus *Fragilariopsis*. Oslo, Norway, Den Norske Videnskaps - Akademi i Oslo.
- Hasle, G.R. (1973). Some marine plankton genera of the diatom family *Thalassiosiraceae*. Second symposium on recent and fossil marine diatoms London, Sept. 4-9, 1972. *Beihefte zur Nova Hedwigia*. **45**: 1-49.

- Hasle, G.R. (1976). The biogeography of some marine planktonic diatoms. *Deep-Sea Research and Oceanographic Abstracts*. **23**: 319-338.
- Hasle, G.R., Syvertson, E.E. (1997). Marine diatoms. In: Tomas, C.R. (Ed.). *Identifying marine phytoplankton*. pp. 5-385.
- Hasle, G.R., Sims, P.A. Syvertsen, E.E. (1988). Two Recent *Stellarima* Species – *Stellarima microtrias* and *Stellarima stellaris* (Bacillariophyceae). *Botanica Marina*. **31** (3): 195-206.
- Hays, J.D. (1967). Quaternary sediments of the Antarctic Ocean. *Progress in Oceanography*. **4**: 117-131.
- Hendey, I. (1937). The plankton diatoms of the southern seas. *Discovery Reports*. **16**: 151-364.
- Hodell, D.A., Kanfoush, S.L., Shemesh, A., Crosta, X., Charles, C.D. Guilderson, T.P. (2001). Abrupt cooling of Antarctic Surface Waters and sea ice expansion in the South Atlantic sector of the Southern Ocean at 5000 cal. yr BP. *Quaternary Research*. **56**: 191-198.
- Hofmann, E.E., Klinck, J.M. (1998a). Hydrography and circulation of the Antarctic continental shelf: 150 degrees E to the Greenwich Meridan. *Coastal Segment. The Sea*. **11**: 997-1042.
- Hofmann, E.E., Klinck, J.M. (1998b). Thermohaline variability of the waters overlying the west Antarctic Peninsula continental shelf. In: Jacobs, S.S., Weis, R.F. (Eds). *Ocean, Ice and Atmosphere: Interactions at the Antarctic Continental Margin*. Antarctic Research Series. **75**: 67–81.
- Holm-Hansen, O., Mitchell, B.G., Hewes, C.D., Karl, D.M. (1989). Phytoplankton blooms in the vicinity of Palmer Station, Antarctica. *Polar Biology*. **10**: 49-57.
- Horner, R.A. (1976). Sea-ice organisms. *Oceanographic Marine Biological Annual Review*. **14**: 167-182.
- Horner, R.A. (1985a). History of ice algal investigations. In: Horner, R.A. (Ed.). *Sea ice biota*. CRC Press, Boca Raton, Florida. pp. 1-19.
- Horner, R.A. (1985b). Taxonomy of sea ice microalgae. In: Horner, R.A. (Ed.). *Sea ice biota*. CRC Press, Boca Raton, Florida. pp. 147-157.
- Hughes, T.J., Denton, G.H., Anderson, B.G., Schilling, D.H., Fastook, J.L., Lingle, C.S. (1981). The last great ice sheets: a global view. In: Denton, G.H., Hughes, T.J. (Eds.). *The Last Great Ice Sheets*. New York, Wiley. pp. 275-317.
- Hunke, E.C., Ackley, S.F. (2001). A numerical investigation of the 1997-1998 Ronne Polynya. *Journal of Geophysical*. **100**: 4751-4760.

Hustedt, F. (1930). Die Kieselalgen Deutschlands, sterreichs und der Schweiz. In: Rabenhorst, L. (Ed.), *Kryptogamen-Flora Deutschlands, sterreichs und der Schweiz*, Reprint 1977. Otto Koeltz Science Publishers, West Germany. pp. 1-920.

Hustedt, F., (1958). Diatomeen aus der Antarktis und dem Sqdatlaktik. Reprinted from "Deutsche Antarktische Expedition 19838/1939" Band II. Geographische-Kartographische Anstalt "Mundus". Hamburg, pp. 191.

## I

Imbrie, J., Boyle, E.A., Clemens, S.C., Duffy, A., Howard, W.R., Kukla, G., Kutzbach, D.G., Martinson, A., McIntyre, A., Mix, A.C., Molino, B., Morley, J.J., Peterson, L.C., Pisias, N.G., Prell, W., Raymo, M.E., Shackleton, N.J., Toggweiler, G.R. (1992). On the structure and origin of major glaciations cycles: 1. Linear responses to Milankovitch forcing. *Paleoceanography*. **7**: 701-738.

Ishman, S.E. (1990). Quantitative analysis of Antarctic benthic foraminifera: Application to paleoenvironmental interpretations. PhD thesis. Ohio State University, Columbus, USA.

Ingólfsson, Ó., Hjort, C., Berkman, P.A., Bjorck, S., Colhoun, E., Goodwin, I.D., Hall, B., Hirakawa, K., Melles, M., Moller, P., Prentice, M.L. (1998). Antarctic glacial history since the Last Glacial Maximum: an overview of the record on land. *Antarctic Science*. **10** (3): 326-344.

Ingólfsson, Ó., Hjort, C., Humlum, O., (2003). Glacial and climate history of the Antarctic Peninsula since the Last Glacial Maximum. *Arctic Antarctic and Alpine Research*. **35** (2): 175-186.

## J

Jacobs, S.S. (1989). Marine controls on modern sedimentation on the Antarctic continental-shelf. *Marine Geology*. **85** (2-4): 121-153.

Jacobs, S.S., Amos, A.F., Bruchhausen, P.M. (1970). Ross Sea oceanography and Antarctic Bottom Water formation. *Deep-Sea Research Part I – Oceanographic Research Papers*. **17**: 935-962.

Jacobs, S.S., Fairbanks, R.G., Horibe, Y. (1985). Origin and evolution of water masses near the Antarctic continental margin. In: Jacobs, S.S. (Ed.). *Oceanology of the Antarctic Continental Shelf*. Antarctic Research Series. **43**: 59-85.

Jaeger, J.M., Nittrouer, C.A., DeMaster, D.J., Dunbar R.B. (1996). Advection of suspended sediment in the Ross Sea and implications for the fate of biogenic material. *Journal of Geophysical Research*. **101**: 18479-18488.

Jim, C.Y. (1985). Impregnation of moist and dry unconsolidated clay samples using Spurr resin for microstructural studies. *Journal of Sedimentary Petrology*. **55**: 597-599.



Johnsen, S.J., Clausen, H.B., Dansgaard, W., Fuhrer, K., Gundestrup, N., Hammer, C.U., Iversen, P., Jouzel, J., Stauffer, B., Steffensen, J.P. (1992). Irregular glacial interstadials recorded in a new Greenland ice core. *Nature*. **359**: 311-313.

Jones, P.D. (1990). Antarctic temperatures over the present century - a study of the early expedition record. *Journal of climate*. **3** (11): 1193-1203.

Jones, G.A., Johnson, D.A. (1984). Displaced Antarctic diatoms in Vema Channel sediments: Late Pleistocene/Holocene fluctuations in AABW flow. *Marine Geology*. **58**: 165-186.

Jones, P.D., Marsh, R., Wigley, T.M.L., Peel, D.A. (1993). Decadal timescale links between Antarctic Peninsula ice-core oxygen-18, deuterium and temperature. *The Holocene*. **3** (1): 14-26.

Jordan, R.W., Pudsey, C.J. (1992). High-resolution diatom stratigraphy of Quaternary sediments from the Scotia Sea. *Marine Micropaleontology*. **19**: 201-237.

Jordan, R.W., Ligowski, R., Nöthig, E.-M., Priddle, J. (1991). The diatom genus *Proboscia* in Antarctic waters. *Diatom Research*. **6** (1): 63-78.

José, A.P., Koroleva, G.S., Nagaeva, G.A. (1962). Diatoms in the surface layer of sediment in the Indian sector of the Antarctic. *Trudy Instituta Okeanologii Akademiyi Nauk SSSR*. **61**: 20-91.

Jouzel, J., Lorius, C., Petit, J.R., Genthon, C., Barkov, N.I., Kotlyakov, V.M., Petrov, V.M. (1987). Vostok ice core: a continuous isotope temperature record over the last climatic cycle (160, 000 years). *Nature*. **329**: 403-408.

Jouzel, J., Masson, V., Cattani, O., Falourd, S., Stievenard, M., Stenni, B., Longinelli, A., Johnsen, S.J., Steffensen, J.P., Petit, J.R., Schwander, J., Souchez, R., Barkov, N.I. (2001). A new 27 ky high resolution East Antarctic climate record. *Geophysical Research Letters*. **28** (16): 3199-3202.

## K

Kaczmarzka, I., Barbrick, N.E., Ehrman, J.M., Cant, G.P. (1993). *Eucampia* Index as an Indicator of the Late Pleistocene Oscillations of the Winter Sea-Ice Extent at the Ocean Drilling Program Leg 119 Site 745b at the Kerguelen Plateau. *Hydrobiologia*. **269**: 103-112.

Kang, S.-H., Fryxell, G.A. (1991). Most abundant diatom species in water column assemblages from five ODP Leg 119 drill sites in Prydz Bay, Antarctica: Distributional patterns. *Proceeding of the Ocean Drilling Program, Scientific Results*, **119**: 645 – 666.

Kang, S.-H., Fryxell, G. (1992). *Fragilariopsis cylindrus* (Grunow) Krieger: The most abundant diatom in the water column assemblages of Antarctic marginal ice-edge zones. *Polar Biology*. **12**: 609-627.

- Kang, S.-H., Fryxell, G.A. (1993). Phytoplankton in the Weddell Sea, Antarctica – composition, abundance and distribution in water-column assemblages of the marginal ice-edge zone during austral autumn. *Marine Biology*. **116** (2): 335-348.
- Kang, S.-H., Fryxell, G.A., Roelke, D.L. (1993). *Fragilariopsis cylindrus* compared with other species of the diatom family Bacillariaceae in Antarctic marginal ice-edge zones. *Nova Hedwigia Beih.* **106**: 335–352.
- Kellogg, D.E., Kellogg, T.B. (1987). Microfossil distributions in modern Amundson Sea sediments. *Marine Micropalaeontology*. **12**: 203-222.
- Kemp, A.E.S. (1990). Sedimentary fabrics and variation in lamination style in Peru continental margin upwelling sediments. *Proceedings of the Ocean Drilling Program, Scientific Results*. **112**: 43-58.
- Kemp, A.E.S. (1996). Laminated sediments as palaeo-indicators. In: Kemp, A.E.S. (Ed.) *Palaeoclimatology and Palaeoceanography from Laminated Sediments*. Geological Society of London Special Publication. **116**: vii –xii.
- Kemp, A.E.S., Pearce, R.B., Koizumi, I., Pike, J., Rance, J. (1999). The role of mat-forming diatoms in the formation of Mediterranean sapropels. *Nature*. **398**: 57-61.
- Kemp, A.E.S., Pike, J., Pearce, R.B., Lange, C.B. (2000). The "Fall Dump" - a new perspective on the role of a "shade flora" in the annual cycle of diatom production and export flux. *Deep-Sea Research Part II – Topical Studies in Oceanography*. **47**: 2129-2154.
- Kennett, J.P. (1978). Development of planktonic biogeography in Southern-Ocean during Cenozoic. *Marine Micropalaeontology*. **3** (4): 301-345.
- Kennett, J.P., Shackleton, N.J. (1976). Oxygen isotopic evidence for development of psychrosphere 38 myr ago. *Nature*. **260**: 513-515.
- King, J.C. (1994). Recent climate variability in the vicinity of the Antarctic Peninsula. *International Journal of Climatology*. **14**: 357-369.
- King, J.C., Marshall, G.J., Connolley, W.M., Lachlan-Cope, T.A. (2003). Antarctic Peninsula climate variability and its cause as revealed by analysis of instrumental records. In: Domack, E., Leventer, A., Burnett, A. Bindschadler, R., Convey, P., Kirby, M. (Eds.). *Antarctic Peninsula climate variability*. Antarctic Research Series. **79**: 17-30.
- Kirby, M.E., Domack, E.W., McClennen, C.E. (1998). Magnetic stratigraphy and sedimentology of Holocene glacial marine deposits in the Palmer Deep, Bellingshausen Sea, Antarctica: implications for climate change? *Marine Geology*. **152** (4): 247-259.
- Kleinschmidt, G., Talarico, F. (2000). The Mertz Shear Zone. *Terra Antarctica Reports*. **5**: 109-115.

Kozlova, O.G. (1966). Diatoms of the Indian and Pacific Sectors of the Antarctic, national Science Foundation, Washington, D.C. by Israel Program for Scientific Translations, Jerusalem.

Krebs, W.N. (1983). Ecology of neritic marine diatoms, Arthur Harbor, Antarctica. *Micropaleontology*. **29**: 267-297.

Krebs, W.N., Lipps, J.H., Burckle, L.H. (1987). Ice diatom floras, Arthur Harbour, Antarctica. *Polar biology*. **7**: 163-171.

Kreutz, K.J., Mayewski, P.A., Meeker, L.D., Twickler, M.S., Whitlow, S.I., Pittalwala, I.I. (1997). Bipolar changes in atmospheric circulation during the little ice age. *Science*. **277**: 1294-1296.

Kulbe, T., Melle, M., Verkulich, S.R., Pushina, Z.V. (2001). East Antarctic climate and environmental variability over the last 9400 years inferred from marine sediments of the Bunger Oasis. *Arctic, Antarctic, Alpine Research*. **33**: 223-230.

## L

Larter, R.D., Vanneste, L.E. (1995). Relict subglacial deltas on the Antarctic Peninsula outer shelf. *Geology*. **23**: 33-36.

Lamoureux, S.F. (1994). Embedding unfrozen lake sediments for thin section preparation. *Journal of Palaeolimnology*. **10**: 141-146.

Lancelot, C., Billen, G., Veth, C., Mathot, S., Becquevort, S. (1991a). Modelling carbon cycling through phytoplankton and microbes in the Scotia-Weddell Sea area during sea ice retreat. *Marine Chemistry*. **35**: 305-324.

Lancelot, C., Veth, C., Mathot, S. (1991b). Modelling ice-edge phytoplankton bloom in the Scotia-Weddell Sea sector of the Southern Ocean during spring 1988. *Journal of Marine Systems*. **2**: 333-346.

Lawver, L.A., Gahagan L.M. (2003). Evolution of Cenozoic sea ways in the circum-Antarctic region. *Palaeogeography, Palaeoclimatology, Palaeoecology*. **198**: 11-37.

Lear, C.H., Elderfield, H., Wilson, P.A. (2000). Cenozoic deep-sea temperatures and global ice volumes from Mg/Ca in benthic foraminiferal calcite. *Science*. **287**: 269-272.

Ledford-Hoffman, P.A., DeMaster, D.J., Nittrouer, C.A. (1986). Biogenic-silica accumulation in the Ross Sea and the importance of Antarctic continental-shelf deposits in the marine silica budget. *Geochimica et Cosmochimica Acta*. **50**: 2099-2110.

Legendre, L., Ackley, S.F. Dieckmann, G.S., Gulliksen, B., Horner, R., Hoshiai, T., Melnikov, I.A., Reeburgh, W.S., Spindler, M., Sullivan, C.W. (1992). Ecology of sea ice biota. *Polar Biology*. **12**: 429-444.

- Leventer, A. (1991). Sediment trap diatom assemblages from the northern Antarctic Peninsula region. *Deep-Sea Research Part A - Oceanographic Research Papers*. **38** (8-9): 1127-1143.
- Leventer, A. (1992). Modern distribution of diatoms in sediments from the George V Coast, Antarctica. *Marine Micropalaeontology*. **19** (4): 315-332.
- Leventer, A. (1998). The fate of Antarctic "sea ice diatoms" and their use as paleoenvironmental indicators. In: Lizotte, M., and Arrigo, K., (Eds.). *Antarctic sea ice biological processes, interactions and variability*. Antarctic Research Series. **73**: 121-137.
- Leventer, A. (2003). Particulate flux from sea ice in polar waters. In: Thomas, D.N., Dieckmann, G.S. (Eds.). *Sea Ice: An introduction to its physics, chemistry, biology and geology*. Oxford, Blackwell Science Ltd. pp. 303-332.
- Leventer, A., Dunbar, R.B. (1987). Diatom Flux in McMurdo Sound, Antarctica. *Marine Micropaleontology*. **12** (1): 49-64.
- Leventer, A., Dunbar, R.B. (1988). Recent diatom record of McMurdo Sound, Antarctica: implications for the history of sea ice extent. *Paleoceanography*. **3**: 259-274.
- Leventer, A., Dunbar, R.B. (1996). Factors influencing the distribution of diatoms and other algae in the Ross Sea. *Journal of Geophysical Research – Oceans*. **101** (C8): 18489-18500.
- Leventer, A., Dunbar, R.B., Demaster, D.J. (1993). Diatom evidence for Late Holocene climatic events in Granite Harbor, Antarctica. *Paleoceanography*. **8** (3): 373-386.
- Leventer, A., Domack, E.W., Ishman, S.E., Brachfeld, S., McClennen, C.E., Manley, P. (1996). Productivity cycles of 200-300 years in the Antarctic Peninsula region: Understanding linkages among the sun, atmosphere, oceans, sea ice, and biota. *Geological Society of America Bulletin*. **108** (12): 1626-1644.
- Leventer, A., Brachfield, S., Domack, E.W., Dunbar, R., Manley, P., McClennen, C. (2001). CHAOS (Coring Holocene Antarctic Ocean Sediments) – NBP0101 Cruise Report.
- Leventer, A., Domack, E., Barkoukis, A., McAndrews, B., Murray, J. (2002). Laminations from the Palmer Deep: A diatom-based interpretation. *Paleoceanography*. **17**: 1-15.
- Ligowski, R. (1993). Marine diatoms (Bacillariophyceae) in the Antarctic ecosystem and their importance as an indicator of food source of krill (*Euphusia superba* Dana). *Wydział Uniwersytetu Łódzkiego*. Łódź (in Polish with English summary).

- Ligowski, R., Godlewski, M., Lukowski, A. (1992). Sea ice diatoms and ice edge planktonic diatoms at the northern limit of the Weddell Sea pack ice. *Proceedings of the National Institute of Polar Research Symposium. Polar Biology*. **5**: 9-20.
- Lisitzin, A.P. (1960). Bottom sediments of the eastern Antarctic and the Southern Indian Ocean. *Deep-Sea Research*. **7** (2): 89-99.
- Loewe, F. (1972). The land of storms. *Weather*. **27**: 110-121.
- Love, L.G. Amstutz, G.C. (1966). Review of microscopic pyrite from the Devonian Chattanooga shale and Rammelsberg Banderz. *Fortschritte der Mineralogie*. **43** (2): 273-309.
- Lowe, J.J., Walker, M.J.C. (1997). *Reconstructing Quaternary Environments*. Harlow, Addison Wesley Longman Ltd. pp. 1-446.
- Lozano, J.A., Hays, J.D. (1976). Relationship of radiolarian assemblages to sediment types and physical oceanography in the Atlantic and Western Indian Ocean Sectors of the Antarctic Ocean. In: Cline, R.M., Hays, J.D. (Eds.). *Investigation of late Quaternary Paleooceanography and Paleoclimatology*. Geological Society of America. pp. 303-336.
- Luz, B. (1977). Late Pleistocene paleoclimates of South-Pacific based on statistical-analysis of planktonic foraminifers. *Palaeogeography Palaeoclimatology Palaeoecology*. **22** (1): 61-78.
- Lynch-Stieglitz, J., Curry, W.B., Slowey, N. (1999). Weaker Gulf Stream in the Florida straits during the last glacial maximum. *Nature* **402**: 644-648.

## M

- Maddison, E.J., Pike J., Leventer, A. and Domack, E.W. (2005). Deglacial seasonal and sub-seasonal diatom record from Palmer Deep, Antarctica. *Journal of Quaternary Science*. **20**: 435-446.
- Maddison, E.J., Pike, J., Leventer, A., Dunbar, R., Brachfeld, S., Domack, E.W., Manley, P., McClennen, C. (in review). Post-glacial seasonal diatom record: an early record of the Mertz Glacier Polynya, East Antarctic Margin. *Marine Micropalaeontology*.
- Makarov, R.R. (1984). Distribution pattern of phytoplankton in the Lazarev Sea. *Hydrobiological Journal*. **20**: 101-106.
- Manabe, S., Broccoli A.J. (1985). A comparison of climate model sensitivity with data from the last glacial maximum. *Journal of Atmospheric Science*. **42**: 2643-2651.
- Manguin, E. (1960). Les diatomées de la Terre Adélie. *Annales des Sciences Naturelles*. **1**: 223- 385.

- Maqueda, M.A.M., Willmott A.J., Biggs, N.R.T. (2004). Polynya dynamics: A review of observations and modeling. *Reviews of Geophysics*. **42** (1): art. no.-RG1004.
- Marra, J., Boardman D.C. (1984). Late winter chlorophyll a distributions in the Weddell Sea. *Marine Ecology Progress Series*. **19**: 197-205.
- Martin, J.H. (1990). Glacial-interglacial CO<sub>2</sub> change: The iron hypothesis. *Paleoceanography*. **5** (1):1-13.
- Martinson, D.G., Pisias, N.G., Hays, J.D., Imbrie, J., Moore, T.C., Shackleton, N.J. (1987). Age dating and the orbital theory of the ice ages: development of a high resolution 0-300000 year chronostratigraphy. *Quaternary Research*. **27**: 1-29.
- Martinson, D.G., Iannuzzi R.A. (1998). Antarctic ocean-ice interactions: implications from ocean bulk property distributions in the Weddell Gyre. **74**: 243-271.
- Massom, R.A., Harris, P.T., Michael, K.J., Potter, M.J. (1998). The distribution and formative processes of latent-heat polynyas in East Antarctica. *Annals of Glaciology*. **27**: 420-426.
- Massom, R.A., Hill, K.L., Lytle, V.I., Worby, A.P., Paget, M., Allison, I. (2001). Effects of regional fast-ice and iceberg distributions on the behaviour of the Mertz Glacier Polynya, East Antarctica. *Annals of Glaciology*. **33**: 391-398.
- Massom, R.A., Jacka, K., Pook, M.J., Fowler, C., Adams, N., Bindoff, N. (2003). An anomalous late-season change in the regional sea ice regime in the vicinity of the Mertz Glacier Polynya, East Antarctica. *Journal of Geophysical Research-Oceans*. **108** (C7): art. no.-3212.
- Masson, V., Vimeux, F., Jouzel, J., Morgan, V., Delmotte, M., Ciais, P., Hammer, C., Johnsen, S., Lipenkov, V.Y., Mosley-Thompson, E., Petit, J.R., Steig, E.J., Stievenard, M., Vaikmae, R. (2000). Holocene climate variability in Antarctica based on 11 ice-core isotopic records. *Quaternary Research*. **54** (3): 348-358.
- Mayewski, P.A. (1975). Glacial geologic investigation of upper Rennick Glacier region, Northern Victoria Land. *Antarctic Journal of the United States*. **10** (4): 164-166.
- Mawson, D. (1915). *The Home of the Blizzard; being the story of the Australasian Antarctic Expedition 1911-1914*. Heinemann, London, pp. 438.
- McConville, M., Wetherbee, R. (1983). The bottom-ice microalgal community from annual ice in the inshore waters of East Antarctica. *Journal of Phycology*. **19**: 431-439.
- McMinn, A. (1994). Preliminary investigation of a method for determining past winter temperatures at Ellis Fjord, eastern Antarctica, from fast-ice diatom assemblages. *Memoirs of the Japanese National Institute of Polar Research, Special Issue*. **50**: 34-40.

- McMinn, A., Henk, H., Harle, K., McOrist, G. (2001). Late Holocene climatic change recorded in sediment cores from Ellis Fjord, East Antarctica. *The Holocene*. **11** (3): 291-300.
- McQuoid, M.R., Hobson L.A. (1996). Diatom resting stages. *Journal of Phycology*. **32**: 889-902.
- Mercer, J.H. (1978). West Antarctic Ice Sheet and CO<sub>2</sub> greenhouse effect - threat of disaster. *Nature*. **271**: 321-325.
- Miller, K.G., Wright, J.D., Fairbanks, R.G. (1991). Unlocking the Ice House: Oligocene-Miocene oxygen isotopes, eustasy, and margin erosion. *Journal of Geophysical Research*. **96**: 6829-6848.
- Mitchell, J.F.B., Grahame, N.S., Needham, K.J. (1988). Climate simulation for 9000 years before present: seasonal variations and the effect of the Laurentide ice sheet. *Journal of Geophysical Research*. **94**: 16097-16114.
- Mix, A.C., Bard, E., Schneider, R. (2001). Environmental processes of the ice age: land, oceans, glaciers (EPILOG). *Quaternary Science Reviews*. **20** (4): 627-657.
- Moisan, T.A., Fryxell, G.A. (1993). The distribution of Antarctic diatoms in the Weddell Sea during austral winter. *Botanica Marina*. **36** (6): 489-497.
- Moore, J.K., Abbott, M.R., (2000). Phytoplankton chlorophyll distributions and primary production in the Southern Ocean. *Journal of Geophysical Research*. **105**: 28,709-28,722.
- Mullan, A.B., Hickman J.S. (1990). Meteorology. In: Glasby, G.P. (Ed.). *Antarctic Sector of the Pacific*. New York, Elsevier. **51**: 21-54.
- Murray, J.W. (1973). *Distribution and ecology of living benthonic Foraminiferids*. Cane, Russak and Company, New York. pp. 1-274.
- Mysak, L.A., Huang, F.T. (1992). A latent-heat and sensible-heat polynya model for the North Water, Northern Baffin-Bay. *Journal of Physical Oceanography*. **22** (6): 596-608.

## N

- Nelson, D.M., Gordon, L.I. (1982). Production and pelagic dissolution of biogenic silica in the Southern Ocean. *Geochimica et Cosmochimica Acta*. **46**: 491-501.
- Nelson, D.M., Smith Jr., W.O. (1986). Phytoplankton bloom dynamics of the western Ross Sea II. Mesoscale cycling of nitrogen and silicon. *Deep-Sea Research Part A - Oceanographic Research Papers*. **33**: 1389-1412.
- Nelson, D.M., Smith, W.O., Gordon, L.I., Huber, B.A. (1987). Spring distributions of density, nutrients, and phytoplankton biomass in the ice edge zone of the Weddell-Scotia Sea. *Journal of Geophysical Research*. **92**: 7181-7190.

Nelson, D.M., Treguer, P., Brzezinsinki, M.A., Leynaert, A., Quéguiner, B. (1995). Production and dissolution of biogenic silica in the ocean: Revised global estimates, comparison with regional data and relationship to biogenic sedimentation. *Global Biogeochemical Cycle*. **9** (3): 359-372.

Neori, A., Holm-Hansen, O. (1982). Effect of temperature on rate of photosynthesis in Antarctic phytoplankton. *Polar Biology*. **1** (1): 33-38.

Niebauer, H.J., Alexander, V. (1985). Oceanographic frontal structure and biological production at an ice edge. *Continental Shelf Research*. **4**: 367-388.

## O

Ohshima, K.I., Kazumasa, Y., Shimoda, H., Wakatsuchi, M., Endoh, T., Fukuchi, M. (1998). Relationship between the upper ocean and sea ice during the Antarctic melting season. *Journal of Geophysical Research*. **103**: 7601-7615.

Omoto, K. (1983). The problem and significance of radiocarbon geochronology in Antarctica. In: Oliver, R.L., James, P.R., Jago, J.B. (Eds.). *Antarctic Earth Science*. Cambridge, Cambridge University Press. pp. 450-452.

Open University course team (1998). *Ocean circulation*. Butterworth-Heinemann, Oxford. pp. 1-238.

Orsi, A.H., Whitworth, T., Nowlin, W.D.J. (1995). On the meridional extent and fronts of the Antarctic Circumpolar Current. *Deep-Sea Research Part I – Oceanographic Research Papers*. **42**: 641-673.

## P

Palmisano, A.C., Garrison D.L. (1993). Microorganisms in Antarctic sea-ice. In: Friedman, I. (Ed.). *Antarctic Microbiology*. New York, Wiley-Liss. pp. 167-218.

Patience, R.L., Clayton, C.J., Kearsley, A.T., Rowlands, S.J., Bishop, A.N., Rees, A. W.G., Bibby, K.G., Hopper, A.C. (1990). An integrated biochemical, geochemical, and sedimentological study of organic diagenesis in sediments from Leg 112. *Proceedings of the Ocean Drilling Program, Scientific Results*. **112**: 135-153.

Pearce, R.B., Kemp, A.E.S, Koizumi, I., Pike, J., Cramp, A., Rowland, S.J. (1998). A lamina-scale, SEM based study of a late quaternary diatom ooze sapropel from the Mediterranean ridge, site 971. In: Robertson, A.H.F., Emeis, K.C., Richter, C., Camerlenghi, A. (Eds.). *Proceedings of the Ocean Drilling Program, Scientific Results*. **160**: 349-363.

Pease, C.H. (1987). The size of wind-driven coastal polynyas. *Journal of Geophysical Research*. **92** (C7): 7049-7059.

Periard, C., Pettre, P. (1993). Some aspects of the climatology of Dumont d'Urville, Adélie Land, Antarctica. *International Journal of Climatology*. **13** (3): 313-327.



- Peterson, G.M., Webb, T.I., Kutzbach, J.E., van der Hammen, T., Wijnstra, T., Street, F.A. (1979). The continental record of environmental conditions at 18,000 yr B.P.: an initial evaluation. *Quaternary Research*. **12**: 47-82.
- Petit, J. R., Briat, M., Royer, A. (1981). Ice-Age aerosol content from East Antarctic ice core samples and past wind strength. *Nature*. **293**: 391-394.
- Petit, J.R., Jouzel, R., Raynaud, D., Barkov, N.I., Barnola, J.-M., Basile, I., Benders, M., Chappellaz, J., Davis, M., Delaygue, G., Delmotte, M., Kotlyakov, V.M., Legrand, M., Lipenkov, V.Y., Lorius, C., Pepin, L., Ritz, C., Saltzman, E., Stievenard, M. (1999). Climate and atmospheric history of the past 420,000 years from the Vostok ice core, Antarctica. *Nature*. **399**: 429-436.
- Pfuhl, H.A., McCave, N. (2005). Evidence for the late Oligocene establishment of the Antarctic Circumpolar climate. *Earth and Planetary Science Letters*. **235**: 715-728.
- Phleger, F.B. (1960) Ecology and distribution of recent Foraminifera. The John Hopkins Press, Baltimore. pp. 1-297.
- Pichon, J.J., Labeyrie, L.D., Bareille, G., Labracherie, M., Duprat, J., Jouzel, J. (1992a). Surface water temperature changes in the high latitudes of the southern hemisphere during the last glacial-interglacial cycle. *Paleoceanography*. **7**: 289-313.
- Pichon, J.-J., Bareille, G., Labracherie, M., Labeyrie, L.D., Baudrimont, A., Turon, J.L. (1992b). Quantification of the biogenic silica dissolution in Southern Ocean sediments. *Quaternary Research*. **37** (3): 361-378.
- Pickard, G.L., Emery, W.J. (1990). Descriptive physical oceanography: an introduction. Pergamon Press. pp. 1-320.
- Pierrehumbert, R.T. (1999). Huascarán delta O-18 as an indicator of tropical climate during the Last Glacial Maximum. *Geophysical Research Letters*. **26** (9): 1345-1348.
- Pike, J., Kemp, A.E.S. (1996). Preparation and analysis techniques for studies of laminated sediments. In: Kemp A.E.S. (Ed.). *Palaeoclimatology and Palaeoceanography from Laminated Sediments*. Geological Society Special Publication. **116**: 37-48.
- Pike, J., Moreton, S.G., Allen, C.S. (2001). Data report: microfabric analysis of postglacial sediments from Palmer Deep, Western Antarctic Peninsula. *Proceedings of the Ocean Drilling Program, Scientific Results*. **178**: 1-17.
- Piotrowski, A.M., Goldstein, S.L., Hemming, S.R., Fairbanks, R.G. (2004). Intensification and variability of ocean thermohaline circulation through the last deglaciation. *Earth and Planetary Science Letters*. **225** (1-2): 205-220.
- Piotrowski, A.M., Goldstein, S.L., Hemming, S.R., Fairbanks, R.G. (2005). Temporal relationships of carbon cycling and ocean circulation at glacial boundaries. *Science*. **307**: 1933-1938.

- Pokras, E.M., Molfino, B. (1986). Oceanographic control of diatom abundances and species distributions in surface sediments of the Tropical and Southeast Atlantic. *Marine Micropalaeontology*. **10**: 165-188.
- Polysciences Inc. (1986). Spurr Low-Viscosity Embedding Media. Polysciences Data Sheet. **127**.
- Pondaven, P., Ragueneau, O., Tréguer, P., Hauvespre, A., Dezileau, L., Reyss, J.L. (2000). Resolving the 'opal paradox' in the Southern Ocean. *Nature*. **405**: 168-172.
- Potter, J.R., Paren, G. (1985). Interaction between ice shelf and ocean in George VI Sound, Antarctica. In: Jacobs, S.S. (Ed.). *Oceanology of the Antarctic Continental Shelf*. Antarctic Research Series. **43**: 35-58.
- Prasad, A.K.S.K., Nienow, J.A. (1986). Marine diatoms of sediments from Croft Bay, Antarctica. *Antarctic Journal of the United States*. **21**: 157-159.
- Presti, M., De Santis, L., Buseti, M., Harris, P.T. (2003). Late Pleistocene and Holocene sedimentation on the George V Continental Shelf, East Antarctica. *Deep-Sea Research Part II-Topical Studies in Oceanography*. **50** (8-9): 1441-1461.
- Priddle, J., Fryxell, G. (1985). *Handbook of the Common Plankton Diatoms of the Southern Ocean. Centrales except the Genus Thalassiosira*. Cambridge, British Antarctic Survey. pp.1-159.
- Priddle, J., Thomas, D.P. (1989). *Coscinodiscus bouvet* Karsten - a distinctive diatom which may be an indicator of changes in the Southern-Ocean. *Polar Biology*. **9** (3): 161-167.
- Priddle, J., Jordan, R.W., Medlin, L.K. (1990). Family *Rhizosoleniaceae*. In: Medlin L.K., Priddle, J. (Eds.). *Polar marine diatoms*. British Antarctic Survey, Cambridge. pp. 115-127.
- Pudsey, C.J., Barker, P.F., Larter, R.D. (1994). Ice sheet retreat from the Antarctic Peninsula shelf. *Continental Shelf Research*. **14**: 1647-1675.
- Pye, K., Krinsley, D.H. (1984). Petrographic examination of sedimentary rocks in the SEM using backscattered electron detectors. *Journal of Sedimentary Petrology*. **54**: 877-888.

## R

- Rebesco, M., Camerlenghi, A., Zanolla, C. (1998a). Bathymetry and morphogenesis of the continental margin west of the Antarctic Peninsula. *Terra Antarctica*. **5** (4): 715-725.
- Rebesco, M., Camerlenghi, A., De Santis, L., Domack, E., Kirby, M.. (1998b). Seismic stratigraphy of Palmer Deep: a fault-bounded late Quaternary sediment trap

on the inner continental shelf, Antarctic Peninsula Pacific margin. *Marine Geology*. **151**: 89-110.

Reynolds, J.M. (1981). The distribution of mean annual temperatures in the Antarctic Peninsula. *British Antarctic Survey Bulletin*. **54**: 123-133.

Rignot, E. (2002). East Antarctic glaciers and ice shelves mass balance from satellite data. *Annals of Glaciology*. **34**: 217-227.

Rintoul, S.R. (1998). On the origin and influence of Adélie Land bottom water. In: Jacobs, S.S., Weiss, R.F. (Eds.). *Ocean, Ice and Atmosphere: Interactions at the Antarctic Continental Margin*. Antarctic Research Series. **75**: 151-171.

Rolfe, W.D.I., Brett, D.W. (1969). Fossilization Processes. In: Eglinton, G., Murphy, M.T.J. (Eds.). *Organic Geochemistry Methods and Results*. New York / Heidelberg / Berlin (Springer-Verlag). pp. 213-244.

Romero, O., Hensen, C. (2002). Oceanographic control of biogenic opal and diatoms in surface sediments of the Southwestern Atlantic. *Marine Geology*. **186** (3-4): 263-280.

Rott, H., Skvarca, P., Nagler, T. (1996). Rapid collapse of northern Larsen Ice Shelf, Antarctica. *Science*. **271**: 788-792.

Rott, H., Rack, W., Nagler, T., Skvarca, P. (1998). Climatically induced retreat and collapse of northern Larsen Ice Shelf, Antarctic Peninsula. *Annals of Glaciology*. **27**: 86-92.

Round, F.E. (1971). Benthic marine diatoms. *Oceanography and Marine Biology Annual Review*. **9**: 83-139.

Round, F.E., Crawford, R.M. Mann, D.G. (1990). *The diatoms: biology and morphology of the genera*. Cambridge University Press. pp. 1-747.

## S

Sakshaug, E., Holm-Hansen, O. (1984). Factors governing pelagic production in polar oceans. In: Holm-Hansen, O., Bolis, L., Gilles., R. (Eds.). *Marine phytoplankton and productivity, lecture notes coastal and estuarine studies*. **8**: 1-18.

Sakshaug, E., Skjoldal, H.R. (1989). Life at the Ice Edge. *Ambio*. **18**: 60-67.

Sambrotto, R.N., Matsuda, A., Vaillancourt, R., Brown, M., Langdon, C., Jacobs, S. S., Measures, C. (2003). Summer plankton production and nutrient consumption patterns in the Mertz Glacier Region of East Antarctica. *Deep-Sea Research Part II-Topical Studies in Oceanography*. **50** (8-9): 1393-1414.

Sancetta, C. (1999). Diatoms and marine paleoceanography. In: Stoermer, E.F., Smol, J.P. (Eds.). *The Diatoms: Applications for the environmental and earth sciences*, pp. 374-386.

- Sarnthein, M. (1978). Sand deserts during the glacial maximum and climatic optimum. *Nature*. **272**: 43-46.
- Scambos, T.A., Hulbe, C., Fahnstock, M., Bohlander, J. (2000). The link between climate warming and break-up of ice shelves in the Antarctic Peninsula. *Journal of Glaciology*. **46**: 516.
- Scambos, T., Raup, R., Bohlander, J. (2001). Images of Antarctic ice shelves, March 2004. Boulder, CO: National Snow and Ice Data Center. Digital media. [http://nsidc.org/data/iceshelves\\_images/mertz.html](http://nsidc.org/data/iceshelves_images/mertz.html) (07/09/05).
- Schallreuter, R. (1984). Framboidal pyrite in deep-sea sediments. *Initial Reports of the Deep Sea Drilling Project*. **75**: 875-891.
- Scherer, R.P. (1994). A new method for the determination of absolute abundance of diatoms and other silt-sized sedimentary particles. *Journal of Paleolimnology*. **12**: 171-179.
- Schimmelmann, A., Lange, C.B., Berger, W.H. (1990). Climatically controlled marker layers in Santa Barbara Basin sediments and fine-scale core-to-core correlation. *Limnology and Oceanography*. **35**: 165-173.
- Schloss, I., Estrada, M. (1994). Phytoplankton composition in the Weddell-Scotia confluence area during austral spring in relation to hydrography. *Polar Biology*. **14** (2): 77-90.
- Schrader, H.J., Schütte, G., (1981). Marine diatoms. *The Sea*. **7**: 1179-1232.
- Schwerdtfeger, W. (1984). *Weather and Climate of the Antarctic, Developments in Atmospheric Sciences*. New York, Elsevier. pp. 1-261.
- Scott, P., McMinn, A., Hosie, G. (1994). Physical parameters influencing diatom community structure in eastern Antarctic sea ice. *Polar biology*. **14**: 507-517.
- Sedwick, P.N., Harris, P.T., Robertson, L.G., McMurty, G.M., Cremer, M.D., Robinson, P. (2001). Holocene sediment records from the continental shelf of Mac. Robertson Land, East Antarctica. *Paleoceanography*. **16** (2): 212-225.
- Selph, K.E., Landry, M.R., Allen, C.B., Calbet, A., Christensen, S., Bidigare, R.R. (2001). Microbial community composition and growth dynamics in the Antarctic Polar Front and seasonal ice zone during late spring 1997. *Deep-Sea Research Part II-Topical Studies in Oceanography*. **48** (19-20): 4059-4080.
- Semina, H.J. (2003). SEM - studied diatoms of different regions of the World Ocean. *Iconographia Diatomologica*. **10**: 1-362.
- Shackleton, N.J. (1987). Oxygen isotopes, ice volume and sea level. *Quaternary Science Reviews*. **6**: 183-190.

- Shemesh, A., Burckle, L.H., Froelich, P.N. (1989). Dissolution and preservation of Antarctic diatoms and the effect on sediment thanatocoenoses. *Quaternary Research*. **31** (2): 288-308.
- Shepherd, A., Wingham, D., Fahnestock, M., Bohlander, J. (2003). Larsen ice shelf has progressively thinned. *Science*. **302**: 856-859.
- Shevenell, A.E., Domack, E.W., Kernan, G.M. (1996). Record of Holocene palaeoclimate change along the Antarctic Peninsula: evidence from glacial marine sediments, Lallemand Fjord. *Papers and Proceedings of the Royal Society of Tasmania*. **130**: 55-64.
- Sievers, H.A., Nowlin, W.D.J. (1984). The stratification and water masses at Drake Passage. *Journal of Geophysical Research*. **89**: 10489-10514.
- Simmonds, I., Murray, R.J. (1999). Southern extratropical cyclone behaviour in ECMWF analyses during the FROST special observing periods. *Weather and Forecasting*. **14**: 878-891.
- Simmonds I. (2003). Regional and large-scale influences on Antarctic Peninsula climate. In: Domack, E., Leventer, A., Burnett, A., Bindschadler, R., Convey, P., Kirby, M. (Eds). *Antarctic Peninsula Climate Variability*. Antarctic Research Series. **79**: 31-42.
- Sjunneskog, C., Taylor, F. (2002) Postglacial marine diatom record of the Palmer Deep, Antarctic Peninsula (ODP Leg 178, Site 1098) I: Total diatom abundance. *Paleoceanography*. **17** (3): Art. No. 8003.
- Skvarca, P., De Angelis, H. (2003). Impact assessment of regional climatic warming on glaciers and ice shelves of the northeastern Antarctic Peninsula. In: Domack, E., Leventer, A., Burnett, A., Bindschadler, R., Convey, P., Kirby, M. *Antarctic Peninsula Climate Variability*. Antarctic Research Series. **79**: 69-78.
- Smayda, T.J. (1970). The suspension and sinking of phytoplankton in the sea. *Oceanography and Marine Biology Annual Reviews*. **8**: 353-414.
- Smetacek, V. (1985) Role of sinking in diatom life history cycles: ecological, evolutionary and geological significance. *Marine Biology*. **84**: 239-251.
- Smetacek, V., Scharek, R., Gordon, L.I., Eicken, H., Fuhtbach, E., Rohardt, G., Moore, S., (1992). Early spring phytoplankton blooms in ice platelet layers of the southern Weddell Sea, Antarctica. *Deep-Sea Research Part A – Oceanographic Research Series*. **39**: 153-168.
- Smetacek, V., DeBaar, H.J.W., Bathmann, U.V., Lochte, K., VanderLoeff, M.M.R. (1997). Ecology and biogeochemistry of the Antarctic Circumpolar Current during austral spring: A summary of Southern Ocean JGOFS cruise ANT X/6 of RV Polarstern. *Deep-Sea Research Part II-Topical Studies in Oceanography*. **44** (1-2): 1-21.

- Smetacek, V., Assmy, P., Henjes, J. (2004). The role of grazing in structuring Southern Ocean pelagic ecosystems and biogeochemical cycles. *Antarctic Science*. **16** (4): 541-558.
- Smith, W.O., Nelson, D.M. (1985). Phytoplankton bloom produced by a receding ice edge in the Ross Sea - spatial coherence with the density field. *Science*. **227**: 163-166.
- Smith, W.O., Nelson, D.M. (1986). Importance of ice edge phytoplankton production in the Southern Ocean. *Bioscience*. **36**: 251-257.
- Smith, D.A., Hofmann, E.E., Klinck, J.M., Lascara, C.M. (1999a). Hydrography and circulation of the west Antarctic Peninsula continental shelf. *Deep-Sea Research Part I - Oceanographic Research Papers*. **46**: 925-949.
- Smith, R.C., Ainley, D., Baker, K., Domack, E., Emslie, S., Fraser, B., Kennett, J., Leventer, A., Mosley-Thompson, E., Stammerjohn, S., Vernet, M. (1999b). Marine ecosystem sensitivity to climate change. *Bioscience*. **49** (5): 393-404.
- Smith, R.C., Fraser, W.R., Stammerjohn, S.E., Vernet, M. (2003). Palmer long-term ecological research on the Antarctic Peninsula. In: Domack, E., Leventer, A., Burnett, A., Bindschadler, R., Convey, P., Kirby, M. (Eds.). *Antarctic Peninsula Climate Variability*. Antarctic Research Series. **79**: 131-144.
- Sommer, U. (1991). Comparative nutrient status and competitive interactions of two Antarctic diatoms (*Corethron criophilum* and *Thalassiosira antarctica*). *Journal of Plankton Research*. **13**: 61-75.
- Spurr, A.R. (1969). A low-viscosity epoxy resin embedding medium for electron microscopy. *Journal of Ultrastructure Research*. **26**: 31-43.
- Steig, E.J., Brook, E.J., White, J.W.C., Sucher, C.M., Bender, M.L., Lehman, S.J., Morse, D.L., Waddington, E.D., Clow, G.D. (1998). Synchronous climate changes in Antarctica and the North Atlantic. *Science*. **282**: 92-95.
- Stickley, C.E., Brinkhuis, H., Schellenberg, S.A., Sluijs, A., Rohl, U., Fuller, M.D., Grauert, M., Huber, M., Warnaar, J., Williams, G.L. (2004). Timing and nature of the deepening of the Tasmanian Gateway. *Paleoceanography*. **19**: 1-18.
- Stickley, C.E., Pike, J., Leventer, A., Dunbar, R., Domack, E.W., Brachfeld, S., Manley, P., McClennen, C. (2005). Deglacial ocean and climate seasonality in laminated diatom sediments, Mac. Robertson Shelf, Antarctica. *Palaeogeography, Palaeoclimatology, Palaeoecology*. **227**: 290-310.
- Stillwell, F.L. (1918). The metamorphic rocks of Adélie Land. Australian Antarctic Expedition 1911-1914. Science Report A III. pp. 7-230.
- Stock, J., Molnar, P. (1987). Revised history of early Tertiary plate motion in the south-west Pacific. *Nature*. **325**: 495-499.

- Stockwell, D.A., Kang, S.-H., Fryxell, G.A. (1991). Comparisons of diatom biocoenoses with Holocene sediment assemblages in Prydz Bay, Antarctica. *Proceedings of the Ocean Drilling Program, Scientific Results*. **119**: 667-673.
- Stuiver, M., Pearson, G.W., Braziunas, T. (1986). Radiocarbon age calibration of marine samples back to 9000 cal yr BP. *Radiocarbon*. **28**: 980-1021.
- Stuiver, M., Reimer, P.J., Reimer, R.W. (2005). CALIB 5.0. (www program and documentation). <http://radiocarbon.pa.qub.ac.uk/calib/>.
- Sullivan C.W., McClain, C.R., Comiso, J.C., Smith, W.O. (1988). Phytoplankton standing crops within an Antarctic ice edge assessed by satellite remote sensing. *Journal of Geophysical Research*. **93**: 12487–12498.
- Sundström, B.G. (1986). The marine diatom genus *Rhizosolenia*. A new approach to taxonomy. Lund, Lund University, Sweden. PhD thesis.
- Swan, A.R.H. Sandilands, M. (1995). Introduction to geological data analysis, Blackwell Science Limited.
- T**
- Tanimura, Y., Fukuchi, M., Watanabe, K., Moriwaki, K. (1990). Diatoms in water column and sea-ice in Lutzow-Holm Bay, Antarctica, and their preservation in the underlying sediments. *Bulletin of the National Science Museum (Japan)*. Series C. **16** (1): 15-39.
- Taylor, F. (1999a). Sedimentary diatom assemblages of Prydz Bay. PhD Thesis. University of Tasmania, Hobart, Australia.
- Taylor, F. (1999b). Sedimentary diatom assemblages of Prydz Bay and MacRobertson Shelf, East Antarctica, and their use as paleoecological indicators. Senior thesis, Hamilton College, USA.
- Taylor, F.W., Sjunneskog, C. (2002). Postglacial marine diatom record of the Palmer Deep, Antarctic Peninsula (ODP Leg 178, Site 1098) 2. Diatom assemblages. *Paleoceanography*. **17** (3): 8001, doi:10.1029/2000PA000564.
- Taylor, F., McMinn, A., Franklin, D. (1997). Distribution of diatoms in surface sediments of Prydz Bay, Antarctica. *Marine Micropalaeontology*. **32**: 209-229.
- Taylor, F., Whitehead, J., Domack., E. (2001). Holocene paleoclimatic change in the Antarctic Peninsula: evidence from the diatom, sedimentary and geochemical record. *Marine Micropalaeontology*. **41**: 25-43.
- Taylor, F., McMinn, A. (2002). Late Quaternary diatom assemblages from Prydz Bay, Eastern Antarctica. *Quaternary Research*. **57**: 151-161.
- Thomas, C.W. (1966). Vertical circulation off the Ross Ice Shelf. *Pacific Science*. **20**: 239-249.

Tréguer, P., Nelson, D.M., Van Bennekom, A.J., DeMaster, D.J., Leynaert, A., Queguiner, B. (1995). The silica balance in the World Ocean: A reestimate. *Science*. **268**: 375-379.

Truesdale, R.S., Kellogg, T.B. (1979). Ross Sea Diatoms: Modern assemblage distributions and their relationship to ecologic, oceanographic and sedimentary conditions. *Marine Micropaleontology*. **4**: 13-31.

Tuncel, G., Aras, N.K., Zoller, W.H. (1989). Temporal variations and sources of elements in the South Pole atmosphere. 1. Non-enriched and moderately-enriched elements. *Journal of Geophysical Research*. **94**: 13025-13038.

## V

Van Bennekom, A.J., Berger, G.W., Van der Gaast, S.J., De Vries, R.T.P. (1988). Primary productivity and the silica cycle in the Southern Ocean (Atlantic Sector). *Palaeoceanography, Palaeoclimatology, Palaeoecology*. **67**: 19-30.

Vandergoes, M.J., Newnham, R.M., Preusser, F., Hendy, C.H., Lowell, T.V., Fitzsimons, S.J., Hogg, A.G., Kasper, H.U., Schluchter, C. (2005). Regional insolation forcing of late Quaternary climate change in the Southern Hemisphere. *Nature*. **436**: 242-245.

van Iperen, J.M., Weering, T.C.E., Jansen, J.H.F., van Bennekom, A.J. (1987). Diatoms in surface sediments of the Zaire deep-sea fan (SE Atlantic Ocean) and their relation to overlying water masses. *Netherlands Journal of Sea Research*. **21** (3): 203–217.

Vaughan, D.G., Doake, C.S.M. (1996). Recent atmospheric warming and retreat of ice shelves on the Antarctic Peninsula. *Nature*. **379**: 328-331.

Vaughan, D.G., Marshall, G.J., Connolley, W.M., King, J.C., Mulvaney, R. (2001). Devil is in the detail. *Science*. **293**: 1777-1779.

Vaughan, D.G., Marshall, G.J., Connolley, W.M., Parkinson, C., Mulvaney, R., Hodgson, D.A., King, J.C., Pudsey, C.J., Turner, J. (2003). Recent rapid regional climate warming on the Antarctic Peninsula. *Climatic Change*. **60** (3): 243-274.

Villareal, T.A. (1988). Positive buoyancy in the oceanic diatom *Rhizosolenia debyana* H. Peragallo. *Deep-Sea Research Part A - Oceanographic Research Papers*. **35**: 1037-1045.

Villareal, T.A., Fryxell, G.A. (1983). Temperature effects on the valve structure of the polar diatoms *Thalassiosira antarctica* and *Porosira glacialis*. *Polar Biology*. **2**: 163-169.

Villareal, T.A., Altabet, M.A., Culver-Rymsza, K. (1993). Nitrogen transport by vertically migrating diatom mats in the North Pacific Ocean. *Nature*. **363**: 709-712.



Villareal, T.A., Woods, S., Moore, J.K., Culver-Rymsza, K. (1996). Vertical migration of *Rhizosolenia* mats and their significance to NO<sub>3</sub> fluxes in the central North Pacific gyre. *Journal of Plankton Research*. **18**: 1103-1121.

Vimeux, F., Masson, V., Jouzel, J., Petit, J.R., Steig, E.J., Stievenard, M., Vaikmae, R., White, J.W.C. (2001). Holocene hydrological cycle changes in the Southern Hemisphere documented in East Antarctic deuterium excess records. *Climate Dynamics*. **17** (7): 503-513.

von Bodungen, B. (1986). Phytoplankton growth and krill grazing during spring in the Bransfield Strait, Antarctica - Implications from sediment trap collections. *Polar Biology*. **6**: 153-160.

## W

Wagenbach, D. (1996). Coastal Antarctica: atmospheric chemical composition and atmospheric transport. In: Wolff, E.W., Bales, R.C. (Eds.) *Chemical Exchange between the Atmosphere and Polar Snow*. NATO ASI Series 143, Springer-Verlag, Berlin. pp. 173-199.

Watanabe, K. (1982). Centric diatom communities found in the Antarctic sea ice. *Antarctic Record*, National Institute of Polar Research. **7**: 119-126.

Watanabe, K. (1988). Sub-ice microalgal strands in the Antarctic coastal fast ice area near Syowa Station. *Japanese Journal of Phycology*. **36**: 221-229.

Weaver, A.J., Saenko, O.A., Clark, P.U., Mitrovica, J.X. (2003). Meltwater pulse 1A from Antarctica as a trigger of the Bølling- Allerød warm interval. *Science*. **299**: 1709-1713.

Weertman, J. (1973). Can a water-filled crevasse reach the bottom surface of a glacier? Symposium on the Hydrology of glaciers; water within glaciers, II. Stelczer-Karoly, International Association of Scientific Hydrology-Association Internationale d'Hydrologie Scientifique (International Union of Geodesy and Geophysics-Union de Geodesie et de Geophysique Internationale). **95**: 139-145.

Wendler, G., Pritchard, D. (1991). Temperature increase observed in Adélie Land, East Antarctica? *Antarctic Journal of the United States*. **26** (5): 281-284.

Wendler, G., Ahlnas, K., Lingle, C.S. (1996a). On Mertz and Ninnis glaciers, East Antarctica. *Journal of Glaciology*. **42** (142): 447-453.

Wendler, G., Ahlnas, K., Lingle, C. (1996b). On the Mertz and Ninnis glaciers, Eastern Antarctica. *Antarctic Journal of the United States*. **31**: 75-76.

Wendler, G., Gilmore, D., Curtis, J. (1997). On the formation of coastal polynyas in the area of Commonwealth Bay, Eastern Antarctica. *Atmospheric Research*. **45** (1): 55-75.

Whitaker, T.M. (1982). Primary production of phytoplankton off Signy Island, South Orkneys, the Antarctic. *Proceedings of the Royal Society of London. Series B: Biological Sciences.* **214**: 169–189

Whitehead, J.M. McMinn, A. (1997). Paleodepth determination from Antarctic benthic diatom assemblages. *Marine Micropaleontology.* **29**: 301-318.

Williams, G.D., Bindoff, N.L. (2003). Wintertime oceanography of the Adélie Depression. *Deep-Sea Research Part II-Topical Studies in Oceanography.* **50** (8-9): 1373-1392.

Wilson, A.T. Hendy C.H. (1971). Past wind strength from isotope studies. *Nature.* **234**: 344-345.

Wright, J.D., Miller, K.G. (1993). Southern Ocean influences on Late Eocene to Miocene deepwater circulation. In: Kennett, J.P., Warnke, D.A. (Eds.). *The Antarctic Paleoenvironment: A Perspective on Global Change.* Antarctic Research Series. **60**: 1-25.

## Y

Yoder, J.A., Ackleson, S.G., Barber, R.T., Flament, P., Balch, W.M. (1994). A Line in the Sea. *Nature.* **371**: 689-692.

## Z

Zachos, J.C., Quinn, T.M., Salamy, K.A. (1996). High-resolution ( $10^4$  years) deep-sea foraminiferal stable isotope records of the Eocene-Oligocene climate transition. *Palaeoceanography.* **11**(3): 251-266.

Zielinski, U. (1993). Quantitative estimation of palaeoenvironmental parameters of the Antarctic surface water in the Late Quaternary using transfer functions with diatoms. *Berichte zur Polarforschung.* **126**: 1-148.

Zielinski, U., Gersonde, R. (1997). Diatom distribution in Southern Ocean surface sediments (Atlantic sector): Implications for paleoenvironmental reconstructions. *Palaeogeography, Palaeoclimatology, Palaeoecology.* **129**: 213-250.

Zwally, H.J., Comiso, J.C., Gordon, A.L. (1985). Antarctic offshore leads and polynyas and oceanographic effects. In: Jacobs, S.S. (Ed.) *Oceanology of the Antarctic Continental Shelf.* Antarctic Research Series. **43**: 203-226.

